

**N 70 37560**

**CR 112789**

REPORT NO. 12411-6012-ROOO

JULY 1970

# **CASE FILE COPY**

## **ADVANCED SPACECRAFT VALVE TECHNOLOGY COMPILATION**

### **VOLUME I MECHANICAL CONTROLS**

*Prepared for*

*THE JET PROPULSION LABORATORY  
PASADENA, CALIFORNIA 91103*

*under*

*NATIONAL AERONAUTICS AND SPACE ADMINISTRATION  
Contract NAS 7-717*

**TRW**  
SYSTEMS GROUP

ONE SPACE PARK • REDONDO BEACH • CALIFORNIA



REPORT NO. 12411-6012-ROOO

JULY 1970

# ADVANCED SPACECRAFT VALVE TECHNOLOGY COMPILATION

## VOLUME I MECHANICAL CONTROLS

*Prepared for*

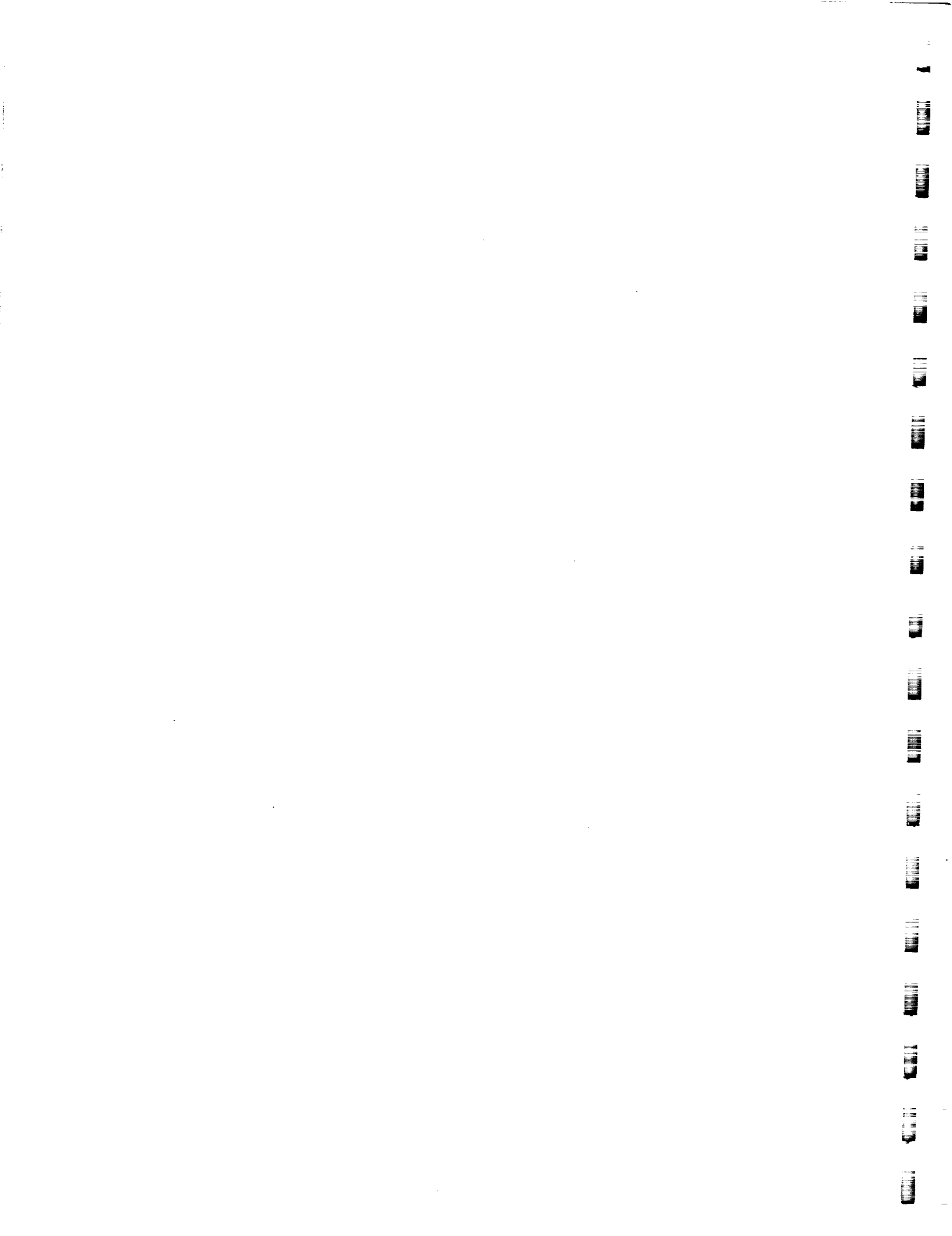
THE JET PROPULSION LABORATORY  
PASADENA, CALIFORNIA 91103

*under*

NATIONAL AERONAUTICS AND SPACE ADMINISTRATION  
Contract NAS 7-717

**TRW**  
SYSTEMS GROUP

ONE SPACE PARK • REDONDO BEACH • CALIFORNIA





## FOREWORD

The Advanced Valve Technology Compilation was prepared by TRW Systems Group, Redondo Beach, California. The compilation represents the results of work undertaken on a series of programs having the main objective of advancing the art of valve technology used on liquid chemical propulsion spacecraft engines. The series of program efforts began in 1962 and continued to 1970, and were performed for the Chief, Liquid Propulsion Technology, Code RPL, Headquarters, National Aeronautics and Space Administration, Washington, D. C. Mr. Frank E. Compitello was the Headquarters Project Manager. The program was administered under the technical direction of Mr. Louis R. Toth of the Jet Propulsion Laboratory, Pasadena, California.

The compilation was prepared within the TRW Science and Technology Division. Mr. R. J. Salvinski of the Applied Technology Department was responsible for the preparation. The compilation represents several years of technical effort, including consultation and efforts on the part of many NASA and Air Force agencies, universities, and industrial companies. The TRW technical staff responsible for the results of the work presented in the compilation are listed below.

J. Alter	D. Hill	S. N. Prescott
A. Ambruso	G. W. Howell	J. L. Reger
C. Armstrong	L. J. Hynek	L. Rosales
R. J. Berg	S. Lieberman	Dr. A. Rosen
Dr. P. Bhuta	R. Lovejoy	C. Salts
K. A. Bloom	J. E. Magallanes	Dr. R. Sayano
B. P. Brady	M. J. Makowski	W. A. Schaal
Dr. H. Burge	C. Mangion	J. R. Smirra
Dr. J. M. Denney	Dr. H. T. Mann	Dr. V. Srinivasan
N. H. Doshi	F. L. Merritt	J. L. Vogl
R. G. Downing	W. Miller	T. M. Weathers
O. O. Fiet	P. Mitchell	M. Weiner
M. H. Goodrow	Dr. J. Neff	D. Yates
Dr. A. Grenall	D. L. Perkins	L. D. Young
R. L. Hammel	R. Porter	

# VOLUME I - MECHANICAL CONTROLS

## CONTENTS

	<u>Page</u>
1.0 INTRODUCTION	1-1
1.1 Background	1-1
1.2 Purpose and Scope	1-2
1.3 References	1-4
2.0 OPERATIONAL, FUNCTIONAL AND ENVIRONMENTAL CONSIDERATIONS	2-1
2.1 Introduction	2-1
2.2 Operational Considerations	2-1
2.2.1 Fluid Operating Temperatures	2-1
2.2.2 Fluid Operating Pressure	2-2
2.2.3 Acceleration, Vibration and Shock	2-3
2.2.4 Contamination	2-5
2.2.5 Gaseous Flow Media	2-5
2.2.6 Liquid Propellants	2-6
2.2.7 Leakage	2-7
2.2.8 Sterilization	2-7
2.3 Functional Parameters	2-12
2.3.1 Response Time	2-12
2.3.2 Weight	2-12
2.3.3 Power Requirements	2-13
2.3.4 Operating Life	2-14
2.4 Space Environment Considerations	2-15
2.4.1 Vacuum	2-15
2.4.2 Radiation	2-23
2.4.3 Zero Gravity	2-36
2.4.4 Time	2-36
2.4.5 Temperature in Space	2-39
2.4.6 Space Maintenance	2-39
2.4.7 Meteoroids	2-40
2.5 References	2-49

## ILLUSTRATIONS

<u>Figure</u>		<u>Page</u>
2-1	Temperature Vs. Vapor Pressure.....	2-16
2-2	Fission Energy Spectrum.....	2-25
2-3	Isointensity Contours of the Inner Radiation Zone.....	2-25
2-4	Spectral Distribution of Protons in the Edge of the Inner Radiation Zone.....	2-25
2-5	Electron Isointensity Contours Before and After The Storm.....	2-27
2-6	Electron Spectrum in the Outer Radiation Zone.....	2-27
2-7	Differential Energy of Decay of Sept. 28 Event.....	2-30
2-8	Gamma-Ray Absorption at 1 Mev Energy.....	2-32
2-9	Gamma-Ray Absorption at 4 Mev Energy.....	2-32
2-10	Range-Energy Relation for Electrons to 10 Mev.....	2-33
2-11	Range-Energy Relation in Aluminum for Electrons to 10 Mev.....	2-33
2-12	Range-Energy Relation for Protons to 100 Mev.....	2-35
2-13	Range-Energy Relation for Protons to 100 Mev.....	2-35
2-14	High-Velocity Penetration in Aluminum.....	2-44
2-15	Rear Surface Damage in Relatively Thick Targets.....	2-44

## TABLES

<u>Table</u>		
2-1	Estimated Decelerations Upon Planetary Entry.....	2-3
2-2	Representative Values of Acceleration, Vibration and Shock.....	2-4
2-3	Properties of Elastomers Exposed to 12% Ethylene Oxide-88% Freon 12 for 24 Hours.....	2-10
2-4	Properties of Lexan, Kel-F and DC 4 Grease Exposed to 12% Ethylene Oxide - 88% Freon 12 for 24 Hours.....	2-11
2-5	Effect of Exposure to 12% Ethylene Oxide - 88% Freon 12 for 24 Hours on Metals and Metal Coatings.....	2-11
2-6	Radiation Dose Rates for Various Orbits.....	2-30
2-7	Relationship of Time and Effects of Functional and Environmental Parameters.....	2-38
2-8	Hypervelocity Impact in Semi-Infinite Metallic Targets.....	2-42
2-9	Hypervelocity Impact in Thin Multilayer Targets.....	2-46

## CONTENTS

	<u>Page</u>
3.0 MATERIALS	3-1
3.1 Introduction	3-1
3.2 Discussion	3-2
3.3 Materials Compatibility Test Methods	3-6
3.4 Recommendations	3-9
3.5 Propellant Rating Chart (Table 3-2)	3-10
3.6 Earth Storable Propellants	3-12
3.6.1 Fuels	3-12
3.6.2 Oxidizers	3-39
3.7 Space Storable Propellants	3-58
3.7.1 Fuels	3-58
3.7.2 Oxidizers	3-64
3.7.3 Nitrogen-Fluorine Compounds	3-76
3.8 Hard Cryogenics	3-77
3.8.1 Liquid Fluorine	3-77
3.8.2 Liquid Oxygen	3-81
3.8.3 Liquid Hydrogen	3-83
3.8.4 Liquid Oxygen-Liquid Fluorine Mixtures	3-86
3.9 Gelled Propellants	3-87
3.9.1 Liquid Gelled Propellants	3-87
3.9.2 Metallized Gelled Propellants	3-89
3.10 References	3-91

TABLES

<u>Table</u>		<u>Page</u>
3-1	Rating Chart for Macroscopic and Microscopic Examination of Corrosion Behavior of Metals (After Champion)	3-4
3-2	Propellant Rating Chart	3-11
3-3	Hydrazine ( $N_2H_4$ )	3-14
3-4	Monomethylhydrazine	3-20
3-5	Unsymmetrical Dimethylhydrazine (UDMH)	3-23
3-6	Aerozine-50 (50% Hydrazine/50% UDMH)	3-28
3-7	Hydrazine-Hydrazine Nitrate	3-33
3-8	Pentaborane	3-36
3-9	Nitrogen Tetroxide	3-42
3-10	Physical Appearance of One and Four Month Aluminum Specimens Prior To and After Removal of Propellant ( $N_2O_4$ )	3-51
3-11	Physical Appearance of One and Four Month Stainless Steel Specimens Prior To and After Removal of Propellant ( $N_2O_4$ )	3-52
3-12	Physical Appearance of One and Four Month Titanium Specimens Prior To and After Removal of Propellant ( $N_2O_4$ )	3-53
3-13	Rating Chart for Macroscopic and Microscopic Examination of Corrosion Behavior of Metals (After Champion)	3-54
3-14	Results of One and Four Month Storage of 6061 T6 Aluminum Specimens With Neat and Contaminated $N_2O_4$ at 165°F	3-55
3-15	Results of One and Four Month Storage of 347 Stainless Steel Specimens With Neat and Contaminated $N_2O_4$ at 165°F	3-56
3-16	Results of One and Four Month Storage of Ti-6Al-4V Alloy Specimens With Neat and Contaminated $N_2O_4$ at 165°F	3-57
3-17	Diborane	3-59
3-18	Hybaline A-5	3-61
3-19	Chlorine Trifluoride ( $ClF_3$ )	3-66
3-20	Chlorine Pentafluoride	3-68
3-21	Oxygen Difluoride	3-71
3-22	Perchloryl Chloride	3-75
3-23	Liquid Fluorine ( $LF_2$ )	3-80
3-24	Liquid Hydrogen ( $H_2$ )	3-85
3-25	Liquid Fluorine Liquid Oxygen (FLOX)	3-86

## CONTENTS

	<u>Page</u>
4.0 VALVES	4-1
4.1 Introduction	4-1
4.2 Valve State Of The Art	4-1
4.2.1 Valve Component Rating Analysis Chart	4-1
4.2.2 Surveys and Searches	4-2
4.2.3 Valve Problem Areas	4-5
4.2.4 Valve Review	4-11
4.3 Valve Design Consideration	4-20
4.3.1 Propellant Valve Requirements	4-20
4.3.2 Feed System Component Definition	4-33
4.3.3 Valve Redundancy	4-40
4.4 Conceptual Valve Designs	4-45
4.4.1 Semi-Toroidal Diaphragm Valve	4-45
4.4.2 Diaphragm Valve	4-47
4.4.3 Radial Shutoff Valve	4-49
4.4.4 Valves With Thermally Generated Seat Stress	4-51
4.4.5 Microvalves	4-52
4.4.6 Electrofluid Interaction in Valves	4-55
4.4.7 Electroseat Valve	4-55
4.4.8 Surface Tension Valve Concepts	4-58
4.4.9 Radioisotope Heated Valves	4-61
4.4.10 Fusion Valve	4-62
4.4.11 Diffusion Valve	4-64
4.5 Zero G Vent Valve Study	4-66
4.5.1 Introduction	4-66
4.5.2 Survey of Zero G Vent Techniques	4-67
4.5.3 Consideration of Thermodynamic Processes	4-69
4.5.4 Experimental Zero G Thermal Vent System	4-70
4.5.5 Vent System for Liquid Hydrogen	4-73
4.6 In-Tank Design Study	4-76
4.6.1 Advantages	4-76
4.6.2 Disadvantages	4-78
4.7 References	4-79

## ILLUSTRATIONS

<u>Figure</u>		<u>Page</u>
4-1	Typical Bipropellant Spacecraft Propulsion System.....	4-6
4-2	Typical Attitude Control for Spacecraft.....	4-6
4-3	Prototype Cone Labyrinth Valve.....	4-12
4-4	Pneumatic Pressure Regulator for Mariner C.....	4-14
4-5	Chemically Etched Filter Wafer.....	4-14
4-6	Cavitating Flow Control Valve.....	4-19
4-7	Cavitating Venturi Throttle Valve Performance With LN <sub>2</sub> ..	4-19
4-8	Pulse Width Time History.....	4-23
4-9	Pressure-Fed Engine Schematic.....	4-26
4-10	Bipropellant Feed System With Turbine Flowmeters.....	4-26
4-11	Bipropellant System With Cavitating Control Valve.....	4-26
4-12	Bipropellant Cavitating Venturi Valve.....	4-28
4-13	Relationships Between Opening Signal, Valve Stroke, and Chamber Pressure.....	4-28
4-14	Valve Stroke-Flow Characteristic Curves.....	4-28
4-15	Chamber Pressure Versus Valve Closing Time.....	4-32
4-16	OF <sub>2</sub> /B <sub>2</sub> H <sub>6</sub> Propellant Feed System.....	4-34
4-17	OF <sub>2</sub> /B <sub>2</sub> H <sub>6</sub> Mass Flowrates @ I <sub>sp</sub> of 400 Sec.....	4-41
4-18	OF <sub>2</sub> /B <sub>2</sub> H <sub>6</sub> Volumetric Flowrates @ I <sub>sp</sub> of 400 Sec.....	4-41
4-19	Propellant Head Loss Versus Flow Area at I <sub>sp</sub> of 400 Sec.	4-42
4-20	Propellant Flow Area Vs. Thrust at I <sub>sp</sub> of 400 Sec.....	4-42
4-21	B <sub>2</sub> H <sub>6</sub> Critical Flow Velocities.....	4-42
4-22	OF <sub>2</sub> Critical Flow Velocities.....	4-42
4-23	OF <sub>2</sub> -B <sub>2</sub> H <sub>6</sub> Line Diameter Vs. Thrust at I <sub>sp</sub> of 400 Sec.....	4-44
4-24	Mean Helium Flowrate Vs. Engine Thrust.....	4-44
4-25	Helium Pressure Drop Vs. Flow Area.....	4-44
4-26	Helium Flow Area Vs. Thrust.....	4-44
4-27	Semi-Toroidal Diaphragm Seal Detail.....	4-46
4-28	Lightweight Semi-Toroidal Propellant Valve Concept.....	4-46
4-29	Integral Semi-Toroidal Bipropellant Valve Configuration.	4-46
4-30	Coaxial Variable Thrust Injector With Semi-Toroidal Valve	4-46
4-31	Mixture Ratio Controller With Semi-Toroidal Valve.....	4-48
4-32	Bipropellant Diaphragm Valve.....	4-48
4-33	Integrated Venturi and Radial Shutoff Valve Concept.....	4-50

<u>Figure</u>		<u>Page</u>
4-34	Thermal Shutoff Valve With High Compression Poppet Seating.....	4-53
4-35	Thermal Shutoff Valve - Wagon Wheel Concept.....	4-53
4-36	Two-Way Normally Closed Thermally Actuated Microvalve..	4-53
4-37	Dual Two-Way Thermally Actuated Microvalve.....	4-54
4-38	Three-Way Snap Action Thermally Actuated Valve.....	4-54
4-39	Piezoelectrically Actuated Three-Way Valve.....	4-54
4-40	Electroseal Valve Concept.....	4-57
4-41	Electroseal No-Moving Part Valve Concept.....	4-57
4-42	Electroseal Valve Test Model.....	4-57
4-43	Electroseal Valve Test Setup.....	4-57
4-44	Electromagnetic Capillary Valve Concept.....	4-59
4-45	Electromagnetic Capillary Valve Test Unit.....	4-59
4-46	Capillary Relief Valve.....	4-59
4-47	Capillary Check Valve.....	4-59
4-48	Radioisotope Heated Valve Seat.....	4-63
4-49	Prototype Fusion Valve.....	4-63
4-50	Diffusion Valve Concept for Use With a Microthruster...	4-65
4-51	Centaur Vapor/Liquid Separator.....	4-68
4-52	Saturn IV Vapor/Liquid Separator.....	4-68
4-53	Vent Valve and In-Line Heat Exchanger Arrangement.....	4-68
4-54	Vent Valve and In-Line Heat Exchanger With Turbine.....	4-71
4-55	Zero G Venting Process With Secondary Compression/ Expansion Cycle.....	4-71
4-56	Experimental Zero G Thermal Vent System.....	4-72
4-57	Zero G Thermal Vent System.....	4-72
4-58	LH <sub>2</sub> Zero G Vent Test Tank Assembly.....	4-74
4-59	LH <sub>2</sub> Pressure Vessel With Heat Exchanger.....	4-74
4-60	Pressure Vessel Installation in Vacuum Tank.....	4-74
4-61	TRW Pneumatic Operated (Pierce Valve) External Design Configuration.....	4-77
4-62	TRW Pneumatic Operated (Pierce Valve) Internal Design Configuration.....	4-77



## TABLES

<u>Table</u>		<u>Page</u>
4-1	Valve Component Rating Analysis Chart.....	4-3
4-2	Electromechanical Valve Characteristics.....	4-16
4-3	Factors Influencing Valve Selection and Design.....	4-23
4-4	Relationships Between Valve Parameters, Engine Parameters and Control Mode.....	4-23
4-5	Engine Pressure Schedule.....	4-26
4-6	OF <sub>2</sub> /B <sub>2</sub> H <sub>6</sub> Feed System Components.....	4-34
4-7	Component Problems in Baseline OF <sub>2</sub> -B <sub>2</sub> H <sub>6</sub> Feed System....	4-36
4-8	Critical Component Performance Parameters.....	4-38
4-9	Component and System Leakage Criteria.....	4-39
4-10	Component Pressure Drop Allowances.....	4-41
4-11	Component and Line Size Summary.....	4-43
4-12	Diffusion Valve Estimated Thrust Level.....	4-65

## CONTENTS

	<u>Page</u>
5.0 LEAKAGE AND SEALING TECHNOLOGY	5-1
5.1 Leakage Technology	5-1
5.1.1 Leakage Considerations and Criteria	5-1
5.1.2 Leakage Phenomena	5-2
5.1.3 Gas and Liquid Leakage Correlations	5-6
5.1.4 Effects of Wear Particles and Temperature	5-7
5.1.5 The Effect of Ultrasonic Disturbance on Leakage	5-14
5.1.6 Propellant Leakage in Vacuum	5-20
5.1.7 Permeation Seal Leakage	5-47
5.2 Sealing Technology	5-53
5.2.1 State Of The Art Evaluation	5-53
5.2.2 Teflon Seal Improvements	5-54
5.2.3 Wet Seal Study	5-56
5.2.4 Metal-to-Metal Seals	5-82
5.2.5 Thin Film Studies	5-87
5.2.6 Energized Seal Development	5-117
5.3 References	5-124

## ILLUSTRATIONS

<u>Figure</u>		<u>Page</u>
5-1	Mechanism of Clogging - Zero Liquid Leakage.....	5-3
5-2	Definition of Zero Gas Leakage as a Function of Upstream Gas Pressure.....	5-3
5-3	Theoretical Nitrogen Flow Through Flat-Seat Valve Model	5-4
5-4	One-Inch Flat Poppet and Seat Model.....	5-4
5-5	Thick Cylindrical Shell Subjected to a Steady State Thermal Gradient.....	5-15
5-6	Displacement Vs. Polar Angle.....	5-15
5-7	Ultrasonic Leakage Test Schematic.....	5-17
5-8	Case I - Maximum Adiabatic Leakage Rates Without Solid Phase Formation - Hydrazine.....	5-30
5-9	Case I - Maximum Adiabatic Leakage Rates Without Solid Phase Formation - Monomethylhydrazine.....	5-30
5-10	Case I - Maximum Adiabatic Leakage Rates Without Solid Phase Formation - Aerozine-50.....	5-30
5-11	Case I - Maximum Adiabatic Leakage Rates Without Solid Phase Formation - Unsymmetrical Dimethylhydrazine.....	5-30
5-12	Case I - Maximum Adiabatic Leakage Rates Without Solid Phase Formation - Pentaborane.....	5-31
5-13	Case I - Maximum Adiabatic Leakage Rates Without Solid Phase Formation - Diborane.....	5-31
5-14	Case I - Maximum Adiabatic Leakage Rates Without Solid Phase Formation - Chlorine Trifluoride.....	5-31
5-15	Case I - Maximum Adiabatic Leakage Rates Without Solid Phase Formation - Perchloryl Fluoride.....	5-31
5-16	Case I - Maximum Adiabatic Leakage Rates Without Solid Phase Formation - Nitrogen Tetroxide.....	5-32
5-17	Case I - Maximum Adiabatic Leakage Rates Without Solid Phase Formation - Liquid Hydrogen.....	5-32
5-18	Case I - Maximum Adiabatic Leakage Rates Without Solid Phase Formation - Liquid Fluorine.....	5-32
5-19	Case I - Maximum Adiabatic Leakage Rates Without Solid Phase Formation - Liquid Oxygen.....	5-32
5-20	Case I - Maximum Adiabatic Leakage Rates Without Solid Phase Formation - Oxygen Fluoride.....	5-33
5-21	Case II - Minimum Flow Rate Vs. Injector Orifice Area - $N_2H_4$ .....	5-33
5-22	Case II - Minimum Flow Rate Vs. Injector Orifice Area - MMH.....	5-34

ILLUSTRATIONS ( CONT. )

<u>Figure</u>		<u>Page</u>
5-23	Case II - Minimum Flow Rate Vs. Injector Orifice Area - UDMH.....	5-34
5-24	Case II - Minimum Flow Rate Vs. Injector Orifice Area - Aerozine-50.....	5-35
5-25	Case II - Minimum Flow Rate Vs. Injector Orifice Area - B <sub>2</sub> H <sub>6</sub> .....	5-35
5-26	Case II - Minimum Flow Rate Vs. Injector Orifice Area - B <sub>5</sub> H <sub>9</sub> .....	5-36
5-27	Case II - Minimum Flow Rate Vs. Injector Orifice Area - CTF .....	5-36
5-28	Case II - Minimum Flow Rate Vs. Injector Orifice Area - ClO <sub>3</sub> F.....	5-37
5-29	Case II - Minimum Flow Rate Vs. Injector Orifice Area - N <sub>2</sub> O <sub>4</sub> .....	5-37
5-30	Case II - Minimum Flow Rate Vs. Injector Orifice Area - LH <sub>2</sub> .....	5-38
5-31	Case II - Minimum Flow Rate Vs. Injector Orifice Area - LO <sub>2</sub> .....	5-38
5-32	Case II - Minimum Flow Rate Vs. Injector Orifice Area - LF <sub>2</sub> .....	5-39
5-33	Case II - Minimum Flow Rate Vs. Injector Orifice Area - OF <sub>2</sub> .....	5-39
5-34	Case II - Environmental Heating Rate Vs. Injector Orifice Area - N <sub>2</sub> H <sub>4</sub> .....	5-40
5-35	Case II - Environmental Heating Rate Vs. Injector Orifice Area - MMH.....	5-40
5-36	Case II - Environmental Heating Rate Vs. Injector Orifice Area - UDMH.....	5-41
5-37	Case II - Environmental Heating Rate Vs. Injector Orifice Area - Aerozine-50.....	5-41
5-38	Case II - Environmental Heating Rate Vs. Injector Orifice Area - B <sub>2</sub> H <sub>6</sub> .....	5-42
5-39	Case II - Environmental Heating Rate Vs. Injector Orifice Area - B <sub>5</sub> H <sub>9</sub> .....	5-42
5-40	Case II - Environmental Heating Rate Vs. Injector Orifice Area - CTF.....	5-43
5-41	Case II - Environmental Heating Rate Vs. Injector Orifice Area - ClO <sub>3</sub> F.....	5-43
5-42	Case II - Environmental Heating Rate Vs. Injector Orifice Area - ClO <sub>3</sub> F.....	5-44

ILLUSTRATIONS (CONT.)

<u>Figure</u>		<u>Page</u>
5-43	Case II - Environmental Heating Rate Vs. Injector Orifice Area - LH <sub>2</sub> .....	5-44
5-44	Case II - Environmental Heating Rate Vs. Injector Orifice Area - LO <sub>2</sub> .....	5-45
5-45	Case II - Environmental Heating Rate Vs. Injector Orifice Area - LF <sub>2</sub> .....	5-45
5-46	Case II - Environmental Heating Rate Vs. Injector Orifice Area - OF <sub>2</sub> .....	5-46
5-47	Radial Leakage Model.....	5-49
5-48	Axial Leakage.....	5-49
5-49	Final Permeation Leakage Model.....	5-49
5-50	Simplified Final Permeation Leakage Model.....	5-49
5-51	Plot of Flow Per Unit Length and Pressure Vs. $\alpha$ , The Ratio of Gland Thickness to Leakage Gap.....	5-52
5-52	Model of Seal Configuration.....	5-52
5-53	Capillary Pressure $\Delta P$ Vs. Spacing D Between Parallel Plates.....	5-58
5-54	Preliminary Leak Test Configuration.....	5-64
5-55	High Pressure Cell Assembly.....	5-64
5-56	Photo of High Pressure Test Cell Assembly.....	5-65
5-57	Summarization of High Pressure Tests.....	5-70
5-58	Diffraction Pattern of Unknown Compound.....	5-72
5-59	Photomicrograph of Wetting with Gallium Alloy.....	5-73
5-60	Photomicrograph of Wetting with Gallium Alloy.....	5-74
5-61	Photomicrograph of Wetting with Gallium Alloy.....	5-75
5-62	Photomicrograph of Wetting with Gallium Alloy.....	5-76
5-63	Schematic of Dynamic Wet Seal Leak Test.....	5-77
5-64	Interference Fit Ball Seal Test Fixture.....	5-83
5-65	Seat Specimen for Thin Film Leakage Tests.....	5-103
5-66	Valve Seal Leakage Fixture.....	5-103
5-67	Leakage Test Data Showing Effect of Thin Films.....	5-113
5-68	Energized Seal.....	5-119
5-69	Valve and Seal Test Fixture.....	5-119

TABLES

<u>Table</u>		<u>Page</u>
5-1	Size of Wear Particles and Related Functions Under Standardized Conditions of Ambient Atmosphere.....	5-9
5-2	Wear of Copper in Various Environments.....	5-9
5-3	Combination of Weldable Materials using Ultrasonics....	5-16
5-4	Test Results Showing Decrease in Leakage Rate Following Long Period of Ultrasonic Excitation.....	5-19
5-5	Test Results Showing Decrease in Leakage Rate Following Short Period of Ultrasonic Excitation.....	5-19
5-6	Temperature °C for Good Corrosion Resistance.....	5-60
5-7	Permanent Properties of Liquid Metal System.....	5-61
5-8	Materials Tested - High Pressure Test.....	5-65
5-9	Wetted Material Couples Showing No Leakage With Helium Probe Techniques.....	5-65
5-10	Test 440C SN1 O-Ring E515-8.....	5-67
5-11	Test 440C SN1 O-Ring E515-8.....	5-68
5-12	Test O-Ring Compound E515-8.....	5-69
5-13	Test 4340 Vs. BC SN 6.....	5-69
5-14	Test 4340 Vs. HSS SN1.....	5-70
5-15	Interplanar Spacing of Unidentified Compound.....	5-72
5-16	Summary of Test Results for Stainless Steel Tubes.....	5-85
5-17	Summary of Test Results for Aluminum Tubes.....	5-85
5-18	Original Thin Films Coated Specimen Test Results.....	5-89
5-19	Thin Film Coated Teflon Helium Permeation Test Results.	5-90
5-20	Task A Formation Conditions.....	5-93
5-21	Task A Test Results.....	5-93
5-22	Task B Formation Conditions.....	5-95
5-23	Task B Test Results.....	5-95
5-24	Metal-to-Metal Seal Test Results.....	5-100
5-25	Effect of Thin Films on Seal Leakage.....	5-106
5-26	Effect of Thin Films on Seal Leakage.....	5-107
5-27	Effect of Thin Films on Seal Leakage.....	5-108
5-28	Effect of Thin Films on Seal Leakage.....	5-109
5-29	Effect of Thin Films on Seal Leakage.....	5-110
5-30	Effect of Thin Films on Seal Leakage.....	5-111
5-31	Effect of Thin Films on Seal Leakage.....	5-112
5-32	Valve Leakage Test Data Using Energized Seal.....	5-121
5-33	Valve Contamination Test Leakage Data, Teflon Seat.....	5-123

## CONTENTS

	<u>Page</u>
6.0 VALVE ACTUATORS	6-1
6.1 Introduction	6-1
6.2 Actuator State Of The Art	6-1
6.2.1 Valve Actuator Rating Analysis Chart	6-1
6.2.2 Valve Actuator Review	6-3
6.2.3 Electromechanical Actuators	6-3
6.2.4 Pneumatic Valve Actuators	6-7
6.2.5 Hydraulic Actuators	6-8
6.2.6 Chemical Actuators	6-8
6.2.7 Thermal Actuators	6-9
6.2.8 Manual Overrides	6-10
6.3 Electromagnetic Actuator Design Considerations	6-10
6.3.1 Solenoid Actuator Response Time	6-10
6.3.2 High Temperature Electromagnetic Actuators - Materials and Practices	6-13
6.3.3 High Temperature Solenoid Design Criteria	6-19
6.3.4 High Speed Solenoid Valve Drive Circuits	6-19
6.4 Conceptual Actuator Designs	6-33
6.4.1 Monopropellant Chemical Actuator Concept	6-33
6.4.2 Bipropellant Chemical Actuator Concept	6-35
6.4.3 Electrodynamic Actuators	6-35
6.4.4 Piezoelectric Actuators	6-39
6.4.5 Superconductive Actuators	6-41
6.4.6 Thermal Actuators	6-43
6.5 Lightweight Solenoid Actuator	6-46
6.5.1 Introduction	6-46
6.5.2 Beryllium Technology	6-47
6.5.3 Solenoid Actuator Evaluation	6-54
6.6 Thermal Expansion Actuator	6-56
6.6.1 Conceptual Design	6-56
6.6.2 Prototype Evaluation	6-57
6.6.3 Test Results and Conclusions	6-59
6.7 Electropyrotechnic Actuator Cartridge Study	6-62
6.7.1 Background	6-62
6.7.2 Electropyrotechnic Cartridge Environmental Tests	6-66
6.8 References	6-83

## ILLUSTRATIONS

<u>Figure</u>		<u>Page</u>
6-1	Diaphragm Sealed Solenoid Valve.....	6-4
6-2	Time Relationships in Solenoid Actuated Valve.....	6-11
6-3	Saturation Flux Density Ratio Vs. Temperature for Ferromagnetic Materials.....	6-18
6-4	Solenoid Actuator Circuit.....	6-20
6-5	Typical Current Transient Characteristic Curve for Solenoid Valve Actuator.....	6-21
6-6	Capacitor Impulse Actuator Driver.....	6-24
6-7	Ideal Solenoid Drive Impulse.....	6-32
6-8	Monopropellant Chemical Actuator (Normally Open Valve).	6-34
6-9	Monopropellant Chemical Actuator Test Schematic.....	6-34
6-10	Monopropellant Chemical Actuator - Performance Curve...	6-34
6-11	Monopropellant Chemical Actuator Test Unit.....	6-34
6-12	Bipropellant Chemical Actuator (Normally Closed Valve).	6-34
6-13	Typical Electrodynamic Actuator Configurations.....	6-37
6-14	Relative Magnetization Change with Temperature.....	6-37
6-15	Equivalent Circuit of a Piezoelectric Transducer.....	6-40
6-16	Piezoelectric Ceramic Disc Test Installation.....	6-40
6-17	Piezoelectric Actuator Using Stacked Discs.....	6-40
6-18	Piezoelectric Helical Actuator.....	6-40
6-19	Critical Field Curves of Some Superconductors.....	6-42
6-20	Variation of Critical Temperature with Number of Valence Electrons.....	6-42
6-21	Differential Expansion Actuated Valve.....	6-45
6-22	Fluid Expansion Actuated Valve.....	6-45
6-23	Snap Action Differential Expansion Actuated Valve.....	6-45
6-24	State Change Actuator for Multicycle Operation.....	6-45
6-25	State Change Actuator for Single Cycle Operation.....	6-45
6-26	Resistivity of Ultra Pure Beryllium and Copper.....	6-49
6-27	Resistivity - Density Product of Pure Beryllium and Copper.....	6-49
6-28	Beryllium Film Deposited on Beryllium Oxide Substrate..	6-53
6-29	Bulk Resistivity Data for Evaporated Beryllium Thin Films.....	6-53
6-30	Thermal Expansion Actuator Parameters.....	6-58
6-31	Prototype Thermal Expansion Actuator.....	6-58



ILLUSTRATIONS (CONT.)

<u>Figure</u>		<u>Page</u>
6-32	Thermal Expansion Actuator Assembly.....	6-58
6-33	Thermal Expansion Actuator Subcomponents.....	6-58
6-34	Test Setup for Thermal Actuator Evaluation.....	6-60
6-35	Thermal Actuator Stroke Vs. Time with 80 Lb Load.....	6-60
6-36	Thermal Actuator Stroke Vs. Time for Several Loads....	6-60
6-37	Thermal Actuator Temperature Rise Time.....	6-61
6-38	Thermal Actuator Stroke Vs. Temperature Rise.....	6-61
6-39	Thermal Actuator Stroke Vs. Time from Power Off.....	6-61
6-40	Low Voltage Electropyrotechnic Cartridge and Associated Firing Circuit.....	6-63
6-41	Exploding Bridgewire (EBW) Pyrotechnic Cartridge and Associated Firing Circuit.....	6-63
6-42	Electropyrotechnic Cartridge S/N 592 After Six 300°F 24-Hr Temperature Cycle Sterilization Test.....	6-72
6-43	Photomicrograph of Electropyrotechnic Cartridge S/N 583 Showing Ceramic Insert After Firing.....	6-75
6-44	Photomicrograph of Electropyrotechnic Cartridge S/N 584 Showing Ceramic Insert After Firing.....	6-75
6-45	Photomicrograph of Electropyrotechnic Cartridge S/N 585 showing Ceramic Insert After Firing.....	6-75
6-46	Photomicrograph of Electropyrotechnic Cartridge S/N 591 Showing Ceramic Insert After Firing.....	6-75
6-47	Horex #72 Propellant Before 300°F Thermal Exposure...	6-82
6-48	Horex #72 Propellant After 300°F Thermal Exposure....	6-82

## TABLES

### Table

6-1	Valve Actuator Rating Analysis Chart.....	6-2
6-2	Definition of Solenoid Valve Response Time.....	6-11
6-3	Radiation Exposure and Temperature Limits for Electromagnetic Materials.....	6-14
6-4	Comparison of Magnetic Assemblies.....	6-37
6-5	Comparison of Solenoid and Electrodynamic Actuators (Power = 5 watts).....	6-38
6-6	Comparison of Solenoid and Electrodynamic Actuators (Force = 5 pounds).....	6-38
6-7	Data on Electrical Conductors and Ceramic Insulators...	6-48
6-8	Comparison of Beryllium and Copper.....	6-48
6-9	Comparison of Beryllia and Alumina.....	6-48
6-10	Characteristics of Beryllium Films on Quartz.....	6-53
6-11	Electrical Properties of Beryllium Films on Quartz.....	6-53
6-12	Resistivity of Beryllium Film on Beryllium Oxide.....	6-53
6-13	Summary of Thermal Actuator Test Runs.....	6-61
6-14	Relative Advantages and Disadvantages of Exploding Bridgewire and Low Voltage Elements.....	6-65
6-15	Electropyrotechnic Cartridge Group I Test Results.....	6-68
6-16	Flow Chart - Electropyrotechnic Cartridge Group II Test	6-72
6-17	Data Sheet - 3511-1 Electropyrotechnic Cartridge Group II Test Results.....	6-73
6-18	3511-1 Electropyrotechnic Cartridge Group II Test.....	6-76
6-19	4360-1 Electropyrotechnic Cartridge Group IV Test.....	6-76
6-20	Temperature Extremes During Radiation Exposure $10^5$ r/hr	6-77
6-21	3511-1 Group III Thermal Cycle Vacuum Soak Test Description.....	6-77
6-22	3511-1 Group III Vacuum Firing Test Description.....	6-77
6-23	Group IV 4360-1 Electropyrotechnic Cartridge Sterilization-Thermal Cycle Test.....	6-79
6-24	4360-1 Thermal Cycle Vacuum Soak Test Description.....	6-80
6-25	4360-1 Vacuum Firing Test Description.....	6-80
6-26	Electropyrotechnic Cartridge Helium Leak Check.....	6-81
6-27	Weight Loss of Electropyrotechnic Cartridges Materials.	6-82

## CONTENTS

	<u>Page</u>
7.0 INSTRUMENTATION AND MEASUREMENT	7-1
7.1 Introduction	7-1
7.2 Valve Position Indicators	7-1
7.2.1 Solenoid Valve Position Indicators	7-1
7.2.2 Radioactive Proximeter	7-6
7.3 Flow and Leakage Measurement	7-11
7.3.1 In-Flight Leakage Measurement	7-11
7.3.2 Electromagnetic Flowmeter	7-14
7.3.3 Acoustic Flowmeters	7-16
7.3.4 Acoustic Pressure - Leakage Measurement Technique	7-18
7.3.5 Accelerometer Valve Control Concept	7-19
7.4 Leakage Measurement Concept - ABLEAK	7-21
7.4.1 Introduction	7-21
7.4.2 ABLEAK Concept	7-23
7.4.3 Valve Leak Investigations	7-25
7.4.4 Evaluation of ABLEAK 100	7-27
7.5 Electropyrotechnic Cartridge Tester	7-29
7.5.1 Introduction	7-29
7.5.2 Advantages of the Dynamic Tester	7-29
7.5.3 Test Instrumentation	7-31
7.5.4 Evaluation	7-32
7.6 Corrosion Measurement by Holography	7-33
7.6.1 Test Setup	7-33
7.6.2 Test Results	7-35
7.6.3 Conclusions	7-39
7.7 References	7-40

## VOLUME II - NONMECHANICAL CONTROLS

### 8.0 FLUIDICS (SEE VOLUME II)

## ILLUSTRATIONS

<u>Figure</u>		<u>Page</u>
7-1	Solenoid Actuator On-Off Transient Test Setup.....	7-3
7-2	Typical Current Voltage Transient Characteristics of a Solenoid Valve.....	7-3
7-3	Solenoid Valve With Built-in LVDT Position Sensor.....	7-5
7-4	LVDT Position Error Measuring System.....	7-5
7-5	Solenoid Valve With Built-in Magneto Resistance Position Sensors.....	7-5
7-6	Magneto Resistance Position Error Measuring System.....	7-5
7-7	Alpha Source, Beryllium Target Positioner.....	7-7
7-8	Linear Displacement Proximeter in LEM Valve Actuator...	7-7
7-9	Four Quadrant Position Indicator.....	7-7
7-10	Four Quadrant Position Indicator Installation.....	7-7
7-11	Linear Output Rotational Source With Split Detector....	7-7
7-12	Radioisotope Positioner Electronic Components.....	7-7
7-13	AC Electrohydrodynamic Flowmeter.....	7-15
7-14	Acoustic Flowmeter Concept.....	7-15
7-15	Acoustic Pressure Measuring Device.....	7-15
7-16	Accelerometer Control System for Spacecraft Engine Valves.....	7-20
7-17	Definition of Zero Gas Leakage.....	7-22
7-18	Schematic of ABLEAK 1.....	7-24
7-19	ABLEAK 1 Mass Leak Measurement System.....	7-24
7-20	ABLEAK LMDE Valve Test Arrangement.....	7-26
7-21	LMDE Oxidizer Shutoff Valve Test Setup.....	7-26
7-22	LMDE Valve N <sub>2</sub> O <sub>4</sub> Leakage.....	7-28
7-23	ABLEAK 100 Mass Leak Measurement System.....	7-28
7-24	Dynamic Squib Tester.....	7-30
7-25	Stored Beam Holographic Interferometer Technique.....	7-34
7-26	Stored Beam Holographic Interferometer Apparatus.....	7-34
7-27	Holographic Interferometer Photographs of Steel Corrosion In Nitric Acid.....	7-36
7-28	Holographic Interferometer Photographs of Thin Film Protected Steel Corrosion in Nitric Acid.....	7-36
7-29	Arrangement of Coated Specimens in Cell.....	7-38
7-30	Representation of Nitric Acid Attack on Coated Steel Specimens.....	7-38

## 1.0 INTRODUCTION

### 1.1 BACKGROUND

The first rocket propelled aircraft, as were the first rocket propelled missiles, simple in design, yet advanced in concept. The valves and controls used in these rocket engines were simple, reliable, and few in number. As airplanes were developed, they became more complex and valve requirements became more stringent, which resulted in more complicated components. However, this evolution took place over a long period of time, which permitted an orderly development of the valves in keeping with the development of the aircraft. In the event of a valve malfunction during flight, alternatives were usually available to the pilot; thus, catastrophic failures because of malfunction were few compared with the number of missions carried out.

With the advent of the ICBM, the industry was confronted with vastly different and far more severe requirements. Permissible leakage was reduced, even though more difficult-to-seal media such as helium were being used. Cryogenic propellant used in conjunction with gaseous pressurization systems greatly extended the band of operating temperatures, ranging in some cases from  $-423^{\circ}$  to  $+300^{\circ}$ F. Higher acceleration and vibration levels were encountered, and aerodynamic heating imposed new requirements on designers. Because of the extremely high cost of missiles, great emphasis was placed on reliability to reduce the possibility of failure. Greater efforts were made to reduce weight and power requirements of the components. This, it became necessary to develop whole new families of valves and controls to satisfy the critical needs of missiles.

The developments were very costly, and did not proceed at a rapid enough rate to prevent numerous failures of the early missiles. In addition to the inflight catastrophic failures, preflight failures added tremendously to the expense of the programs and caused serious delays.

A report on malfunctions of airborne valves, regulators, and disconnects covering the period of 1 January to 30 September 1959 showed a total of 431 failures of varying degrees of severity in these three categories alone (Reference 1). New processes had to be developed to produce the necessary hardware, and on occasion apparently simple problems proved to be major stumbling blocks. Fittings were difficult to seal, especially when used over wide temperature ranges. Removal of contaminants such as oil vapors, water, air, and solids proved to be especially difficult. However, most of the problems were solved, or at least greatly mitigated, through the large expenditure of time and money.

Space vehicle requirements imposed an additional increment of performance and reliability upon components. Missile valves were required to operate for a maximum time of five minutes. Space valves were required which could operate for as long as two years and are presently planned to operate for 10 to 15 years, and withstand the rigors of high vacuum, radiation, space debris, temperatures extremes, and highly reactive propellants. These environments, in general, deteriorate materials; hence, functional performance

is degraded. The very low pressures of space can cause evaporation and sublimation of materials to the point where the normal function is impaired or destroyed. For instance, liquids would boil away completely in a short time. The more volatile constituents of elastomers will escape, effecting a change in the mechanical properties of materials. Friction coefficients increase with the removal of the gas film that is always present on parts in the earth's atmosphere, and the loss of the electrical insulating properties of air tends to lead to the electric breakdown of insulators.

The effects of radiation on materials in vacuum have not been completely known, and it is known that certain polymers (e.g., Teflon) are adversely affected in the presence of oxygen to the point where its use has been prohibited on some projects.

Space debris has been a subject of much concern, since it can cause deleterious effects on spacecraft performance ranging from total mechanical failure from a puncture to a less severe performance degradation such as upset by thermal balance by erosion of surfaces.

Such temperature extremes may range from near absolute zero to several hundred degrees, it is necessary to have accurate information on the probable temperatures to be encountered and to provide for proper operation of the equipment.

The problems flowing extremely reactive fuels and oxidizers and maintaining zero leakage, low weight and high reliability imposed severe requirements in advancing the state of the art of propulsion valves.

Not only did the technology of rocket controls need improvement, but the associated disciplines such as instrumentation and measurement, materials, and the definition of criteria needed improvement.

## 1.2 PURPOSE AND SCOPE

The purpose of the Advanced Valve Technology Compilation is to document in a single source the results of the efforts expended during the past several years on advancing the state of the art of valves and controls used on liquid chemical rocket engines for manned and unmanned space exploration vehicles. The valves studied were those used with earth and space storables and cryogenic propellants at pressures to 1000 psia and operate for periods of up to ten years. The ten year requirement was considered in conjunction with missions beyond Jupiter to the outer planets, Saturn, Uranus, Neptune and Pluto. Considerations were given to electrical, pneumatic (hot and cold gas) and hydraulic actuated valves and actuator concepts.

Functional requirements for valves and actuators include zero leakage, service life (1,000 to 10,000 cycles), low weight, minimum size, minimum pressure drop and minimum power consumption. Environmental parametric requirements include zero gravity, radiation, shock and vibration, sterilization (300°F temperature soak, and/or ethylene oxide sterilant), thermal shock, thermal cycling, vacuum and other effects anticipated by operating

for periods of two, five and ten years in the space and planetary environments. Thrust levels used for specific valve and control applications were 50 lb, 200 lb and 1000 lb.

Two broad classes of valve and controls technology are emerging which find application to controlling the flow of gaseous pressurants and liquid propellants. The two classes flow are: 1) Mechanical Controls (moving parts and 2) Nonmechanical Controls (no moving parts).

The first class includes those valves represented by mechanical elements such as diaphragms, seals, hydraulic, pneumatic and electrical actuators. The second class represents a group of fluid controls that have no sliding or moving parts and include fluidics and electric and magnetic fluid interaction devices.

The valve compilation is produced in two volumes, Volume I Mechanical Controls and Volume II Nonmechanical Controls. The compilation is divided into eight sections which make up the two volumes.

#### Volume I - Mechanical Controls

- 1.0 Introduction
- 2.0 Operational, Functional and Environmental Considerations
- 3.0 Materials
- 4.0 Valves
- 5.0 Leakage and Seal Technology
- 6.0 Valve Actuators
- 7.0 Instrumentation and Measurement

#### Volume II - Nonmechanical Controls

- 8.0 Fluidics

The major source of the material used in compiling these volumes were taken from the following references:

TRW Systems Group, Redondo Beach, California, Contract NAS 7-107 and 7-436

1. Advanced Valve Technology for Spacecraft Engines, Final Report No. 8651-6016-RU000, March 1963, Contract NAS 7-107.
2. Advanced Valve Technology for Spacecraft Engines, Final Report No. 8651-6032-SU000, Volume I, Valve Study and 8651-6033-SU000, Volume II, New Concepts, July 1964, Contract NAS 7-107.
3. Advanced Valve Technology for Spacecraft Engines, Final Report No. 8651-6042-SU000, August 1965, Contract NAS 7-107.
4. Advanced Valve Technology, Interim Report No. 06641-6004-R000, November 1966, Contract NAS 7-436.

5. Advanced Valve Technology, Interim Report No. 06641-6014-R000, Volume I, Spacecraft Valve Technology, Volume II, Materials Compatibility and Liquid Propellant Study, November 1967, Contract NAS-7-436.
6. Advanced Valve Technology, Interim Report No. 06641-6023-R000, Volume I, Mechanical Controls, Volume II, Nonmechanical Controls, January 1969, Contract NAS 7-436.

Other studies which included the definition of the environments and the investigation of fundamental mechanism of leakage heavily used in the work reported above were taken from the following reports:

1. Aerojet-General Corporation, Azusa, California, Contract NAS 7-98  
 "Engine Operating Problems in Space," Vol. I "The Space Environment," by D. Christensen; Vol. II "Environmental Effects on Engines and Components," by W. W. Howard and J. M. Bauer; and Vol. III "Improvement of System Reliability," by G. K. Cornelius, W. W. Howard and J. D. O'Donnell. Report No. 2824, April 1964.
2. General Electric Company, Schenectady, New York, Contract NAS 7-102  
 "Study of Dynamic and Static Seals for Liquid Rocket Engines," Vol. 1 "Description of Program and Results of Evaluation of Currently Available Sealing Methods," Vol. 2 "Studies of Special Topics in Sealing," Vol. 3A "Bibliography of ASTIA Literature on Seals," and Vol. 3B "Bibliography of Open Literature of Seals," by R. C. Elwell, et al., 26 February 1962 - 25 February 1963; also Vol. 2 "Studies of Special Topics in Sealing," Final Report for Period 26 February 1963 to 30 November 1963 and "Study of Dynamic and Static Seals for Liquid Rocket Engines," Final Report for Period 1 January 1965 to 1 September 1965.
3. General Electric Company, Schenectady, New York, Contract NAS 8-4012  
 "Design Criteria for Zero-Leakage Connectors for Launch Vehicles," Final Report, Vol. 1 "Summary, Conclusions and Design Examples," Vol. 2 "Leakage Flow," Vol. 3 "Sealing Action at the Seal Interface," Vol. 4 "Design of Connectors," Vol. 5 "Pressure Energized Seals," and Vol. 6 "Environmental Effects," by T. P. Goodman, et al., March 1962 through February 1963.
4. General Electric Company, Schenectady, New York  
 "Leakage Measurement and Evaluation," by J. W. Marr, Report No. 64GL163, October 12, 1964.
5. General Electric Company, Schenectady, New York, Contract NAS 7-434  
 "Study of Dynamic and Static Seals for Liquid Rocket Engines," Final Report for Period 1 April 1967 to 1 April 1968.
6. General Electric Company, Schenectady, New York, Contract NAS 7-396  
 "Leakage Testing Handbook," Revised Edition, July 1969

### 1.3 REFERENCES

1. Boeing Aircraft Company. "Propulsion System Optimization Study", Report No. DGR-TOR-33.



## 2.0 OPERATIONAL, FUNCTIONAL AND ENVIRONMENTAL CONSIDERATIONS

### 2.1 INTRODUCTION

The design and utilization of flow control components in spacecraft necessitates a wide variety of operational and environmental considerations relative to each intended application. Of particular concern are the design constraints imposed by the system, i.e., the operational, functional, and environmental factors which affect component operation.

The bulk of this section is taken from the report reference "Advanced Valve Technology for Spacecraft Engines, TRW Report No. 8651-6016-RU-000, March 1963. Although the information is applicable much of the contents in this section requires updating and in certain areas such as environments new information has been generated as a result of flight experience. However, the information is presented to maintain continuity of the overall objectives of the program and which provided an important base for developing technology areas.

### 2.2 OPERATIONAL CONSIDERATIONS

#### 2.2.1 Fluid Operating Temperatures

The operating temperatures discussed under this heading refer to the temperatures of the flowing media and are considered independently of temperature effects from space environments.

2.2.1.1 Cryogenic and Low Temperatures (-100°F to -423°F) - The effects cryogenic fluid temperatures on valves and valve materials may be summarized as follows:

1. Dimensional changes in subcomponents, such as seats and seals.
2. Greatly increased viscosity in lubricants with conventional lubricants reaching the solid state.
3. Change in the structural properties of materials with some properties being enhanced and some being degraded.
4. Contamination resulting from the solidification of gases. Carbon dioxide solidifies at -110°F, and air or nitrogen becomes solid at approximately -350°F.

2.2.1.2 Moderate temperatures (-100°F to +400°F) - If devices such as gas generators are excluded from consideration, the temperature range of the various flow media encountered on spacecraft using storable propellants may vary from approximately -100°F to +400°F. These flow media include pressurant gases which may be heated by engine exhaust to obtain an increase in the specific volume, which serves to reduce the weight of gas required for pressurizing applications.

Valves have been successfully operated in missile applications for several years in temperature ranges of -423°F to +450°F. Because of the extensive development work that has been accomplished in this field, valves operating within this temperature range are considered within the state of the art.

2.2.1.3 High Temperatures (400°F - 2000°F) - Requirements for valves to operate in the range of 400°F to 2000°F arise from the use of products of combustion, obtained either from rocket engine combustion chamber bleed or from auxiliary gas generators. The gases may be used to operate mechanical devices such as pumps or may be used as tank pressurants in fluid transfer systems. The effects produced by these hot gases vary with the materials that are being used and with the duration of the exposure. The significant effects are as follows:

1. All metals experience a reduction in strength as the temperature is varied. Additional material must therefore be provided for operation at high temperature, thus incurring a weight penalty.
2. Extreme changes in temperature can cause relatively large changes in dimensions, which may be critical for a given part. If severe gradients exist across the valve, seizure of movable parts can occur because of differential expansion.
3. Products of combustion may contain large quantities of particulate contamination. These contaminants, in conjunction with the gases which also may be corrosive in nature, can produce severe erosion.

#### 2.2.2 Fluid Operating Pressure

The internal pressure at which a valve is required to operate will govern several aspects of the design of a given component. For example, gas pressures of 300 to 600 psia are normally required for a pressure operated propellant rocket engine feed system. For a turbopump fed system gas pressures as low as 25 to 85 psia are usually required. Gases are typically stored at 5000 psi and regulated to from 150 to 660 psi to pressurize liquid propellants. Gas storage pressures of 3000 psi are regulated from 5 to 50 psi for a typical attitude control system. Typical design considerations relative to these conditions include:

1. When the operating pressure is sufficiently high to require significant actuating forces, a balanced poppet design may be required.
2. In addition to internal pressure, external or ambient pressure must be considered relative to seals and housing structures if the valve or system is to be operated in atmospheres such as those of Venus (16 atmospheres) or Jupiter (several thousand psi). For these operating conditions the initial system pressure would have to be higher by the increment of the planetary ambient pressure to permit overboard discharge of a gas, as is done with an altitude control valve.
3. In the event that system pressure is depleted prior to entry into a high-pressure planetary atmosphere, the structural design of the tanks, valves, tubing, etc. would have to be such that components would not be collapsed because of the high external ambient pressure. Care must be taken to insure that seals used on the various components are effective in both directions of pressure application if seepage of a planetary atmosphere into any part of the system would be objectionable.

### 2.2.3 Acceleration, Vibration and Shock

2.2.3.1 Launch Loads - Acceleration is usually considered to be more severe in the launch phase than for the space flight condition. Acceleration levels measured on a typical rocket engine dome range from 10 to 30 g with the maximum occurring between 600 to 1600 hertz. Valves attached to the combustion chamber of the launch missile may experience up to four times this load through amplification in the mount. Valves located in the tankage area may experience from 5 to 20 g.

During the first few seconds of engine firing, severe excitation of most of the valves located at some distance from the rocket engine occurs due to acoustical noise.

2.2.3.2 Space Flight Loads - Vibration and shock may be more serious for the space flight phase within varying degrees depending on the orbit or space mission, such as lunar landing. At present, vibration and shock requirements are usually most severe under rocket engine ground test conditions.

Acceleration is normally considered more pronounced in the launch phase than for the space flight condition. It should be noted, however, that a valve used on the space vehicle will not be operating at the time of the earth launch, but will be operative in the space orbit and under this condition the valve is more susceptible to adverse effects from the acceleration.

2.2.3.3 Reentry and Recovery Loads - Accelerations and dynamic pressures up to 10 times the launch values can be experienced by spacecraft during reentry. Shock loads imposed by parachute recovery of equipment would also have to be considered, although ascent loads usually predominate.

Expected values for deceleration during planetary entry are given in Table 2-1.

2.2.3.4 Other Loads - An important shock source could be the impact load on the valve or spacecraft from meteorites, and consideration of this possibility should be included in the design analysis. Additional information on meteorites is given in Section 2.3.

Representative values of acceleration, vibration and shock for space vehicles are given in Table 2-2.

Table 2-1. Estimated Decelerations Upon Planetary Entry

Planet	Direct Entry at Escape Velocity			Direct Entry at Orbital Velocity			Entry by Decay From Satellite Orbit
	$\theta=5^\circ$	$\theta=20^\circ$	$\theta=90^\circ$	$\theta=5^\circ$	$\theta=20^\circ$	$\theta=90^\circ$	
Venus	28.6	112	326	14.3	56	163	8.9
Earth	28.3	111	324	14.2	55.5	162	9.5
Mars	1.6	6.3	18.3	0.8	3.2	9.2	9.2

NOTES: 1.  $\theta$  is the reentry angle with the horizontal  
 2. Decelerations are given in earth g's.

Table 2-2. Representative Values of Acceleration, Vibration and Shock

Mission	Acceleration or Deceleration	Vibration	Shock	Acoustical Noise
Earth Launch	up to 7g to 775 sec. 20-30g for 150sec.	10g rms 600 to 1600 cps	15 to 20g for 6 to 12 milliseconds	Field outside of payload 150 db 60 sec duration
Low Earth Orbit	1 to 3g longitudinal for increments of 5 min. or longer	to 50g peak >1000 cps 5 min. duration	Secondary stage ignition shock levels to 50g for approximately 10-3 sec.	None
Lunar Orbit	Deceleration to 2g up to 10 min. for lunar injection	50g peak to >1000 cps for 10 min. duration	Engine ignition levels to 40g for 6-12 ms	None
Lunar Landing	0.5 to 72g for landing approach		Engine ignition levels to 40g for 12 ms. Soft landing shock of 10 to 100g for several ms - Hard landing shock to >1000g for several ms.	None

#### 2.2.4 Contamination

2.2.4.1 Summary - There are normally two sources of contamination, "built-in" and system generated. The built-in contamination is caused during the manufacture and handling of the parts and at installation of the components in the system. Also, contamination may be introduced by the propellants and pressurants. Generated contamination is contamination created within the system, and is caused by wear and chemical action of the propellants on the materials. Also, freezing of small amounts of water or other constituents mixed with the propellants can cause serious problems. Internal spalling which results from meteoroid impact can also be a source of contamination.

2.2.4.2 Filter Contamination - Filters are normally used to protect the mechanical function of the valve from contamination and are usually found in the line and sometimes in the valve itself. Filters, however, can be a contamination source in that the filter industry has not yet solved the problem of producing a clean filter. Also, filters cannot protect the moving parts from the wear particles created by the parts. The valve seats themselves will contain wear particles created by bearings, actuators, etc., upstream of the seats. Extensive test programs recently conducted on filters of various types have indicated that many filters contained built-in dirt or contamination particles that were in excess of the absolute rating of the filter. It is necessary, therefore, to be aware of the fact that it is possible for a filter to be a contaminant generator and thus defeat the very purpose for which the filter was installed. Cognizant personnel should also be aware of SAE document, ARP 599, which defines the various procedures in cleaning and inspecting filters.

#### 2.2.5 Gaseous Flow Media

Commercial gases commonly used in spacecraft for pressurization and component actuation are hydrogen, helium, nitrogen, oxygen and argon. In addition to these, boiloff vapors from propellants such as  $N_2O_4$  and  $F_2$  may be used, and combustion product gases from engines and squibs find applications. Typical operational considerations relative to gases include particulate or vapor contaminants, chemical impurities, and ice crystals.

It is essential that the commercial gases be free of contaminants such as fine rust particles because of the erosive effects these particles may have upon component parts in the gas stream, e.g., valve seats. This is especially true of hydrogen and helium because of the very high velocities that are attained under sonic conditions. Normal care in maintaining system cleanliness and use of adequate filters will obviate problems with such particulate contamination. Chemical impurities in the gases, such as water vapor, carbon dioxide and air can create contamination problems that are more difficult to identify and correct. As is the case with liquid flow media, care must be taken to avoid contamination of the gases with traces of other gases, such as air or carbon dioxide. In some space applications, gases are cooled in heat exchangers operating at cryogenic temperatures, to facilitate loading and storage. Ice crystals formed from water vapor or  $CO_2$  flakes can interfere with the process by clogging filters and orifices. Significant amounts of contamination can also cause erroneous readings on flow meters that are calibrated on the basis of a pure gas as the flowing medium.

Among the problems peculiar to individual gases are the following:

1. Hydrogen and helium are extremely difficult to seal and will leak through exceedingly fine openings in threaded connectors, body seals, and valve seats. The erosive effects of these gases on seats in the nearly closed position can be very significant.
2. Boiloff gases from the various propellants such as  $N_2O_4$  and fluorine may be both corrosive and toxic, and adequate provisions must be made to insure compatibility of the materials in contact with the vapors and to prevent hazard to personnel. Section 3.0 of this report presents detailed data on fluid compatibility.
3. Products of combustion contain sizable particulate matter, and the gases may or may not be corrosive. However, devices that use these gases, e.g., turbine-driven power supplies, are normally designed to cope with this type of contamination.

#### 2.2.6 Liquid Propellants

2.2.6.1 Newtonian Fluids - A more difficult problem usually exists with a liquid flow medium than with a gas, because of more stringent compatibility problems with the valve materials, especially the seals. Difficulty can arise because of chemical reactions, as in the case of storables, or because of temperature extremes as in the case of cryogenic fluids.

Purity of the liquid flow media must be maintained to avoid problems. This is of special significance in the case of cryogenic fluids that may become contaminated with gases whose melting point is above the temperature of the cryogenic fluid. For example,  $CO_2$  solidifies at  $-110^\circ F$ , which is well above the boiling point of LOX at atmospheric pressures ( $-297^\circ F$ ). Excess  $CO_2$  in liquid oxygen has been known to clog filters in transfer systems, which poses a difficult problem for diagnosis, since the filter will appear to be perfectly clean when it is warmed up and dismantled for inspection. The same condition could be experienced in a liquid hydrogen system, with the added possibility of having solid air as a contaminant in addition to  $CO_2$ .

A detailed discussion of the compatibility of these various propellants with valve materials is presented in Section 3.0 of this report.

2.2.6.2 Gels - A liquid propellant which has been conditioned so that it exhibits non-Newtonian properties is normally called a gel. For spacecraft propulsion the gels are classified into two types: nonmetallized and metallized. In a nonmetallized gel the additives used to cause gelling (carbon black, silica, etc.) do not normally modify the chemical characteristics of the propellant, whereas a metallized gel is generally prepared with propellant mixed with metal having an average particle size range of 5 to 50 microns and it has been necessary to gel the mixture in order to suspend the metal in the propellant. The gels are characterized by thixotropic properties, i.e., the viscosity decreases with increasing shear rate

and stress decreases with time at constant shear. As the gel flows through lines and components, the shear becomes greater, the viscosity becomes less and the gel behaves more like a low viscosity liquid.

With gelled propellants, pressure drops through lines and elements are larger than those of comparable liquids and are unpredictable, i.e., the viscosity keeps varying. Throttling can cause evaporation of the liquid phase of the gel, which leaves a solid matrix as a residue that can hinder and restrict the flow. The abrasive action of metal particles can cause erosion of nozzles, passages, and valve seats. The compatibility of gelled propellants with the materials of construction is generally comparable to the base liquid propellant.

### 2.2.7 Leakage

Leakage is a primary problem in most valves, and a difficult one to solve. Soft seats give better leakage control than hard seats where fluid compatibility and temperature limits are suitable, but hard seats must be used in cases where fluid media and operating temperature would cause problems.

The detrimental effects associated with leakage include the following:

1. Loss of propellants and pressurants
2. Corrosive effect on materials
3. Interference with experiments
4. Fire and explosion hazard
5. Toxic properties of propellants

The loss of propellants may or may not be a serious problem, depending upon the system and mission duration. The corrosive effects resulting from propellant loss may be a more severe problem than would be the reduction in total thrust. A significant leak could envelop components within the spacecraft with corrosive vapors and cause failure of the mission. Such an envelope could cause interference with experiments and perhaps degrade materials and equipment. For manned missions and ground handling, possible danger from toxic vapors would have to be considered.

In addition to macroscopic leakage, seepage permitted by permeability of materials must be considered.

In general, leakage requirements for unmanned missions, obtained from interviews with the prime manufacturers, vary from 1 cc/day to zero for  $N_2O_4$  to from 30 cc/hr to 0.5 cc/hr for gases. Zero leakage is defined in Section 5.0.

### 2.2.8 Sterilization

One important consideration in those space vehicles and probes with even a remote possibility of extraterrestrial impact is that of complete biological sterilization.

Sterilization is required since, to the best of our present knowledge, micro-organisms from earth not only might survive on other planetary surfaces, but they might find nutrient there, thrive and multiply. Thus, with these planets, there is concern with the problem of possible infection, as well as pollution.

Generally, the penetrating radiations of outer space are not of sufficient intensity to assure sterility. The ultraviolet radiation is intense enough, but is so easily shielded that only organisms uncovered on the surface of the space vehicle would be exposed. Cold, even down to a slight fraction of a degree above absolute zero, has no lethal effect (Reference 1). Heat is lethal, even if the resistance of organisms in an evacuated dehydrated state is greater than was supposed (Reference 2), but the temperature within space vehicles is carefully controlled at more or less room temperature so that instruments will perform satisfactorily. Vacuum has not resulted in a deleterious effect on all micro-organisms. As for the hazards in landing on an extraterrestrial body, the momentary heat and pressure of a high-velocity landing on a hard surface should not exceed those achieved for brief fractions of a second in explosions, which bacteria have survived, nor can it be assumed that the atmosphere of Mars or Venus will consume a space vehicle coming in at a high speed, as micro-meteorites are heated and consumed in earth's atmosphere. In short, only by seeing that the space vehicles are sterile as they leave earth can it be assured that living earth forms will not be transported to other celestial bodies.

2.2.8.1 Methods of Sterilization - The possible methods of sterilization include heat, chemical, and radiation. In choosing the optimum method one must consider the materials of construction, the methods of fabrication and assembly, and the handling necessary following fabrication and assembly.

The presently accepted heat sterilization methods consist of soaking the components, subassemblies, or perhaps the entire vehicle at temperatures of 300°F for 60 hours - 6 cycles. The principal advantage of heat is its ability to permeate hermetic seals, container walls, and encapsulated components or assemblies. This allows sterilization of commercial components such as valves, actuators, motors, solenoids, capacitors, resistors, and transformers. It has been demonstrated that such components are not internally sterile and could be a source of extraterrestrial contamination should they fracture upon impact. Other advantages of heat sterilization are the absence of personnel hazards and the availability of the necessary facilities and technology.

Disadvantages of the heat sterilization method include the degradation in performance and reliability of valves, some electronic components and assemblies, materials, propellants, and pressurized propellant storage systems. An additional disadvantage, and one less susceptible to solution, arises from the difficulties that would be incurred in sterilizing cryogenic propellants. Bacteria and spores are not killed by cryogenic temperatures, and as it may be possible to impact the earth's moon with residual propellants on board, contamination of the moon could result. Producing sterile cryogenic propellants would require extra steps in the manufacturing process (e.g., heating the gas in a sterilizing heat exchanger prior to liquefaction).



Such a process would be difficult and expensive, at best; perhaps impossible in the case of liquid hydrogen. If sterilization of the vehicle is to be effective, a means must be found to sterilize those cryogenic propellants in which bacteria and spores could survive.

The effectiveness of chemical sterilizers is limited in that they must contact the surfaces to be sterilized. This rules out their usage in sterilizing hermetically sealed components, valves or subassemblies as well as in cases of bulk contamination of a solid such as encapsulated electronic modules where heat may be the only effective sterilizer. Of the chemicals, gaseous sterilizers, such as ethylene oxide mixtures, readily lend themselves to surface sterilization (References 3, 4 and 5).

The ease of handling, storage, applications, and above all the ability to sterilize a probe or a spacecraft mounted on the booster vehicle immediately prior to launch are among the advantages of a gaseous sterilizer. Compatibility of ethylene oxide mixtures with most materials and components (Reference 6) has led to its general acceptance. Limited compatibility data for various engineering materials are shown in Tables 2-3 through 2-5.

The use of hard radiation as a sterilizer is limited due to the radiation sensitivity of various materials and components as well as the handling and facilities requirements (Reference 7).

Applying the previous discussion to a propulsion system, it is evident that a combination of sterilization techniques would be necessary. These sterilization techniques would impose certain design requirements.

Three alternative methods exist for insuring sterilization of a complete propulsion system including the associated valving. These are:

1. Terminal heat sterilization of a complete system without fuel and oxidizer, which were added subsequently under aseptic conditions.
2. Terminal heat sterilization of a completely fueled system.
3. Subassembly sterilization using various techniques and subsequent assembly and propellant loading under aseptic conditions.

In the first two cases, while valves, with the possible exception of squibs, do not pose any unusual problems outside of insuring the valves can withstand a heat sterilization cycle, the following problem areas exist:

For liquid propellant systems:

- Insuring that no leaks occur due to differential expansion at sealing points and valves.
- Venting the increased tank pressure due to the increased temperature during sterilization or over-designing the tankage to accommodate this increase. Both methods impose a payload penalty.

- Accounting for the decrease in the strength of the structural materials at the higher temperature.

The third method of sterilization of a propellant system, involving the sterilization of subassemblies and final assembly under aseptic conditions, requires the sterilization, by heat, of all the subassemblies or components with surfaces not accessible to a chemical sterilizer. Those components such as flared tubing, nuts and bolts in which before assembly all surfaces are exposed are internally aseptic, may be sterilized by either heat or chemical sterilizers. Storage and final assembly procedures must be devised to insure the maintenance of these aseptic conditions until the assembly is hermetically sealed to prevent internal recontamination.

After installation of the system in the space vehicle, surface resterilization may be effected by the use of a gaseous sterilizer such as ethylene oxide.

Certainly separate sterilization of subsystems with subsequent sterile assembly implies more complicated ground equipment and ground operations than does terminal sterilization. However, the reliability and performance to be gained by the use of highly developed propulsion systems and propellants makes the former method worthy of strong consideration.

Table 2-3. Properties of Elastomers Exposed to 12% Ethylene Oxide - 88% Freon 12 for 24 Hrs.

Elastomer	% Weight Change	% Volume Change	Hardness Shore "A"		Tensile Strength, psi			Ultimate Elongation		
			Unexposed	Exposed	Unexposed	Exposed	%	Unexposed	Exposed	%
Neoprene Parco 363-70	0.00	+0.02	68	70	1583	1324	-16.4	313	251	-19.8
LS-53, TH TH1057	-0.09	-0.48	66	67	841	691	-17.8	105	86	-18.4
Buna N, Precision 758-70	+0.21	+0.33	not measured	not measured	1142	1133	- 0.7	272	234	-13.9
Viton A	+0.1	+0.5	-	-	2467	2267	- 8.1	137	137	0
AMS 3303 Silicone Rubber	-0.08	-	-	-	-	-	-	-	-	-

Table 2-4. Properties of Lexan, Kel-F and DC 4 Grease Exposed to 12% Ethylene Oxide - 88% Freon 12 for 24 Hours.

Lexan		
% Weight Change		+3.3
Elastic Modulus, Control		3.81 x 10 <sup>5</sup> psi
	Exposed Specimens	3.61 x 10 <sup>5</sup> psi
Kel-F		
% Weight Change		0.0
% Volume Change		-0.1
Hardness, Shore D, Control		81
	Exposed Specimens	79
DC 4 Silicone Grease		
% Weight Change		-0.37

Table 2-5. Effect of Exposure to 12% Ethylene Oxide - 88% Freon 12 for 24 Hours on Metals and Metal Coatings.

Specimen	Weight Change mg/cm <sup>2</sup>	Film Adhesion Test	
		Unexposed	Exposed
MIL-A-8625, Type I Anodized Al	+0.01	-	-
MIL-A-8625, Type II Anodized Al	+0.04	-	-
Molybdenum disulfide lubricant on MIL-A-8625, Type I Anodized Al	0.00	No removal of film	No removal of film
Molybdenum disulfide lubricant on MIL-A-8625, Type II Anodized Al	-0.06	No removal of film	No removal of film
AZ 31 B Magnesium	+0.01	-	-
Dow 17 lite on AZ 31B Magnesium	0.00	-	-
Dow 17 heavy on AZ 31B Magnesium	+0.01	-	-
DU lead Teflon coating on steel	0.00	No removal of coating	No removal of coating
Rokide on 321 CRES	+0.02	-	-
Rokide on Molybdenum	-0.03	-	-

## 2.3 FUNCTIONAL PARAMETERS

### 2.3.1 Response Time

The response time of a typical solenoid valve is affected by the mass of the moving parts, pressure differential, armature travel, coil winding, applied current, and friction of the moving parts. An examination of these variables suggests that a requirement for higher response time than is actually necessary will incur penalties in cost and weight, i.e., the size of the coil and the power required to operate the valve would be larger. Furthermore, high response produces high seat and poppet loads, since a suddenly applied load will produce a much higher stress than if the load had been applied gradually. A valve having a higher poppet velocity will incur high seat stresses which tend to reduce the life expectancy of the unit.

The speed with which a modulating valve can respond to a signal will be governed by the available actuator force, mass of moving parts, spring force, friction forces, and forces due to the dynamic effects of the flowing medium. In addition to these factors, the signal transport time must be included in the case of a valve having pneumatic actuation if the sensing point is remote from the valve and the signal is transmitted by pneumatic lines.

The response of a regulator or a vent valve must be sufficiently fast to compensate for the most rapid change that could occur in the system. Normally, a vent or regulator valve is subjected to relatively slow changes in demand. However, at the instant of application of inlet pressure to a regulator, a high speed transient may be imposed, especially if the downstream ullage is very small. Similarly, a vent valve could be subjected to a transient condition if a sudden application of pressure could be effected in a small ullage. The response of the valves would therefore have to be equal to the rise time of these pressure applications.

Typical response requirements are 5 to 50 milliseconds for liquid bipropellant shutoff valves and 12 to 200 milliseconds for gaseous shutoff valves. A response time of 1 to 2 milliseconds is not uncommon for valves used in low thrust pulse width modulated engine systems.

### 2.3.2 Weight

One method of increasing the useful payload per given launch vehicle for equivalent launch cost is by reducing the weight of the components in a payload, such as valves, lines, brackets, flanges, fittings, etc.

One attempt to provide a basis for the design and manufacture of subcomponents on space payloads is presented here. The basis is the dollars per pound of payload for the mission (e.g., earth orbit, lunar orbit, lunar landing, Venus flyby). For example, if an engineer designing a gas regulator or valve for an earth-orbited satellite could, by an additional machining process, reduce the valve weight by one pound, the additional machining process would be worth approximately \$150 to \$200 because this

is the additional launch vehicle cost to place that amount into orbit. Similarly, if the payload were placed into lunar orbit or a Venus or Mars flyby, then this same machining process would be worth considerably more.

### 2.3.3 Power Requirements

Present sources of power available for operation of components include the following:

- Batteries and Fuel Cells
- Solar Cells
- Compressed Gas
- Hydraulic Accumulators
  - a) Liquid gas combination
  - b) Liquid compressibility devices
- Mechanical Springs
- Chemical devices (gas generators and squibs)

Each source of power has its advantages and limitations, and the choice of system depends upon the specific requirements. Batteries have a relatively short life, do not operate well at low temperature or under heavy loads, and are essentially low-voltage devices. Solar cells depend upon constant input from the sun and thus are used in conjunction with batteries to provide power.

A limited amount of energy may be stored in pressure vessels as compressed gas, or a combination of gas and liquid can be used, as in a conventional hydraulic accumulator. Cocked mechanical or liquid springs may also be used as a source of energy. Finally, chemical devices such as squibs are useful for some applications.

Efforts are required to determine means of reducing electrical power requirements for spacecraft applications. It is quite probable that improvements could be obtained in the efficiency of solenoid actuators by taking measures that are available but not generally considered because of the added cost that would be incurred. However, as is shown in Section 2.3.2, it may be well worthwhile to pay more for a lighter component through additional machining steps to reduce the total payload weight, as the extra cost of the machining may be insignificant compared to launch costs per pound of the total system. Therefore, a reduction in total power requirements, which would result in a reduction in weight through use of lighter equipment, appears to have a very attractive potential. Specific areas to be investigated include the following:

## 1. Electrical and Magnetic

- a) Use of silver, aluminum or beryllium wire
- b) Use of higher permeability material in flux path
- c) Variation in coil shape, wire shape, flux path size
- d) Improvement of insulation - reduction of bulk.

## 2. General

Care in specifying the operating temperature is required to achieve optimum efficiency and lowest weight. Military specification values should not be used if the temperature range of the specification is greatly different than the expected operating range of the actuator. For example, a specification requiring a range of  $-65^{\circ}\text{F}$  to  $160^{\circ}\text{F}$  will impose a needless weight requirement if the actual operating temperature will be significantly below the upper limit of  $160^{\circ}\text{F}$ , because a smaller unit can be constructed for a given force requirement if the operating temperature is reduced.

### 2.3.4 Operating Life

Operating life can vary from one cycle for a pierce diaphragm valve to many hundreds of thousands of cycles for a solenoid valve. Many factors and combinations of factors affect the life expectancy of a valve, among which are operating temperature, operating pressure, rate of cycling, number of cycles, loads on members, materials of construction, and exposure to space environments.

Pressure will govern seat loads required, and operating temperature in the higher ranges has a very direct bearing on the life of the valve. The rate of cycling may be important if the temperature rise as a result of the operation becomes significant. As with any piece of mechanical equipment, the higher the structural loads, the shorter the life.

Exposure to the space environments will tend to shorten the life of valves because of the deleterious effects of vacuum, radiation and erosion from space debris. The degree to which this occurs depends upon the design of the valve and the location and length of time in the environment.

The survey of prime manufacturers indicated life requirements varying from several hours in the space environment and one cycle of operation to three years in space and 500,000 cycles. The requirements for a particular application must be carefully analyzed and the appropriate compromises or "tradeoffs" must be made to permit specification of an optimum life requirement for a component.

## 2.4 SPACE ENVIRONMENT CONSIDERATIONS

A space environment includes vacuum, on board and solar radiation, zero gravity, and meteoroidal impact conditions. The problems inherent to these environments are discussed in the following sections.

### 2.4.1 Vacuum

Interplanetary space consists of a low-density gas mixture consisting primarily of hydrogen and helium. The estimated gas pressure in interplanetary space is about  $10^{-16}$  mm Hg, and in interstellar space, pressures lower than  $10^{-25}$  mm Hg may be encountered. The lowest pressure that has been produced in the laboratory is about  $10^{-14}$  mm Hg; however, pressures of  $10^{-9}$  to  $10^{-10}$  mm Hg are currently considered practicable for the best vacuum pumps available.

In order to maintain an orbit in the gravitational fields of the planets, the space vehicle must be traveling at some determined velocity, and as a result, the pressure near the spacecraft will be different than the static pressure of space. Also, streams of molecules will emanate from the sun and thereby influence the space vacuum. Gas molecules leaving the surface of the space vehicle will for the most part escape into space, but some may collide with other gas molecules and return.

A vacuum environment may affect the functional characteristics of valves and their related equipment in the following areas:

- Sublimation and evaporation of materials
- Cold welding
- Friction and wear
- Strength of materials

2.4.1.1 Sublimation and Evaporation of Materials - The effects of high vacuum on the sublimation rates of metals can be calculated from the Langmuir Equation, assuming that none of the molecules leaving the surface return to it.

$$G = \frac{P}{17.14} \sqrt{\frac{M}{T}}$$

where: G = rate of loss per unit area of exposed surface in  $\text{g.cm}^{-2}\text{sec}^{-1}$

P = vapor pressure at temperature T in mm Hg

M = molecular weight of the metal in the gas phase

T = absolute temperature ( $^{\circ}\text{K}$ )

The higher the vapor pressure of the material, the higher the rate of sublimation. A plot of vapor pressure against temperature is presented in Figure 2-1. Cadmium, which is often used for plating of parts, is a poor material to use in space vacuum. Metals that sublimate from a warm surface will have a tendency to plate on a cooler surface, possibly causing electrical

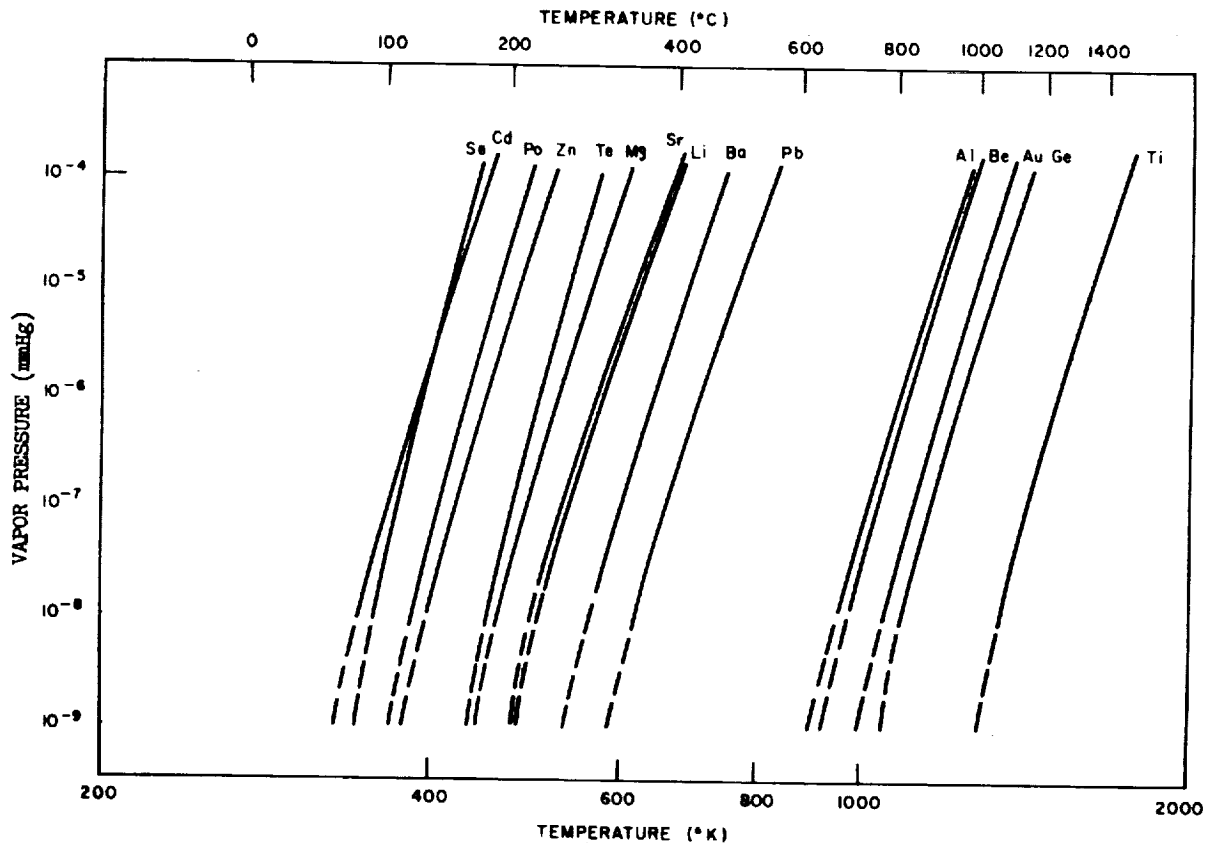


Figure 2-1. Temperature Vs. Vapor Pressure

short circuiting, change of surface emissivities, or change of optical properties of mirrors and lenses. Sublimation can be retarded by selection of surface coatings with low-vapor pressures or inorganic coatings such as oxides, which often have lower vapor pressures than the metals from which they are formed.

The Langmuir Equation is not applicable to the organic materials of interest to the valve designer; therefore, experimental studies of weight loss of organic materials are necessary.

In recent years considerable study has been devoted to the investigation of the mechanisms and kinetics of the degradation of polymers. Such degradation or breakdown can be caused by various factors, including heat, light, and nuclear radiation, as well as various substances, such as oxidizing agents (Reference 8). Results of these studies indicate:

- Polymers of relatively high molecular weight useful in spacecraft applications do not evaporate or vaporize in a vacuum, but when supplied with sufficient thermal energy, decompose or depolymerize by one of several possible mechanisms. That is to say, these polymers have such low vapor pressures that the thermal energy required to cause evaporation exceeds that required to break chemical bonds of the polymer. Thus, many polymers of engineering importance do not sublime or evaporate in high vacuum environments



and will probably not decompose at the moderate interior temperatures anticipated in many spacecraft applications. Furthermore, since in a high vacuum environment many deleterious contaminants such as oxygen and moisture will not be present, at least in the quantities found in the earth's atmosphere; it might be further concluded that the thermal stability of these polymers should be at least as good in high vacuum as at earth ambient conditions.

The very pure polymers necessary for scientific investigation and research are not those commonly used in engineering applications. Most commonly used polymeric materials are commercially formulated products. Investigation of these products in vacuum environment has revealed varying results. From these data it becomes immediately evident that the purity variations of molecular weight and formulation additives significantly influence the weight-loss characteristics of a plastic. Low molecular weight, high vapor pressure fractions of the polymer may be expected to evaporate from the surface of the material. Also, a wide variety of additives may be expected in many instances to evaporate from the surface. Common additives include diluents, plasticizers, dyes, antioxidants, flexibilizers, flame retardants, accelerators and catalysts. For most plastics of engineering interest, the quantities and vapor pressures of these materials and other contaminants such as adsorbed and absorbed gases, moisture, solvents, cleaners, and mold releases will be primarily responsible for the weight loss or outgassing which is detected in engineering studies. Additional factors which may influence the weight loss of materials in vacuum are the degree of cure of the material and any by-products of the polymerization reaction. If the material is inadequately or improperly cured, fragments of low molecular weight and high vapor pressure may remain uncombined in the product. These will evaporate when the material is subjected to a vacuum environment. The same effect may be anticipated for reaction by-products, such as water in many condensation polymerization reactions.

It is obvious that property changes may be expected to occur as a result of the loss of these various additives and contaminants. First, there is the loss or degradation of that property for which the additive was initially placed into the formulation. For example, the loss of a flexibilizer by evaporation in a vacuum environment will produce a more rigid, perhaps brittle, plastic with a corresponding decrease in elongation and impact strength and increased tensile and flexural strength. On the other hand, loss of a dye may result merely in a color change, which may not be significant.

- The loss of an antioxidant or fire retardant may not result in any serious property degradation since these factors are not generally considered to be serious problems in space applications. On the other hand, the loss of a radiation-resistant (anti-rad) compound may result in a very definite change in the ability of the material to withstand the space radiations.

- The loss of accelerators or catalysts from materials may result in a beneficial effect. These materials are generally of high reactivity added initially to initiate and/or accelerate the polymerization of the material and are also capable of serving to accelerate any depolymerization or degradation reaction. Consequently, the loss of these materials could prove to be quite beneficial in many instances.

In addition to degrading that property for which an additive may have been used in the formulation, other property changes may be produced and must be considered. For example, the loss of these materials may change significantly the electrical properties of the polymer, such as dielectric strength, dielectric constant, dissipation factor, and resistivity. Because of the loss of contaminants, moisture, and absorbed gases, many polymers, such as Teflon, used as seals in a valve may experience an increase in their permeability to the propellant.

Based on the postulates that the thermal stability of the basic pure polymers is at least as good in vacuum as in air and that the molecular weights of these polymers are too great to allow evaporation, the rate at which the various materials (additives and contaminants) will evaporate from the plastic is dependent upon at least two factors: the vapor pressures of these various constituents and their diffusion rates through the plastic to its surface. It is to be expected that the weight-loss rate of materials in vacuum will be initially high during the time that surface "contaminants" evaporate and then should steadily decrease to the rate determined by the diffusion rates of these "contaminants" to the surface.

2.4.1.2 Cold Welding - "Cold welding" or pressure bonding, as the term implies, refers to the joining of two solid objects without the presence of a gross liquid or melt phase at the interface. If the bulk temperatures of the objects in question are near ambient, the problem is of great concern to the spacecraft designer utilizing components or subsystems relying on the process of mechanical motion at some specific time in the space environment.

Examinations of the controlling factors in considering such a rate phenomenon reveals at least the following for consideration:

- The atomic species and interatomic bonds
- The surface energy

Clearly the greatest difficulty lies in qualitatively and quantitatively describing the variables associated with the surface energy condition. Three of the most obvious are:

- The absolute temperature - for both the bulk and differential volumes at the surface
- Contamination of the surface
- Crystalline perfection of the surface.

Since under the stated conditions in the earth atmosphere "solid state bonding" does not occur in the same time scale the designer is to be concerned with, the role of surface contaminants is indeed important. Likewise, it is quite clear that if clean surfaces are established in space, they will remain so.

Thus, two rate processes must be quantitatively described to reliably predict either joining or nonjoining of two surfaces by solid state bonding: First, if contaminated surfaces are placed in the space environment, how rapidly and by what mechanisms may the contaminations be removed? Second, if the contaminants are removed, will the two surfaces in question form a bond of sufficient strength, during the contact period, to be of consequence?

Absorbed contaminants are conventionally described as physisorbed or chemisorbed on the surface. Physisorption does not involve the species in question by any strong chemical bond and only rather long-range but relatively weak Van der Waal type forces are involved. Chemisorption does involve strong atomic bonds. The difference in energy between the two types of bonding is very significant - Van der Waal bonds have energies of less than one electron-volt and chemical bonds involve energies of a few electron-volts. The exact role played by contaminants is not clear or necessarily simple. In some cases, the most important role may be satisfaction of available surface bonds. In other instances, an equally important role might be the presentation of an inert barrier serving to retard or prohibit diffusion across the interface.

With this very simple background, examination of desorption mechanisms to be found in space is possible.

- Mechanical Motion

A high efficient means of breaking down or providing sufficient energy to the surface to be desorbed is mechanical motion. What happens to the contaminants upon this additional energy could be one of several processes or combinations thereof. Microscopic plastic deformation can produce short-time, high-surface temperatures without a detectable change in bulk temperatures. Continuous mechanical motion is a different situation than one-time contact. However, in both cases small volumes at the interface will develop high instantaneous surface temperatures resulting in desorption.

- Ultraviolet and/or Low Energy Electron Desorption

Radiation of suitable character to interact at the surface has been demonstrated (Reference 9) as a suitable mechanism for producing clean surfaces. If two surfaces are in static contact with each other in the contaminated condition, such desorption mechanisms would not operate since the penetrating power of such radiation limits desorption to exposed surfaces.

2.4.1.3 Sublimation - Sublimation, dissociation, and chemical reaction are all removal mechanisms. Each process is temperature dependent and usually one is the dominant rate-controlling process. The limitation on the assessment of the loss rate of contaminants in the use of bulk thermodynamic criteria applies to very thin layers. The problem is further complicated by lack of any reasonable estimates of the initial thicknesses of surface contaminants associated with engineering surfaces.

Any rationalization of loss rates in a specific experiment will have a significant geometrical factor. Solid-angle considerations must then be taken into account. The question of two-dimensional mobility and surface diffusion clearly is significant in determining the loss rate process for the contaminants in many instances.

Examination of the bonding processes between two clean surfaces indicates bulk diffusion\* to be the most probable. Before this is discussed in more detail, one other possibility will be considered. This will be termed coherent bonding. Coherent bonding would involve no diffusion. The joining would be effected by attachment of surface bonds by both interfaces which were previously involved in the first monolayer. If the first monolayer bond strength is not pure Van der Waal, then the bond strength could be significant. For coherent bonding, a number of surface conditions must be considered in determining how many individual bonds contribute to the gross bond strength. Consideration of the degree of registry required for appreciable bond formation shows that only lattices with metallic bonds could conceivably establish at least an initial joining of this sort. Lattices consisting of covalent or ionic bonds would require such a precise degree of registry as to make such a bond highly improbable (Reference 10).

Coherent bonding of this nature would be nearly instantaneous. However, three-dimensional atomic mobility of few atom distances could likewise be almost instantaneous compared with the time span of a few seconds to minutes representative of the most rapid experiments which have been reported. Contemporary experiments do not permit distinguishing between the two mechanisms.

Of significance is that neither short-time diffusion bonds nor coherent bonds have occurred for metallic elements placed in contact in which the metals in question were immiscible with each other as determined from the appropriate phase diagram. Also all couples in which adhesion has been demonstrated have had either complete or partial solid solution exhibited in their phase diagrams.

A few experimental observations which have been performed in vacuo are summarized as follows:

---

\*Bulk diffusion is considered only to involve three-dimensional atomic mobility, at least at small microscopic sites at the interface, not necessarily gross diffusion.

OFHC copper (Reference 11) fractured at a bulk temperature of 200°C could be rejoined under high compressive pressures to strengths of approximately 95 percent of the original in repeated operations. Bonding was achieved in seconds in some cases. Gross plastic deformation was incurred during the compressive cycle of rejoining the surface.

Other materials tested by the same investigator with similar techniques were 1018 steel and 52100 steel; only 1018 steel showed measurable rebonding. Steel by another investigator also showed adhesion (Reference 12).

Copper was also the subject of investigation in other studies in which the copper in question was the needles of Project Westford. Subjection to ultra-high vacuum resulted in partial cold welding of the needles.

The primary investigations supporting a solubility-immiscibility hypothesis were performed by Spalvins and Keller, in which adhesion was found only where solubility of some degree was indicated by the phase diagrams. Conversely, no joining was noted in the remaining couples, which showed no solubility or, in one instance, had covalent bonds.

<u>Complete Adhesion</u>	<u>No Adhesion</u>
FE-AL	Cu-Mo
Ag-Cu	Ag-Mo
Ni-Cu	Ag-Fe
Ni-Mo	Ag-Ni
	Ge-Ge (single crystal)

Because of the uncertainty in predicting rate processes, practical techniques to minimize the possibility of cold welding can only be generalized. Reliance on maintaining a contaminated surface may be suitable or mandatory in some instances. This could be in the form of strictly natural chemisorbed layers or preferentially treated solid lubricants, oils, or greases. With exception of the naturally occurring contaminants, other forms could be placed on the surface to permit and justify to a greater extent use of bulk thermodynamic properties in predicting loss rates.

Cold welding is no different than common fusion welding or brazing of metal parts. The oxides of the metals joined are removed by heat or acids. The melt phase of the metals to be joined are not important in the joining mechanism except to provide complete area of contact at the interface. The heat does, however, remove the protective oxides producing clean surfaces. As a rule, any weldable materials using conventional welding techniques are potential candidates for cold welding.

2.4.1.4 Friction and Wear - The tendency of a vacuum to permit clean surfaces (surface contamination removed) will, as a result, increase the friction forces between metals in sliding contact. After initial sliding has begun, the oxide film is broken, and because of the absence of an oxidizing atmosphere, these oxide layers are not reformed and consequently many more metallic junctions are formed at the interface. Since adhesive friction is considered to be the result of shearing of these cold welded metallic junctions, any methods that can be devised to prevent the junction formations will be helpful in reducing friction.

If the oxide films are completely removed from the metal surfaces, the metal can weld together and sliding is impossible. Any amount of gases or vapors produces some contamination to a surface whereby the friction will decrease. For valve closures exposed to vacuum, leakage through the seat interface would alleviate cold welding and decrease the friction on seats which are in sliding contact, such as the ball-type configuration.

Wear is aggravated when the oxide layers are removed between surfaces in sliding contact. The wear debris formed between metallic surfaces in contact also change in size, depending on the atmosphere the wear surfaces are exposed to. With the absence of an atmosphere, the wear particle size is believed to be a maximum. The surfaces in contact and exposed to the vacuum of space, such as a valve closure or valve actuator part, may experience larger wear debris than is found when they are operated in the earth's atmosphere. Because of a change in wear particle size, a change in leakage in the "last" valve in the system (shutoff valve) may occur, or seizure may develop between the surfaces of the moving parts of an actuator.

2.4.1.5 Strength of Materials - The absence of an oxidizing atmosphere and the loss of the initial oxide films on the surface of structural parts may influence the fatigue strength of the parts.

Investigators have shown that the fatigue life of many metals increased substantially when the metals were tested in a vacuum, as compared to when they were tested in air. A flexure pivot is an interesting application to a mechanism that requires a bearing or hinge supports. A flexure pivot is basically a thin, flat beam which will bend easily under a load and thereby act as a hinge point. An increase in fatigue properties of metals in a vacuum supports this means of providing a pivot joint and also eliminates the need for lubricants.

The tensile strength of fine metal wires in a vacuum is slightly greater than in air, but in general the strength of metals in a vacuum does not differ significantly.

- The Effects of Vacuum on Electrical Components

For many electrical components the effect of vacuum must be considered. A motor that operates satisfactorily in air may not perform its task in vacuum. A switch may short-circuit in vacuum because of the change of the dielectric. A motor or solenoid winding, when exposed to vacuum, may fail because of the loss of insulation. Capacitors may change in value

if the insulation materials used in their construction lose moisture or other contaminants entrapped during their manufacture. Preliminary studies have indicated changes in the electrical characteristics of some components (Reference 13).

Additional problems may be presented when the components must operate in the atmosphere of another planet. A component may have to meet test procedures in air, but in addition, work in the vacuum of space and then again operate satisfactorily in the atmosphere of Mars, Venus, or Jupiter.

Some of the various environmental problems may be eliminated, for instance, by providing the solenoid actuator for a valve with its own atmosphere, such as the propellants. An actuator buried in the propellant would not be exposed to vacuum, but care should be taken to ensure that the materials exposed to the propellants are compatible.

## 2.4.2 Radiation

2.4.2.1 Introduction - The usual division of the space radiation environment is into four zones, described as follows:

The Inner Radiation Zone

The Outer Radiation Zone

The Auroral Zone

The Interplanetary Zone

The characteristics of each of these zones will be discussed below in terms of the type and energy spectrum of the radiation present, as well as the temporal and spacial variations of this radiation. A few brief definitions of the units employed in the following calculations will first be presented.

### 2.4.2.2 Definitions

Flux - The omnidirectional flux of particles at any point in space is the number of particles of a particular type that would traverse a test sphere of  $1 \text{ cm}^2$  cross sectional area in one second. It has the units of particles/ $\text{cm}^2 \text{ sec}$ . The unidirectional flux is the flux arriving at the test sphere per unit solid angle from any particular direction and has the units of particles/ $\text{cm}^2 \text{ sec steradian}$ . If the incident radiation is isotropic, the unidirectional flux equals the omnidirectional flux divided by  $4\pi$ . Under this same assumption, the flux of particles incident from one hemisphere on a plane surface is one-fourth the omnidirectional flux.

The results of laboratory radiation damage experiments are usually quoted in units of particles/ $\text{cm}^2$  required to produce some effect in a given sample. This unit should not be confused with the omnidirectional flux, however, since the laboratory measurements are almost always made with a unidirectional beam of particles. Thus, to obtain the omnidirectional flux corresponding to this laboratory flux, the laboratory flux should be multiplied by four.

Dosage Units - There are four units generally used to describe the amount of energy lost in a material by incident radiation. The roentgen (r) is defined precisely as the quantity of gamma radiation that will produce one electrostatic unit of electrical charge in 1 cc of dry air at standard conditions of temperature and pressure. This corresponds to the absorption of 87.7 ergs of energy per gram of air. A more useful unit, the roentgen-equivalent-physical(rep), which is independent of the type of radiation, refers to tissue damage and is defined as the radiation dose which produces an energy absorption of 93 ergs/cm<sup>3</sup> in aqueous tissue. Still more useful is the rad which is independent of the material being irradiated and the type of radiation and is the radiation dose which produces an energy absorption of 100 ergs/cm<sup>3</sup>. The roentgen-equivalent-man (rem) is useful in discussing biological effects and will not be considered here.

Geomagnetic Coordinates - Since the trapping of charged particles and the behavior of extraterrestrial particles in the earth's vicinity is characterized by the shape and strength of the earth's magnetic field, it is quite convenient to plot the radiation intensities in geomagnetic rather than geographic coordinates. The origins of these coordinate systems coincide, but the geomagnetic axis is tilted by 11.5 degrees with respect to the axis of rotation of the earth. Since isointensity contour maps presented herein, as well as the sample vehicle trajectories, are in geomagnetic coordinates, it will be necessary to consider the differences between the two systems when the radiation in an actual trajectory is being predicted.

2.4.2.3 The Inner Radiation Zone - Until recently the inner radiation zone was primarily characterized by a high proton flux. However, the high altitude nuclear test bomb blast of July 9, 1962 above Johnston Island resulted in the trapping of a large number of fission electrons in this zone. Measurements of these fission electrons indicate a peak omnidirectional intensity of 10<sup>9</sup> electrons/cm<sup>2</sup> sec extending from an altitude of 1300 km to an altitude of 5500 km (Reference 14). The differential spectrum of fission electrons, shown in Figure 2-2, can be approximated by  $N_0 \exp[-0.575 E - 0.055 E^2]$  for the range  $1 \leq E \leq 7$  Mev,  $N_0$  being the normalizing factor. Approximately half of these fission electrons have energies below 1 Mev. The figure of 10<sup>9</sup> electrons/cm<sup>2</sup> sec quoted above represents the total number of electrons of all energies that are trapped based on the assumption that a fission spectrum does indeed exist. The isointensity contours of this artificial electron belt based on this assumption are shown in the bottom half of Figure 2-3. There have not yet been any measurements of the temporal decay of the fission electrons in the inner zone. (For the sixty days following July 7, no decrease was observed).

The proton isointensity contours for  $E > 40$  Mev are shown in the top half of Figure 2-3. The spectral distribution of these protons is based on data analyzed by Freden and White (References 15 and 16), Naugle and Kniffen (Reference 17), and Heckman and Armstrong (Reference 18) from vehicles skirting the edge of the inner radiation zone, which is shown in Figure 2-4. The most reasonable assumption that can be made at this time is that the spectral distribution in the heart of the inner zone is given by the spectral observed on the fringes. The distribution is well approximated by an



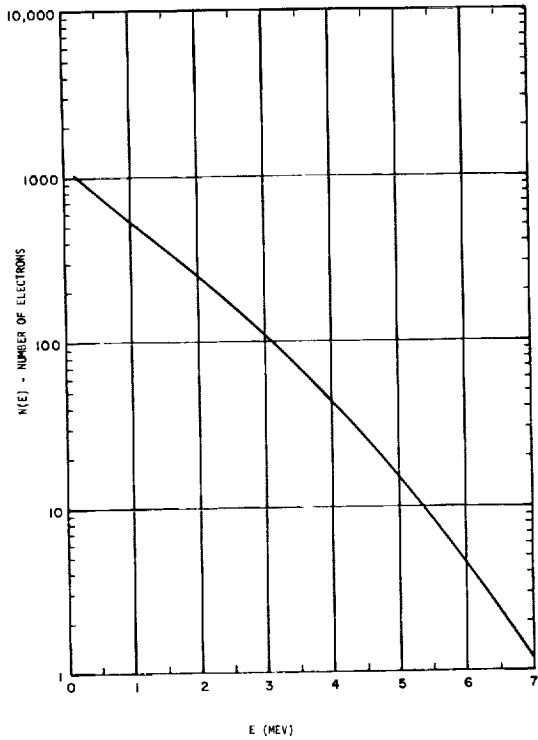


Figure 2-2. Fission Energy Spectrum

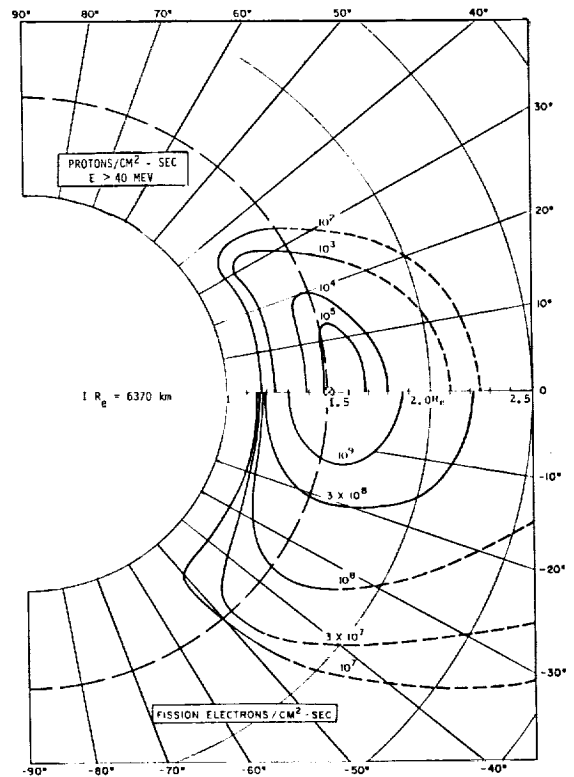


Figure 2-3. Isointensity Contours of the Inner Radiation Zone

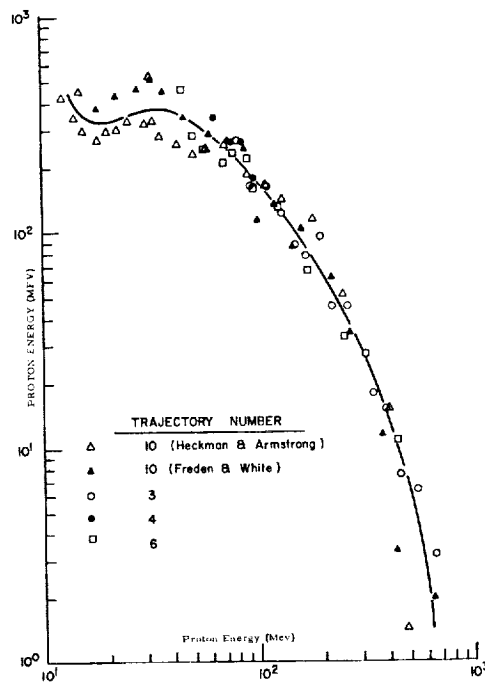


Figure 2-4. Spectral Distribution of Protons in the Edge of the Inner Radiation Zone

integral spectrum of the shape

$$kE^{-0.8} \text{ for } E \geq 20 \text{ Mev}$$

$$k'E^{-3.5} \text{ for } \geq 20 \geq E \geq 8 \text{ Mev}$$

Observations during magnetically quiet days indicate that changes in intensity in the inner radiation zone are of the order of several percent. However, time variations involving as much as a factor of 3 increase in intensities have been observed to occur in temporal correlation with major solar events and/or major geomagnetic storms (Reference 19). On the other hand, the geomagnetic field acts as an excellent shield in deflecting solar protons from the inner radiation zone, since protons of energies less than 6.8 Bev are excluded from the equatorial plane at altitudes below 1.25 Re (earth radii).

2.4.2.4 The Outer Radiation Zone - The outer radiation zone is characterized by the absence of high intensities ( $>100$  particles/cm<sup>2</sup> sec) of geomagnetically trapped protons with energies greater than 10 Mev. The trapped radiation consists principally of electrons and soft protons ( $E < 10$  Mev). In the equatorial plane the outer zone begins at 2.3 Re and extends to 8 to 10 Re. In a meridian plane the outer zone boundary dips down to lower altitudes with increasing geomagnetic latitude. The intensities at the heart of the outer zone (3.6 Re) are:

Electrons	$E > 500$ kev	$2 \times 10^7$ electrons/cm <sup>2</sup> sec
Protons	$E > 100$ Mev	$< 1$ proton/cm <sup>2</sup> sec
Protons	$E > 140$ kev	$\sim 10^8$ protons/cm <sup>2</sup> sec

The isointensity electron contours are plotted in the top half of Figure 2-5. In the bottom half of this figure are shown the contours after the magnetic storm of August 16, 1959, which increased the intensities 20-fold to  $4 \times 10^8$  electrons/cm<sup>2</sup> sec of energy greater than 500 kev. In addition to these large changes wrought by magnetic storms, 3-fold increases and decreases not clearly correlated with solar activity are observed above 6 Re. In the heart of the outer zone the spectrum of electrons is given by an expression of the form  $\text{const.} \times \exp(-4.26 E)$ , and is shown in Figure 2-6.

2.4.2.5 The Auroral Zone - The auroral zone is located roughly between 60 and 65 degrees geomagnetic latitude, but moves toward lower latitudes during strong magnetic disturbances. The auroral displays are caused by energetic electrons entering the atmosphere, although protons may or may not be present.

Since the particle flux, the energy spectrum of each component, and the directional characteristics of the particles are characteristic of the observed aurora, the auroral zone cannot be described in as definite a fashion as the inner and outer radiation zones. The maximum proton intensity seen in the auroral zone, which was observed during an aurora with the fading ray structure, is given by an integral spectrum of the form  $J(>E) = 75E^{-3.2}$  protons/cm<sup>2</sup> sec steradian where the energy is in Mev.

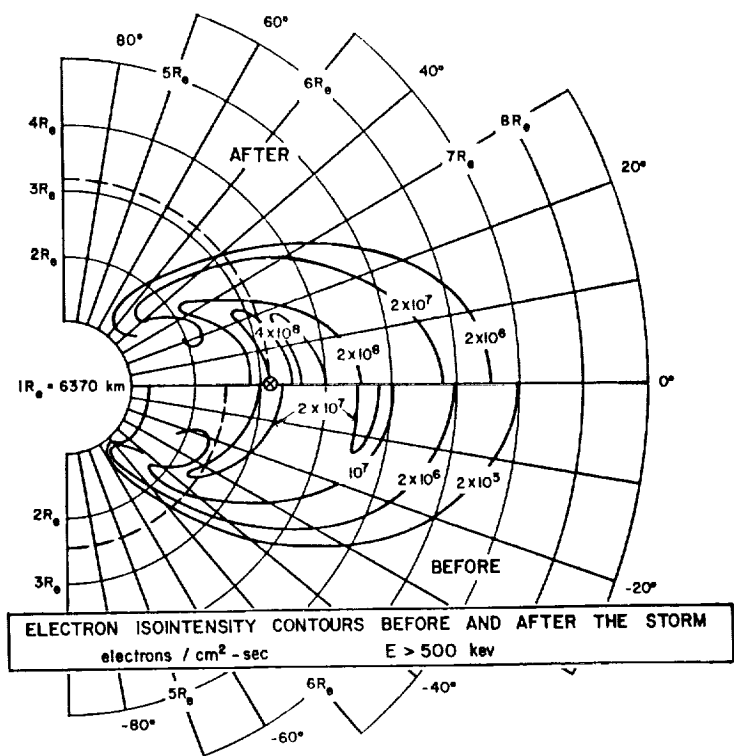


Figure 2-5. Electron Isointensity Contours Before and After the Storm

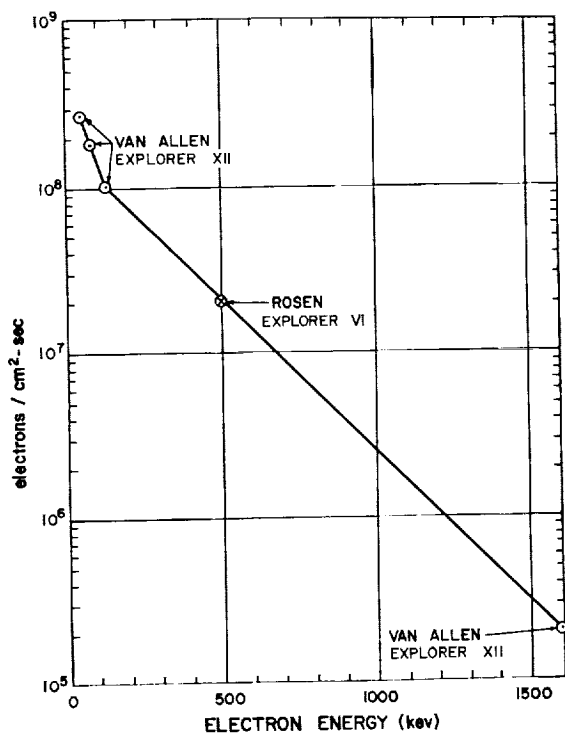


Figure 2-6. Electron Spectrum in the Outer Radiation Zone

For this type of aurora the electron spectrum is of the form  $J(>E) \frac{1}{E}$  for energies where  $5 \text{ kev} \leq E \leq 50 \text{ kev}$ . The intensity above 10 kev was measured to be  $(4+2) \times 10^7$  electrons/cm<sup>2</sup> sec ster. Since the particle fluxes in the auroral zone are much smaller than those observed in the equatorial radiation zone, the damage done to these particles has been neglected in the calculations below. Of course, for special trajectories that leave the earth near a geomagnetic pole, the auroral zone radiation could become important.

2.4.2.6 The Interplanetary Zone - Energetic radiation in interplanetary space consists of an extremely high energy, temporally stable component, the primary cosmic flux, and pulses of radiation of a few days' duration associated with solar flares which occur at random intervals. The largest flares, designated 3+, include the relativistic flares in which enormous amounts of energy are carried away by highly relativistic protons. These flares are extremely rare, only nine having been observed in the last 23 years. However, the smaller flares occur with increased frequency--the smallest, a flare of importance occurring eight times per day (Reference 14). In addition to these two sources of interplanetary radiation there also exists a continuous ejection of low energy particles (primarily protons and electrons) from the sun to form what is called the solar wind. These particles generally have energies of the order of a few kev and need not be considered in any radiation damage estimates.

Galactic cosmic rays consist primarily of protons (~93%) and alpha particles (~7%) along with small amounts of heavier elements. The energy spectrum of the galactic protons is well represented by  $N(>E) = 0.3/(1+E^{1.5})$  protons/cm<sup>2</sup> sec ster for energies where  $500 \text{ Mev} \leq E \leq 20 \text{ Bev}$ . The energy E is in Bev. This gives the free space flux of particles as 2.5 particles/cm<sup>2</sup> sec. This flux is quite small and needs to be considered only in very long space flights; although shielding such high energy particles would be extremely difficult to achieve, since small thicknesses are likely to cause increased damage from the secondaries produced.

The effect of solar flares is very difficult to estimate because of time variations in their intensity and the temporal randomness of the occurrence. The integral energy spectrum at peak intensity of the type 3 solar flare of September 29, 1961, was measured to be  $N(>E) = kE^{-\gamma} = 6.33 \times 10^4 E^{-1.77}$  protons/cm<sup>2</sup> sec ster for E between 100 and 1000 Mev. The temporal variation of this spectrum is shown in the series of spectra in Figure 2-7. Solar flares of intensity 3 or higher have a frequency of approximately 1 per 20 days. To obtain the radiation intensity in space from solar flares one could take 1/20 of the intensity of the above flare as an average for flights of long duration away from the earth. This is, of course, only a very rough approximation because any particular flight may see radiation from flares that is far from average.

Typical Maximum Intensity Orbits - Several circular orbits, passing through either the heart of the inner or outer radiation zone, have been considered in making calculations of the integrated radiation intensity on a spacecraft. For a circular orbit the period is given by

$$T = 2\pi \sqrt{\frac{R_E}{g}} \left(\frac{R}{R_E}\right)^{3/2}$$

where  $g$  is the acceleration due to gravity at the earth's surface,  $R_E$  is the earth's radius and  $R$  is the radius of the orbit (altitude +  $R_E$ ). This expression leads to  $T = 85 (R/R_E)^{3/2}$  minutes, for  $R_E = 6370$  km and  $g = 9.8 \times 10^{-3}$  km/sec.

There are, in all, six different orbits that were considered. The first two were the equatorial and polar orbits passing through the heart of the inner zone. The next four were the equatorial and polar orbits passing through the heart of the outer zone, two for before the storm and two for after the storm. All of these orbits are shown on Figures 2-3 and 2-5. Note that the outer zone equatorial orbit before the storm is identical with the outer zone equatorial orbit after the storm. Calculations of the radiation intensities in these orbits lead to the results presented in Table 2-6.

#### 2.4.2.7 Dose Rates

Bremsstrahlung - The calculation of the dose rates produced by an incident electron flux is complicated by the existence of gamma rays that are produced whenever electrons pass through an absorber. The gamma radiation thus produced is termed "Bremsstrahlung." An exact calculation of the dose rate produced by the Bremsstrahlung is complicated by a number of factors:

1. Angular dependence of the Bremsstrahlung with respect to the incident electron.
2. Partial absorption of the Bremsstrahlung by the electron absorber.
3. Variation of the mass absorption coefficient with Bremsstrahlung energy.
4. Electron straggling and scattering in the absorber.

To simplify the calculation a number of approximations can be made which will lead to results that for reasonable absorber thicknesses, e.g., less than 5 inches of aluminum, will yield answers accurate to approximately + 50 percent, a result probably more accurate than the estimates of the incident electron intensity. The calculation will assume that:

1. The Bremsstrahlung is produced isotopically
2. None of the Bremsstrahlung is absorbed in the material that produces it
3. The mass absorption coefficient for aluminum is taken as a constant
4. The electrons are all assumed to stop in the absorber.

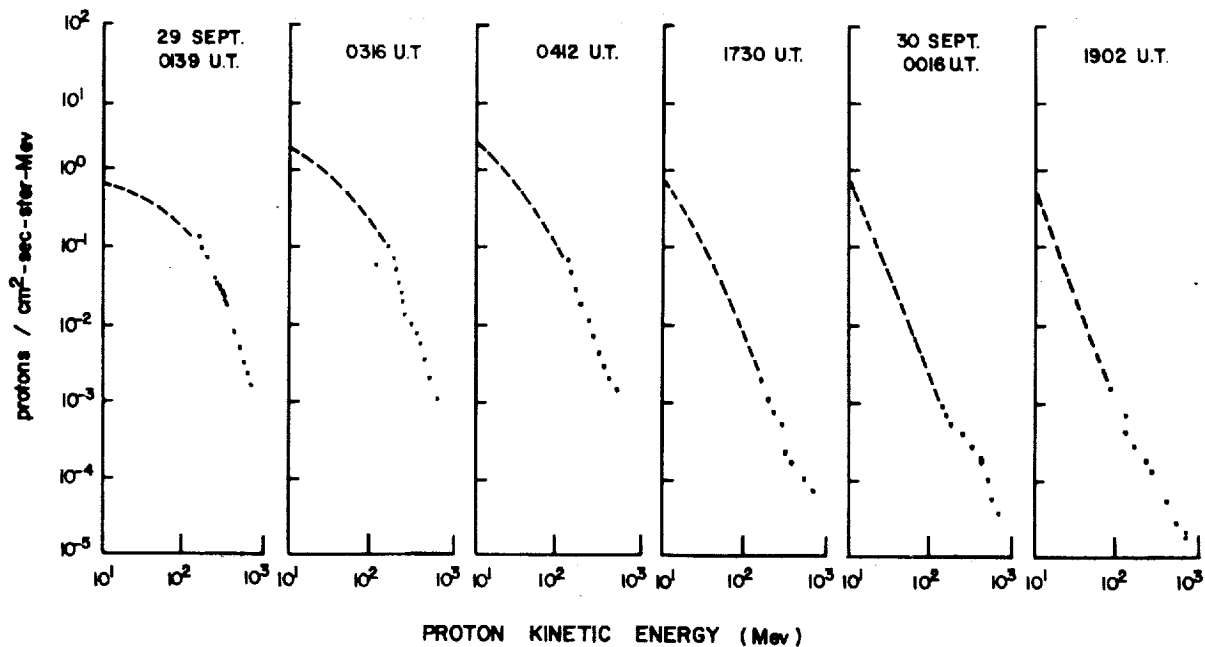


Figure 2-7. Differential Energy of Decay of Sept. 28 Event

Table 2-6. Radiation Dose Rates for Various Orbits

Type	Radius $R_e$	Period Min.	Electrons/cm <sup>2</sup> Orbit	Protons/cm <sup>2</sup> Orbit	Electrons/cm <sup>2</sup> Day	Protons/cm <sup>2</sup> Day
Polar	1.5	156	$2.3 \times 10^{12}$	$1.7 \times 10^8$	$2.1 \times 10^{13}$	$1.55 \times 10^9$
Equat	1.5	156	$9.4 \times 10^{12}$	$9.4 \times 10^8$	$8.6 \times 10^{13}$	$8.6 \times 10^9$
Polar Before	3.5	557	$2.45 \times 10^{11}$	--	$6.2 \times 10^{11}$	--
Equat Before	4.2	731	$6.8 \times 10^{11}$	--	$1.7 \times 10^{12}$	--
Polar After	4.2	731	$4.8 \times 10^{12}$	--	$9.5 \times 10^{12}$	--
Equat After	4.2	731	$1.8 \times 10^{13}$	--	$3.4 \times 10^{13}$	--

Of these assumptions, the last is the only one that will yield a large error in the answer, and this only for those cases where the shielding thickness is less than 1 g/cm<sup>2</sup> (approximately 0.17 inches). In any case, assuming that all the electrons are stopped can only lead to a dose rate estimate that is larger than one that is calculated without using this assumption. That assumption (2) is an excellent approximation can be seen by referring to Figures 2-8 and 2-9 which present the absorption of gamma rays in various materials. As can easily be seen, gamma rays suffer very small absorptions in aluminum, 1 inch of which decreases the intensity by only 20 percent. Under the above assumptions, the expression for the dose rate becomes

$$R = 6.1 \times 10^{-8} \int_{E=0}^{\infty} \int_{T=E}^{\infty} (T-E) N(T) dT dE$$

where R is in rad/day, N(T) dT is the differential incident electron spectrum as a function of the kinetic energy T, and E is the Bremsstrahlung energy. If the electrons are not stopped in the absorber, the upper limits in this double integral will be T<sub>MAX</sub>, the energy of the electron whose range is the thickness of the absorber. Figures 2-10 and 2-11 indicate this range as a function of electron energy. For the outer zone one can use

$$N(T) dT = 36 k e^{-4.26T} dt$$

and for the inner zone

$$N(T) dT = 1.1 k e^{-0.93T} dT$$

where k is the number that appears in Table 2-6 in the column labeled "Electrons/cm<sup>2</sup> Day." Using these two expressions, we obtain:

$$R = 3.3 \times 10^{-13} k \text{ rad/day (Outer Zone)}$$

$$R = 9.7 \times 10^{-12} k \text{ rad/day (Inner Zone)}$$

Electrons - A calculation of the dose rates produced by an electron flux after passing through an absorber is complicated by the energy variation of the range. If, however, we approximate the range as proportional to the energy, the calculation becomes much simpler. This is a quite good approximation for electrons as can be seen by studying Figures 2-10 and 2-11. With this approximation the dose rate becomes:

$$R = 3.2 \times 10^{-8} k \beta \int_0^{\infty} e^{-\alpha(E + 13.3t)} dE \text{ rad/day}$$

where k again is obtained from the column labeled "Electrons/cm<sup>2</sup> Day" in Table 2-6, t is the thickness of the aluminum shield in inches, and

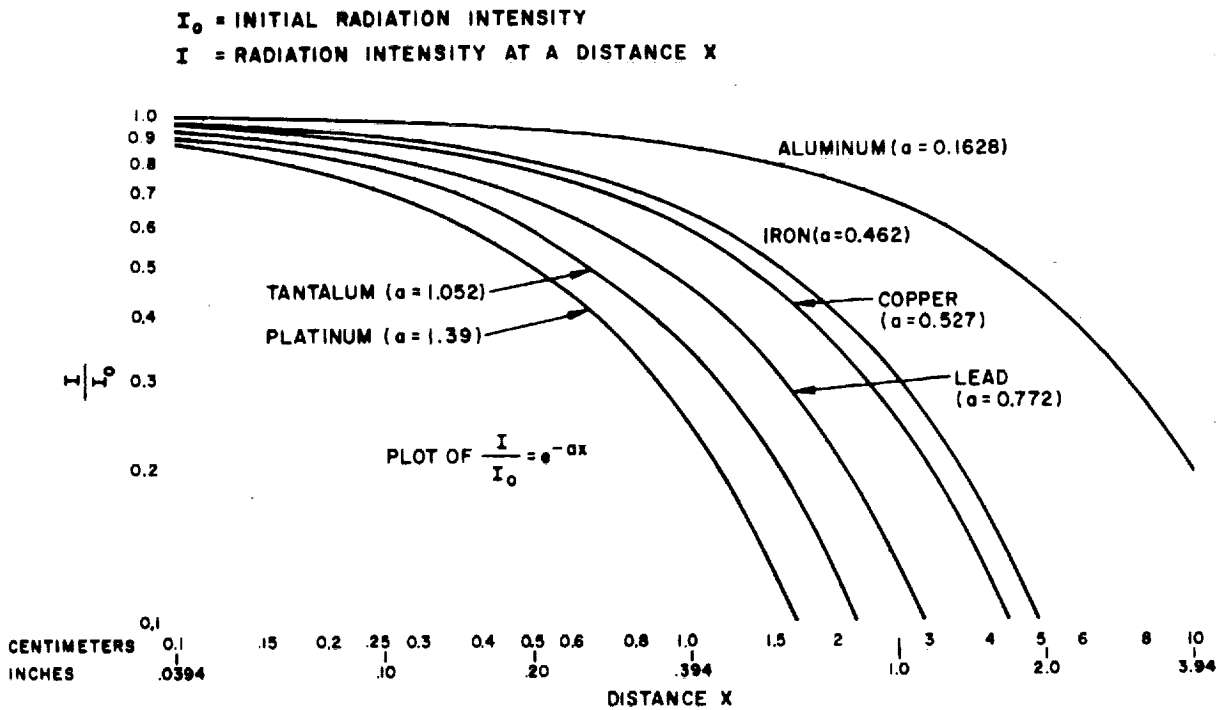


Figure 2-8. Gamma-Ray Absorption at 1 Mev Energy

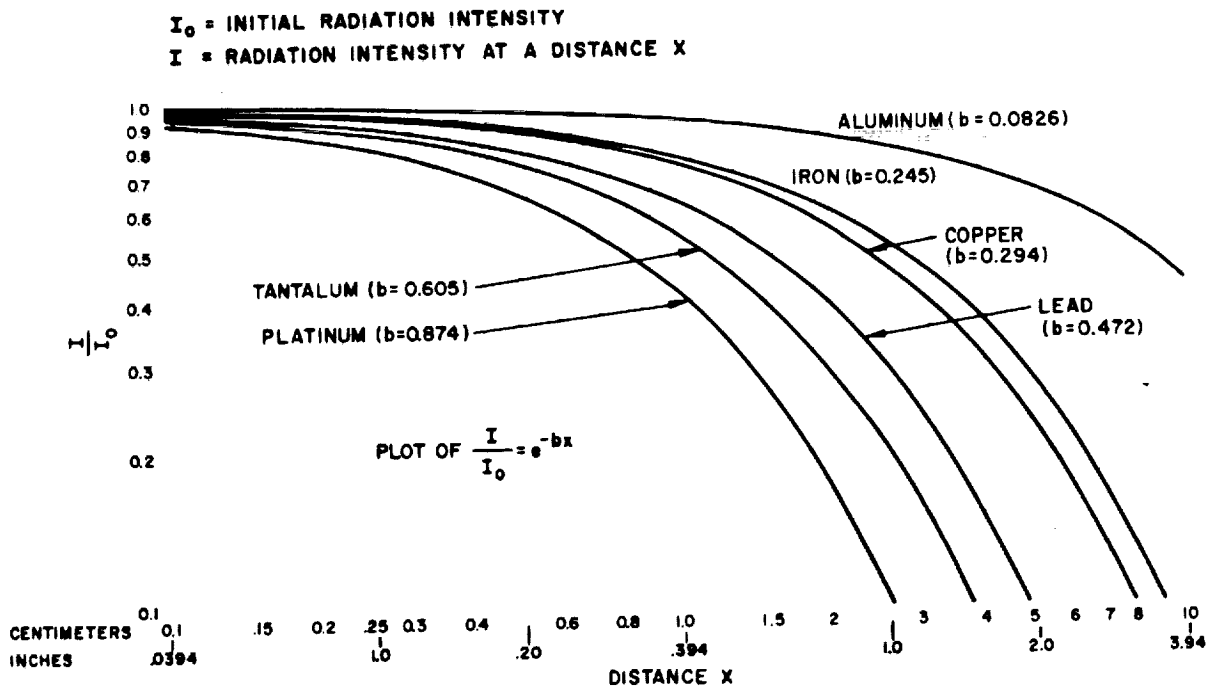


Figure 2-9. Gamma-Ray Absorption at 4 Mev Energy



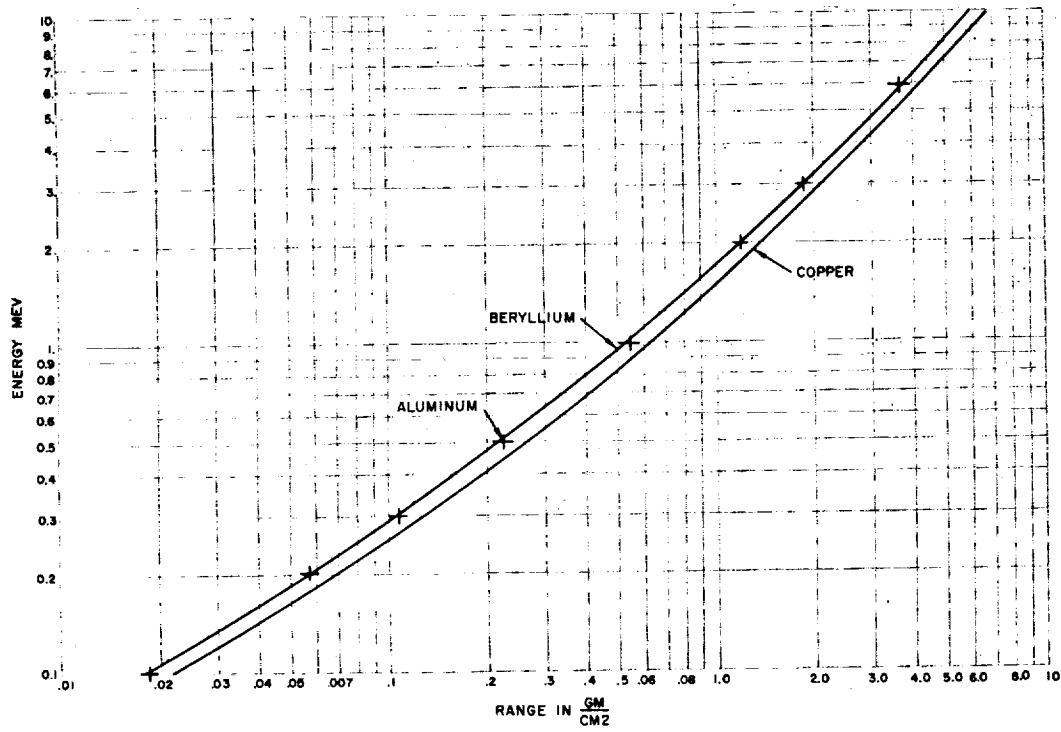


Figure 2-10. Range-Energy Relation for Electrons to 10 Mev

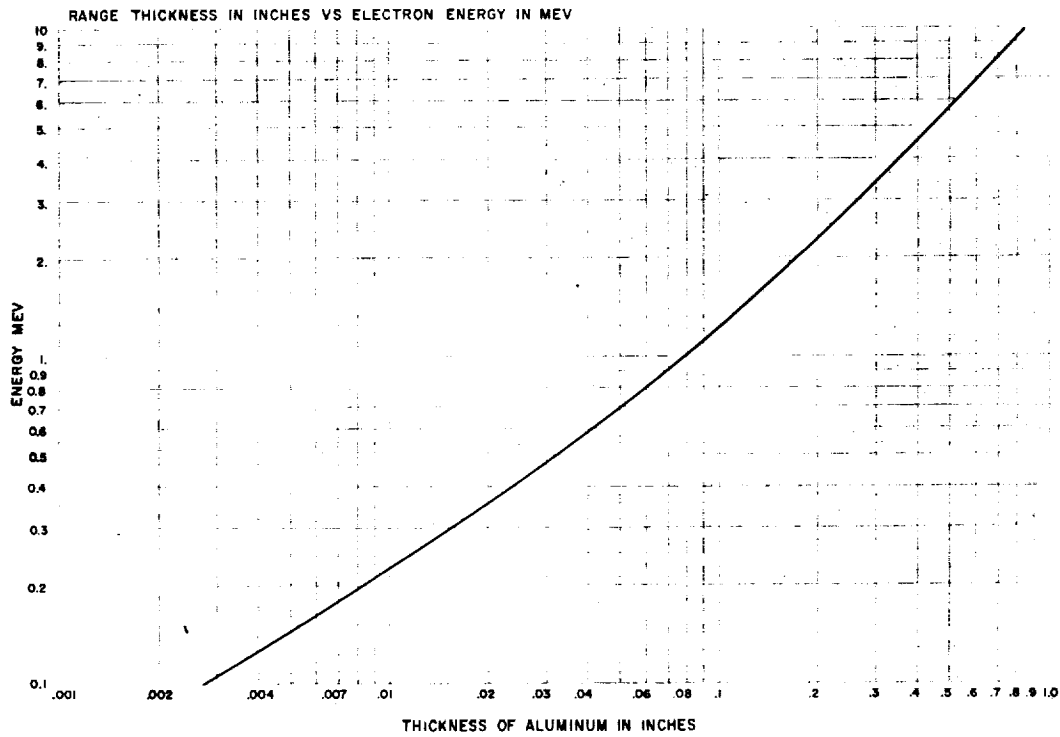


Figure 2-11. Range-Energy Relation in Aluminum for Electrons to 10 Mev

$\alpha = 4.264$ ,  $\beta = 36$  in the outer zone;  $\alpha = 0.93$ ,  $\beta = 1.1$  in the inner zone. For a thickness of aluminum absorber  $t = 0.06$  inches, the above integral for R gives:

$$R = 8.9 \times 10^{-8} \text{ k rad/day (Outer Zone)}$$

$$R = 1.8 \times 10^{-8} \text{ k rad/day (Inner Zone)}$$

Protons - The calculation for protons is more difficult than for electrons because the range energy relation and energy loss rate for protons cannot be approximated by as simple an expression as was used above for the electrons. A power law fits the curves of Figures 2-12 and 2-13 quite well, but a function of this form will not yield an answer in closed form. A sample calculation has been previously performed for an inner radiation zone orbit that can be used here, however (Reference 20). The calculation was carried out quite accurately for a shielding thickness of  $1 \text{ g/cm}^2$ , which gave, for an integral energy spectrum of  $1.8 \times 10^4 E^{-0.8}$  protons/cm<sup>2</sup> sec for E between E and 1000 Mev, a dose rate of 1.00 rad/hr. To use this number for the orbits chosen here we simply note that the integral spectrum used in the calculation referred to gives an intensity of  $9.4 \times 10^2$  protons/cm<sup>2</sup> sec of energies greater than 40 Mev. The dose rate for the orbits of Table 2-6 thus becomes:

$$R = 2.9 \times 10^{-7} \text{ k rad/day}$$

This result is for an aluminum thickness of  $1 \text{ g/cm}^2$  or 0.146 inches of aluminum. Looking at Figures 2-12 and 2-13 we note that this thickness of aluminum will just stop 28 Mev protons. A thickness of 0.060 inches will stop 15 Mev protons. Thus  $(28/15)^{0.8} = 1.65$  times as many protons penetrate 60 mils of aluminum as penetrate 146 mils. Since the energy loss rate for protons of this energy is not strongly energy dependent, a good approximation for the dose rate under 60 mils of aluminum would be:

$$R = 4.6 \times 10^{-7} \text{ k rad/day.}$$

Interplanetary Space - The dose rate in interplanetary space due to galactic cosmic rays was measured on the Pioneer V space probe below  $1 \text{ g/cm}^2$  of low Z shielding materials, and was found to be 14 mrad/day. The dose rate from solar flares, on the other hand, cannot easily be measured and so must be calculated. Calculating this dose rate is a formidable task because (1) the temporal variations of the particle intensities as well as the energy spectrum of these ejected particles are not known accurately, and (2) calculations would be difficult, requiring a computer, even if the flare characteristics were well known.

An estimate of the dose rate can be made by fitting the differential energy spectrum of 0412 U.T. in Figure 2-7, to a power law in energy of the form  $kE^{-\gamma}$  which gives a value for  $\gamma$  of 1.7. In the inner radiation zone a value of  $\gamma = 1.8$  has been used for the differential energy spectrum to give the dose rates reported under Protons above. To obviate the necessity of performing a separate computer calculation for the solar flare contributions

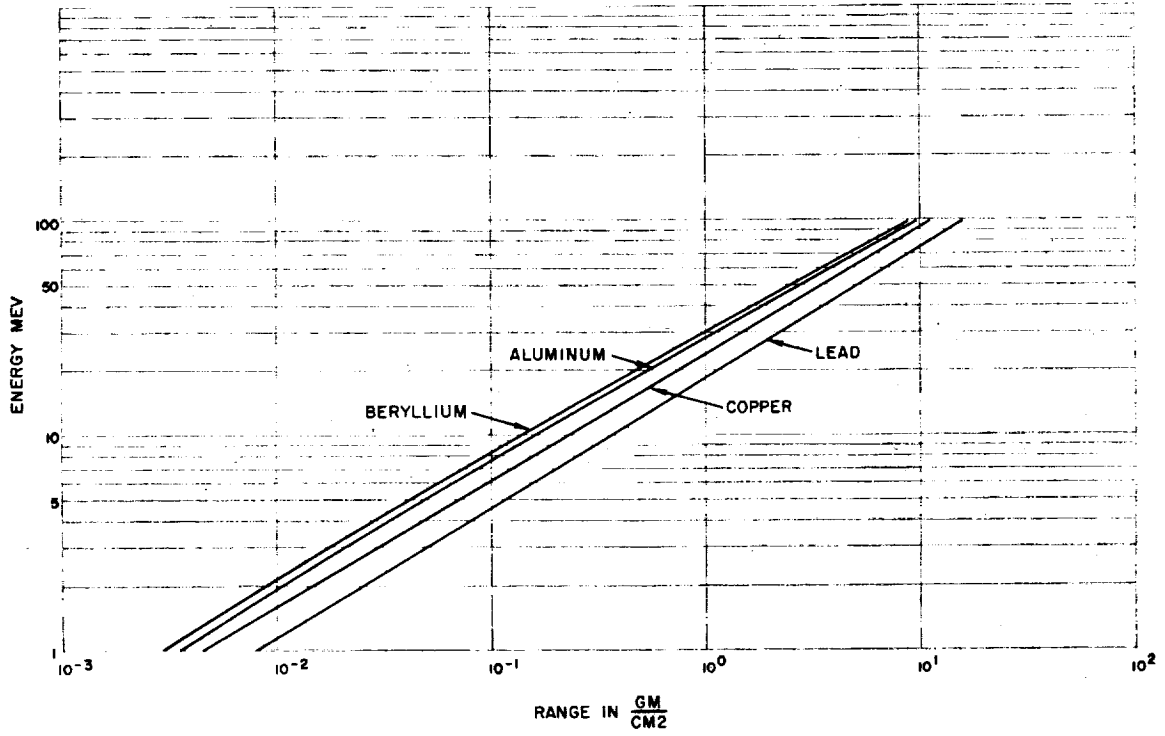


Figure 2-12. Range-Energy Relation for Protons to 100 Mev

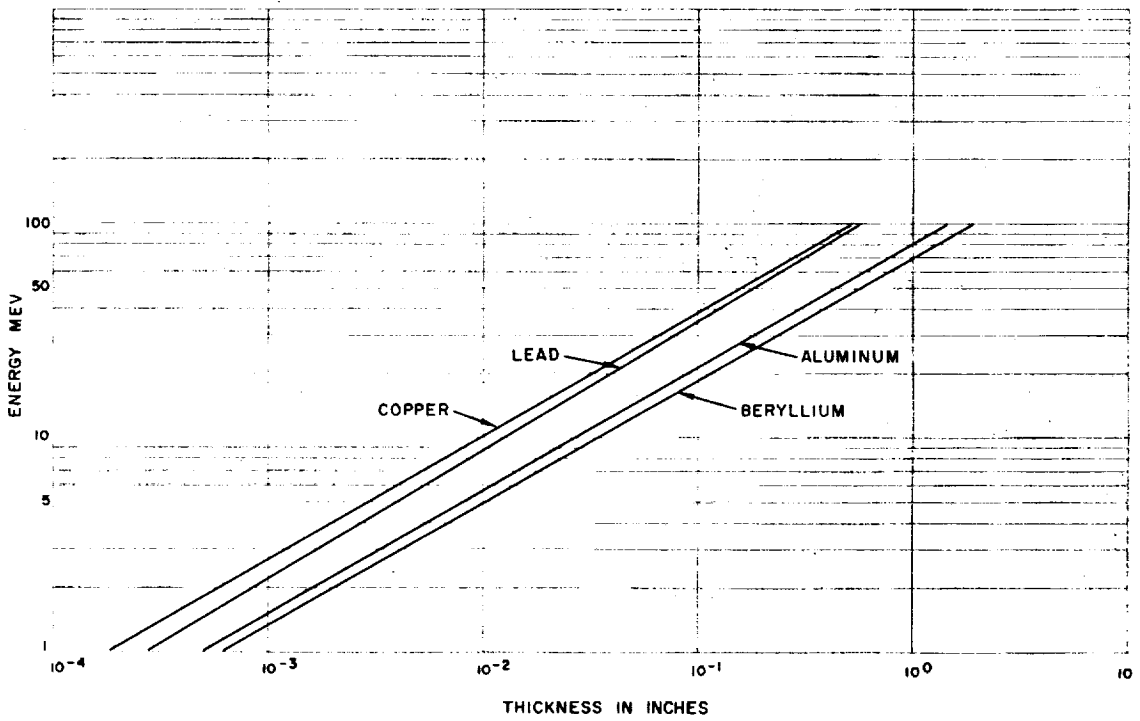


Figure 2-13. Range-Energy Relation for Protons to 100 Mev

to dose rates, an approximate result can be obtained using  $\lambda = 1.8$  for this case as well. With this approximation and assuming the peak flare intensity yields twenty times the average intensity, the average number of protons/cm<sup>2</sup> sec greater than 40 Mev is 6.3. The dose rate is thus

$$R = 4.6 \times 10^{-7} \times [6.3 \times 8.64 \times 10^4] \text{ rad/day}$$

or

$$R = 0.25 \text{ rad/day}$$

#### 2.4.3 Zero Gravity

Noted below are several problems associated with a zero-gravity field:

1. Fluid heat transfer must depend on mechanisms other than convection, such as film boiling, conduction and diffusion. Heat transfer by convection is not possible in a zero-gravity field. Design depending on weights and liquid-liquid or liquid-vapor separating to some predictable orientation will be useless in the zero-gravity field.
2. Venting the gas from a liquid-vapor phase requires techniques to prevent loss of the liquid. A vent valve capable of this without special design of the tank is a problem. A thermal zero-g vent system for liquid hydrogen is described in Section 4.0.
3. Transfer or flow of fluids, such as propellants and lubricants, must be made without dependence upon gravity. The behavior of contained liquids in a zero-gravity field may depend on the wettability of the liquids with the container walls. Liquids which do not wet the container walls will tend to contract to a spherical shape and leave the wall to be suspended in space. Liquids which do wet the container walls will tend to spread out over the wall, leaving the gas pocket in the center.
4. Spring mass system characteristics are subject to change. For example, the resultant force on a regulator controller could be altered in going from 1g field to a zero-g field, with a consequent shift in the regulator output values.

#### 2.4.4 Time

Although time is not usually thought of as an environmental parameter, it will be considered as such for purposes of this report. Probably in all cases time works in the direction of performance degradation, and its effect is, of course, more pronounced with less stable materials such as the polymers than with metals.

Several mission durations are presented as follows (Reference 21).

	<u>Nominal Velocity (ft/sec)</u>	<u>Nominal Duration</u>
Earth Orbit, 300-n. mi. Orbit	30,000	90 minutes
Earth Escape, Circumlunar	40,000	5 days
Lunar Landing, One Way	50,000	2-1/2 days
Lunar Landing Earth-Return	60,000	1 - 2 weeks
Mars Cargo Mission, One Way	64,000	9 months
Mars Reconnaissance Mission (1-Year Duration, No Landing, No Martian Orbit)	85,000	12 months
Close Solar Probe, One- Way Instrumented	90,000	4-1/2 months
Mars Reconnaissance, Planetary Orbit and Return to Earth	98,000	2-1/2 years
Venus Reconnaissance, Planetary Orbit and Return to Earth	104,000	1-1/4 years
Solar System Escape, Ecliptic	120,000	----
Mercury Reconnaissance, Planetary Orbit and Return to Earth	150,000	1-1/2 years
Solar System Escape 45° Out of Ecliptic	245,000	----
Jupiter Reconnaissance, Planetary Orbit and Return to Earth	250,000	3-2/3 years
Saturn Reconnaissance, Planetary Orbit and Return to Earth	400,000	4-1/2 years

Table 2-7 presents the functional and environmental parameters with related comments on the effect of the time parameter

Table 2-7. Relationship of Time and Effects of Functional and Environmental Parameters

Functional and Environmental Parameter	Effects of Parameter	Time Relationship
Meteoroids	Penetration and Erosion	Probability increase with exposure to time
Radiation	Degradation and surface changes on materials	Direct and cumulative relationship; also periodic depending on space flight path
Thermal radiation	Temperature balance and gradients	Constant or varying for heliocentric orbits and periodic for planetary orbits
Zero gravity	Venting of gases, spring mass systems, and fluid systems	Independent
Space vacuum	Sublimation and evaporation of materials and increase in friction	Direct relationship
Planetary atmospheres	Material effects and friction variations	Direct and periodic relationship
Flow media	Corrosion of materials, chemical changes and boiloff of propellant	Increases with exposure to time
Leakage	Loss of propellant corrosion and loss of range	Direct relationship
Contamination	Decreases reliability of the valves	Direction relationship due to corrosion; periodic due to meteoroidal impact and generated wear debris
Space maintenance	_____	Direct relationship
Acceleration, vibration, shock	Valve performance	Periodic

#### 2.4.5 Temperature in Space

The primary sources of thermal energy for a space system within the solar system are the sun and the internal energy generated by the equipment housed within the space vehicle. Other sources may be the earth, moon, or other planets, and may be of greater importance for orbiting vehicles or reentry conditions.

Temperature control is attained primarily through heat transfer by radiation and may be accomplished by the use of reflecting materials or reflection devices such as rotating louvers. In some instances the temperature requirements for valves are governed by the temperature control requirements of the space vehicle, since the propulsion control system is normally housed within the space vehicle.

Heat energy derived from the total electromagnetic spectrum is 7.4 Btu/ft<sup>2</sup> min. at a distance of 1 au (astronomical unit). At any given distance, the amount of heat energy is inversely proportional to the square of that distance from the sun. The propellants such as those used in cryogenic systems or hot gas systems may be the most important source of heat energy or in some cases the sterilization temperatures may be the most critical design temperature.

For the general case of heat energy to a body in space, the design parameters to consider are the  $\alpha_s/\epsilon$  ratio and the  $A_t/A_p$  ratio. For any specific valve on a spacecraft, the heat transfer analysis<sup>p</sup> is more complicated and each case should be analyzed separately. However, considering the general case of spheres, cylinders and parallelepipeds, the  $\alpha_s/\epsilon$  ratio is important and the analyses indicate that the finish and the surface materials should be selected for optimum temperatures. For example, hard anodized aluminum closely represents a black body, but for many materials used in valves, organic coatings or insulation such as aluminized mylar ( $\alpha_s/\epsilon \approx .25$ ) should be considered.

where:  $\alpha_s$  = absorptivity  
 $\epsilon$  = emissivity  
 $A_t$  = total area  
 $A_p$  = projected area

#### 2.4.6 Space Maintenance

Maintenance and repair of both manned and unmanned spacecraft is a requirement that will demand new designs, techniques and procedures. Additionally, repairs of a major nature may be required of vehicles that have landed on the moon or other celestial body.

The need for such repairs imposes particular constraints on component materials, assembly processes, mounting and accessibility. For example, conventional threaded tubing fittings may not be satisfactory in systems where replacement of components may be probable, because of the possibility of cold welding. Means of joining tubing to components and tubing to tubing must be devised

that will permit uncoupling of fittings under the numerous handicaps imposed by the space environment. A weightless environment imposes unusual difficulties on an astronaut who is attempting to exert a torque on a fitting in that the man will tend to rotate about the fitting unless he is anchored in some manner to the surrounding structure. Space clothing, required because of the vacuum conditions, is bulky and cumbersome and thus not conducive to performing mechanical tasks that would be simple routine on earth. Validation of the repair by a component on system check will require ingenious test procedures and equipment.

Conventional shop processes, e.g., filing, drilling, sawing, gas welding, and brazing may require modifications to varying degrees of space applications. The effects of vacuum on such operations as filing, sawing, and drilling are not well understood.

Gas welding and brazing techniques may require attention because of a combination of effects of vacuum and zero gravity. Lack of atmospheric pressures may significantly alter the size and shape of the flame, which may require resizing or redesign of the tips for a given task.

Special problems in maintenance may be encountered on the various planets and these problems may differ from those encountered in interplanetary space. For instance, the problems caused by maneuvering in a zero gravity field would be mitigated on the moon and Mars because of the existence of gravity fields on these bodies. The atmosphere may conceivably pose maintenance problems that differ from those encountered in space or on the moon.

One possible problem that might be encountered on either the planets or in space is that of igniting a gas torch in the absence of oxygen, as conventional lighters, e.g., flints and matches, depend on oxygen for operation. A possible solution to this problem might be an electrically heated wire. This, and other potential problems, will require further investigation.

#### 2.4.7 Meteoroids

2.4.7.1 Introduction - One hazard of space about which there is much theoretical and actual test data is the meteoroidal penetration of materials and meteoroidal flux which may be encountered in space travel.

In design of valves for space application it is apparent that much thought should be given to protecting the valves not only from meteoroidal penetration, but from any other ill effects that could result from meteoroids impinging on the valve body; e.g., spalling on inner surface, deformation of cylinder walls, and loss of heat balance of the system.

2.4.7.2 Origin - It is believed, at the present time, that meteoroids are of two origins, meteoroids from asteroids and meteoroids from comets.

Meteoroids of asteroidal origin constitute approximately 10 percent of the total influx of particles that enter the earth's atmosphere. Since the particles are of asteroidal origin, their concentration lies in the asteroidal belt located between the orbits of Mars and Jupiter, and the particles



enter the earth's atmosphere only when their devious orbits cross the path of earth's orbit and pass sufficiently close to earth to be trapped by its gravitational field. Meteoroids are believed to be the result of continual colliding and grinding of bodies in the asteroidal belt, and for the most part they maintain the same orbit around the sun in or near the ecliptic plane. For this reason, the flux is relatively low at the earth's atmosphere and does not constitute a hazard to spacecraft. However, when interplanetary travel is considered, meteoroids of this extraterrestrial origin may be considered to be hazardous to the spacecraft. Information regarding the flux and concentrations of these particles is too limited to determine analytically what the effects could be. Therefore, information that has been obtained about other particles that frequent the earth's atmosphere must be used as criteria in space vehicle design. These particles, about which there is some valid information, are believed to be of cometary origin.

Most meteoroidal material in the solar system is believed to be associated with existing or extinct comets. Approximately 90 percent of the total influx into the earth's atmosphere is thought to be of cometary origin. It is known that a comet is not a very dense mass, but is, instead, a loose accumulation of particles. A present hypothesis is that comets are formed originally at large distances from our sun by a gradual accumulation of atoms and particles which are wandering randomly in space. The distribution of meteoroidal particles is a result of typical comet orbits about the sun; the comets are constantly modified by the effects of sputtering, sublimation from solar radiation, breakage and disruption by mutual collisions among the small particles themselves, planetary perturbations and collisions, solar pressure, and solar radiation drag.

2.4.7.3 Meteoroidal Penetration - One of the main interests of the valve designer in providing protection against meteoroidal impingement on a valve is the penetration capability of a single meteoroid. For unprotected structures or components, Bjork's Penetration Equation on a Semi-infinite Target (Reference 22) relates meteoroidal penetration to the one-third power of the momentum  $(mv)^{1/3}$  of the meteoroid. Bjork's calculations are restricted to a projectile and target of the same material and are based somewhat conservatively on the density of a meteoroid to be 2.7 gm/cc, or that of stone. From observations made in the photographic range, where the mass is larger, there is good indication that the density would be considerably lower, possibly even as low as 0.05 gm/cc.

In tests performed by Aerojet General Corporation (Reference 23), velocities of projectiles up to 30,000 ft/sec were achieved. These velocities are still in a range below the estimated average velocity of a meteoroid (30 km/sec, or  $10^5$  ft/sec). However, this is the most definitive information available at the present. Aluminum projectiles (density approximately that of stone, 2.7 gm/cc) were impinged on different target materials with the results given in Table 2-8 as extracted from the report. From actual test specimens that were used (see Table 2-8) for aluminum projectiles impinging on aluminum targets, estimated penetration depths were calculated using the following common penetration equations:

Table 2-8. Hypervelocity Impact in Semi-Infinite Metallic Targets

Target Data			Particle Data						Crater Data								
Test No.	Data Point	Target Material	Thickness (in.)	Brinell Hardness	Velocity (ft/sec)	(km/sec)	L/D	Average Dia. (in.)	Mass (gm)	(lb x 10 <sup>-4</sup> )	Angle of Incidence (1) (deg)	Silhouette Area (2) (in. <sup>2</sup> )	Mean Dia. (in.)	Depth (in.)	Depth/Dia. Ratio	Volume (in. <sup>3</sup> )	Remarks
AC 11	1	Aluminum 2024-T4	1.0	135	32,000	9.75	(3)	.125	.0453	.997	(3)	(3)	.62	.27	.436	.0427	
	2				→			.0898	.0170	.375			.53	.22	.415	.0244	
	3				→			.0661	.147	.147			.35	.144	.411	.0122	
	4				→			.0337	.000884	.0195			.32	.134	.388	.091	
	5				→			.145	.0740	1.63			.50	.145	.290	-	
	6				→			.144	.0687	1.51			.72	.28	.389	.0427	
	7				→			.206	.201	4.42			.82	.32	.390	.0548	
	8			4.0		→		.248	.545	12.0			1.35	.57	.416	.555	
	9			→		→		.239	.311	6.85			1.22	.61	.500	.378	
	10			→		→		.146	.0714	15.7			.66	.28	.444	.0548	
AC 12	A	Stainless 321	1.0	167	31,800	9.69	5.1	.163	.765	16.83	0	.137	1.05	.350	.333	.163	
	B				→			.128	.223	4.89	24	.052	.60	.235	.392	.051	
AC 13	A	Stainless 347	1.0	195	32,400	9.88	4.8	.148	.543	11.95	36	.090	1.00	.406	.406	.078	(4)
	B				→			.126	.140	3.07	79	.018	.50	.297	.549	.045	
	C				→			.144	.269	5.85	6	.052	.58	.204	.352	.035	
AC 14	A	Stainless 347	1.0	195	30,400	9.27	5.8	.151	.702	15.46	30	.117	1.20	.391	.326	.252	(4)
	B				→			.147	.432	9.52	14	.085	1.00	.391	.391	.156	(4)
	C				→			.122	.0754	1.66	59	.019	.53	.266	.502	.038	(4)
	D				→			.122	.0931	2.05	55	.022	.45	.204	.454	.027	(4)
AC 15	A	Aluminum 6061-T4	1.0	65	31,200	9.41	1.4	.119	.0819	1.81	83	.016	.50	.204	.408	.026	
	B				→			.109	.249	5.50	62	.044	1.45	.844	.582	.738	(4)
	C				→			.106	.144	3.13	0	.035	.80	.484	.606	.038	(4)
	D				→			.077	.0455	1.01	17	.014	.40	.235	.587	.017	(4)
	E				→			.118	.127	2.81	18	.027	.60	.375	.625	.082	(4)
AC 16	A	Titanium RS55	1.0	185	30,800	9.39	3.2	.0943	.0627	.1383	24	.022	.60	.281	.468	.051	
	B				→			.168	.519	11.43	4	.087	1.10	.360	.327	.196	(4)
	D				→			.110	.0738	1.63	11	.012	.63	.297	.472	.041	(4)
AC 16B	E				→			.083	.0803	1.77	26	.028	.58	.282	.486	.053	(4)
	C				→			.093	.0749	1.65	0		.58	.188	.324	.024	(4)
	D				→			.084	.0300	6.60	48	.083	.50	.360	.720	.034	(4)
AC 17	A				→			.151	.443	9.76	27	.034	1.05	.360	.343	.099	(4)
	B				→			.127	.171	3.78	40	.034	.75	.250	.333	.046	(4)
	C				→			.110	.100	2.22	27	.027	.50	.187	.374	.015	(4)

NOTES: (1) angle measured between longest axis of particle and plane of target.  
 (2) area of particle as viewed from target.  
 (3) data not available.  
 (4) impact caused slight bulge on back of target.

Bjork:  $P = 1.09 (mv)^{1/3}$

Charters-  
Summers:  $P = 2.28 \left[ \left( \frac{\rho_p}{\rho_T} \right)^{2/3} \left( \frac{V}{C_t} \right)^{2/3} \right] d$

Herrman-  
Jones:  $P = (0.35 \pm 0.07) \left[ \left( \frac{\rho_p}{\rho_t} \right)^{2/3} \left( \frac{\rho_t V^2}{H_t} \right)^{1/3} \right] d$

The resulting predicted penetration depths were plotted along with the actual crater depth observed from the tests (Figure 2-14). By observation it can be seen that a wide variation in values can exist, dependent on the penetration equation chosen. It is then the designer's responsibility to justify usage of a chosen equation and any weight penalty that may result.

It can also be seen in Table 2-8 that the use of high-strength materials such as steel in place of aluminum as a protective material is not warranted. The possible exception to this would be the use of beryllium, with a strength-to-weight ratio greater than that of aluminum.

2.4.7.4 Meteoroid Bumper as a Method of Shielding - To alleviate the weight penalty involved to prevent meteoroid penetration, Whipple (Reference 24) suggested the use of a meteoroid bumper. The meteoroid bumper, a thin external shield spaced some distance from the main structure, would intercept and shatter the meteoroid far enough away from the main surface to enable the impact to be spread over a larger area and at a somewhat reduced velocity. For this purpose, the bumper should be as thin as possible, perhaps limited only by fabrication procedures. Experiments show (Reference 25) that an aluminum projectile will shatter when it is impinged on an aluminum plate 1/10 of its own thickness at velocities of 6-20 km/sec.

The shattering of the particles stopped by a thin shield produces a "spray cone" effect on the target. The cone effect is a result of the dispersion of the shattered fragments leaving the shield. An optimum shield thickness, approximately 0.4 times the projectile length, would produce a spray cone angle of approximately 55 degrees from the direction of travel of the center particles. At this shield thickness the total penetration (shield plus target) reaches a minimum.

Total penetration is also seen to decrease with an increase in shield spacing until an optimum spacing is obtained where no further reduction in penetration is achieved. Beyond the optimum spacing, each particle in the spray strikes a different portion of the target, while at smaller spacings several spray particles may strike the same location on the target. If the shattered fragments are so spread out that they act independently upon hitting the target, the momentum and energy transmitted to the target at each point of impact are reduced in proportion to the number of fragments. Experiments indicate that approximately 33 percent of the original thickness of the target is required to prevent penetration if an adequate spacing

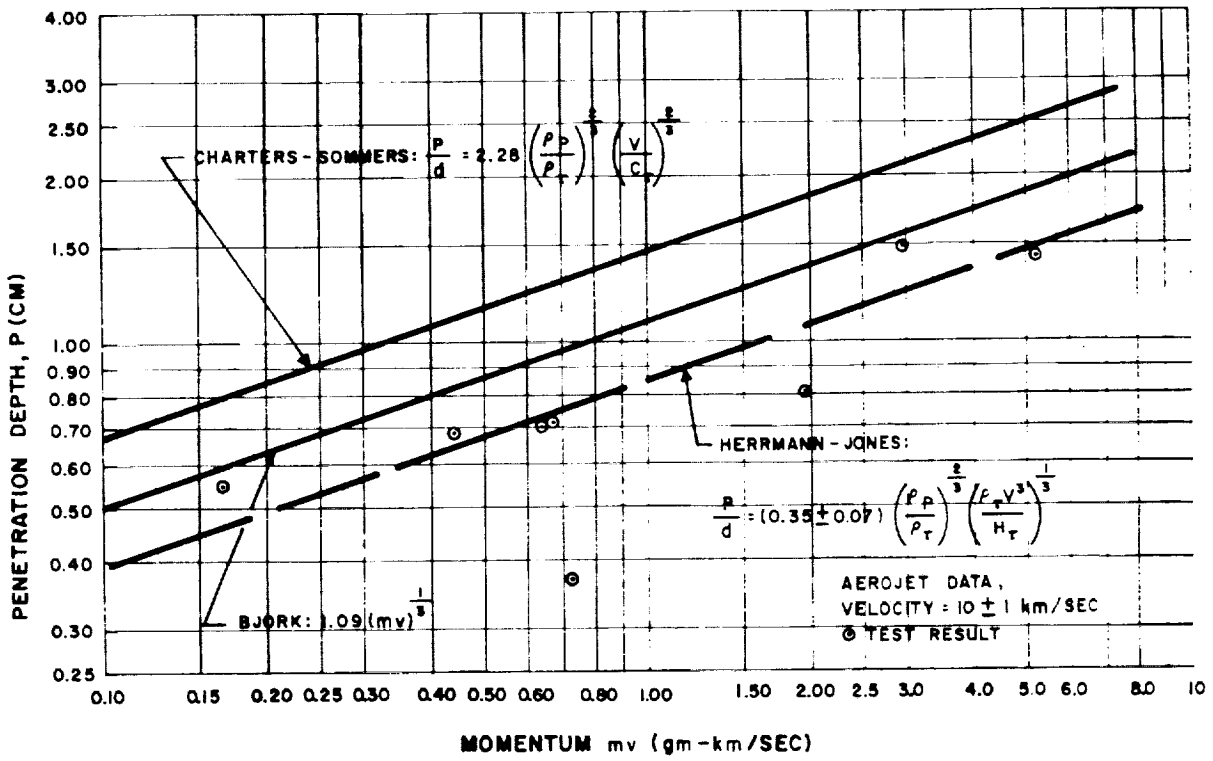


Figure 2-14. High-Velocity Penetration in Aluminum

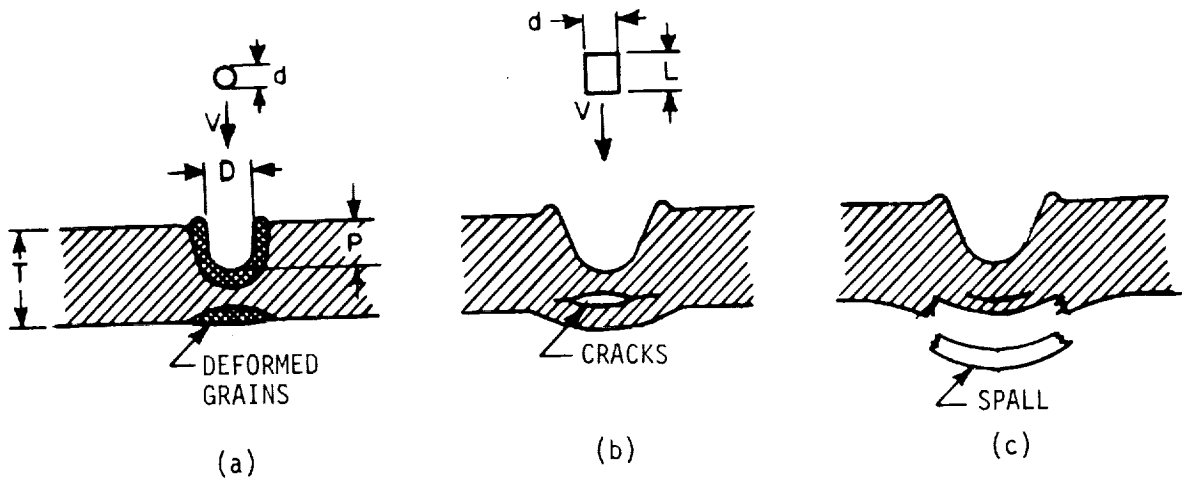


Figure 2-15. Rear Surface Damage in Relatively Thick Targets

between bumper and target is provided (Reference 25). Applying this criterion, an elastic analysis (Reference 25) shows that spacing of a bumper may be determined by the equation:

$$S = 2t_t \sqrt{t_t/t_b \rho_b}$$

where: S = bumper spacing (distance away from target)

$t_t$  = thickness of main target

$t_b$  = thickness of bumper

$\rho_b$  = density of bumper, in gm/cm<sup>3</sup>

This indicates that an aluminum bumper 1 percent of the thickness of the target should have a spacing from the target approximately equal to 12 times the target thickness.

Because of clearances and handling conditions, the problem of obtaining optimum spacing between the bumper and a valve body may possibly be lessened by the use of insulation placed between them. Investigations have been made (Table 2-9 from Reference 23) using such a configuration, and results using NRC-2 insulation proved quite favorable. The use of NRC-2 insulation by itself as a meteoroid bumper may be possible.

2.4.7.5 Spalling by Meteoroids - The effects of spalling and deformation of the inner surface of the valve body when struck by a meteoroid are difficult to predict theoretically, due to the complex wave propagation that occurs on hypervelocity impact. When a meteoroid hits a plate, it not only makes a hemispherical crater on the front surface, but also initiates a strong compressive shock wave which travels through the plate. When this wave reaches the free surface (inner surface) of the target, a reflected plastic wave of tension occurs. Interaction occurs between the reflected tension wave and the remainder of the compression wave propagating in the direction of impact. The result is that at some depth from the free surface of the target, the tensile stress may exceed the fracture stress. If this occurs, a spall is formed on the free (inner) surface and ejected inward at high velocity (Figure 2-15 from Reference 26). The diameter of the spall is usually several times the plate thickness, varying from 1/10 to 1/2 of the plate thickness. There is a definite tendency for spall thickness to increase with velocity of impact and also increase with decreasing plate thickness (Reference 26).

From investigations on the spalling of materials (Reference 27) it was noted that the thickness required to avoid spalling varies approximately as the 1/3 power of the impact energy, or the 1/3 power of the number of fragments into which a meteoroid is broken by a bumper. This is the same dependence as that for penetration. Indications are that spacings of bumper and targets which spread the impact particles over a larger area and thus decrease penetration of the main target should also separate the pulse waves, which the shattered particles generate in the main target, sufficiently to avoid serious pulse overlap at the inner surface of a valve body.

Table 2-9. Hypervelocity Impact in Thin Multilayer Targets

Particle Data										Target Data			
Test No.	Data Point	Velocity (ft/sec)	Velocity (km/sec)	L/D	Average Dia. (in.)	Mass (gm)	Mass (10 <sup>-4</sup> gm)	Angle of Incidence (deg)	Silhouette Area (in. <sup>2</sup> )	Material	Thickness (in.)	Separation (in.)	Penetration (in.)
<b>Single-Sheet Target</b>													
AC 7	A	32,800	10.0	4.9	.121	.258	5.67	41	.045	Aluminum 6061-T4	.016	2	.24 (1)
9	C	30,900	9.43	1.7	.110	.0858	1.84	50	.025	Titanium 45A	.015	2	.09 (1)
	D	30,600	9.33	2.8	.092	.0766	1.68	11	.023	Aluminum 2024-T4	.016	2	.11 (1)
10C	A	30,100	9.18	2.1	.126	.129	2.86	47	.036	Titanium 45A	.016	2	.07 (1)
	B	30,100	9.18	1.5	.0664	.0153	.337	40	.008	Aluminum 2024-T4	.016	2	.03 (1)
	C	30,600	9.33	2.5	.037	.00427	.094	41	.003	Stainless 321	.016	2	.02 (1)
										Aluminum 2024-T4	1.0		
<b>Double-Sheet Target</b>													
AC 5	C	30,600	9.33	1.9	.106	.0785	1.68	28	.024	Stainless 321	.016	2	.08 (1)
										"	.016	2	None
										Aluminum 2024-T4	1.0		
AC 6	A	31,900	9.73	3.0	.204	.870	19.25	6	.126	Titanium 45A	.016	2	.25 (1)
										"	.016	2	1.33 (1)
										Aluminum 2024-T4	1.0		
<b>Double-Sheet Target with Super-Insulation</b>													
AC 20	A	30,600	9.33	2.1	.105	.0822	1.82	18	.024	Aluminum 6061-T4	.016	0	.08 (1)
										Linde SI-44	.025	0	4.3 (1)
										Aluminum 6061-T6	.125	2	.33 (1)
										Aluminum 2024-T4	1.0		
AC 26	A	31,800	9.69	6.5	.091	.172	3.78	36	.030	Stainless 321	.016	0	.08 (1)
	B	31,800	9.69	1.5	.037	.00278	.064	90	.003	"	.016	0	.0031 (1)
	C	31,500	9.61	2.0	.045	.00629	.139	47	.004	"	.016	0	.0078 (1)
										NRC-2	.250	0	5.5 (1)
										Stainless 321	.125	2	.05 (1)
										Aluminum 2024-T4	1.0		
AC 30	A	31,600	9.64	4.0	.085	.0849	1.87	3	.028	Aluminum 6061-T4	.016	0	.12 (1)
										Linde SI-44	1.0	0	4.1 (1)
										Aluminum 6061-T6	.125	2	.08 (1)
										Aluminum 2024-T4	1.00		

NOTE: (1) no crater formed; splash or pitting only.

2.4.7.6 Other Effects of Meteoroids on Valves - Penetration of meteoroids smaller than  $10^{-6}$  gm is not considered to be a problem, as noted. However, impingement of micrometeoroids on a valve body may remove enough material from an unprotected exterior surface through erosion (removal of material by cratering) to alter the absorptivity ( $\alpha$ ) and emissivity ( $\epsilon$ ) value of the material enough to create a heat balance problem. Estimates show that total volume lost by meteoric erosion is approximately 1 Å/yr in the vicinity of the earth to as much as 200 Å/yr at low satellite altitude. Deposition of meteoroidal dust on the valve body may also produce the same result.

Another possible effect of meteoroidal impacts would be the generation of pressure pulses transmitted to and through the liquid in the valve, causing internal damage.

Propellant containers and lines may also experience extensive damage from pressure pulses transmitted to and through the liquid from meteoroidal impact.

2.4.7.7 Conclusions - It has been shown that meteoroidal hazard to valves in space could exert a definite influence on the design of a valve body, but that protective measures can be taken to prevent damage to the valve without imposing an extremely high weight penalty.

A statistical solution to the problem involves the probability of meteoroidal encounter during the mission and the damage phenomena of a single meteoroidal impact.

The likelihood of encounter of meteoroids depends on:

1. The reliability required of the valve, which may vary with a given mission (e.g., manned or unmanned).
2. The duration and path of the mission.
3. Size of the valve body (exposed area -in<sup>2</sup>).
4. The proper choice of flux distribution.

Present quantitative knowledge of flux distribution is far from adequate. In the area of concern to the designer (mass range of  $10^{-6}$  to  $10^{-3}$  gm), extrapolation from recorded data is the only means of estimation of the flux intensity.

Damage phenomena of a meteoroidal impact also warrants more investigation before definite design criteria can be established. At the present time sufficient knowledge relating depth of penetration or fragmentation mechanics of bumpers to material properties is lacking. Similarly, insufficient information is available to correlate depth of penetration with velocity of a particle at impact on metal surfaces. The velocity of impact of meteoroids with space vehicles (in this case, a valve body) is assumed to be approximately 30 km/sec ( $10^5$  ft/sec), a considerably higher velocity than any extensive laboratory data that has been obtained to date on high

velocity impact. Many theoretical penetration equations for high-velocity impact have been proposed, ranging from very conservative predictions, thereby imposing a weight penalty, to nonconservative predictions requiring no protection for a valve. Bjork's penetration equation appears to be between the extremes, and predicted results from the equation follow closely to test data obtained to date for target and projectile restricted to the same material (Figure 2-14).

Until more definitive information is obtained concerning flux intensity, fragmentation of particles on impact, and penetration characteristics of hypervelocity particles, the designer must use the information available. Discretion in choice of flux distribution and penetration equation should result in a conservative but reasonable prediction of protection needed to protect a valve from meteoroidal impingement. The use of a meteoroid bumper should definitely be considered as a means of reduction in weight, either for protection against penetration or protection against spalling. If only a minimal amount of shielding is necessary, the proper use of an insulation could be accomplished. The insulation may also be required for thermal properties, thus serving a dual purpose.



## 2.5 REFERENCES

1. Keilin, D., The Leeuwenhock Lecture. The Problems of Anabiosis or Latent Life: History and Current Concept. Proc. of Royal Society 150, 1959.
2. Zamenhof, S., Effects of Heating Dry Bacteria and Spores on Their Phenotype and Genotype, Proc. National Academy Science 46, 1960.
3. Phillips, C. R., Gaseous Sterilization. In Antiseptics, Disinfectants, Fungicides and Sterilization, edited by G. F. Reddish, Lea and Febiger, Philadelphia, Pa., 1957.
4. Phillips, C. R. and Warshowsky, B., Chemical Disinfectants, Ann Rev. Microbiol. 12, 1958.
5. Schley, D. G., Hoffman, R. K., and Phillips, C. R., Simple Improvised Chambers for Gas Sterilization with Ethylene Oxide, Applied Microbiol. 8, 1960.
6. Willard, M., Entreken, V. K., and Alexander, A., Hughes Research Studies RS 277, RS 283, RS 292, RS 293 Surveyor Sterilization Parts I to 4, 1962.
7. Development of International Efforts to Avoid Contamination of Extra-terrestrial Bodies, Science, V. 128, 1958.
8. Jellinek, H.H.G., Degradation of Vinyl Polymers, Academic Press, Inc., New York, 1955.
9. Lange, W. J., and Riemersma, H., Desorption of Gas by Photons, Transactions of the Eighth Vacuum Symposium and Second International Congress, Vol. 1, 1961.
10. Spalvins, T., and Keller, D. V., Adhesion Between Atomically Clean Metallic Surfaces, Final Report NSG-159-61, NASA, July 1962.
11. Private Communications with J. L. Ham, NRC, Cambridge, Mass.
12. Colner, W. H., Space - A New Environment for Materials, Materials Research and Standards, August 1962.
13. Brueschke, E. E., The Effects of the Space Environment on Electronic Components and Materials, Special Research Study SRS-367, Hughes Aircraft Company, Culver City, Calif., 15 June 1960.
14. Project Relay Quarterly Technical Progress Report of 1 June 1962 to 31 August 1962, TRW Report No. 8614-6037-SU-000.
15. Freden, S. C. and White, R. S., Protons in the Earth's Magnetic Field, Phys. Rev. Letters, 3, 1959.
16. Freden, S. C. and White, R. S., Particle Fluxes in the Inner Radiation Belt, UCRL-5877-T.

17. Naugle, J. E. and Kniffen, D. A., Flux and Energy Spectra of the Protons in the Inner Van Allen Belt, Phys. Rev. Letters, 7, 1961.
18. Heckman, H. H. and Armstrong, A. H., Spectrum of Geomagnetically Trapped Protons, J. Geophys. Research, 67, 1962.
19. Pizella, G., McIlwain, C. E. and VanAllen, J. A., Time Variations of Intensity in the Earth's Inner Radiation Zone, October 1959 through December 1960, J. Geophys. Research, 67, 1962.
20. Rosen, A., Eberhard, C. A. Farley, T. A. and Vogl, J. L., A Comprehensive Map of the Space Radiation Environment, TRW Systems Report No. 8644-6003-RU-000.
21. Hazard, Al B., The Space Mission Planning Chart, Space-General Corp., El Monte, Calif.
22. Whipple, F. C., The Meteoritic Risk to Space Vehicles, Seventh International Astronautical Congress, Barcelona, Spain, 1957.
23. Summers, J. L., Investigation of High-Speed Impact, NASA TN-94, October 1959.
24. Whipple, F. C., Dust and Meteorites, ARS Report 2253-61, 9-15 October, 1961.
25. Gray, P. D., et al., Rockets in Space Environments - Phase II Individual Component Investigation, April 1962, Report No. 2263, Aerojet-General Corporation.
26. Jaffe, L. D., and Rittenhouse, J. B., Behavior of Materials in Space Environments, JPL TR-32-150, November 1, 1961.
27. Bjork, R. L., Meteoroids Versus Space Vehicles, ARS Paper No. 1200-60, May 9-12, 1960.

## 3.0 MATERIALS

### 3.1 INTRODUCTION

The information contained in this section has been extracted from the best technical sources available; these sources are referenced in the bibliography at the end of the section. Materials compatibility data derived from these sources are generally the result of laboratory scale bottle tests involving immersion of materials in propellants under static conditions. For the most part, these data are fairly consistent, but many instances exist where data are contradictory or differing in degree of compatibility. Also, in most cases the data report only the effects of propellant exposure, and do not reflect the functionality of the material after exposure.

Where differences are noted, acceptance of information was based on multiple sources, appropriate procedures, availability of service data, and recentness of evaluation. Unless specifically noted, data not meeting these criteria have not been included.

Propellant compatibility data contained in the following reference is included:

"Advanced Valve Technology," Interim Report No. 06641-6014-R000, Volume II, Materials Compatibility and Liquid Propellant Study, Contract NAS 7-436, November 1967.

The work presented in this report represents a continuation of the referenced study, however, where possible the data was updated to include more recent information.

## 3.2 DISCUSSION

In the course of the literature search performed, several areas requiring early additional effort became apparent. Basically, it was noted that the testing performed to obtain the desired data shared a common failing: there was no conformity of method, no procedural approach to the problem of the compatibility test, and little assessment of the effects of impurities in the propellants. For example, some long term compatibility data were generated based on actual immersion for one year periods, while others were conducted for shorter periods of time, and data extrapolated to one year. Short term compatibility, in some cases, denotes ability to survive propellant exposure for two to four weeks. In other cases, it is defined as the ability to withstand propellant splash or fumes for designated periods of time. In very few cases, has the effect of the material on the propellants been determined, and the initial processing of the test specimen is seldom recorded. The variations do not reflect on the multitude of investigators, but rather on the void which exists with respect to test standards to which work has been performed.

The compatibility of materials to the liquid propellants primarily takes on three aspects:

- Slow to rapid chemical or electrochemical reaction between metals and the propellants leading to corrosion and loss of strength of the metals and/or degradation of the propellants.
- Slow to rapid chemical reaction between non-metals and the propellants leading to degradation and loss of strength.
- Rapid chemical reaction between all types of materials and the propellants leading to explosion or fire within the system.

Each of these undesirable aspects of materials compatibility have been investigated by various organizations, and the data reported. However, there are quite often differing and sometimes conflicting points of view concerning the compatibility and use of a specific material. This conflict of opinion frequently arises not from incorrect data or interpretation, but rather from a lack of a common reference point. In particular, failure to delineate all of the testing parameters and procedures, and of not characterizing the test fluid sufficiently, can lead to widely different results, each of which, however, are valid within the context of the experiment performed. Two illustrations are presented as cases in point:

### 1. Corrosion

Most of the data on corrosion of metals are given in terms of depth of material removed per unit time. Usually the data are presented as penetration in mils per year (MPY). Not so frequently, however, is a description given of the type of corrosion, or of the localized severity. Inasmuch as a MPY removal figure implies a general, overall corrosion of the metal, failure of the investigator to remark that the greatest amount of corrosion occurred as pitting or intergranular attack could lead a designer, using the compatibility data,

to arrive at an erroneous conclusion regarding the service life of the metal with respect to the propellant in question. It is suggested that a common corrosion description, such as that proposed by Champion\*, should be employed when reporting data of this nature. Table 3-1 presents the rating parameters recommended by Champion. In this method the corrosion that has occurred between the metal and the corrodant is segregated into two main classes: general and local. These classes are then further subdivided into various categories, depending on the average ratio of width to the depth of each type of corrosive attack.

General corrosion is attack to an approximately uniform depth of the whole of the surface under consideration, but it may vary from a reasonably uniform attack, such as from acidic substances, to a more uneven attack as is usually experienced in oxygen-water environments.

Semilocal corrosion is somewhat similar to general attack, but is confined to areas of restricted size which are still large compared to the depth of the attack. This type of attack does not normally degrade the metal by perforation due to corrosion, but may affect the use of the metal in applications such as valve seats, sliding surfaces, etc.

Pitting corrosion is determined to be present when the area of attack is so localized that the width is of the same order as the depth of the attack. In such cases the liability of the metal to fail by perforation is serious and hence the depth of attack is of major importance.

In some cases, the corrosion attack results in cracking of the metal, particularly if stress has been applied to the specimen. These are regarded as the most highly localized form of corrosion. It must be emphasized that the differences between these types of corrosion are in degree rather than kind and that as corrosion proceeds it may change from one type to another, i.e., the corrosion may change in character as well as in severity with continued exposure.

## 2. Propellant and Test Specimen Characterization

It is well known that relatively minor impurities can cause gross changes in the characteristics of liquid propellants. Failure to properly analyze and report the chemical makeup of the test fluid utilized in the experiments can lead to unwarranted conclusions. As an example, several metals are compatible with  $OF_2$ . If, however, the  $OF_2$  is contaminated with water, hydrogen fluoride is formed which is particularly reactive toward metals which cannot form adherent, passive protective films against the fluoride ion. Thus, failure to analyze the HF content of the  $OF_2$  can lead to erroneous conclusions regarding its compatibility.

\* General Reference, No. 1

Table 3-1. Rating Chart for Macroscopic and Microscopic Examination of Corrosion Behavior of Metals (After Champion)

No.	Number of Pits		Size of Pits		Intensity of Corrosion			Factors Affecting Corrosion (% Influence)
	Chart A		Chart B		Chart C			
	Standard Term	No. Per Sq. cm	Standard Term	Area (Sq. cm)	Standard Term	Depth of General Attack (cm)	Depth of Pitting or Cracking (cm)	
1	Very few	33	Minute	0.0006	Minute trace	0.0001	0.004	9
2	Few	100	Very small	0.003	Very small	0.0004	0.01	13
3	Small number	330	Small	0.016	Slight	0.0016	0.025	20
4	Moderate number	1,000	Moderate	0.08	Moderate	0.006	0.06	30
5	Considerable number	3,300	Considerable	0.4	Considerable	0.024	0.15	45
6	Numerous	10,000	Large	2.0	Severe	0.10	0.4	70
7	Very numerous	33,000	Very large	10.0	Very severe	0.40	1.0	100

This same type of problem has occurred in the testing of the impact sensitivity of LOX with various metals. Lack of close control in insuring contamination free metal samples and the testing apparatus has led to some conflict of data in this area.

Since contamination can occur during transport and handling of samples and test equipment, it is suggested that the test fluids be analyzed as used, and any possible contamination path be noted.

From the standpoint of the valve designer involved in the process of material selection as one portion of the component design, the available data do not provide the necessary information from which to make rapid and automatic selections. In order for such information to be intelligently used, it must be supplemented in areas which are currently lacking.

For example, the data presently available do not normally distinguish between static and dynamic compatibility, either in respect to the test methods employed, or where a material's use is approved, in respect to that material's potential application. In many instances it may be assumed that the mechanism for potential failure of a particular material is augmented by the mechanical action of adjoining component materials and/or the erosive effects of the flowing propellant itself. Specifically, a material appropriate for use as a static parking within a given valve assembly may be completely incompatible, in the identical propellant service, when used as a sliding seal or an impact seal. For example, butyl rubber seals and O-rings have proven to be excellent static seals for containment of nitrogen tetroxide, even though the material itself is completely incompatible with the propellant. The sealing ability of the material is enhanced by the fact that it swells and becomes gummy in contact with  $N_2O_4$ . On the other hand, once the material has been exposed to  $N_2O_4$ , it could never survive a sliding motion. Data regarding these conditional aspects of compatibility are not presently documented. Similarly, the effects of temperature, pressure and propellant phase variations have seldom been treated in establishing compatibility.

A second distinct information void, with respect to material compatibility, exists in the area of historical data accumulation. The primary source of the data presented is the laboratory test. This is seldom supplemented by field information which should be extensive.

A search of the actual materials employed in varying configurations, environments, and propellant service would greatly aid in establishing a realistic confidence level for new valve designs. A detailed search, though beyond the scope of the present program, would not only serve as an early source of dynamic use-data, but would provide confirmation of, and give direction to, successive laboratory test effort. An attempt was, therefore, made in the course of the Advanced Valve Technology Program, to survey briefly the available experience through direct interview of cognizant personnel.

The data presently contained in this survey report attempt to correct some of these shortcomings by including what supplementary information could be readily obtained. It is felt that a more extensive program will permit sounder initial component designs with a minimum expenditure of development time and cost and is, therefore, warranted.

### 3.3 MATERIALS COMPATIBILITY TEST METHODS

There is a serious lack of precise compatibility data for both short term and long term storage of the more energetic propellants in the accepted materials of construction. The shortcomings of present compatibility data and the lack of standard, unified test methods, reporting and compilation has been discussed in the Introduction. The more serious problem is that of obtaining reliable data for long term requirements necessary for upcoming spacecraft missions, which have operating lifetimes of up to ten years. It is generally accepted that short term, accelerated storage and testing do not give data which can be reliably extrapolated to longer mission lives. Compatibility testing in real time is prohibitively expensive, and may be outmoded by state of the art advances from the initiation of testing, which may render the evaluation obsolete.

Under this program a laser technique was studied which may prove to circumvent the traditional shortcomings of conventional compatibility testing. This technique is holographic interferometry. This test method records the fringe pattern of the propellant adjacent to the sample. The distortion of the fringe pattern with time represents corrosion mapping. The theory of holographic processes have been extensively discussed in the literature\* and will not be detailed.

However, it is significant to note that a hologram is able to record a complex optical wave so that when the hologram is reilluminated later, another optical wave is created identical to the original in both phase and amplitude. It is this property which makes it possible to use a hologram to generate either the test beam, or a comparison beam, or both as an interferometric analytical technique.

Holographic interferometry may be considered as a form of common path interferometry (normally not used with conventional light sources due to cell size, configurations, optical inhomogeneities, etc.), except that the test and comparison beams are separated in time. It is the use of this feature, either double exposure or "stored beam" interferometry, that is of interest in their application to compatibility and corrosion investigation.

Thus far, the techniques have been utilized in applications to electro-mechanical processes\*\*. In the case of double exposure interferometry, the holographic record represents only one instant of time, and it is not possible to view changes as they occur in the subject without making new holograms. However, if only the comparison beam is holographically recorded and "stored", and the reconstructed comparison beam is compared with the

---

\*E. N. Leith and J. Upatnieks, J. Opt. Soc. Amer., 52, 1123 (1962; 53, 377 (1963); 54, 1295 (1964).

\*\*L. O. Heflinger, R. F. Wuerker and R. E. Brooks, Appl. Phys., 37, 642 (1966).

R. W. Brooks, L. O. Heflinger and R. F. Wuerker, Appl. Phys., Letters, 7, 248 (1965).



actual subject and test beam, then the real time behavior of the subject can be seen interferometrically. Thus, "stored beam" holographic interferometry offers not only real time information, but provides a means for acquiring time-lapse or moving picture records during the course of the reaction.

There are several advantages of the "stored beam" holographic interferometric method over the classical methods: alignment and preparatory procedures are far less critical, the common path nature provides significant flexibility and irregular shaped and imperfect optic elements and cells may be used. Furthermore, by the use of diffusers, three-dimensional information may be obtained. Thus, investigation of localization of corrosion and non-rotational symmetrical activities can be observed, as well as the use of assymetric samples.

These advantages then, enable one to observe changes which occur in a subject as a function of time, and since the aspects of the subject do not change the interference pattern as a function of time, a technique is available which is able to measure subtle changes in very complex samples incapable of being explored with any of the classical methods of interferometry.

While it is true that this method has thus far been utilized only for electromechanical changes with an external driving force, there is no reason that subtle interactions between materials and their potentially corrosive environment cannot be observed also. Thus, elucidation of the onset and nature of corrosion should be observable.

In addition to the technique mentioned above, two other methods of studying the interaction between the environment and the component should be examined for their applicability to the study of corrosion behavior. These methods are: 1) the electrical-resistance method, and 2) the electrochemical polarization technique. Each of these are described below.

- Electrical-Resistance Method - This method was developed at TRW and is based on the use of a probe with two sensing elements of different initial thickness. The probe is constructed of the material to be studied to avoid problems with contact corrosion. Since the entire probe is unprotected and immersed in the liquid of interest, corrosion takes place uniformly over the entire surface of the probe. As corrosion occurs, the cross-sections become thinner by equal amounts but, because of the different geometries, the resistances of the two sensing elements increase at different rates. By monitoring the change in resistance ratio as a function of time, it is possible to calculate the corrosion rate. It is possible to detect corrosion rates of less than one mil per year (MPY), and has the advantage of being a rapid method of monitoring metallic materials which comprise the component of interest.

- Electrochemical Polarization Techniques - There are three basic ways that these techniques can be utilized to determine corrosion rate. They include: a) linear polarization, b) transient linear polarization, and c) galvanostatic charging. These methods are based primarily on the fact that a linear relation exists between an applied current and a potential when an electrode system including the corrosive environment is changed by an application of a small external constant current. By these methods, it has been demonstrated that real time corrosion rates as low as 0.0005 MPY can be measured in 20 minutes. The sensitivity and time required for such measurements are limited only by instrumental sensitivity. However, even with these limitations, these electrochemical methods offer a means by which very low corrosion rates can be determined with relative ease and rapidity.

### 3.4 RECOMMENDATIONS

To provide greater utility for the valve component designer, a recommended program could be implemented which will achieve the following results:

1. Establishment of realistic criteria for valve component materials and definition of parameters which can affect performance under those conditions.
2. Establishment of test methodology, the test fluid and test specimen, and which will provide more meaningful information to the designer relative to the performance of materials under specified conditions.
3. Establishment of a procedure for documenting and reporting compatibility data such that extraneous data will be minimized, and pertinent data will be presented in their most useable form.

The program would not only take advantage of all existing data, but would identify the effects of material processing variables as well as propellant impurities. It could also introduce advanced concepts of testing to more accurately determine the functionality of materials during and after propellant exposure, and under static and dynamic conditions.

Consideration should be given to the long duration mission such as the ten year space flight to the outer planets. Past applications have usually involved storage and operation times on the order of days, weeks or months. This has generally enabled design personnel to instigate full duration tests of new materials during the design phase. Full duration tests of materials for a ten year space flight might well become obsolete during the test phase due to rapid technological advances in material developments. Consequently, the program should attempt to generate accelerated test methods that will provide valid data applicable to long term materials and component compatibility with propellants.

It is felt that the outlined program will provide a significant advance in an area of vitally needed data where the approach taken to date has been seriously inadequate.

### 3.5 PROPELLANT RATING CHART (TABLE 3-2)

In this chart the severity of the problems associated with each propellant were assessed and values assigned to the various combinations of propellants and parameters according to the following definitions:

<u>RATING</u>	<u>DEFINITION</u>
1	A value of 1 was assigned to those combinations with which a serious problem exists; i.e., one for which there is no satisfactory solution.
2	A value of 2 was assigned to those combinations with which a problem exists, but for which a remedy may be available. This is, the combination of component and parameter is deemed to be acceptable, <u>with qualifications</u> .
3	A value of 3 was assigned to those combinations which were deemed to be satisfactory; i.e., within the present state of the art.
U	A designation of U was made where the necessary information upon which to base a judgment was unavailable.
NA	Where a parameter was not applicable, the letters NA were used.

Following the Propellant Rating Chart is a discussion of the more serious problem areas (with ratings of 1 or 2) for each propellant type.

TABLE 3-2. Propellant Rating Chart

LEGEND 1 POOR 2 FAIR 3 GOOD NA - NOT APPLICABLE U - UNAVAILABLE INFORMATION (NO TEST DATA)	COMPATIBILITY					VALVE TYPES										OVERALL PROBABLE RATING IN 10 YEARS				
	METALS	CERAMICS	POLYMERS	NET LUBES	DRY LUBES	SHOCK SENSITIVITY	LUBRICITY	VISCOSITY	RADIATION TOLERANCE	EFFECTS OF LEAKAGE	CONTROL OF FLOW	SOFT SEATS	HARD SEATS	COMPONENT STERILIZATION*	REGULATORS		SHUTOFF	FLOW METERING	VENT (ZERO-G)	DISCONNECT
EARTH STORABLES																				
FUELS																				
	3	3	3	2 <sup>c</sup>	2	3	1	2	2	1-2	3	3	3	2-3	3	3	3	NA	3	3
	3	3	2	2 <sup>c</sup>	1	3	U	3	2	1	3	U	U	2-3	3	3	3	NA	3	3
	3	3	2	2 <sup>c</sup>	1-2	3	3	3	2	1-2	3	3 <sup>a</sup>	3	1-2	3	3	3	NA	3	3
	3	3	2	2 <sup>c</sup>	1-2	3	3	2	2	1-2	3	3 <sup>a</sup>	3	2-3	3	3	3	NA	3	3
	3	3	2	2 <sup>c</sup>	1-2	3	2	2	2	1	3	3 <sup>a</sup>	U	1-2	3	3	3	NA	3	2-3
	3	2	2-3	2	3	3	U	3	2	1	3	2-3	U	2-3	3	2-3	2-3	2-3	3	2-3
	3	3	2	2	2	3	3	3	3	1-2	3	1-2	3	2-3	3	3	3	NA	3	3
SPACE STORABLES																				
FUELS																				
	3	2	2-3	2	3	3	U	3	3	1	3	2-3	2	U	2-3	2-3	2-3	2-3	3	2-3
	3	3	3	2-3	2-3	3	3	2	2	2	3	3	3	U	3	1-2 <sup>b</sup>	3	2	3	3
	3	2	1-2	1	1	2	U	3	3	1	3	1-2	3	U	3	2 <sup>b</sup>	3	NA	3	2-3
	3	2	1-2	1	1	2	U	3	3	1	3	1-2	3	U	3	2 <sup>b</sup>	3	NA	3	2-3
	3	2	2	1-2	1	2	U	2-3	U	1-2	3	2	3	U	3	2 <sup>b</sup>	3	NA	3	2-3
	3	2	1-2	1	1	3	1-2	2-3	U	1	3	1-2	2-3	U	3	1 <sup>b</sup>	1-2	1-2	2	2-3
	3	2	1-2	1	1	3	2	U	U	1	3	1-2	2-3	U	3	1 <sup>b</sup>	1-2	1-2	2	2
	3	2	1-2	1	1	3	2	3	U	1	3	1-2	2-3	U	3	1 <sup>b</sup>	1-2	1-2	2	2
HAZD CRYOGENICS																				
	3	2	1-2	1	1	3	1-2	3	3	1	3	1-2	2-3	U	3	1 <sup>b</sup>	1-2	1-2	2	2
	3	3	2	1	1	3	2	3	3	2	3	2-3 <sup>a</sup>	3	U	3	2 <sup>b</sup>	3	2-3	2	3
	3	3	1-2	1	1	3	2	3	3	2	3	2-3 <sup>a</sup>	3	U	3	1-2 <sup>b</sup>	3	2-3	2	2-3
	3	2	1-2	1	1	3	1-2	3	3	1	3	1-2	2-3	U	3	1 <sup>b</sup>	1-2	1-2	2	2
GELS																				
	3	2	2	2	2	3	2	2	2	2	2	3 <sup>a</sup>	3	1	U	1	2	NA	U	2
	2	2	2	1-2	1-2	3	1	2-3	2	1	1	2	2	1	U	1	1	NA	U	2

a. THESE RATINGS, UNLIKE THOSE UNDER ORGANIC POLYMERS, WERE BASED ON THE USE OF A SPECIFIC POLYMERIC MATERIAL, IN MOST CASES TEFLON, FOR SOFT SEATS.  
 b. RATINGS BASED ON LEAKAGE CONTROL.  
 c. THESE RATINGS ARE BASED ON THE USE OF DUPONT FLUORINATED GREASE KRYTOX 240.  
 d. LIQUIFIED PETROLEUM GASES, METHANE, PROPANE, BUTENE.  
 e. 300°F, 60 HRS., 6 CYCLES.

### 3.6 EARTH STORABLE PROPELLANTS

#### 3.6.1 Fuels

3.6.1.1 Hydrazine ( $N_2H_4$ ) - Hydrazine is a clear liquid used as a high-energy propellant that is insensitive to mechanical shock or friction and exhibits excellent thermal stability at ambient temperatures. It is considered a hazardous propellant, however, due to its toxicity, reactivity, and flammability. Since it is thermodynamically unstable (i.e., a monopropellant), hydrazine will decompose under elevated temperatures when catalyzed by graphite or a metal oxide such as iron oxide or copper oxide, and will release considerable energy resulting in a possible explosion or fire. In addition, liquid hydrazine exerts sufficient vapor pressure above 100°F to form flammable air mixtures. Its freezing point is 35°F. Hydrazine is hygroscopic and readily forms flammable mixtures in air; therefore, a nitrogen blanket is required.

In assessing the compatibility of a material with hydrazine, the specific application for its use must be considered. Materials satisfactorily used with hydrazine where air oxidation of the surface can be prevented may not be satisfactory for service where prolonged exposure to air cannot be avoided. Factors to consider when selecting materials to use with hydrazine for any given exposure condition are: 1) corrosiveness of the material in contact with hydrazine, and 2) the effect of the material and/or its corrosion products formed on the rate of decomposition of hydrazine.

These factors to be considered are particularly true for carbon steel, low-alloy steels, copper alloys, and molybdenum. From the corrosion standpoint, these metals are satisfactory for use in hydrazine; however, these metals and/or their oxides may catalyze hydrazine decomposition at elevated temperatures. At one time it was thought that 316 stainless (containing molybdenum) caused excessive hydrazine decomposition rates at elevated temperatures. However, it is now generally agreed that the hazard at typical operating (<200°F) temperatures is no greater with 316 stainless than with any of the other 300 series stainless steels.

Evidence of chloride embrittlement of titanium exposed to hydrazine after cleaning with Freon has been noted. Isopropyl alcohol should be considered in lieu of Freon for cleaning titanium.

Table 3-3 lists those materials considered to be compatible with hydrazine for long-term application.

#### PHYSICAL PROPERTIES

Specific Gravity	1.00 (60°F)
Molecular Weight	32.048
Freezing Temperature °F	35.1
Normal Boiling Point °F	236.3
Critical Temperature °F	716
Critical Pressure psia	2131
Heat of Vaporization Btu/lb <sub>m</sub>	540

Discussion of Problem Areas -  
Hydrazine (N<sub>2</sub>H<sub>4</sub>)

Wet Lubes (2)\* - Most wet lubes either wash off or are attacked by hydrazine. For limited use, some silicone lubricants and "Q-Seal," Quigley Company, have been used with fair results. A fluorinated grease by DuPont, Krytox 240, appears to be compatible. Krytox 143 AB oil has been reported compatible with MMH and should be considered for N<sub>2</sub>H<sub>4</sub> services.

Dry Lubes (2) - Most dry film lubricants are attacked or removed by hydrazine. Electrofilm 1000G and Lubeco 2029-3 are partially compatible and can be used, although wear life after propellant exposure is somewhat reduced.

Lubricity (1) - Unsatisfactory lubricating performance was found for hydrazine in a series of low-load short duration ball bearing and gear tests at 24,600 rpm. The poor lubricity, resulting in degradation of the component metals surveyed, was attributed to its active solvent and reducing properties.

Viscosity (2) - The viscosity of hydrazine presents a problem only at low temperatures. The freezing point of commercial hydrazine is approximately 30°F, which is relatively high for operation under cold climatic conditions. Three methods of preventing N<sub>2</sub>H<sub>4</sub> from freezing have been employed: 1) the addition of freezing point depressant, 2) insulation of container and components, and 3) insulation plus tracing with heat elements, steam, or hot water.

Radiation Tolerance (2) - Hydrazine, UDMH, and Aerozine 50, subjected to an irradiation dose of  $1 \times 10^9$  erg/g, which is the maximum space radiation dose likely to be incurred in two years of operation in the Van Allen belts, showed that the composition of the propellants was not significantly affected. However, a pressure increase resulted, accompanied by the evolution of insoluble gases, due to slight decomposition. It is therefore recommended that tanks be designed to minimize this problem.

Effects of Leakage (1-2) - Anhydrous hydrazine is a flammable liquid, hence leakage may initiate a fire; it is hypergolic with most oxidizing agents and decomposes on contact with catalytic materials including iron rust. Vapors of hydrazine can be detonated by an electric spark or an open flame.

Since this propellant is a strong chemical reducing agent, leakage may result in malfunction of other elements in the system or injury to man. Prolonged exposure to this toxic material produces damage to the liver and kidneys and, to a lesser extent, anemia and lowering of blood sugar concentrations. The threshold value which has been adopted by the American Conference of Governmental Industrial Hygienists is 1 ppm.

---

\*Parenthetical enclosures refer to Propellant Rating Chart, Page 3-11.

TABLE 3-3. HYDRAZINE ( $N_2H_4$ )  
 COMPATIBILITY OF MATERIALS FOR  
 LONG TERM APPLICATION (NOTE 1)

MATERIAL	TEST TEMP °F
<u>ALUMINUM ALLOYS</u>	
1100	140
2014	80
2017	160
2024	70
3003	80
4043	160
5052	80
5456	140
6061	160
6061-T6	110
6066	80
716	140
356	160
*356-T6	110
40E	75
Tens 50	-
<u>STAINLESS STEEL</u>	
410	80
416	200 (pits)
430	68
440C	80
302	80
304	140
316	200
317	80
321	140
347	200
17-4 PH	140
17-7 PH	75
AM 350	160
AM 355	160

\*Reported noncompatible for period > 1 year based on limits of decomposition of hydrazine, see specific Reference 128.



HYDRAZINE (N<sub>2</sub>H<sub>4</sub>) (Continued)

MATERIALS	TEST TEMP °F
<u>MISCELLANEOUS METALS</u>	
Chromel A	80
Chromium Plating	70
Gold	75
Hastelloy C	125
Inconel	200
Inconel X	80
K-Monel	140
Monel	80
Nichrome Braze	80
Platinum	110
Silver	80
Silver Solder	75
Stellite 21	75
Tantalum	80
Tin	80
Titanium, Al10AT	140
*Titanium, 6Al-4V	160
Zirconium	75
<u>NON-METALS</u>	
Butyl Rubber Compound 805-70	140
Butyl Rubber Compound 823-70 (Parco)	-
Butyl Rubber Compound B480 (Parker)	-
Butyl Rubber Compound 9257 (Precision)	-
Ethylene Propylene Co-polymer	110
Kel-F	80
Polyethylene	80
Teflon	140
Teflon Coatings	-

\*Has been reported noncompatible for period >1 year at 110°F based on limits of decomposition of hydrazine, see specific Reference 128.

HYDRAZINE (N<sub>2</sub>H<sub>4</sub>) (Continued)

<u>MATERIAL</u>	<u>TEST TEMP °F</u>
<u>NON-METALS</u>	
Asbestos	80
Delanium	140
Glass	80
Polypropylene	-
SBR	75
Silicone Grease DC-11	-

Note 1. Metals listed above are rated compatible on a corrosion rate of less than 1 mil per year and the material does not cause decomposition, and is free from impact sensitivity. Non-metals are rated for satisfactory service for general use.

HYDRAZINE (N<sub>2</sub>H<sub>4</sub>) (Continued)

INCOMPATIBLE MATERIALS

INCOMPATIBLE MISCELLANEOUS METALS	INCOMPATIBLE NON-METALS
Cadmium	Buna-N Rubber
Cobalt	Cellulose Acetate
Lead	Diallyl Phthalate
Magnesium	Epons
Zinc	Kel-F 300 @140°F
Brass*	Kel-F @160°F
Bronze*	Kel-F Grease @212°F
Copper*	Natural Rubber
Iron*	Neoprene Rubber
Molybdenum*	Nylon
Mild Steel*	Mylar
6A-4V Ti (110°F, <1 year)**	Polyester
	Polyvinyl Alcohol
	Polyvinyl Chloride
	Saran
	Silastic LS-53
	Tygon

\*The oxide of these metals act as catalysts for decomposition of hydrazine at elevated temperatures.

\*\*Outside limit for decomposition rate of hydrazine, see specific Reference 128.

3.6.1.2 Monomethylhydrazine ( $\text{CH}_3\text{NHNH}_2$ ) - Monomethylhydrazine (MMH) is a clear, water white liquid with a strong amine odor detectable in concentrations of 1 to 3 ppm. It is a fairly volatile liquid; the vapor pressure, 0.96 psia at 77°F, is higher than that of hydrazine and hence creates a more hazardous health problem than hydrazine. The maximum allowable concentration of MMH vapor in air has not been established, but it has been suggested that it be set within 0.1 and 0.5 ppm.

Liquid MMH is not sensitive to impact or friction and is more stable than hydrazine under conditions of mild heating. The flammability characteristics of MMH with air are close to those of hydrazine and UDMH; consequently it should be maintained under a nitrogen blanket at all times. MMH must be stored away from any oxidizers and from possible sources of ignition. All metallic equipment employed for storage and handling of MMH requires grounding to prevent an accumulation of static charge.

An extensive compilation of compatibility data for metals and non-metals is not available. Due to the similarity in catalytic oxidation and chemical activity for MMH and hydrazine, those metals found satisfactory for hydrazine should suffice for MMH. In general, monomethylhydrazine attacks organic materials more readily than does hydrazine. Only short-term studies on a selected few plastics have been reported; no long-term compatibility tests have been done. Vydax, a telomer of teflon plus Freon, has been used for a lubricant however as a result deposits on close tolerance fits have been reported to cause problems. Krytox 143 AB oil is recommended.

Table 3-4 lists the materials which have been found to be satisfactory for use in the storage and handling of MMH.

#### PHYSICAL PROPERTIES

Molecular Weight	46.075
Freezing Temperature °F	-63
Normal Boiling Point °F	189
Critical Temperature °F	609
Critical Pressure psia	1195
Heat of Vaporization Btu/lb <sub>m</sub>	377

Discussion of Problem Areas -  
Monomethylhydrazine

Organic Polymers (2)\* - In general, monomethylhydrazine attacks organic materials more readily than does hydrazine. Materials satisfactory for limited use include Teflon, some silicone rubbers, and high density polyethylene.

Wet and Dry Lubes (2) - Because monomethylhydrazine is a better solvent than UDMH and  $N_2H_4$ , it also has attendant undesirable lubricant and "wash-out" effects. DuPont's Krytox 143 AB oil has been reported compatible with MMH. Electrofilm 2406 and 1000 G dry film lubricants have shown an ability to withstand attack. However, lubricity after exposure is undetermined. Cico 200-029-3 dry film lubricant has shown an increase in wear life after 72 hours exposure to monomethylhydrazine.

Radiation Tolerance (2) - This rating was made by analogy to hydrazine and UDMH, which have very similar chemical structure and physical and chemical properties.

Effects of Leakage (1) - Monomethylhydrazine is somewhat more toxic than UDMH or hydrazine; its flammability characteristics are similar. MMH vapors detonate on ignition by static sparking. Iron rust promotes the catalytic decomposition, resulting in spontaneous ignition. For effects of space vacuum, see the discussed effects of leakage for hydrazine.

---

\*Parenthetical enclosures refer to the Propellant Rating Chart, page 3-11

TABLE 3-4. MONOMETHYLHYDRAZINE

COMPATIBILITY OF MATERIALS  
FOR SHORT TERM USE<sup>a</sup>

<u>MATERIAL</u>	<u>TEMPERATURE</u>
<u>ALUMINUM ALLOYS</u>	
3003	
5052	
5154	
6061-S	Satisfactory below 160°F
<u>MISCELLANEOUS ALLOYS</u>	
Titanium 6Al-4V	
Columbium C 103	
<u>STEELS</u>	
303 Stainless Steels	
304 Stainless Steels	
321 Stainless Steels	
347 Stainless Steels	
17-7 PH Stainless Steels	
4130 <sup>b</sup>	Satisfactory below 160°F
<u>BRAZES</u>	
Aerobrazo-T	
82 Au-18 Ni Braze Alloy	
<u>PLASTICS AND ELASTOMERS</u>	
Natural Rubber	Intermediate <sup>d</sup> below 160°F, 1 wk
Neoprene	Intermediate <sup>d</sup> below 160°F, 1 wk
Polyethylene (high density)	Good <sup>c</sup> below 160°F, 1 wk
Silicone Rubber	Intermediate <sup>d</sup> below 160°F, 1 wk
Teflon	Intermediate <sup>d</sup> below 160°F, 1 wk
Some unplasticized trichlorofluoroethylenes	
Butyl Rubber	Below 95°F

a Two to four weeks.

b Very susceptible to rusting.

c Negligible weight change (0.5%); no change in elasticity.

d Moderate weight change (0.5 - 2.5%); change in elasticity of 25-40%.

3.6.1.3 Unsymmetrical Dimethylhydrazine  $(\text{CH}_3)_2\text{NNH}_2$  - UDMH is a derivative of hydrazine and is a moderately toxic, shock insensitive, storable liquid propellant. It exhibits excellent thermal stability and resistance to catalytic breakdown. It has a lower freezing point and higher boiling point than hydrazine.

Due to an extremely wide flammable range in air and the possibility that explosive vapor-air mixtures may be found above the liquid, UDMH should not be exposed to open air. Instead, it should be stored in a closed container under a nitrogen blanket.

At the present time test results imply that lubricants which are compatible for use with UDMH are still in the development stage. Lubricants such as APS C-407, Parkerlube 6PB, Molykote, and Peraline 12-4 may cause decomposition, while petroleum and silicone greases which do not react but are dissolved by the UDMH.

Table 3-5 lists those materials which are considered to be compatible with UDMH for long-term application.

#### PHYSICAL PROPERTIES

Specific Gravity	0.785 (60°F)
Molecular Weight	60.078
Freezing Temperature °F	-72
Normal Boiling Point °F	146
Critical Temperature °F	480
Critical Pressure psia	880
Heat of Vaporization Btu/lb <sub>m</sub>	250.7

Discussion of Problem Areas -  
Unsymmetrical Dimethylhydrazine (UDMH)

Organic Polymers (2)\* - In view of the variable nature of the service in which organic polymeric materials might be employed, it is difficult to be specific regarding their performance. Because of the excellent solvent properties of UDMH, most polymeric materials prove unsatisfactory. Numerous plastics and rubbers are rated "good" (suitable for repeated short-term exposure). Of the references cited, all indicated that Teflon was not attacked by UDMH and rated it as suitable for long-term storage or exposure.

Wet and Dry Lubes (2) - Because of the excellent solvent properties of UDMH, most lubricants are incompatible. Several lubricants, litharge, glycerine paste, X-Pando, and Q-Seal, are compatible and have been employed for pipe threads and other similar applications involving minimum contact with UDMH. Petroleum and silicone greases do not react, however, they tend to "wash-out" under dynamic conditions. DuPont's fluorinated grease, Krytox 240 is compatible. Krytox 143 AB oil has been reported compatible with MMH and should be considered for UDMH use.

Lubricity (1) - UDMH was found to have unsatisfactory lubricating properties when subjected to bearing and gear tests. The performance was thought to be related to the excellent solvent and reducing properties of UDMH.

Radiation Tolerance (2) - See hydrazine.

Effects of Leakage (2) - Being chemically similar to hydrazine, the same hazards are encountered as with that material. The maximum allowable concentration is somewhat less (0.5 ppm) than hydrazine. It is flammable in air, hypergolic in the presence of oxidizers; its excellent solvent properties may cause malfunction of components constructed of incompatible organic plastics with which it may come in contact. For space conditions, see the discussion on effects of leakage for hydrazine.

---

\*Parenthetical enclosures refer to Propellant Rating Chart, Page 3-11.



TABLE 3-5. UNSYMMETRICAL DIMETHYLHYDRAZINE (UDMH)

COMPATIBILITY OF MATERIALS FOR  
LONG TERM APPLICATIONS (NOTE 1)

MATERIALS	TEST TEMP °F
<u>ALUMINUM ALLOYS<sup>a</sup></u>	
1100	160
1100-H14	145
1260-H14	145
2014	140
2017	75
2024	75
2024-T3	145
3003	86
3003-H14	145
3004-H34	145
5052	160
5052-H34	145
5086	85
5086-H34	145
5154-H34	145
5456	140
6061	160
6061-T6	145
6063-T6	145
7075	160
7075-T6	145
356	160
356-T6	85
43	145

<sup>a</sup> Aluminum is attacked by UDMH if water is present, with the attack being directly proportional to the amount of water present.

UNSYMMETRICAL DIMETHYLHYDRAZINE (UDMH) (Continued)

<u>MATERIALS</u>	<u>TEST TEMP °F</u>
<u>STAINLESS STEEL</u>	
302	160
303	160
304	160
316	140
321	160
347	160
410	160
416	250
422	145
17-7 PH	160
Carpenter 20	140
PH15-7 Mo	85
A286	85
AM350	
AM355 CRT	100
17-4 PH Cond H925	
17-4 PH Cond H1151	
<u>MISCELLANEOUS METALS</u>	
Copper	145
Hastelloy (B, C, X, F)	145
Haynes Alloy 25	140
Inconel	140
Magnesium Alloy AZ-31B-0	85
Magnesium Alloy AZ-31B, AZ-61A	130
Magnesium Alloy AZ-92-F	85
Mild Steel	140
4130 Steel	85
Monel	140
Nickel	140

UNSYMMETRICAL DIMETHYLHYDRAZINE (UDMH) (Continued)

<u>MATERIALS</u>	<u>TEST TEMP °F</u>
<u>MISCELLANEOUS METALS (Cont.)</u>	
Tantalum	140
Titanium Alloy 6Al-4V	
Titanium A-55 (Commercially Pure)	145
Titanium Alloy B-120VCA	145
Titanium Alloy C-120AV	160
Columbium C 103	
<u>PLASTICS AND ELASTOMERS</u>	
Butyl Rubber	140
Kel-F (Unplasticized)	140
Nylon	130
Polyethylene	80
Teflon (FEP)	160
Teflon (TFE)	160
<u>MISCELLANEOUS MATERIALS</u>	
Delanium	75
Glass Pyrex	160
Graphitar No. 2	140
Graphite	75

Note 1: Materials listed above are rated compatible based on a corrosion rate of less than 1 mil per year and the material does not cause decomposition, and is free from impact sensitivity. Non-metals are rated for satisfactory service for general use.

3.6.1.4 Aerozine-50 (50% Hydrazine/50% UDMH)- The storable fuel blend of a nominal 50 percent by weight of hydrazine ( $N_2H_4$ ) and 50 percent by weight of unsymmetrical dimethylhydrazine (UDMH) is a hygroscopic (readily capable of absorbing moisture) liquid which is insensitive to mechanical shock but flammable in both liquid and vapor states. When combined, there is a definite tendency for each to dissolve in the other. Since the vapor above the fuel blend at 72°F is predominately UDMH, the flammability hazards of the mixture are the same as for UDMH. Explosion hazards can be minimized, however, by maintaining the fuel in closed systems.

Most common metals which might be used for valve construction, with the exception of the magnesium and copper alloys, are compatible with the 50/50 fuel blend providing they are clean. Care should be exercised when using ferrous alloys because of the possible catalytic decomposition of the fuel blend due to rust. Titanium alloy 6AL-4V has been reported non-compatible based on hydrazine decomposition rate limits (see specific Reference 128).

Table 3-6 lists those materials which are considered to be compatible with the 50/50 fuel blend for long term application.

#### PHYSICAL PROPERTIES

Molecular Weight	41.797
Freezing Temperature °F	18
Normal Boiling Point °F	170
Critical Temperature °F	634
Critical Pressure psia	1696
Heat of Vaporization Btu/lb <sub>m</sub>	425.8

Discussion of Problem Areas -  
Aerozine-50 (N<sub>2</sub>H<sub>4</sub> and UMDH)

Organic Polymers (2)\* - Most organic polymers either dissolve or deteriorate in the presence of Aerozine-50. Teflon has proved most successful for some uses; butyl rubbers are being used for most dynamic seals.

Wet Lubes (2) - Certain silicone-base greases, polyglycol oils, and powdered Teflon have been used for limited service. The fluorolubes react; many dissolve. DuPont's fluorinated grease, Krytox 240 is compatible.

Dry Lubes (1-2) - Graphite has been used, but found susceptible to washing out under dynamic conditions. Electrofilm 2406 and 1000 have shown resistance to propellant attack. However, lubricity after exposure is unknown.

Lubricity (1) - Being a mixture of hydrazine and UDMH, Aerozine-50 would have properties similar to the two components.

Viscosity (2) - Because of the high freezing temperature (18°F) of the Aerozine-50 mixture and the rapid increase in viscosity as this temperature is approached, it is desirable to maintain fuel temperature well above this point to insure proper flow characteristics.

Radiation Tolerance (2) - See hydrazine

Effects of Leakage (1-2) - The leakage effects will be similar to those discussed for the components of the fuel blend.

---

\*Parenthetical enclosures refer to Propellant Rating Chart, Page 3-11.

TABLE 3-6. AEROZINE-50 (50% HYDRAZINE/50% UDMH)

COMPATIBILITY OF MATERIALS FOR  
LONG TERM APPLICATION

<u>MATERIAL</u>	<u>TEST TEMP °F</u>
<u>ALUMINUM ALLOYS</u>	
1100	55-60
2014-T4	55-60
*2014-T6	160
*2024-T6	160
2219-T81	55-60
3003-H14	150
5086-H36	160
5254-F	160
5456-H24	55-60
5456-H321	160
6061-T6	160
6066	160
*7075-T6	160
356	160
Tens 50	160
<u>STAINLESS STEEL</u>	
303	160
304L	
*316	160
321	160
347	160
PH15-7 Mo (Cond. A)	160
*17-4 PH	160
17-4 PH (Cond. A)	160
*AM355 (Cond. H)	160
*AM350 SCT	160
*410H and T	160
440C	160

\*Disagreement exists among authorities as to acceptability.

## AEROZINE-50 (Continued)

<u>MATERIALS</u>	<u>TEST TEMP °F</u>
<u>OTHER METALS</u>	
*Anodize Coatings on Aluminum	160
Berlyco 25	160
Cadmium Plate	60
Columbium C 103	
Non-porous Chromium Plating	55-60
Gold Plate	160
Monel	80
Nickel	160
Non-porous Electrolytic Nickel Plating	55-60
*Electroless Nickel Plating	160
Silver	55-60
Silver Solder	60
Stellite 6K	160
*Stellite 21	160
Stellite 25	160
A286 Steel (rust free)	55-60
*1020 Steel (rust free)	55-60
4130 Steel (rust free)	55-60
Ti Alloy A110-AT	160
Ti Alloy C 120AV	160
Ti Alloy B 120VCA	55-60
**Titanium 6Al-4V	110
Tin	55-60
Titanium Carbide (Ni Binder)	160
Tungsten Carbide	160
<u>PLASTICS AND ELASTOMERS</u>	
Enjay 035	80
Fluorobestos filled with Asbestos	55-60
Fluorogreen	55-60

\*Disagreement exists between authorities as to acceptability.

\*\*Reported noncompatible based on limits of decomposition rate of hydrazine, see specific Reference 128.

AEROZINE-50 (Continued)

<u>MATERIALS</u>	<u>TEST TEMP °F</u>
<u>PLASTICS AND ELASTOMERS (Cont.)</u>	
Hadbar SB800-71 Rubber	160
Kel-F 300 (15% Glass Filled)	75
Kel-F 300 (Unfilled)	75
Parker B496-7 Rubber	160
Low-density Polyethylene	60
Polypropylene	160
Precision Rubber 9257, 940, X559	80
Teflon (FEP)	70-80
Teflon (TFE)	70-80
Teflon filled with Graphite	55-60
Teflon filled with Molydisulfide	55-60
Teflon filled with Asbestos	55-60
Zytel 31 Nylon	70-80
Zytel 101 Nylon	60
<u>LUBRICANTS AND GRAPHITE</u>	
Flake Graphite	80
Graphitar 39	70-80
Graphitar 84	70-80
Graphitar 86	160
Microseal 100-1 (dry lube)	80
National Carbon CCP-72	160
Purebon P3N	160
Reddy Lube 100	80
Reddy Lube 200	80
Silicone DC 11	80
Water Glass Graphite	80
Krytox 240	80



AEROZINE-50 (Continued)

<u>MATERIALS</u>	<u>TEST TEMP °F</u>
<u>CERAMICS</u>	
Rockflux	75
Sauereisen P-1	60
Sauereisen 31	60
Temporall 1500	60
<u>ADHESIVES</u>	
Epon 422	80

3.6.1.5 Hydrazine-Hydrazine Nitrate (HHN) - Hydrazine-hydrazine nitrate is a mixture of hydrazine, nitrated hydrazine ( $N_2H_5NO_3$ ), and a small amount of water. As such, it is more energetic, and more sensitive to impact than the regular hydrazine fuels and mixtures.

An extensive compilation of compatibility data for metals and nonmetals is not available. All iron and nickel based alloys are incompatible with hydrazine-hydrazine nitrate mixtures from gas evolution data and should not be used. The most comprehensive testing of compatible metals thus far has been done by Stanford Research Institute under contract to JPL. In general, aluminum and titanium alloys are compatible with the hydrazine-hydrazine nitrate mixtures, although some variability in compatibility and corrosion is noted when the two types of alloys are stored together.

Most nonmetals that are compatible with other hydrazine fuels can be used for hydrazine-hydrazine nitrate mixtures, although the compatibility varies with the composition of the mixture.

Due to the presence of hydrazine nitrate, greater susceptibility to catalytic decomposition is present, therefore, strict cleaning of materials in contact with the mixture, and careful handling procedures are necessary.

Table 3-7 lists those metals which have been tested, and their compatibility with hydrazine-hydrazine nitrate mixtures.

#### Discussion of Problem Areas - Hydrazine-Hydrazine Nitrate (HHN)

Organic Polymers (2)\* - In view of the variable nature of the service in which organic polymers might be employed, it is difficult to be specific regarding their performance. In general, HHN attacks organic materials more readily than the other hydrazine fuels. Teflon is rated satisfactory, with some silicone rubbers and high density polyethylene suitable for limited use.

Wet and Dry Lubes (2) - HHN, as other hydrazine fuels, has undesirable lubricant and "wash out" effects. DuPont's Krytox 240 grease appears compatible.

Viscosity (2) - The viscosity behavior of HHN is similar in nature to the other hydrazine fuels.

Radiation Tolerance (2) - This rating was made by analogy to hydrazine which is the major constituent of HHN, and the fact that the thermal and catalytic decomposition mechanism appears similar.

Effects of Leakage (1-2) - This rating was also made by analogy to hydrazine, with the added hazard of greater susceptibility to catalytic decomposition.

---

\*Parenthetical enclosures refer to Propellant Rating Chart, Page 3-11.

TABLE 3-7. HYDRAZINE-HYDRAZINE NITRATE

COMPATIBILITY OF METALS FOR LONG TERM APPLICATION

<u>COMPATIBLE</u>	<u>NOT COMPATIBLE</u>
<p><u>ALUMINUM ALLOYS</u></p> <p>6061-T6<sup>a,b</sup></p> <p>2014-T6</p> <p>1100</p> <p><u>TITANIUM ALLOYS</u></p> <p>Ti-6Al-4V (ELI)<sup>b</sup></p> <p>Ti-5Al-2.5 Sn (ELI)<sup>b</sup></p> <p>Ti-6Al-6V-2 Sn (HT)<sup>b</sup></p> <p>Ti-6Al-6V-2 Sn<sup>b</sup></p>	<p><u>IRON BASED ALLOYS</u></p> <p>AM 355 PH</p> <p>17-4 PH</p> <p>301 Full Hard</p> <p>AFC-77 PH</p> <p>Carpenter Custom 455 Maraging</p> <p><u>NICKEL BASED ALLOYS</u></p> <p>Inco 718</p>

<sup>a</sup> Compatibility is variable when stored with some titanium alloys - Base (NaOH) passivation decomposes HHN.

<sup>b</sup> Stored from 2.6 to 4.5 years in HHN at 110°F.

3.6.1.6 Pentaborane ( $B_2H_9$ ) - Pentaborane is a high energy fuel which is an extremely hazardous pyrophoric compound which is insensitive to mechanical shock and in an inert atmosphere, exhibits satisfactory (to 77°F) thermal stability. It exhibits hypergolicity with the high-energy oxidizers, and behaves as a strong reducing agent in oxidation-reduction reactions.

The boranes have a pungent, sickeningly sweet odor, and are toxic to a high degree. Toxic concentrations are reached before any odor can be detected and special detectors must be used. Any substance which will function as a potential oxidizer will react with the boranes. Materials such as water, air, metal oxides, and reducible organic compounds are in this category. For this reason, considerable care should be exercised in the selection of materials to be used with pentaborane, so as to avoid use of any organic compounds containing a reducible functional group. Teflon, Viton, Kel-F, and Fluorosilica rubber are among the compatible polymers.

Organic materials such as gaskets, lubricants, and seals must be chemically inert if they are to be used. High-porosity castings and gaskets should be avoided. Because of the ability of the boranes to reduce some metal oxides, welded joints should be avoided in pipe constructions. To date, no metals are known to be incompatible with pentaborane at ordinary room temperatures and atmospheric pressures. Pentaborane forms shock-sensitive mixtures with many highly chlorinated organic compounds such as carbon tetrachloride or trichloroethylene and with organic compounds containing reactive carbonyl groups such as acetone, other ketones and aldehydes. Thus, strict house-keeping rules and thorough solvent removal procedures must be employed when cleaning components such as valves, etc., in propellant systems using pentaborane.

Table 3-8 lists those materials which are considered to be compatible with the pentaborane for long-term application.

#### PHYSICAL PROPERTIES

Molecular Weight	63.17
Freezing Temperature °F	-52
Normal Boiling Point °F	136
Critical Temperature °F	435
Critical Pressure psia	557
Heat of Vaporization Btu/lb <sub>m</sub>	219
Density, gm/cc	0.643 (32)

Discussion of Problem Areas -  
Pentaborane (B<sub>5</sub>H<sub>9</sub>)

Ceramics (2)\* - Because of their strong reducing properties, pentaboranes will reduce some metal oxides and also precipitate some heavy metals from solutions of their salts.

Wet Lubes (2) - A number of lubricants are satisfactory for short-term service; however, pentaborane, being soluble in these lubricants, presents problems of cleaning, disposal, and "wash-out" of lubricant from components. Generally, non-lubricated valve designs acceptable for use with other toxic and corrosive liquids may be used successfully with the boranes.

Effects of Leakage (1) - The toxicity of the boranes, with a tentative threshold limit of 0.005 ppm, would constitute a severe hazard to humans in the event of leakage. The pyrophoricity of pentaborane in air has been a controversial subject; however, it is generally agreed pentaborane must be treated as if it were spontaneously flammable in air under most conditions. For leakage in space, see the discussion on effects of leakage for hydrazine.

Hard Seats (2) - Because of the necessity of eliminating all leakage, soft seat materials compatible with the boranes are recommended. Particle migration occurring where valve parts rub on plastic seals may cause problems of seal life, plugging or opening and fouling up close tolerance fits.

---

\*Parenthetical enclosures refer to Propellant Rating Chart, Page 3-11.

TABLE 3-8. PENTABORANE

COMPATIBILITY OF MATERIALS FOR  
LONG TERM APPLICATIONS

<u>MATERIAL</u>	<u>TEMPERATURE °F</u>
<u>ALUMINUM ALLOYS</u>	
2024-T3	75
3003-H14	75
5052-S	75
6061-T6	75
7075-T6	75
356-T6	75
Cadmium Coated Aluminum	75
Chromated Aluminum	75
<u>STAINLESS STEELS</u>	
302	75
304	75
321	75
347	75
<u>OTHER METALS</u>	
Brass	75
Cadmium Plated Steel	75
Copper	75
Hastelloy No. X-1258	75
Iron	75
K-Monel	75
Magnesium Alloy, AZ63A	
Magnesium Alloy, AZ318	

PENTABORANE (Continued)

<u>MATERIAL</u>	<u>TEMPERATURE °F</u>
<u>OTHER METALS (Cont.)</u>	
Monel, Soft, M-8330-B	
Nichrome "V"	75
Steel	75
Titanium Alloy C-110M	75
Titanium Alloy C-130AM	75
<u>NON-METALS</u>	
Fluoroflex T	75
Fluorosilicone Rubber	75
Graphitar No. 39	75
Graphite Impregnated Asbestos	75
Kel-F No. 5500	75
Kel-F & Glass Cloth	75
Kel-F & Glass Yarn	75
Molybdenum Disulfide	75
Pure Carbons	75
Rockwell Nordstrom Lube No. 921	75
Teflon	75
Viton	75
Viton A	75

Note 1: Materials listed above are rated compatible based on corrosion rate of less than 1 mil per year and the material does not cause decomposition, and is free from impact sensitivity. Non-metals are rated for satisfactory service for general use.

• PENTABORANE

INCOMPATIBLE MATERIALS

INCOMPATIBLE NON-METALS

INCOMPATIBLE LUBRICANTS

Foamglass  
Dow Corning R7002 Foam  
Dow Corning R7003 Foam  
Napco F10 Foam  
Napco B49  
Natural Rubber  
Nitrile Rubber on Nylon  
Dow Corning 9283 Rubber  
Saran  
Nylon  
Mylar  
Tygon  
Rubatex G-2027 N  
Rubatex R-103 J  
Fiberfrax No. XSW  
Fiberfrax No. SIF  
Dow Corning Silastic 80-24-480  
Garlock Silastic 250

Rockwell Nordstrom Lube 356  
Rockwell Nordstrom Lube 833  
Rockwell Nordstrom Lube 860  
Rockwell Nordstrom Lube 852-S  
Rockwell Nordstrom Lube P-21  
Rockwell Nordstrom Lube P-55  
Rockwell Nordstrom Lube 942-S



### 3.6.2 Oxidizers

3.6.2.1 Nitrogen Tetroxide (NTO) ( $N_2O_4$ ) - Nitrogen tetroxide is a highly reactive, toxic oxidizer, insensitive to all types of mechanical shock and impact. It is a dense brown or green liquid, depending on the NO content, and although it is nonflammable itself, it will support combustion and will react hypergolically upon contact with certain high-energy fuels such as the hydrazines.  $N_2O_4$  can cause spontaneous ignition with common materials such as leather and wood. The fumes are extremely toxic. Nitrogen tetroxide is used as a storable propellant oxidizer and is used in the Titan II missile and many spacecraft propulsion systems.

Dry nitrogen tetroxide is compatible with many metals and alloys used in space vehicle construction. However, water contamination present in the nitrogen tetroxide causes the formation of nitric acid, which is corrosive to many metals; therefore, materials selected for use in  $N_2O_4$  should be compatible with nitric acid as well. Gold and a few types of stainless steel have been satisfactory as materials in nitric acid storage containers and so should be best for long-term  $N_2O_4$  containment.

In general, aluminum alloys and stainless steels are most suitable for use as materials in contact with dry nitrogen tetroxide. The resistance to corrosion exhibited by the various aluminum alloys is a function of water content in the nitrogen tetroxide and the aluminum content of the alloy in question. As the water content in the nitrogen tetroxide exceeds 0.3 percent, highly alloyed aluminum (e.g., 7075 Aluminum Alloy) shows a sharp increase in corrosion rates as contrasted by the purer aluminum alloys (e.g., 1100 Aluminum Alloy), whose increase in corrosion rate is much less pronounced. For stainless steel, however, the corrosion rate in nitrogen tetroxide varies directly with water content.

Stress corrosion of titanium tanks has been experienced with the use of Mil Spec grade  $N_2O_4$  (MIL-P-26539A). Addition of small amounts of NO (>1.0%) in order to scavenge the dissolved oxygen has given dramatic evidence of reducing the incidence of stress corrosion in titanium tanks containing NTO. Shot peening the inside of titanium tanks in order to produce a surface under compression also has been effective in reducing corrosion by brown NTO. Thus, the true nature of the factors producing stress corrosion in titanium by NTO are still incompletely resolved. Copper, magnesium and nickel alloys are not recommended for use because of their poor corrosive resistance to nitric acid.

The chloride content of NTO may also give rise to pitting corrosion, which is a particularly serious matter with respect to very thin walled containers and/or bellows which must have long-term service life. This, coupled with the demonstrated problems of nitric acid production from moisture present and the uncertain role of  $O_2$  in NTO, clearly dictate that the aerospace designer should consider his choice of materials carefully in order to minimize failure due to materials incompatibility.

Most nonmetallic materials show poor resistance to nitrogen tetroxide and are considered unsatisfactory for use. Reaction of nitrogen tetroxide with nonmetals can result in decomposition of the materials, causing degradation

or complete destruction, or it can alter the physical properties such as volume and/or hardness of the material. In certain cases, this reaction can be advantageous as in the case of butyl rubber seals. Reaction of the butyl rubber with NTO results in tackiness and swelling which seems to augment the sealing characteristics of the material. This type of seal has been reported successful in service for over one year. The propellant may also be affected in its physical characteristics. Of all the plastics available for use, Teflon and Teflon products exhibit the best resistance to nitrogen tetroxide; however, nitrogen tetroxide permeates and is absorbed by Teflon. Results from permeability tests conducted show that the permeability rate for Teflon TFE is three times greater than Teflon FEP. Under certain conditions, Teflon in conjunction with NTO has caused increased corrosion rates. This may be due to the water content of NTO; however, no long-term storage data are available. Recently, the cyclized polybutadienes (HYSTL) and some of the nitroso copolymers ( $\text{CF}_3\text{NO}/\text{C}_2\text{F}_4$ ), and terpolymers ( $\text{CF}_3\text{NO}/\text{C}_6\text{F}_5\text{NO}/\text{C}_2\text{F}_4$ ) have shown promise as organic materials for use with NTO.

Another method of circumventing seal problems with NTO has been to design the O-ring groove such that less than 2% seal exposure is allowed. The swelling of the polymer then closes the gap and does not allow further interaction of the seal with the NTO. It has been claimed that over ten months storage life without leaks has been accomplished by this procedure.

Most lubricants in contact with nitrogen tetroxide are either dissolved and washed off or undergo a substantial change in hardness. DuPont's fluorinated grease, Krytox 240 and Krytox 143 AB and several dry lubricants such as Molykote Z, Drilube 703, and Electrofilm 66-C have been rated as compatible with nitrogen tetroxide. Microseal 100-1 is rated as compatible with nitrogen tetroxide and does not undergo any physical changes.

The formation of a gelatinous material has been reported and occurs during high velocity flow on  $\text{N}_2\text{O}_4$  through small clearances. Investigation of this phenomena is being carried out at several agencies and companies. The formation of the clogging material seems to be correlatable to various impurities in  $\text{N}_2\text{O}_4$  introduced either during the manufacture, storage, or conditioning of the oxidizer. The materials that appear to be responsible are metal- $\text{N}_2\text{O}_4$  reaction products and, possibly, organic species formed subsequent to the actual usage of the  $\text{N}_2\text{O}_4$ .

Table 3-9 lists those materials which are considered to be compatible with nitrogen tetroxide for long-term application. It should be noted that temperatures, temperature ranges and percent of water contamination are parameters of conducted tests and are not necessarily temperature limits or moisture content limits.

## PHYSICAL PROPERTIES

Specific Gravity	1.49 (60°F)
Molecular Weight	92.016
Freezing Temperature °F	11.8
Normal Boiling Point °F	70
Critical Temperature °F	316
Critical Pressure psia	1470
Heat of Vaporization Btu/lb <sub>m</sub>	178.2

### Discussion of Problem Areas - Nitrogen Tetroxide (N<sub>2</sub>O<sub>4</sub>)

Organic Polymers (2)\* - No completely satisfactory nonmetallic material has yet been found for use as valve seats. Most organic polymers have some disadvantages, principally that of swelling when exposed to N<sub>2</sub>O<sub>4</sub>. Polymers of promise have not been fully characterized as yet in NTO service.

Wet Lubes (2) - Most lubricants absorb N<sub>2</sub>O<sub>4</sub>, rendering them useless. Certain silicone greases have limited use because they tend to absorb N<sub>2</sub>O<sub>4</sub> slowly. DuPont's fluorinated grease, Krytox 240 and Krytox 143 AB has been rated compatible.

Dry Lubes (2) - A number of dry lubricants, including graphite and molybdenum disulfide, show good compatibility, but tend to wash out under flow conditions.

Effects of Leakage (1) - N<sub>2</sub>O<sub>4</sub> is a highly toxic substance and thus is classified as a poison on ICC regulations. The maximum allowable concentration of 5 ppm in air is accepted by the American Conference of Government Hygienists. Because of its corrosive nature and reaction with, or absorption in organic materials, adjacent components may easily be affected by N<sub>2</sub>O<sub>4</sub> leakage. The hypergolic nature of N<sub>2</sub>O<sub>4</sub> with many fuels constitutes a potential fire problem if leakage allows the two propellants to mix. Effects of leakage in space are discussed under the propellant hydrazine.

Soft Seats (1-2) - A limited number of nonmetallic materials are satisfactory for short-term use, but it is recommended that polymeric seals be avoided whenever possible. Teflon and Kel-F are the more resistant plastic materials. Teflon, when compatible with N<sub>2</sub>O<sub>4</sub>, absorbs N<sub>2</sub>O<sub>4</sub> vapors slowly. The resultant swelling may result in component malfunction.

---

\*Parenthetical enclosures refer to Propellant Rating Chart, Page 3-11.

TABLE 3-9. NITROGEN TETROXIDE  
 COMPATIBILITY OF MATERIALS FOR  
 LONG TERM APPLICATION

MATERIAL	TEST TEMP °F	% MOISTURE CONTENT
<u>ALUMINUM ALLOYS</u>		
1060	80	0.2 to 1.0
1100	60	0.3
1100-0	60	0.2 to 1.0
2014-T6	60	0.2 to 1.0
2014-T6 (Hardas Anodize)	60	
2014-T6 (H <sub>2</sub> SO <sub>4</sub> Anodize)	65	
2014-T6 (Iridite)	60	
2014-T6 (Welded)		
2024	140	0.2 to 1.0
2024-0	150	
2219-T6	60	
2219-T81	60	0.2 to 1.0
3003-H14	150	0.6
4043	80	
5052	130	0.2 to 1.0
5086-H34	165	
5086-H36	65	
5254-F	65	
5456	60	
5456 H-24	60	0.2 to 1.0
5456 H-24 (Iridite)	60	
5456 H 321	65	0.2 to 1.0
6061	130	
6061-T6	130	0.2 to 1.0
6061-T6 (Welded)	65	
6066	65	
7075	60	
7075-0	150	
7075-T6	150	

NITROGEN TETROXIDE (Continued)

MATERIAL	TEST TEMP °F	% MOISTURE CONTENT
<u>ALUMINUM ALLOYS (Cont.)</u>		
7075-T6	60	0.2 to 1.0
356	80	
356-T6 (See Incompatible Listing)	80	0.2 to 1.0
Tens 50	65	
<u>STAINLESS STEELS</u>		
410	110	
416	110	
430	110	
440C	110	
302	100	
303	80	0.2 to 1.0
304	140	0.2 to 1.0
304L	165	3.2
316	65	
321 (Incl. Welded)	60	3.0
347 (Incl. Welded)	100	10.0
17-4PH (Cond. A)	65	
17-4PH (H1000)	100	0.3
17-4PH	65	3.0
17-7PH (TH950)	100	
17-7PH (RH950)	100	
AM-350 (Annealed)	100	10.0
AM-355 (Cond. H)	100	
Titanium*		
<u>MISCELLANEOUS METALS</u>		
Chromium Plate	60	
Haynes Stellite 1	100	
Haynes Stellite 12	100	
Haynes Stellite 6K	65	
Haynes Stellite 21	65	
Haynes Stellite 25		

\*Compatible with Mil Spec grade  $N_2O_4$  containing NO as an inhibitor.

NITROGEN TETROXIDE (Continued)

MATERIAL	TEST TEMP °F	% MOISTURE CONTENT
<u>MISCELLANEOUS METALS (Cont.)</u>		
Haynes Stellite 93	100	
Gold	75	
Gold Plate	60	
Cast Iron	80	
Carbon Steel	80	
Mild Steel	140	
1020 Steel	130	
A-285 (Grade C)	165	3.2
8630 Steel	140	
A286 (Annealed) Steel	100	
A286 (Aged)	60	
PH15-7 Mo (Cond. A)	165	3.2
Magnesium, 100A	60	
Magnesium, HM21A-T8	60	
Nickel Electroplate	60	
Electroless Nickel Plate	100	
Inconel	65	
Monel	65	
Ni-Span-C	60	
Inconel X	75	
Platinum	75	
718 Braze 6061-T6A1	65	
Pure Tin Solder on 303SS	65	
Easy Flo Braze on 347SS	65	
Tantalum	75	
Tin	80	
Columbium	75	

NITROGEN TETROXIDE (Continued)

MATERIAL	TEST TEMP °F	% MOISTURE CONTENT
<u>NON-METALS</u>		
Microseal 100-1 on 2014-T6A1	100	
Teflon TFE	75	
Teflon FEP	160	0.2 to 1.0
Teflon Graphite	75	
Teflon MoS <sub>2</sub>	75	
Teflon Asbestos	75	
Teflon Glass Filled	80	
Alcar 191	67	
Armalon 7700	75	
Armalon 7700B	75	
Fluorobestos	60	
Fluogreen	60	
Genetron GCX-3B	80	
Genetron XE-2B	65	
Kynar	80	
Raythene N. (Irradiated)	65	
Tedlar	67	
<u>LUBRICANTS</u>		
		0.2
XC 150	65	
Molykote Z	60	
Microseal 100-1	67	
Lox Safe	80	
Flake Graphite	80	
Graphitar 2, 14, 39, 50, 86	67	
CCP-72		
Fluorolube MG6D0	80	
Fluoroethane G	80	
Krytox 240	80	
Krytox 143 AB		

NITROGEN TETROXIDE (Continued)

<u>MATERIAL</u>	<u>TEST TEMP °F</u>	<u>% MOISTURE CONTENT</u>
<u>SEALANTS AND POTTING COMPOUNDS</u>		0.2
Reddy Lube 100	160	
Reddy Lube 200	160	
Waterglass-Graphite	67	
Oxylube Sealant	80	
Teflon Tape (Unsintered)	80	
Crystal M&CF	60	
4-3	60	
Sauereisen P-1	60	
Proseal 333	60	



NITROGEN TETROXIDE  
INCOMPATIBLE MATERIALS - Note 1

INCOMPATIBLE METALS

Cadmium  
Lead  
356-T6 Aluminum Alloy (110°F, 1.9 yr)  
Copper  
K-Monel  
Silver  
Sintered Molybdenum  
Zinc  
Zirconium  
Cobalt  
Hastelloy B (110°F)  
Magnesium A231C (110°F)

INCOMPATIBLE NON-METALS

ELASTOMERS

Natural Rubber  
Butyl Rubber  
Buna-N  
Neoprene  
Viton  
Chloroprene  
Ethylene Propylene  
Silicones  
Kel-F  
Hypalon  
Polyurethane

INCOMPATIBLE NON-METALS

PLASTICS

Kel-F  
Polyethylene  
Nylon  
Mylar  
Polyvinylidene Chloride  
Acrylics  
H-Film  
Polypropylene  
Silicone Laminates  
Epoxy Laminates  
Phenolic Laminates  
Polyester Laminates  
Polyvinyl Chloride  
Epon Resins  
Acetal Resins  
Vinyl

NITROGEN TETROXIDE

INCOMPATIBLE MATERIALS Note 1

INCOMPATIBLE NON-METALS

LUBRICANTS

DC 11  
DC 33  
DC 510  
DC 550  
Molykote M-8800  
Molykote X-106  
Drilube 7  
Drilube 1  
Surfkote N-1284  
Rayco 30  
Electrofilm 66C  
Johns Manville No. 60

INCOMPATIBLE SEALANTS  
AND POTTING COMPOUNDS

Polysulfides  
RTV Silicones  
Epon Resins  
Polyesters  
Polyurethanes

Note 1 - Plastics, elastomers and sealants are generally listed by chemical family. While not all commercial products have been tested, it has generally been determined that these chemical families are incompatible. Lubricants included are rated on basis of wash-out tendencies or failure to maintain lubricity after propellant exposure.

3.6.2.2 Corrosion of Materials with Impure N<sub>2</sub>O<sub>4</sub> - TRW Systems performed corrosion testing using engineering materials at elevated temperatures with impure N<sub>2</sub>O<sub>4</sub> for NASA (General Reference No. 18). It was the intent of the NASA program to enhance corrosion, not suppress it, for purposes of determining the effect of corrosion products on contaminating the N<sub>2</sub>O<sub>4</sub>. However, this information and test data generated is valuable, since it represents the only known matrix testing done showing the effects of impurities in the propellant on corrosion. The work also included a different rating analysis on reporting corrosion not generally used by investigators. The test specimens were unstressed samples of 6061-T6 aluminum, 347 stainless steel and Ti-6Al-4V alloy subjected to one and four months duration at 165°F. The specimens measured nominal 0.025 inch thickness x 3/4 inch x 4 inch long and were placed in glass capsules containing the N<sub>2</sub>O<sub>4</sub> and sealed. The impurities individually added to the N<sub>2</sub>O<sub>4</sub> are listed as follows:

<u>ADDED IMPURITY</u>	<u>PRE-STORAGE CONCENTRATION, % w/w</u>
Chlorine (Cl <sub>2</sub> )	0.10
Water (H <sub>2</sub> O)	0.91
Oxygen (O <sub>2</sub> )	0.04
Nitrosyl Chloride (NOCl)	0.025
Nitrosyl Chloride + O <sub>2</sub> (NOCl + O <sub>2</sub> )	0.054 NOCl + 0.050 O <sub>2</sub>

The effects of the selected impurities in the corrosivity of N<sub>2</sub>O<sub>4</sub> showed no significant increase in dissolved metal content with time. Of all the impurities, water resulted in the greatest increase in corrosivity. Tables 3-10, 3-11, and 3-12, present a visual description of the appearance of the one and four month specimens. Tables 3-14 through 3-16 list the results of the corrosion testing for all three metals. Table 3-13 gives the definitions of the rating analysis used in the corrosion results of Tables 3-14 through 3-16. The rating analysis is taken from Champion, General Reference 1.

6061-T6 Aluminum - The water contaminated N<sub>2</sub>O<sub>4</sub> caused the greatest weight change in the aluminum and also caused the greatest structural damage to the metal. A significant decrease in water content after the four month storage period is noted. The samples were covered with a very thick, white coating which was easily removed by washing. Greatest damage appeared to be concentrated in the rolling marks left in the metal during sheet fabrication. Oxygen and O<sub>2</sub>/NOCl impurities caused general dark discoloration and pitting, with no deposit buildup. In the case of the oxygenated N<sub>2</sub>O<sub>4</sub>, no change in oxygen content occurred after one month storage whereas four month storage apparently resulted in O<sub>2</sub> depletion. An unexpectedly large negative oxygen value was obtained for the one month O<sub>2</sub>/NOCl fluid, reported as a positive nitric oxide (NO) content. Apparently either an impurity was present or spurious reaction occurred to cause consumption of oxygen. It is not possible that the oxygenation apparatus leaked, however, it is conceivable that an error in weighing caused the anomalous value. No change in NOCl content was detectable in the O<sub>2</sub>/NOCl fluid after one or four months.

Of interest is the very small degree of corrosion caused by the  $\text{Cl}_2$  and  $\text{NOCl}$  contaminated  $\text{N}_2\text{O}_4$ , because it has been postulated that the chloride ion and/or molecular chlorine may be one of the principle species responsible for metal degradation in  $\text{N}_2\text{O}_4$ . The slight decrease in chlorine content is not considered significant in view of the fact that the specimens were not corroded significantly. Furthermore, they were extremely similar to the specimens exposed to uncontaminated  $\text{N}_2\text{O}_4$ . The larger values for  $\text{NOCl}$  content after storage are not particularly surprising as many instances of chloride buildup are reported in the literature.

347 Stainless Steel - The most severe attack was obtained in the  $\text{O}_2$ ,  $\text{H}_2\text{O}$ , and  $\text{O}_2/\text{NOCl}$  contaminated  $\text{N}_2\text{O}_4$  test fluids. Crystals formed on the specimen surface in the  $\text{H}_2\text{O}$  contaminated  $\text{N}_2\text{O}_4$  were of a green color when viewed by reflected light, but were red when viewed by transmitted light. The crystals formed in the  $\text{O}_2/\text{NOCl}$  contaminated  $\text{N}_2\text{O}_4$  were red when viewed by either light mode, and in addition, reacted vigorously (effervesced) when exposed to either atmospheric oxygen or water vapor. A significant water decrease and complete consumption of oxygen in the stainless steel tests were the most notable changes in contaminant additive. Once again an anomalous positive NO content results for the one month fluid contaminated with  $\text{O}_2/\text{NOCl}$ . The chlorine and  $\text{NOCl}$  contents changed moderately and insignificantly, respectively.

The general mode of corrosion for the stainless steel specimens was primarily minute pitting. Some surface roughening was also evident, however, since the objective of this task was to enhance, not suppress corrosion, none of the specimens were passivated prior to storage. The stainless steel specimens, however, did passivate to an extent, as can be noted from the thickness changes in the one and four month storage samples.

Ti-6Al-4V Alloy - The titanium alloy specimens were the least affected of any of the alloy systems by the corrodent fluids. The specimens appear somewhat darker than normal due to their high reflectivity. Some surface discoloration was evident on the specimens but they did not appear to be affected otherwise. No evidence of pitting or general attack was found in any of the specimens, and the only effect of the corrodent fluids noted was to slightly roughen the surface. In general, slight to moderate changes in contaminant level occurred with the exception of the four month  $\text{O}_2$  and water concentrations which decreased markedly, though no corresponding increase in corrosion was found.

TABLE 3-10. Physical Appearance of One and Four Month Aluminum Specimens Prior To and After Removal of Propellant ( $N_2O_4$ )

Added Contaminant	Appearance of One Month Capsules		Appearance of Four Month Capsules	
	Before Propellant Removal	After Propellant Removal	Before Propellant Removal	After Propellant Removal
None	No noticeable corrosion.	No noticeable corrosion.	No noticeable corrosion.	Some oily substances on bottoms of tubes.
$H_2O$	Specimens covered with white salts.	Specimens covered with white salts.	White crystals on bottom of tubes. Specimens covered with white salts.	Specimens covered with white salts. Some crystals on walls and bottoms of tubes.
$O_2$	Slight spotted discoloration of specimens.	Slight spotted discoloration of specimens.	Slight discoloration.	Slight spotted discoloration of specimens. Yellow crystals at tops of the tubes. White powdery coating on the walls of the tubes.
$NOCl$	No noticeable corrosion.	No noticeable corrosion.	No noticeable corrosion.	No noticeable corrosion.
$NOCl + O_2$	Specimens slightly tarnished. One tube contained yellow gelatinous material.	Specimens appeared corroded. One tube had a yellow powdery coating at the top of the tube and a yellowish-brown gelatinous material, adhering to the walls.	Slight corrosion of specimens. One tube had yellow-green spots at the top of the liquid.	Specimens were slightly corroded. One tube had yellow particles at the top and a few on the bottom.
$Cl_2$	No noticeable corrosion.	No noticeable corrosion of specimens. One tube had a yellow ring at the $N_2O_4$ liquid-vapor interface.	No noticeable corrosion.	No noticeable corrosion.

TABLE 3-11. Physical Appearance of One and Four Month Stainless Steel Specimens Prior To and After Removal of Propellant ( $N_2O_4$ )

Added Contaminant	Appearance of One Month Capsules		Appearance of Four Month Capsules	
	Before Propellant Removal	After Propellant Removal	Before Propellant Removal	After Propellant Removal
None	No noticeable corrosion.	No noticeable corrosion.	No noticeable corrosion.	Some gelatinous material on the bottoms of the tubes. One tube had yellow coating on wall.
$H_2O$	Specimens were black with few black crystals on them. Greenish colored immiscible droplets on sides of tubes.	Specimens were black with few black crystals on them. Greenish colored immiscible droplets on sides of tubes.	Specimens were black with black crystals on them. Greenish colored immiscible droplets on sides of tubes.	Black salt crystals on specimens. Green oily substance on walls and bottom of tubes.
$O_2$	Specimens were black. Some yellow crystals on specimens and walls of the tubes. One tube had a few immiscible droplets.	Specimens were black and had some yellow crystals on them and on the tube walls. One tube had green immiscible droplets on it.	Specimens were black. Reddish-Brown crystals on walls of tubes above the liquid $N_2O_4$ .	Specimens were black. Reddish-brown crystals on the walls of the tubes.
$NOCl$	No noticeable corrosion.	No noticeable corrosion.	Gelatinous material on the walls of the tubes. No noticeable corrosion of specimens.	Specimens are slightly discolored. Coating on the walls. No sign of gelatinous material.
$NOCl + O_2$	Specimens were black. Yellow crystals at the top of the liquid. Clear crystals on the bottoms of the tubes.	Specimens were black. Some yellow crystals and coating on the tops of the tubes.	Specimens were black. One tube had reddish-brown gelatinous material above and 1/2" below the liquid. Some gelatinous material on the tube wall.	Specimens were black and tube walls were coated. One tube had yellow crystals on the wall and the other tube had black spots.
$Cl_2$	Clear crystals on the tube walls. No noticeable corrosion of the specimens.	Slight discoloration of specimens.	No noticeable corrosion.	Slight discoloration of specimens. Reddish-brown crystals on bottoms of tubes.

TABLE 3-12. Physical Appearance of One and Four Month Titanium Specimens Prior To and After Removal of Propellant (N<sub>2</sub>O<sub>4</sub>)

Added Contaminant	Appearance of One Month Capsules		Appearance of Four Month Capsules	
	Before Propellant Removal	After Propellant Removal	Before Propellant Removal	After Propellant Removal
None	No noticeable corrosion.	No noticeable corrosion.	No noticeable corrosion.	A few crystals on the walls of the tubes.
H <sub>2</sub> O	Specimens slightly spotted.	Specimens slightly spotted.	No noticeable corrosion.	Small amount of oily substance on bottoms of tubes. Clear crystals on walls of tubes.
O <sub>2</sub>	No noticeable corrosion of the specimens. Tube walls covered with a yellowish-white material.	No noticeable corrosion of specimens. Tube walls coated with a yellowish-white substance.	No noticeable corrosion of specimens. One tube had reddish-yellow crystals on the wall above the liquid.	No noticeable corrosion. One tube had reddish-brown crystals above the liquid level.
NOCl	No noticeable corrosion.	No noticeable corrosion.	No noticeable corrosion.	No noticeable corrosion.
NOCl + O <sub>2</sub>	A few clear crystals on the walls of the tubes.	No noticeable corrosion.	Clear colorless gelatinous material at the top of the liquid on the tube walls.	No noticeable corrosion. Yellowish-green immiscible droplets at the tops of the tubes and a few crystals on the bottoms.
Cl <sub>2</sub>	No noticeable corrosion.	No noticeable corrosion.	No noticeable corrosion.	No noticeable corrosion.

TABLE 3-13. Rating Chart for Macroscopic and Microscopic Examination of Corrosion Behavior of Metals (After Champion)

NO.	Number of Pits		Size of Pits		Intensity of Corrosion			Factors Affecting Corrosion (% Influence)
	Chart A		Chart B		Chart C			
	Standard Term	No. Per Sq. cm	Standard Term	Area (Sq. cm)	Standard Term	Depth of General Attack (cm)	Depth of Pitting or Cracking (cm)	
1	Very few	33	Minute	0.0006	Minute trace	0.0001	0.004	9
2	Few	100	Very small	0.003	Very small	0.0004	0.01	13
3	Small number	330	Small	0.016	Slight	0.0016	0.025	20
4	Moderate number	1,000	Moderate	0.08	Moderate	0.006	0.06	30
5	Considerable number	3,300	Considerable	0.4	Considerable	0.024	0.15	45
6	Numerous	10,000	Large	2.0	Severe	0.10	0.4	70
7	Very numerous	33,000	Very large	10.0	Very severe	0.40	1.0	100



TABLE 3-14. Results of One and Four Month Storage of 6061 T6 Aluminum Specimens With Neat and Contaminated  $N_2O_4$  at 165°F.

FLUID CHARACTERIZATION				POST TEST METAL CHARACTERIZATION						
Added Impurities	Pretest Concentration % w/w	Storage Period, Months	Post Test Concentration % w/w	Weight Change mg	Thickness Change mil	Rating (b)			Remarks	
						A	B	C		D
None	--	One	--	-0.3	-0.2	0	0	2	0	Little Discoloration.
		Four	--	-0.4	-0.1	1	1	0	0	Slight Discoloration.
Cl <sub>2</sub>	0.101	One	0.060	+0.4	+0.4	0	0	(c)	0	Little or No Discoloration.
		Four	0.094	-0.2	-0.2	0	0	2	0	Slight Discoloration.
H <sub>2</sub> O	0.91	One	0.82	-102.4	-0.6	3	2	3	2	Thick white coating on metal surface. General light discoloration after washing.
		Four	0.29	-111.1	-0.5	5	3	3	3	As Above.
O <sub>2</sub>	0.04	One	0.04	-0.5	-0.3	4	2	2	3	General Dark Discoloration.
		Four	0	+1.4	-0.1	4	3	0	3	As Above.
NOCl	0.024	One	0.035	+0.2	-0.3	0	0	2	0	Little Discoloration.
		Four	0.030	-0.1	0.0	1	1	0	1	Slight Discoloration
NOCl + O <sub>2</sub>	0.054 0.05	One	0.056 NOCl + 0.43 NO (a)	+1.0	-0.3	4	2	2	2	General Dark Discoloration.
		Four	0.054 NOCl + 0.07	+1.4	0.0	5	3	0	3	General Dark Discoloration.

- (a) Oxygen apparently depleted and species formed which react with O<sub>2</sub>.
- (b) Rating of zero indicates negligible corrosion. See Table 1-11 for rating definitions.
- (c) Corrosion rating not applicable because of deposit build-up.

TABLE 3-15. Results of One and Four Month Storage of 347 Stainless Steel Specimens With Neat and Contaminated  $N_2O_4$  at 165°F.

FLUID CHARACTERIZATION				POST TEST METAL CHARACTERIZATION						
Added Impurities	Pretest Concentration % w/w	Storage Period, Months	Post Test Concentration % w/w	Weight Change mg	Thickness Change mil	Rating (b)				Remarks
						A	B	C	D	
None	--	One	--	-2.3	-0.1	0	0	0	0	No Discoloration.
		Four	--	-2.2	+0.1	0	0	(c)	0	No Discoloration.
Cl <sub>2</sub>	0.101	One	0.075	-1.6	-0.1	0	0	0	0	No Discoloration.
		Four	0.068	-2.5	+0.2	0	0	(c)	0	Slight Discoloration.
H <sub>2</sub> O	0.91	One	1.1	5.6	-0.4	1	1	3	1	Small crystals on metal surface. General dark discoloration.
		Four	0.48	-54.1	-0.1	4	1	0	2	As Above.
O <sub>2</sub>	0.04	One	0.07 NO(a)	-24.0	-0.2	4	2	2	3	Small crystals on metal surface. General dark discoloration.
		Four	0.01 NO(a)	-28.8	0.0	4	2	0	3	As Above.
NOCl	0.024	One	0.020	-0.8	-0.2	0	0	2	0	No Discoloration.
		Four	0.020	-1.5	+0.1	0	0	(c)	0	No Discoloration.
NOCl + O <sub>2</sub>	0.054	One	0.072 NOCl 0.33 <sup>+</sup> NO(a)	-37.2	-0.2	2	2	2	2	Small crystals on metal surface. General dark discoloration.
		Four	0.053 NOCl 0.03 <sup>+</sup>	-33.5	+0.1	4	2	(c)	2	As Above.

(a) Oxygen apparently depleted and species formed which react with O<sub>2</sub>.  
 (b) Rating of zero indicates negligible corrosion. See table 1-11 for rating definitions.  
 (c) Corrosion rating not applicable because of deposit build-up.

TABLE 3-16. Results of One and Four Month Storage of Ti-6Al-4V Alloy Specimens With Neat and Contaminated N<sub>2</sub>O<sub>4</sub> at 165°F.

FLUID CHARACTERIZATION				POST TEST METAL CHARACTERIZATION						
Added Impurities	Pretest Concentration % w/w	Storage Period, Months	Post Test Concentration % w/w	Weight Change mg	Thickness Change mil	Rating (b)				Remarks
						A	B	C	D	
None	--	One	--	-0.2	-0.1	0	0	0	0	Minute Discoloration.
		Four	--	-0.1	+0.2	0	0	(c)	0	Slight Discoloration.
Cl <sub>2</sub>	.0101	One	0.084	-0.3	+0.4	0	0	(c)	0	Minute Discoloration.
		Four	0.058	-0.0	+0.2	0	0	6	0	Slight Discoloration.
H <sub>2</sub> O	0.91	One	1.37	0.0	0.0	0	0	0	0	General Medium Discoloration.
		Four	0.52	+0.2	+0.2	0	0	(c)	0	As Above.
O <sub>2</sub>	0.04	One	0.12	-3.6	-0.1	0	0	0	0	No Discoloration.
		Four	0.04 NO <sup>(a)</sup>	-0.6	+0.2	0	0	(c)	0	Slight Discoloration.
NOCl	0.024	One	0.018	-0.2	0.0	0	0	0	0	No Discoloration.
		Four	0.017	-0.1	+0.1	0	0	(c)	0	Slight Discoloration.
NOCl + O <sub>2</sub>	0.054 0.05	One	0.060 NOCl 0.09 +	-6.0	-0.1	0	0	0	0	Minute Discoloration.
		Four	0.043 NOCl 0.09 +	-4.1	0.0	0	0	0	0	Slight Discoloration.

(a) Oxygen apparently depleted - oxygen reactive species present.  
 (b) Rating of zero indicates negligible corrosion. See table 1-11 for rating definitions.  
 (c) Corrosion rating not applicable because of deposit build-up.

### 3.7 SPACE STORABLE PROPELLANTS

#### 3.7.1 Fuels

3.7.1.1 Diborane ( $B_2H_6$ ) - Diborane is used as a high energy fuel. It is extremely toxic. Diborane is insensitive to mechanical shock and exhibits satisfactory (77°F) thermal stability in an inert atmosphere. It exhibits hypergolicity with the high energy oxidizers and behaves as a strong reducing agent in oxidation reduction reactions.

Diborane as a liquid is water clear and is considered to be a mild cryogen normally kept at temperatures below 0°F. Diborane has a distinctive odor described as rotten eggs, sickly sweet and musty or foul. The recommended threshold limit is 0.1 ppm for an 8 hour exposure. Toxic concentrations are reached before any odor is detected. The ability to detect the odor decreases with exposure, therefore, special detectors must be used. Any substance which will function as a potential oxidizer will react with diborane including such materials as water, air, some metal oxides and reducible organic compounds. Diborane decomposes slowly at room temperature to hydrogen and high-molecular weight boron hydrides. Diborane is completely hydrolyzed by water:



The compatibility of diborane with other materials is similar to those listed under pentaborane except that diborane is somewhat more reactive than pentaborane at normal storage temperatures. In comparing chemical compatibility of pentaborane with diborane considerations should be given to problems associated with the lower temperature of the gaseous state of diborane.

Diborane must be stored and transferred in totally closed systems that are clean, dry, and free of air. Gases for purging and pressurizing diborane systems include nitrogen and helium (carbon dioxide is not suitable). The pressure over diborane should be greater than atmospheric to minimize the probability of air seeping into the system. Double-walled storage and transfer systems are sometimes used where leaks pose a serious hazard; purge gas circulated between the walls is passed through a detector that signals the presence of diborane should a leak develop through the inner wall. Special precautions must be observed in cleaning hardware for diborane services as diborane may react explosively with residual halogenated solvents such as carbon tetrachloride.

Table 3-17 lists the materials considered to be most recommended for diborane. In all cases, these materials are suitable only if strict control of surface contamination and careful attention to minimize thermal fluctuations above -20°C are maintained.

PHYSICAL PROPERTIES

Molecular Weight	27.69
Freezing Temperature °F	-265
Normal Boiling Point °F	-134
Critical Temperature °F	62
Critical Pressure psia	581
Heat of Vaporization Btu/lb <sub>m</sub> at NBP	222
Viscosity of Liquid at NBP	$9 \times 10^{-5}$ lb/ft - sec.
Specific Gravity of Liquid at NBP	.437

TABLE 3-17. DIBORANE

COMPATIBILITY OF MATERIALS FOR LONG TERM APPLICATION

COMPATIBLE MATERIALS

Metals

Stainless Steel 18-8 Series  
 Low Carbon Steels  
 Nickel  
 Monel  
 Brass  
 Titanium

Non-Metals

50-50 Polyethylene Polyisobutalene  
 Kel-F  
 Glyptal  
 Vaseline-Paraffin-Graphite  
 Asbestos-Graphite-Copper Packings

INCOMPATIBLE MATERIALS

Non-Metals

Most Natural and Synthetic  
 Elastomers  
 Silicone Grease <sup>a</sup><sub>—</sub>  
 Fluorolube FS <sup>a</sup><sub>—</sub>

<sup>a</sup> These materials absorb small quantities of diborane and thus are suitable for limited service only.

3.7.1.2 Hybaline A-5 - Hybaline A-5 is a pyrophoric, high energy fuel blend, of low volatility and reacts violently with water. Its composition is classified.

Cursory tests have been performed on some materials, although no definitive evaluation has as yet been conducted. Two separate investigations have been performed on the compatibility and corrosion rates of structural materials in Hybaline A-5 liquid and vapor at 50°C (122°F). Some discrepancy is noted on the compatibility of copper and brass toward the decomposition of Hybaline A-5, thus, caution is recommended until extensive investigation resolves these differences. The primary corrosion agents in the mixture are chlorides, utilized in the synthesis, which are not completely removed from the product.

The results of the two investigations are listed in Table 3-18. Materials listed as compatible have low (0.1 MPY avg.) corrosion rates and/or do not catalyze the decomposition of Hybaline A-5.

Discussion of Problem Areas -  
Hybaline A-5

Metals, Ceramics, Organic Polymers, Wet and Dry Lubes (2)\* - There is not sufficient data available on Hybaline A-5 to enable a reliable assessment of materials compatibility, but it would appear that no serious problems exist with these materials.

---

\*Parenthetical enclosures refer to Propellant Rating Chart, Page 3-11.

TABLE 3-18. HYBALINE A-5  
 COMPATIBILITY OF MATERIALS AT 122°F

<u>COMPATIBLE METALS</u>	<u>NON-COMPATIBLE METALS</u>
<u>ALUMINUM</u>	Copper <sup>a</sup>
1100 <sup>a</sup>	Brass <sup>a</sup>
2104-T6	
2024-T3	
6061-T6	
7075-T6	
7075-T73	
356-T6	
Titanium Alloy A-110 AT <sup>a</sup>	
<u>STAINLESS STEELS</u>	
17-7 PH <sup>a</sup>	
17-4 PH	
302	
304L <sup>a</sup>	
316	
321	
347	
410	
<u>NON-METALS</u>	<u>NON-METALS</u>
Mylar <sup>a</sup>	Neoprene
Teflon (TFE and FEP) <sup>a</sup>	Viton-A
Kynar <sup>a</sup>	Tygon
Polyethylene <sup>a</sup>	Ke-F 90
Buna-N <sup>a</sup>	Fluorolube 362
Halocarbon Grease <sup>a</sup>	Dow Corning Valve
Dow Corning Hi-Vac Oil <sup>a</sup>	Seal Aerochlor 1254

a - exposure for 2 months. Other data is for a static, twenty-one day test.

3.7.1.3 Liquid Petroleum Gases (LPG) Propellants - The LPG propellants are colorless, flammable hydrocarbons, which are normally gaseous at room temperature and atmospheric pressure. The primary pure materials of interest are methane, propane, and butene. A pentane blend has also been proposed for use. The LPG propellants are not considered toxic gases. Methane acts physiologically as a simple asphyxiant. Butene and propane, in higher concentrations, also have an anesthetic action. Self-contained breathing apparatus, therefore, should be used if there is a suspected high concentration of these gases present, as in the case of a spill, etc. The LPG propellants should be stored away from any oxidizer and from possible sources of ignitions. All metallic equipment required for storage and handling should be grounded in order to prevent an accumulation of static charge.

Since the LPG propellants are non-corrosive, any common or commercially available metal may be used if the propellant is in the gaseous state. Metals having acceptable low temperature physical properties must be utilized in storing liquid methane, however, since it boils at  $-259^{\circ}\text{F}$  (1 atm).

Inasmuch as the propellants are hydrocarbons, they exert a solvent action on many greases, plastics and rubbers. Thus, consideration must be given to the types of organic materials which may come in contact with the propellants. Teflon, nylon, and the alkylene polysulfides are all resistant to attack, with the neoprene and butadiene-acrylonitrile rubbers being slightly less resistant.

#### PHYSICAL PROPERTIES

	Methane	Propane	1-Butene
Molecular Weight	16.04	44.10	56.10
Freezing Point $^{\circ}\text{F}$ at 1 atm	-296	-306	-303
Normal Boiling Point $^{\circ}\text{F}$ at 1 atm	-259	-44	20.7
Critical Pressure, psia	693	617	583
Latent Heat of Vaporization, cal/g	121.9	101.8	93.4



Discussion of Problem Areas -  
Liquified Petroleum Gases (LPG) Propellants

Radiation Tolerance (2)\* - Since butene is an unsaturated hydrocarbon, reactions such as polymerization or molecular rearrangement can occur. Polymerization by free radical extension is normally carried out using catalysts, but can be induced by ionizing radiation. If the polymerization initiation is widespread throughout the storage tank, a violent and uncontrollable reaction may take place. Slow polymerization may result in the formation of sludge or varnish, leading to system malfunction.

Wet and Dry Lubes (2-3) - Because of the solvent properties of the propellants, there tends to be undesirable "wash-out" effects on lubricants. These problems can be minimized by the use of glands and seals. Experience in the petroleum industry with such lubricants as Plastilube #1 (Lubrication Company of America), John Crane Insoluble Gasoline Lubricant (Crane Packing Company), and Dow Corning Valve Seal (Dow Corning), indicated that these materials may be satisfactory for use.

Effects of Leakage (2) - Because of the extensive flammability of the propellants, the main hazard lies in the accumulation of vapors in confined areas, where the possibility of accidental ignition can occur. However, inasmuch as the gases are non-toxic, possess low flammability limits and since reliable vapor detectors are available, proper ventilation and elimination of sources of ignition reduce the danger of fire or explosion.

---

\*Parenthetical enclosures refer to the Propellant Rating Chart, Page 3-11.

### 3.7.2 Oxidizers

3.7.2.1 Chlorine Trifluoride (CTF) (ClF<sub>3</sub>) - Chlorine trifluoride, like fluorine, is among the most active chemicals known. Being a very strong oxidizing agent, it reacts vigorously with most oxidizable substances at room temperature and with most common metals at elevated temperatures. Under ordinary conditions, chlorine trifluoride reacts violently with water or ice. It is, however, insensitive to mechanical shock, nonflammable in dry air, and shows good thermal stability at ambient temperatures. Although some surface staining has occurred in tests employing impact, there has been no evidence of ignition utilizing aluminum, copper, magnesium or titanium in either gaseous or liquid CTF. Since CTF is probably the most corrosive and toxic of the interhalogens, the materials and precautions given for it are sufficient for use with the other halogen fluorides.

The corrosion resistance of all materials of construction used with chlorine trifluoride depends on the formation of a passive metal fluoride film which protects the metal from further attack. It is important that this film exhibits a tenacious bond with the parent material and not be easily removed or soluble in the CTF. Successive wearing operations can destroy the film and result in a "pseudo-corrosion rate" which is due to the inability of the film to withstand the operation and not due to a basic incompatibility of the material. The ability of some metals such as Monel, copper, nickel, stainless steel, etc., to form this tenacious, passive, metal-fluoride film makes them resistant to attack by chlorine trifluoride. Among the metals mentioned, Monel and nickel are preferred because of their resistance to hydrogen fluoride and hydrogen chloride, which are formed by the reaction of chlorine trifluoride with water. Aluminum alloys, 18-8 stainless steels and K Monel have been used for bellows materials. Gaskets have been made from sterling silver and lead-indium alloys, copper braid backed in Teflon, and calcium fluoride filled Teflon. Tin, indium carbon and boron carbide have been used for rotating seals.

Table 3-19 lists those materials which are considered to be compatible with chlorine trifluoride under most conditions for long-term application. However, materials that are listed in the table must be thoroughly cleaned and passivated (in the case of metal) to insure a contamination-free surface. All chlorine trifluoride systems must also be dry and leak proof.

#### PHYSICAL PROPERTIES

Specific Gravity	1.83 (60°F)
Molecular Weight	92.46
Freezing Temperature °F	-105
Normal Boiling Point °F	53
Critical Temperature °F	345
Critical Pressure psia	838
Heat of Vaporization Btu/lb <sub>m</sub>	128

Discussion of Problem Areas -  
Chlorine Trifluoride (ClF<sub>3</sub>)

Organic Polymers (1-2)\* - Most organic polymers undergo spontaneous ignition and/or absorption of ClF<sub>3</sub> to form detonable mixtures, hence use of components incorporating plastic materials is not recommended. Teflon and Kel-F have been found acceptable under static propellant (nonflow) conditions; however, they may ignite when heated.

Wet and Dry Lubes (1) - No completely satisfactory lubricant is known. Most lubricants ignite spontaneously and/or form detonable mixtures with chlorine trifluoride. However, see remarks under fluorine.

Effects of Leakage (1) - Leakage cannot be tolerated in valves used with chlorine trifluoride. Although ClF<sub>3</sub> is nonflammable in air and exhibits excellent thermal stability at ambient temperatures, it does represent an extremely hazardous propellant due to its toxicity and extreme reactivity with the vast majority of organic and inorganic compounds. At elevated temperatures it will react vigorously with most common metals; the propellant readily ignites organic materials such as solvents and lubricants. Space leakage is discussed under hydrazine.

Soft Seats (1-2) - Soft seats made of plastic materials generally are unsuitable for service with chlorine trifluoride. Some success has been found using Teflon impregnated with 40% calcium fluoride.

Hard Seats (2) - A very limited number of soft metals (principally aluminum 1100 and copper) have been found satisfactory for valve seat use. The seats should be thoroughly cleaned and propellant passivated prior to installation.

---

\*Parenthetical enclosures refer to Propellant Rating Chart, Page 3-11.

TABLE 3-19. CHLORINE TRIFLUORIDE (ClF<sub>3</sub>)

<u>MATERIAL</u>	<u>TEMP °F</u>	<u>MATERIAL</u>	<u>TEMP °F</u>
<u>ALUMINUM ALLOYS</u>		<u>OTHER METALS</u>	
1060	85	A-Nickel	85
1100	85	Copper	85
2014	85	Incoloy	85
2024	85	Inconel	85
3003	85	Indium	
5052	85	Lead Indium Alloy	
6061 (Welded)	85	Tin Indium Alloy	
6063		Magnesium AZ-31B	85
6066		Magnesium HM-21A	85
356		Magnesium HK-31A	85
Tens 50		Monel	85
		K. Monel	
		Nitralloy	
		Silver Solder	
		Sterling Silver	
		Tin	
<u>STAINLESS STEEL</u>		<u>NON-METALS</u>	
301		Boron Carbide	
302		Carbon	
303	85	Kel-F (Under Static Cond. Only)	
304	85	Teflon (Under Static Cond. Only)	
316	85	Teflon-40% CaF <sub>2</sub>	
321			
347	85		
403	85		
PH 15-7 Mo	85		
410	85		

Note 1: Materials listed above are rated compatible based on a corrosion rate of less than 1 mil per year and the material does not cause decomposition, and is free from impact sensitivity. Non-metals are rated for satisfactory service for general use.

3.7.2.2 Chlorine Pentafluoride - Chlorine pentafluoride is among one of the most energetic oxidizers in use as a rocket propellant.

Immersion of TFE Teflon and Kel-F in liquid chlorine pentafluoride up to 86°F resulted in moderate weight gains, particularly for Kel-F. Complete and rapid reaction of columbium and molybdenum and degradation of blocks of carbon and graphite to powders resulted from immersion in this propellant. There was no change in titanium from immersion in chlorine pentafluoride, however. Ignition could not be initiated by impassing aluminum 2014-T6, magnesium AZ 31B, nickel 200, or 347 stainless at 65 ft-lbs in the liquid at 86°F. Teflon TFE violently reacted when impacted under similar circumstances with 410 stainless. Table 3-20 lists those materials which showed minimal corrosion rates at 86°F or 150°F.

Discussion of Problem Areas -  
Chlorine Pentafluoride

Organic Polymers (1-2)\* - Most organic polymers undergo spontaneous ignition and/or absorption to form detonable mixtures, hence use of components incorporating plastic materials is recommended. Teflon TFE and FEP have been found satisfactory under static propellant conditions; however, they may ignite when heated or impacted.

Wet and Dry Lubes (1) - No completely satisfactory lubricant is known. Most lubricants ignite spontaneously and/or form detonable mixtures.

Effects of Leakage (1) - Leakage through valves presents a serious hazard, due to its toxicity and reactivity with most known materials. In addition, the effect of leakage is usually to increase the size of the leakage passage and thus present an increasing exposure threat to its surrounding environment. Space leakage is discussed under hydrazine.

Soft Seats (1-2) - Soft seats made of plastic are unsuitable for service.  $\text{CaF}_2$  - filled Teflon might be applicable under special conditions.

Hard Seats (2) - No data is available, but probably valve seats found suitable for use in the more energetic oxidizers would prove satisfactory.

---

\*Parenthetic enclosures refer to Propellant Rating Chart, Page 3-11.

TABLE 3-20. CHLORINE PENTAFLUORIDE

MATERIAL	CORROSION RATE	
	MPY 86°F	(21 day storage) 150°F
Aluminum 2014-T6	0.03	0.00
Aluminum 6061-T6	0.01	0.00
Yellow Brass, 1/2 Hard	0.13	0.66
Copper ETP, Soft Temper	0.07	0.17
Magnesium AZ 31B-0	0.06	0.07
Monel 400, Annealed	0.00	0.00
Nickel 200, Annealed	0.00	0.01
347 SS, Hot-rolled	0.00	0.00
410 SS, 180-200 ksi T.S.	0.00	0.67

3.7.2.3 Oxygen Difluoride (OF<sub>2</sub>) - Oxygen difluoride is a colorless gas at room temperature and atmospheric pressure, condensing to a yellow liquid at -229°F. It has a foul odor. The limit of detectability appears to be in the range of 0.1 ppm; 0.5 ppm in air is easily detected. Based on present knowledge, oxygen difluoride must be regarded as a highly toxic gas, possessing the same lethal characteristics as phosgene.

Oxygen difluoride is a powerful oxidizing agent similar to fluorine and the halogen fluorides, but is generally considered to be much less reactive than fluorine. It is capable of reacting with a majority of inorganic and organic compounds provided sufficient activation energy is available.

When reaction with OF<sub>2</sub> occurs, high heats of reaction are common, many sufficiently energetic to cause ignition. Reports on hypergolicity of fuels such as hydrazine, ammonia and monomethylhydrazine give varying conclusions; hence, the materials should be treated as potentially hypergolic at all times. Oxygen difluoride and diborane are unquestionably hypergolic. Oxygen difluoride is a relatively stable compound in that it does not detonate by sparking and was found to be insensitive to shock at -320°F. It does, however, begin to decompose thermally at approximately 480°F.

The data for materials compatibility are limited but they do show that no major problems are to be expected with the majority of metals. It has been reported that a few metals including Titanium 110 AT, tantalum, magnesium and lead, exhibit moderate-to-violent reactions when subjected to shock loading in the presence of OF<sub>2</sub>, but the data is limited and somewhat inconclusive. Some references indicate both magnesium and titanium can be utilized, whereas others reject these metals due to impact sensitiveness. In no cases, however, has titanium demonstrated shock sensitivity to the point of flame propagation, as it does with oxygen.

Another important aspect to be considered is the purity of  $OF_2$ . In "pure"  $OF_2$ , titanium exhibits one of the lowest corrosion rates of all metals; however, in doped  $OF_2$ , particularly with  $O_2$  and HF present, extensive corrosion occurs, General Reference 20. Thus, more complete testing with actual propulsion components is indicated.

In like manner, Teflon, Kel-F and graphite indicate shock sensitivity. Parts made of these materials are not suitable for  $OF_2$  applications if shock or impact loading is a requirement. On the other hand, there exists some service experience with valves containing fluorinated polymers such as Teflon, Alcar and Halon in contact with the liquid phase.\* These data are insufficient, but results are reported to be encouraging. Oxygen difluoride can be handled readily in most common metals and glass, with the choice dependent upon the service requirement. Metals such as stainless steel, copper, aluminum, Monel, and nickel may be used for gas and liquid service from cryogenic temperatures to approximately 400°F.

Table 3-21 lists the materials considered to be compatible with oxygen difluoride. Tests were conducted with liquid  $OF_2$  at -109°F.

#### PHYSICAL PROPERTIES

Specific Gravity	1.496 (-288.8°F)
Molecular Weight	54.00
Freezing Temperature °F	-370.8
Normal Boiling Point °F	-288.6
Critical Temperature °F	-72.8
Critical Pressure psia	719

---

\*Although most data indicate that these materials are recommended for gas phase service only.

Discussion of Problem Areas -  
Oxygen Difluoride (OF<sub>2</sub>)

Ceramics (2)\* - Oxygen difluoride exhibits a strong oxidizing power similar to that of fluorine, and thus reacts with the vast majority of inorganic and organic materials. Extreme care should be taken to select materials compatible with the propellant under the temperature extremes of its environment.

Organic Polymers (2) - Polymers such as Teflon (TFE and FEP), Kel-F-81, the fluorosilicones, the vinyl silicone elastomers and Cis 1-4 polybutadiene have been utilized for limited service at moderate temperatures.

Wet and Dry Lubes (1) - There is no known lubricant for use in contact with liquid or gaseous oxygen difluoride. Because of the high reactivity of OF<sub>2</sub> with organic materials, conventional lubricants should definitely be avoided. Even the most likely candidates, the normally unreactive perfluorinated hydrocarbon lubricants, are degraded in the presence of liquid or gaseous OF<sub>2</sub>. It is therefore recommended that all valves be designed so as to eliminate the use of a lubricant in intimate contact with this oxidizer.

Soft Seats (1) - Soft seat materials are often used at cryogenic temperatures, however, this use is normally limited to polymers rather than elastomers. Extreme care must be used with polymers in OF<sub>2</sub> service due to possible reaction with the propellant. The use of polymers should be limited to static seals not exposed to the flow stream. All metal valves with metal to metal seats are preferred.

Effects of Leakage (1) - Oxygen difluoride displays properties similar to those of liquid fluorine, but is generally considered to be less reactive and easier to handle. It is a relatively stable material in that it does not detonate by sparking, but it does begin to decompose thermally at elevated temperatures (about 480°F). Tests of reactivity to fuels such as hydrazine, ammonia, and monomethylhydrazine have given varied results as to its hypergolic nature. However, it should be assumed that the oxidizer is hypergolic with all fuels because of its very strong oxidizing power. The data on toxicity are quite limited, but OF<sub>2</sub> must be regarded as a highly toxic material, similar to phosgene. Space leakage problems are similar to those discussed for hydrazine.

---

\*Parenthetical enclosures refer to Propellant Rating Chart, Page 3-11.



TABLE 3-21. OXYGEN DIFLUORIDE  
 COMPATIBILITY OF MATERIALS AT -109°F<sup>(a)</sup>

<u>MATERIAL</u>	<u>MATERIAL</u>
<u>METALS</u>	<u>OTHER METALS</u>
<u>ALUMINUM</u>	PH 15-7 Mo
1100-0	AM-350
2014-T6	Nickel 200
2219-T6	Inconel X
6061-T6	Rene 41
7079-T6	Cufenloy 40
	Cufenloy with electroless Ni plate
<u>STAINLESS</u>	Copper
301	Brass 7030
316	Columbium
347	
410	

(a) Metals listed above are rated compatible based on a corrosion rate of less than 1 mil per year, and the material does not cause decomposition and is free of impact sensitivity.

COMPATIBILITY OF MATERIALS FOR SHORT TERM USE

<u>MATERIAL</u>	<u>REMARKS</u>
<u>ALUMINUM ALLOYS</u>	
2024-T3	*
2024-T3 (Alclad)	*
<u>STAINLESS STEEL</u>	
301	*
304	
Maraging AM 355	*(No change for gas at ambient temperature)
Maraging AM 367	*

\*Fluoride coatings formed, but weight gain was considered insignificant.

OXYGEN DIFLUORIDE  
 COMPATIBILITY OF MATERIALS FOR SHORT TERM USE  
 (Continued)

<u>MATERIAL</u>	<u>REMARKS</u>
<u>OTHER METALS</u>	
Beryllium Copper (2%)	*
Inconel X750	
Magnesium AZ 31B, H24	*
Monel 400	*
Monel K500	*
Titanium Alloy 5Al-2.5 Sn	**
 <u>NON-METALS</u>	
Glass	Above 390°F, glass is attacked by OF <sub>2</sub>

\*Fluoride coatings formed, but weight gain was considered insignificant.  
 \*\*May be impact sensitive

INCOMPATIBLE MATERIALS\*

<u>INCOMPATIBLE METALS</u>	<u>INCOMPATIBLE NON-METALS</u>
Lead	Graphite
	Teflon TFE
Tantalum	Teflon FEP
	Kel-F 5909
Magnesium HM21A-T8	Kel-F Resin
	Oxylube 701

\*Incompatibility with OF<sub>2</sub> is based on impact sensitivity.

3.7.2.4 Perchloryl Fluoride (PF) ( $\text{FClO}_3$  or  $\text{ClO}_3\text{F}$ ) - Perchloryl fluoride is a colorless gas at ambient conditions with a characteristic sweetish odor. Under pressure or low temperature it is storable in liquid form. The toxic action of perchloryl fluoride is derived from its pronounced oxidizing properties and results in respiratory irritation, oxidation of hemoglobin and absorption of fluoride into the body. The toxicity threshold limit for perchloryl fluoride in air is 3 ppm.

Perchloryl fluoride is thermally stable up to 849°F in absence of air. It is nonflammable but, being a strong oxidizing agent, readily supports combustion of many organic materials. Although not shock sensitive itself, in combination with porous organic or inorganic materials it can produce a potentially shock-sensitive mixture. Combinations of perchloryl fluoride and most rocket fuels constitute explosion hazards.

Reactions of perchloryl fluoride with water is very slow up to about 575°F. However, in the presence of water, perchloryl fluoride becomes more corrosive. The corrosion resistance of metals of construction therefore depends largely on the quantity of moisture present, hence selection must be governed by the moisture content. Under moisture conditions, types 304, 310, and 314 stainless steel have shown good resistance at room temperature.

Teflon and Kel-F are very resistant to attack by perchloryl fluoride. Other plastics which are suitable are unmodified phenolic resins and epoxy resins. Under mild conditions of heat shock, Teflon, Kel-F and Kaynar can be used, but may undergo structural changes when moderate amounts of perchloryl fluoride are absorbed. These plastics should not be used under dynamic flow conditions such as would result in their use with valves, since the resultant swelling of seal materials so constituted presents problems of physical interference.

Table 3-22 lists materials suitable for use with perchloryl fluoride.

#### PHYSICAL PROPERTIES

Specific Gravity	1.69 (-52.2°F)
Molecular Weight	102.457
Freezing Temperature °F	-231
Normal Boiling Point °F	-52.2
Critical Temperature °F	202
Critical Pressure psia	779
Heat of Vaporization Btu/lb <sub>m</sub>	84.0

Discussion of Problem Areas -  
Perchloryl Fluoride (FC10<sub>3</sub>)

Metals (2-3)\* - Although anhydrous perchloryl fluoride (less reactive and corrosive than other halogen-containing oxidants) at ordinary temperatures is not reactive to most common metals, selection of a metal for use with this propellant should be governed by the moisture content. In the presence of water, perchloryl fluoride is corrosive to most metals. The readily oxidized metals will burn in perchloryl fluoride under severe conditions; therefore, extreme care must be taken in selecting metals with thorough knowledge of propellant purity, compatibility, and potential environmental extremes.

Organic Polymers (2) - Many organic materials do not react with perchloryl fluoride at ambient temperature, but if ignited, will burn violently; some are hypergolic. Hence, materials compatibility is extremely important in the selection of a polymeric material. Teflon and Kel-F appear to be resistant to attack, but tend to absorb the fuel. Some phenolic and epoxy resins have found limited use.

Wet and Dry Lubes (1-2) - Fluorocarbons are the only suitable lubricants. Perchloryl fluoride must not be brought into contact with any other conventional valve grease or oil.

Effects of Leakage (1-2) - Perchloryl fluoride leakage represents an acute toxic hazard. Because of its strong oxidizing effect, it readily supports combustion with oxidizable materials such as organic compounds; it is hypergolic with some fuels such as hydrazine, and in combination with most other fuels may detonate. Space effects of leakage are discussed under hydrazine.

Soft Seats (2) - Teflon and Kel-F seats are recommended for limited use; however, consideration must be given to their ability to absorb perchloryl fluoride.

---

\*Parenthetical enclosures refer to Propellant Rating Chart, Page 3-11.

TABLE 3-22. PERCHLORYL CHLORIDE  
 COMPATIBILITY OF MATERIALS FOR  
 LONG TERM APPLICATION (NOTE 1)

<u>MATERIALS</u>	<u>TEST TEMP °F</u>	<u>MATERIALS</u>	<u>TEST TEMP °F</u>
<u>ALUMINUM ALLOYS</u>		<u>MAGNESIUM ALLOYS</u>	
1060	85	AZ-31B	85
1100	85	HK-31A	85
2014	85	HM-21A	85
2024	85		
3003	85	<u>NICKEL ALLOYS</u>	
5052	85	"A" Nickel	85
6061	85	Nickel 200	85
7079	85	Inconel	85*
		Incoloy	85*
		Monel	85
		Ni-o-Nel	85*
<u>STAINLESS STEELS</u>		<u>LOW CARBON STEELS</u>	
304	85*	1010	85
316	85*	1010 (Coated w/Fosbond 40)	85
347	85	1010 (Coated w/Fosbond 27)	85
403	85		
410	85		
Carpenter No. 20-Cb	85*		
PH 15-7 Mo (Cond. RH 950)	85		
PH 15-7 Mo (Cond. TH 1050)	85		
AM 350 (Welded)	85		
<u>COPPER ALLOYS</u>		<u>MISCELLANEOUS METALS</u>	
Aluminum Bronze, 8% Ampco 8	85	Gold	85*
Beryllium Copper, 2%	85	Platinum	85*
Nickel Silver, 18% Alloy A	85	Silver	85*
Phosphor Bronze, 5% Grade A	85		
Rule Brass	85		
Yellow Brass	85		
Copper, ETP	85		
Copper, DHP	85		
		<u>PLASTICS AND ELASTOMERS</u>	
		Teflon	
		Kel-F	
		Polyethylene	

\*Moisture content to 1%.

NOTE 1: Metals listed above are rated compatible based on a corrosion rate of less than 1 mil per year and the material does not cause decomposition, and is free from impact sensitivity. Non-metals are rated for satisfactory service for general use.

### 3.7.3 Nitrogen-Fluorine Compounds

This family of chemical compounds includes three oxidizers which have limited usage as storable propellants. Included are nitrogen trifluoride ( $\text{NF}_3$ ), tetrafluorohydrazine ( $\text{N}_2\text{F}_4$ ) and nitryl fluoride ( $\text{NO}_2\text{F}$ ). Usage is limited because these oxidizers present most of the normal problems associated with corrosive cryogenic propellants but do not yield as high a specific impulse as other oxidizers such as liquid fluorine and oxygen difluoride. The main interest in these oxidizers stems from the fact that they have become building blocks toward the production of other N-F compounds that have higher boiling points, hence, are more easily storable. Inasmuch as compatibility data is limited, separate compatibility tables are not included, but discussed under each propellant.

3.7.3.1 Nitrogen Trifluoride ( $\text{NF}_3$ ) - Nitrogen trifluoride is a colorless gas at room temperature and atmospheric pressure which condenses to a liquid at  $-200^\circ\text{F}$ . As a gas it is fairly stable and noncorrosive. As a liquid it is similar to liquid fluorine in that it is highly reactive with certain fuels. Materials compatibility is very limited. Glass, stainless steel, nickel, copper and monel are suitable for use with this oxidizer.

3.7.3.2 Nitryl Fluoride ( $\text{NO}_2\text{F}$ ) - Nitryl fluoride is a gas at room temperature and atmospheric pressure which condenses to a liquid at  $-82^\circ\text{F}$ . It is highly reactive, even attacking glass. Reaction with metals and nonmetals differs from the above two oxidizers because of the oxygen present. Most metals, including aluminum, steel, and titanium react to form both an oxide and a fluoride. Most nonmetals react to form nitronium salts. Beryllium, magnesium, and gold do not react with nitryl fluoride below  $300^\circ\text{F}$ .

3.7.3.3 Tetrafluorohydrazine ( $\text{N}_2\text{F}_4$ ) - This oxidizer is similar to nitrogen trifluoride but is slightly heavier. At room temperature and atmospheric pressure it is a gas, and condenses to a liquid at  $-100^\circ\text{F}$ . Compatibility data is scarce, but will be similar to that supplied for  $\text{NF}_3$ .

### 3.8 HARD CRYOGENICS

#### 3.8.1 Liquid Fluorine (LF<sub>2</sub>)

Fluorine is the most powerful chemical oxidizing agent known. It reacts with practically all organic and inorganic substances, with a few exceptions being the inert gases, some metal fluorides and a few uncontaminated fluorinated organic compounds. It exhibits excellent thermal stability and resistance to catalytic breakdown, thereby presenting little or no problem in these areas. Compatibility ratings are, therefore, based primarily on the reaction of the fluorine with the various materials used.

Although fluorine is the most chemically reactive of all elements, many of the common metals can be considered for use in liquid fluorine service.

Fluorine is a liquid at atmospheric pressure only in the short temperature range of -306°F to -363°F, therefore requiring insulation of all valves. At these low temperatures chemical reactions in general tend to take place rather slowly, thus corrosive attack by the liquid fluorine is generated at a slower rate. Another factor responsible for low rate of attack by liquid fluorine on the common metals is that protective films of fluoride compounds tend to form on metal surfaces and act as a barrier to further reaction. These films, however, must be tenaciously held by the parent material in order to retain their effectiveness.

The effectiveness of the protective film formed on the metals by the liquid fluorine also is based on the solubility of the various metal fluorides that form in the film in fluorine. It is believed that, as a protective film builds up and the rate of reaction slows down, an equilibrium between reactive rate and solubility of the film will be reached and a relatively steady corrosion rate will result. Lack of solubility data for fluorine compounds and corrosion rates for long periods of exposure can only be supplemented by actual service data and extrapolation of existing data. Service data indicate that the fluorides of nickel, copper, chromium and iron are relatively insoluble in liquid fluorine. Also, metals such as Monel, nickel and stainless steels exhibit satisfactory performance in liquid fluorine and indications are that much lower rates of corrosion can be expected for long-term exposure where equilibrium rates are reached, than for short-term laboratory exposure. Some experiments, however, have shown that there is no increased corrosion of specimens immersed in liquid fluorine and wirebrushed to remove any films. This suggests that either not all the passivating effect is from formation of a metal fluoride film, or that the thickness of the film necessary for protection can be extremely thin.

Several lightweight metals such as the alloys of aluminum, titanium and magnesium are also known to produce protective films in liquid fluorine. Of these, titanium probably exhibits the lowest rate of corrosion; however, tests have shown it to be impact sensitive in fluorine, but tests have not demonstrated flame propagation as with oxygen.

Other factors to consider in selecting materials for use in a liquid fluorine system are: 1) flow rates, 2) water contamination in the system, and 3) mechanical properties of the material at the low temperatures experienced with liquid fluorine. The rate of flow of the liquid fluorine in a valve and through an orifice is considered to be an important factor in maintaining the protective film on the materials being attacked. Fluoride coatings on some metals that are less resistant to fluorine, such as low-alloy steels, are sometimes very brittle or porous and powdery. High flow rates tend to remove these coatings and thus increase corrosive action. In restricted flow applications "flaking" of the coating may result in contamination of the propellant, thus creating leakage problems at the valve seat.

Teflon has withstood exposure to liquid fluorine in a static condition. However, Teflon tends to react with fluorine to break down the polymers and form unsaturated low molecular weight fluorocarbons which do not adhere to the surface. Any flow of the propellant or movement of material over the surface of Teflon will remove these fluorocarbons, thus leaving them valueless as a protective film. Impurities introduced in the manufacturing process appear to be responsible for accelerated decomposition of Teflon in liquid fluorine service.

Fluorine will react with any water present in the system to form hydrofluoric acid. This acid tends to attack some materials that are normally resistant to uncontaminated fluorine. Of all the metals showing resistivity to fluorine attack, Monel is generally preferred for use because of its inherent resistivity to the hydrofluoric acid.

In selecting materials for use in fluorine systems, consideration should also be given to the effects of flow temperature environment on the mechanical properties of the materials. Some metals, such as the martensitic stainless steels, become brittle at these low temperatures.

Table 3-23 lists those materials which are considered to be compatible for service with liquid fluorine. However, as previously stated, insufficient information on prolonged usage of these materials in liquid fluorine restricts any rating for long-term application. Also, before using any material with fluorine, extreme care should be exercised in cleaning the material thoroughly to remove all possible contamination that may be present. Pre-treatment or conditioning treatment is also recommended. After thoroughly cleaning the material, a conditioning treatment exposes the material at room temperature to pure fluorine gas or a mixture of fluorine diluted with an inert gas. This, it is believed, initiates the formation of a relatively inert fluoride film. With the use of a diluted gas, the reaction that may take place with any traces of contamination remaining after cleaning would be less violent in nature. This treatment will then permit the material to withstand attack by full strength fluorine with much less reaction.



## PHYSICAL PROPERTIES

Specific Gravity	1.69 (-52.2°F)
Molecular Weight	102.457
Freezing Temperature °F	-231
Normal Boiling Point °F	-52.2
Critical Temperature °F	202
Critical Pressure psia	779
Heat of Vaporization Btu/lb <sub>m</sub>	84.0

### Discussion of Problem Areas - Liquid Fluorine (F<sub>2</sub>)

Ceramics (2-3)\* - There are few ceramic materials which are completely satisfactory for use with liquid fluorine, although some have found limited use. Ceramic materials such as calcium fluoride and alumina are resistant to attack by gaseous fluorine even at high temperatures, but these lack mechanical strength. Both materials exhibited corrosion rates lower than metals tested at the same temperature and can be used where physical properties of ceramic materials can be tolerated. Recent work using TiC cermet and fused coatings of CaF<sub>2</sub> + LiF + NiF<sub>2</sub> on alumina has been encouraging.

Organic Polymers (1-2) - Organic polymeric materials are generally not suitable for service in liquid fluorine. Some fluorinated polymers have found limited service at moderate pressures with gaseous fluorine. Impurities introduced in the manufacturing process appear to be responsible for accelerated decomposition of Teflon in liquid fluorine service.

Lubricity (1-2) - Recent work at NASA Lewis on pumping of liquid fluorine has shown excellent results using liquid fluorine as the lubricant and alumina and titanium carbide as the rotating shaft seals. These materials showed no reaction with liquid fluorine and adequately performed their functions as seal materials.

Effects of Leakage (1) - Leakage of fluorine represents potential toxic, fire, and explosion hazards. The threshold limit value of fluorine is 0.1 ppm; it reacts vigorously with most substances at ambient temperatures, frequently with immediate ignition. Space leakage of propellants is discussed under the section for hydrazine.

Soft Seats (1-2) - Under static conditions, fluorocarbon plastics are satisfactory for liquid fluorine service. Limited applications of some fluorinated soft seat materials (Teflon) have been found for dynamic flow conditions; however, it is recommended that the material be shielded and a minimum of surface area exposed to liquid fluorine.

---

\*Parenthetical enclosures refer to Propellant Rating Chart, Page 3-11.

Hard Seats (2) - Valves having metal-to-metal seats have been used quite extensively in handling fluorine. It is desirable to use dissimilar materials to obtain a good seal and to prevent galling or binding when the valve is operated. Because metal valve seats are not as leak tight as those which utilize a resilient material, the use of double valving is recommended for critical applications.

Disconnect (2) - Further availability tests and evaluations are required before a more realistic prediction of performance can be made. Icing due to water vapor in the atmosphere can cause problems in disengagement of the separable units.

TABLE 3-23. LIQUID FLUORINE (LF<sub>2</sub>)  
COMPATIBILITY OF MATERIALS

<u>ALUMINUM ALLOYS</u>	<u>TEMP °F</u>	<u>CLASS</u>	<u>OTHER METALS</u>	<u>TEMP °F</u>	<u>CLASS</u>
1100	-320	1	A-Nickel	-320	1
2017	-320	11	Brass (Yellow)	-320	1
5052	-320	11	Brass (Cartridge)	-320	1
6061	-320	1	Brass (Casting)	-320	11
7079	-320	1	Copper	-320	1
			Copper-10% Nickel	-320	1
			Copper-30% Nickel	-320	1
<u>STAINLESS STEELS</u>			Everdur 1010	-320	1
304	-320	1	Magnesium Alloy		1
316	-320	1	AZ-31	-320	
347	-320	1	Magnesium Alloy		
410	-320	1	HK-31	-320	1
420	-320	1	Magnesium Alloy		
PH 15-7 Mo	-320	1	HM-31	-320	1
AM 350-C,CX,D,DX	-320	1	Monel	-320	1
Carpenter 20	-320	1			

NOTE: Materials listed above are rated compatible based on corrosion resistance and shock sensitivity; they do not include effects of cryogenic temperatures on the materials mechanical properties.

Class 1 Metals listed above are rated compatible based on a corrosion rate of less than 1 mil per year and the material does not cause decomposition, and is free from impact sensitivity. Nonmetals are rated for satisfactory service for general use.

Class 11 Materials which exhibit corrosion rates as great as 5 mils per year.

### 3.8.2 Liquid Oxygen (LOX)

Liquid oxygen is a non-toxic, nonflammable, and non-explosive oxidizing agent having a reactivity much lower than gaseous oxygen. Mixing of liquid oxygen with a hydrocarbon fuel will cause the latter to solidify. The resulting mixture is extremely shock sensitive.

Most metals are not corroded by liquid oxygen; however, the low temperature of liquid oxygen (-300°F) does cause embrittlement of some metals, especially the body-centered ferrous alloys. As a result, the alloys most commonly used in liquid oxygen handling equipment are nickel, Monel, copper, aluminum, the 300-series of stainless steels, brass, and silver solder.

Of all the metals studied to date, titanium exhibits the greatest sensitivity to impact when immersed in LOX. Battelle Memorial Institute studied the reactivity of metals with liquid and gaseous oxygen and found that only zirconium shows similar reactions to that of titanium. Aluminum and the stainless steels were found to exhibit almost no reactivity in oxygen, although aluminum will ignite under conditions of high explosive shock. Magnesium shows reactivity to explosive shock lying about midway between that of aluminum and titanium. Following is a partial summary of the results reported by Battelle for titanium.

The sensitivity of titanium approaches that of many organic materials, particularly when the surfaces are not completely cleaned or particles of dirt or grit are present. Reactivity is observed in liquid oxygen and mixtures of liquid oxygen and liquid nitrogen and mixtures of liquid oxygen and liquid nitrogen at impact forces of 20 ft-pounds until the LOX concentration is reduced to 30 percent. Titanium can be partially protected from reactivity in LOX under impact by certain protective coatings, provided these coatings are not broken. Electroless copper and nickel coatings are best, although protection also is provided by nitroding which adds a protective film, and by annealing which increases the oxide film thickness.

When a titanium vessel containing LOX or gaseous oxygen is ruptured by a bullet, a simulated micrometeoroid, or other mechanical puncture, violent burning begins at almost zero pressure (gauge). If the vessel is not fractured by application of external impact, vibration, acoustic or thermal energy, no reactivity is noted. Slowly propagated cracks, such as fatigue cracks, also do not cause reactivity.

The mechanism for the Ti-O<sub>2</sub> reaction is described as a reaction between a freshly formed titanium surface and gaseous oxygen. Titanium exhibits no great reactivity in LOX when deformed by compression, by exposure of a fresh surface by machining or rupture, or by exposure of bulk titanium to high-pressure or high-velocity LOX. In gaseous oxygen, however, titanium is highly reactive when a freshly formed surface is exposed at even moderate pressures. Under conditions of tensile rupture, a pressure of approximately 100 psig will initiate a violent burning reaction with titanium from about -250°F up to room temperature. When 2 percent HF is added as an inhibitor or 5 percent argon as a diluent, the pressure must be increased approximately twofold at room temperature before reaction occurs. Titanium could not be made to react even at very high pressure when the oxygen content was 35 percent or less.

All valves require insulation to avoid evaporation losses. Drainage of condensed water on valves should be provided to avoid water entrapment which may cause corrosion, or valve malfunction if the water refreezes.

Discussion of Problem Areas -  
Liquid Oxygen (O<sub>2</sub>)

Organic Polymers (2)\* - Organic materials should be avoided whenever possible with both liquid and gaseous oxygen because of possibilities of explosion. Currently there are no tests which give a reliable compatibility rating for organic materials in liquid oxygen. Although there are several lists of organic materials rated as suitable for use with liquid oxygen, specific conditions such as compatibility, impact sensitivity, and embrittlement at cryogenic temperatures should be thoroughly and carefully studied before any organic material is utilized. Sources of energy also may be from operation of mechanical parts, such as 1) heat produced by friction of metal surfaces, 2) heat from shearing of liquids, 3) shock waves, and 4) heat generated by the catalytic breakdown of an organic material in contact with the metal surface, etc.

The most reliable organic materials for liquid oxygen applications are the fluorinated organic compounds (the more highly fluorinated the compound, the more stable\*\* to attack by liquid oxygen). In special applications many other organic compounds are used, even though these materials have shown to be sensitive to LOX. However, investigations with satisfactory testing procedures are needed before organic materials can be used with liquid oxygen with any great assurance of success.

Currently, there is no single test or group of tests which gives a reliable, uniform compatibility rating for materials suitable for use with liquid oxygen because of difficulty in determining impact sensitivity. Much of the data which are available were based on the ABMA 70 ft-lb acceptance level for impact sensitivity. This requirement was designed for application to materials used in missiles, based on the impact threshold level of a particular lubricant which, at the time, was considered to be the only safe available lubricant. Because of the lack of a technical basis for the establishment of the 70 ft-lb as an acceptance test parameter, and because the size, shape and cleanliness of the sample and test apparatus, as well as the design of the testing machine affect the detonation results, little can be assigned to published compatibility tables. Battelle has indicated that Teflon and Kel-F are the preferred plastics; with a combination of the two most desirable from the standpoint of ductility and strength. Picatinny reports that a polyurethane adhesive has been found to be LOX compatible under ABMA procedure. A TFE-FEP hot melt adhesive was also reported to be the only insensitive adhesive when used in direct contact with LOX, but requires a 700°F bonding temperature. Because of the apparent need of individual use-tests for each design, no compatibility tables are included in this report.

\*Parenthetical enclosures refer to Propellant Rating Chart, Page 3-11.

\*\*The word stable here is more applicable than resistant because it deals with impact sensitivity and not resistance to corrosion.

Wet and Dry Lubes (1)\* - No completely compatible lubricants have been found. Selected perfluorinated hydrocarbon and dry lubricants have found limited use; however, the possibility of detonation still exists.

Lubricity (2) - Satisfactory low-load, short-life bearing and gear operation was possible where liquid oxygen was used as a lubricant. While some of the metals of construction proved satisfactory for use with liquid oxygen, others, under stress, tend to become brittle.

Effects of Leakage (2) - Liquid or gaseous oxygen does not display hazards similar to those encountered with most other oxidizers. Pure oxygen is incapable of burning or detonating, but mixed with a material that will burn, the resulting fire is intensified. Gaseous mixtures of oxygen and fuels form a potentially dangerous mixture which can be ignited by any form of spark. Liquid oxygen, when in contact or mixed with any form of combustible material, such as fuels, wood, plastics, oil, lubricants, or paper, forms an explosive mixture and even when frozen may be detonated by static electricity, mechanical shock, or similar energy source. Oxygen is non-toxic; however, contact with liquid or gaseous oxygen close to its boiling temperature will cause severe frostbite. Space conditions and leakage are discussed under this section for hydrazine.

Soft Seats (2) - Because of the composition of soft seat materials, they should be avoided in liquid oxygen service. Although some fluorinated plastics have been found reliable, until satisfactory testing procedures are available, there remains doubt about compatibility tests.

Disconnects (2) - Pneumatically operated disconnected valves used on missiles presented problems due to icing caused by condensed water vapor in the atmosphere, requiring extensive effort to disengage. In space transfer of the propellant, "freeze-up" should not be a problem due to the absence of water vapor in space atmospheres. Disconnects of the pull-away type during liftoff caused few problems, except for minor leakage.

### 3.8.3 Liquid Hydrogen (H<sub>2</sub>)

Liquid hydrogen is a colorless, odorless liquid that normally does not present an explosive hazard when it evaporates and mixes with air in an unconfined space. However, an unconfined mixture of hydrogen gas and air will burn if exposed to an ignition source such as a spark. Liquid hydrogen is not in itself explosive, but reacts violently with strong oxidizers. If it is contaminated with oxygen, it becomes unstable and an explosion is likely to occur. Reaction with fluorine and chlorine trifluoride is spontaneous. Two species of liquid hydrogen exist: ortho-hydrogen and para-hydrogen.

---

\*Parenthetical enclosures refer to Propellant Rating Chart, Page 3-11.

At the low temperature (-423°F) at which hydrogen is a liquid, corrosive attack on materials is not considered to be an important factor in selecting materials to be used. A more important factor in selecting the materials for use with liquid hydrogen is the embrittlement of some materials by the low temperature of the liquid. Embrittlement of some materials by the low temperature of the liquid requires selection of materials on the basis of their structural properties, i.e., yield strength, tensile strength, ductility, impact strength, and notch sensitivity. The materials must also be metallurgically stable so that phase changes in the crystalline structure will not occur either with time-or temperature-cycling. It is known that body-centered metals (such as low-alloy steels) undergo a transition from a ductile to brittle behavior at low temperatures; therefore, such metals are generally not suitable for structural applications at cryogenic temperatures. Face-centered metals, such as the austenitic stainless steels, normally do not show a transition from a ductile to a brittle behavior at low temperatures. For this reason, these types of materials are desirable for use in cryogenic applications; however, care should be exercised in selection of face-centered metals. Low temperature toughness is not a characteristic of all face-centered metals, nor is it a characteristic of all conditions of a specific metal. For example, severely cold-worked or sensitized (carbide precipitation at grain boundaries) austenitic stainless steels can become embrittled at low temperatures.

Table 3-24 lists those materials which are considered to be compatible with liquid hydrogen for long-term application.

Discussion of Problem Areas -  
Liquid Hydrogen (H<sub>2</sub>)

Organic Polymers (1-2)\* - The ability of polymeric materials to maintain satisfactory physical properties and to withstand thermal stress caused by large temperature changes is of prime importance. The use of a selected few organic plastics is thus limited to service where embrittling effect at the low temperatures of liquid hydrogen is minimized. Specifically, lip seals constructed of Teflon and Kel-F, static seals and some rubbers, and diaphragm seals from Mylar have proven serviceable. Studies at the National Bureau of Standards have shown that some elastomeric seals under compression retain their sealing capabilities effectively well below the normal brittle point of the polymer without compression.

Wet and Dry Lubes (1) - Lubricants are generally not practical in the presence of liquid hydrogen since they solidify and become brittle at the temperatures involved.

Lubricity (2) - Liquid hydrogen can be utilized as a lubricant under low-load, short-life conditions. Severe surface failure will occur, however, if the service conditions are such that local heating of the contact surface is allowed. The stainless steels are particularly susceptible to surface failure, as are other materials with low thermal conductivities.

---

\*Parenthetical enclosures refer to Propellant Rating Chart, Page 3-11.

(Wear rates are reduced drastically by coating one of the surfaces with Teflon or Kel-F). Coldwelding has also been found to occur in gate valves having seats and wedges of 304 stainless in cryogenic service.

Effects of Leakage (2)\* - The leakage of hydrogen gas does not appear to present problems of an unusual nature, even though the composition limits for combustion are very wide. Hydrogen, being very light, tends to dissipate rapidly. Proper ventilation and elimination of sources of ignition reduce danger of detonation. An explosion hazard exists when the hydrogen-air mixture is completely or partially confined. Effects of leakage in space are discussed under this section for hydrazine.

Disconnects (2) - See comments under Liquid Oxygen.

TABLE 3-24. LIQUID HYDROGEN (H<sub>2</sub>)

COMPATIBILITY OF MATERIALS  
FOR LONG-TERM APPLICATION

<u>ALUMINUM ALLOYS</u>	<u>OTHER METALS</u>
1100	Molybdenum
1100T	Nickel
2024T	Monel
4043	Inconel
5052	Low Carbon Steel
	High Nickel Steel
	Titanium
<u>STAINLESS STEEL</u>	<u>NON-METALS</u>
301	Nitryl Rubber
302	Silicone Rubber
303	Teflon
304	Garlock Packing
304L	Bakelite
316	Micarta
321	Lucite
347	Graphite
410	
Haynes 21	

NOTE: The above listed materials were rated compatible primarily for their embrittlement properties at cryogenic temperatures. Non-metals shown as being compatible should be restricted for "warm" joint application or equivalent.

\*Parenthetical enclosures refer to Propellant Rating Chart, Page 3-11.

### 3.8.4 Liquid Oxygen-Liquid Fluorine Mixtures (FLOX)

Mixtures of liquid fluorine and liquid oxygen (FLOX) have received some consideration as oxidizers. A typical mixture contains 80 percent fluorine and 20 percent oxygen. There is limited compatibility data for these mixtures, but results of work done at various installations suggests that any material that performs well in liquid fluorine service will also work in FLOX. Evaluation of Atlas components showed no serious problems, except for the replacement of valves with constricted passageways.

The problem areas for FLOX are considered to be the same as those for fluorine, and the reader is referred to that section. Table 3-25 lists the limited compatibility data accumulated to date for FLOX.

TABLE 3-25. LIQUID FLUORINE-LIQUID OXYGEN (FLOX)  
COMPATIBILITY OF MATERIALS AT  $-320^{\circ}\text{F}^{(a)}$

FLOX-40 (40%F<sub>2</sub> - 60% O<sub>2</sub>)

FLOX-20 (20% F<sub>2</sub> - 80% O<sub>2</sub>)

MATERIAL

MATERIAL

Aluminum 2014-T6

Aluminum 2014

Aluminum 5052-H34

Aluminum 6061-T6

Cadmium Plated 4037 Steel

4340 Steel

301 Stainless

304 Stainless

347 Stainless

Monel

Inconel X

(a) These materials exhibited less than 1 mil per year corrosion rate, do not cause decomposition, and are impact insensitive.



### 3.9 GELLED PROPELLANTS

#### 3.9.1 Liquid Gelled Propellants

A gelled propellant is any liquid propellant which has been conditioned so that it exhibits non-Newtonian properties. So many propellants have been gelled (e.g., hydrazine, RP-1, nitrogen tetroxide, etc.) that it is impossible to make any generalized statements about the compatibility of the gels, as such, with other materials. However, as a rule the additives needed to cause gelling (carbon black, silica, etc.) are not reactive and do not modify the chemical characteristics of the parent propellant, so that the compatibilities of gel can be considered to be the same as those of the parent propellant with respect to the action of the propellant on the system. Recently, studies on some gelled systems has indicated that the degradation of the propellant by system materials or impurities has been decreased by the gellation. Current work has been concentrated on finding more efficient gellation agents, in order to increase combustion efficiency and storage life.

One type of gelled propellant is characterized by thixotropic properties; that is, the viscosity of the propellant decreases with increasing shear and stress decreases with time at constant shear. These properties are of interest for several reasons. For example, when the propellant is locked in a tank, there is no shear being applied and the propellant is very viscous. When pressure is applied and the propellant valve is opened, shear stresses are induced, viscosity is reduced, and the propellant flows. As the propellant flows through the tank, valves, feed lines, and injector orifices, the shear becomes greater, the viscosity becomes less and the propellant behaves more like a low-viscosity liquid. From the standpoint of safety, the highly viscous state of the propellant when locked in a nonpressurized tank is advantageous.

The properties of gelled propellants also presents some problems. For example, a relatively thick coating of propellant may adhere to tank and valve walls. Pressure drops through lines, valves and other components are larger than those of comparable liquids. Valve maintenance and cleaning may be difficult if there are inaccessible cavities where gel may collect. Gels also may break down under the influence of radiation, temperature extremes, or inclusion of impurity electrolytes.

Excessive cold working (i.e., pumping into run tanks, over-mixing, etc.) can reduce the strength of the gel to an unacceptable value. Evaporation of the propellant can leave a fine powdery residue which could interfere with the normal action of moving parts such as valve stems.

Gelled propellant systems will probably be schematically similar to liquid propulsion systems which perform the same task. In general, it can be stated that the interaction between typical valve configurations and gelled propellants is not overly severe and that the associated problem areas can be circumvented through the use of proper design techniques.

Discussion of Problem Areas -  
Liquid Gelled Propellants

Metals and Ceramics (3)\* - No real problem is envisioned with selecting metals suitable for use with liquid gels. It has been demonstrated that metals compatible with the liquid constituent will serve equally as well for gelled propellants.

Organic Polymers (2) - As with metals, it is necessary to select polymeric material based on the compatibility of the liquid constituent since the gelling agents are present in very small quantity and are normally inert materials.

Wet and Dry Lubes (2) - Compatibility of lubricants with gelled liquids depends on the compatibility of the liquid constituent.

Lubricity (2) - Experimental flow systems on both real and simulated systems has shown that it is reasonable to consider that the gelled liquid will have lubricating properties similar to those of the liquid constituent. These properties are the result of solvent characteristics and reducing properties of the liquid constituent under a frictional force.

Viscosity (2) - Viscosity varies with shear force (i.e., velocity, tube diameter). This presents a definite problem of retention in pockets and cavities of components, resulting in poor propellant utilization and difficulties in cleaning. As discussed previously, proper mechanical design should eliminate most of these difficulties.

Radiation Tolerance (2) - While no major problems have been envisioned for the liquid constituents under consideration for gels, some gelling agents appear to break down under various types of radiation and, in turn, cause the gel to be degraded.

Effects of Leakage (2) - The vapor pressure of the parent propellant is unaffected by gelling, hence toxic hazards of the liquid constituent must be considered. The rate of vapor evolution, however, is reduced, which in turn will reduce fire and explosion possibilities. Leakage, predominantly from volatilization of the high vapor pressure liquid constituent of the gel, will leave a residual powder, the gelling agent, creating problems such as sticking or malfunction of valves.

Control of Flow (2) - Difficulties in accurately measuring flow rate are anticipated; however, it may be expected that pressure drop will generally be higher than for the parent propellant and design allowances may be necessary.

Shutoff (1) - A very serious problem exists with the last valve in a system exposed to space environment. Rapid volatilization of the liquid component of a gelled liquid would leave a solid residue possibly of sufficient quantity to produce leakage or sticking of the valve on subsequent operations.

---

\*Parenthetical enclosures refer to Propellant Rating Chart, Page 3-11.

### 3.9.2 Metallized Gelled Propellants

In order to increase the thermochemical performance of rocket propellants, or to increase propellant bulk density for volume-limited propulsion system applications, powdered metals have been added to liquid propellants. The solid phase of these mixtures can be anywhere from 10 to 90 percent by weight. The metallic gel is generally prepared with metal having an average particle size range of 5 to 50 micron so that: 1) its effect on the flow characteristics of the propellant will be minimized, 2) burning in the combustion chamber will be less difficult, 3) suspension in the liquid will be easier. It has been necessary to gel the mixtures in order to suspend the metal powder in the propellant. Like gelled propellants, these metallized gelled propellant often exhibit thixotropic properties. Another similar case of gels employ metal containing compounds as gellants. These systems are more energetic than the straight metallized ones, but exhibit some storage instability.

Because of the solid particles, metallized gelled propellants present problems which are not encountered with standard propellants. For example, abrasive action of the particles could cause galling of the valve stems or scarring of valve seats and plugs. Particles may become trapped between a valve seat and plug, allowing the valve to leak. Evaporation of the liquid phase of the propellant will leave a solid matrix as a residue which can hinder valve operation and restrict propellant flow. The presence of solid particles in the propellant can result in the galvanic corrosion of certain standard materials of construction, particularly in the presence of impurities which allow electrolytic activity to occur. Any intimate contact of the propellant with lubricants could result in the transfer of particles to the lubricant, thereby reducing the effectiveness of the lubricant. In addition, the problems listed previously for non-metallized gels are applicable. Although it is not certain whether special components will be necessary to utilize metallized gels in propulsion systems, modified designs of standard components will be required to reduce the effects of the undesirable characteristics.

#### Discussion of Problem Areas - Metallized Gelled Propellants

Metals and Ceramics (2)\* - Metallized gels subject certain metal components (i.e., aluminum, nickel, copper) to erosion and/or galling under dynamic conditions. Suitable metals for construction require compatibility with the liquid carrier and relatively high hardness for erosion resistance against the metal constituents of the gel.

Organic Polymers (2) - Considerably greater erosion and galling of plastic materials are anticipated under dynamic conditions. Generally, polymeric materials compatible with the liquid constituent are expected to serve as well under static conditions.

---

\*Parenthetical enclosures refer to Propellant Rating Chart, Page 3-11.

Wet and Dry Lubes (1-2)\* - Gels containing metal particles have considerably greater abrasive action under dynamic flow resulting in greater "wash-out" of lubricants. For static conditions, the restrictions placed upon the liquid constituent dictate selection of a compatible lubricant.

Lubricity (1) - The incorporation of metal particles in a gelled propellant tends to decrease the lubricating properties due to the added abrasive nature of such metals.

Viscosity (2-3) - As with gelled liquid propellants, viscosity varies with shear force and presents problems of propellant utilization, cleaning and greater pressure drop in components. Recent tests were performed by Edwards AFB on metallized propellant simulants in order to define the problem areas in pumping a metallized gelled propellant. Prior to testing, the pump start transient performance was considered to be the greatest potential problem area. Test results indicate, however, that pump start transients with a metallized gel compared favorable with those obtained with a Newtonian fluid. The pump cavitation performance was unaffected by the presence of solid particles in the test fluid. Considerable erosion of the aluminum pump hardware was encountered during testing with the simulated propellant; however, they considered that there was a good indication that the use of steel hardware would solve the problem.

Radiation Tolerance (2) - Some gelling agents appear to deteriorate under radiation and in turn cause the gel to be degraded.

Effects of Leakage (1) - Loss of the liquid component of the gel by leakage will leave a solid matrix to interfere with proper operation of a component. The volatile liquid component will still present toxic, fire, and explosion hazards, but to a lesser extent due to the probable slower rate of evolution.

Control of Flow (1) - No satisfactory way has been found to measure flow rate accurately.

Soft Seats (1-2) - It is anticipated that the metal particles of gels will have detrimental effects on soft seats. Metal particles, trapped against the valve seat when the valve is closed, can cause the valve to leak initially or after several cycles. Selection of seat material should be based principally on compatibility with the liquid constituent of the gel.

Hard Seats (2) - Metal particles of the gel may prevent valves utilizing hard seats from complete sealing, and under dynamic flow the metal particles may result in considerable erosion of the seat by abrasive action.

Shutoff (1) - As with liquid gels, metallized gels present a serious problem for valves exposed to vacuum conditions because there would remain a greater quantity of residue on volatilization of the liquid constituent.

---

\*Parenthetical enclosures refer to Propellant Rating Chart, Page 3-11.

### 3.10 REFERENCES

A number of the propellants of interest have similar compatibility behavior and degradation mechanisms. Because of this, it is felt that the references should be listed numerically and the number referred to for the propellant of interest. Some of the references were general enough in nature to warrant inclusion under a general heading. These references normally include either a general treatise on materials compatibility, or else deal with a large number of the listed propellants. As such, these references should be examined in conjunction with the references for the specific propellants of interest. A compilation of reference numbers for specific propellants given in Section B, unless otherwise noted, are listed as follows:

#### EARTH STORABLE PROPELLANTS

1. Hydrazine: 8, 13, 14, 15, 16, 17, 18, 19, 20, 21, 22, 23, 24, 25, 26, 128.
2. Monomethylhydrazine: 27, 28, 29, 30.
3. Unsymmetrical Dimethylhydrazine: 8, 31, 32, 33.
4. Aerozine-50: 8, 20, 34, 35, 36, 37, 38, 39, 40, 128.
5. Hydrazine-Hydrazine Nitrate: 128, 132.
6. Pentaborane: 3, 4, 5, 6, 7, 8, 9, 10, 11, 12, 54.
7. Nitrogen: 8, 20, 23, 38, 59, 60, 61, 62, 63, 64, 65, 66, 67, 68, 69, 70, 71, 72, 73, 76, 127.

#### SPACE STORABLE PROPELLANTS

1. Diborane: 54
2. Hybaline A5: 1, 2, 12, 51.
3. Liquified Petroleum Gases: 126; General References Section A - 5, 10.
4. Chlorine Trifluoride: 8, 24, 44, 45, 46, 47, 48, 49, 50.
5. Chlorine Pentafluoride: 24, 51.
6. Oxygen Difluoride: 52, 53, 106, 108, 109, 110, 111, 112, 113, 133, 134.
7. Perchloryl Fluoride: 24, 48, 49, 55, 56, 57, 58.
8. Nitrogen Trifluoride: 21, 129, 130.
9. Nitryl Trifluoride: 21, 129, 130.
10. Tetrafluorohydrazine: 21, 129, 130.
11. Liquid Fluorine: 50, 96, 97, 98, 99, 100, 101, 102, 103, 104, 105, 106, 107, plus Section C: "Bibliography of Fluorine Reports."
12. Liquid Oxygen: 40, 83, 84, 85, 86, 87, 88, 89, 90, 91, 92, 93, 94, 95.
13. Liquid Hydrogen: 74, 75, 76, 77, 78, 79, 80, 81, 82.
14. Liquid Oxygen-Liquid Fluorine Mistures: 106, 113, 114, 115, 116, 117, 118, 119, 131
15. Liquid and Metallized Gelled Propellants: 120, 121, 122, 123, 124, 125.

#### A. GENERAL REFERENCES

1. F. Champion, "Corrosion Testing Procedures," John Wiley and Sons, Inc., 1965, 2nd Ed.
2. NASA, "Lubrication, Corrosion and Wear, A continuing Bibliography," Jan. 1962 - March 1965, NASA SP-7020, N65-29845
3. CPIA, "Chemical Propulsion Abstracts - 1965," (U) CPIA Publication No. 116, August 1966, (CONFIDENTIAL)
4. NASA, "Handling Hazardous Materials," NASA SP-5032, September 1965
5. NASA, "Advanced Valve Technology," NASA SP-5019, February 1965
6. NASA, "High Energy Propellants, A Continuing Bibliography," NASA SP-7002, 1964
7. NASA "High Energy Propellants, A continuing Bibliography," NASA SP-7002 (01), March 1965
8. NASA, "High Energy Propellants, A continuing Bibliography," NASA SP-7002 (03), April 1966
9. Defense Metals Information Center, "Combatibility of Materials with Rocket Propellants and Oxidizers," DMIC Memo: No. 201, Jan. 29, 1965
10. S. Sarnar, "Propellant Chemistry," Reinhold Publishing Corp., New York, 1966
11. N. Tomashov, "Theory of Corrosion and Protection of Metals," The Macmillan Co., N.Y., 1966
12. R. M. McClintock and H. P. Gibbons, "Compilation of Mechanical Properties of Materials at Cryogenic Temperatures," NBS Report 6064
13. "Conference on Elastomers," Sixth Joint Army, Navy, Air Force, AD250916, Volume 2
14. Evans, George R., "Construction Materials for Containers of Liquid Propellants; Hydrogen, Fluorine, Hydrazine and Nitrogen Tetroxide: An Annotated Bibliography," AD 271034, April 1960, Lockheed Aircraft Company, Technical Information Center, Research Section.
15. Masteller, R. D. and others, "Design Criteria--Materials," 804-1001001, March 1960, The Martin Company, Denver Division

16. Howell, G. W. and Weathers, T. M., "Aerospace Fluid Component Designers' Handbook," Revision B, RPL-TDR-64-25, Vol. I (AD 809182), Vol. II (AD 809183), March 1967, TRW Systems
17. Beach, N. E., "Compatibility of Plastics with Liquid Propellants, Fuels and Oxidizers," Plastic Report 25, January 1966, Plastics Technical Evaluation Center, Picatinny Arsenal
18. "Investigation of the Formation and Behavior of Clogging Material In Earth and Space Storable Propellants," Interim Report No. 08113-6007-R000, Contract No. NAS 7-549, October 1967.
19. "Investigation of the Formation and Behavior of Clogging Material in Earth and Space Storable Propellants," Interim Report No. 08113-6016-R000, Contract NAS 7-549, October 1968.
20. "Investigation of the Formation and Behavior of Clogging Material in Earth and Space Storable Propellants," Final Report No. 08113-6025-R000, Contract NAS 7-549, November 1969.

## B. SPECIFIC REFERENCES

1. Union Carbide Chemicals Co., "Research and Development of Metal Hydride Organic Nitrogen Complexes," (U), Rocket Propulsion Department Quarterly Progress No. 3, Sept. 1962, South Charleston, West Virginia, (CONFIDENTIAL)
2. Telecon, M. W. Wong, TRW and Capt. K. F. Illies, Edwards AFB, 16 Oct. 1963
3. S. S. Miller, "Pentaborane," Unit 4, Liquid Propellant Manual, Liquid Propellant Information Agency, March 1961
4. Rocketdyne, "Pentaborane Handling Manual," AF/SSD TR-61-110, R-3137, Sept. 1961
5. Rocketdyne, "Mechanical System Design-Criteria Manual for Penaborane," AF/SSD TR-61-3, R-3233, Sept. 1961
6. A. V. Jensen and B. B. Goshgarian, "A Study of Pentaborane," AFFTC-TR-61-3, R-3233, Sept. 1961
7. Gallery Chemical Company, "Pentaborane," Technical Bulletin CT-1300, October 1961
8. P. D. Gray, et al. "Rockets in Space Environment, Vol. I - The Experimental Program," Aerojet-General Corporation, RTD-TDR-63-1050, Contract AF04(611)-7441, Feb. 1963
9. F. Ward, "Pentaborane Handling and Safety Procedures," American Rocket Society Missile and Spacecraft Testing Conference, Los Angeles, March 13-16, 1961, Paper No. 1638-61
10. B. Dawson and R. Schreib, "Investigation of Advanced High Energy Space Storable Propellant System -  $\text{OF}_2/\text{B}_2\text{H}_6$ ," AIAA Summer Meeting, Los Angeles June 17-20, 1963, Paper No. 63-238
11. CPIA, "Boron Hydrides and Derivatives. An Indexed Bibliography of Unclassified Titles for 1952-1959." CPIA (LPIA Publication LBH-1), June 1962; AD-468981
12. AFML, "Evaluation of Elastomers as O-Ring Seals for Liquid Rocket Fuel and Oxidizer Systems," Technical Documentary Report No. ASD-TDR-63-496, Part VI, August 1964; AD-607240
13. E. W. Cox, "Hydrazine," Unit 2, Liquid Propellant Manual, Liquid Propellant Information Agency, March 1961



14. Bell Aerosystems Company, "Titan II Storable Propellant Handbook," Bell Report No. 8182-933004 for AFBSD, Contract No. AF04(694)-72, March 1962
15. Bell Aerosystems Company, "Titan II Storable Propellant Handbook," Bell Report No. 8182-933004, AFBSD TR-62-2, Contract AF04(694)-72, March 1963
16. Arthur D. Little, Inc., "The Problems of Toxicity, Explosivity, and Corrosivity Associated with the WS 107A Mark II Operational Base Facility," Report to the Ralph M. Parsons Co., May 1960
17. Rocketdyne, "Hydrazine Handling Manual," AF/SSD-TR-61-7, R-3134, September 1961
18. Rocketdyne, "Mechanical System Design-Criteria Manual for Hydrazine," AF/SSD-TR-61-6, R-3130, September 1961
19. Department of the Air Force, "The Handling and Storage of Liquid Propellants," AFM 160-39, March 1961
20. Martin Company, "Propellant Compatibility Report," CR-64-88, November 1964.
21. D. J. Simkin, G. C. Szego and P. J. Valentine, Advances in Space Propulsion, U.C.L.A. Course Test, 1961.
22. JPL, "Supporting Research and Advanced Development," 31 Aug. 1965, Space Programs Summary No. 37-34, Vol. IV
23. C. Grelicki and S. Tannenbaum, "Survey of Current Storable Propellants," ARS Journal, 32, 1189 (1962)
24. S. N. Levine, W. Sheehan, and J. Green, "Elastomeric and Compliant Materials for Liquid Rocket Fuel and Oxidizer Application," Technical Report ML-TDR-64-107, Part II, Feb. 1965 (See Also Chemical Engineering Progress Symposium Series, No. 52, Vol. 60, p. 45)
25. K. Carroll, "Hydrazine - Chemical Properties, Decomposition," Report No. SB-59-63, 15 June 1959, AD-462732
26. Bell Aerosystems, "Handling and Storageability of Liquid Rocket Propellants - Tank Storage Tests," Report No. 02-989-020, Jan. 23, 1956, AD-455098
27. Olin Mathieson Chemical Corporation, "Mathieson Monomethylhydrazine - MMH," Product Bulletin, 1961
28. S. S. Miller, "Monomethylhydrazine," Unit II, Liquid Propellant Manual, Liquid Propellant Information Agency, December 1961

29. S. Sarnier, "Monomethylhydrazine (MMH)," Astronautics, 5, 86 (July 1960)
30. O. Knight, "Monomethyl Hydrazine," Hydrocarbon Processing and Petroleum Refiner, 41, 179 (1962)
31. S. S. Miller, "Unsym. Dimethylhydr-zine," Unit 5, Liquid Propellant Manual, Liquid Propellant Information Agency, March 1961
32. Department of the Air Force, "The Handling and Storage of Liquid Propellants," AFM 160-39, March 1961
33. M. F. Butner, "Final Report - Proepllant Lubrication Properties Investigation," Rocketdyne, WADD-TR-61-77, June 1961
34. E. W. Cox, "Hydrazine/Unsym. Dimethylhydrazine (50:50)," Unit 7, Liquid Propellant Manual, Liquid Propellant Information Agency, July, 1961
35. Bell Aerosystems Company, "Titan II Storable Propellant Handbook," Bell Report No. 8182-933004, for AFBSD, Contract No. AF04(694)-72, March 1962
36. Bell Aerosystems Company, "Titan II Storable Propellant Handbook," AFFTC TR-61-32, Contract No. AF04(611)-6079, June 1961
37. E. M. Tomlinson, "Materials Selector for Propellant Systems," Aerospace Management, 4, 24 (February 1961)
38. S. Lewis and J. P. Cooper, "Materials Compatibility with Storable Propellants," Space/Aeronautics R&D Handbook, July 1962
39. Aerojet-General Corporation, "Storable Liquid Propellants - Nitrogen Tetroxide/Aerozine 50, LRP 198, June 1962
40. W. D. Smith and O. C. Bender, "Comparison of Storable and Cryogenic Propellants," AIAA Summer Meeting, Los Angeles, California, June 1963
41. J. Messina, "Greases Nonreactive with Missile Fuels and Oxidizers," Fourth National SAMPE Symposium, Los Angeles, Calif., Nov. 13-15, 1962
42. C. Wong, "Design for Material Compatibility and Corrosion Control Problems Associated with Typical Storage Propellants," SAE, Nat'l Aeronautic and Space Engineering and Manufacturing Meeting, Los Angeles Oct. 5-9, 1964, Paper No. 916C
43. K. Fisch, L. Peale, J. Messina, and H. Gisser, "Compatibility of Lubricants with Missile Fuels and Oxidizers," ASLE Trans. 5, 287 (1962); N63-13326
44. E. W. Cox, "Chlorine Trifluoride," Unit 3, Liquid Propellant Manual, Liquid Propellant Information Agency, March 1961

45. Rocketdyne, "Chlorine Trifluoride Handling Manual," AF/SSD TR-61-9, R-3136, Sept. 1961
46. Rocketdyne, Mechanical System Design-Criteria Manual for Chlorine Trifluoride," AF/SSD TR-61-4, R-3132, Sept. 1961
47. Rocketdyne, "Semiannual Program Progress Report for Product Engineering," (U), Report No. R-5652-2P, 31 July 1964 (CONFIDENTIAL)
48. J. Grigger and H. Miller, "The Compatibility of Materials with Chlorine Trifluoride, Perchloryl Fluoride, and Their Mixtures," Materials Protection 3, 53 (1964)
49. C. Grelecki and S. Tannenbaum, "Survey of Current Storable Propellants," ARS Journal 32, 1189 (1962)
50. W. English, S. Pohl, and N. Tines, "Corrosion Behavior of Structural Materials with Fluorine - Containing Liquid Oxidizers," SAMPE Nat'l Symp. on Mat'ls for Space Vehicle Use, 6th, Seattle, Wash., Nov. 18-20 1963, Vol. 3; AD 65-11524
51. J. Grigger and H. Miller, "The Compatibility of Structural Materials with Hybaline A-5 and Compound A," Pennsalt Co., Technical Report No. AFML-TR-64-391, Dec. 1964, AD-458159, X65-15579
52. N. A. Tiner, W. D. English and S. M. Toy, "Compatibility of Structural Materials with High Performance O-F Liquid Oxidizers," November 1965, AFML-TR-65-414.
53. N. A. Tiner, W. D. English, and S. K. Asunmaa, "Investigation of Explosive Reactions Involving Oxygen Difluoride," July 1965, AFML-TR-65-222.
54. R. L. Hughes, I. C. Smith, and E. L. Lawless, "Production of the Boranes and Related Research," Academic Press, New York, 1967.
55. Department of the Air Force, "The Handling and Storage of Liquid Propellants," AFM 160-39, March 1961
56. L. B. Piper, "Perchloryl Fluoride," Unit 19, Liquid Propellant Manual, Liquid Propellant Information Agency, January 1963
57. B. Kit and D. S. Evered, "Rocket Propellant Handbook," The Macmillan Co., New York, N.Y., 1960
58. W. English, S. Pohl, and N. Tiner, "Corrosion Behavior of Structural Materials with Fluorine-Containing Liquid Oxidizers," SAMPE Nat'l Symposium on Materials for Space Vehicle Use, 6th, Seattle, Wash., Nov. 18-20, 1963, Vol. 3; AD 65-11524

59. E. W. Cox, "Nitrogen Tetroxide," Unit 1, Liquid Propellant Manual, Liquid Propellant Information Agency, March 1961
60. Allied Chemical, Nitrogen Division, "Nitrogen Tetroxide," Product Bulletin
61. Bell Aerosystems Company, Titan II Storable Propellant Handbook," Bell Report No. 8182-933004 for AFBSD, Contract No. AF04(694)-72, March 1962
62. Arthur D. Little, Inc., "The Problems of Toxicity, Explosivity, and Corrosivity Associated with the WS 107A Mark II Operational Base Facility," Report to the Ralph M. Parsons, Co., May 1960
63. Rocketdyne, "Nitrogen Tetroxide Handling Manual," AF/SSD-TR-61-8, R-3135, September 1961
64. Rocketdyne, "Mechanical System Design-Criteria Manual for Nitrogen Tetroxide," AF/SSD-TR-61-5, R-3131, September 1961
65. Bell Aerosystems Company, "Titan II Storable Propellant Handbook," Bell Report No. 8111-933003, AFFTC TR-61-32, Contract No. AF04(611)-6079, June 1961
66. Aerojet-General Corporation, "Storable Liquid Propellants, Nitrogen Tetroxide/Aerozine 50," Report No. LRP 198, June 1962
67. E. M. Tomlinson, "Material Selection for Propellant Systems," Aerospace Management, 4, 24, February 1961
68. W. D. Smith and O. C. Bender, "Comparison of Storable and Cryogenic Propellants," AIAA Summer Meeting, Los Angeles, Calif., June 1963
69. R. Wallner, B. Williams, and A. Simmons, "Compatibility of Titanium and Nitrogen Tetroxide," Mat'ls. Prot. 4, 55, (1965)
70. AFRPL, "Methods for Elimination of Corrosion Products of Nitrogen Tetroxide," AFRPL-TR-66-209, August 1966
71. R. Wood, "Review of Recent Developments: Titanium and Titanium Alloys," DMIC Technical Note, April 6, 1966
72. G. Curran, "Metallurgical Investigation of Leakage in Missile B-58 Stage I Oxidizer Feed Line Bellows (SIN-47)," Martin Co. Report No. Cr-65-9, 31 Dec. 1964
73. J. Marcus, W. Day, and J. Jelinek, "Design and Development of an Elastomer Seal for Long-Term Hazardous Propellant Storage," SAMPE Journal, 2, 34, (1966)
74. B. M. Bailey, et al., "Handbook for Hydrogen Handling Equipment," WADC TR-59-751, February 1960

75. A. W. Adkins, et al., "Storage, Servicing, Transfer and Handling of Hydrogen," AFFTC TR-61-18, May 1961
76. M. F. Butner, "Final Report - Propellant Lubricating Properties Investigation," Rocketdyne, WADD-TR-61-77, June 1961
77. Department of the Air Force, "The Handling and Storage of Liquid Propellants," AFM 160-39, March 1961
78. Arthur D. Little, Inc., "Liquid Propellant Losses During Space Flight," Contract No. NAS5-664, January 1961
79. S. S. Miller, "Liquid Hydrogen," Unit 6, Liquid Propellant Manual, Liquid Propellant Information Agency, March 1961
80. Arthur D. Little, Inc., "Hydrogen Handbook," AF33(616)-6710, AFFTC TR-60-19, April 1960
81. J. Jackson, "Permeability of Titanium to Hydrogen," DMIC Technical Note, July 29, 1964, AD-609339
82. A. Jeffs, D. Lidster, and F. Luptou, "A Vacuum-Insulated Pipe to Carry Liquid Hydrogen at High Pressure," Rocket Propulsion Establishment (UIC) Technical Memo No. 321, July 1964, AD-454507
83. W. D. Smith and O. C. Bender, "Comparison of Storable and Cryogenic Propellants," AIAA Summer Meeting, Los Angeles, Calif., June 1963
84. Arthur D. Little, Inc., "Liquid Propellant Losses During Space Flight," Contract No. NAS5-664, January 1961
85. Department of the Air Force, "The Handling and Storage of Liquid Propellants," AFM 160-39, March 1961
86. W. K. A. Gallant, "Liquid Oxygen," Unit 8, Liquid Propellant Manual, Liquid Propellant Information Agency, July 1961
87. F. W. Fink and E. L. White, Corrosion Effects of Liquid Fluorine and Liquid Oxygen on Materials of Construction, NACE Paper Submitted at the 16th Annual Conference, 22 March 1960
88. The Martin Company, "Compatibility of Materials with Liquid Oxygen," November 1958, Report No. M-M-MI-58-66
89. A. Landrock, "Properties of Plastics and Related Materials at Cryogenic Temperatures," Picatinny Arsenal Report No. PLASTEC Report 20, July 1965, AD-469126
90. J. Jackson, W. Boyd, and P. Miller, "Reactivity of Metals with Liquid and Gaseous Oxygen," DMIC Memorandum No. 163, Jan. 15, 1963

91. E. Brady, "Compatibility of Metallic Materials with Liquid Oxygen," Aerojet-General Report No. DVR-64-459, 19 Oct. 1964, AD-459269
92. C. Dey and J. Gayle, "Effect of Liquid Nitrogen Dilution on LOX Impact Sensitivity," J. Spacecraft, 3, 274 (1966)
93. D. Weitzel, R. Robbins, and P. Ludtke, "Elastomeric Seals and Materials at Cryogenic Temperatures," AFML Report TDR-64-50, Part 2, March 1965, AD-485555
94. V. Chinberg and H. Perkins, "Preliminary Studies of Liquid Oxygen Explulsion Bladders," NASA Technical Memorandum No. NASA-TM-X-53005, Oct. 12, 1964, N65-12314
95. P. Schuman, "Development of Vulcanizable Elastomer Suitable for Use In Contact with Liquid Oxygen," Peninsular ChemResearch Inc., Gainesville, Fla., 8 June 1965
96. P. S. Gakle, et al., "Design Handbook for Liquid Fluorine Ground Handling Equipment, Aerojet-General Corp., WADD TR-60-159, December 1960
97. J. M. Siegmund, "Research on the Production, Storage and Handling of Liquefied Fluorine," Allied Chemical Corp., Contract No. AF33(616)-2229, June 1955
98. H. G. Price and H. W. Douglas, "Non-Metallic Material Compatibility with Liquid Fluorine," NACA RM-E57G18, October 1957
99. C. J. Sterner and A. H. Singleton, "The Compatibility of Various Metals with Liquid Fluorine," Air Products, Inc., WADD TR-60-819, March 1961
100. R. L. DeWitt and H. W. Schmidt, "Experimental Evaluation of Liquid Fluorine System Components," Lewis Research Center, NASA TN-D-1727, June 1963
101. H. R. Neumark, "Fluorine and Advanced Rocket Propulsion," Missiles and Space, 7, 18, July 1961
102. Aerojet-General Corp., "Design Handbook for Liquid Fluorine Ground Handling Equipment," 2nd Ed., Technical Report AFRPL-TR-65-133, August 1965
103. W. Osborn, "Investigation of a Liquid-Fluorine Inducer and Main-Stage Pump Combination Designed for a Suction Specific Speed of 20,000," NASA TMX-1070, March 1965
104. W. Hady, G. Allen, H. Sliney, and R. Johnson, "Friction, Wear, and Dynamic Seal Studies in Liquid Fluorine and Liquid Oxygen," NASA TN D-2453, 1964

105. J. Flanagan and F. Stephanson, "Fluorine Propulsion Technology," AIAA Annual Meeting, 2nd, San Francisco, July 1965, AIAA Paper No. 65-536
106. Defense Metals Information Center, "Compatibility of Materials with Fluorine and Fluorine-Base Oxidizers," DMIC Technical Note, April 8, 1965
107. J. Cabiness and J. Williamson, "A Literature Survey of the Corrosion of Metal Alloys in Liquid and Gaseous Fluorine," NASA TM-X-54612; N64-17691, 31 Dec. 1963
108. Allied Chemical, General Chemical Division, "Oxygen Difluoride," Product Data Sheet, July 1962
109. D. S. Smith and D. J. Mann, "OF<sub>2</sub> Looks Promising as Space-Storable Propellant," Space/Aeronautics, 39, 103, January 1963
110. B. E. Dawson, A. F. Lum, and R. R. Schreib, "Investigation of Advanced High Energy Space Storable Propellant System," Thiokol Chemical Corp., RMD Report 5507-F, Contract NASw-449, November 1962
111. B. E. Dawson, A. F. Lum, and R. R. Schreib, "Investigation of Advanced High Energy Space Storable Propellant System - OF<sub>2</sub>/B<sub>2</sub>H<sub>6</sub>," AIAA Summer Meeting, Los Angeles, Calif., June 1963
112. B. Dawson and R. Schreib, "Investigation of Advanced High Energy Space Storable Propellant System - OF<sub>2</sub>/B<sub>2</sub>H<sub>6</sub>," AIAA Summer Meeting, Los Angeles, June 17-20, 1963, Paper No. 63-238
113. J. Cakiness, "Bibliography on Fluorine and Fluorine-Oxygen Oxidizer for Space Applications," 16 Oct. 1964, NASA TM-X-53149
114. General Dynamics/Astronautics, "Feasibility Testing 30% FLOX with Atlas Oxidizer System Components," 24 July 1964, Report No. GD/A-Bgm-64-0021, Final (CONFIDENTIAL)
115. General Dynamics/Astronautics, "Feasibility Testing 50% FLOX with Atlas Oxidizer System Components," 20 Nove. 1964, Report No. GD/A-BHV64-011, Final (CONFIDENTIAL)
116. D. Spicer, "Liquid Fluorine and FLOX Immersion Tests of Alloys Under Static Stress," Laboratory Report No. MP30, 450, Douglas Aircraft Co., Inc., (March 3, 1964)
117. D. Spicer, "Static Immersion of Non-Metallic Materials in Gaseous FLOX," Laboratory Report No. MP30, 451, Douglas Aircraft Co., Inc., (March 23, 1964)
118. General Dynamics/Astronautics, "Atlas 77D Oxidizer Tank Storage Test After Exposure to 30% FLOX," (U) GD/C-CHB65-009, Final (CONFIDENTIAL)

119. Rocketdyne, "Atlas Mark 4 Turbopump Seal FLOX Test Program," (U) Report R-5889, 9 Jan. 1964 (CONFIDENTIAL)
120. Edwards AFB, California, Proceedings of the Metallized Gelled Propellants Conference, June 1963 (CONFIDENTIAL)
121. A. J. Aitken, "Metallized Thixotropic Propellants," Aerojet-General Corporation Report No. 652/SA4-2.2-F1, Vol. 5, Air Force Contract No. AF04(647)-652/SA4, June 1963 (CONFIDENTIAL)
122. W. B. Tarpley, C. D. McKinney and R. Pheasant, "Research and Development Program on Thixotropic Propellants," Aeroprojects Incorporated, Research Report 62-15, Navy Contract NOW-61-0506-c, May 1962 (CONFIDENTIAL)
123. Packaged Liquid Propulsion Symposium, October 1962, CPIA Publication No. 13, March 1963, (CONFIDENTIAL)
124. J. Chlapek and R. Probst, "Metallized Propellant Simulant Pumping," Technical Report AFRPL-TR-65-67, April 1965
125. CPIA, "2nd Metallized Gelled Propellants Conference, 26-28 August 1964," (U), Silver Spring, Md., Pub. No. 64 (CONFIDENTIAL)
126. The Matheson Company, "Matheson Gas Data Book," Newark, Calif., 1961
127. Muraca, R. F. and J. S. Whittick, "The Results of Long-Term Storage Tests for Compatibility of Nitrogen Tetroxide with Various Spacecraft Materials," JPL Contract No. 951581 (Under NASA NAS 7-100), Special Report No. 2., May 15, 1967.
128. R. F. Muraca and J. S. Whittick, "The Results of Long-Term Storage Tests for Compatibilities of Spacecraft Materials with Hydrazine and Hydrazine Mixtures," JPL Contract No. 951581 (Under NASA NAS 7-100), Special Report No. 951581-6, October 1, 1967.
129. J. H. Simmons, Fluorine Chemistry, Volume 5, Academic Press, New York, N.Y., 1961.
130. M. Stacey, J. C. Tatlow and G. G. Sharpe, Advances in Fluorine Chemistry, Volume 5, Butterworth, Washington, D. C. 1965.
131. Harold W. Schmidt, Handling and Use of Fluorine and Fluorine-Oxygen Mixtures in Rocket Systems, NASA SP 3037, Lewis Research Center, Cleveland, Ohio.
132. "Advanced Packaged Liquid Propellant Research (U)", RMD Report No. 5074-Q1, Contract NOW 65-0575-C, Report Period: 12 May 1965 - 12 August 1965.
133. "Elastomeric and Compliant Materials for Liquid Rocket Fuel and Oxidizer Applications," Contract AF33(657)-11093, Thiokol Report No. ML-TDR-64-107, March 1964.
134. "Design Handbook for Oxygen Difluoride," Contract No. AF04(611)-8400, Thiokol Report No. RTD-63-1084, November 1963.



### C. BIBLIOGRAPHY OF FLUORINE REPORTS

1. Aerojet Engineering Corporation, Azusa, California, Investigation of Liquid Rocket Propellants, by S. B. Kilner, et al., Report No. 577 (Annual), 7 February 1952
2. Aerojet-General Corporation, Sacramento, California. Design Handbook for Liquid Fluorine Ground Handling Equipment, WADD Technical Report No. 60-160, February 1961
3. Research Study on Ground Handling Equipment for Transporting Service Storing, and Handling Liquid Fluorine, WADD Technical Report No. 60-160, February 1961
4. Air Products, Inc. Allentown, Pennsylvania. Compatibility of Liquid Fluorine with Various Structural Materials and Carbon, by Alan H. Singleton and Charles J. Sterner, Progress Report VI, August 1960
5. Air Products, Inc., Emmaus, Pennsylvania. Compatibility of Liquid Fluorine with Various Structural Metals and Carbon, by Charles J. Steiner, Bi-Monthly Progress reports 1 through 6, Contract AF33(616)-6515
6. Allied Chemical Corporation, General Chemical Division. Fluorine Elemental F.
7. Allied Chemical and Dye Corporation, General Chemical Division. Fluorine Study for Experimental Rocket Engine Test Laboratory, by J. M. Siegmund, AD 147621, 15 May 1956 (C)
8. Fluorine-Properties and Methods of Handling
9. Research on the Production and Handling of Liquified Fluorine, Vol. I, Research on the Production of Liquified Fluorine, 10 June 1955 (C) AD 77312
10. Fluorine, PD-TA-85413, Revised 15 August 1958
11. Liquid Fluorine Unloading Procedure, PD-TB-85411, July 1958
12. Altman, D. "A Review of Liquid Propellant Oxidizers," Symposium on Liquid Propellants, Vol. I, Office of the Assistant Secretary of Defense, R&D, Washington, D.C., 23-24 May 1955
13. American Medical Association Archives of Industrial Hygiene and Operational Medicine, June 1954, as given in "Threshold Limit Values for 1954," and adopted at the 16th Annual Meeting of the American Conference of Governmental and Industrial Hygienists, Chicago, Illinois, 24-27 April 1954

14. Anonymous. Chemical and Engineering News, 35, 7, 18, March 1957
15. Anonymous. Chemical and Engineering News, 36, 35, 1958
16. Anonymous. "Atomic Weights, 1948," Journal of the American Chemical Society, 70, 11, 1948
17. Aoyama, S. and E. Kanda, "Studies on F<sub>2</sub> at Low Temperatures," Bulletin of the Chemical Society of Japan, 12, 416, 1937
18. Aoyama, S. and E. Kanda, "Studies of Fluorine at Low Temperatures, Vapor Pressure of Fluorine," Bulletin of the Chemical Society of Japan, 12, 417-18, 1937
19. Argonne National Laboratory, Lemont, Illinois, Corrosion of Metals in the Presence of Fluorine at Elevated Temperatures, by M. J. Steindler and R. C. Vogel, January 1957
20. Barrow, R. F. and D. C. Count, "The Ultra-Violet Absorption Spectra of Some Gaseous Alkali-Metal Halides and the Dissociation Energy"
21. Barrow, R. F. and A. D. Count, "The Heat of Solution of Thallous Fluoride and the Dissociation of Fluorine," Transactions of the Faraday Society, 46, 154-6, 1950
22. Battelle Memorial Institute, Columbus, Ohio. Physical Properties and Thermodynamic Functions of Fuels, Oxidizers, and Products of Combustion II, Oxidizers," Report to the Rand Corporation, Santa Monica, California, February 1949
23. Battelle Memorial Institute, Division of Chemical Engineering, Columbus, Ohio, Liquid Propellants Handbook, Volume 3, Experience with Fluorine Systems," December 1958
24. Liquid Propellants Handbook, Volume 2, Properties of Fluorine," Compiled by D. E. Sparrow, 13 August 1956
25. Bell Aerosystems Company, Launch Area Servicing of a Fluorine-Hydrogen Upper Stage, Report No. 8031-982-003, 31 December 1962
26. Areas of Proposed Investigations Rocket Technology, Status Report, August 1962
27. Summary of Bell Fluorine Propulsion Experience and Design Studies, Report No. S-128857, January 1962
28. Research and Development to Advance the State-of-the-Art of Fluorine High-Energy Propulsion Systems, Final Report No. SSD-TR-61-2, 24 July 1961 (C)

29. Research and Development to Advance the State-of-the-Art of Fluorine High-Energy Propulsion Systems, Report No. 8136-920001, (Supplement to SSD-TR-61-2), 24 July 1961 (C)
30. Fluorine Hydrogen Rocket Engine Feasibility Investigations, Report No. 8031-982-002, 28 February 1961 (C)
31. Fluorine-Hydrogen Propulsion Data, Report No. D8217-953001, 3 January 1962 (C)
32. 35,000 Lb Fluorine/Ammonia Thrust Chamber Feasibility Investigation, Final Report No. 123-982-002, May 1958
33. Summary of High Energy Propellant Programs at Bell Aircraft Corporation, Report No. 7-59-0452-001, 30 January 1959 (C)
34. High Energy Propellant Program, Final Report, Report No. 8031-982-001, 1959 (C)
35. Bernstein, R. B. and M. Metlay, "Note of the Electron Affinity of Fluorine," Journal of Chemical Physics, 19, 1612, 1954
36. Bird, R. B., J. O. Herschfelder, and E. L. Spatz, "The Transport Properties of Nonpolar Gases," J. Chem. Physics, 16, 968, 1948
37. Booth, H. S. and J. P. Pinkston, Jr. Chemical Reviews, 41, 421-37, 1947
38. Borg-Warner Corporation, Chicago, Illinois, Investigation of Propellant Systems and Components Utilizing a High-Energy Oxidizer, Final Report, Volume 2, May 1960, AFPTC Technical Report 60-9
39. Bureau of Ordnance. Safety Regulations for Guided Missile Propellants, (Including Revisions of April 21, 1949, prepared by Ad Hoc Committee on Safety Code for Guided Missile Propellants for Inter-Bureau Technical Committee, July 1948
40. Burford, W. D., III, et al. "Solubility of Fluorine Gas in Various Fluorocarbons and Concentrated Acids," as given in Preparation, Properties and Technology of Fluorine and Organic Fluoro Compounds, Chapter II by Slesser (Ed.), McGraw-Hill, New York, 1951
41. Buthov, K. V. and R. B. Rozenbaum, "Vibration Frequency of the Atoms in a Fluorine Molecule, the Thermodynamic Functions of Fluorine and the Equilibrium Constant  $F_2 \rightleftharpoons 2F$  in a Temp Interval of 298.1 to 5000°K," Translation under auspices of State University Research Foundation, Columbus, Ohio, 35th Progress Report, 1 September 1951, p. 11 of translation

42. California Institute of Technology, Jet Propulsion Laboratory, Pasadena, California, The Heat of Dissociation of Fluorine by R. N. Doescher, Report No. 20-61, November 1951; also Journal of Chemical Physics, 20, 334, 1952
43. Gallery Chemical Company, Gallery, Pennsylvania, Background Chemistry for Development of Liquid Rocket Oxidizers, by J. O. Collins, P. A. Joyner and L. S. Stone, Report No. 000-52208-SR-1, 1963
44. Cody, G. H. "Reaction of Fluorine with Water Hydroxides," J. Am. Chem. Soc., 57, 246-9, 1935
45. Cody, G. H. and J. H. Hildebrand, "The Vapor Pressure and Critical Temperature of Fluorine," J. Am. Chem. Soc., 52, 3839-43, 1930
46. Claussen, W. H., "The Vapor Pressure of Fluorine," J. Am. Chem. Soc., 56, 614, 1934
47. Coe, C. S. and G. P. Sutton, "The Effect of Liquid Propellant Properties on Rocket Engine and Missile Design and Operation," Symposium on Liquid Propellants, Office of the Assistant Secretary of Defense, R and D, Washington, D.C., 23-24- May 1955
48. Cole, L. G., G. W. Elverum, Jr., and M. Farber, "Thermodynamic Properties of the Fluorine Atom and Molecule and Hydrogen Fluoride to 5000°K," J. Am. Chem. Soc., 20, 586-90, 1952
49. Davenport, S. J. and G. C. Margis, "Review of Health Hazards of Fluorine and Fluorine Compounds in the Mining and Allied Industries," Bureau of Mines Circular 7687, 1954
50. Doescher, R. N. "The Heat of Dissociation of Fluorine," J. Chem. Phys., 19, 1070-1, 1951
51. Doescher, R. N. and G. W. Elverum, Jr., "Physical Properties of Liquid Fluorine," J. Chem. Phys., 20, 1834-6, 1952
52. Dykstra, J., W. E. Paris, and J. Thompson, "A Twenty-Five Pound per Hour Fluorine Plant," Ind. Eng. Chem., V50, No. 2, February 1958
53. Dykstra, J., A. P. Huber, and B. H. Thompson, "Multi-Ton Production of Fluorine for Manufactur of Uranium Hexafluoride," Second United Nations Internaitonal Conference on the Peaceful Uses of Atomic Energy, Paper No. A/Confidential 15/p/524, U.S.A., 1958
54. Eucken, A. and E. Wieke, "The Dissociation Energy of Fluorine," Die Naturwissenschaften, 36, 233-4, 1950
55. Evans, W. H., T. R. Munson, and W. D. Wagman, "Therodynamic Properties of Some Gaseous Halogen Compounds," J. Res. NBS, 55, 154-4, 1955

56. Evans, M. G., E. Warhust, and E. Whittle, "The Dissociation Energy of Fluorine," J. Chem. Soc. (London), 1524-34, 1950
57. Ferry, J. L., The Toxicity of Fluorine, AECD 3776, 1955, Declassified.
58. Franch, E. V., "A Determination of the Refractive Index of Fluorine Vapor," Die Naturwissenschaften, 41, 36, 1954
59. Fritz, H. and E. Wieke, "The Dissociation Energy of Fluorine by the Explosion Method," Zeitschrift fur Elektrochemie, 57, 9-16-1953, as given in Chemical Abstracts, 1953
60. Gainer, C. S. and D. M. Yost, "An Attempt to Determine the Electrode Potential and Raman Spectrum of Fluorine," J. Am. Chem. Soc., 59, 2738, 1937
61. Gall, John F., "Recent Advances in Fluorine Chemistry and Technology," ARS J., February 1959, Vol. 29, No. 2
62. Gaydon, A. G., Dissociation Energies and Spectra of Diatomic Molecules, John Wiley and Sons, Inc., New York, 1947
63. Gilles, P. W. and J. L. Margrave, "The Dissociation Energy of Fluorine," J. Chem. Phys., 21, 381-2, 1953
64. Glocker, G. Physical Review, 46, 111, 1934
65. Unpublished Results, as given by J. F. Simmons (Ed.) in Fluorine Chemistry, Volume I, Academic Press, Inc., New York, 1950
66. Godwin, T. W. and C. F. Lorenzo, "Ignition of Several Metals in Fluorine," 13th Annual ARS Meeting, Hotel Statler, New York, 17-21 November 1958
67. Harshaw Chemical Company, Cleveland 6, Ohio, Unloading Anhydrous Hydrofluoric Acid from Tank Cars, Manufacturing Chemists Association Manual Sheet TC-5, Reprinted in Hydrofluoric Acid Anhydrous, 1952
68. Hazeldine, R. N. and A. G. Sharpe, Fluorine and Its Compounds, Methuen and Company, London, 1951
69. Hodgman, C. D., Ed. Handbook of Chemistry and Physics, 36th Edition Chemical Rubber Publishing Company, Cleveland, 1955
70. Holloway, F. L. and H. R. Neumark, "Fluorine....Tamed for Rockets," Missiles and Rockets, September 1957
71. Hu, J., H. L. Johnston, and D. White, "Condensed Gas Calorimetry Vs. Heat Capacities, Latent Heats and Entropies of Fluorine from 13 to 85°K; Heats of Transition, Fusion, Vaporization, and Vapor Pressures of the Liquid," J. Am. Chem. Soc., 75, 5642-45, 1953

72. "The Density and Surface Tension of Liquid Fluorine Between 66 and 80°K," J. Am. Chem. Soc., 76, 2584-6, 1954
73. Industrial and Engineering Chemistry, January-June 1947, Vol. 39, Pages 236-434
74. Jarry, R. L. and H. C. Miller, "The Density of Liquid Fluorine 67 and 103°K," J. Am. Chem. Soc., 78, 1552-3, 1956
75. Jones, W. L. and R. J. Lubick, "Performance Characteristics of Hydrogen Fluorine Rocket Engines at Various Chamber Pressures and Nozzle Area Ratios," (paper presented at LPIA JANIS meeting at San Diego, California, November 1960)
76. Kanda, E., "Studies of Fluorine at Low Temperatures, Determination of Dielectric Constants of Condensed Gases," Bull. Chem. Soc. Japan, 12, 477, 1937
77. "Studies of Fluorine at Low Temperatures, Surface Tension of Liquid Fluorine," Bull. Chem. Soc. Japan, 12, 472, 1937
78. "Studies of Fluorine at Low Temperatures, Determination of Molecular Heat, Heat of Fusion of Condensed Fluorine and the Entropy of Fluorine," Bull. Chem. Soc. Japan, 518, 1937.
79. "Studies of Fluorine at Low Temperatures, Viscosity of Fluorine Gas at Low Temperatures," Bull. Chem. Soc. Japan, 12, 463, 1937
80. "Studies of Fluorine at Low Temperatures, Boiling Point of Fluorine," Bull. Chem. Soc. Japan, 12, 463, 1937.
81. Kapustinskii, A. R., "Dissociation Energy of Fluorine Molecules Vs. the Rule of Thermochemical Logarithmicity," Trudy, Moskov, Khim..... ..Tekhnol Inst. im. D. E. Mendelew, 1956, 22, 17-20, as given in Chemical Abstracts, 1957
82. Kimball, G. E. and M. Metlay, "Ionization Processes on Tungsten Filaments, the Absorption of Fluorine on Tungsten," J. Chem. Phys., 16, 779, 1948
83. Landau, R. and R. Rosen, "Industrial Handling of Fluorine," Chapter VII in Preparation, Properties, and Technology of Fluorine and Organic Fluor Compounds by C. Slessor (ed.), McGraw-Hill, New York, 1951, p. 136
84. Leech, H. R., "Some Advances in Fluorine Chemistry," Research, 5, 449-55-1952
85. Liquid Propellant Information Agency, Applied Physics Laboratory, Liquid Propellant Safety Manual, October 1958

86. Arthur D. Little Company, An Investigation and Evaluation of Methods and Equipment to Transport, Transfer, and Store Liquid Fluorine, Report to Army Ballistic Missile Agency, 31 January 1957, C-60516
87. Lubick, R. J. and W. L. Jones, "Performance Characteristics of Hydrogen-Fluorine Rocket Engines at Various Chamber Pressures and Nozzle Area Ratios," Bulletin of 2nd Meeting of Joint Army, Navy, Air Force Liquid Propellant Group, San Diego, California, 1-3 November 1960, LPIA, APL, Johns Hopkins University, Silver Spring, Maryland, p. 437
88. The Martin Company, Baltimore, Liquid Fluorine-Oxidant for Rocket Engines, by James Stebbins and George Morris, RM38, Aug. 1959
89. Murphy, G. M. and J. E. Vana, "Thermodynamic Properties of Hydrogen Fluoride and Fluorine from Spectroscopic Data," J. Chem. Phys., 7, 807, 1939
90. "Standard Entropy of Fluorine Gas," J. Chem. Phys., 18, 1514, 1950
91. Murphy, G. M. and E. Rubin, "The Entropy of Fluorine," J. Chem. Phys., 20, 1179-80, 1952
92. National Advisory Committee for Aeronautics, Lewis Flight Propulsion Laboratory, Cleveland, Ohio, Rocket Laboratory Safety and Design Manual
93. NACA, Theoretical Rocket Performance of JP-4 Fuel with Several Fluorine-Oxygen Mixtures Assuming Equilibrium Composition, NACA RM E57K22, by S. Gordon, 1958
94. NACA, Theoretical Rocket Performance of JP-4 Fuel with Several Fluorine-Oxygen Mixtures Assuming Frozen Composition by S. Gordon and K. S. Drellishak, NACA RM E57G16a, 1957
95. NACA, Theoretical Performance of Liquid NH<sub>2</sub> and Liquid Fluorine as a Rocket Propellant by S. Gordon and V. N. Huff, NACA RM53A26, March 1953
96. NACA, Theoretical Performance of Liquid Hydrazine and Liquid Fluorine as a Rocket Propellant by S. Gordon and V. N. Huff, NACA RM53E12, July 1953
97. NACA, Theoretical Performance of Mixture of Liquid Ammonia and Hydrazine as Fuel with Liquid Fluorine as Oxidant for Rocket Engines by S. Gordon and V. N. Huff, NACA RM53F08, July 1953
98. NACA, Theoretical Performance of JP-4 Fuel with a 70 Percent Fluorine-30 Percent O<sub>2</sub> Mixture as a Rocket Propellant, I-Frozen Composition by S. Gordon and V. N. Huff, NACA RM56A13a, 11 April 1956

99. NACA, Theoretical Performance of JP-4 Fuel with 70-30 Mixture of Fluorine and O<sub>2</sub> as a Rocket Propellant, II-Equilibrium Composition by S. Gordon and V. N. Huff, NACA RM E56F04, 2 October 1956
100. NACA, Theoretical Performance of Lithium and Fluorine as a Rocket Propellant by S. Gordon and V. N. Huff, NACA RM E51C01, May 1957
101. NACA, Theoretical Performance of Liquid Methane with Several Fluorine-Oxygen Mixtures Assuming Frozen Composition by S. Gordon and M. E. Kastner, NACA RM E58B20, 1958
102. NACA, Theoretical Maximum Performance of Liquid F<sub>2</sub> - Liquid O<sub>2</sub> Mixtures with JP-4 Fuel as Rocket Propellants by S. Gordon and R. L. Wilkins, NACA RM E57H09, October 1954
103. NACA, A Study of Injection Processes for 15 Percent Fluorine - 85 Percent O<sub>2</sub> and Heptane in a 200-Pound-Thrust Rocket Engine by M. F. Heidman, NACA RME56J11, 15 January 1957
104. NACA, Theoretical Rocket Performance of JP-4 Fuel with Mixtures of Liquid Ozone and Fluorine by S. Gordon and V. N. Huff, NACA RM E56K14, 28 January 1957
105. NACA, Investigation of Liquid Fluorine and Hydrazine-Ammonia Mixture in 100 Pound-Thrust Rocket Engines by P. M. Ordin, E. A. Rothenberg, and W. H. Rowe, NACA RM E52H22, October 1952
106. NACA, Preliminary Investigation of the Performance and Starting Characteristics of Liquid Oxygen-Liquid Fluorine Mixtures with JP-4 Fuel by P. M. Ordin and E. A. Rothenberg, NACA RM E53J20, January 1954
107. NACA, Experimental Performance of a 500-Pound-Thrust Rocket Chamber Using a 20 Percent Fluorine - 80 Percent Oxygen Mixture with RP-1 by F. J. Kutina, Jr., E. A. Rothenberg, and W. A. Tomanic, NACA RM E57B08, 1957
108. NACA, Compatibility of Metals with Liquid Fluorine at High Pressures and Flow Velocities by H. W. Schmidt, NACA RM E58D11, 1958
109. NACA, Reaction of Fluorine with Carbon as a Means of Fluorine Disposal by H. W. Schmidt, NACA RM E57E02, 1957
110. NACA, Nonmetallic Material Compatibility with Liquid Fluorine by Harold G. Price, Jr., and Howard W. Douglass, NACA RM E57G18, 2 October 1957
111. NACA, Material Compatibility with Gaseous Fluorine by H. W. Douglass and H. G. Price, Jr., NACA RM E56K21, 23 January 1957



112. NACA, Theoretical Performance of Liquid Hydrogen and Liquid Fluorine as a Rocket Propellant for a Chamber Pressure of 600 psia by A. Fortini and V. N. Huff, NACA RM E56L10a, 25 January 1957
113. NACA, Theoretical Performance of Liquid H<sub>2</sub> and Liquid Fluorine as a Rocket Propellant by S. Gordon and V. N. Huff, NACA RM E52L11, February 1953
114. NACA, Investigation of the Liquid Fluorine-Liquid Diborane Propellant Combination in a 100-Pound Thrust Rocket Engine, by H. W. Douglass, P. M. Ordin, and W. H. Roew, NACA RM E51104, November 1951
115. NACA, Investigation of the Liquid Fluorine-Liquid Ammonia Propellant Combination in a 100-Pound Thrust Rocket Engine by H. W. Douglass and E. A. Rothenberg, NACA RM E53E08, July 1953
116. NACA, Experimental Performance of Fluorine-Ammonia in 1000-Pound-Thrust Rocket Engines, by H. W. Douglass, RM E54C17, May 1954
117. NACA, Experimental Performance of Fluorine-Oxygen with JP-4 Fuel in a Rocket Engine, by H. W. Douglass, NACA RM E55D27, July 1955
118. NACA, Experimental Rocket Performance with 15% Fluorine-85% Oxygen and JP-4, by E. A. Rothenberg and W. A. Tomaxic, NACA RM E55D29, 29 August 1955
119. NACA, Investigation of the Corrosion of Metals of Construction by Alternate Exposure to Liquid and Gaseous Fluorine by C. E. Feiler and R. M. Gundzik, NACA TN 333, December 1954
120. NACA, Transportation of Liquid Fluorine by P. M. Ordin, NACA RM E55123, 8 November 1955
121. NACA, Preliminary Evaluation of a Very High Energy Rocket Propellant by Howard W. Douglass, ASTIA No. 152273, for presentation at the Institute of Aeronautical Sciences Annual Flight Propulsion Meeting, Cleveland, 13-14 March 1958
122. NASA, Lewis Research Center, Cleveland, "Hydrogen-Fluorine and Hydrogen-Oxygen Rocket Research" by H. W. Douglass, R. J. Salmo, and W. A. Tomazic for IAS-NASA-Air Force Meeting, 9 March 1961
123. NASA, Investigation of Injectors for a Low-Chamber-Pressure Hydrogen-Fluorine Rocket Engine by R. J. Lubick, H. G. Price, Jr., and A. M. Shinn, Jr., NASA TM X-485, July 1962
124. NASA, Investigation of the Effects of Fluoride on Corrosion at 170°F of 2S-O Aluminum and 347 Stainless Steel in Fuming Nitric Acid by C. E. Feiler and G. M. Morrell, NASA RM E53L17b, February 1954
125. NASA, (Unpublished Data) by Fletcher and Hubbard

126. NASA, Control of Combustion-Chamber Pressure and Oxidant-Fuel Ratio for a Regeneratively Cooled Hydrogen-Fluorine Rocket Engine by R. A. Flage and E. W. Otto, NASA TN D-82, 1959
127. NASA, Rate of Reaction of Gaseous Fluorine with Water by E. A. Fletcher and V. A. Slabery, NASA, Washington, D.C. Report TN 4374, 1958
128. NASA, Ignition of Hydrogen-Oxygen Rocket Engine with Fluorine by E. A. Rothenberg and D. M. Straight, NASA RM X-101, 1959
129. NASA, Analytical Comparison of Hydrazine with Primary Propellants as the Turbine Drive Fluid for Hydrogen-Fluorine and Hydrogen-Oxygen Altitude Stage Rockets by W. T. Wintucky, NASA TN D-78, 1959
130. NASA, Field Experiments on Treatment of Fluorine Spills with Water or Soda Ash by G. R. Kinney, L. C. Leopold, and R. J. Rollbuhler, NASA TN D-63, 1959
131. NASA, Design and Operating Criteria for Fluorine Disposal by Reaction with Charcoal by H. W. Schmidt, NASA Memo 1-27-59E, 1959
132. NASA, Experimental Performance of Liquid Hydrogen and Liquid Fluorine in Regeneratively Cooled Rocket Engines by H. W. Douglass, G. Hennings, and H. G. Price, Jr., NASA TM X-87, 1959
133. NASA, Performance of a JP-4 Fuel with Fluorine-Oxygen Mixtures in 1000-Pound-Thrust Rocket Engines, by H. W. Douglass and D. L. Nored, NASA RM E58C18, 1958
134. NASA, Investigation of Small-Scale Hydrazine-Fluorine Injectors by R. J. Rollbuhler and W. A. Tomazic. NASA Memo 1-23-59E. 1959
135. NASA, Analysis of Effects of Rocket-Engine Parameters on Regenerative-Cooling Capabilities of Several Propellants by A. N. Curren, H. W. Douglass, and H. G. Price, Jr., NASA TN D-66. 1959
136. National Bureau of Standards. Circular No. 467
137. National Nuclear Energy Series, Division VI, Vol. I, Pharmacology and Toxicology of Uranium Compounds, Manhattan Project, "Toxicity Following Inhalation of Fluorine and Hydrogen Fluorine" by H. C. Hodge and C. Voegtlin, McGraw-Hill, New York, 1021, 1949
138. Noland, R. L. "Rockets and Missiles," Chem. Eng., 65, 10, 145. 1958
139. North American Aviation, Inc., Fluorine as a Rocket Propellant, by T. F. Dixon, PC-143P, September 1955
140. NAA, A Study of Rocket Engines Using Liquid Fluorine as the Oxidizer by W. R. Edmondson, R-371-4, December 1957 (C)
141. NAA, Development of a Prototype Liquid Fluorine Pump, R-172, March 1956

142. NAA, A survey of Liquid Rocket Propellants by T. F. Dixon, J. W. Parsons, and T. L. Thompson, NAA Report NA-47-95, April 1947 (C)
143. NAA, Rocket Research on Fluorine-Oxygen Mixtures--Final Report by H. Grossaclus, SI Greenfield, and R. Osborn, PC 21, 1 February 1955 (C)
144. NAA, Evaluation of the Performance of Liquid Fluorine-Ammonia Propellant System, AL-1517-1 through -7 and AL-1800, Contract AF33(616)-62, covering period Sept. 1952 - Oct. 1953
145. NAA, Rocket Research on Fluorine-Oxygen Mixtures, Report PC-74-4, Downey, California, Period Ending Sept. 1955 (C)
146. NAA, Rocketdyne, Component Development and Research for Rocket Engines Using High-Performance Propellants, Report R-371-2, Canoga Park, Calif., Quarterly Progress Report for period ending 31 Dec 1956 (C)
147. NAA, Rocketdyne, Research in Fluorine Chemistry, Summary Report No. R-3505, Canoga Park, Calif., Period 16 March 1961 to 15 March 1962
148. NAA, Rocketdyne, High Energy Upper Stage Propulsion System, Canoga Park, Calif. (C)
149. NAA, Rocketdyne, Nomad Quarterly Technical Program Report, Report No. R-2278-1, Canoga Park, Calif., 30 April 1960 (C)
150. NAA, Rocketdyne, Nomad Monthly Technical Report, Report No. R-1090-8, Canoga Park, Calif., 28 Feb 1959 (C)
151. NAA, Rocketdyne, Rocket Research on Fluorine-Oxygen Mixtures, Final Report No. R-171, 30 March 1956
152. NAA, Rocketdyne, Physical Properties of Fluorine-Oxygen Mixtures, Report No. R-398, 28 Nov 1956
153. NAA, Rocketdyne, Nomad Semiannual Technical Program Report, Contract AF04(647)-171, 31 Dec 1959 (C)
154. NAA, Rocketdyne, Nomad Program Review, Report No. BCI 60-51 7 June 1960 (C)
155. Ohio State Univ., Dept. of Chem., Cryogenic Laboratory, Kinetics, Thermodynamics, Physico-Chemical Properties and Manufacture of Fluorine in Its Volatile Inorganic Compounds, By E. Fultz, H. L. Honston, and D. White, 18 Aug 1952
156. The Ralph M. Parsons Company, Final Report High Energy Test Facility Study, Contract AF04(611)-1047, 30 Nov 1956 (C)

157. Potter, R. L., "Thermodynamic Properties of Oxygen Fluoride and Chlorine Fluoride from Spectroscopic Data," J. Chem. Phys., 17, 957-9, 1949
158. Potter, R. L., "Thermodynamic Properties of Some Simple Fluorine Compounds," J. Chem. Phys., 26, 394-6, 1957
159. Pritchard, H. O., "The Determination of Electron Affinities," Chem. Rev., 52, 529, 1953
160. Pritchard, H. O. and H. A. Skinner, "Extrapolation of Electric Affinities," J. Chem. Phys., 22, 1936, 1954
161. Rand Corporation, Propellants for Supersonic Vehicles, Liquid Fluorine, by S. J. Kiehl and J. R. Moore, No. PA-15047, Aug 1947
162. Reaction Motors, Inc., Theoretical, Laboratory and Experimental Investigations of High-Energy Propellants: A Review of the Physical and Chemical Properties of Fluorine and Certain of Its Compounds, by D. Horvitz, Report No. RMI-293-55, Rockaway, New Jersey, Sept 1950 (LP 4755)
163. Republic Aviation Corporation, Cooling Equipment, Design Study Part 8, The Thermodynamics of Oxygen, Hydrazine, and Fluorine by E. F. Fricke, Report No. F-5028-101, Farmingdale, L. I., N.Y.
164. Rogers, M., V. Schomaker, and D. P. Stevenson, "The Internuclear Distance in the Fluorine Molecular," J. Am. Chem. Soc., 63, 2610, 1941
165. Rosen, F. D. "Magnetic Pumps for Corrosive Gases and Liquids," Rev. Sci. Instr., 24, 1061-2, 1953
166. Sanderson, R. T. "The Dissociation Energy of Fluorine," J. Chem. Phys., 22, 345-6, 1954
167. Schmidt, H. W. and E. A. Rothenberg, "Some Problems in Using Fluorine in Rocket Systems," Proceedings of the Propellant Thermodynamics and Handling Conference held at Ohio State University, Columbus, Ohio, Special Report No. 12, June 1960
168. Schram, S. R. and C. Slessor, Preparation, Properties, and Technology of Fluorine and Organic Fluoro Compounds, McGraw-Hill, New York, 1951
169. Sharpe, A. G. "Some General Aspects of the Inorganic Chemistry of Fluorine," Quart. Rev. (London), 49-60, 1957
170. Simons, J. F., Ed. Fluorine Chemistry, Vol. I., Academic Press, Inc., New York, 1950

171. Thompson, G. U. E. "Cost and Availability of High Energy Rocket Propellants," J. Brit. Interplanet, Soc., 11, 333-41, 1952
172. Thompson, F. J., Jr., "Rocket Propellants," Chem. Eng. News, 36, 62-7, 1958
173. Tormey, J. F. "Liquid Rocket Propellants...Is There An Energy Limit?" Ind. Eng. Chem., 49, 1339-43, 1957
174. U. S. Dept. of Commerce, NBS, Selected Values of Chemical Thermodynamic Properties, Circular 500, U. S. Govt. Prtg. Office, Washington, D.C., 1 Feb 1952
175. U. S. Naval Ordnance Test Station, China Lake, Calif. Selection of Oxidizers for Pre-Loaded Liquid Propellant Missiles, by S. Singer, Report No. 2020, Navord Report No. 5881, 5 May 1958
176. Univ. of Rochester, A Study of the Toxicological Effects of the Inhalation of Gaseous Fluorine at a Concentration of Approximately 25 MG/MP; 8 MG/MP; 3 MG/MP (3 reports) by Nils Eriksen, Division of Pharmacology, Reports No. 397, 407 and 427, Manhattan Project, Contract W-7401-eng-49, 1945
177. Univ. of Rochester, A 31-Day Study of the Toxicological Effects of the Inhalation of Gaseous Fluorine at a Concentration of Approximately 0.8 MG/MP, Manhattan Project, Contract W-7401-eng-49, 1945
178. Univ. of Rochester, A Study of the Lethal Effect of the Inhalation of Gaseous Fluorine at Concentrations from 100 ppm to 10,000 ppm, by Nils Eriksen. Manhattan Project, Contract W-7401-eng-49, 1945
179. Wieke, E., "The Dissociation Energy of Fluorine," J. Chem. Phys., 56, 358-60, 1952
180. Wise, H., "Measurement of the Heat of Dissociation of Fluorine by the Effusion Method," J. Phys. Chem., 58, 389-91, 1954, also J. Chem. Phys., 20, 927, 1952
181. Wright-Patterson AFB, Dayton, Ohio, The Thermodynamic Functions of the Halgens and Halgen Halides, by R. Edse, Technical Intelligence Dept. AMC, Technical Report No. F-TR-2250-IA (Preprint), Oct 1948
182. Wright-Patterson AFB, Dayton, Ohio, Simplified Method for Rating Liquid Rocket Propellants, by W. C. Noeggeiath, Technical Report No. F-TR-2191-ND. May 1948
183. Zaehring, A. F., "Propulsion Engineering," Missiles and Rockets, 4, 5, 27, 4 Aug 1958
184. Harold W. Schmidt, Handling and Use of Fluorine and Fluorine-Oxygen Mixtures in Rocket Systems, NASA SP-3037, Lewis Research Center, Cleveland, Ohio.



## 4.0 VALVES

### 4.1 INTRODUCTION

The Valves Section compiles the results of work performed to investigate the performance, applications, and limitations of propellant valving and studies concentrated on the evolution of new valve concepts. A Valve Component Rating Analysis Chart was used as an aid to define the areas where advancement in valve technology is required. This chart was constructed based on the results of industry surveys, literature and patent searches. Valve performance was based on their operation with propellants and the space environment.

A study was also made of a pressure-fed bipropellant feed system for an  $OF_2/B_2H_6$  propulsion system. The design facets relative to component definition and sizing are defined in detail.

This section includes several advanced propellant valve designs. Micro-valves are defined and concepts evolved which are suitable for use in fluidic systems and in the control of small thrusters.

### 4.2 VALVE STATE OF THE ART

This section contains a Valve Component Rating Analysis Chart which defines the areas where an advancement in valve technology is required. The results of surveys, valve problem areas, and a review of important state of the art valves are also discussed.

#### 4.2.1 Valve Component Rating Analysis Chart

The valve analysis chart is used as an aid in defining the areas where advancement in valve technology is required. A reliability rating method was used for defining and evaluating problems relating to the state of the art of valves used on liquid chemical propulsion systems. The reliability rating is assigned to each valve and valve element which make up a valve assembly and qualitatively relates to a functional parameter; the performance of the valve or valve elements operating in a propellant; and the space environment.

Reliability ratings assigned to various combinations of components and parameters have the following definitions:

#### Rating

- |    |   |
|----|---|
| 1  | A serious problem exists for which there is no satisfactory solution.                         |
| 2  | A problem exists, but a refinement in technology may be required within the state of the art. |
| 3  | Satisfactory, i.e., within the state of the art.  |
| U  | Necessary information upon which to base a judgment was unavailable.                          |
| NA | Parameter is not applicable.  |

The planetary characteristics and mission parameters presented in the chart were considered for mission durations of five to ten years. These missions may be categorized as those in earth orbit such as communications satellites and those planned for planetary explorations such as missions to Jupiter and beyond to the outer planets. The significant parameters considered for long term missions relate to the effects of leakage and materials' compatibility with propellants and pressurants.

The ratings depicted on the analysis chart, Table 4-1, were based on the results of surveys, studies and work performed under this program. The functional parameters and the space and planetary environments that affect valve operation are discussed in Section 2.0. Propellant properties and materials compatibility are covered in Section 3.0.

#### 4.2.2 Surveys and Searches

The initial efforts to ascertain the state of the art of spacecraft valves consisted of searches and surveys to determine the extent of existing data and evaluate major areas of concern to help supply the direction for the conduct of the program. These efforts included a literature and patent search, a survey of the manufacturing industry, and interviews with cognizant personnel of the prime valve contractors.

4.2.2.1 Literature Search - Since the space environment was of primary interest on this program, information relating to the various space environments, such as vacuum, radiation, meteoroids, and temperature was obtained. This information was required for determination of the environmental problems that valves would encounter in space. The sources for the information included ASTIA documents, NASA Technical Publication Announcements, scientific and technical journals, and industrial reports. One specific reference used extensively was "Engine Operating Problems in Space," Aerojet-General Corp. Report No. 2824, Contract NAS 7-98, April 1964.

From this survey, sufficient information was extracted and compiled to present a reasonably accurate description of the space environments and their relationships to components used on space vehicles. The information on these environments is summarized in Section 2.0 of this report, and covered in detail in References 1 and 2.

4.2.2.2 Patent Search - A search was made of the U.S. Patent Files to determine if any new and useful valve concepts not already applied to space vehicles might be discovered. The search included five general classes of valves, i.e., flow control, vent, relief, shutoff and disconnects. Patents granted prior to 1945 were excluded. Copies of approximately 600 patents were reviewed. The patent numbers are tabulated and presented in Reference 1 by component categories. Each patent was examined to the extent necessary to determine its applicability. Of the entire list of patents examined, there was only one or two basic ideas that might be of some interest to current valve technology.

The low yield of useful ideas was attributed to the exceptionally long time between the conception of an idea and the granting of a patent (about 5 years).



APPLICABILITY			GASES								EARTH STOR.				
			HYDROGEN	HELIUM	NITROGEN	OXYGEN	ARGON	CO <sub>2</sub>	PROPELLANT BOILOFF	COMBUSTION PRODUCTS TO 1500°F	MON 10	NITROGEN TETROXIDE	AEROZINE 50	HYDRAZINE	
FM	VALVE TYPE	FLOW METERING	3	3	3	3	3	3	3	2-3	3	3	3	3	
S		SHUTOFF	2 <sup>e</sup>	2 <sup>e</sup>	3	3	3	3	2-3	2-3	3	3	3	3	
V		VENT OR RELIEF	2 <sup>e</sup>	2 <sup>e</sup>	3	3	3	3	2-3	2-3	3	3	3	3	
CR		COLD GAS REGULATOR	2 <sup>e</sup>	2 <sup>e</sup>	3	3	3	3	2-3	NA	NA	NA	NA	NA	
HR		HOT GAS REGULATOR	2-3	2-3	2-3	U	2-3	2-3	NA	2	NA	NA	NA	NA	
LF		LIQUID FILL OR DISCONNECT	2	2	2-3	2-3	2-3	NA	2-3	NA	2 <sup>b</sup>	2 <sup>b</sup>	2 <sup>b</sup>	2 <sup>b</sup>	
PF		PNEUMATIC FILL OR DISCONNECT	2-3 <sup>b</sup>	2-3 <sup>b</sup>	2-3 <sup>b</sup>	2-3 <sup>b</sup>	2-3 <sup>b</sup>	2-3 <sup>b</sup>	2-3 <sup>b</sup>	NA	NA	NA	NA	NA	
S	CLOSURE	BALL (POLYMERIC SEAL)	3	3	3	3	3	3	3	1	2	2	3	3	
S,V,CR,HR,LF,PF		POPPET	3	3	3	3	3	3	3	3	3	3	3	3	
FM,S		BUTTERFLY	3	3	3	3	3	3	3	3	2	2	3	2	
S		BURST DIAPHRAGM	3	3	3	3	3	3	3	2	3	3	3	3	
S,V,CR,HR,LF,PF	POLYMERIC SEALS	VALVE CLOSURE	2-3	2 <sup>e</sup>	3	3	3	3	3	1-3	2	2	2	2	
ALL		STATIC SEALS	2-3	2-3	3	3	3	3	3	1-3	2	2	3	3	
ALL		DYNAMIC SEALS	2-3	2 <sup>e</sup>	3	3	3	3	3	1-3	2	2	3	3	
S,V,CR,HR,LF,PF		VALVE CLOSURE	1-2 <sup>e</sup>	1-2 <sup>e</sup>	1-2 <sup>e</sup>	1-2 <sup>e</sup>	1-2 <sup>e</sup>	1-2 <sup>e</sup>	1-2 <sup>e</sup>	1-2 <sup>e</sup>	3	3	3	3	
ALL	METAL SEALS	STATIC SEALS	3	3	3	3	3	3	3	3	3	3	3	3	
ALL		DYNAMIC SEALS	1-2 <sup>e</sup>	1-2 <sup>e</sup>	3	3	3	3	3	3	3	3	3	3	
S		SOLENOID	3	3	3	3	3	3	3	3	1	2-3	3	3	
FM,S		PNEUMATIC	3	3	3	3	3	3	3	3	NA	NA	NA	NA	
FM,S	ACTUATORS	HYDRAULIC	NA	NA	NA	NA	NA	NA	NA	2	2	2	2		
FM,S		ELECT. MOTOR	3	1-3	3	3	3	3	3	1	2	2	2	U	
S		SQUIB	3	3	3	3	3	3	3	1	NA	NA	NA	NA	
ALL		SCREW DRIVES	3	3	3	3	3	3	1-3	1-3	U	U	1 <sup>f</sup>	1 <sup>f</sup>	
ALL	DRIVE MECHANISMS	BALL SCREW DRIVES	3	3	3	3	3	3	2-3	2-3	U	1 <sup>f</sup>	1 <sup>f</sup>	1 <sup>f</sup>	
ALL		LINEAR BALL DRIVES	3	3	3	3	3	3	2-3	2-3	U	1 <sup>f</sup>	1 <sup>f</sup>	1 <sup>f</sup>	
ALL		GEARED	3	3	3	3	3	3	2-3	1-2	U	1 <sup>f</sup>	1 <sup>f</sup>	1 <sup>f</sup>	
ALL		PISTON	3	3	3	3	3	3	3	1-3	3	3 <sup>f</sup>	1 <sup>f</sup>	1 <sup>f</sup>	
ALL	BEARINGS AND BUSHINGS	BALL-ROTARY	3	3	3	3	3	3	3	2	U	3 <sup>f</sup>	1 <sup>f</sup>	1 <sup>f</sup>	
ALL		POLYMERIC	3	3	3	3	3	3	3	1	1	1	U	U	
ALL		METAL	2 <sup>f</sup>	2 <sup>f</sup>	2 <sup>f</sup>	2 <sup>f</sup>	2 <sup>f</sup>	2 <sup>f</sup>	3 <sup>f</sup>	1	U	3 <sup>f</sup>	1 <sup>f</sup>	1 <sup>f</sup>	
ALL		FLEXURE PIVOTS	3	3	3	3	3	3	3	2-3	3	2	3	3	
ALL	HERMETIC SEALS	BELLOWS	3	3	3	3	3	3	3	2-3	3	3	3	3	
ALL		DIAPHRAGMS (METAL)	3	3	3	3	3	3	3	2-3	3	3	3	3	
ALL	LUBES	DRY FILM	3	3	3	3	3	3	3	1-2	U	2	2-3	2	
ALL		LIQUID	3	3	3	3	3	3	3	1-2	1	1	1	2	2
ALL		COIL	3	3	3	3	3	3	3	3	3	3	3	3	
ALL	SPRINGS	BELLVILLE	3	3	3	3	3	3	3	2-3	3	3	3	3	
ALL		LIQUID	3	3	3	3	3	3	3	1	U	2 <sup>h</sup>	3 <sup>h</sup>	2 <sup>h</sup>	
FM,S,CR,HR		AN FLARE AND MS FLARELESS	3	3	3	3	3	3	3	3	3	3	3	3	
ALL	FITTINGS AND FASTENERS	WELDED	3	3	3	3	3	3	3	3	3	3	3	3	
ALL		BOLTS AND SCREWS	3	3	3	3	3	3	3	3	3	3	3	3	
ALL		FILTERS	3	3	3	3	3	3	3	1-3	3	3	3	3	







60 HRS. 6 CYCLES	FUNCTIONAL PARAMETERS								ENVIRONMENTAL PARAMETERS										
	POWER REQUIREMENTS	OPERATING LIFE 1000 CYCLES	CONTAMINATION	RESPONSE	VIBRATION AND SHOCK	LEAKAGE	SPACE MAINTAINANCE					SPACE RADIATION			SPACE VACUUM	ZERO G	METEOROIDS	PROD. OF COMBUSTION (TURN AROUND)	
												ON BOARD NUCLEAR POWER SOURCES	VAN ALLEN BELT	SOLAR FLARE					INDUCED BREMSTRAHLUNG
2-3	3	3	3	3	3	2-3	U					2-3	3	3	2	3	3	2/1M	3
2	3	1-2	2	3	1-2	U						2	2	2	2	2-3	3	2/1M	2
3	3	1-3	2	2	1-2	U						2	2	2	2	2-3	3	2/1M	2
3	3	1-2	2	2	1-2	U						2-3	3	3	2	3	3	2/1M	3
3	3	1-2	2	2	1-2	U						2-3	3	3	2	3	3	2/1M	3
NA	3	2	NA	3	1-2	U						2	2	2	2	2	3	2/1M	1-2
NA	3	2	NA	3	1-2	U						2	2	2	2	2	3	2/1M	1-2
2	3	2-3	1-2	3	2-3	U						2	3	3	3	2	3	2/1M	3
3	3	2	3	2	3	U						3	3	3	3	3	3	2/1M	3
2	3	2-3	2	3	1-2	U						3	3	3	3	3	3	2/1M	3
3	NA	1-2 <sup>b</sup>	3	3	3	U						3	3	3	3	3	3	2/1M	3
NA	3	2-3	NA	3	3	U						1-2	1-2	1-2	1-2	2	3	2/1M	2
NA	2	3	NA	3	3	U						1-2	2	1-2	2	2	3	2/1M	3
1-2	3	2-3	2	3	3	U						1-2	1-2	2	1-2	2	3	2/1M	2
NA	3	1	NA	1-3	1-2	U						3	3	3	3	2	3	2/1M	1-2
NA	1	3	NA	3	3	U						3	3	3	3	3	3	2/1M	3
2	2	1	2	3	1-2	U						3	3	3	3	1	3	U	1-2
2	3	2-3	2-3	2-3	NA	U						1-2	2	2	3	1-2	3	2/1M	3
2-3	3	2-3	2-3	2-3	1-3	U						3	3	3	3	3	3	2/1M	3
2-3	3	2-3	2-3	3	3	U						3	3	3	3	3	3	2/1M	3
2	3	1-3	2	3	NA	U						1-2	2	2	2	1-2	3	2/1M	3
3	1	3 <sup>g</sup>	3	3	1	1						U	U	U	U	U	3	U	3
2	3	2	2	3	NA	U						2-3	2-3	2-3	2-3	2	3	2/1M	3
3	3	2	2-3	3	NA	U						3	3	3	3	2	3	2/1M	2
3	3	2	2-3	3	NA	U						3	3	3	3	2	3	2/1M	2
2	3	2	2	3	NA	U						3	3	3	3	2	3	2/1M	2
2-3	3	2	3	3	2	U						3	3	3	3	2-3	3	2/1M	2-3
3	3	2	NA	3	NA	U						3	3	3	3	2	3	2/1M	2
2	2-3	3	NA	3	NA	U						3	3	3	3	2	3	2/1M	2
2	2-3	1-2	NA	3	NA	U						3	1-2	2	2	2	3	2/1M	2-3
2	2-3	1-2	NA	3	NA	U						3	3	3	3	1-2	3	2/1M	1-2
3	3	3	NA	3	NA	U						3	3	3	3	3	3	2/1M	3
2	3	2	2	2	3	U						3	3	3	3	3	3	2/1M	3
2	3	2	3	3	3	U						U	3	3	3	3	3	2/1M	3
2	3	2	NA	2	NA	U						U	U	U	U	2	3	2/1M	2-3
2-3	3	2-3	NA	2-3	NA	U						2	2	2	2	2	1-3	2/1M	2-3
NA	3	3	2-3	2	NA	U						3	3	3	3	3	3	2/1M	3
NA	3	3	2-3	3	NA	U						3	3	3	3	3	3	2/1M	3
NA	3	3	2-3	3	1-2	U						U	U	U	U	2	3	2/1M	3
NA	1-2	2	NA	2	2-3	2						3	3	3	3	3	3	2/1M	3
NA	1	1-3	NA	3	3	U						3	3	3	3	3	3	2/1M	3
NA	1-2	3	NA	2	NA	U						3	3	3	3	3	3	2/1M	3
NA	1-3	1	NA	2	NA	U						3	3	3	3	3	3	2/1M	3

LEGEND:

RATING CHARACTERISTICS

1- POOR  
2- FAIR  
3- GOOD

U- UNAVAILABLE INFORMATION  
NA- NOT APPLICABLE  
UNMANNED (DIGIT ONLY)

2/1M MANNED

VALVE DESIGNATION

FM- FLOW METERING  
S- SHUTOFF  
V- VENT OR RELIEF  
CR- COLD GAS REGULATOR  
HR- HOT GAS REGULATOR  
LF- LIQUID FILL OR DISCONNECT  
PF- PNEUMATIC FILL OR DISCONNECT

NOTES:

a) FREEZING OF CONDENSED MOISTURE AT INTERFACE OF DISCONNECT

b) RATING FOR SERVICE IN VACUUM ENVIRONMENT

c) RATING FOR SHUTOFF VALVE EXPOSED TO SPACE VACUUM

d) NON CAVITATING FLOW CONTROL

e) RATING BASED ON LEAKAGE CONTROL

f) RATING BASED ON PROPELLANT LUBRICATION DATA AT LOW LOADS, SHORT DURATION

g) CONTAMINATION GENERATOR

h) PROPELLANT USED AS COMPRESSIBLE FLUID

i) RATING BASED ON POOR RELIABILITY ASSOCIATED WITH PASSIVATION

j) LIQUIFIED PETROLEUM GAS, METHANE, PROPANE, BUTENE

k) n.d., NEUTRONS RADIOISOTOPE NUCLEAR POWER SOURCES

m) RATING BASED ON FORMATION OF CLOGGING MATERIAL

Table 4-1. Valve Component Rating Analysis Chart 4-3



**RATING CHARACTERISTICS:**

- 1 - POOR
- 2 - FAIR
- 3 - GOOD
- U - UNAVAILABLE INFORMATION
- NA - NOT APPLICABLE

**NOTES:**

- (a) ESTIMATED
- (b) ASSUMED TO BE SMALL
- (c) ASSUMED MUCH GREATER THAN VAN ALLEN LEVEL
- (d) ASSUMED INERT GASES

**APPLICABILITY**

		EARTH MOON						MERCURY						VENUS								
		ATMOSPHERIC PRESSURE ≈ 10 <sup>-8</sup> TORR	TEMPERATURE -243°F TO 240°F	MISSION TIME ≈ 3 - 6 DAYS	SOLAR RADIATION	LUNAR DUST	LUNAR MAINTENANCE	ATMOSPHERIC COMPOSITION HEAVY RARE GASES	ATMOSPHERIC PRESSURE ≈ 4E EARTH (≈ 2.4 TORR)	TEMPERATURE -426°F TO 750°F	MISSION TIME ≈ 2 YEARS	SOLAR RADIATION	RADIATION BELT ≈ 4E EARTH	MERCURY DUST	MERCURY MAINTENANCE	ATMOSPHERIC COMPOSITION CO <sub>2</sub> , N <sub>2</sub> , H <sub>2</sub> O, H <sub>2</sub>	ATMOSPHERIC PRESSURE ≈ 10 - 20 EARTH ATM.	TEMPERATURE ≈ 600 - 800°F	MISSION TIME ≈ 1 1/2 YEARS	RADIATION BELT < 0.01 EARTH	VENUS DUST	
FM	VALVE TYPE	FLOW METERING	3	2	3	2	2	U	3	3	2	2	U	3	2	U	3	3	2	2	3	2
		SHUTOFF	1	2	3	2	2	U	3	1	2	2	U	3	2	U	3	3	2	2	3	2
V	VENT OR RELIEF	2	2	3	2	2	U	3	2	2	2	U	3	2	U	3	3	2	2	3	2	
CR	COLD GAS REGULATOR	3	2	3	2	2-3	U	3	3	2	2	U	3	2-3	U	3	3	2	2	3	2-3	
HR	HOT GAS REGULATOR	3	2	3	2	3	U	3	3	2	2	U	3	3	U	3	3	2	2	3	3	
LF	LIQUID FILL OR DISCONNECT	2	2	3	2	1	U	3	2	1	2	U	3	1	U	3	3	1	2	3	1	
PF	PNEUMATIC FILL OR DISCONNECT	2	2	3	2	1	U	3	2	1	2	U	3	1	U	3	3	1	2	3	1	
S	CLOSURE	BALL (POLYMERIC SEAL)	1	2	3	1-2	2-3	NA	3	2	1	U	1	3	2-3	NA	3	3	1	U	3	2-3
S, V, CR, HR, LF, PF		POPPET	2	3	3	2-3	2-3	NA	3	2	2	3	U	3	2-3	NA	3	3	2	3	3	2-3
FM, S		BUTTERFLY	2	3	3	2-3	2-3	NA	3	2	2	3	U	3	2-3	NA	3	3	2	3	3	2-3
S		BURST DIAPHRAGM	3	3	3	2-3	3	NA	3	3	2	3	U	3	3	NA	3	3	2	3	3	3
S, V, CR, HR, LF, PF	POLYMERIC SEALS	VALVE CLOSURE	2	1-2	3	1-2	2	NA	3	2	1	2	1	3	2	NA	3	3	1	2	3	2
ALL		STATIC SEALS	2	1-2	3	1-2	3	U	3	2	1	3	1	3	3	U	3	3	1	3	3	3
ALL		DYNAMIC SEALS	2	1-2	3	1-2	2	U	3	2	1	2	1	3	2	U	3	3	1	2	3	2
S, V, CR, HR, LF, PF	METAL SEALS	VALVE CLOSURE	2	2	3	2	1	NA	3	2	2	U	2	3	1	NA	3	2	2	U	3	1
ALL		STATIC SEALS	3	2-3	3	2-3	3	U	3	3	2	3	2-3	3	3	U	3	3	2	3	3	3
ALL		DYNAMIC SEALS	1	2	3	2	1	U	3	1	2	U	2	3	1	U	3	3	2	U	3	1
S	ACTUATORS	SOLENOID	1-2	3	3	3	2	U	3	1-2	2	2	2-3	3	2	U	3	3	2	2	3	2
FM, S		PNEUMATIC	3	3	3	3	2	U	3	3	3	3	3	2	U	3	3	3	3	3	2	
FM, S		HYDRAULIC	3	1-2	3	1-2	2	U	3	3	2	3	1	3	2	U	3	3	2	3	3	2
FM, S		ELECT. MOTOR	1-2	1	3	1	2	U	U	1-2	1-2	U	1	3	2	U	U	U	1-2	U	3	2
S		SQUIB	U	2-3	3	2-3	U	1	2	U	1	U	2	3	U	1	3	U	1	U	3	U
ALL	DRIVE MECHANISMS	SCREW DRIVES	2	2	3	2	1	U	2	2	1	2	1-2	3	1	U	2	3	1	2	3	1
ALL		BALL SCREW DRIVES	2	2	3	2	1	U	2	2	1	2	1-2	3	1	U	2	3	1	2	3	1
ALL		LINEAR BALL DRIVES	2	2	3	2	1	U	2	2	1	2	1-2	3	1	U	2	3	1	2	3	1
ALL		GEARED	2	2	3	2	2	U	2	2	1-2	2	1-2	3	2	U	2	3	1-2	2	3	2
ALL		PISTON	2-3	2-3	3	2-3	2	U	2	2-3	2	3	2	3	2	U	3	3	2	3	3	2
ALL	BEARINGS AND BUSHINGS	BALL-ROTARY	1-2	2	3	2	1	U	2	1-2	2	3	3	3	1	U	2	3	1	2	3	2
ALL		POLYMERIC	2	2	3	2	2	U	3	2	1	2	1	3	2	U	3	3	1	2	3	1
ALL		METAL	1	2	3	2	1	U	2	1	1-2	2	1-2	3	1	U	2	3	1-2	2	3	1
ALL	HER-METIC SEALS	FLEXURE PIVOTS	3	3	3	2-3	3	U	3	3	3	3	3	3	U	3	3	3	3	3	3	
ALL		BELLOWS	3	3	3	3	3	U	3	3	3	3	3	3	U	3	3	3	3	3	3	
ALL	DIAPHRAGMS METALS	3	3	3	3	3	U	3	3	3	3	3	3	U	3	3	3	3	3	3		
ALL	LUBES	DRY FILM	2	2	3	1	1-2	1	3	2	2	1-2	2	3	1-2	1	3	3	2	1-2	3	1-2
ALL		LIQUID	2	1	3	1	2-3	1	3	2	1	1-2	1	3	2-3	1	3	3	1	1-2	3	2-3
ALL		COIL	3	3	3	3	3	U	3	3	2	3	2-3	3	3	U	3	3	2	3	3	3
ALL	SPRINGS	BELLVILLE	3	3	3	3	3	U	3	3	2	3	2-3	3	3	U	3	3	2	3	3	3
ALL		LIQUID	2	1	3	1-2	3	U	3	2	1	1-2	1	3	3	U	3	3	1	1-2	3	3
FM, S, CR, HR	FITTINGS AND FASTENERS	AN FLARE AND MS FLARELESS	3	3	3	3	1-2	3	3	2	3	3	3	3	U	3	3	2	3	3	3	
ALL		WELDED	3	3	3	3	3	1	3	3	3	3	3	3	U	3	3	3	3	3	3	
ALL		BOLTS AND SCREWS	3	3	3	3	3	1-2	3	3	3	3	3	3	U	3	3	3	3	3	3	
ALL		FILTERS	3	3	3	3	1	U	3	3	3	U	3	3	1	U	3	3	3	U	3	1





PLANETARY MISSIONS

VENUS MAINTENANCE		MARS							JUPITER							SATURN										
		ATMOSPHERIC COMPOSITION N <sub>2</sub> , CO <sub>2</sub> , A	ATMOSPHERIC PRESSURE & EARTH (= 19 TORR)	TEMPERATURE = -190°F TO 80°F	MISSION TIME ≈ 3 YEARS	RADIATION BELT (NEGLECTABLE)	MARTIAN DUST	MARTIAN MAINTENANCE	ATMOSPHERIC COMPOSITION CH <sub>4</sub> , NH <sub>3</sub>	ATMOSPHERIC PRESSURE > 1 EARTH ATM. (g)	TEMPERATURE = -230°F	MISSION TIME ≈ 4 YEARS	RADIATION BELT (g) (UNKNOWN)	JOVIAN DUST	JOVIAN MAINTENANCE	ATMOSPHERIC COMPOSITION CH <sub>4</sub> , NH <sub>3</sub> , O <sub>3</sub> , SO <sub>2</sub>	ATMOSPHERIC PRESSURE > 1 EARTH ATM (g)	TEMPERATURE = -320°F	MISSION TIME ≈ 5 YEARS	RADIATION BELT (UNKNOWN) (g)	SATURN DUST	SATURN MAINTENANCE	ATMOSPHERIC COMPOSITION CH <sub>4</sub> , O <sub>3</sub> , SO <sub>2</sub>	ATMOSPHERIC PRESSURE > 1 ATM (g)	TEMPERATURE	
U		3	3	2	2	3	2	U																		
U		3	2	2	2	3	2	U																		
U		3	3	2	2	3	2	U																		
U		3	3	2	2	3	2-3	U																		
U		3	3	2	2	3	3	U																		
U		3	2	2	2	3	1	U																		
U		3	2	2	2	3	1	U																		
U		3	2	2	2	3	1	U																		
NA		3	2	1-2	U	3	2-3	NA																		
NA		3	3	3	3	3	2-3	NA																		
NA		3	3	3	3	3	2-3	NA																		
NA		3	3	3	3	3	3	NA																		
NA		3	2-3	1-2	U	3	2	NA																		
U		3	3	1-2	3	3	3	U																		
U		3	2-3	1-2	U	3	2	U																		
NA		3	2	2	U	3	1	NA																		
U		3	3	2-3	3	3	3	U																		
U		3	1-2	2	U	3	1	U																		
U		3	3	3	3	3	2	U																		
U		3	3	3	3	3	2	U																		
U		3	3	1-2	3	3	2	U																		
U		1-3	2-3	1	U	3	2	U																		
U		3	2-3	2-3	U	3	U	1																		
U		2-3	2	2	2	3	1	U																		
U		2-3	2	2	2	3	1	U																		
U		2-3	2	2	2	3	1	U																		
U		2-3	2	2	2	3	2	U																		
U		2-3	2-3	2-3	2-3	3	2	U																		
U		2-3	2-3	2	3	3	1	U																		
U		3	2-3	2	2	3	2	U																		
U		2-3	1-2	2	2	3	1	U																		
U		3	3	3	3	3	3	U																		
U		3	3	3	3	3	3	U																		
U		3	3	3	3	3	3	U																		
U		3	3	2	1-2	3	1-2	1																		
U		3	2	1	1-2	3	2-3	1																		
U		3	3	3	3	3	3	U																		
U		3	3	3	3	3	3	U																		
U		3	3	3	3	3	3	U																		
U		3	2	1	1-2	3	3	U																		
U		3	3	3	3	3	3	U																		
U		3	3	3	3	3	3	U																		
U		3	3	3	3	3	3	U																		
U		3	3	3	3	3	3	U																		
U		3	3	3	U	3	1	U																		







4.2.2.3 Agency Surveys - Interviews were arranged with the cognizant personnel at most of the prime manufacturers for the purpose of determining present and future valve requirements and to determine what current valve problems existed. As an aid to the conduct of these interviews, typical systems schematics (Figures 4-1 and 4-2) were used in the discussion.

A list of approximately 500 valve manufacturers was compiled from the various buyer's guides, trade journals, and technical magazines, and a form letter, including a questionnaire, was mailed to each of the manufacturers. The questionnaire requested that the recipient note the type of valve or valves produces, the actuator that could be used with it, and the class of service for which the valve was intended, such as high temperature, high pressure, or cryogenic. A tabulated list of typical valve requirements by function, a list of aerospace valve manufacturers, and a breakdown of valve types by manufacturer and service are presented in Reference 1.

#### 4.2.3 Valve Problem Areas

An analysis of the problems associated with state of the art valves and subcomponents was made. Conclusions were drawn on the basis of the information on functional parameters and the space and planetary environments obtained during the surveys (see Section 2.0). The material discussed in this area is also tabulated in Reference 1.

4.2.3.1 Fill Valves (Disconnects) - Fill valves may assume numerous configurations with respect to the type of valve used, and the method of connecting and disconnecting. In the simplest case the valve can be of almost any type of manual shutoff, particularly at low pressures. For added insurance against leakage, a secondary closure such as a cap can be attached and locked in place. An example of such a fill valve for a low-pressure gas system, consists of an AN bulkhead union fitted with a conventional aircraft tire valve core which is capped after filling. This fill valve represents the ultimate in simplicity and the leakage is essentially zero. As the requirements become more rigorous, fill valves become more complex. High pressures and toxic, corrosive, or cryogenic fluids must be transferred by more elaborate couplings which may include requirements for remote operation, balanced valve design, and very low spillage upon engagement or disengagement.

Disconnects are required to meet stringent leakage requirements because of the necessity of preventing pressurant or propellant loss and the hazards to personnel that might result from leakage. To meet the requirements, soft seats are used in these valves almost exclusively. A problem arises from the fact that no known polymers are compatible with fluorine and fluorine vapors, and thus all metal construction would be required for these propellants. However, metal-to-metal closures are very sensitive to contamination.

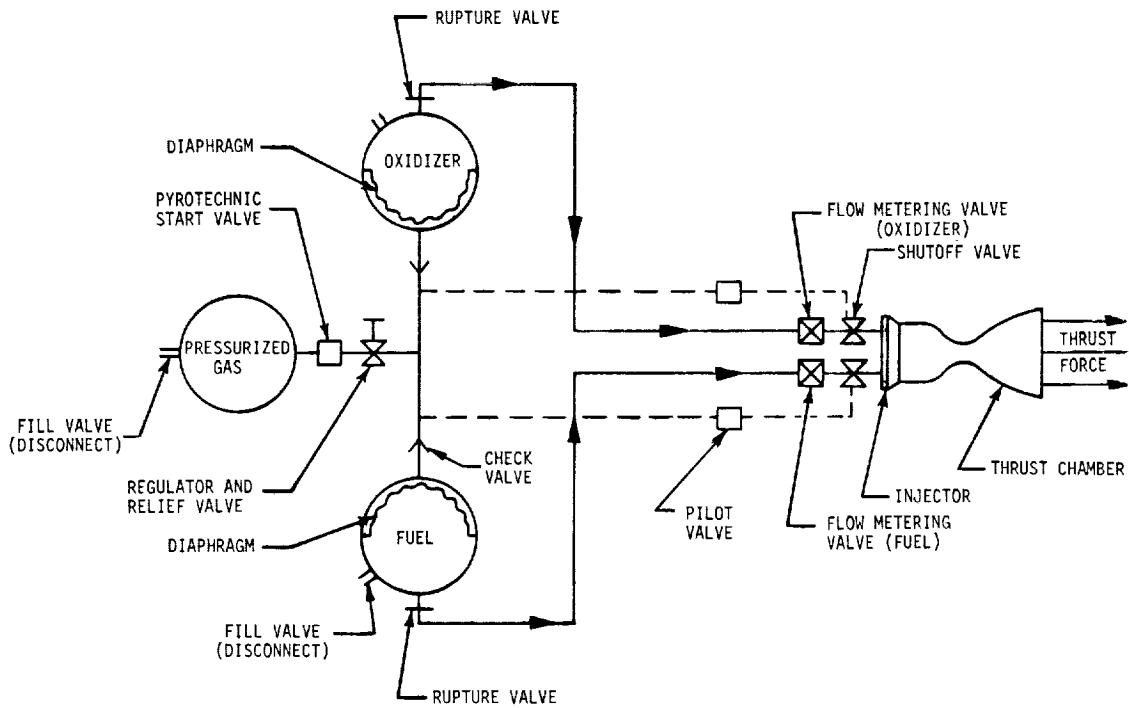


Figure 4-1. Typical Bipropellant Spacecraft Propulsion System

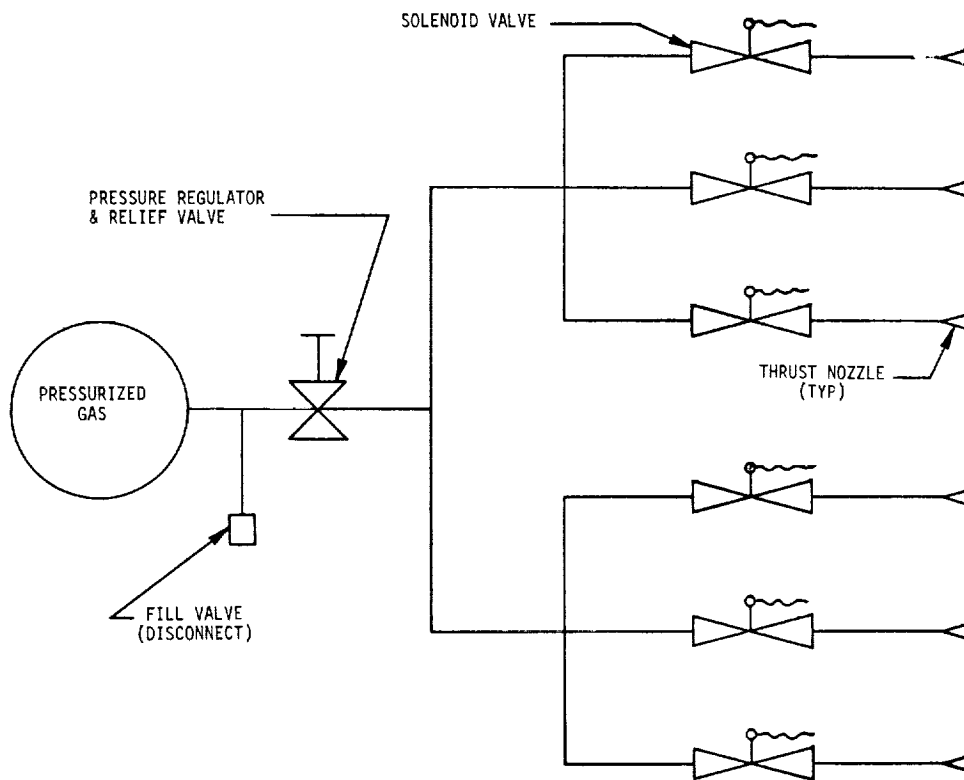


Figure 4-2. Typical Attitude Control For Spacecraft

Other problems with fill valves include that of the effects of sterilization temperatures on soft seats in contact with propellants. It is probable that the combination of high sterilization temperature for long periods (36 hours) and propellant contact may degrade elastomeric seals or seats. If the disconnect port is exposed to space vacuum, sublimation of the material would occur to some degree, and radiation effects could degrade the polymers if the dosage became sufficiently high.

4.2.3.2 Shutoff Valves - The term shutoff valve is general. It usually means a valve that has only an on-off function, i.e., it does not modulate pressure or control flow in a variable way. A great variety of shutoff valves exists, since such a valve may be of almost any configuration and still satisfy the function. It can be a simple petcock, commonly called a plug valve, or it can use any of numerous other closure mechanisms, e.g., butterfly, poppet, slide, pinch, etc. The closures may use elastomers for sealing or a metal-to-metal seat. The valve can have a variety of actuators - manual, electrical, hydraulic, electrohydraulic or pneumatic.

The particular configuration selected for a given system depends upon the detail requirements of the application. The choice of seat material, for instance, depends upon the degree of contamination that must be contended with, the operating and ambient temperature ranges the valve will experience, and the flow medium the valve is required to control. The choice of actuator is also strictly dependent upon system requirements. From this almost limitless number of combinations, it is possible to select and procure an adequate shutoff valve for most applications. However, there remains distinct and pressing problems to be solved with shutoff valves intended for use on space vehicles. Many of the problems encountered by shutoffs are identical to those encountered by disconnects, e.g., those of sterilization, contamination susceptibility and the possibility of damage from radiation. In addition, the shutoff valve will be required to operate at higher temperatures than a disconnect, and above 500°F the choice of seat material is usually restricted to metals only. Continuously operating attitude control valves may use significant amounts of electrical energy, and the response of a valve for this application must be quite high. If metal-to-metal seats are used, the possibility of cold welding in high vacuum exists. Contamination from space debris and lunar dust could contribute to failure, and measures must be taken to exclude such dirt from the valve.

Shutoff valves are available for performing a wide variety of tasks. Valves are available for "in line" operation of a space vehicle, where the valve is immersed in the operating fluid and does not have its internal parts exposed to space. However, the "last valve" in the system, which will have one port exposed to the space environment, may be degraded from the effects of vacuum, radiation, space debris and other external contaminants.

4.2.3.3 Flow Metering Valves - The function of a flow metering valve is to control the flow of a propellant to the engines at some specific rate. The control may be effected by a sharp-edged orifice in the line with a shutoff valve upstream, or the orifice may be incorporated into the valve itself. Variable thrust rocket engines employ a movable variable area pintle in a fixed orifice. Bipropellant engines employ a dual pintle arrangement in which the pintles are operated in tandem through a linkage. The valves also can be designed to operate in the cavitating regime, which makes the flow rate independent of changes in the downstream pressure. Flow metering valves are not subject to failure from contamination to the same degree as shutoff valves, because stringent leakage requirements are eliminated.

Flow metering valves can be of all metal construction or can be designed to include polymers, the choice being dependent upon the particular application and propellants used. All metal construction permits a higher range of operating temperature, and alleviates the concern with propellant compatibility, especially for long-term missions. The use of all metal construction would involve bellows, seals, and may also incorporate a hermetically sealed lubrication system. If polymers are used in the construction, the previous comments regarding the limitations imposed by temperature, propellant compatibility, radiation, and vacuum apply.

4.2.3.4 Vent Valves - A vent valve is required to perform to exacting requirements under widely varying conditions of ambient temperature, vibration, and acceleration. It must be able to handle the large flow rates resulting from boiloff during propellant loading, and it must have a high response to maintain tank pressures within close limits after loading and cooldown. Cryogenic vent valves presented one of the most severe problems encountered in the ICBM program.

Valves have been produced to satisfy the vent function on ICBM's after a development program of more than five years. The techniques of design, manufacture, test, and operation that evolved during this program can be utilized in supplying a vent valve for space operations. Some of the problems that must still be considered with cryogenic vent valves are:

1. Care must be taken to insure that the tank is purged of all water vapor prior to loading. If this is not done, the vapor may freeze in the vent valve causing failure.
2. If plastic liners or other components are used for seals, the plastics must be dimensionally stable over the expected range of temperatures. Ideally, this stability is achieved through the proper selection of material. However, if stable material is not available, suitable processing techniques must be used to achieve the desired result.



3. Under zero gravity conditions, the location of the liquid in the tank may be random and indeterminate unless a positive expulsion system is used. To avoid the excessive loss of oxidizer which would result if liquid were vented instead of gas, it will be necessary to insure that only the vapor phase has access to the discharge ducting. Studies have indicated that the liquid tends to collect in the center of the tank under zero g conditions. If additional tests substantiate this position, it may only be necessary to provide an annular collector ring inside the tank to effect the separation of liquid and gas. A zero g thermal vent valve system is discussed in Section 4.5.
4. If polymers are used in the construction, the effects of the propellants, sterilization, temperature, vacuum, and radiation must be considered.

Vent valves for spacecraft must perform under adverse conditions. As one port will be posed to the space environment, sublimation of polymers, if used in the closure, must be considered. If all metal seats are used, the possibility of cold welding exists. Radiation and contamination from external sources could also impair or destroy the valve. In addition to these normal environmental effects with which the valve must contend, the vent valve is faced with a unique problem peculiar to the venting function, i.e., the zero gravity condition. The valve must be capable of discriminating between a gaseous and liquid flow medium, or must be capable of separating the two phases so that only the gas is relieved. During the vendor survey, only two manufacturers were found who have attempted to design a vent valve capable of meeting the requirements imposed by the zero gravity field. Because of the difficulty of testing such devices, little or no test data is available.

It must be concluded that considerable development time and effort would be required to produce a satisfactory valve for a venting operation. Additional studies are also needed to determine the actual valve requirements. For instance, some tank studies have indicated that the location of the liquid in the tank can be predicted or controlled, and temperature studies have indicated that venting may not be necessary for some specific missions.

4.2.3.5 Pneumatic Cold-Gas Regulators - The function of a pressure regulator is to reduce a higher pressure fluid to a lower pressure within rather narrow limits of accuracy. The regulator must perform this task in spite of many variables that occur during the process. For example, the upstream pressure decays with time and the temperature of the flowing medium may increase or decrease. The flow rate may vary from zero to the maximum capacity of the regulator. The temperature in the ullage downstream of the regulator may vary widely with time, and the regulator may be subjected to extremely variable environmental conditions, such as abrupt changes in ambient temperature and pressure and variable conditions of acceleration, vibration, and shock.

The development of ICBM pressure regulators was conducted concurrently with the development of vent valves. The requirements for regulators are more severe in several respects than are those for the vent valves, in that the operating temperature range is wider (from -300° to +400°F) and the valves must control helium gas which imposes stringent seal requirements.

Two general types of regulators have been employed in tank pressurization, the modulating and the on-off, sometimes called the "bang-bang" type. In the former, tank pressure is sensed and a pneumatic signal is fed to a controller on the regulator. In brief, the controller matches the tank pressure signal against a preset reference pressure signal (spring or bellows) and the main valve within the regulator responds to eliminate any error between the signals. In the bang-bang control system, tank pressure is sensed by a pressure switch, which in turn actuates a solenoid valve. A particular advantage of the bang-bang concept is that the sensing elements, i.e., the pressure switch, can be isolated from the temperature effects of the flowing medium, as it can be located remotely from the valve.

The following problems must be considered with cold gas regulators:

1. Contamination - This is the largest source of trouble reported. The close fits of the moving parts and the small orifices that are often used in the control sections dictate that the flowing medium be exceptionally clean. In addition, extreme care must be used in the final cleansing of the tanks, lines, and fittings upstream of the regulator prior to installation.
2. Sterilization Temperature - This temperature is sufficiently high (270°F, 36 hours) to cause damage to polymers and elastomers, and possibly permanent dimensional change in some metal parts.
3. Radiation - Long term exposure to space radiation and on-board nuclear radiation could result in the degradation of nonmetallic parts. All metal regulators may be necessary for the 10 year missions.

Satisfactory regulators can be produced which will operate with relatively clean gas for short duration runs in the 1500 to 1700°F range. However, extended operation at these temperatures and an extension of the operational temperature to 2000°F, for even short duration runs, would require an advance in the state of the art.

The use of the on-off (bang-bang) concept for hot gas regulation is particularly attractive because the control section can be isolated from the high temperature. The valve actuator could also be isolated to a degree, by means of a standoff or other insulation method, which would permit use of conventional actuation means such as solenoids.

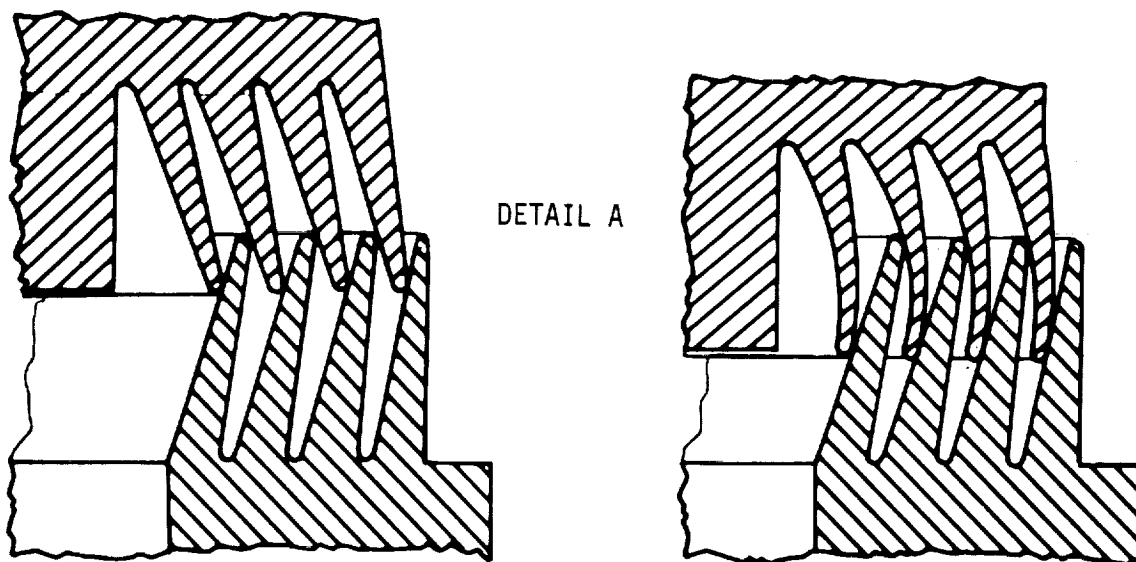
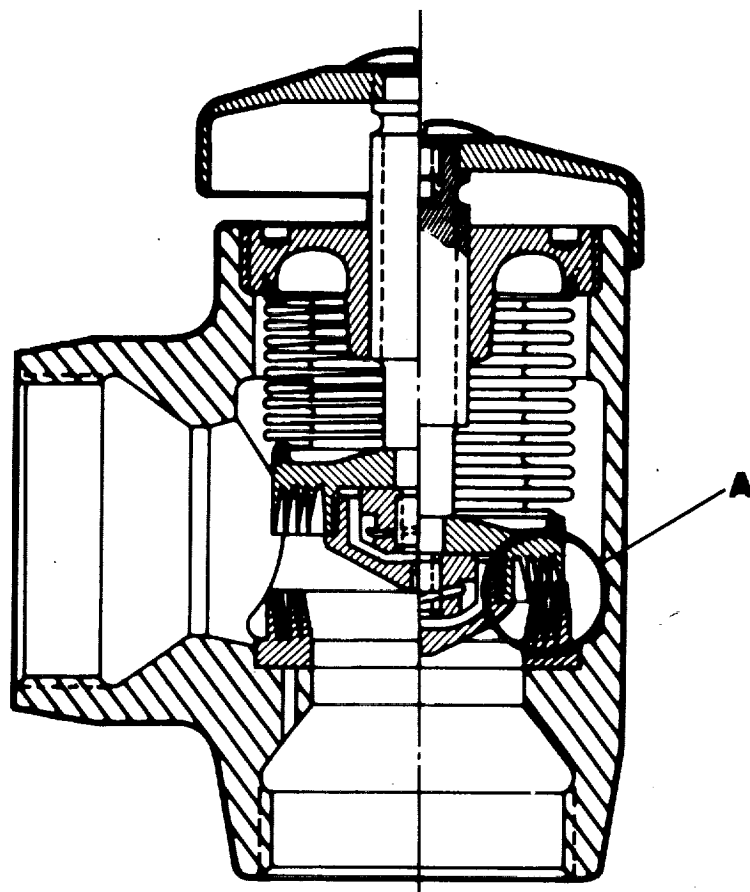
#### 4.2.4 Valve Review

Some of the important state of the art valves which may be used on liquid chemical spacecraft rocket engines are briefly described. The advantages and limitations of each of the valves are emphasized.

4.2.4.1 Cone Labyrinth Valve - This valve was investigated during the survey of present valve technology, because it employed an original method of sealing. The novel means of seat surface contact in the "Cone Labyrinth Valve" promises improvements in contamination insensitive, leak-tight sealing coupled with an unusual method for throttling over a wide flow range.

The flow control element of the Cone Labyrinth Valve (Figure 4-3) accomplishes both throttling and shutoff by the use of two concentric sets of flexible metal blades. Throttling is effected by forcing capillary flow through the labyrinth created in closing and sealing action results from the engagement of resilient metallic sliding surfaces. The concentric blades approach each other with an intermeshing action which tends to be self adjusting and finally provides shearing contact. The advantages, individually or in combination, over existing flow control devices are:

1. The maximum possible corrosion resistance which is afforded by the material choices possible with an all-metal design. Corrosion resistance is further reduced by minimizing the erosive cavitation normally associated with deep throttling but which is almost nonexistent in capillary throttling.
2. Extreme service temperature capability (cryogenic liquids, nuclear reactor liquid metals) resulting from the all-metal design. Radiation and vacuum problems associated with the use of elastomers and plastics are similarly eliminated.
3. Contamination insensitivity due to the fact that impurities are scraped away instead of being crushed or imbedded, which is particularly desirable when controlling metallized propellants.
4. Extended seal life due to the self adjusting feature which results in both cleaning and self-lapping of the seat contact surfaces.
5. Sealing redundancy due to the use of multiple seats.
6. Wide range pressure throttling resulting from the division and spread of the energy conversion process over several labyrinth stages.



LABYRINTH SEAL AFTER  
INITIAL CONTACT

LABYRINTH SEAL NEAR  
TOTAL ENGAGEMENT

Figure 4-3. Prototype Cone Labyrinth Valve  
(Courtesy of Smirra Development Co.)

4.2.4.2 Cold Gas Pressure Regulator - A lightweight pneumatic pressure regulator (Figure 4-4) was developed for use on Mariner C by the Jet Propulsion Laboratory, Pasadena. A sapphire ball poppet operating against an aluminum seat is used for valve closure. Seat leakage requirements of 4 cc/hr of nitrogen are easily met with this configuration. Output pressure is regulated to about 360 psia from a 3600 psia blowdown supply. Except for the belleville springs and filter, all valve elements of the assembly are fabricated from aluminum. All external connections are of the welded type, providing zero external leakage. This regulator incorporates three unique design concepts:

1. The filter employed on the inlet side of the regulator consists of a series of stainless steel (type 347) annular wafers, each having one face chemically etched to provide a flow path for the fluid as shown in Figure 4-5. The fluid enters the outer radial channels, which are 0.0004 inch deep, and then flows in and around the baffles or maze and out through the inner radial channel. On passing through the maze, contaminants are trapped and held. The filter can be disassembled, cleaned, and reused.
2. A flexure diaphragm support ring (Figure 4-4) is used directly behind the low (reference) pressure side of the aluminum diaphragm which is used as the sensing element. The flexure is an annular ring containing a series of fine saw slits running radially part way through the ring. This ring supports the thin diaphragm structurally, yet allows the diaphragm to move the 0.015 inch required for actuation. The backup ring and diaphragm replace the bellows normally used in this type of regulator.
3. Belleville springs, stacked in parallel, are used to provide high force, low deflection characteristics which are desirable in a regulator reference spring. Stacked belleville springs, because of their inherently high friction and hysteresis forces are normally impractical for such a sensitive system. Spacer washers of flat or torus-type rings have been used to alleviate this problem. All had disadvantages because the load varied on each spacer, with the last spacer supporting the combined load of the assembled stack of springs. The load path of the belleville spring assembly shown in Figure 4-4 is taken through the cylindrical carriers provided for both the inner and outer support. The cylinders are grooved to equally space the springs as well as contain them. The belleville spring washers are also silver plated to provide dry film lubrication, since relative motion exists between the outer and inner edges and the grooved carriers.

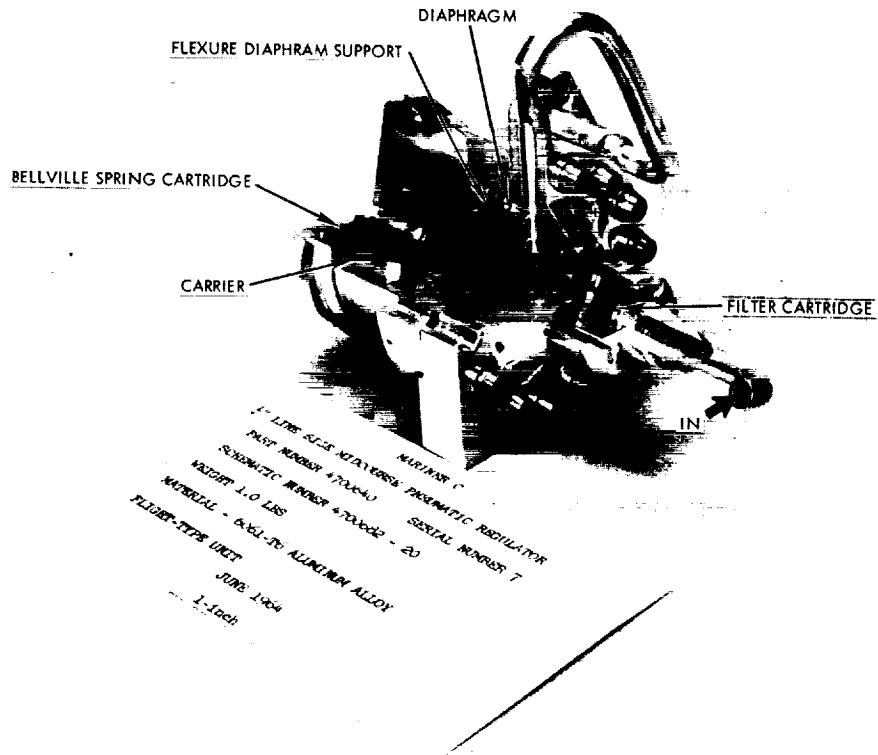


Figure 4-4. Pneumatic Pressure Regulator for Mariner C

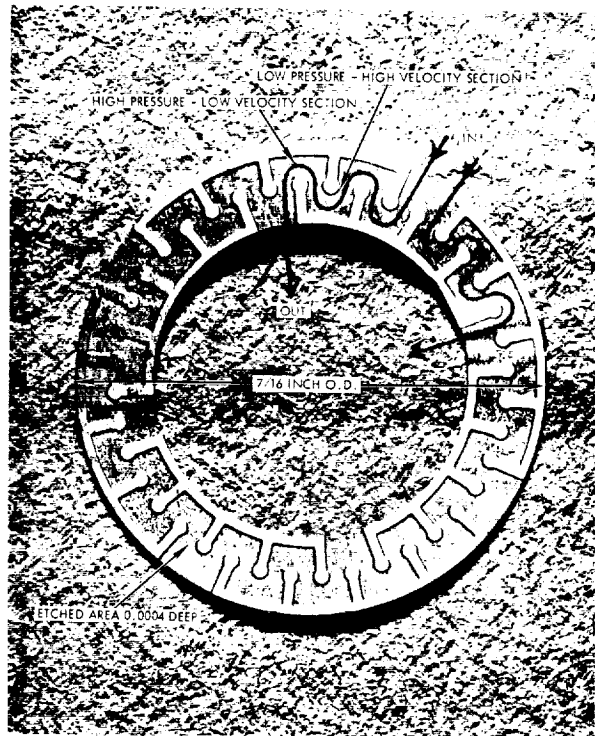


Figure 4-5. Chemically Etched Filter Wafer

4.2.4.3 Electromechanical Valves - Data collected from the aerospace valve suppliers on a number of small, direct-acting, electrically-operated valves is summarized in Table 4-2. Line sizes refer to the connector or tube size. Flow characteristics are given either by  $C_v$ , rated flow vs. pressure loss, or equivalent orifice size. Most of the valves are suitable for a variety of fluids but in most cases the service for which the valve was designed is stated.

The propellants commonly listed in the literature are nitrogen tetroxide ( $N_2O_4$ ), chlorine pentafluoride ( $ClF_5$ ), hydrazine ( $N_2H_4$ ), and monomethylhydrazine (MMH). Nitrogen tetroxide is generally passive to metals unless water is present but restricts the use of plastics and elastomers.  $ClF_5$  must be treated much as if it were "room-temperature" fluorine and requires extreme cleanliness. Passive metals must be used with hydrazine to avoid decomposition of the fuel and few elastomers are suitable.

These considerations have led the industry to gradually depend more and more on stainless steel, Teflon, and Kel-F as universally suitable materials. To some extent, the tendency to use these materials and to avoid dynamic seals has shaped the direction taken in valve development. For example, the torque motor design with a flexible stainless steel tube controlling the poppet is chosen because there are no static seals and no sliding surfaces exposed to the propellant.

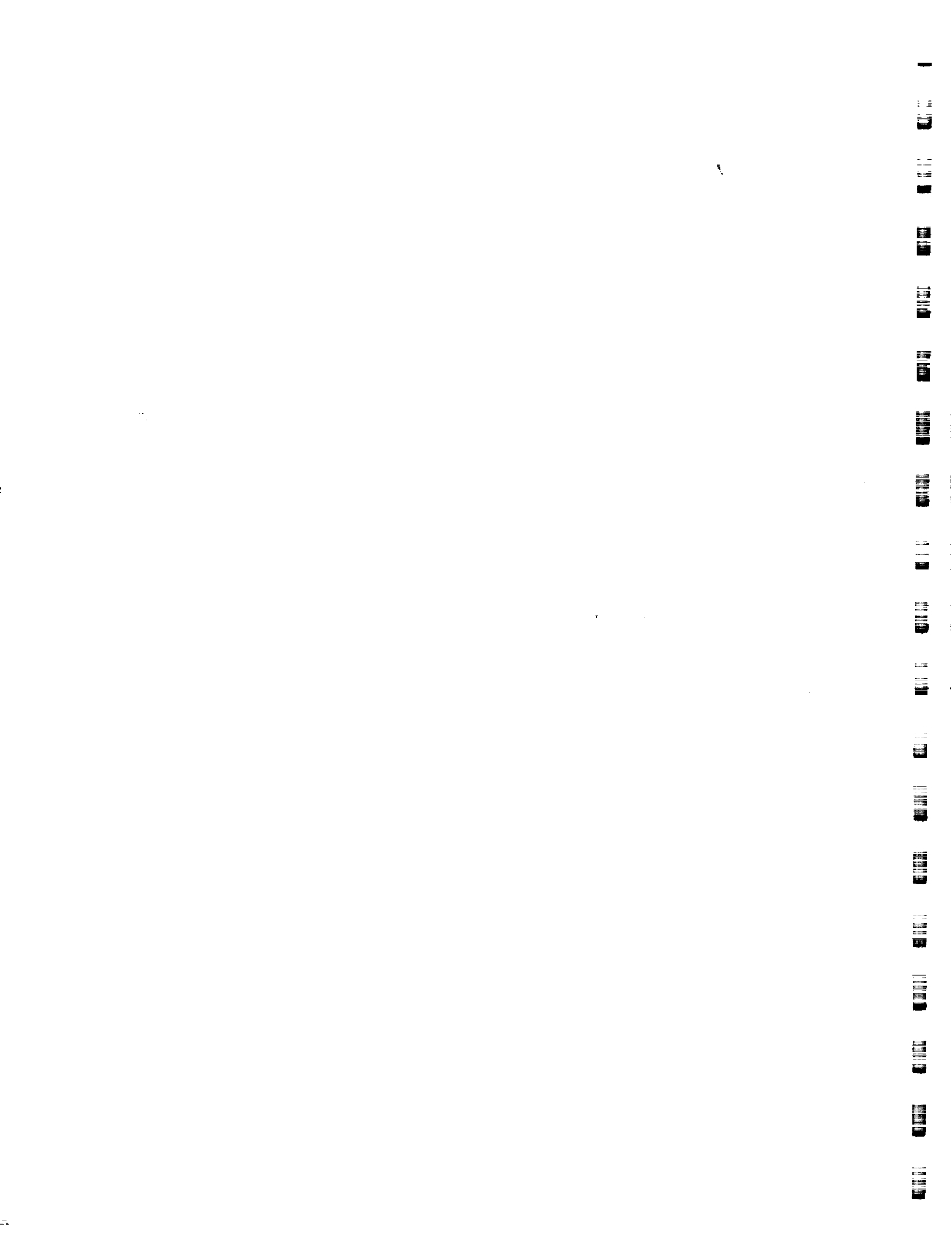
Valve response has been a critical performance parameter for attitude control systems operating in a "bang-bang" mode (pulse width modulation). Relatively high thrust levels are necessary to provide strong corrective moments yet these thrust levels cause a severe problem in minimizing errors unless the thrusters have appropriately fast thrust rise and decay characteristics. Electromechanical valves with fast response (and small manifold dribble volumes) have been used to solve this problem.

Surveys show a wider use of torque motors to achieve fast response rates. Small valves (1/8-inch line size) with responses of less than five milliseconds to open or close are available. Slightly larger valves (1/4-inch to 3/8-inch) have given 5 to 10 milliseconds response, while the larger torque-motor-operated valves require 10 to 30 milliseconds to open.

In prolonged service, a valve can be expected to show a slight (if any) reduction in leak rate, and then gradually increased leakage as wear and damage from hard contaminating particles begins to destroy the surface finishes of the mating parts. This problem has been attacked through the use of (1) soft, compliant seats, (2) hard, scratch-proof seats, and (3) redundant seats.

Soft, compliant seats have been used for years but increasingly severe limitations on materials have restricted their use. The majority of current designs use fluorocarbon seat materials, however, cold-flow is a chronic problem. For high-energy oxidizers (e.g.,  $OF_2$ ), it is questionable whether soft seats can be used safely for dynamic seals.

Hard seats have received more attention in recent years. These parts must be lapped with finishes better than 2 microinches to achieve leakage rates competitive with soft seats. Flat, circular bands that are self-aligning





Manufacturer	P/N	Line Size	Flow Characteristics	Rated Pressure, Psi (g = gauge ) (a = absolute)	Fluid	Rated Internal Leakage		
						scch	Fluid	Pressure psi
James Pond Clark	Circle Seal V4075	1/4	$C_v = 0.4$	1000 g	gas & liquid	1/5	Liquid/Air.	
"	Circle Seal V4175	1/4	$C_v = 0.4$	3600 g	" "	1/5	" "	
"	Circle Seal V4076	3/8	$C_v = 1.0$	1000 g	" "	1/5	" "	
"	Circle Seal V4176	3/8	$C_v = 1.0$	3600 g	" "	1/5	" "	
"	Circle Seal V4077	1/2	$C_v = 1.4$	1000 g	" "	1/5	" "	
"	Circle Seal V4177	1/2	$C_v = 1.4$	3600 g	" "	1/5	" "	
Parker Aircraft	5640054	1/8	0.0012 lb/sec @ 3 psid		$N_2H_4$	100	He	50 a
"	5650031	1/8	0.0012 lb/sec @ 3 psid		$N_2H_4$	5	$N_2$	375 a
"	5677000	3/16	0.0023 lb/sec @ 5 psid		$N_2H_4$	5	$N_2$	350 a
"	564003, 4, 6, 7	3/16	0.008 lb/sec @ 3 psid		$N_2H_4$	40	He	50 g
"	5676210	3/8	0.022 lb/sec @ 30 psid		$N_2H_4$	5	He	350 a
"	5670020	5/16	0.109 lb/sec @ 30 psid		$N_2H_4$	5	$N_2$	350 a
"	5650014	1/4	0.18 lb/sec @ 30 psid		$N_2H_4$	50	He	500 a
"	5640014	5/8	0.73 lb/sec @ 2 psid		$N_2H_4$	50	He	250 g
"	5675210 & 220 5676210 & 220	3/8 inlet, 1/4 tube out	0.0403 inch	350 g	$N_2H_4$	0.4	He	35 g
Moog Inc.	50-315		0.117 lb/sec @ 60 psid	400 g	$N_2O_4$ , MMH	5	$N_2$	
"	52-143		$N_2O_4$ 0.0621 lb/sec @ $48 \pm 5$ psid MMH 0.0388 lb/sec @ $60 \pm 5$ psid	290 g	$N_2O_4$ , MMH	5	$N_2$	
"	50-304		$N_2O_4$ 0.213 lb/sec @ 11 psid MMH 0.133 lb/sec @ 14 psid	325 a	$N_2O_4$ , MMH	5	$N_2$	325 g
"	50-353	3/16	0.025 lb/sec @ 16 psid	450 g	$N_2H_4$	1	$N_2$	250 g
"	52-147		$N_2O_4$ 0.213 lb/sec @ $23 \pm 2$ psid MMH 0.133 lb/sec @ $23 \pm 2$ psid	480 a	$N_2O_4$ , MMH	5	$N_2$	480 g
"	54-102		$N_2O_4$ 0.678 lb/sec @ $33 \pm 4$ psid MMH 0.424 lb/sec @ $33 \pm 9$ psid	290 g	$N_2O_4$ , MMH	5	$N_2$	
Hydraulic Research	300B	5/8	$N_2O_4$ 0.678 lb/sec @ $33 \pm 4$ psid MMH 0.424 lb/sec @ $33 \pm 4$ psid	240 g	$N_2O_4$ , MMH	5	$N_2$	290 g
"	100M	3/8	0.44 lb/sec @ $50 \pm 5$ psid	335 g	$N_2H_4$	5	$N_2$	335 g
"	100B	3/8	$N_2O_4$ 0.216 lb/sec @ $40 \pm 5$ psid MMH 0.132 lb/sec @ $40 \pm 5$ psid	335 g	$N_2O_4$ , MMH	5	$N_2$	335 g
"	50M	special	0.22 lb/sec @ $50 \pm 5$ psid	350 g	$N_2H_4$	5	$N_2$	350 g
"	50B	1/4	$ClF_5$ 0.159 lb/sec @ $45 \pm 5$ psid MMH 0.065 lb/sec @ $45 \pm 5$ psid	450 a	$ClF_5$ , MMH	1	He	435 g
"	25M	special	0.11 lb/sec @ $30 \pm 3$ psid	335 g	$N_2H_4$	5	$N_2$	335 g
"	25B	1/2	$ClF_5$ 0.064 lb/sec @ $27 \pm 3$ psid $N_2H_4$ 0.027 lb/sec @ $27 \pm 3$ psid	350 g	$ClF_5$ , $N_2H_4$	5	$N_2$	350 g
"	5M	1/4	0.022 lb/sec @ $10 \pm 2$ psid	335 g	$N_2H_4$	5	$N_2$	335 g
"	.5M	1/8	0.0022 lb/sec @ $8 \pm 2$ psid	300 g	$N_2H_5$	1	$N_2$	300 g



e,	Rated External Leakage			Rated Response					
	Rate	Fluid	Pressure, psi	Open, ms	Close, ms	Repeatability, ms	VDC	Pressure (d = differential)	Temperature of
"Zero"				14	8		24	1000 d	78
"				17	9		24	3600 d	78
"				12	10		24	1000 d	78
"				29	11		24	3600 d	78
"				19	13		24	1000 d	78
"				13	11		24	3600 d	78
				15	10		28	321 a	150
				10	10	+ 1	28	367 a	70
				12	34	+ 1	21	350 a	200
				10	10	+ 0.5	10	100 a	70
				10	10	+ 1	23	350 a	150
				5	3	+ 0.5	28	375 a	70
				10	10	+ 1	28	300 a	70
				20			23	350 g	150
Zero bubbles in 5 min.	N <sub>2</sub>	400 g							
Zero bubbles in 6 min.	N <sub>2</sub>	435 g		5.5			24	247 g	
<1 x 10 <sup>-6</sup> scc/sec	He	325 g		10				195 g	
<1 x 10 <sup>-6</sup> scc/sec	He	450 g		6	1.8		24	250 g	
<1 x 10 <sup>-6</sup> scc/sec	He	480 g		9				295 g	
Zero bubbles in 6 min.	N <sub>2</sub>	435 g		29	7		24	247 g	
1 x 10 <sup>-6</sup> scc/sec	He	435 g		20	7				
1 x 10 <sup>-6</sup> scc/sec	He	525 g		10	5				
1 x 10 <sup>-6</sup> scc/sec	He	335 g		10	5				
1 x 10 <sup>-6</sup> scc/sec	He	700 g		5	3				
1 x 10 <sup>-6</sup> scc/sec	He	675 a		8	5				
1 x 10 <sup>-6</sup> scc/sec	He	700 g		5	3				
1 x 10 <sup>-6</sup> scc/sec	He	525 g		5	3				
1 x 10 <sup>-6</sup> scc/sec	He	525 g		3	3				
1 x 10 <sup>-6</sup> scc/sec	He	450 g		3	3				

Table 4-2. Electromechanical Valve







have been made to work well if the flatness is true within a fraction of a light band. Leakage rates as low as 0.1 scch are reported to be available. Very hard materials, such as tungsten carbide, have been successfully tested for scratch and erosion resistance by cycling the valves while flowing liquid containing hard, solid particles.

Several forms of redundancy are possible, but a well-established design principle is the use of two complete valving elements in series. In some cases, both elements are actuated by a single driver but in other designs two complete valves are arranged in series. Quad-redundant valves are used for applications where a failed-closed, as well as a failed-open, malfunction must be avoided.

4.2.4.4 Pulsing Bipropellant Valves - The application of pulse width modulated bipropellant rocket engines has resulted in the development of a number of pulsing control valves. The designs include solenoid and torque motor operated, balanced and unbalanced, hard and soft seats, and piloted and direct operating valves. Torque motor actuated valves generally have higher response and force levels for a given electrical power input, although are more complex and costlier than a solenoid valve. Because of cost, the solenoid actuator is preferred over the torque motor for low thrust level engine applications. The approximate engine thrust levels for which each valve type is used are as follows:

<u>Approximate Thrust Level</u>	<u>Valve Type</u>
0-5 lb <sub>f</sub>	Solenoid-unbalanced
5-100 lb <sub>f</sub>	Torque motor unbalanced
>100 lb <sub>f</sub>	Torque motor or solenoid, balanced or piloted.

See Reference 3 for detailed considerations.

4.2.4.5 Cavitating Venturi Throttle - Throttling valves, applying the cavitating venturi concept, were developed for NASA for use in the LM Descent Engine (LMDE), and for the Air Force Rocket Propulsion Laboratory in an advanced program for a 15,000 pound thrust engine.

The cavitating venturi flow control valve applies a variable throat to the conventional cavitating venturi. With reference to the flow equation for a valve in cavitating flow:

$$\dot{W} = C_d A \rho \left[ 2g (P_1 - P_v) \right]^{1/2}$$

The differential pressure across the controlling throat area, is fixed for a given propellant inlet pressure,  $P_1$ , and a given propellant vapor pressure,  $P_v$ . Both density,  $\rho$ , and  $P_v$  are a function of the temperature of the fluid. For a given value of fluid temperature and a constant value of the discharge

coefficient,  $C_d$ , the mass flow,  $\dot{W}$ , will be directly proportional to the throat area. If the control element contour is designed for a linear function of stroke versus control area, the flow will be a linear function of valve position and may be simply adjusted by a proportional actuating device.

To remain in cavitation the throat velocity must be maintained sufficiently high to lower the static pressure to the vapor pressure of the fluid. In the typical throttling application, good pressure recovery at the maximum throttle position is therefore quite important. The pressure recovery of a valve is defined as the percentage of the inlet pressure which is recovered at the outlet as defined in the following equation:

$$\Delta P = P_1 \left[ 1 - \frac{\text{Recovery (\%)}}{100} \right]$$

As the equation shows, the lower the recovery, the higher the pressure drop,  $\Delta P$ , is across the valve. In a pressure fed engine system low-recovery in the propellant valves increases the tank pressure requirement increasing the weights of the tank and the pressurization system. In a pump fed system low valve recovery means an increase in the required delivery pressure from the pump requiring an increase in turbopump weight and propellant consumption to the drive turbine.

As is apparent in the flow equation for cavitating flow, the downstream pressure has no effect on flow. This phenomena is beneficial to accurate and stable flow control inasmuch as pressure pulsations from the combustion chamber or other sources are effectively isolated downstream of the cavitating region.

A liquid fluorine cavitating throttle valve (Figure 4-6) has been developed for Air Force Rocket Propulsion Laboratory and flow tested with water, liquid nitrogen, and liquid fluorine. Predictable performance was demonstrated with all of the liquids. The results of the liquid nitrogen flow tests are shown in Figure 4-7. An inlet pressure of approximately 470 psia was maintained during these runs while downstream pressure was varied in a series of steps from a low to a high differential pressure for each valve flow setting. The important performance characteristics of the valve were as follows:

1. 90% pressure recovery at full flow.
2. A linear flow versus stroke characteristic over a 52:1 throttling range with effective throttling down to 1% flow.
3. A flow coefficient of 0.90 from 10% to 100% stroke.

The application of variable area cavitating valves to mixture ratio control requires an actuating system capable of accurately positioning each of the valves to input signals for throttle position and mixture ratio error compensation. This was accomplished on the LM Descent Engine by interconnecting the valves with a mechanical linkage capable of varying the relative valve stroke in proportion to a mixture ratio control signal and varying the position of the combined valves to a throttle input signal.



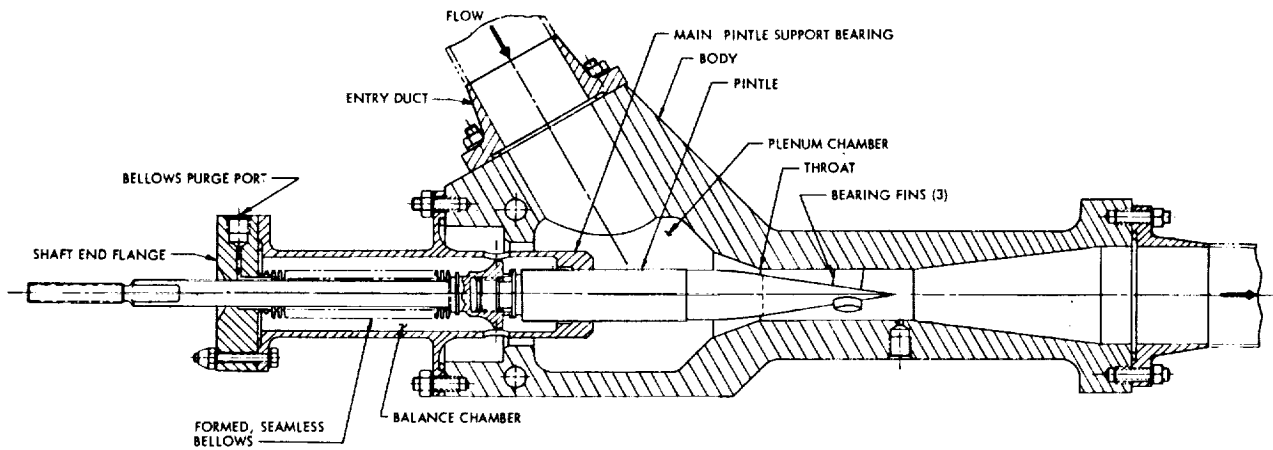


Figure 4-6. Cavitating Flow Control Valve

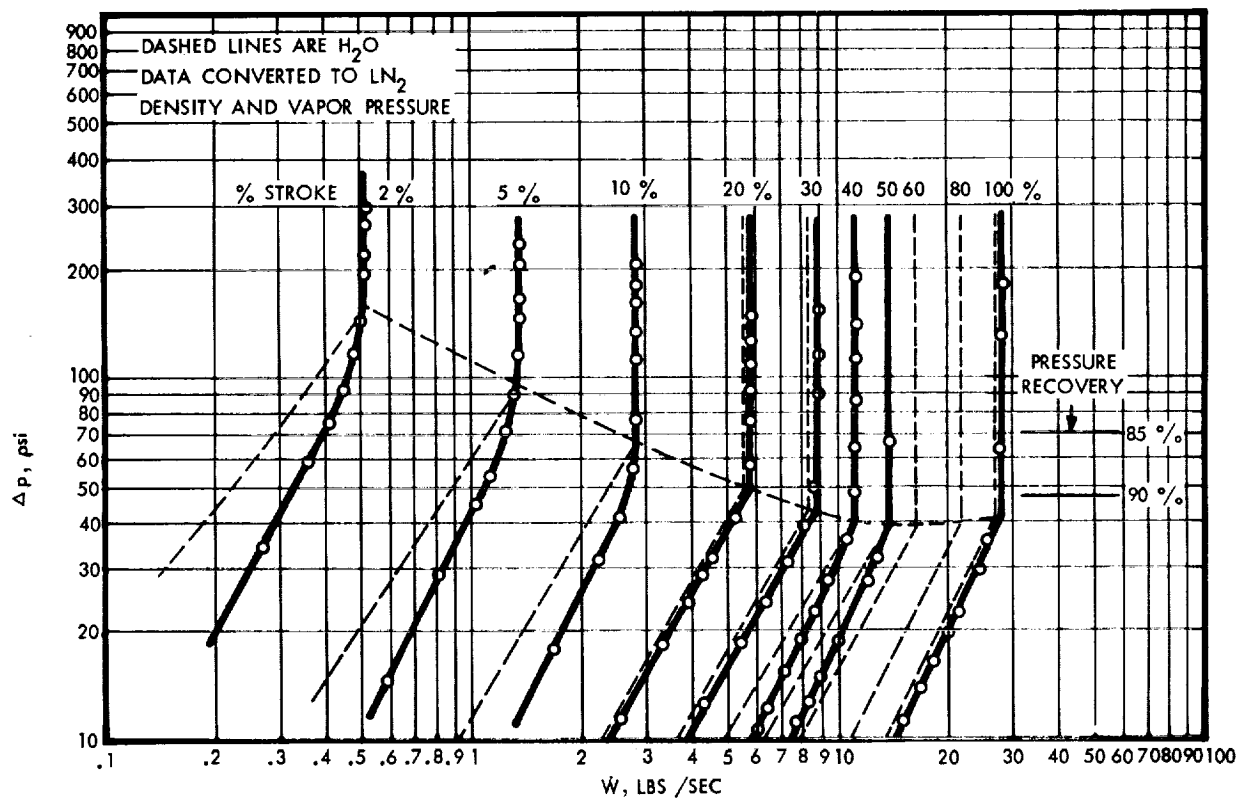


Figure 4-7. Cavitating Venturi Throttle Valve Performance with LN<sub>2</sub>

### 4.3 VALVE DESIGN CONSIDERATION

The the advance of space technology into more complex and extensive missions in space, the requirements for liquid propulsion engines have become more complex. A significant requirement is for rocket thrust modulation, i.e., high response thrust buildup and termination necessary for attitude control and maneuvering in space. In addition, a soft planetary landing without the benefit of an atmosphere requires a rocket engine capable of variable thrust. The Surveyor and LM Descent Engines exemplify this requirement.

Inasmuch as the propellant flow is largely, if not entirely, controlled by the engine valving upstream of the injector, the valving becomes one of the most important elements in the engine system. The general requirements of engine control are: high response pulsing valves for engines below 1000-pound thrust levels, variable area cavitating and noncavitating throttle valves for low and high thrust engines, and valves possessing low leakage shutoff.

This section considers the principles involved in flow control with respect to both engine characteristic requirements and valve capabilities. Valve components used in an  $\text{OF}_2/\text{B}_2\text{H}_6$  propulsion system are defined. Line size, actuator force requirements, and redundancy are also considered.

#### 4.3.1 Propellant Valve Requirements

Propellant valves may be best classed according to their functional application. In general, they perform either shutoff or proportional throttling functions. The shutoff function may be applied to a pulse or time modulated throttling valve or simply to perform the start-stop control function of the engine firing. Proportional throttling, which can be considered amplitude modulation, defines a continuously controllable thrust. Conceivably, the pulsing and proportional throttling modes could be combined. Pulse operation is restricted to application in small engines for attitude control or similar functions because of reasons discussed below. Such operation is likely to be limited to thrust under 1000 pounds. Proportional throttling has been applied or considered for engines ranging from the 150-pound thrust MIRA-150 engine to applications of over 100,000 pounds thrust.

Liquid propellant rocket engines may be monopropellant or bipropellant. The bipropellant engine is at present the one most utilized for space applications, so that bipropellant valving has been given the major consideration. In general, two monopropellant valves could function as a bipropellant valve. The primary consideration with the bipropellant valve is the interrelationship of flow control of the oxidizer and fuel. In most cases, mechanical interconnection of the propellant's flow control function with a highly reliable interpropellant isolation is required. In addition, requirements for mixture ratio control, proportional throttling, and startup and shutdown flow sequencing may be imposed. Propellant compatibility is always a consideration which imposes different problems on the design and material selection for the oxidizer valve and fuel valve. Several specialized areas of bipropellant control are considered in the succeeding sections.

4.3.1.1 Valve Functions - A bipropellant valve is basically any valve which possesses two valving units located in separate, isolated fluid channels and actuated by a single actuator. The function of the valve is to control simultaneously the flow of both fuel and oxidizer. The forms of control include amplitude, pulse width, and frequency modulation, or a combination of the three. A matrix of the combination of parameters which can be varied for achieving flow (thrust) control is as follows:

1. Fixed amplitude - Fixed pulse width - Fixed frequency
2. Fixed amplitude - Fixed pulse width - Frequency control
3. Fixed amplitude - Pulse width control - Frequency control
4. Fixed amplitude - Pulse width control - Fixed frequency
5. Amplitude control - Fixed pulse width - Fixed frequency
6. Amplitude control - Fixed pulse width - Frequency control
7. Amplitude control - Pulse width control - Frequency control
8. Amplitude control - Pulse width control - Fixed frequency

If parallel flow control can be incorporated in a single valve, phasing becomes another control parameter. Phasing can effectively change flow rate by adding individual amplitude (flow) levels, each at a different start time.

In amplitude modulation control, engine thrust level is varied over a range of values by varying the propellant flow rates. The continuous and uniform variation in propellant flow rates is called throttling. Amplitude modulation control is emphasized in soft landing missions such as Surveyor and LM or in manually operated vehicles. The closed loop system with a man closing the loop is less oscillatory if it is amplitude modulated than if it is frequency modulated.

Amplitude modulation is a more sophisticated control system than frequency modulation, involving the use of a servo actuator for achieving positioning accuracy. Mixture ratio control is commonly an attendant requirement in the throttling. Cavitating venturi valves are commonly used because flow rate is independent of change in downstream pressure and, hence, propellant flow changes vary linearly with change in area for constant upstream conditions. The mixture ratio controller assures a proper flow control when propellant inlet pressure and/or temperature vary.

Pulse width modulation is a simple control system because only the on-time of the valve is varied, the engine dynamics and thrust level remaining unchanged. The engine thrust for a given length of time creates an impulse which contributes to a change in vehicle velocity. The valve on-time is usually controlled by pulse width of the electrical signal. Pulse width modulation is used for attitude control, maneuvering, and orbit injection. Minimum impulse bit establishes the lower extreme for incremental changes in velocity and is one of the most important performance parameters in pulse mode engines. To achieve minimum impulse bit the valving element

travel time and total closing time are performance variables which can be minimized. The incremental times which, when summed, contribute to the impulse bit are shown in Figure 4-8. Coil warmup time, valve inertia, dribble volume, and ignition delay establish the time lag from electrical pulse to thrust pulse.

The application may arise in which it is desirable to accomplish orbit injection and then provide attitude control with the same engine or engines. For orbit injection, high thrust levels are desired, while for attitude control minimum impulse bit becomes the desirable performance parameter. In cases such as these a series system of amplitude and frequency modulation can be used. The amplitude modulation may be in discrete steps rather than a throttling function.

By establishing a lower thrust level to achieve minimum impulse bit, greater accuracy can be achieved from pulse to pulse. For example, if a 5 lb-sec impulse bit were necessary with a 1000-pound thrust engine, a variation in valve response time of 1 to 2 milliseconds could cause a variation of 20 to 40 percent in impulse bit, whereas with a 100-pound thrust engine a variation of 1 to 2 milliseconds could cause a variation of only 2 to 4 percent in impulse bit.

4.3.1.2 Engine Control Considerations - Many engine system factors including type of control required must be taken into consideration when developing a bipropellant valve (Table 4-3). Some engine system factors are influenced by the control mode, i.e., pulsing or throttling. For example, such engine system factors as thrust level and method of cooling may be closely related to the control mode used. Presumably, throttling may be used with an engine of practically any rated thrust level, but the type of engine cooling used may present severe limitations to the lower limit of thrust amplitude under throttling. Such limitations are usually associated with engine designs which utilize a large portion of propellant flow for regenerative and/or film cooling of the thrust chamber. With a pulse mode of control, the maximum thrust level of the engine becomes a major criterion because of the increased start and shutdown transient times. Such time requirements limit the practical width of the minimum pulse bit, as compared with low thrust level engines in which a square wave function may be more closely approximated. As the pulse modulated engine is always run at "full throttle," the cooling method becomes somewhat less critical, provided that the engine is designed with multiple start capability in mind. Ablative or radiation cooled thrust chambers significantly reduce the influence of cooling method upon control mode selections.

If the control mode or control function is considered to be essentially represented by a plot of engine thrust versus time, valve response time may be considered to be a small portion of this time. Total valve response time may be considered to be the time interval between the time that the signal to open the valve is received and the time at which the valving element reaches the full open position. A similar response time is associated with the valve closure, of course. With the throttling control mode an additional complicating factor is introduced, since the valving element must be positioned at a location intermediate between the full open and

Figure 4-8. Pulse Width Time History

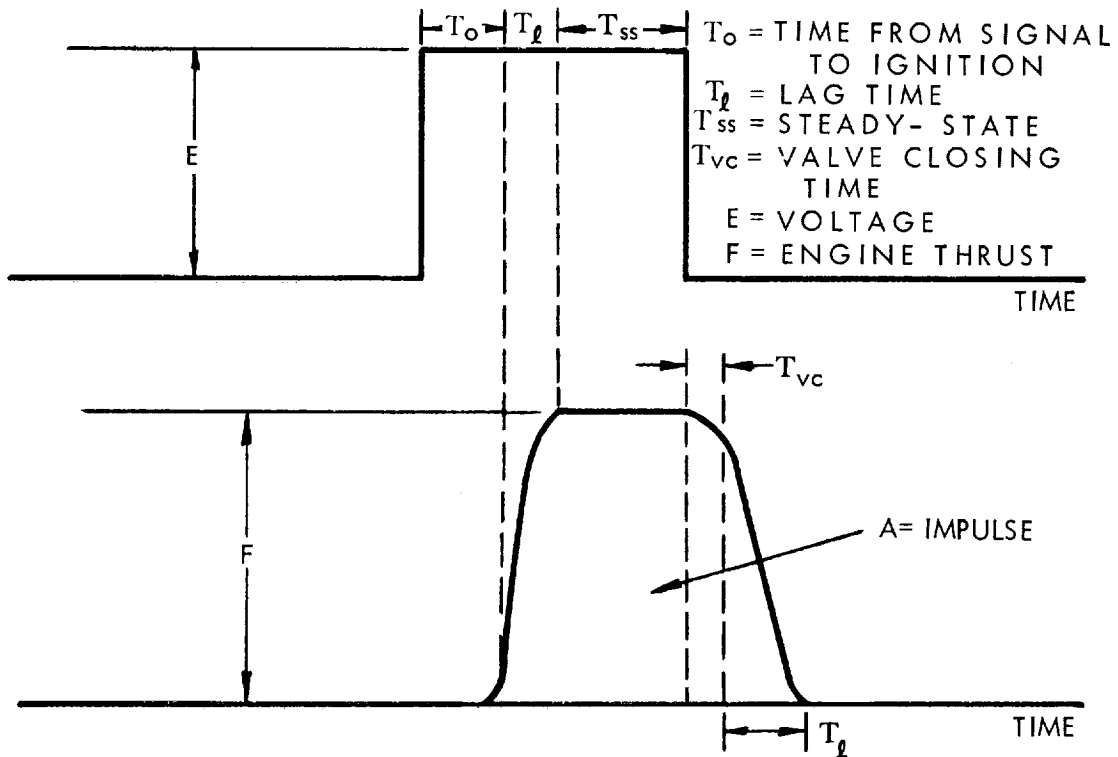


Table 4-3. Factors Influencing Valve Selection and Design

Application	Valve Type	Construction	Electrical	Performance	Reliability	Environmental	Interface
1. Attitude control	1. Piloted	1. All-welded assembly	1. Coil resistance	1. Internal leakage	1. Failure mode	1. Vibration	1. Heat soak-back
2. Maneuvering	2. Direct acting a) balanced b) unbalanced	2. Lubrication	2. Insulation resistance	2. External leakage	2. Service life a) shelf b) propellant service c) cycle d) environmental	a) sinusoidal b) random	2. Voltage suppression
3. Soft landing	3. Actuator	3. Small dribble volume	3. Voltage suppression	3. Inlet pressure		2. Acceleration	3. Contamination levels
4. Orbit injection	a) torque motor	4. Use a mechanical linkage	4. Thermal compensation	4. Pressure drop		3. Vacuum	4. Pressure surges
5. Steady state	b) solenoid	5. Facilitate cleaning	5. Heat generation	5. Pull-in and drop-out voltage		4. Temperature	
6. Pulse mode	c) pneumatic	6. Sliding parts	6. Magnetic flux path a) materials b) temperature	6. Size		5. Sterilization	
7. Size range	d) hydraulic e) electric motor	7. Seat design	7. EMI	7. Weight		6. Fungus	
		8. Electrical cables or connectors		8. Flowrate		7. Humidity	
		9. Inlet filters		9. Response a) opening b) closing		8. Radiation	
		10. Instrumentation		10. Current		9. Shock	
		11. Materials		11. Backpressure		10. Transportation	
				12. Positioning accuracy			
				13. Flow characteristic			

Table 4-4. Relationships Between Valve Parameters, Engine Parameters and Control Mode

KEY C = Critically Related D = Directly Related S = Somewhat Related U = Unrelated	Valve Parameters										Control Mode	
	Response Time	Flow Vs. Stroke	ΔP and Flow Capacity	Size	Weight	Contamination Sensitivity	Wear/Life	Valving Unit Type	Actuation Mode	Actuation Force Requirements	Throttle	Pulse
<b>Engine Parameters</b>												
Thrust Level	U	U	D	D	D	D	U	C	D	C	D	C
Pressure	C	S	S	S	D	U	S	C	D	C	U	U
Propellants	D	U	U	U	U	D	S	S	S	U	S	D
Cooling Mode	C	S	S	U	U	U	U	U	U	U	C	D
Start Transient	C	C	U	U	U	U	U	C	D	S	D	C
Shutdown Transient	C	C	U	U	U	U	U	C	D	S	D	C
Water Hammer	C	C	U	U	U	U	U	C	S	U	D	C
<b>Control Mode</b>												
Throttle	D	C	D	S	S	C	S	C	C	C		
Pulse	C	D	D	S	S	D	C	C	C	C		

full closed or shutoff position. With the exception of some simplified stepped-thrust systems, such throttling modes usually require a feedback system which indicates valving element position to the controller. The relationship between valve response time and engine response time depends largely upon such engine characteristics as fill or dribble volume and ignition time, which in turn are largely functions of the engine thrust level, engine cooling mode, engine configuration and the particular propellants used.

When high-response valves are used for either mode of control, the valve flow characteristic or flow versus stroke characteristic becomes very important. This factor is amplified in larger thrust level engines, particularly with lengthy suction lines in which water hammer on either opening or shutdown may present severe problems. It is reasonable to assume that a control valve response time on the order of 5 milliseconds would require specific engine system design considerations if water hammer effects and start and shutdown stability were to be maintained within reasonable limits for engines approaching 1000 pounds thrust.

The preceding examples of interactions between engine, valve, and control mode factors are merely representative. Table 4-4 presents in abbreviated form some of the relationships between engine and valve parameters and mode of control.

4.3.1.3 Throttling Bipropellant Valve - The difficulties in satisfying the requirements for a high-response throttling bipropellant valve have necessitated a review of the basic function served by propellant valves in rocket engine systems. The relationship of rocket engine operation to valve requirements and of valve operation to engine requirements is a prerequisite for an advancement in valve technology.

The basic functions of a combined throttling and shutoff bipropellant valve are:

1. Meter or control the mass flow rate of each propellant to that value demanded by signal
2. Seal the fuel and oxidizer branches of the system to all propellant flow except when demanded by signal.

Historically, both of these functions have been performed by placing an obstruction of some sort in the flow path. In the case of shutoff, the obstruction totally blocks the flow path, whereas for throttling the flow path is only partially obstructed to provide a certain degree of resistance to flow.

4.3.1.4 Throttling - Throttling involves a complex interaction with total engine system performance. The shutoff function is more straightforward, although an actual design for a high response valve with very low leak rates and low power consumption requirements may present a severe challenge and the start/shutdown transient conditions associated with pulse mode operation can be complex. The throttling function is dependent upon the entire rocket engine system. The techniques used to achieve rocket engine throttling

are numerous and include such approaches as variable-area injectors, momentum exchange, inert fluid injection, pressure-compensated metering valves, cavitating venturi valves, and various combinations of these. The difficulties with rocket engine throttling that have resulted in such a variety of throttling schemes are primarily associated with occurrences within the combustion chamber. Simply reducing the flow rate of propellant to the chamber will not necessarily result in a smooth reduction in chamber pressure and thrust, because mixing efficiency and combustion efficiency are reduced. Most of the throttling techniques employ some means of increasing or maintaining injection velocity (to maintain mixing efficiency) as propellant flow rates are reduced.

A further complication is that different throttling techniques result in different pressure drops across the valve. This may be demonstrated by comparing two similar hypothetical engine systems, one of which utilizes a fixed-area injector while the other uses a variable-area injector designed to provide constant injection velocity. Figure 4-9 is a simplified schematic of such an engine, and Table 4-5 shows the pressure schedules. With the fixed-area injector, practically all of the pressure drop is across the valve at 10 percent thrust, whereas with the variable-area injector, the injector pressure drop remains constant.

For most valves, the flow rate through the valve is a function of not only the valve position but also the pressure upstream and downstream of the valve. With pressure-fed rocket engines it has been found advantageous to utilize cavitating venturi valves for throttling. For any given setting of a cavitating venturi valve, assuming a constant upstream pressure, flow rate will increase as downstream pressure is decreased until the throat pressure reaches the critical or cavitation pressure for the particular fluid and valve setting. Once the valve has gone into cavitation the throat pressure remains constant at the vapor pressure of the liquid and further reductions in downstream pressure will result in no further increase in flow rate. The cavitating venturi valve is therefore insensitive to fluctuations in downstream pressure so long as the critical pressure is not exceeded, and flow rate is a function only of upstream pressure (assumed to be regulated in a pressure-fed system) and valve setting. The cavitating venturi valve, although it eliminates one source of error, provides no panacea to the throttling problem. It presents limitations and restrictions, one of which is the necessity for a relatively large head loss across the valve (usually about 10 percent of the upstream pressure) in the full open position if cavitation is to be maintained over a broad operating range.

A variety of approaches are available whereby a valve may actually control flow to a specified value. In essence these techniques may be categorized as either "sense and position" or precalibrated. The former approach entails measuring certain parameters such as propellant flow rate (mass or volumetric) and using this information in a device which compares it with the demand requirement and adjusts the valve accordingly. Such systems are usually complex and contain inherent lag times which are not usually compatible with the required system response times. An indication of this complexity may be seen in Figures 4-10 and 4-11, which are schematics of systems incorporating mixture ratio control. The system in Figure 4-10

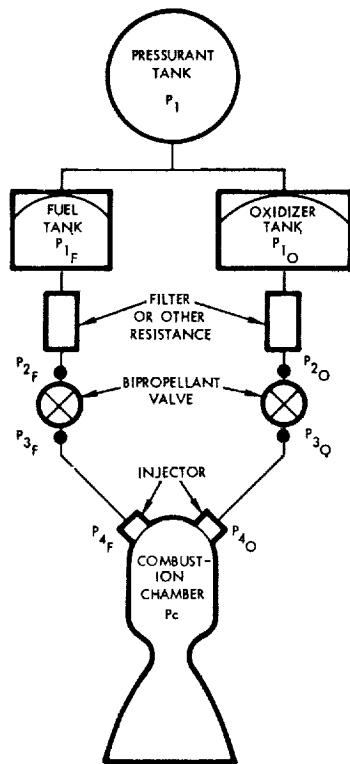


Figure 4-9. Pressure-Fed Engine Schematic

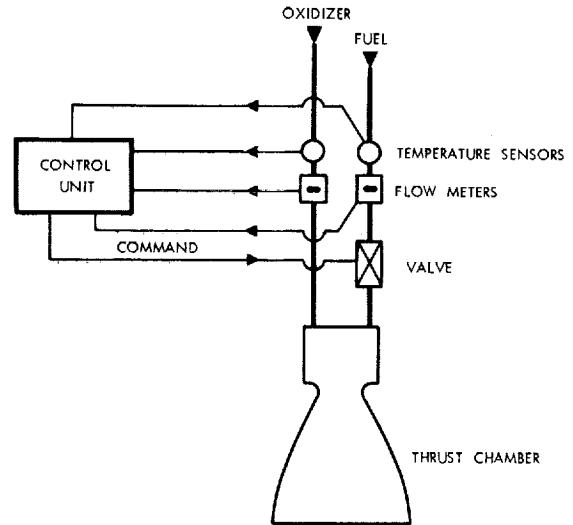


Figure 4-10. Bipropellant Feed System With Turbine Flowmeters

Table 4-5. Engine Pressure Schedule

Thrust Level	100 percent		10 percent	
	Both Fixed and Variable	Fixed	Variable	
Tank Pressure, psia	200.0	200.0	200.0	
Line and Filter $\Delta P$ , psi	20.0	0.2	0.2	
Bipropellant Valve $\Delta P$ , psi	30.0	189.3	139.8	
Injector $\Delta P$ , psi	50.0	0.5	50.0	
Chamber Pressure, psia	100.0	10.0	10.0	

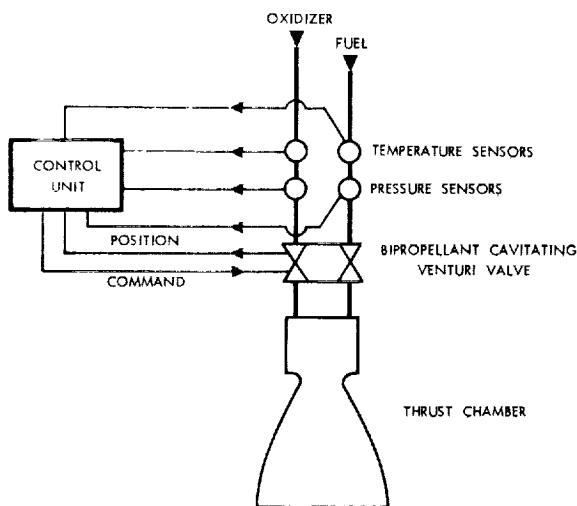


Figure 4-11. Bipropellant System With Cavitating Control Valve



are numerous and include such approaches as variable-area injectors, momentum exchange, inert fluid injection, pressure-compensated metering valves, cavitating venturi valves, and various combinations of these. The difficulties with rocket engine throttling that have resulted in such a variety of throttling schemes are primarily associated with occurrences within the combustion chamber. Simply reducing the flow rate of propellant to the chamber will not necessarily result in a smooth reduction in chamber pressure and thrust, because mixing efficiency and combustion efficiency are reduced. Most of the throttling techniques employ some means of increasing or maintaining injection velocity (to maintain mixing efficiency) as propellant flow rates are reduced.

A further complication is that different throttling techniques result in different pressure drops across the valve. This may be demonstrated by comparing two similar hypothetical engine systems, one of which utilizes a fixed-area injector while the other uses a variable-area injector designed to provide constant injection velocity. Figure 4-9 is a simplified schematic of such an engine, and Table 4-5 shows the pressure schedules. With the fixed-area injector, practically all of the pressure drop is across the valve at 10 percent thrust, whereas with the variable-area injector, the injector pressure drop remains constant.

For most valves, the flow rate through the valve is a function of not only the valve position but also the pressure upstream and downstream of the valve. With pressure-fed rocket engines it has been found advantageous to utilize cavitating venturi valves for throttling. For any given setting of a cavitating venturi valve, assuming a constant upstream pressure, flow rate will increase as downstream pressure is decreased until the throat pressure reaches the critical or cavitation pressure for the particular fluid and valve setting. Once the valve has gone into cavitation the throat pressure remains constant at the vapor pressure of the liquid and further reductions in downstream pressure will result in no further increase in flow rate. The cavitating venturi valve is therefore insensitive to fluctuations in downstream pressure so long as the critical pressure is not exceeded, and flow rate is a function only of upstream pressure (assumed to be regulated in a pressure-fed system) and valve setting. The cavitating venturi valve, although it eliminates one source of error, provides no panacea to the throttling problem. It presents limitations and restrictions, one of which is the necessity for a relatively large head loss across the valve (usually about 10 percent of the upstream pressure) in the full open position if cavitation is to be maintained over a broad operating range.

A variety of approaches are available whereby a valve may actually control flow to a specified value. In essence these techniques may be categorized as either "sense and position" or precalibrated. The former approach entails measuring certain parameters such as propellant flow rate (mass or volumetric) and using this information in a device which compares it with the demand requirement and adjusts the valve accordingly. Such systems are usually complex and contain inherent lag times which are not usually compatible with the required system response times. An indication of this complexity may be seen in Figures 4-10 and 4-11, which are schematics of systems incorporating mixture ratio control. The system in Figure 4-10

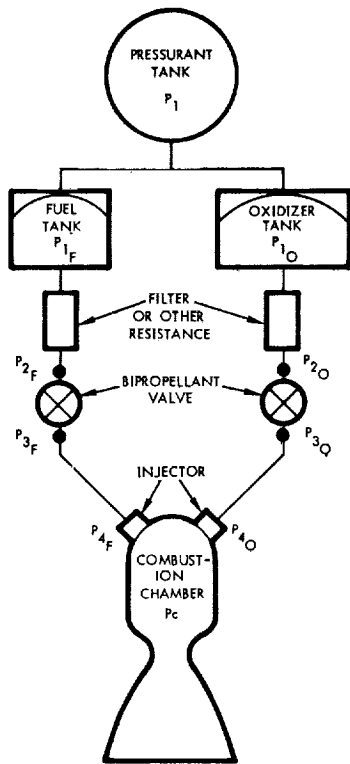


Figure 4-9. Pressure-Fed Engine Schematic

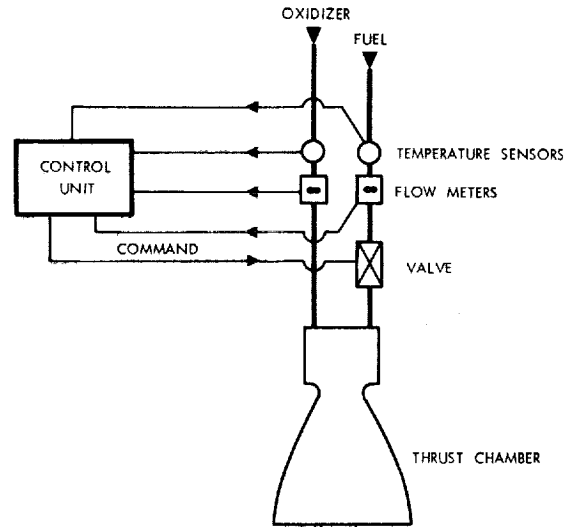


Figure 4-10. Bipropellant Feed System With Turbine Flowmeters

Table 4-5. Engine Pressure Schedule

Thrust Level	100 percent		10 percent
	Both Fixed and Variable	Fixed	Variable
Tank Pressure, psia	200.0	200.0	200.0
Line and Filter $\Delta P$ , psi	20.0	0.2	0.2
Bipropellant Valve $\Delta P$ , psi	30.0	189.3	139.8
Injector $\Delta P$ , psi	50.0	0.5	50.0
Chamber Pressure, psia	100.0	10.0	10.0

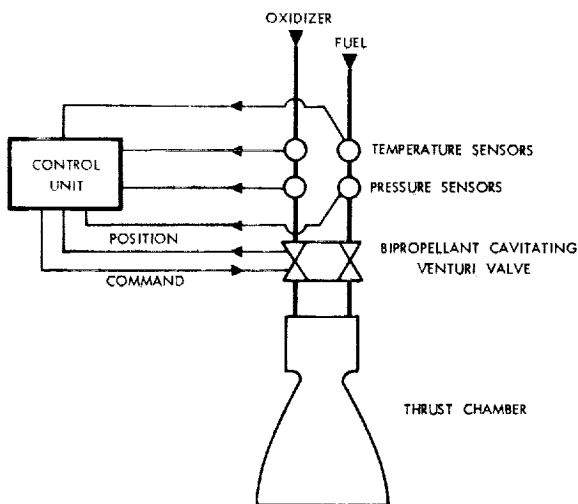


Figure 4-11. Bipropellant System With Cavitating Control Valve

measures mass flow directly (volumetric flow with density correction for temperature) and controls mixture ratio by adjusting the resistance of a single valve. The system in Figure 4-11 accomplishes the same task by measuring pressure and temperature upstream of a bipropellant cavitating venturi valve (flow rate is controlled by valve area) and biasing the relative strokes of two venturi pintles by means of a second actuator and linkage as illustrated in the sketch of a test assembly (Figure 4-12). The unit shown includes a temperature correction applied to both density and vapor pressure. The temperature corrections for both systems can be omitted in some systems if accuracy is not critical or if propellant temperatures are accurately controlled. Corrections for off-design propellant temperatures are more vital in cryogenic systems than in storable propellant systems.

The precalibrated technique entails development testing to relate valve position to flow rate for the pressure conditions under which the valve will be operated. Flow control in this case consists simply of positioning the valve to the calibrated position for the desired flow rate. The disadvantage of this approach is that the precalibrated throttling valve is unable to compensate for variations in operating conditions such as changes in pressure differential due to regulator malfunction or system contamination.

It may be seen from the above that satisfaction of the throttling requirement presents significant problems in addition to those posed by the shutoff function. Most of the preceding has been associated with the problems posed to the valve by the engine system. Attempting to analyze a rocket engine system without knowing the characteristics of the propellant valves can be equally difficult, especially in the case of throttling. Valve resistance characteristics and whether or not a valve is pressure balanced can influence the establishment of pressure levels used and the pressure schedule throughout the engine system. It is for this reason that rocket engines are usually designed with desired system values specified first, followed by the design or selection of valves with characteristics to match the system. More than any other item, the variety in engine system requirements will limit the applicability of any valve concept. For this reason, flexibility in tailoring valve characteristics is of major importance in evolving bipropellant valve designs.

4.3.1.5 Start-Shutdown Response - An interesting example of the interdependence of valve characteristics and engine system characteristics occurs with start and shutdown response times. For the purpose of this discussion a simple on-off shutoff valve such as those associated with pulse-mode operation will be considered. Valve response may be defined as the total elapsed time from receipt of the signal at the actuator until the valving element is stabilized in the throttling position ordered, or full open in this case. Valving element response may be defined as the total elapsed time from initial movement of the valving element until the valving element is stabilized in the ordered position. Figure 4-13 illustrates the relationship of valve and valving element response times to engine response times. The shape of the stroke versus time plots indicates a valving element that accelerates throughout its stroke. The lag between the time the valving

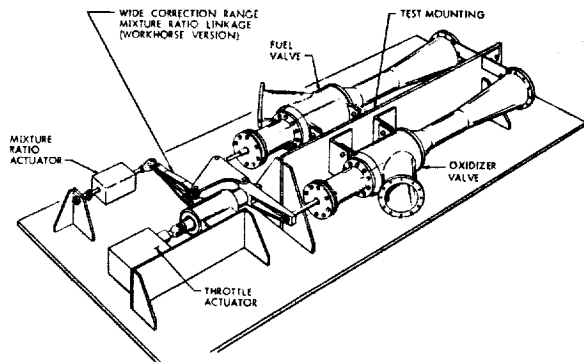


Figure 4-12. Bipropellant Cavitating Venturi Valve

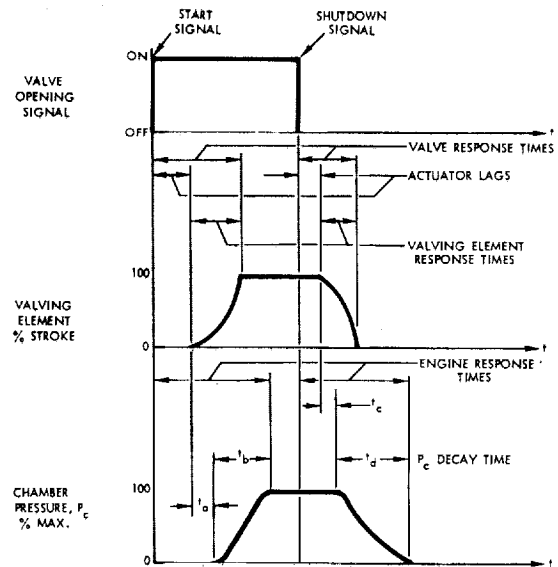


Figure 4-13. Relationships Between Valve Signal, Valve Stroke and Chamber Pressure

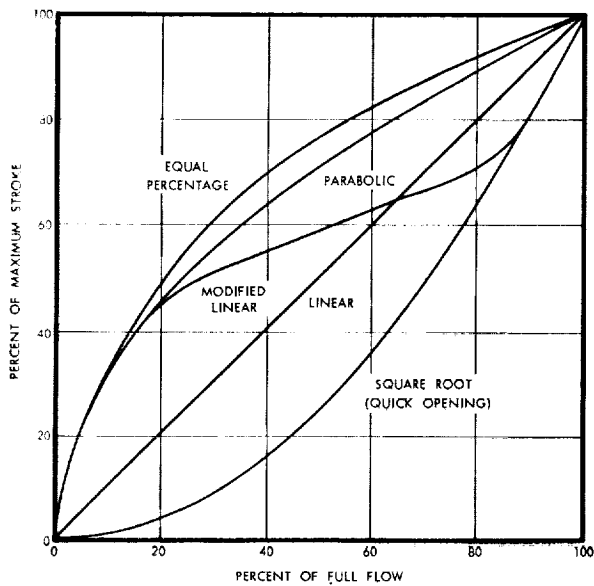


Figure 4-14. Valve Stroke-Flow Characteristic Curves

element starts to move and the time that chamber pressure ( $P_c$ ) starts to rise (shown as time  $t_a$ ) is a relatively complex function of the following:

1. Fill or dribble volume between valve and injector orifices
2. Valve flow versus stroke characteristics
3. Valving element response time
4. Ignition delay characteristics (which in turn are dependent upon propellant characteristics and injector design features).

Similarly, the elapsed time between the start of  $P_c$  rise and the attainment of maximum  $P_c$  is a function of:

1. Valve flow versus stroke characteristic
2. Valving element response time
3. Combustion chamber characteristic length ( $L^*$ )
4. Chemical conversion time ( $\tau$ )
5. Combustion chamber pressure ( $P_c$ )

Similar relationships control the shutdown transient, with the exception that valving element closing response time and the valve flow characteristic when closing replace the respective valve opening parameters.

The manner in which these factors influence engine response is explained briefly in the following paragraphs.

**4.3.1.6 Fill or Dribble Volume** - The larger the dribble volume (injector manifold volume plus any lines between valve and manifold), the longer the response time for either start or shutdown. It is apparent that for given valve characteristics, the larger volume will take longer to fill or blow down. The larger the engine the greater the significance of dribble volume on the shutdown due to the increased line diameters.

**4.3.1.7 Stroke Characteristics** - The more closely the valve characteristic approaches a square root or "quick opening" type (Figure 4-14), the shorter will be the engine response time for a given valving element response time. This results because the total volume of propellant which passes through the valve during the elapsed valving element response time ( $\sim dq/dt$ ) will be greater than with a linear or equal-percentage valve characteristic.

The shorter the time for the valving unit to travel through its entire stroke, the shorter the engine response time. In practically all cases, maximum  $P_c$  cannot be obtained until after the valve is fully open. Conversely, for high response systems,  $P_c$  will not decay to ambient pressures until the valve has completely stopped the flow. In the case of slow, or even moderately fast valving response (50 milliseconds or greater)  $P_c$  may be expected to follow valve flow position rather closely. As valving element response approaches instantaneous opening or closure, other factors govern  $P_c$  rise or decay, as discussed below.

4.3.1.8 Ignition Delay Characteristics - The longer the ignition delay, the longer will be the lag between the start of valve opening and the start of  $P_c$  rise. If propellants of low reactivity are injected through injectors which provide poor mixing at low flow rates, ignition delay can substantially increase total engine response time and add to the danger of a "hard start" (wherein a large quantity of propellant is accumulated in the combustion chamber prior to ignition).

4.3.1.9 Combustion Chamber Characteristic Length ( $L^*$ ) - For a given propellant combination, a chamber of small  $L^*$  will yield more rapid  $P_c$  rise and  $P_c$  decay than will a chamber of greater  $L^*$ .  $L^*$  is a measure of combustion chamber residence time and may be defined by:

$$L^* = V_c/A_t$$

where:  $V_c$  = combustion chamber volume

$A_t$  = throat area

$L^*$  is the length a combustion chamber of the same volume would have if it were a cylindrical tube with a diameter equal to the throat diameter. Engines using slow reacting propellants require a large  $L^*$  chamber, whereas fast reacting propellants may use chambers of lower  $L^*$ . It is apparent that for a given injector and throat, a larger chamber volume (and hence larger  $L^*$ ) will require longer to fill and longer to blow down.

4.3.1.10 Chemical Conversion Time ( $\tau_c$ ) - The shorter the chemical conversion time, the more rapid may be the  $P_c$  rise and decay. Just as  $L^*$  is a measure of steady state gas residence time,  $\tau_c$  is a measure of reaction rate.  $\tau_c$  may be defined by a reaction rate function of the form:

$$q_b/q_o = e^{-t/\tau_c}$$

where:  $q_b/q_o$  = the reduced reaction rate

$q_b$  = the rate of change of gas added  
by distributed time-dependent  
combustion in the chamber

$q_o$  = the steady state nozzle flow rate

L. L. Bixson (Reference 4) relates chemical conversion time and steady state gas residence time ( $\theta$ ) to yield the rate of  $P_c$  decay after propellant flow has been cut off by

$$\frac{P_c}{P_{c1}} = \frac{1}{\tau_c - \theta} \left[ \tau_c e^{-t/\tau_c} - \theta e^{-t/\theta} \right]$$

where:  $P_c$  = chamber pressure at any point during  $P_c$  decay

$P_{c1}$  = steady state chamber pressure

In experiments with near instantaneous propellant shutoff (effective valving element response time of less than one millisecond) using a 5000-pound thrust LOX/RP-1 engine,  $P_c$  was found to decay from 457 psia to ambient pressure in approximately 12 milliseconds. It is interesting to note that  $P_c$  remained steady for about 2 milliseconds after valve closure.

4.3.1.11 Combustion Chamber Pressure ( $P_c$ ) - The rate of  $P_c$  decay has been shown to be dependent upon gas residence time and chemical conversion time. This  $P_c$  decay rate establishes the slope of the  $P_c$  versus time plot. Therefore, the elapsed  $P_c$  decay time becomes directly proportional to  $P_{c1}$ , the steady state value of  $P_c$ .

This view of the relationship between valving element response and engine response gives rise to the questions, "Why a 5-millisecond valve? Why not a one-millisecond or 10-millisecond valve?" A brief look at what happens when valve closing time is varied would appear in order. Figure 4-15a is a simplified plot of valve position and  $P_c$  as a function of time in the case of instantaneous valve closure. Note that no discernable drop in pressure occurs between time a and time b. This corresponds to the 2-millisecond period observed in the experiments of Reference 4 and is not considered in the equation for  $P_c/P_{c1}$ , which gives only the slope of the  $P_c$  plot from b to c.

As a finite valving element response time is considered (Figure 4-15b) it becomes apparent that the  $P_c$  decay time (b to c) is complex and is a function of valve flow versus stroke characteristics. If the other extreme of very gradual valve closures is considered, however, another limit may theoretically be established for any given engine. That limit is established by the point in valve stroke where propellant flow is insufficient to support combustion and  $P_c$  rapidly decays to ambient, probably at the rate depicted from b to c in Figure 4-15a. Obviously this point can vary drastically between throttling engines and non-throttling engines. For a given engine, it can be assumed that there is a situation where  $P_c$  decay time is identical to valving element response time. Such a situation is shown in Figure 4-15c, where it is presumed that combustion cannot be maintained with the bipropellant valve less than 5 percent open. Although some propellant will certainly enter the chamber, it is presumed that this propellant does not burn, and hence does not contribute to  $P_c$ .

Referring back to the rapid response valve closure indicated in Figure 4-15c, it is reasonable to state that total  $P_c$  decay time, a to c will always exceed the valving element response time until these response times become so long that they coincide.

4.3.1.12 Fuel or Oxidizer Lead - The preceding start-shutdown response discussion has treated the simple system wherein both fuel and oxidizer valves are opened and closed simultaneously. This simultaneous operation is common practice on small, high-response engines such as those in the 100-pound thrust range. While it is reasonable to presume simultaneous valve operation when considering response times of 5 milliseconds, consideration should be given to fuel or oxidizer lead on start or shutdown. The

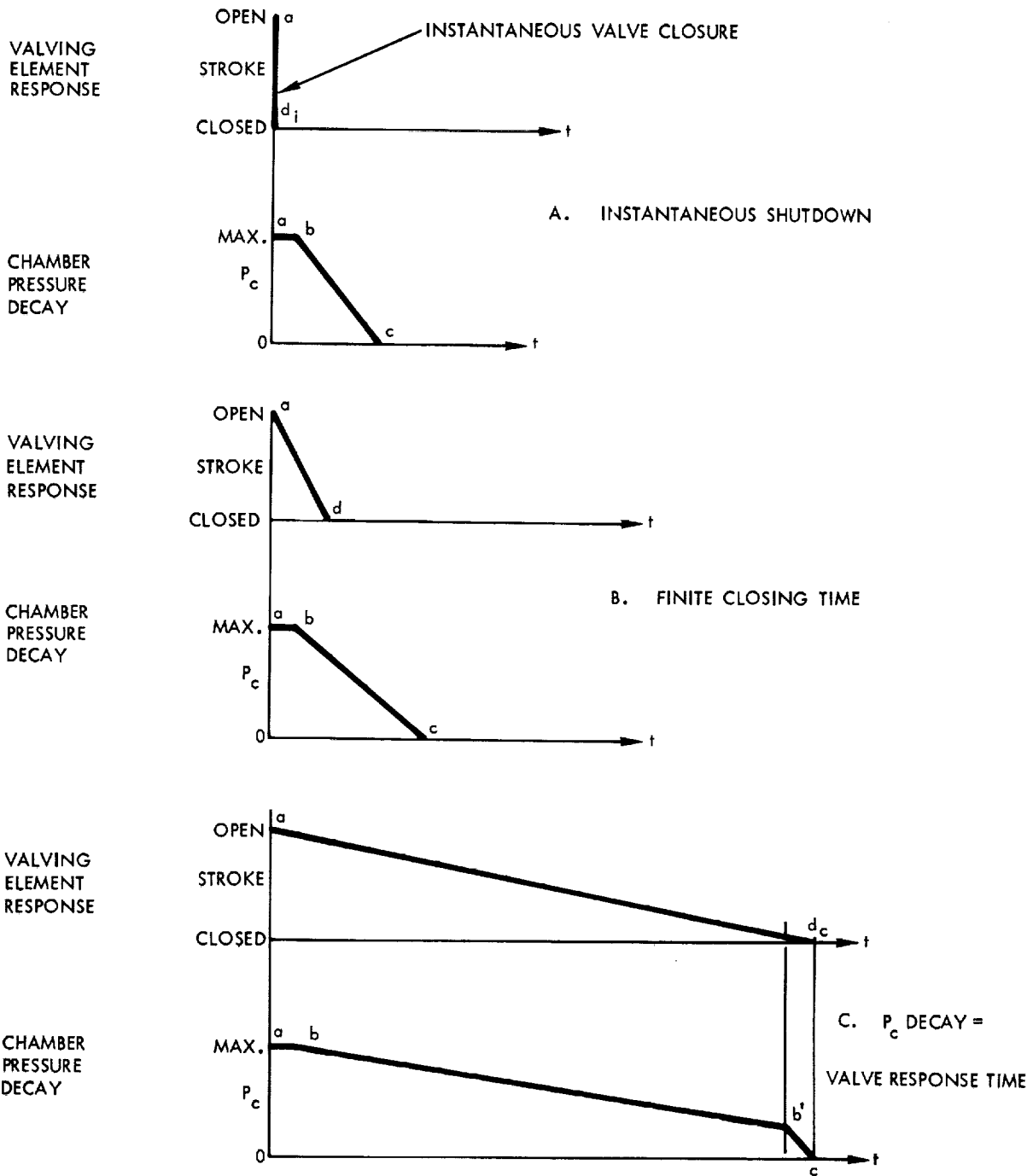


Figure 4-15. Chamber Pressure Versus Valve Closing Time



reasons for incorporating such leads on larger engines may include any of the following:

1. To provide optimum mixture ratio for ignition
2. To provide smooth start or shutdown
3. To avoid potentially explosive residues in the chamber after shutdown
4. To minimize corrosive residues in the chamber after or between firings.

The choice of fuel or oxidizer lead on either start or shutdown is dependent upon the particular propellants involved and operating conditions such as control mode and vacuum or atmospheric environment. The means of achieving such leads with a single-actuator bipropellant valve include the following:

1. Tailoring the flow versus stroke characteristic of each valving unit
2. Varying the valving element response time, either by modifying the valving unit or the linkage connecting the actuator and valving element
3. Adjusting the fill or dribble volumes between the valve and injector orifices
4. The use of a burst diaphragm in one propellant branch.

#### 4.3.2 Feed System Component Definition

A study was made to define the valve components used in an  $\text{OF}_2/\text{B}_2\text{H}_6$  propulsion system, establish component requirements, and develop sizing criteria. In order to accomplish this study, a propellant system configuration was defined, and a parametric study of valve size as a function of engine thrust was performed in the range of 50 to 1000 pounds thrust. Consideration was also given to line sizing and actuator force requirements as a function of line pressure and response.

4.3.2.1 Component Definition - A pressure-fed bipropellant liquid rocket engine feed system was used for component definition as shown in Figure 4-16. Both legs of the system are similar in layout and component requirements although component sizing varied from the fuel to the oxidizer side. The system shown utilizes a single pressurant tank and includes dual fuel and oxidizer tankage. Additional fuel and oxidizer tanks may be connected in at the points indicated by the dotted lines. The fluid control components required in the system are shown in Table 4-6.

Each of the components and their connecting lines were chosen and sized, taking into consideration allowable pressure drops and possible cavitation. Check valves are used to prevent migration of fuel and oxidizer into the pressurant system. Although it was realized that this is not a positive isolation scheme, this approach was used to illustrate the use of check valves in propellant feed systems.

Table 4-6. OF<sub>2</sub>/B<sub>2</sub>H<sub>6</sub> Feed System Components

Symbol	Component Type	Pressurant System	Fuel System	Oxidizer System
FV	Fill Valve	1	2	2
RV	Relief Valve	4	2*	2*
MV	Manual Valve	4	2*	2*
CV	Check Valve	2	-	-
BD	Burst Disc	5	2*	2*
REG	Regulator	1	-	-
PF	Pneumatic Fuse	4	2*	2*
OV	Remotely Operated Valve	4	4**	4**
BV	Bipropellant Valve	-	1/2	1/2
F	Filter	1	1	1

\*Included in the pressurant system total. Fuel or oxidizer vapors may contact the units.

\*\*Two of the valves are accounted for in the pressurant system and will be exposed to fuel or oxidizer vapors.

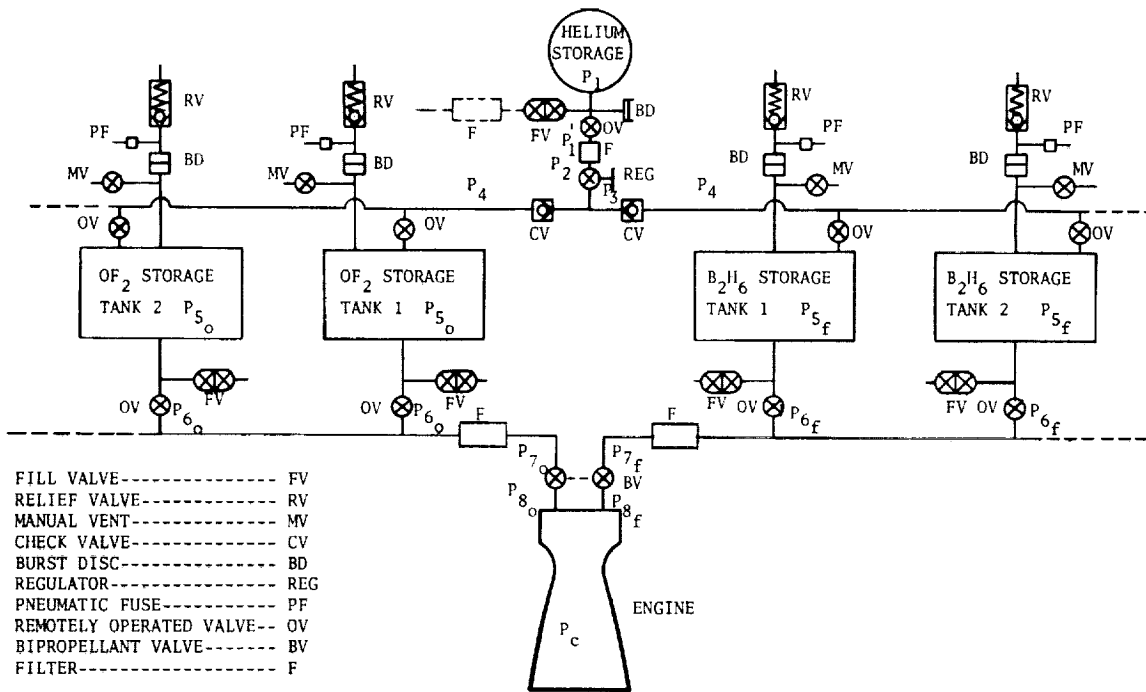


Figure 4-16. OF<sub>2</sub>/B<sub>2</sub>H<sub>6</sub> Propellant Feed System

4.3.2.2 Component Requirements - The purpose of this segment is to examine some of the more critical requirements which must be met by valve components used on spacecraft propulsion systems. This discussion is oriented to view the origin and nature of these requirements from both the designer's and the system engineer's viewpoints.

Aside from the conventional list of specifications, most of which are reflections of a given system's geometry requirements, certain characteristics of components must be matched to the needs of a system, its operation, and its environment, to maximize the probability of success. Figure 4-16 will be used as a baseline system schematic; only selected areas bearing on the more severe problems will be discussed here. The propellant combination oxygen difluoride ( $OF_2$ ) and diborane ( $B_2H_6$ ) has been chosen as the combination of greatest interest but some examples are based on the use of other propellants such as monopropellant hydrazine.

Several of the problems can be directly related to the component parts which are listed in Table 4-7. For the highly reactive propellants, problems appear in the areas of corrosion, contamination, and cleaning. Proper choice of materials will be essential and, in the case of  $OF_2$  and  $B_2H_6$ , there is limited materials compatibility data (see Section 3.0 of this report). Metals that resist erosion where flow impingement occurs should be used while metals which pit or build up coatings should be avoided.

Data on potential sources of contamination are not plentiful. The obvious case of initial contamination during fabrication, assembly, and test will not be discussed here. Moisture, largely due to atmospheric humidity, can increase a propellant's tendency to corrode normally corrosion resistant materials and form ice crystals, or particulate contaminants. The formation of gels (due to metal complexes) within propellant systems while in service has been detected a number of times (Reference 5). Hydraulic unbalance between the fuel and oxidizer legs of flow circuits could be caused by "flow decay." Filter clogging is a possible problem as is injector orifice clogging. Gel formation could also lead to valve malfunction.

Particulate contamination can abrade surfaces and cause excessive forces between close-tolerance sliding parts. The present designs tend toward superfine finishes (less than 2 microinches) on hard seat valves which depend entirely on metal-to-metal alignment for sealing (little deformation). Soft seats can deform to seal around small particles and scratches to some degree, but no material soft enough to provide adequate deformation with low actuation loads is presently recommended for  $OF_2$  service. Self-actuated parts (check valves, regulators, etc.) are particularly prone to jamming or leaking in a system containing particulate contamination.

The particulate contamination problem is more insidious than it seems at first. Most cleaning specifications allow an unlimited number of particles below a lower limiting size, yet there is adequate evidence that certain conditions cause these particles to conglomerate and form large particles within the system. Furthermore, particle generation within working systems has been a chronic problem. The system interconnections and all of the component parts must be designed to permit thorough cleaning and drying.

Table 4-7. Component Performance in Baseline  
OF<sub>2</sub>/B<sub>2</sub>H<sub>6</sub> Feed System

Component	Symbol	Likely Corrosion Problem Areas	Types of Contamination Causing Problems	Likely Cleaning Problems	Likely Dynamic Problems	Critical Performance Parameters
Regulator	REG	Diaphragm Sliding parts Seat	Solids Moisture Propellant vapor	Crevice at diaphragm Under sliding parts Crevice at joint	Seat surface fatigue and galling of sliding parts	Set pressure
Check Valve	CV	Sliding parts	Solids Moisture	Under spring Crevice at joint Under guide	Seat surface fatigue and galling of sliding parts	Cracking pressure Leakage ΔP vs flow
Manual Vent Valve	MV	Seat corrosion and erosion	Solids	Dynamic seal or bellows Crevice at joint	Unload poppet	Leakage
Burst Disc	BD	Disc	---	Crevice at edge of disc and at joint	Generation of particles	Burst pressure Leakage
Pneumatic Fuse	PF	Seat corrosion and erosion Sliding parts	Solids	Under spring Crevice at joint	Seat surface fatigue and galling of sliding parts	Leakage
Relief Valve	RV	Seat Sliding parts	Solids	Crevice at joint Under spring and sliding parts Bellows	Seat surface fatigue and galling of sliding parts	Set pressure Re-seat pressure Leakage
Isolation Valve	OV	Seat corrosion and erosion Sliding parts Bellows	Solids	Under spring Crevice at joint Under sliding parts, Bellows	Seat surface fatigue and galling of sliding parts	Cracking pressure Leakage
Fill Valve	FV	Seat corrosion and erosion	Solids	Dynamic seal or bellows Crevice at joint	Unload poppet	Leakage
Filter	F	Wire in element	Propellant gel	Particles trapped in or generated by element Crevice at joint	Generation of particles and wire breakage	ΔP vs flow
Bipropellant Valve	BV	Seat corrosion and erosion Sliding parts Bellows	Solid Propellant gel	Crevice at joint Bellows Under sliding parts	Seat surface fatigue and galling of sliding parts	Response Leakage

Most valve designs incorporate crevices and have concave corners sharp enough to shield contamination from the flow of cleaning fluids. While the advent of sonic cleaners has increased the ability to clean parts before assembly, crevices and corners within parts cannot be effectively cleaned after the system is assembled. Circulating solvents and drying fluids through the system is the only practical procedure at this time (few systems are small enough, for example, to be vacuum dried in an oven.

In addition to generating particles, moving parts degrade themselves if overloaded. Surface fatigue can occur after many cycles of impact, for example, when fast closing valves seat. Vibration induced either by external forces or instabilities powered by flow interactions can cause pounding to occur, which eventually destroys the surface finish. Galling failure is not too common but still to be considered a hazard since no good lubricants can be used in contact with the propellants.

Table 4-8 lists the more critical component performance parameters in the  $OF_2$ - $B_2H_6$  feed system. Table 4-9 summarizes component and system leakage criteria. The last column in the tables gives a condensed summary of the likely range of values or tolerances on values. Note that "worst case" calculations (based on arbitrary methods or datum points) often lead to values beyond the state of the art, so that the systems engineer must specify the best obtainable.

The most critical problem area is that of leakage. Table 4-9 presents some of the criteria on which a system (or component) designer can base allowable leakage calculations. Samples are given to illustrate how these criteria might be implemented. The examples presented represent real cases, however, the sample cases and calculations are primarily illustrative rather than actual.

The task of determining leakage rates becomes very complex because real systems contain many leak paths, both in series and in parallel, which have different potentials for leakage and produce different effects if leakage occurs. Calculating the "worst case" total leakage allowance, based on all of the likely criteria, then assigning equal shares of the lowest rates to all the leak paths will usually result in very low individual leakage allowables that are often beyond the state of the art.

4.3.2.3 Component Sizing - Sizing data is required to allow a more detailed design study of each valve. A pressure drop allowance has been assigned to each component to be sized starting at the engine and working back to the pressurant tank. These pressure drops are itemized in Table 4-10. A chamber pressure of 150 psi was assumed, and line losses were considered small compared to component losses.

The propellant flow rates were calculated for thrusts of 50, 200 and 1000 pounds, a specific impulse of 400 seconds, and an oxidizer to fuel mixture ratio of 4.0. The theoretical specific impulse ( $I_{sp}$ ) for an O-F mixture ratio of 4.0 is 434 seconds for a 40 to 1 expansion to vacuum and 317 seconds at optimal expansion to sea level for a 300 psi chamber pressure (Reference 6). Gas flow data was determined by adding the volumetric flow rates of fuel and oxidizer with appropriate corrections for gas density.

Table 4-8. Critical Component Performance Parameters

COMPONENT	SYMBOL	PARAMETER	CRITERIA OR PROBLEM	ESTIMATED RANGE OR TOLERANCE
Regulator	REG	Set Pressure	Variation in thrust from nominal.	$\Delta P_{REG} = \frac{(F+\Delta F)^2}{K} + F + \Delta F - P_{REG}$ Typical $\Delta P_{REG} = \pm 0.015 P_{REG}$
Check Valve	CV	Repeatability of cracking pressure	Sequencing of tank pressure rise at start, which if not together, may cause unequal flow which change c.g. and shift mixture ratio.	Typically $\delta(\Delta P_c) \pm 50\%$ of cracking pressure $(\Delta P_c)$
		Leakage	Possible mixing of fuel and oxidizer and corrosion of regulator if isolation valves also leak.	(see Table 4-9) Worst case leakage, $L = 10^{-10}$ to $10^{-8}$ cm <sup>3</sup> /sec
		Repeatability of $\Delta P$ versus flow at full open	Differences in tank pressures causing unequal flows which change c.g., and shift mixture ratio.	Typically $\delta(\Delta P) = \pm 1/2\%$ of overall drop from regulator to chamber pressure, therefore, $\Delta P_{CV} = \Delta P_{NOM} \pm 0.005 (P_{REG} - P_c)$
Manual Vent Valve	MV	Leakage	Hazard of fire, toxicity and corrosion on ground; loss of pressure or propellant in flight, possible torque on spacecraft or interference with optical instruments in flight.	(see Table 4-9) Typically: For toxicity, $L = \frac{10^{-6}}{\text{No. of Leaks}} \text{ cm}^3/\text{sec}$ For torque, $L = \frac{20 \text{ to } 100}{\text{Mission Life in seconds}} \text{ gm/sec}$
Burst Disc	BD	Burst Pressure Leakage	High value fails to protect tank, low value allows unnecessary venting (see Manual Vent Valve)	High value increases tank design weight by $W = K P_R$ is a constant margin of relief pressure to burst pressure is kept. $K = 0.9$ to $0.95$ . Typically $P_R = 2$ to $5\%$ of set pressure. Low value case requires lengthy analysis. For leakage case, see pneumatic fuse.
Pneumatic Fuse	PF	Leakage	Once burst disc has ruptured, leakage may produce torque on spacecraft or interfere with optical instruments, and cause loss of pressure or propellant.	(see Table 4-9) Typically: For torque, $L = \frac{20 \text{ to } 100}{\text{Mission Life in seconds}} \text{ gm/sec}$
Relief Valve	RV	Set Pressure	High value fails to protect tank, low value may allow unnecessary venting, which will cause loss of pressure or propellant, produce a torque on spacecraft, and may interfere with optical instruments.	(See Burst Disc)
		Re-Seal Pressure Leakage	Low value may allow unnecessary venting (see Set Pressure). (see Pneumatic Fuse)	
Isolation Valve	OV	Cracking Pressure & Repeatability of Response	Sequencing of tank pressurization and flows from tanks, which, if not together, may cause unequal flows which change c.g. and momentarily shift mixture ratio.	Typically: $\Delta P_c = \pm 10\%$ of nominal $\Delta t = \pm 25$ msec
Fill Valve	FV	Leakage	(See Manual Vent Valve)	(See Manual Vent Valve)
Filter	F	Particle Size in Efflux	Particles that are too large may jam close tolerance parts, erode surfaces, etc.	To avoid jamming, smallest of two largest dimensions should not exceed approximately $0.75 \times$ diametral clearance. Erosion problem is complex, depending on hardness, stream velocities, etc.
		$\Delta P$ VS Flow	Increase in $\Delta P$ may change flowrates causing shift in mixture ratio, variations in thrust.	Typically $\delta(\Delta P_c) = \pm 1\%$ of overall drop from regulator to chamber pressure, therefore: $\Delta P_F = P_{NOM} \pm 0.005 (P_{REG} - P_c)$
Bipropellant Valve	BV	Response	Slow or non-repeatable response will cause errors in impulse delivered by the engine.	Depends on valve characteristics and system response. For systems where valve is nearly linear and dominant influence, nominal valve travel time can be approximated as: $t_o = \frac{\text{minimum impulse bit}}{\text{rated thrust}}$
		Leakage	May produce torque on spacecraft, interfere with optical instruments, cause loss of pressure or propellant, or freeze the valve poppet.	When the maximum allowable impulse bit (for a minimum impulse maneuver) is stated, the tolerance on travel time can also be calculated from: $\Delta t = \frac{\text{maximum-minimum impulse bit}}{2 \times \text{thrust}}$ (i.e., valve travel time = $t_o + \Delta t$ to yield an impulse bit between the minimum and the maximum allowed for a minimum maneuver). Determining the leakage sufficient to freeze the propellant valve is a lengthy calculation requiring the values of many variables to be known.

Table 4-9. Component and System Leakage Criteria

Criteria	Sample Application	Sample Basis For Choosing Allowable	Sample Calculation (Assuming Only One Leak Path)
(1) "No measurable"	Pin holes in Teflon bladder	No bubbles when bladder is immersed in soap solution while inflated with helium	From JPL TR No. 32-926, Figure 7, this test will detect leaks no smaller than $10^{-5}$ scc/sec of helium
(2) JPL "zero leakage"	Fill valve on propellant tank	Liquid flow blocked by surface tension across leak path	From JPL TR No. 32-926, Figure 5, for P=300 psi, leakage = $4.5 \times 10^{-9}$ cm <sup>3</sup> /sec, equal to $1.2 \times 10^{-6}$ scc/sec of helium
(3) Pressure increase	Pressure rise in pressurization manifold due to helium shutoff valve leakage	Manifold pressure shall not increase more than 50 psi in 200 days	Assume $V=0.01 \text{ ft}^3$ , $T=240^\circ\text{R}$ , $P=300 \text{ psia}$ $\Delta W = \frac{V \Delta P}{RT} = \frac{0.01 \times 50 \times 44}{386 \times 240} = 0.00078 \text{ lb} = 0.35 \text{ g}$ $\frac{\text{scc}}{t} = \frac{\Delta W}{t \rho_{\text{scc}}} = \frac{0.35}{1.7 \times 10^{-7} \times 1.78 \times 10^{-4}} = 1.2 \times 10^{-4} \text{ scc/sec}$
(4) Loss of pressure	Conax "Eager Pak" gas source	Helium loss less than 100 psi in one year	$V=0.1 \text{ ft}^3$ , $P=3000 \text{ psia} = 432000 \text{ psfa}$ , $T=100^\circ\text{F} = 560^\circ\text{R}$ , $t=1 \text{ yr.} = 3.15 \times 10^7 \text{ sec}$ . $\Delta W = \frac{V \Delta P}{ZRT} = \frac{0.1 \times 432000}{1.13 \times 386 \times 560} = 0.18 \text{ lb} = 82 \text{ gm}$ $\frac{\text{scc}}{t} = \frac{\Delta W}{t \rho_{\text{scc}}} = \frac{82}{3.15 \times 10^7 \times 1.78 \times 10^{-4}} = 1.5 \times 10^{-2} \text{ scc/sec}$
(5) Loss of mass	Start slug for monopropellant engine	Less than 10% loss in one year	$V = 15 \text{ cm}^3$ of $\text{N}_2\text{O}_4$ , $\frac{\Delta V}{t} = 1.5 \text{ cm}^3/\text{yr}$ $\frac{\Delta V}{t} = \frac{1.5}{3.15 \times 10^7} = 4.8 \times 10^{-8} \text{ cm}^3/\text{sec}$ of liquid
(6) Perturbation of spacecraft	Attitude control system jet valves	Less than 10% of the nitrogen gas load must be able to counteract torque for 1 year	<20% of load will be lost due to the leak and the counteracting jet. Assume $W = 0.32 \text{ lb} = 145 \text{ gm}$ , $\Delta W = 29 \text{ gm}$ , $\frac{\text{scc} \Delta W}{t \rho_{\text{scc}}}$ $= \frac{29}{3.15 \times 10^7 \times 1.25 \times 10^{-3}} = 7.4 \times 10^{-4} \text{ scc/sec}$
(7) Toxicity	Controlled environment space, during preparation for launch of $\text{OF}_2$ system	Concentration of $\text{OF}_2$ shall not exceed 0.05 ppm	Assume one change of air each 3 minutes, $T=68^\circ\text{F}$ , $V=2000 \text{ ft}^3$ , then $\frac{W_{\text{air}}}{t} = \frac{V \rho_{\text{air}}}{t}$ $\frac{0.075 \times 2000}{3 \times 60} = 0.83 \text{ lb/sec} = 380 \text{ gm/sec}$ , leakage of $\text{OF}_2 = \frac{W_{\text{air}}}{t} \times \frac{\text{ppm}}{\rho_{\text{OF}_2}} \times 10^{-6} = \frac{380 \times 0.05 \times 10^{-6}}{1.48} = 1.25 \times 10^{-6} \text{ cm}^3/\text{sec} \text{ \# NBP}$
(8) Explosion hazard	Leakage through isolation valves in common pressurant line to $\text{OF}_2$ and $\text{B}_2\text{H}_6$ tanks	Accumulated leakage in 200 days shall not cause a peak pressure rise of more than 100 psi if burned at a ratio of 3.8 (ox/fuel)	Assume $V=0.006 \text{ ft}^3$ , $T=7500^\circ\text{R}$ , $M=19.5$ , and initial pressure $P=3000 \text{ psia}$ . Burning gas will occupy 1/4 the total volume, therefore, $V_g = \frac{V}{4} = \frac{0.006}{4} = 0.0015 \text{ ft}^3$ $W_g = \frac{MPV}{RT} = \frac{19.5 \times 400 \times 0.0015}{1545 \times 7500} = 1.5 \times 10^{-4} \text{ lb}$ $W_f = \frac{W_g}{r+1} = \frac{0.3 \times 10^{-4} \text{ lb}}{3.8} = 8 \times 10^{-6} \text{ lb} = 3.8 \times 10^{-3} \text{ gm}$ $1.2 \times 10^{-4} \text{ lb}$ , $\frac{W_f}{t} = \frac{3.8 \times 10^{-3}}{1.7 \times 10^7} = 2.2 \times 10^{-10} \text{ gm/sec}$ $1.8 \times 10^{-12} \text{ lb/sec} = 8 \times 10^{-10} \text{ gm/sec}$ , $\rho_{\text{air}} @ 240^\circ\text{R} = 0.494$ , leakage = $1.6 \times 10^{-9} \text{ cm}^3/\text{sec}$ . By similar calculation oxidizer leakage = $2.1 \times 10^{-9} \text{ cm}^3/\text{sec}$
(9) Flammable air mixture	$\text{B}_2\text{H}_6$ storage system	$\text{B}_2\text{H}_6$ concentration shall not exceed 0.5% by volume	Assume 1 change of air per day in 500 cu ft room, $\frac{\Delta V}{t} = \frac{500 \times 0.005}{60 \times 60 \times 24} = 2.9 \times 10^{-5} \text{ ft}^3/\text{sec}$ $0.82 \text{ cm}^3/\text{sec}$ of vapor @ room temperature or $2.2 \times 10^{-3} \text{ cm}^3/\text{sec}$ of liquid @ NBP
(10) Particle visible to star tracker	Crystal of $\text{OF}_2$ from sudden venting of accumulated leakage	Accumulated leakage over 200 days shall not form a spherical crystal over 1/4 inch in diameter	Volume = $0.00818 \text{ cu in} = 0.134 \text{ cm}^3$ Assume $\rho_{\text{solid}} = \rho_{\text{liq}}$ Leakage = $\frac{0.134}{60 \times 60 \times 24 \times 200} = 8 \times 10^{-9} \text{ cm}^3/\text{sec}$
(11) "Refrigeration" of engine parts	Leakage past on-off valve of monopropellant engine chills on evaporation, cooling catalyst bed below threshold of ignition	Leakage to vacuum shall not reduce catalyst bed temperature below $+40^\circ\text{F}$	(Calculation too complex to give simple example)
(12) Blockage by solids	$\text{B}_2\text{H}_6$ leakage through off-off valve and injector	Total leakage over 72 hour period shall not block a 0.02 in orifice when $\text{H}_3\text{BO}_3$ formed with atmospheric humidity	Assume $\rho_{\text{liq}}$ of 0.02 in thickness, vol $\frac{1}{2} 6 \times 10^{-4} \text{ in}^3 = 9.8 \times 10^{-5} \text{ cm}^3$ , $\rho_{\text{H}_3\text{BO}_3} = 1.8 \text{ gm/cm}^3$ , $W = \rho V = 1.8 \times 9.8 \times 10^{-5} = 1.8 \times 10^{-4} \text{ gm}$ , $M_{\text{B}_2\text{H}_6} = 27.69$ , $M_{\text{H}_3\text{BO}_3} = 61.84$ , $W_{\text{B}_2\text{H}_6} = \frac{W_{\text{H}_3\text{BO}_3} M_{\text{B}_2\text{H}_6}}{2 M_{\text{H}_3\text{BO}_3}}$ $\frac{1.8 \times 10^{-4} \times 27.69}{2 \times 61.84} = 4 \times 10^{-5} \text{ gm}$ , $\frac{W}{t} = \frac{4 \times 10^{-5}}{60 \times 60 \times 72} = 1.5 \times 10^{-10} \text{ gm/sec}$
(13) Corrosion	Leakage past shaft seal into actuation cavity of valve	Critical amount of corrodent shall not enter cavity over period of 200 days	Assume critical amount of corrodent (empirical data) is $0.1 \text{ gm}$ , $\frac{\Delta W}{t} = \frac{0.1}{60 \times 60 \times 24 \times 200} = 6 \times 10^{-9} \text{ gm/sec}$

The valves itemized in Table 4-10 were sized on the basis of pressure drop. This has been done by utilizing the flow equation for incompressible flow with a discharge coefficient of 0.6. While this discharge coefficient may seem somewhat conservative it has been found to be the value realized in most valving applications. The results of these calculations are shown in Figures 4-17 through 4-20. The figures present curves of propellant mass and volume flow versus thrust as well as pressure drop versus area at various thrust levels and areas versus thrust at various allowable pressure drops. The calculations required to develop these curves are presented in Reference 7. The data presented in these curves has been used to determine the required flow areas and equivalent diameters required for the propellant valves in Figure 4-16 and Table 4-10, and are summarized in Table 4-11.

The propellant lines are considered to be minor pressure drops for the purpose of this analysis and will be sized large enough to ensure that actual velocities are well below the critical propellant flow velocities (Figures 4-21 and 4-22), so that the possibility of cavitation in bends and fittings is minimized. Suggested line sizes are based on maintaining one half the critical flow velocities shown in Table 4-11 and Figure 4-23.

The pressurant system components have been sized on the basis of the modified compressible sonic flow equation with a restriction factor introduced to account for pressure ratio in subsonic flow as proposed by Smith (Reference 8). Helium flow was determined from the volumetric propellant flow previously calculated. Curves of helium flow versus thrust, flow area versus pressure drop at various thrust levels, and flow area versus thrust at various pressure drops are presented in Figures 4-24, 4-25 and 4-26. The calculations required to develop these curves are included in Reference 7 and the pressurant component areas and equivalent diameters based on this data are presented in Table 4-11.

#### 4.3.3 Valve Redundancy

In order to achieve the maximum system reliability, space systems are normally analyzed by combining the success (or failure) probabilities of their components in their appropriate series or parallel operating modes. The required elements are then rearranged and redundancies introduced until the required reliability values are obtained. The analytical methods normally used to determine the reliability of series parallel, and series-parallel redundant valve arrays are described in Reference 9. The analysis takes into account the difference which occurs between the fail-open and fail-closed probabilities normally encountered in real valving elements. This gives a better indication of actual system reliability and the most probable overall failure mode.

This study examined the analytical procedure for determining the application of redundant valving arrangements and assessed their merits in relation to functional parameters and the effects on system performance not normally considered in failure analysis. Several functional parameters were considered which are not normally included in the redundancy analysis and which may affect engine performance and valve design.



Table 4-10. Component Pressure Drop Allowances

Item	Pressure Symbol	Media	$\Delta P$	Pressure
Injector	$P_8 - P_c$	O,F	10	$P_8 = 160$ psia
BV Bipropellant Valve	$P_7 - P_8$	O,F	20	$P_7 = 180$ psia
F Filter	$P_6 - P_7$	O,F	5	$P_6 = 185$ psia
OV Remotely Operated Valve	$P_5 - P_6$	O,F	15	$P_5 = 200$ psia
OV Remotely Operated Valve	$P_4 - P_5$	He	5	$P_4 = 205$ psia
CV Check Valve	$P_3 - P_4$	He	5	$P_3 = 210$ psia
REG Regulator (wide open @ min. inlet)	$P_{2_1} - P_3$	He	50	$P_{2_1} = 260$ psia
F Filter	$P_1 - P_2$	He	5	$P_1 = 265$ psia
OV Remotely Operated Valve	$P_1 - P_1$	He	5	$P_1 = 270$ psia (min.)

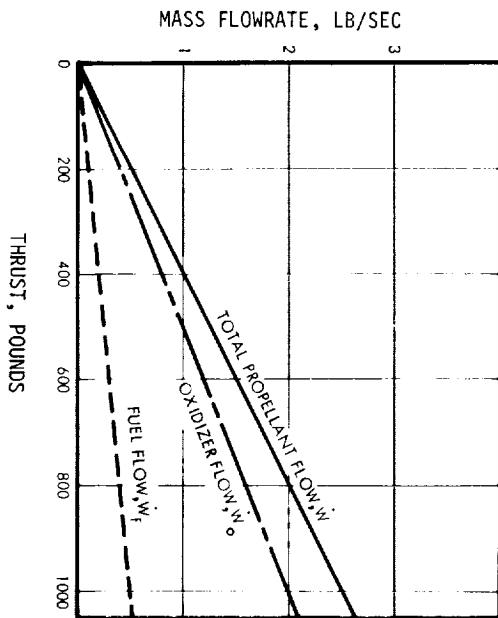


Figure 4-17.  $OF_2/B_2H_6$  Mass Flow-Rates @  $I_{sp}$  of 400 sec.

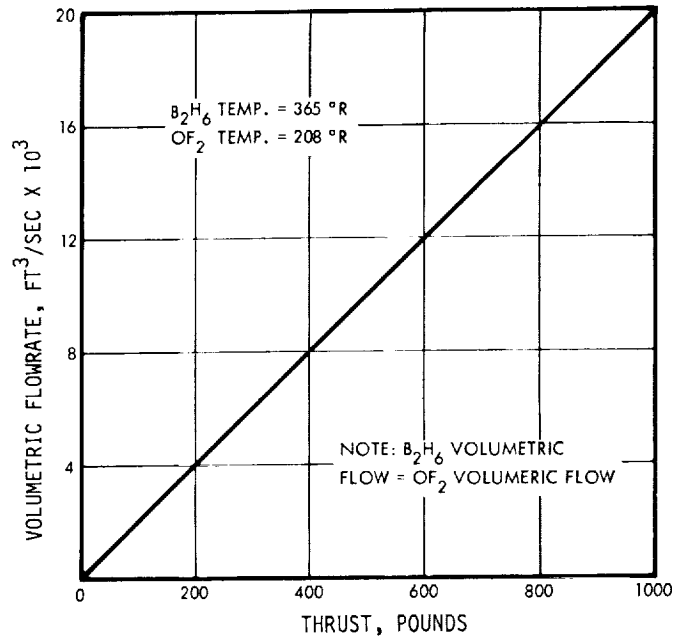


Figure 4-18.  $OF_2/B_2H_6$  Volumetric Flow-Rates @  $I_{sp}$  of 400 sec.

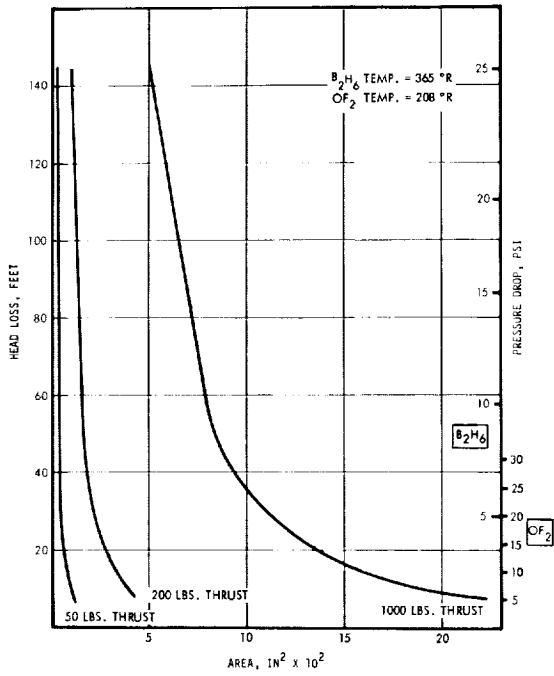


Figure 4-19. Propellant Head Loss Vs Flow Area at  $I_{sp}$  of 400 Sec.

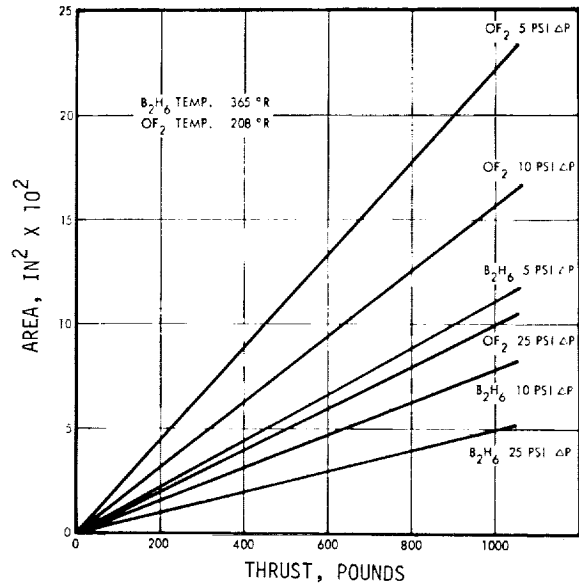


Figure 4-20. Propellant Flow Area Vs Thrust at  $I_{sp}$  of 400 Sec.

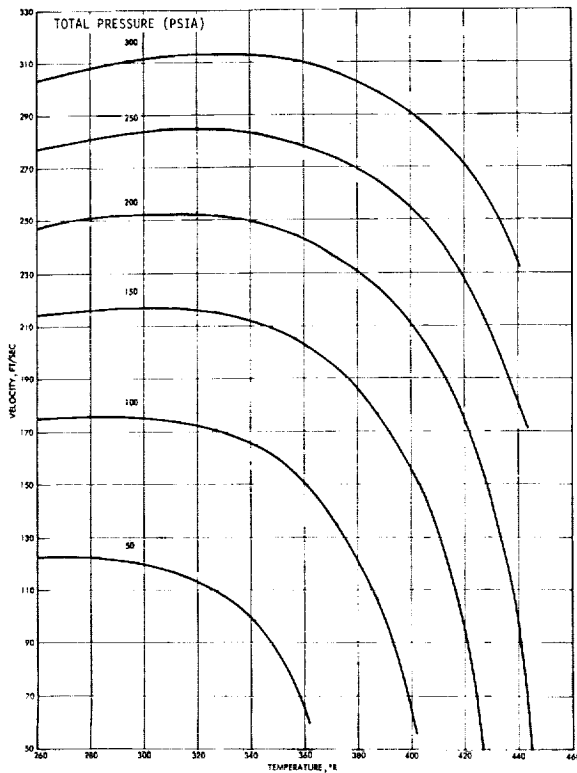


Figure 4-21.  $\text{B}_2\text{H}_6$  Critical Flow Velocity

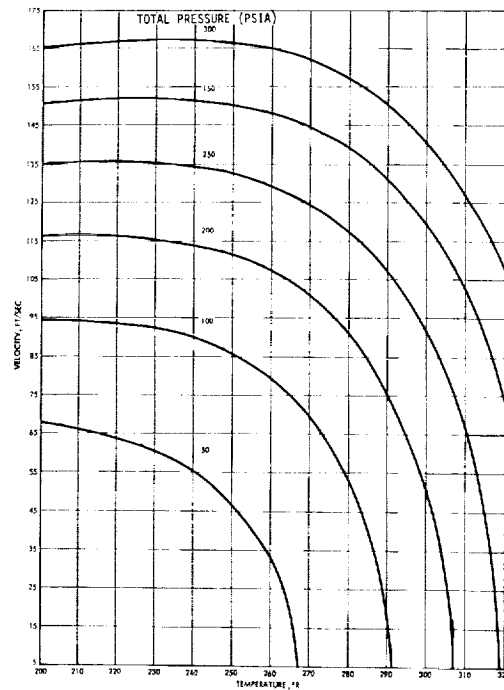


Figure 4-22.  $\text{OF}_2$  Critical Flow Velocity

Table 4-11. Component and Line Size Summary

Symbol	Component Type	Media	Allowed $\Delta P$ (psi)	50 Lb. Thrust		200 Lb. Thrust		1000 Lb. Thrust	
				Area (in <sup>2</sup> )	Eq. Dia. (in.)	Area (in <sup>2</sup> )	Eq. Dia. (in.)	Area (in <sup>2</sup> )	Eq. Dia. (in.)
BF	Bipropellant Valve	F	20	$.30 \times 10^{-2}$	.062	$1.20 \times 10^{-2}$	.124	$6.2 \times 10^{-2}$	.281
		O	20	$.50 \times 10^{-2}$	.079	$2.20 \times 10^{-2}$	.167	$11.2 \times 10^{-2}$	.378
F	Filter	F	5	$.56 \times 10^{-2}$	.085	$2.23 \times 10^{-2}$	.169	$11.14 \times 10^{-2}$	.377
		O	5	$1.11 \times 10^{-2}$	.118	$4.45 \times 10^{-2}$	.238	$22.28 \times 10^{-2}$	.533
OV	Remotely Operated Valve	F	15	$.35 \times 10^{-2}$	.067	$1.30 \times 10^{-2}$	.129	$6.75 \times 10^{-2}$	.294
		O	15	$.60 \times 10^{-2}$	.087	$2.65 \times 10^{-2}$	.184	$13.10 \times 10^{-2}$	.409
OV	Remotely Operated Valve	He	5	$3.38 \times 10^{-5}$	.007	$13.52 \times 10^{-5}$	.014	$67.6 \times 10^{-5}$	.030
CV	Check Valve	He	5	$3.38 \times 10^{-5}$	.007	$13.52 \times 10^{-5}$	.014	$67.6 \times 10^{-5}$	.030
REG	Regulator (worst case)	He	50	$3.18 \times 10^{-5}$	.007	$12.70 \times 10^{-5}$	.013	$63.60 \times 10^{-5}$	.029
F	Filter	He	5	$3.38 \times 10^{-5}$	.007	$13.52 \times 10^{-5}$	.014	$67.6 \times 10^{-5}$	.030
OV	Remotely Operated Valve	He	5	$3.38 \times 10^{-5}$	.007	$13.52 \times 10^{-5}$	.014	$67.6 \times 10^{-5}$	.030
FV	Fill Valve	F	-	$2.83 \times 10^{-5}$	.06	$12.27 \times 10^{-3}$	.125	$49.09 \times 10^{-3}$	.250
		O	-	$2.83 \times 10^{-3}$	.06	$12.27 \times 10^{-3}$	.125	$49.09 \times 10^{-3}$	.250
MV	Manual Valve	He	-	$2.83 \times 10^{-3}$	.06	$12.27 \times 10^{-3}$	.125	$49.09 \times 10^{-3}$	.250
		He	-	$2.83 \times 10^{-3}$	.06	$12.27 \times 10^{-3}$	.125	$49.09 \times 10^{-3}$	.250
-	Propellant Lines	F	-	$5.03 \times 10^{-3}$	.080	$14.31 \times 10^{-3}$	.135	$30.17 \times 10^{-3}$	.196
		O	-	$5.03 \times 10^{-3}$	.080	$14.31 \times 10^{-3}$	.135	$51.47 \times 10^{-3}$	.256
-	Pressurant Lines	He	-	$5.03 \times 10^{-3}$	.080	$5.03 \times 10^{-3}$	.080	$5.03 \times 10^{-3}$	.080

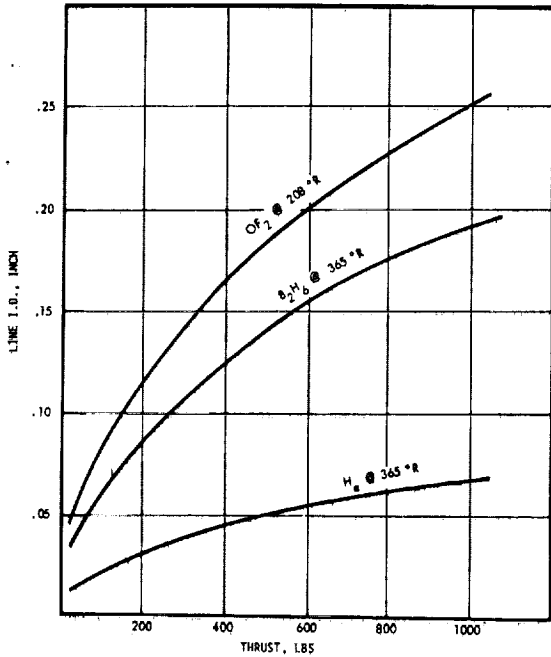


Figure 4-23.  $OF_2$ - $B_2H_6$  Diameter Vs. Thrust at  $I_{sp}$  of 400 sec.

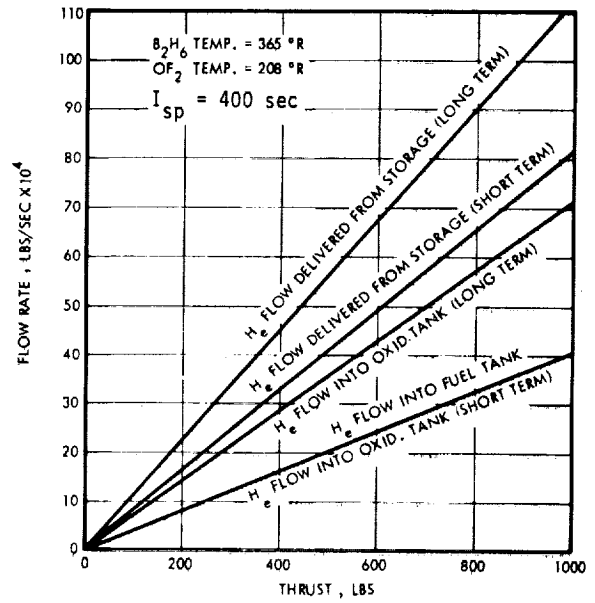


Figure 4-24. Mean Helium Flowrate Vs. Engine Thrust

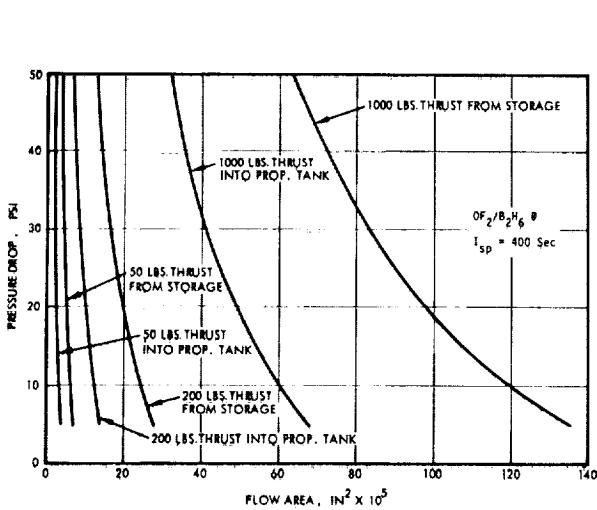


Figure 4-25. Helium Pressure Drop Vs. Flow Area

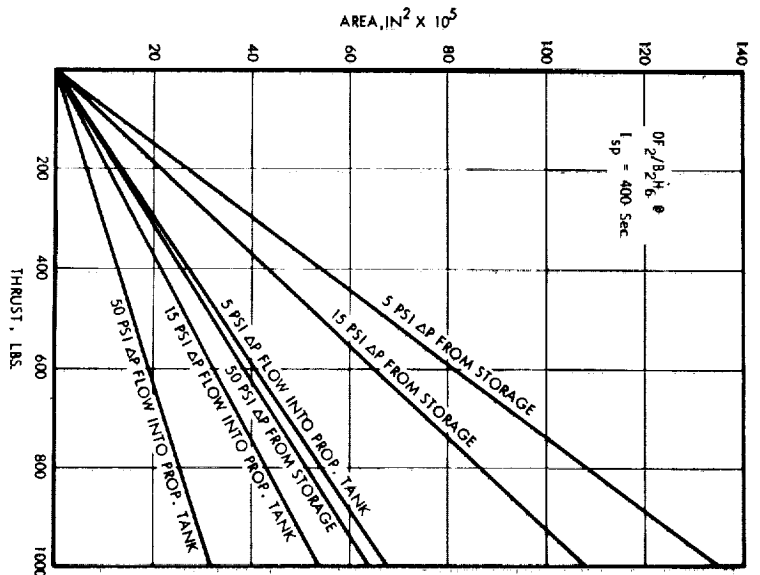


Figure 4-26. Helium Flow Area Vs. Thrust

#### 4.4 CONCEPTUAL VALVE DESIGNS

Studies were performed with the objective of evolving new propellant valve concepts for space application. Primary consideration was given to valves for hydrazine and oxygen-difluoride/diborane service, and engine sizes up to 1000 pound thrust. Extremely small microvalves were also considered for use in fluidic systems and small thrusters. This section presents the new valve concepts evolved and evaluated during the study.

##### 4.4.1 Semi-Toroidal Diaphragm Valve

This valve concept utilizes a semi-toroidal diaphragm and a contoured annular protrusion in the central valve housing to perform flow control (Figure 4-27). The semi-toroidal diaphragm is attached to two annular rings; one is fixed and the other is a moveable control ring. Flow control is achieved by axially moving the control ring to vary the gap between the diaphragm and the annular protrusion of the valve housing. The seal gap can also be designed to operate in cavitation, to provide isolation from downstream pressure variations. Shutoff is accomplished by forcing the diaphragm against the annular protrusion.

A preliminary design of a semi-toroidal lightweight propellant valve is shown in Figure 4-28. In this design the diaphragm is pressure balanced to reduce the required operating forces.

An integral bipropellant valve configuration is shown in Figure 4-29. The propellants enter axially, pass through the throttling area, and proceed out radially. This concept is shown integrated with a coaxial propellant injector in Figure 4-30. In this case, the propellants enter radially into a supply annulus before passing through the throttling area and exit coaxially through the pintle into the combustion chamber. A schematic of a mixture ratio controller utilizing the bipropellant semi-toroidal diaphragm valve is shown in Figure 4-31.

Since the success of the concept is heavily dependent upon the proper function of the diaphragm seals, their limitations must be carefully determined. The relationship between size, radius ratio, pressure, strike, and stress is extremely important. The total membrane stress is made up of two components, that which results from pressure acting on the cylindrical annulus and the bending stress resulting from the displacement of one edge with respect to the other. Limiting values of radii and membrane thickness for various displacements and pressures are given in Reference 3.

A test model of the semi-toroidal metallic diaphragm valve demonstrated the feasibility of this concept in the areas of cavitation and throttling. Shutoff tests conducted were inconclusive, because of the doubtful quality of the test diaphragm itself and the desirability of preventing damage to the diaphragm. There is some doubt that zero ( $10^{-7}$  ccs He) leakage can be achieved without severely overstressing the diaphragm or resorting to the use of a non-metallic resilient seat, however, an order of magnitude of improvement in diaphragm quality must be achieved to prove or disprove this point.

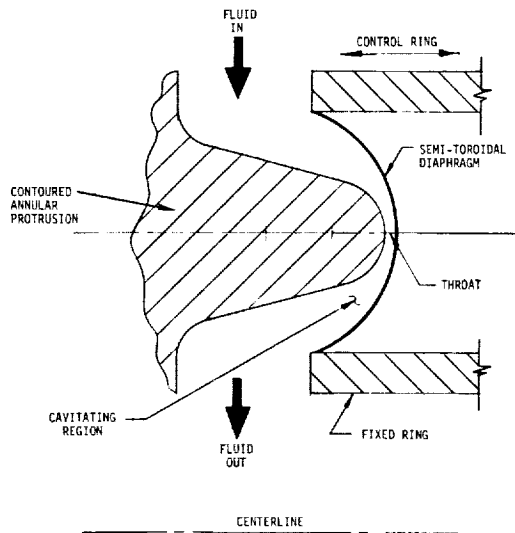


Figure 4-27. Semi-Toroidal Diaphragm Seal Detail

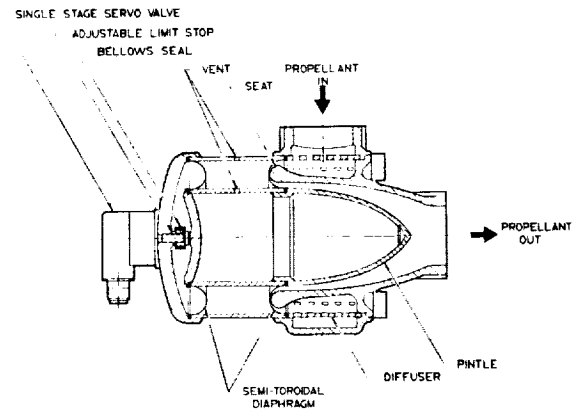


Figure 4-28. Lightweight Semi-Toroidal Propellant Valve Concept

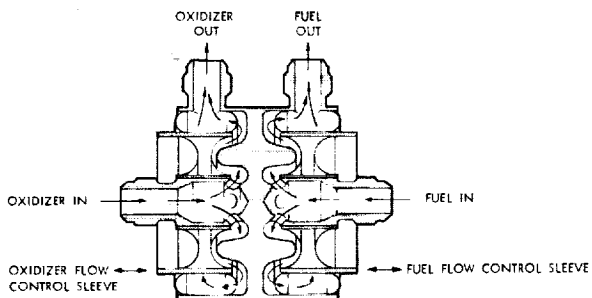


Figure 4-29. Integral Semi-Toroidal Bipropellant Valve Configuration

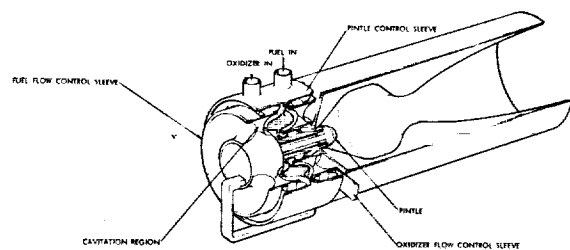


Figure 4-30. Coaxial Variable Thrust Injector with Semi-Toroidal Valve

The advantages of this concept include:

1. no static or dynamic seals or sliding surfaces,
2. all metal construction,
3. cavitation of propellant,
4. 10 to 1 throttle range,
5. simplicity of construction,
6. compactness,
7. large flow rate variation with short stroke.

It should be noted that the semi-toroidal seal design appears to lend itself to fluidic control because the diaphragms represent a natural barrier between the operating fluids. The absence of such barriers has been a problem on some control concepts, as the addition of a separator involves extra weight and the separator usually performs no other useful function. It is possible that a completely fluidic control system could initiate flow and perform the required throttling and shutoff functions.

#### 4.4.2 Diaphragm Valve

A conceptual design of a throttling valve incorporating a simple diaphragm closure is presented in Figure 4-32. The valve has no sliding parts. One metal diaphragm is used as the control element and to effect a seal in the shutoff condition. This feature is utilized to design a compact single or dual propellant valve.

The valve can be used for throttling and flow shutoff in conjunction with fluidic or conventional piloting methods. Diaphragm mass is extremely low, allowing high response in pulsing applications. The control diaphragms can be welded to the seal plates resulting in a hermetically sealed valve design. Only the metal diaphragm and seal plate are exposed to the flow, minimizing materials compatibility problems. With proper material choice the valve may be used from cryogenic to elevated temperature services. Leakage should be comparable to lapped metal-to-metal seal valves. Improved leakage characteristics may be obtained through polymeric coatings on the diaphragm and the seal plate.

The valve operation is described for the oxidizer side; the fuel side operation is identical. The oxidizer flows in through the inlet port and, with control pressure off, deflects the diaphragm upward allowing free flow through the outlet port. When reduced flow is required, pressure is applied to the control port, deflecting the diaphragm toward the seal plate reducing flow. The seal plate may be shaped to allow cavitation. When complete shutoff is required the pressure at the control port is raised so that the diaphragm is firmly pressed against the seal plate, thus sealing the outlet port.

Analysis has shown that a valve with a 2-inch diameter diaphragm could operate with a full stroke of .012-inch without overstressing the diaphragm based on a fatigue life of over a million cycles. If the seat diameter

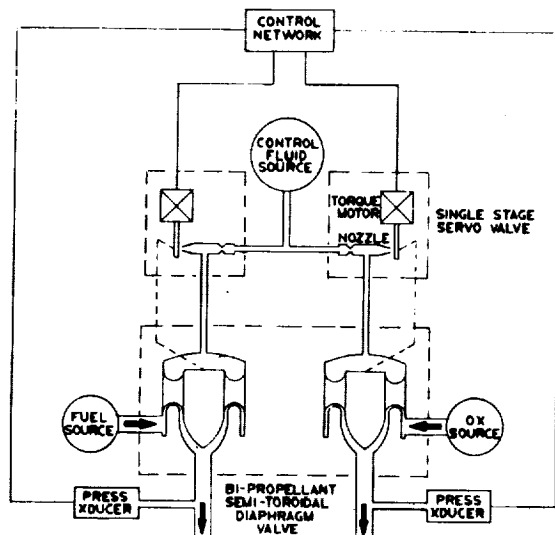


Figure 4-31. Mixture Ratio Controller With Semi-Toroidal Valve

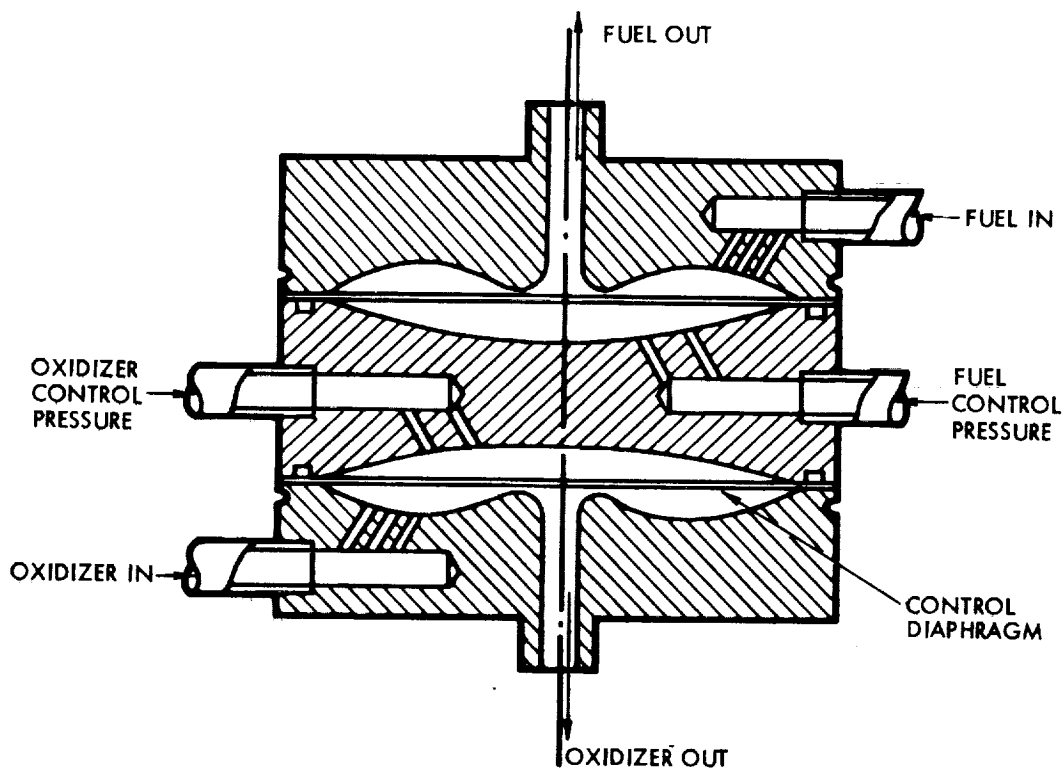


Figure 4-32. Bipropellant Diaphragm Valve



is 0.125 inch the flow area is  $4.72 \times 10^{-3} \text{ in}^2$  or equivalent to a 0.078 diameter hole. The seat diameter may be increased further without hindering valve action. It is felt that an equivalent orifice in excess of 0.093 diameter using a 2-inch diaphragm is entirely possible.

The valving arrangement described has advantages in single as well as bipropellant applications. Its shape makes it attractive for use as a "built in" propellant valve, where it could form part of the propellant tank or engine structure. This would reduce weight and minimize injector dribble volume.

#### 4.4.3 Radial Shutoff Valve

Incorporation of a leak-free flow shutoff function within the venturi injector of a rocket engine can eliminate a separate shutoff valve. The concept described herein can perform the shutoff function by either expanding an internal radial poppet against a circular seat or contracting an outer radial poppet against an internal seat. In either case, the seating force can be derived by an overtravel movement of the venturi or injector pintle actuator with no wiping movement between the poppet and its seat.

Figure 4-33 illustrates a concept of an outwardly expanding radial poppet valve integrally mated to a cavitating venturi flow control valve. The valve is conceived as a flightweight version of a throttle valve for a bipropellant engine applicable to thrust ranges greater than 800 pounds. The venturi is shown in the minimum flow position. To control propellant flow the control rod is moved to the left of this position. To achieve shutoff the following sequence of events takes place:

1. The control rod is moved to the right until the slider contacts the slider stop. During this movement the poppet cap contacts the cap stop, allowing the poppet to move to the right of the cap. At this point the poppet is axially positioned in line with the seat in the venturi throat, with a small radial clearance between the poppet and the seat.
2. The control rod is moved further to the right to achieve the shutoff function. As the inner part of the belleville type disc spring is moved to the right the outer part is forced radially outward, expanding the poppet against the seat.

The opposite sequence is used to open the valve. As the control rod is moved to the left the disc spring contracts, allowing the poppet to contract radially inward away from the seat. Further movement of the rod to the left moves the poppet to the left and allows the cap to cover the poppet.

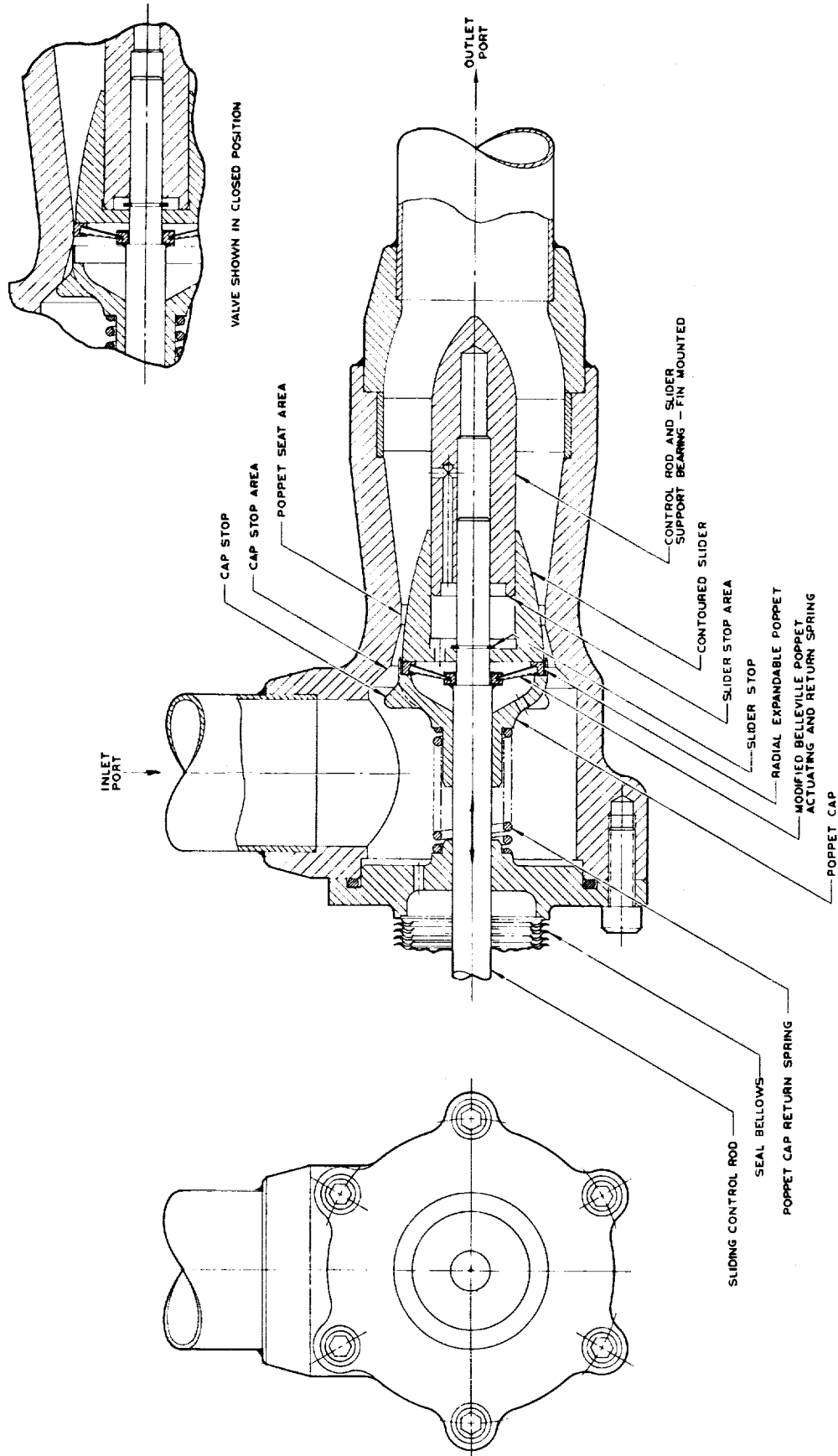


Figure 4-33. Integrated Venturi and Radial Shutoff Valve Concept

The advantages of this arrangement are:

1. Elimination of the need for separate shutoff and throttle valves
2. Reduction in engine weight
3. Longer seal life because the poppet is seated in direct compression
4. Bubble-tight shutoff due to the high closure pressures.

#### 4.4.4 Valves With Thermally Generated Seat Stress

The application of high bearing loads at a valve seat will result in lower leakage rates. Although the degree of leakage as a function of seat stress has not been established, limited tests have demonstrated reduced leakage at relatively high (5000 psi) seat stresses. Consideration was given to the use of temperature variation to stress a valve seat.

The temperature gradient necessary to produce a thermally generated force, positive or negative, can be obtained by the following methods.

1. Electrical heating
2. Convective heating or cooling using hot or cold fluids
3. Thermoelectric cooling
4. Exothermic or endothermic chemical reaction.

Two valve shutoff designs using electrical heating and convective cooling are presented. The valve designs were sized for use on a 1000 pound thrust engine using  $OF_2/B_2H_6$  propellants (see Reference 7 and Section 4.3.2).

4.4.4.1 In-Line Design - The in-line design (Figure 4-34) incorporates a pneumatic actuator for main valve actuation and a thermally strained material providing the high bearing stresses at the valve seat interface. The valve seat is locked by a ball detent locking mechanism. The valve stem is heated prior to closing. The plunger is then locked in position and when the thermal element cools it will contract and generate a high force at the valve seat. The design is also adaptable to heating the valve stem (in the full closed position), expanding the plunger until the ball detent falls into the locked position.

To open the valve the actuator is pressurized and the piston is displaced 0.100 inch allowing the ball to fall into the cavity, thereby unlocking the plunger assembly. It is not necessary to heat the valve stem to open. To close the valve the thermal strain element is heated to raise its temperature by 32°C. The actuator pressure is relieved and the plunger is returned by the spring force. The approximate time to generate 90 percent of the required temperature differential between the valve body and stem is one minute. The total change in length of a free stem is 0.0023 inch.

4.4.4.2 Wagon Wheel Design - The wagon wheel concept (Figure 4-35) employs a thermally contracted rim or ring, around a cylindrical seat design. In the closed position, sealing is initially provided by face shutoff. After cooling the circumferential portion of the poppet contracts around the tubular constructed seat. The design of Figure 4-35 does not include the actuator configuration, since any suitable actuator can be used.

#### 4.4.5 Microvalves

Several valves utilizing thermal and piezoelectric actuation methods were conceived which are suitable for controlling fluidic logic systems or microthrusters. These designs are based on the actuator work presented in Section 6.0. Both two and three way valve configurations were studied.

4.4.5.1 Thermally Actuated Microvalves - Figure 4-36 describes a two way, normally closed electrothermally actuated microvalve with an equivalent orifice of 0.062 inch. The valve is designed to permit the welding of all external joints for hermetic sealing. The envelope measures 0.80 inch long by 0.25 inch diameter. The valve uses a thermal actuator (see Section 6.4.6) which consists of a quantity of heat sensitive amorphous material, in this case a silicone rubber encased in a metal housing. The rubber material used has a thermal volume expansion coefficient of about  $3 \times 10^{-4}$  in<sup>3</sup>/in/°F while the housing volume expansion is  $3 \times 10^{-5}$  in<sup>3</sup>/in/°F. This difference in expansion coefficients results in relatively large deflections when the rubber is heated. The forces are limited by the volume expansion bulk modulus of the material. The actuator shown utilizes an electric heating coil embedded in the heat sensitive material to supply the actuation energy.

Figure 4-37 illustrates a dual two-way valve which may be used to perform a three way function. Two actuators similar to the ones shown above are used to control the two poppets, so that each poppet can be opened separately or together. A similar valve can be built using solenoid actuators, however, they must be considerably larger to provide an equivalent force output.

4.4.5.2 Snap Action Thermally Actuated Valve - A three way valve concept utilizing a bimetal disc actuator is shown in Figure 4-38. The use of a snap acting bimetal disc electrically heated actuator has the advantages of providing relatively high seating loads and good vibration resistance in either of the two valve positions. Since its thermal inertia is very low, response times may be shorter with this type of thermal actuator than with the thermal expansion actuator. The disc is stable in both the cold and hot positions.

4.4.5.3 Piezoelectrically Actuated Valve - A piezoelectrically actuated (see Section 6.4.4) three way valve for moderate pressures is shown in Figure 4-39. This unit employs a single piezoelectric beam or disc to push one ball or the other off its seat. This allows a compact stacking of two valves to accomplish the three way function.

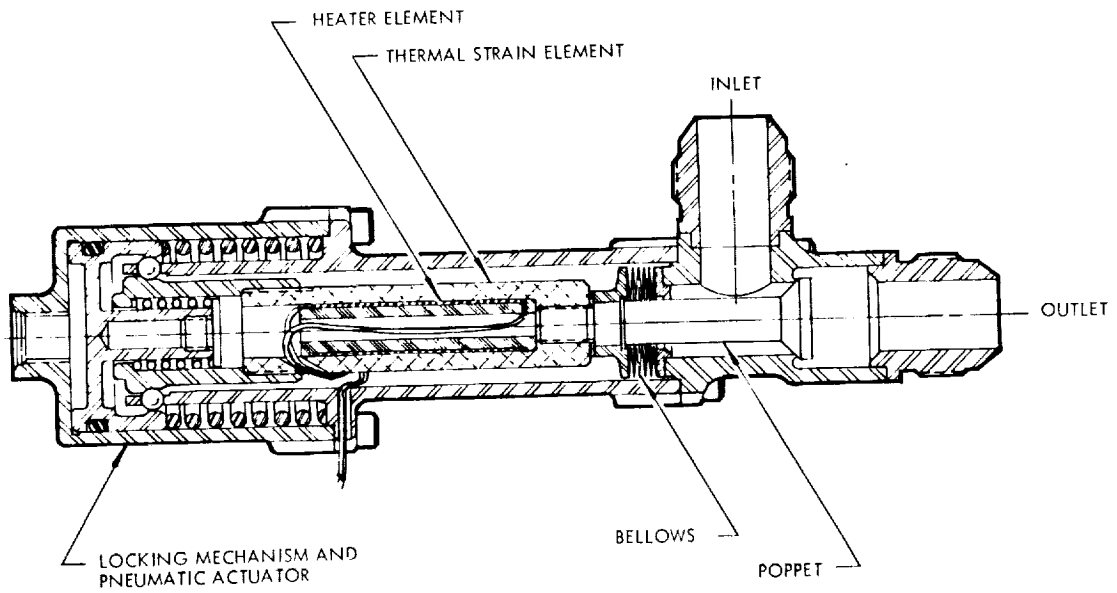


Figure 4-34. Thermal Shutoff Valve With High Compression Poppet Seating

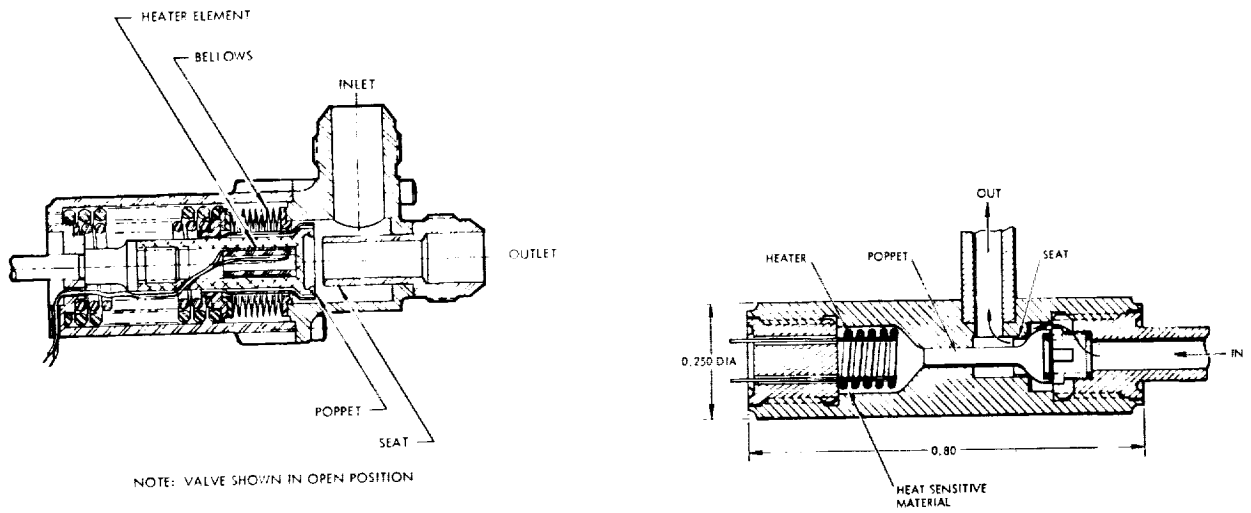


Figure 4-35. Thermal Shutoff Valve - Figure 4-36. Two-Way Normally Closed Thermally Actuated Microvalve Wagon Wheel Concept

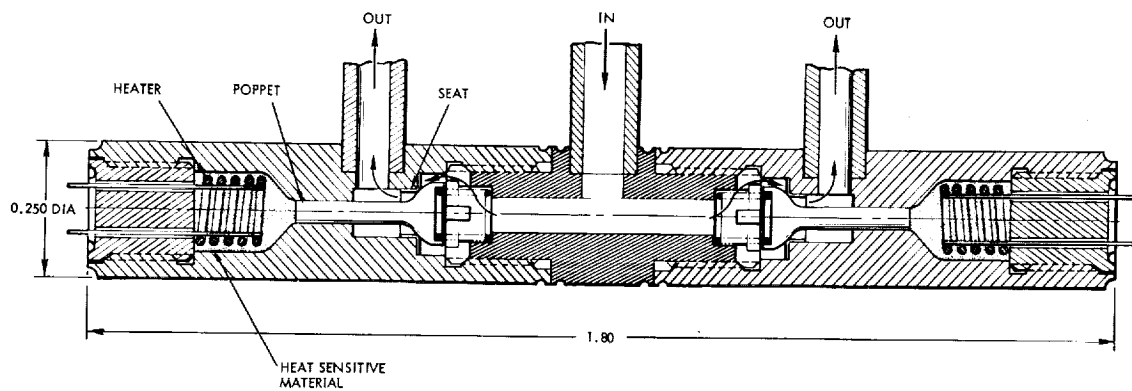


Figure 4-37. Dual Two-Way Thermally Actuated Microvalve

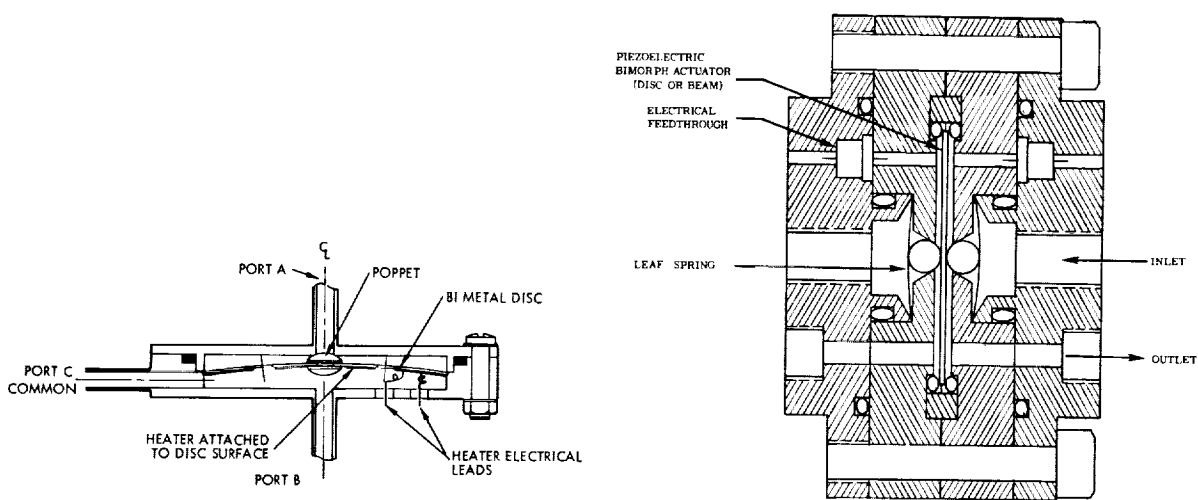


Figure 4-38. Three-Way Snap Action Thermally Actuated Valve

Figure 4-39. Piezoelectrically Actuated Three-Way Valve

#### 4.4.6 Electrofluid Interaction in Valves

The use of direct electrofluid interaction was investigated to determine its potential in applications to a valve with no moving parts. Various mechanisms of electrofluid interaction have been examined and some testing performed.

Interactions between liquids and electrical fields usually are considered to be electrostatic phenomena. This terminology, with respect to liquids, loosely connects phenomena concerned with the deformation or physical change of the fluid by an electric field. The deformation occurs because one or more of the following phenomena takes place: direct ionization or conduction charging of the fluid or one of its components, interaction due to the differential dielectric constants of the fluid constituents, or interaction due to the induced polarization of one or more of the molecular species of the material. In addition, there are also conditions wherein an electric field is produced by the movement of the fluid. The presence of ionizing radiation and impurities in the liquids complicates the understanding of the phenomena, and it is sometimes difficult to determine the exact interaction process.

It must be emphasized that the categorization of the various phenomena as discussed above has been somewhat arbitrary. It was felt that the following characterization would prove useful since the usage of the terms in the past has been applied to a number of quite different liquids, and in view of the disagreements among investigators.

Three general types of fluids have been utilized in studying these interactions: "pure" liquids (in that the impurity content is minimized as much as possible), regular solutions where the solute is evenly distributed in the solvent, and liquid systems containing dispersed particles, such as colloids, charged particles, or "cybotatic regions." A more detailed discussion concerning these systems can be found in Reference 9, and possible electrofluid valve configurations are covered in Section 8.4.10.

#### 4.4.7 Electroseal Valve

In order to obtain a zero leakage valve, the poppet and seat must be in intimate contact so that all the surface asperities which form leakage paths between them are filled. A possible method of eliminating these leak paths is to electroplate the interface of the seal and poppet. A schematic representation of a valve utilizing this technique is shown in Figure 4-40. To effect a zero leakage seal, the valve is closed and a coating of some material, such as copper or gold, is electroplated across the interface between the seat and poppet. To open the valve the material is either plated back onto the source electrode or the joint may be broken open by the valve actuation.

The electroseal concept can be utilized in the design of a no-moving parts valve as shown in Figure 4-41. In this valve, a porous plug, screen, or any system of fine passages is placed in the flow stream. When valve closure is required, material is electroplated over the porous element, shutting off the flow. Valve opening is obtained by plating the material back onto the source electrode. This technique may also be used to throttle flow.

An electrolyte is required in the plating process. Preliminary investigations indicate that some currently used propellants contain enough water to act as effective electrolytes. Experimental verification of the use of propellants as electrolytes in the plating process is required. In certain systems where the propellant is not a suitable electrolyte, an additional electrolyte might be required. The introduction of an electrical potential into the fluid lines could possibly cause long term corrosion problems. These must also be investigated and control measures instituted if required.

The use of chemical deposition might also be possible as an alternate sealing technique. This would be particularly applicable to one shot systems.

A no-moving parts electroseal valve (Figure 4-42) was fabricated and tested. It consisted of a copper anode and stainless steel cathode. The cathode was a porous stainless steel plug, and the anode had several drilled holes to allow flow of the solution. The cathode and anode were insulated from one another by a Lucite plate. Lucite plates were also used for the end pieces in order to eliminate short circuits through the bolts holding the unit together.

To evaluate the test model, it was decided to operate the unit in a copper sulphate solution with approximately 5 percent sulphuric acid added. In actual practice, propellants such as hydrazine could probably provide an effective electrolyte for the plating operation. The test setup (Figure 4-43) consisted of a recirculating system with a pump, flowmeter, throttle valve, electroseal valve, and a catch tank for the electrolyte solution. It was originally planned to observe the flow decay with the flowmeter, however, the flowmeter malfunctioned shortly after the beginning of the test and all flow observations were made visually at the exit tube from the electroseal valve.

The initial flow through the electroseal valve was greater than 1000 ccm and at the end of a 2-hour test period the flow had been reduced to approximately 1-1/2 ccm. The valve at this point was left to sit overnight in the solution. In the morning some added power was applied; however, a growth of copper crystals was observed within the unit. The unit was therefore disassembled and examined. Copper crystals had deposited on the stainless steel anode to a height where they could contact the copper cathode. This was probably caused by the essentially saturated solution of copper sulphate and the acid balance which renders an extremely effective plating solution. After examination, the loose crystals were removed and the test unit was reassembled. The flow in the test unit was found to be unchanged after reassembly, i.e., 1-1/2 ccm. The polarity on the plates was reversed, making the stainless steel porous member the anode and the copper plate the cathode. The unit was operated in this mode for approximately 3 hours with a steadily increasing flow as the copper was plated back from the stainless steel anode to the copper plate.



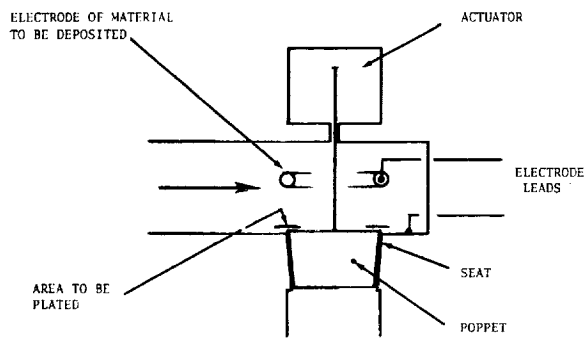


Figure 4-40. Electroseal Valve Concept

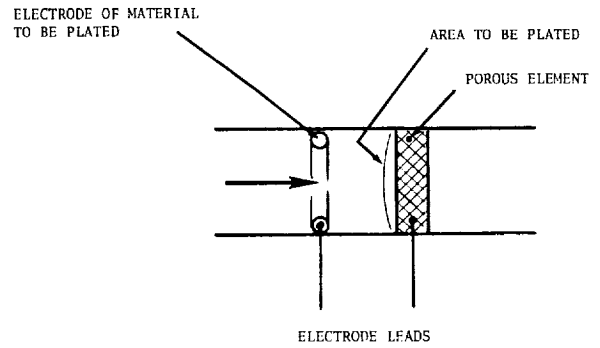


Figure 4-41. Electroseal No-Moving Part Valve Concept

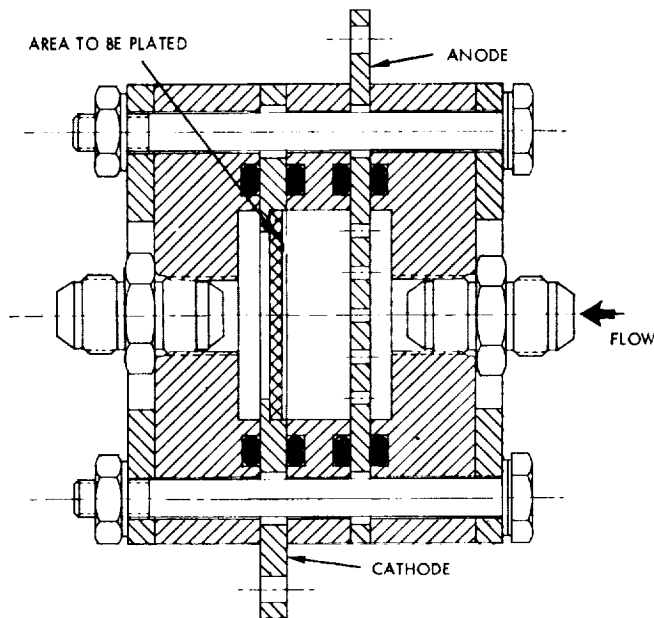


Figure 4-42. Electroseal Valve Test Model

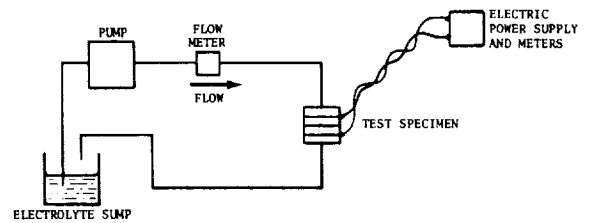


Figure 4-43. Electroseal Valve Test Setup

While this test did not demonstrate flow shutoff, it has demonstrated the feasibility of the electroseal concept. The quantity of copper which must be deposited to reinforce the sealing of a moving parts electroseal valve with a conventional poppet should be considerably less than that required for the no moving parts design tested. Such a unit might be extremely useful where tight shutoff for long periods of time is required. Capability of bridging the gap between the poppet and seat by plating remains to be demonstrated.

#### 4.4.8 Surface Tension Valve Concepts

A study was performed to gain a better understanding of surface tension and the part it plays in the function of fluid components and in leakage phenomena. The results of a literature search, analysis, and surface tension tests are presented in Reference 9. The application of these surface tension effects has resulted in several new valve concepts which are applicable to spacecraft valving.

4.4.8.1 Electromagnetic Capillary Valve - An electromagnetic capillary valve concept utilizing mercury or another high surface tension conductive liquid actuated by an electrical signal has been originated. This valve approach is applicable for use as a fluidic system shutoff and may be adaptable to other low pressure gas systems.

As shown in Figure 4-44, a conductive high surface tension liquid, such as mercury, is trapped in a channel between two fine screens (which also can be slits or porous plugs). The channel is constructed so that the Hg either blocks the main valve flow channel or is withdrawn into a storage chamber. When the Hg is in the flow channel, it is held in place because its surface tension will not allow it to penetrate the pores of the screen until some critical pressure is reached. When the Hg is withdrawn, the working fluid is free to flow through the screens with no more than the normal pressure drop for a filter of equivalent size. The motion is imparted to the mercury by placing it in a magnetic field, and then flowing a current through it, perpendicular to the direction of the field. The current through the mercury need only be applied long enough to accomplish the shutoff function.

Two test models (Figure 4-45) of the valve concept described were built and feasibility testing has been performed. Planar construction was used in producing the test models which is similar to the construction used for integrated fluidic circuits. The valves were fabricated from two sheets of Lucite between which are sandwiched two pieces of stainless steel shim stock, which were shaped to the desired flow channels. Due to the geometry selected, these pieces of shim stock are also used as the electrodes for applying a current through the mercury.

In the first valve, the mercury channel was produced by milling a groove approximately 0.03 inch deep into one of the Lucite plates. The shim used to separate the Lucite plates was 0.001 inch thick and no porous element was used in the gas flow channel. A large permanent magnet was used for applying the required field.

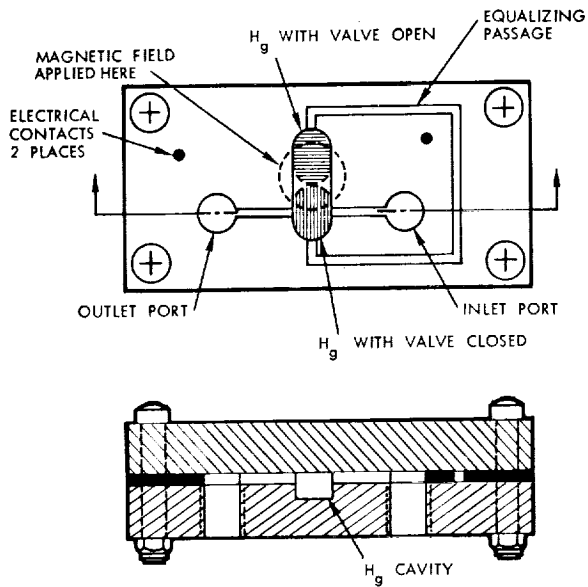


Figure 4-44. Electromagnetic Capillary Valve Concept

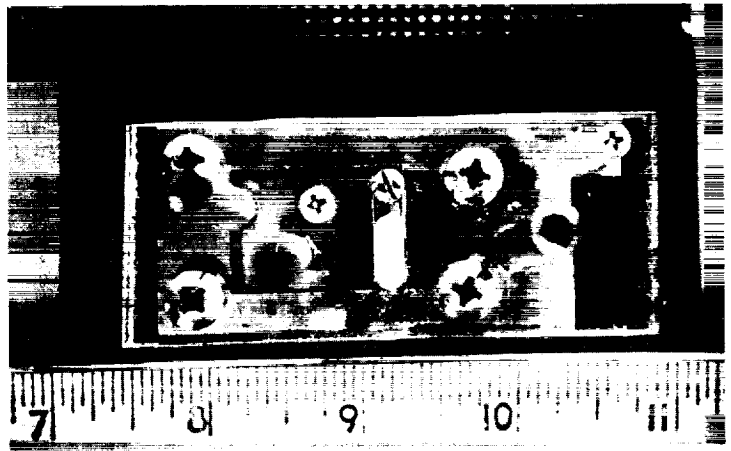


Figure 4-45. Electromagnetic Capillary Valve Test Unit

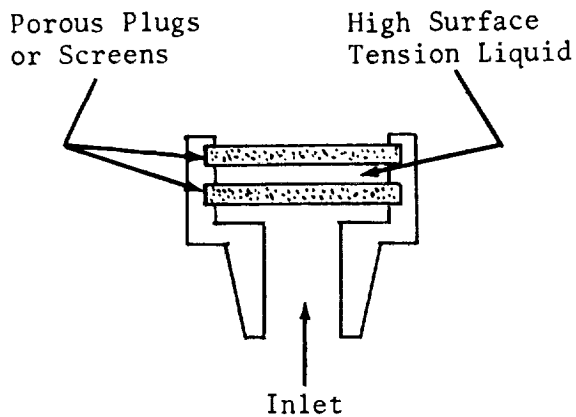


Figure 4-46. Capillary Relief Valve

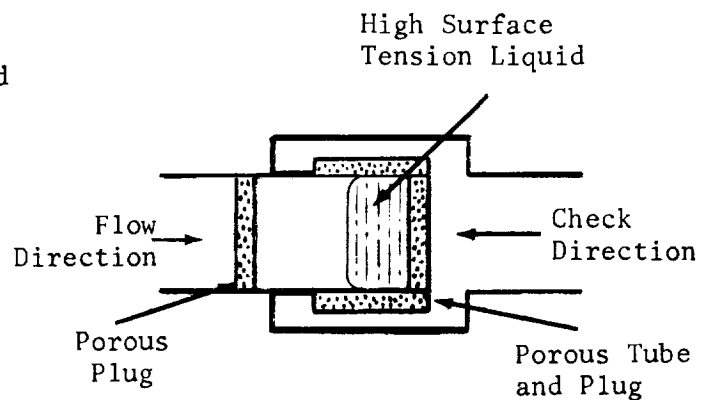


Figure 4-47. Capillary Check Valve

Testing demonstrated an ability to move the mercury from the open to the closed position by applying a current pulse of approximately eight amperes to the electrodes. With nitrogen as the test fluid, flow changes of a factor of three, from closed to open, were accomplished at a pressure of 4.5 psi. Since the slit holding the mercury in place was 0.001 inch thick, this was close to the maximum pressure capability of this particular unit.

The second valve utilized a mercury channel formed between 0.04 inch thick pieces of stainless steel sheet spaced approximately 0.080 inch apart. The mercury was isolated from the gas passages by a pair of 12 micron absolute retention porous stainless steel filter plugs which were bonded into slots in the stainless steel sheet. The spacer plates were cut to allow four electrodes rather than two as formerly used, so that proper current could be applied to the segment of mercury to be moved without short circuits due to the mercury that has already been transferred.

Testing performed demonstrated the ability to move the mercury from the open to the closed position by applying current to the proper pair of electrodes. The mercury was retained in place after opening or closing by a restriction between the two chambers. The mercury was contained in the closed position with pressures of 15 psi applied to the gas inlet ports. The valve exhibited leakage characteristics considerably superior to the first unit, including leak-free shutoff at low pressures.

It is felt that the initial testing done has demonstrated the electromagnetic capillary valve concept to be a feasible and promising one. The pressure sealing capability is adequate for many applications including low pressure fluidic and gas thruster applications.

4.4.8.2 Capillary Relief Valve - A relief valve can be made by trapping a high surface tension liquid between two restrictions, such as fine screens or porous plugs as shown in Figure 4-46. The liquid will form a seal preventing any fluid applied to the inlet port from leaking through until a critical pressure is reached. This critical pressure is a function of the pore size of the plug or screen, the surface tension of the sealing liquid, and the contact angle between the sealing liquid and the plug or screen material.

A device such as this would have application as a replacement for burst discs and similar devices. If required, a combined temperature-pressure relief function may be supplied by using a sealing material that is solid below a certain pressure or exhibits particularly large changes in surface tension with temperature. A test model was fabricated and feasibility tests performed. Relief pressures of approximately 10 psi were obtained using porous stainless steel plugs and up to 30 psi using porous Teflon plugs with mercury as the sealing fluid.

4.4.8.3 Capillary Check Valve - A possible check valve configuration is shown in Figure 4-47. If pressure is applied in the flow direction, the high surface tension liquid is blown into the cup-shaped cavity, formed by a porous tube and plug. There is not sufficient liquid to completely fill the porous tube, and the working fluid flows freely through the unfilled portion. When pressure is applied in the check direction, the high surface tension liquid is blown against the porous plug and forms a seal preventing further flow.

#### 4.4.9 Radioisotope Heated Valves

Radioisotopes can be used to heat valves so as to prevent propellant freezing due to propellant discharge or thermal loss through the attaching structure. Figure 4-48 illustrates the application of a radioisotope to heating of a valve seat. Such an installation would be sized so that the fluid temperature during flow would not be noticeably affected.

Consideration of the radiation characteristics of alpha and beta source radioisotopes favors the alpha source radioisotopes for all valve heating applications. The advantage has attendant restrictions in the form of cost and availability which may restrict the use of alpha sources to spacecraft applications.

The radioisotope enclosure may be shaped in some simple form which will meet aerospace safety requirements and the valve application geometry. The enclosure must be clamped or fastened to the valve assembly to provide adequate thermal conduction to the desired surfaces for heat application. The separate radioisotope enclosure will permit removal and installation of the heat source when required, enabling many operations and tests to be performed without the heat source installed. A mechanical or electrical interlock system could prevent inadvertent omission of the heat source when it is required for a fully operating system.

The use of radioisotopes is controlled by the Atomic Energy Commission, who desire to develop and extend the application of radioisotopes. Spacecraft applications of radioisotopes are numerous and arrangements have been made between the AEC and spacecraft user agencies for their use, provided specific safety procedures are followed.

Radioisotope valve heaters provide several advantages including:

1. For a given power level, a radioisotope heat source costs less and weighs less than an equivalent solar cell power supply with resistive heaters.
2. Radioisotope power sources are inherently simpler and more reliable than electrical heaters with any type of space electrical power supply.
3. Long life alpha-emitting radioisotopes permit a mission life of approximately ten years without temperature control devices.
4. Radioisotope heat sources have a higher mass-energy density than any chemical heat source.

#### 4.4.10 Fusion Valve

Evaluation of existing shutoff valves, pointed out a specific need for a multi-cycle shutoff valve with zero leakage for extended durations. This valve should have the following capabilities:

1. Seal any fluid at substantially any working pressure
2. Maintain zero leakage for extended periods of time
3. Be capable of many cycles of operation
4. Be relatively insensitive to contamination
5. Be operable at temperatures up to 1000°F.

An examination of existing closure mechanisms revealed that each failed to meet these requirements in one respect or another. Soft seats are eliminated by temperature considerations and, in addition, no known plastics are compatible with fluorine. Metal to metal seats can be produced that will give excellent leakage control, approaching zero depending upon the quality of the seating surfaces. However, the slightest contamination from the fluid, the system, or from the moving parts within the valve itself can raise the leakage rates very quickly to an unacceptably high level.

The fusion valve presents a novel approach to meeting the above requirements. This valve (Figure 4-49), provides a zero leakage seal by fusing the mating parts of the valve together with a solder by the application of heat from an electrical heating element. Demating is accomplished by the reapplication of heat to raise the solder to the melting point. Provision is made to prevent the loss of solder from the valve closing mechanism. The isometric drawing (Figure 4-49) shows the valve in the closed position. The flow path is through the hollow lower shaft which incorporates drilled passages at one end. Sealing is effected by bonding the sleeve and sealing ring with a suitable low melting point alloy. To open the valve, the heating element is energized to melt the alloy, so that the lower shaft can be inserted in the housing up to the lock nuts. The drilled passage in the lower shaft is then coincident with the output annulus in the valve body.

The testing accomplished with the prototype fusion valve consisted primarily of cycling the valve from open to closed and closed to open with supply pressures varying from 15 to 1200 psi. No failure or significant loss of solder was observed during 25 consecutive cycles. No measurable leakage was observed in any of the above tests. The minimum time required to open the valve was approximately 3 seconds. Power levels ranging from 200 to 1000 watt-seconds were used for operation.

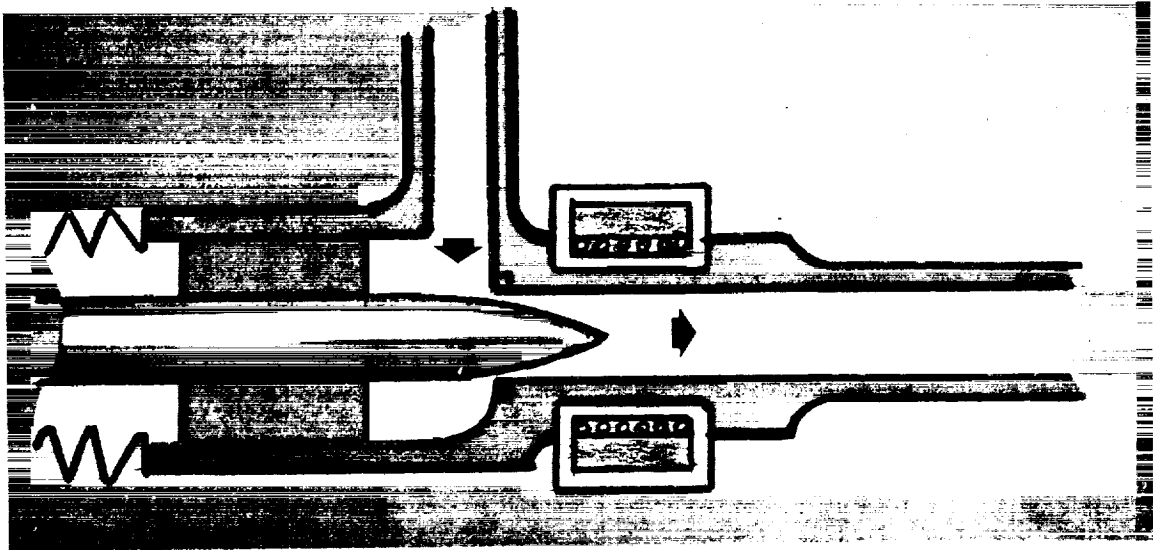


Figure 4-48. Radioisotope Heated Valve Seat

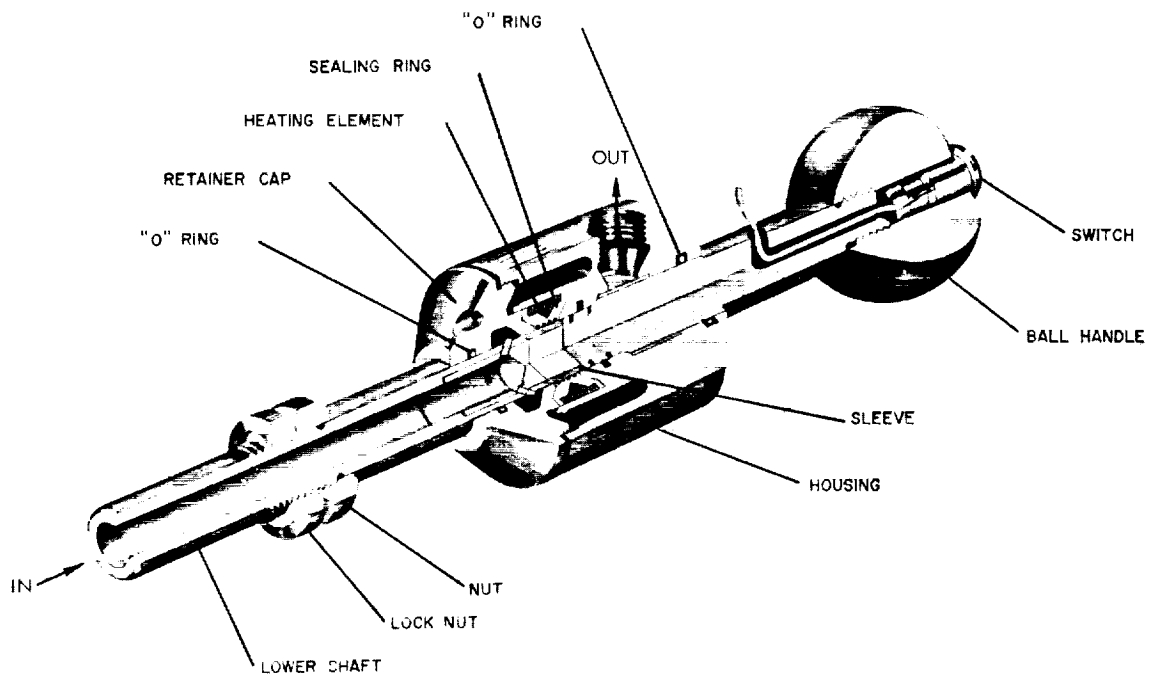


Figure 4-49. Prototype Fusion Valve

Tests on the prototype fusion valve indicated that a zero leak, multi-cycle, contamination insensitive valve is feasible. A wide variation of valve and actuator configuration is possible for use on systems operating at substantially any pressure. Many refinements of the present prototype are possible including one in which the valve seal would be sheared by impact from the actuator, thus providing a very rapid opening time and reducing the amount of electrical power required for actuation. Other possible improvements include a large reduction in the mass of the heating element which would provide an increase in response and a decrease in power consumption.

#### 4.4.11 Diffusion Valve

It is possible to develop a flow control device which utilizes the techniques of permeation of gases through porous structure to produce low thrust force for satellite applications. The porous structure is the static flow control device requiring no moving parts. An on-off or varying flow rate may be accomplished by heating the porous structure. Investigation of the diffusion of hydrogen through palladium-silver alloys (Reference 10) has shown the feasibility of such a device.

A preliminary design of a diffusion valve, from Reference 10, is shown in Figure 4-50. The diffusion element consists of 0.045 inch O.D. by 0.003 inch wall palladium-silver tubing. Table 4-12 lists estimated power-thrust levels which can be achieved with the diffusion valve controlling a microthruster.



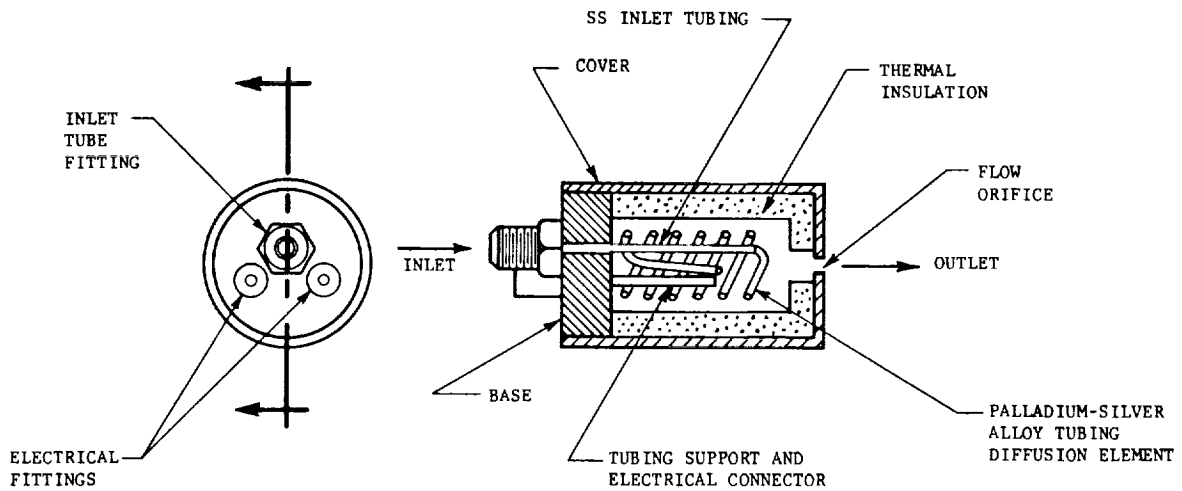


Figure 4-50. Diffusion Valve Concept For Use With a Microthruster

Table 4-12. Diffusion Valve Estimated Thrust Level

Length of Tube (in.)	Tube Temperature (°F)	Power (watts)	Thrust ( $\mu$ lb)
35	390	17	73
35	300	10	34
11	300	4	10.5
11	300	2.5	10.5

## 4.5 ZERO G VENT VALVE STUDY

### 4.5.1 Introduction

Heat leakage to a cryogenic propellant storage tank results in an increase in tank pressure and eventually causes over pressurization which may be decreased by venting a portion of the stored fluid from the tank. Under zero-gravity conditions, the orientation of the liquid or vapor phase is unpredictable resulting in the possible loss of liquid during venting. The problem can be approached by (1) fluid orientation using centrifugal or other gas-liquid separating techniques such as dielectrophoresis and surface-tension devices, or (2) zero g thermal venting techniques in which a liquid vented from the tank is expanded to a lower temperature and by means of a heat exchanger transfers the necessary heat of vaporization from the tank system, allowing only vapor to be overboarded.

Among the problems associated with orientation of fluids are the stability of the device to disturbances such as accelerations imparted from various sources, the time constant required to orient the liquid following a disturbance, weight penalty associated with the device, compatibility with the attitude control system used for the mission, and the hazards associated with the use of the device.

Preliminary studies indicated that surface tension and dielectrophoretic devices have universal applicability. Dielectrophoretic devices also have other secondary advantages in that they provide an improved heat transfer rate and faster reorientation (Reference 11). The disadvantages of the dielectrophoretic devices are weight penalties and safety hazards. Attempts are being made to develop better analytical means of predicting performance of the devices. The static and dynamic behavior of the liquid-vapor interface need to be studied so as to better predict the behavior of the liquid propellant motion during zero and low gravity conditions (References 12 through 15).

Efficient venting of cryogenic propellants in a zero-gravity field utilizing a thermal vent valve system is accomplished by extracting heat from propellant in the tank or directly from the heat leak through the insulation. The heat energy is used to convert vented liquid to vapor by use of a lightweight heat exchanger, thereby insuring that only the vapor phase is ultimately allowed to be vented overboard. By allowing only propellant vapor to be overboarded regardless of the initial propellant orientation, the system permits indifference to the phase initially vented. The thermal vent valve allows liquid to be vented as efficiently as vapor. A throttle valve upstream of the heat exchanger provides the means by which the temperature of the vented propellant is reduced below the temperature of the propellant in the tank.

During engine firings using hydrogen fuel it may be necessary to pressurize the propellant with helium. To avoid loss of the helium, it may be desirable to specifically remove the liquid hydrogen from the tank utilizing a heat exchanger to vaporize the propellant before it is vented overboard. With a thermal vent system, it then only becomes necessary to locate the amount of liquid needed for boiloff when under conditions of weightlessness.

Valves and systems useful for zero g venting were investigated during this study. A state of the art survey was performed and the general problem of venting cryogenics was studied. Preliminary testing of a thermal vent system was completed on a workhorse model utilizing Freon 12 as the vent fluid. Subsequent efforts included the design, fabrication, and test of a zero g thermal vent valve concept. The system included a lightweight heat exchanger and the tankage system which was tested with both liquid nitrogen and liquid hydrogen. Results of the tests conducted verified the feasibility of the thermal vent system concept and, in particular, its use as a means of controlling tank pressures for long term storage of liquid hydrogen in a zero g environment.

The Zero G Vent Valve studies are covered in detail in References 2, 16 and 17.

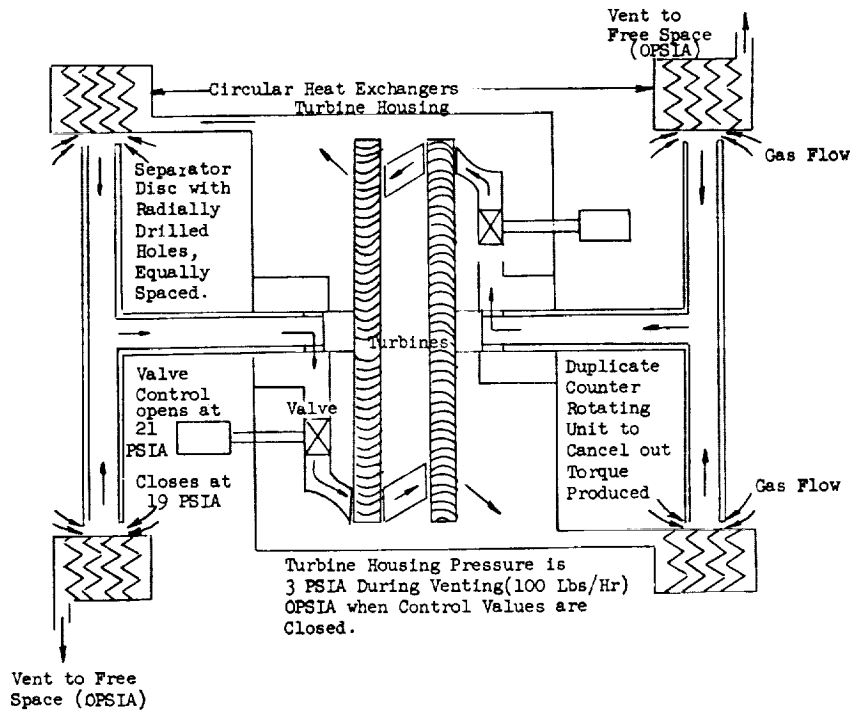
#### 4.5.2 Survey of Zero G Vent Techniques

Studies performed on the subject of weightless fluid behavior related to venting seem to conclude that without absolute knowledge of magnitude and direction of forces exerted on a spacecraft, liquid vapor orientation is unpredictable. Even if ullage orientation with respect to forces were predictable, the use of conventional venting is impractical for a variety of orientations.

NASA's Lewis Research Center has completed and monitored many studies of the behavior of rocket engine propellants stored in space-vehicle tanks while exposed to weightlessness, and solar and planetary radiant heat sources. They have indicated that an efficient vent process, not dependent upon the vapor/liquid separation prediction, is highly desirable. It was also indicated that a vapor/liquid interface can be determined, via computer analysis, if the magnitude and direction of the forces exerted on the fluids are known.

Much information has been published by NASA-Lewis (References 18 through 22) reporting the effects of both flight and analytically simulated zero g on the behavior of liquid propellant orientation. Most of the studies done on weightless fluid behavior assume ideal tank configuration and loading, both of which are variable in space propulsion design. The shape of spacecraft tanks is affected by the purpose for which the mission and design are optimized, the type of propellant quantity measuring device employed, pressurization technique, and many other system design parameters.

The survey has shown that centrifugal separators can be designed to return a portion of the liquid back to the tank when a minimum of five percent vapor is contained within the venting mixture. General Dynamics/Astronautics has developed a dynamic separator for Centaur (Figure 4-51), and the Pesco Division of Borg-Warner Corporation has worked on a vapor/liquid separator for Saturn IV (Figure 4-52). See Reference 2 for details of this survey.



Nominal Operating Speed of the Separator Disc is 4000 RPM: This Speed Climbs to 8850 RPM when Surrounded by 100 Percent Quality Vapor.

Figure 4-51. Centaur Vapor/Liquid Separator

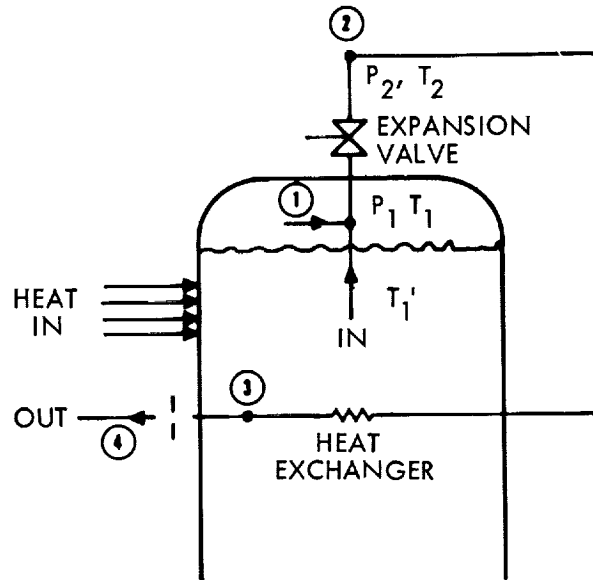
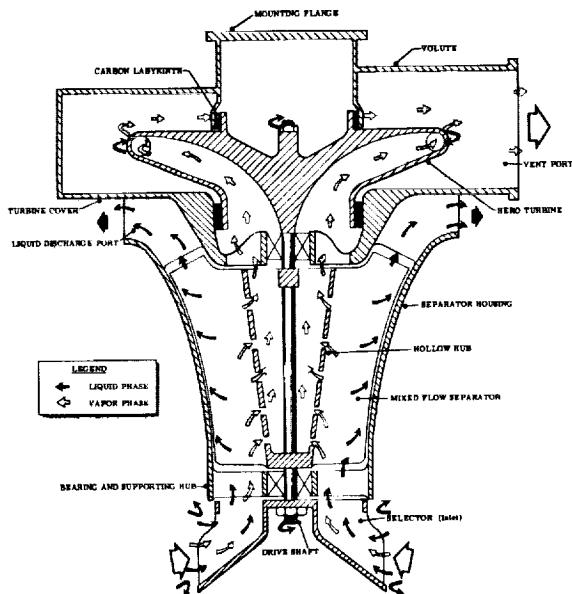


Figure 4-52. Saturn IV Vapor/Liquid Separator

Figure 4-53. Vent Valve and In-Line Heat Exchanger Arrangement

In addition to the performance of a state of the art survey of venting techniques, the general problem of venting cryogenics was studied. It was felt that the need to vent is generally created by the accumulation of energy within the propellant. This energy is transferred through the tank wall, or by pressurants injected at temperatures higher than that of the propellant. Venting is essentially the process of removing this energy deposit in order to maintain constant liquid properties.

#### 4.5.3 Consideration of Thermodynamic Processes

Cryogenic propellants contained within space vehicles usually accept or give off heat to the environment. Cases where heat is absorbed and converted to support propellant evaporation will result in increasing tank pressure. Without some control of heat flow into the tank, it is necessary to return the heat absorbed to the outside of the tank, preferably by means of venting gas. Like most systems, efficiency is important in the operation; so that the heat must be removed as cheaply as possible.

Conventional venting methods depend on the availability of gas or vapor to carry off energy to the outside. Normal venting is effective only when the vapor/liquid interface location is defined and can be consistently positioned by applying acceleration to the tank in the same direction. With the absence of gravity, acceleration must be applied with the settling rocket or other means which lowers the efficiency of the process. Without the use of acceleration to settle the propellant vapor/liquid mixture, the probability of venting liquid is high. Venting may be considered effective if the heat absorbed by the propellant is released with saturated or superheated vapor instead of liquid, or if a favorable balance of flow exists between the heat leaving the tank and that entering the tank.

Several thermodynamic processes of heat exchange or possible compression and expansion can be employed to provide an effective transfer of energy from the tank. The use of the compression/expansion cycle depends on a secondary heat transport system for operation. However, for most cryogenics it is theoretically feasible to depend on constant enthalpy expansion process and heat exchange between the venting fluid and the bulk propellant to achieve efficient venting. Figure 4-53 is a simplified schematic of a vent valve and in-line heat exchanger arrangement. Inlets are shown in both the liquid and vapor, only to show that the system is indifferent to the fluid phase entering the vent valve. The pressurized fluid at  $T_1$ ,  $P_1$ , pressure and temperature, respectively, expands across the expansion valve at constant enthalpy, thus discharging at a lower temperature and pressure ( $T_2$ ,  $P_2$ ). With good heat exchange and distribution, it is possible to extract heat from the propellant faster than it is transferred through the tank wall from the outside.

A more complex version of the above system is shown in Figure 4-54. Liquid or gaseous propellant enters the system at point (1) and is expanded to a lower pressure in the expansion valve. Joule-Thompson cooling from expansion causes a lowering of temperature at point (2), then expanded propellant passes through a low pressure heat exchanger, thus extracting energy from the bulk propellant remaining in the tank. It may be desirable to continue the venting of fluid through the throttle valve actuator for thermal control

purposes at point (3), where the throttle control "C" varies the throttle position such as to increase or decrease flow, so as to maintain constant temperature through the actuator. The venting fluid further expands isentropically across the turbine and is then discharged to the atmosphere. The turbine, if necessary, provides torque for the circulation fan which enhances heat transfer in the heat exchanger. It has been shown that venting with the heat exchanger is about 8.5 percent more efficient than just venting saturated vapor.

A similar, but still more complex zero g venting process is shown in Figure 4-55. This concept employs a secondary technique which by means of a compression/expansion further superheats the venting gases. The fluid in the secondary system used for transporting heat must be either a liquid or gas whose boiling point is near that of the propellant being vented. For this example, helium gas is used as the secondary fluid, and hydrogen liquid or gas is the propellant under consideration.

In Figure 4-55, the process begins at the helium tank, which is submerged in hydrogen at 42°R, at which temperature the thermal properties at point (1) are obtained. The venting fluid in the first system expands via constant enthalpy from point (5) to (6) to 27°R. While both fluids are flowing through the external heat exchanger, the helium is cooled to 27°R at point (3), thus producing a  $\Delta T$  of 15° between the helium and the remaining propellant. The heated hydrogen at 72°R discharging from the heat exchanger at point (7), and by reversible adiabatic expansion across the turbine thus providing compressor torque. The motor shown supplements the compressor during start and for makeup.

The heat absorption potential from point (6) to (7) as shown on Figure 4-55 is

$$\Delta H_{6-7} = h_7 - h_6 = 397.0 - 130 = 267 \text{ Btu/lb}$$

Thus, this system is theoretically 46 percent more effective than venting saturated vapor. However, the inefficiencies of such a system will tend to degrade the theoretical value.

#### 4.5.4 Experimental Zero G Thermal Vent System

A breadboard zero g thermal vent system (Figures 4-56 and 4-57) was designed, fabricated, and tested with Freon 12 to demonstrate the effectiveness of the vent process. The system (including tankage) was precooled with LN<sub>2</sub> prior to filling with the Freon 12. After filling, the fuel tank was heated to 90°F and 100 psig prior to the start of testing. During the test run, Freon 12 was vented from the tank to maintain pressure at 100 psig with a controlled heat input of 1000 Btu/hr. Gaseous and liquid Freon 12 were vented exclusively from the tank during separate runs. This was accomplished by physical orientation of the tank.

POINT	TEMPERATURE (°R)	ENTHALPY (Btu/lb)	PRESSURE (psia)
1	42	130	30.0
2	27	130	2.0
3	42	330	2.0
4	27	295	~0

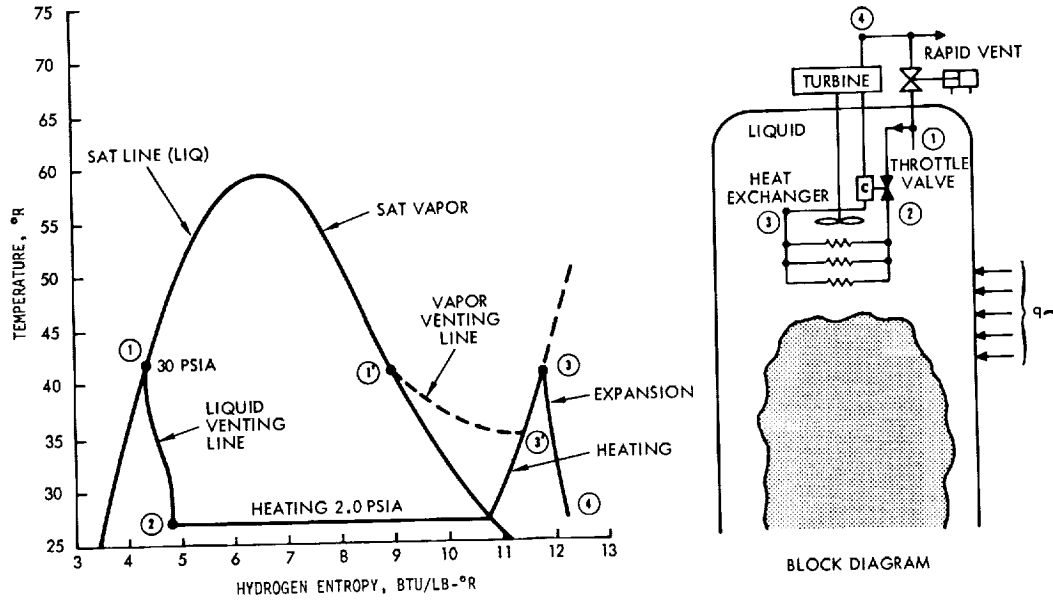


Figure 4-54. Vent Valve and In-Line Heat Exchanger With Turbine

POINT	TEMPERATURE (°R)	ENTHALPY (Btu/lb)	PRESSURE (psia)
1	42	58.5	29.4
2	72	96.2	294.0
3	27	35.0	294.0
4	-	58.5	-
5	42	130.0	30.0
6	27	130.0	2.0
7	72	397.0	2.0
8	20	293.0	~0

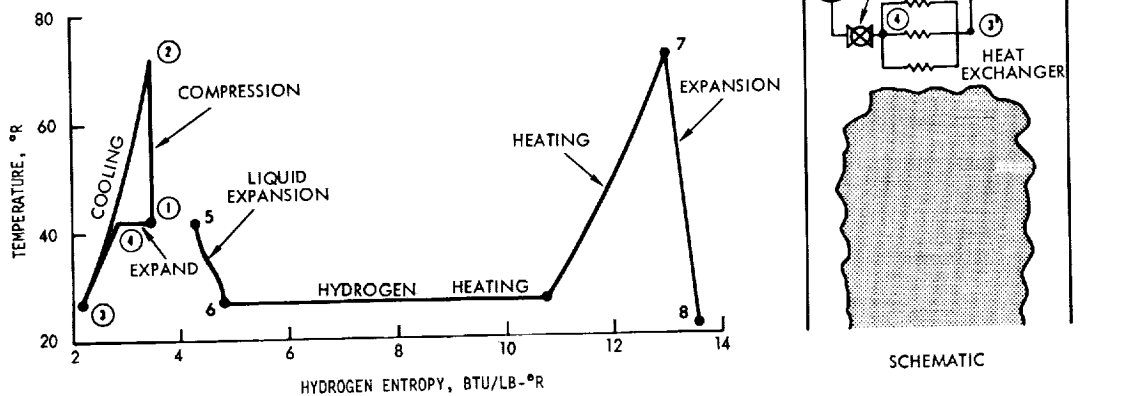


Figure 4-55. Zero G Venting Process With Secondary Compression/Expansion Cycle

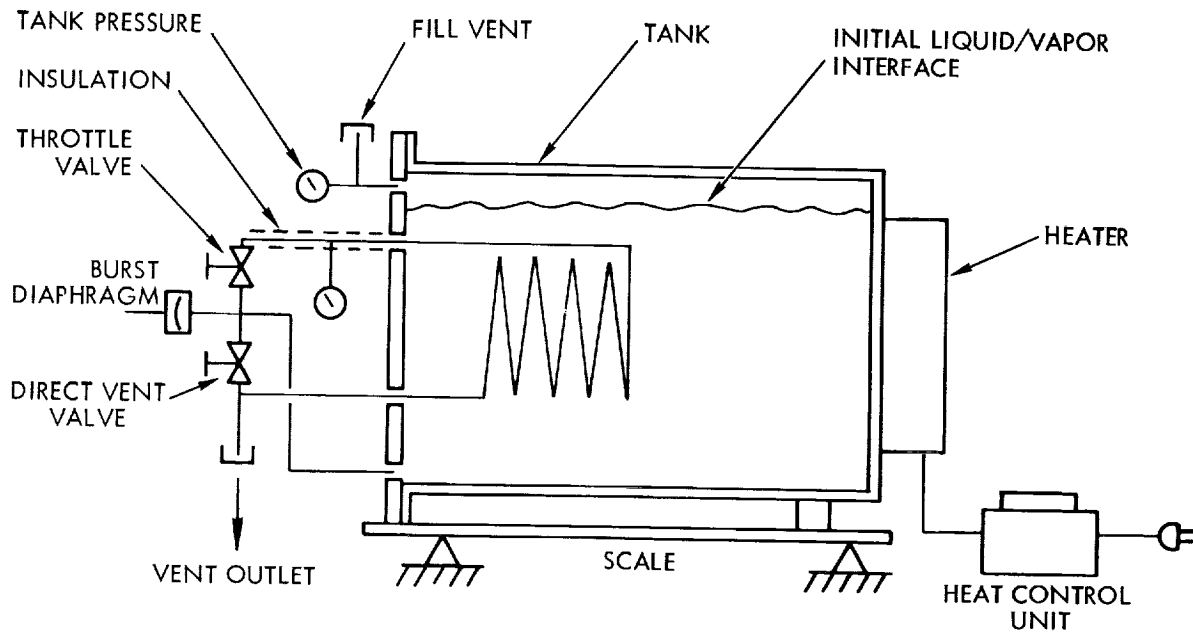


Figure 4-56. Experimental Zero G Thermal Vent System

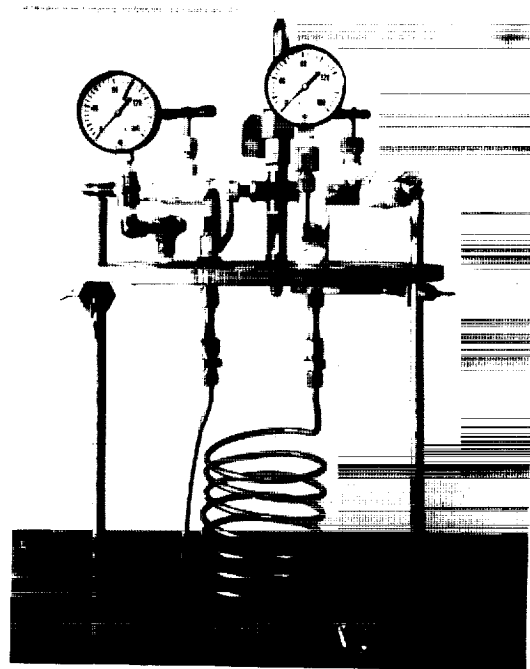


Figure 4-57. Zero G Thermal Vent System



These tests indicated no significant difference in the Freon 12 vent rate when venting either in the gaseous or liquid state. Analysis showed a net gain over a process which vents gas or saturated vapor directly from the tank. Since the vent rate was the same for both liquid and gaseous Freon 12, it was postulated that a thermal vent system of this type would operate equally well in space when venting a mixed phase propellant. See Reference 17 for details.

#### 4.5.5 Vent System For Liquid Hydrogen

Systems analysis and further testing on the experimental system (Section 4.5.4) with  $LN_2$  were accomplished prior to the design of a vent system for use with liquid hydrogen. Consideration was given to the size and location of the heat exchanger, zero g heat transfer, throttle valve, system pressure drops, and the thermodynamic processes.

Liquid hydrogen vent tests were then planned with the primary objective of establishing the feasibility of a tank pressure control throttle valve system venting liquid and utilizing a lightweight tank surface mounted heat exchanger for vaporization of the vented fluid. Determination of approximate weight values for the heat exchanger and performance of the throttle valve were part of this objective. Secondary objectives were to obtain as much pressure and temperature data as possible to provide a better understanding of the thermodynamic processes involved to facilitate the future design of flight systems.

To attain these objectives a system was designed and fabricated providing a liquid hydrogen pressure vessel incorporating a pressure regulating throttle valve and an external tank mounted, lightweight heat exchanger configuration (Figures 4-58, 4-59 and 4-60). A multilayer aluminized Mylar vacuum insulation system was installed around the pressure vessel to obtain heat leak and consequently vent rate characteristics simulating processes expected in a space flight system. In addition, a separate liquid hydrogen container was installed in the pressure vessel so as to isolate the  $LH_2$  from contact with the vessel walls and thus approach the critical case condensation mode of heat transfer. Pressure, temperature, and flow rate instrumentation were provided to obtain process data.

Results of the tests conducted verified the feasibility of the vent system as a means of controlling tank pressures for long term storage of liquid hydrogen in a zero g environment. A total heat leak rate of 45 Btu/hr was measured for the test system resulting in a vapor vent rate of 0.24 lb/hr at near atmospheric pressure. The average insulation conductivity for the tank reduces to  $3.92 \times 10^{-4}$  Btu-ft/ft<sup>2</sup>-°F-hr, indicating a heat leak through the insulation well within the predicted range.

A comparison of the vent rate through the test vent system with that obtained directly from the vapor space of the tank indicated nearly identical flow rates. The performance of the heat exchanger in vaporizing all of the liquid was established. Temperature data obtained was inconclusive in establishing the length of heat exchange tube required for vaporization. The average heat

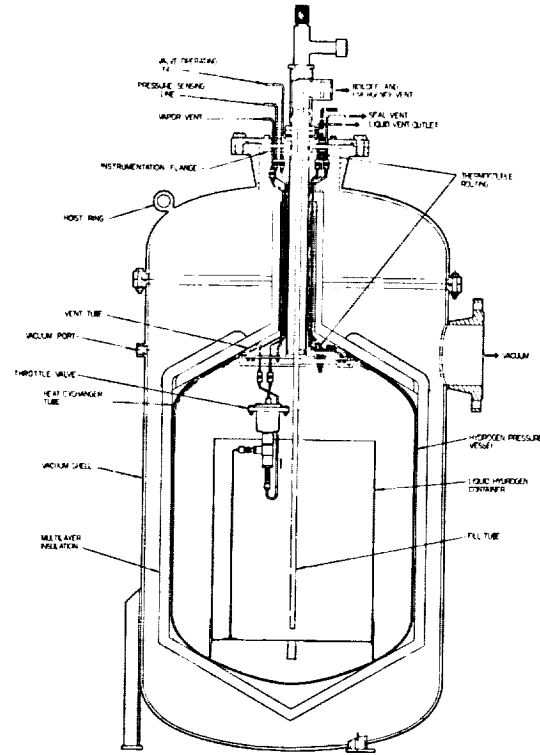


Figure 4-58. LH<sub>2</sub> Zero G Vent Test Tank Assembly



Figure 4-59. Liquid Hydrogen Pressure Vessel With Heat Exchanger



Figure 4-60. Pressure Vessel Installation in Vacuum Tank

exchanger coverage for the overall tank surface was 1.76 feet of tube per square foot of tank surface. The weight of the heat exchanger tube was 0.238 lb or 0.0139 lb/ft<sup>2</sup> of tank surface. Pressure drop through the heat exchanger was measured as 0.6 psi at a flow rate of 42.5 ft<sup>3</sup>/hr gaseous hydrogen at STP or 0.221 lb/hr mass flow rate.

The capability of the vent valve to accurately control set pressures was verified. The minimum throttling flow rate attainable by the valve was higher than expected and; consequently, to demonstrate control at pressures above 7 psig the tank venting rate had to be increased. This was done by degrading the vacuum level in the insulation by introducing helium.

See Reference 16 for details of analysis, design, fabrication and test.

## 4.6 IN-TANK DESIGN STUDY

A study was made (Reference 1) to determine the advantages and disadvantages of locating certain spacecraft valves inside the propellant and pressurization tanks rather than outside as is conventionally done. The advantages and disadvantages of this plan are as follows.

### 4.6.1 Advantages

External leakage through the valve housing seals or through the tubing connectors would be zero. While external leakage through a well designed housing is not common, leakage difficulty with the various tubing connectors is quite common so this consideration is of significance.

Contamination potential is reduced by the elimination of tubing and fittings upstream of the valve. Threaded fittings are a common source of contamination unless care is used in assembly.

Exposure to the several hazards of the space environments, e.g., vacuum, micrometeoroids, and radiation is reduced or eliminated.

More usable space would be available with the valve installed inside the tank than outside. For an internal installation the volume required would be precisely equal the volume of the valve, and if this volume were significant, the volume of the tank would have to be increased accordingly. An external installation requires brackets and the valve location may be such as to make portions of the surrounding area unusable because of lack of accessibility.

Stable temperatures would be provided for the valve which would simplify the design as the operating temperature would be known within close limits. In the case of solenoid valves operating in cryogenic fluids, the power requirements would be very significantly less because of the lower resistance of the coil wire. A smaller coil could be employed if it were known that the solenoid would be actuated under low temperature conditions.

Pressure drop characteristics would be improved because of the reduction in entrance losses to the valve due to the absence of upstream tubing, fittings, changes of fluid direction within the valve, etc.

Weight of the valve system would be reduced because of the absence of the valve housing and the tubing fittings. In place of the housing, a guide or support would have to be provided for the closure mechanism, but this assembly would be significantly lighter than a complete housing. Greater weight savings are possible with higher pressure systems than with low pressure systems for the same valve size.

A study was made of the potential weight savings possible based on a TRW pierce diaphragm valve, assuming that it were modified for an internal tank installation, and a weight reduction of 37 percent was indicated. Figure 4-61 shows the valve mounted in the conventional manner, and Figure 4-62 shows the modified valve in an internal installation.

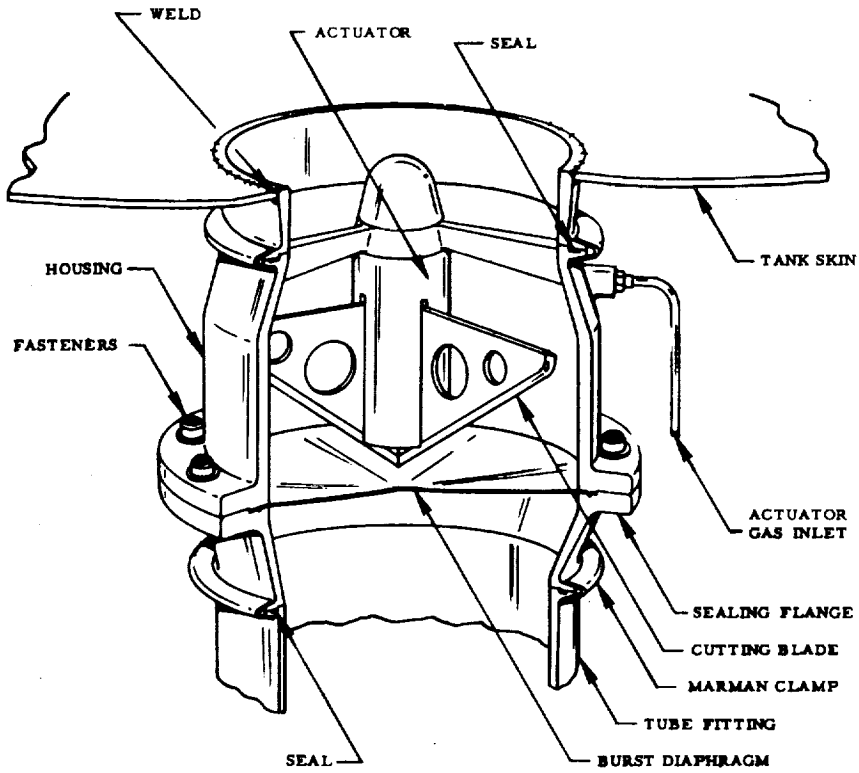


Figure 4-61. TRW Pneumatic Operated (Pierce Valve) External Design Configuration

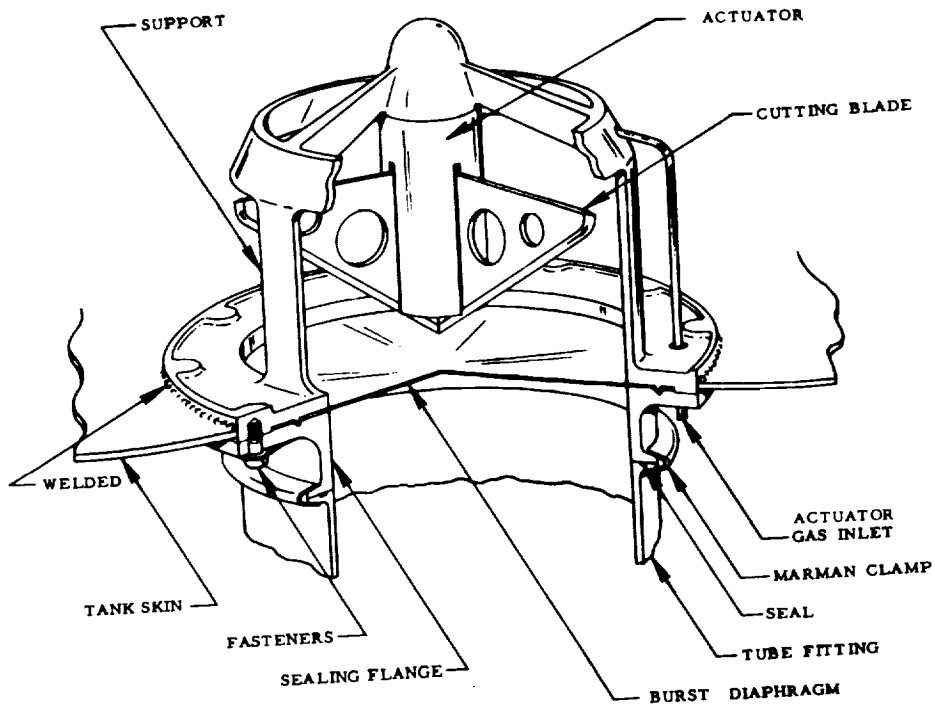


Figure 4-62. TRW Pneumatic Operated (Pierce Valve) Internal Design Configuration

#### 4.6.2 Disadvantages

The most obvious disadvantage of an in-tank design is inaccessibility for maintenance. This would be especially true if a valve were installed in a tank prior to final assembly, for example, installed inside a hemisphere after which the mating half is joined by welding. An alternative installation could be made in which the valve is mounted on a flange and the flange is then bolted to the tank. With this latter method, however, some of the weight savings would be lost and an even greater probability of leakage through the flange would exist than would leakage through the valve housing.

Only valves with a known high reliability should be considered for an in-tank installation and the greatest possible care would be taken to be certain that the unit was operating properly before the installation was made. In addition, the penalty that would be incurred if it became necessary to discard a tank because of a valve failure, would have to be considered. However, in many instances pressurization tankage consists of small spheres which can normally be removed readily, and in cases where this is true the risk does not seem to be great.

An additional penalty may be imposed if the qualification test procedures for the tank were altered because of the addition of the valve. For example, if vibration and shock tests were required of the valve it might be necessary to perform these tests with the valve in its normal mounting, i.e., in the tank. However, such a requirement is not considered to be of great consequence.

#### 4.7 REFERENCES

1. Advanced Valve Technology for Spacecraft Engines, Final Report No. 8651-6016-RU-000, TRW Systems, March 1963.
2. Advanced Valve Technology for Spacecraft Engines, Final Report No. 8651-6032-SU000, Volume I Valve Study, TRW Systems, July 19, 1964.
3. Advanced Valve Technology, Interim Report No. 06641-6004-R000, TRW Systems, November 1, 1966.
4. Bixson, L. L., Analysis and Measurement of Chemical Conversion Time in a Liquid Fuel Rocket Engine With Distributed Combustion, Sunstrand Turbo S/TD No. 1855 Technical Note No. 8, AF OSRTN No. 60-886, 26 July 1960.
5. Investigation of the Formation and Behavior of Clogging Materials in Earth and Space Storable Propellants, Interim Report No. 08113-6007-R000, TRW Systems, October 1967.
6. TRW Space Data, 3rd Edition, TRW Systems Group, 1967.
7. Advanced Valve Technology, Final Report No. 06641-6023-R000, Volume I, Mechanical Controls, TRW Systems, January 1969.
8. Smith, C. W., Calculation of Flow of Air and Diatomic Gases, Journal of the Aeronautical Sciences, June 1946.
9. Advanced Valve Technology, Interim Report No. 06641-6014-R000, Volume I Spacecraft Valve Technology, TRW Systems, November 1967.
10. Gee, L. J., Research on Diffusion of Hydrogen Through Palladium, ATL-D-1136, American Standard Advanced Valve Technology Laboratories, October 29, 1963.
11. Markels, M., Jr. and R. L. Durfee, The Effect of Electrical Potential on Boiling Heat Transfer, Proceedings of 1st Space Vehicle Thermal and Atmospheric Control Symposium, Report No. ASD-TDR-63-260, April 1963.
12. Bhuta, P. G. and L. R. Koval, Sloshing of a Liquid in a Draining or Filling Tank Under Variable G Conditions, Proceedings of AFOSR/Lockheed Symposium on Fluid Mechanics and Heat Transfer Under Low Gravitational Conditions, Palo Alto, Calif. 24-25 June 1965.
13. Yeh, G.C.K. and R. E. Hutton, Fluid Mechanics at Low Gravity Environments, TRW Systems Report No. EM 15-4, December 1964.
14. Yeh, G.C.K. and R. E. Hutton, Static Configuration of the Liquid-Vapor Interface in an Axisymmetric Tank in Various Gravitational Fields, TRW Systems Report No. EM 15-2, March 1965.

15. Koval, L. R. and P. G. Bhuta, A Direct Solution for Capillary-Gravity Waves in a Cylindrical Tank, TRW Systems Report No. EM 15-1, March 1965.
16. Advanced Valve Technology for Spacecraft Engines, Final Report No. 8651-6042-SU-000, TRW Systems, August 1965.
17. Advanced Valve Technology for Spacecraft Engines, Final Report No. 8651-6033-SC000, Volume II New Concepts, TRW Systems, July 19, 1964.
18. Experimental Study of the Effects of Weightlessness on the Configuration of Mercury and Alcohol in Spherical Tanks, NASA Technical Note D-1197.
19. Effects of Surface Energy on Liquid-Vapor Interface Configuration During Weightlessness, NASA Technical Note D-1582.
20. Effects of the Acceleration Disturbances Encountered in the MA-7 Spacecraft in a Baffled Tank During Weightlessness, NASA Technical Note D-1577.
21. Effects of Contact Angle and Tank Geometry on the Configuration of the Liquid-Vapor Interface During Weightlessness, NASA Technical Note D-2075.
22. Benedikt, E. T., General Behavior of a Liquid in a Zero or Near Zero Gravity Environment, Report No. ASG-TM-60-926, Northrop Corporation, Norair Division, May 1960.



## 5.0 LEAKAGE AND SEALING TECHNOLOGY

A significant portion of the Advanced Valve Technology Program effort has been devoted to the analysis of the single greatest problem with spacecraft valves—leakage through the valving unit—and the study of advanced sealing techniques to control this leakage. Most of this effort has been associated with poppet-type valving units, because poppet valves are used on virtually all unmanned and manned spacecraft in small valve applications and appear to be the most probable choice for the larger valves of future spacecraft when more exotic propellants are used.

Most of the work has been concerned with primary leakage, i.e., leakage through the valving unit or between the seat and poppet. These results are, in many instances, equally applicable to the analysis and control of secondary leakage of fluid from the flow conduit to outside of the flow path, such as past a static seal in the connection between the valve and the line.

### 5.1 LEAKAGE TECHNOLOGY

The earliest phases of the AVT program in 1962 brought three factors into sharp focus:

- Leakage was the most critical problem in the development of spacecraft engine valves.
- There existed a serious dearth of knowledge concerning leakage phenomena, the factors influencing leakage, and even criteria for acceptable leakage rates.
- The satisfactory control of valve leakage would require major advances in sealing technology.

The following discussion of leakage technology briefly describes the state of the art and summarizes those aspects of the technology which were studied under the AVT program. The control of leakage is treated under Section 5.2, Sealing Technology.

#### 5.1.1 Leakage Considerations and Criteria

Leakage through spacecraft engine valves has long been recognized as a critical design problem because of the following consequences:

- Reduced overall propulsion system efficiency from loss of propellant
- Fire and explosion hazard (particularly with hypergolics)
- Interference with spacecraft experiments
- Toxicity hazard
- Corrosion potential

Accordingly, a general goal of zero leakage evolved early in the space program. This indefinite term found its way into the advertising of valve manufacturers whose products happened not to drip too much as well as into the titles of such sophisticated programs as "Design Criteria for Zero-Leakage Connectors for Launch Vehicles." This latter program (performed by General Electric Company for the NASA under Contract NAS 8-4012 between 1962 and 1968) is representative of the comprehensive efforts undertaken to improve the understanding of leakage and devise sealing solutions. Another closely related effort also performed by General Electric's Research and Development Center was Contract NAS 7-396 which culminated in Leakage Testing Handbook (Reference 1). This handbook emphasized the costs and problems associated with specifying such vague terms as "no detectable leakage," "no measurable leakage," "no leakage," and "zero leakage."

When the confusion associated with the zero leakage term became apparent early in the Leakage Testing Handbook Program, Jet Propulsion Laboratory published The Basic Criteria and Definitions for Zero Fluid Leakage (Reference 2). This brief (14 page) report makes two rather evident but often overlooked and previously unpublished definitions:

- Zero liquid leakage is that value of liquid leak or flow rate at which the surface tension of the liquid has just overcome the pressure acting on the liquid (Figure 5-1) and no flow occurs - assuming a given pressure and leak diameter.
- Zero gas leakage as such does not exist as far as laboratory measurements have thus far been able to determine because of the limitations of laboratory instruments. Therefore, an arbitrary curve was constructed as shown in Figure 5-2 for use as a specification standard.

Reference 2 has since become not only the accepted standard on zero leakage but also a basic reference on the subject of gas/liquid leakage correlation (Section 5.1.3 below).

References 3 and 4 are representative examples of the use of the zero leakage term in NASA documentation prior to the publication of Reference 2.

#### 5.1.2 Leakage Phenomena

The precise mechanism whereby a fluid leaks past a sealing interface has been the subject of numerous investigations (References 5, 6, 7 and 8). The various flow regimes (nozzle, turbulent channel, laminar, transition, and molecular) have been observed and defined by G. F. Tellier (References 7 and 8) of Rocketdyne under contract to the Air Force Rocket Propulsion Laboratory. A representative example based upon nitrogen flow through a one-inch flat seat poppet valve is shown in Figures 5-3 and 5-4. This work substantiated that at General Electric by concluding that most leakage through closed valves is in the laminar or molecular flow regime, or a combination of the two.

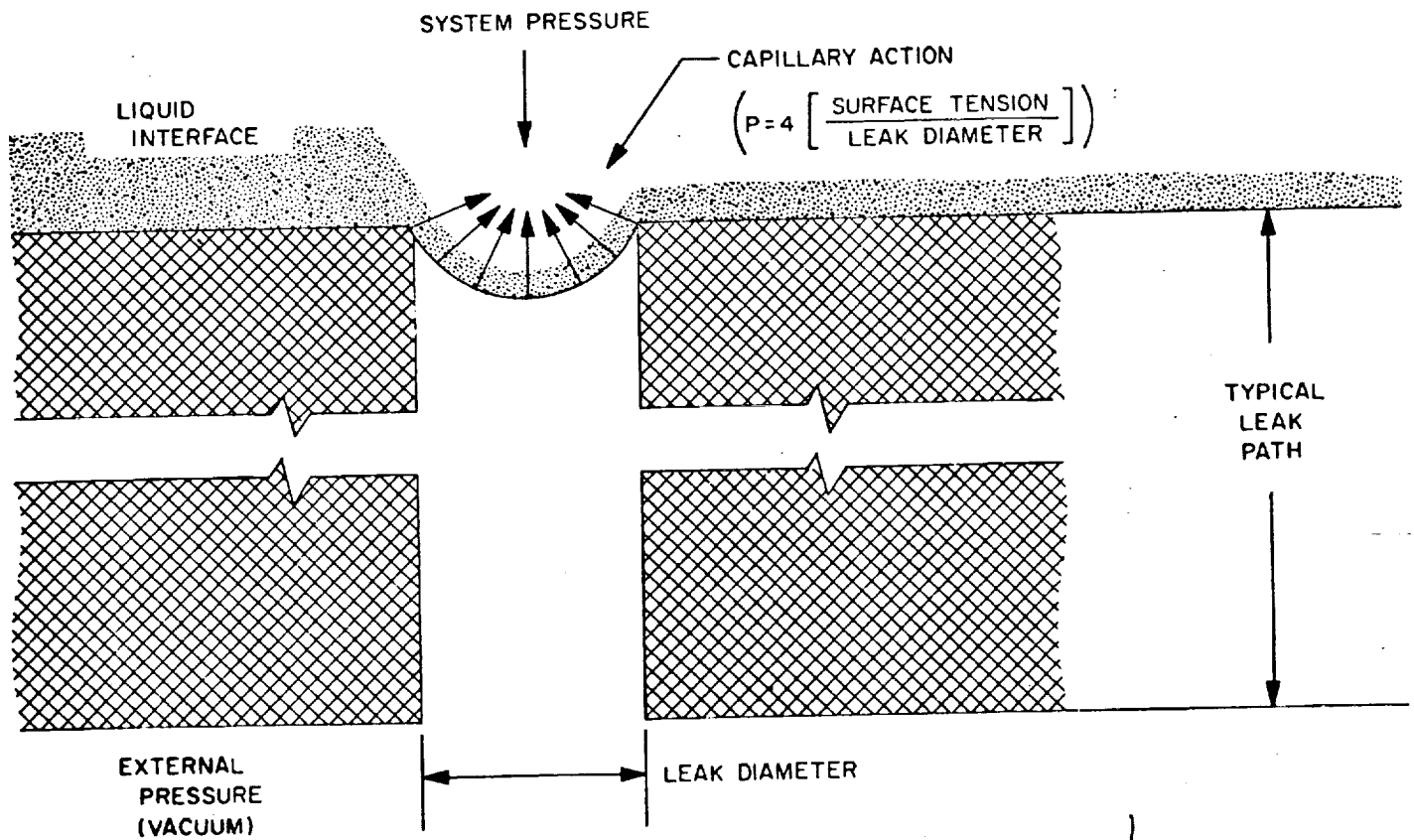


Figure 5-1. Mechanism of Clogging - Zero Liquid Leakage (Reference 2)

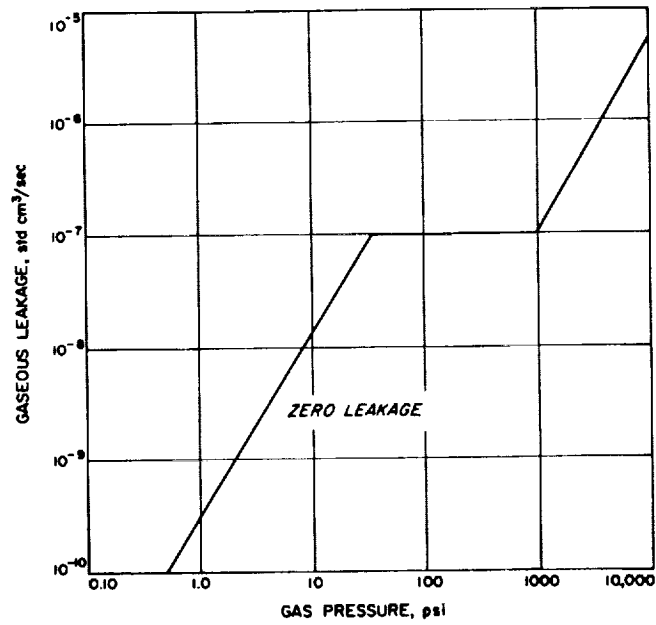


Figure 5-2. Definition of Zero Gas Leakage as a Function of Upstream Gas Pressure (Reference 2)

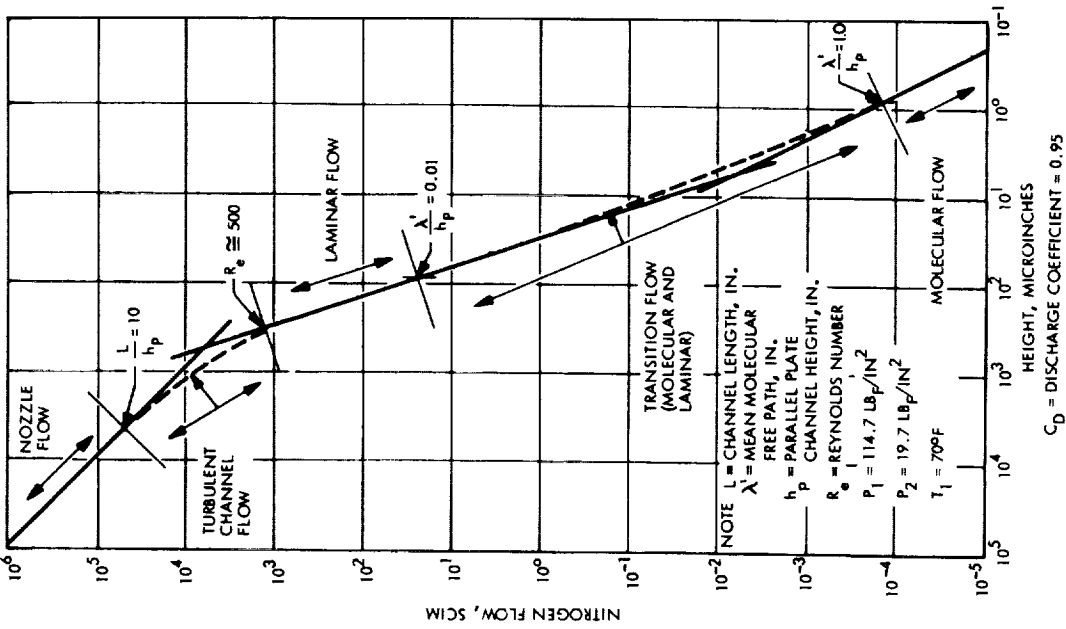
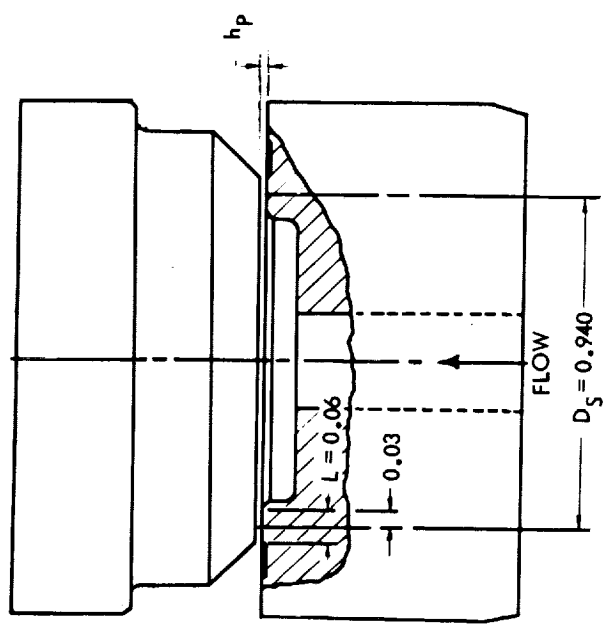


Figure 5-3. Theoretical Nitrogen Flow Through Flat-Seat Valve Model



$D_s$  = MEAN SEAT DIAMETER  
 $L$  = CHANNEL LENGTH, IN.  
 $h_p$  = PARALLEL PLATE CHANNEL HEIGHT, IN.

Figure 5-4. One-Inch Flat Poppet and Seat Model

The only studies to date which have precisely defined flow regimes have been laboratory programs wherein the leakage flow path has been very clearly defined and carefully produced. Much of the leakage and sealing technology work under the AVT Program has taken into consideration the fact that in the great majority of valve leakage situations the precise geometry is unknown and other provisions must be made to analyze valve leakage.

Leakage past a tightly closed valve seat or other seal interface is through a leak path comprised of the interstitial peaks and valleys and extending completely across the width of the interface. References 6 and 9 describe some of the sophisticated techniques which have been applied in attempts to model seal interfaces mathematically. Reference 9 probably represents the current state of the art in the mathematical modelling of interface sealing phenomena.

Reference 1 presents equations representing the various possible modes of flow that can prevail in a leak, and suggests a manner whereby it is possible to determine the mode of flow in any situation.

The dimensionless ratio of mean free path to a characteristic lateral dimension of the flow channel is known as the Knudsen number:

$$N_K = \lambda/d$$

where:  $N_K$  = Knudsen number, dimensionless

$\lambda$  = mean free path, in.

$d$  = flow channel width or diameter, in.

Laminar flow exists for values of  $N_K < 0.01$  and molecular flow exists for values of  $N_K > 1.0$ . The region of transition from one mode to the other lies between values of 0.01 and 1.0.

The Reynolds number can be used to distinguish between turbulent and laminar flow. Turbulent flow exists at values of  $N_{Re} > 2100$ ; laminar flow exists for values of  $N_{Re} < 1200$ . For values of  $1200 < N_{Re} < 2100$  the flow mode can be either turbulent or laminar, depending upon the channel roughness.

As a rule of thumb, it is possible to predict the mode of flow through a leak channel from a knowledge of the rate at which a gas passes through the leak under a differential pressure in the order of one atmosphere:

<u>Mode</u>	<u>Leakage Rate (atm-cc/sec)</u>
Turbulent	$>10^{-2}$
Laminar	$10^{-1}$ to $10^{-6}$
Transition	$10^{-4}$ to $10^{-7}$
Molecular	$<10^{-7}$

These values apply when the leak is essentially through a single hole, such as a nozzle or orifice. When the leak is through a valve seat, for example, the transition from one flow regime to another may of course be expected to vary, as in the valve seat example illustrated in Figures 5-3 and 5-4.

Permeation flow is still another mode of flow and is defined in Reference 1 as the passage of a fluid into, through, and out of a solid barrier having no holes large enough to permit more than a small fraction of the molecules to pass through any one hole. The process involves adsorption, diffusion, dissociation, solution, migration, and desorption. Permeation flow has been the subject of several studies during this program, most notably the early Teflon seal improvement work discussed in Section 5.2.2 and seal permeation leakage study described in Section 5.1.7.

### 5.1.3 Gas and Liquid Leakage Correlations

The present state of the art of leakage correlation leaves a great deal to be desired. Leakage correlation in this case refers to the inference of leakage of a given fluid from known leakage of another test fluid across a given leak path. Current literature on the subject (References 1, 2, 5, 6, 10-16) emphasizes the lack of consistent correlation and the problems associated with knowing that leak path geometry remains the same. Reference 1 appears to be the most up to date and useful reference presently available on the subject.

The most useful leakage correlation techniques such as those presented in References 1 and 2 are limited to an assumption of laminar flow and are based on the 1956 work at General Electric reported by Santeler and Moller in Reference 10.

It is very important to appreciate that a prediction of liquid propellant leakage based upon a gaseous test can be expected to predict only the maximum leakage that could possibly occur, assuming the very same leak path geometry and identical pressures. This may well yield an unrealistically conservative test specification. According to Reference 1, it was found that leaks having a gas conductance in the  $10^{-5}$  atm cc/sec range had a liquid leakage approximately 1/20 of that predicted by the laminar flow equation. Two reasons suggested in Reference 1 for this phenomenon are:

1. No correction was made for the molecular flow component of the measured gas leakage.
2. Physical adsorption completely immobilized a layer of liquid adjacent to the leak wall and therefore reduced the apparent leak diameter.

No comprehensive analysis of leakage correlation was undertaken during the AVT Program, however, some particularly interesting data were obtained as a result of tests conducted with the ABLEAK leak detection instrument described in Section 7.4. These preliminary data showed a high probability that the mass leak flow rate through an actual Lunar Module Descent Engine ball valve shaft seal was essentially the same regardless of which of some

four test fluids were used. These test fluids included both liquids and gases. The applicability of a direct measuring device such as the ABLEAK in future gas/liquid leakage correlation studies is readily apparent from a review of the test results shown in Section 7.4.

#### 5.1.4 Effects of Wear Particles and Temperature

One of the earliest studies under this program was directed toward the influence of wear particles and temperature upon valve leakage (Reference 17).

5.1.4.1 Wear Particle Study - When the normal load between two metals in contact exceeds a certain minimum, adhesive wear takes place and loose wear particles are formed. It was considered possible that a study of this phenomenon of particle production could result in the following:

1. Determination of a relationship between leakage and materials used in metal-to-metal seats including poppet, ball and spool configurations.
2. Prediction of the optimum filter size for use in valves or in valve-controlled systems.
3. Determination of the minimum clearance between moving parts before seizure can occur, or determination of the optimum materials for close-fitted parts in sliding contact.
4. Determination of the final surface finish that can be expected for sliding surfaces given a long period of time, or determination of the materials that will develop the best finish after wear-in.
5. Determination of the type of motion between sliding materials that will optimize roughness. This could prove useful for ball-type seat configurations.
6. Determination of the minimum normal load materials will sustain before wear takes place or when loose wear particles will not be formed.

The mechanism of friction is related to the phenomenon of adhesion. When two clean surfaces (surfaces in a vacuum) are brought together, contact is made at the tips of the many microscopic asperities and consequently the pressure at the junctions is high. Adhesions or cold welding takes place at these junctions and, when the surfaces slide relative to each other, these junctions must be sheared (Reference 18).

When a junction shears during sliding, and depending on the materials, the shear will take place within one of the surface layers and a wear particle is formed that will adhere to the other surface. Wear particles between surfaces in contact are first developed by adhesive wear, that is, there is adhesion between the asperities. The asperity of the softer material is sheared and retained by the harder material. In the shearing process

the particle is deformed and strain energy is stored in the particle. The vertical component of the strain force is relieved but the particle is strained in the horizontal plane and the surface is restrained from contracting at the adhered joint. However, if the strain or surface energy is greater than the adhesive energy of the joint, the joint will fail, creating a loose wear particle.

The theoretical diameter of a particle may set an upper limit on the spacing between the surfaces in contact. It may be an indicator in setting an upper limit on leakage of a valve seat configuration and may predict the screening size of the filters used in the valve or in the plumbing.

A relationship between particle size and adhesive energy has been developed by E. Rabinowicz (Reference 19) at Massachusetts Institute of Technology, and is given by the equation:

$$d = 60 E W_{ab} / \delta_{yp}^2$$

where:  $d$  = the average diameter of the particle

$E$  = Young's modulus

$W_{ab}$  = the work of adhesion of the contacting materials  $a$  and  $b$  and is defined as:

$$W_{ab} = \gamma_a + \gamma_b - \gamma_{ab}$$

where:  $\gamma_a$  = surface free energy of material  $a$  per unit area

$\gamma_b$  = surface free energy of material  $b$  per unit area

$\gamma_{ab}$  = interface free energy per unit area

$\delta_{yp}$  = yield stress of the material in compression.

It is found that  $\delta_{yp}$  is about one-third the hardness  $p$  and that  $\delta_{yp}/E$  is about  $3 \times 10^3$  for many materials.

then,

$$d = 60,000 W_{ab} / p$$

Experimental results showing a relation between material and an average wear particle diameter, obtained by E. Rabinowicz (Reference 20) are given in Table 5-1. It can be seen that the average of the  $W/pd$  ratio is close to  $16 \times 10^6$ , as predicted by the equation  $d = 60,000 W_{ab}/p$ . Table 5-1 also shows the relation between some non-metals and their corresponding particle size. Extensive testing of nylon on nylon produced no apparent wear. With Teflon on Teflon the wear fragments were fibrous and had fairly uniform cross-sectional diameters varying from  $40\mu$  to  $150\mu$ , with the average taken as  $90\mu$ .



Table 5-1. Size of Wear Particles and Related Functions Under Standardized Conditions of Ambient Atmosphere

Metal	p	W	W/p	d	W/p/d
Lead	$4 \times 10^8$	440	$110 \times 10^{-8}$	$270 \times 10^{-4}$	$42 \times 10^{-6}$
Tin	6	540	90	120	75
Bismuth	12	375	31	50	62
Woods Alloy	16	400?	25	400	6.2
Cadmium	23	600	26	320	8
Aluminum	30	900	30	140	21
Zinc	30	750	25	440	5.6
Antimony	45	380	85	400	22
Copper	60	1100	18	250	7.3
Brass	120	700?	5.8	100	5.8
Mild Steel	200	1000	5	60	8.3
Iron (oxide)	2000?	600?	.3	1	30
Aluminum (oxide)	2000	900	.45	1	7.5
Teflon	4	15?	3.8	90	42
Nylon	20	30?	1.5	?	?
Babbitt	30	400?	13	350	3.7
Silver	80	920	11.5	330	3.5
Nickel	260	1650	6.3	35	18
Glass	550	200?	.36	1	36

NOTE: p is the penetration hardness in dynes/cm<sup>2</sup>  
W is the work of adhesion of the system in ergs/cm<sup>2</sup>  
d is the diameter of the average wear particle in cms.

Table 5-2. Wear of Copper in Various Environments

<u>Atmosphere</u>	<u>Average Fragment Diameter</u>
Nitrogen	480
Helium	380
Carbon Dioxide	300
Dry Air	224
Oxygen	201
Laboratory Air	177
Wet Air	144
<u>Lubricant</u>	
Cetane	12.0
Silicone DC 200	9.5
Ucon LB-70X	9.5
Palmitic Acid in Cetane	8.0

Table 5-1 also shows that the smaller average wear particle diameters are obtained for the harder materials. It is interesting to note that the harder materials also appear to be more successful in limiting leakage in metal-to-metal seats used in valves. It would appear that one parameter influencing leakage in valve seat closures would be the particle size generated between the seated surfaces.

Wear experiments carried out by Rabinowicz (Reference 20) show that the size of copper wear particles are essentially independent of surface velocity and that the wear particle size tends to increase with the load. At higher loads a large percent of the particles were greater than  $500\mu$  in diameter, and for the lower loaded specimens there were no particles greater than  $350\mu$ , with the largest percent of particles being less than  $44\mu$  in diameter. Tests made with 1020 steel on 1020 steel showed that at low loads the wear debris was oxides while at higher loads the wear debris was metallic.

Atmospheric composition also has an effect on particle size. Wear experiments on copper conducted by John N. Elliott (Reference 21) support the theory of E. Rabinowicz that the average particle size should vary inversely as the reactivity of the atmosphere. Table 5-2 gives the results of Elliott's work and includes the effect of some lubricants on copper wear particles.

After the "wear in" period between any two connecting surfaces has been accomplished, the surface finish will reach a value that is characteristic of the wear particle size, which in time is a function of the materials. If the finish is initially very fine but the wear particle size is relatively coarse, the surface finish will degrade to a lower value (higher RMS No.). (This phenomenon was later substantiated during the superfinish seal effort reported in Reference 22). Conversely, if the initial surface has a relatively poor finish, the wear-in process will refine the finish to a lower RMS value.

Although no experimental work or further wear particle analyses were performed under the AVT Program, the following conclusions of this early study have remained valid:

- Friction force can be reduced for materials in sliding contact in a vacuum by proper selection and combination of materials. The optimum would be a hard material sliding on a softer material plated to a harder material. However, the softer material will produce large wear particles that may influence the leakage.
- A parameter to consider in selecting a material for a valve seat is the wear particle size generated by the seat materials. By selecting hard materials which produce the smaller wear particles, leakage should be minimized.
- Normally, a valve seat or closure is protected by a filter in the system, usually located as close as possible to the valve, sometimes being integral with the valve. The size of the wear particles generated by the operating action of the valve

may dictate the micron size of the filter to be used. For example, if the wear particles generated by the closure were equal to or greater than  $10\mu$ , there would be no justification to use a  $5\mu$  filter upstream of the closure.

- A knowledge of the effects that various planetary atmospheres have on wear particle size may be essential to component design. For the atmosphere of the planet Venus, which is estimated to be 90 to 95% nitrogen, the mean particle size would be greater than if it were produced in the earth's atmosphere. The significance of this can be important for many mechanical functions; for instance, in close-fitted moving parts such as a shaft sliding in a bushing, the clearance should be larger than the expected wear particle size. For close-fitted parts seizure may take place in the Venus atmosphere or in the space vacuum, while working perfectly in the earth's atmosphere. A tolerable leak rate for a given value in an earth atmosphere may increase for the same valve operating in the atmosphere of Venus or Mars due to the larger particle size produced.
- The surface finish on valve seats is important for leakage control. The initial surface finish should then be comparable or better than the characteristic wear particle size for the softer material.

5.1.4.2 Temperature and Structural-Mechanical Effects - This study evaluated potential fluid leakage problems due to temperature gradients that may be imposed on the valve closure. The study consisted of a review of the general structural-mechanical-thermal problems of fluid valve designs and a detailed study of the relative importance of thermal distortions of a valve seat due to nominal thermal gradients that would be expected from the radiation space environment.

General Structural-Mechanical-Thermal Valve Problems - Various valve designs were reviewed for potential structural-mechanical-thermal problems. Design areas which were felt to be possible potential problems and therefore require design attention are discussed below.

Valve Seat Design Problems - Valve seat design problems include maintaining mechanical stability in the anticipated operating environment. In-plane and out-of-plane distortions were considered to be the major design problems. These distortions can be minimized by:

1. Selecting basically stable valve seat materials
2. Reducing thermal gradients by proper structural thermal design (preliminary study results as presented in this study show that these effects are small for nominal gradients)
3. Allowing controlled material deformations to take place in the valve seat itself
4. Modifying the seat contact line detail to include a slight arc to allow a minute rotational seat misalignment.

Valve Stem Design Problems - Valve stem design problems are similar to the valve seat design problems, i.e., achieving mechanical stability. Mechanical stability can be achieved by:

1. Selecting basically stable valve stem materials
2. Minimizing thermal gradients by proper structural-thermal design
3. Permitting controlled material deformations to take place in the valve stem itself
4. Designing the valve stem housing so that the stem support redundancy is minimized
5. Minimizing the active valve stem length
6. Incorporating the use of a limited "self-centering" stem-seat design arrangement.

Analysis of Thermal Distortions of a Valve Housing - The relative importance of thermal distortions of a valve seat due to nominal thermal gradients was investigated in detail. The idealized solution is summarized below, followed by a numerical example. Results indicate that nominal thermal gradients do not impose any serious distortions of the valve seat.

Analysis - A review of analytical solutions for thermal distortions of a valve housing indicated that a precise three-dimensional solution including edge effects was extremely complicated and unavailable at this time. However, a two-dimensional analysis (based on References 24 and 25) was performed, in which a valve housing was idealized as a thick cylindrical shell subjected to a steady state thermal gradient. It is believed that this idealization is sufficiently accurate for the initial study phase (Figure 5-5).

The two-dimensional analysis assumes that in steady state the temperatures on the inner and outer boundaries of the shell can be expanded in a Fourier series of sines and cosines. However, it can be shown that stresses and deformations in the cross section depend only on the terms of the Fourier series involving the first harmonic. Inasmuch as the valve seat temperature due to solar radiation over 180 degrees of its circumference is symmetric about axis A-A, (Figure 5-5), only cosine terms were considered in the following calculations.

The specialized Fourier series for this problem has the form

$$T(r, \theta) = \sum_{n=1}^{\infty} (a_n r^n + b_n r^{-n}) \cos n\theta + T_{(ref)}$$

and for the purposes of the stress and displacement calculations the only term of interest is

$$T(r, \theta) = (a_1 r + \frac{b_1}{r}) \cos \theta$$

The coefficients  $a_1$  and  $b_1$  are obtained from assumed boundary temperature variations. The only significant terms of these variations for purposes of the following illustrative calculation are

$$T_{r=a} = C_1 \cos \phi$$

$$T_{r=b} = C_2 \cos \phi$$

where  $C_1$  and  $C_2$  denote the maximum amplitude of the temperature variation on the two boundaries.

Solving for  $a_1$  and  $b_1$  in terms of  $C_1$  and  $C_2$  one obtains

$$a_1 = \frac{aC_1 - bC_2}{a^2 - b^2}$$

$$b_1 = \frac{ab (aC_2 - bC_1)}{a^2 - b^2}$$

It is to be noted that the actual boundary temperature variations may contain terms in the higher harmonics when expanded in Fourier series. However, as indicated above, the in-plane deformations do not depend on the latter and the precise form of the temperature distribution is not required.

With the above boundary equations and constants, the resulting in-plane radial and tangential deflections  $u$  and  $v$  are respectively,

$$u = \frac{\alpha}{2} \frac{1+\mu}{1-\mu} \frac{\cos \phi}{a^2 - b^2} \left\{ \frac{3}{4} r^2 (aC_1 - bC_2) + ab (aC_2 - bC_1) \right\}$$

$$v = - \frac{\alpha}{2} \frac{1+\mu}{1-\mu} \frac{\sin \phi}{a^2 - b^2} \left\{ \frac{r^2}{4} (aC_1 - bC_2) + ab (aC_2 - bC_1) \log r \right\}$$

where:  $r$  = radius to point in question

$\phi$  = polar angle

$a$  = inner radius

$b$  = outer radius

$\alpha$  = Thermal coefficient of expansion

$\mu$  = Poisson's Ratio

Numerical Example - With the preceding analytical expressions, a numerical example was selected and calculations conducted for a valve housing idealized as in Figure 5-5, and assuming values for the valve parameters shown below. A temperature gradient of 50°F across the valve was considered.

1. Valve Seat Dimensions and Temperature Coefficients

Inner radius  $a = 0.375$  inches

Temperature coefficient at inner radius  $C_1 = 12.5^\circ\text{F}$

Outer radius  $b = 0.75$  inches

Temperature coefficient at outer radius  $C_2 = 25^\circ\text{F}$

Both outer and inner radii temperature coefficients were estimated based on isolated valve body in space exposed to radiation from the sun.

2. Valve Seat Material

Stainless Steel 440A

Thermal coefficient of expansion  $\alpha = 5.8 \times 10^{-6}$  in/in/°F

Poisson's Ratio  $\mu = 0.33$

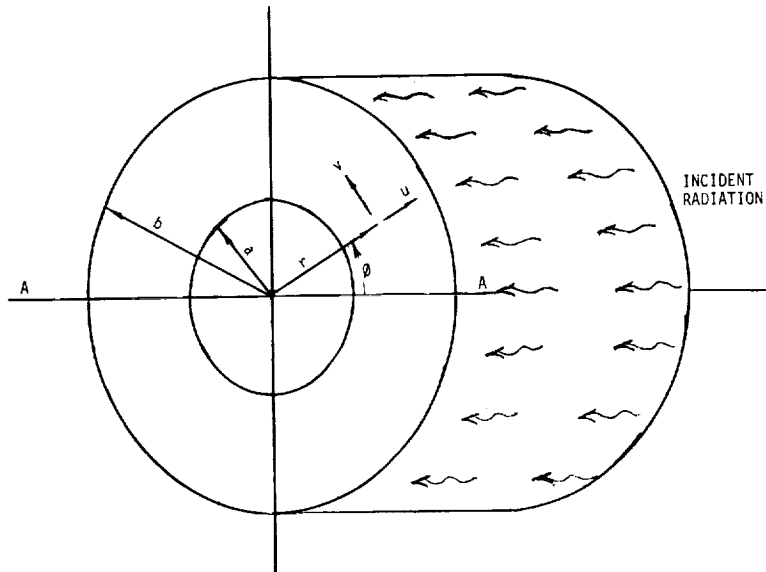
Figure 5-6 shows the computed radial and tangential displacements versus polar angle. With these displacements it may be shown geometrically that the maximum out-of-roundness is less than  $2.4 \times 10^{-10}$  inches, whereas out-of-roundness is defined as the difference between the internal radii at  $\theta = 0^\circ$  and  $\theta = 90^\circ$ . The computed value is extremely small, and negligible from the stress and manufacturing standpoints.

Therefore, it may be concluded that the effects of nominal thermal gradients on the in-plane distortions of valve seats may be considered insignificant.

5.1.5 The Effect of Ultrasonic Disturbance on Leakage

The objective of this investigation was to determine the effect on leakage of ultrasonic disturbance at the interface of metal valve seats. It was postulated that the shear component at the seat interface would affect leakage between the metal surfaces. The approach taken in this task was to apply ultrasonic techniques used in the art of ultrasonic welding of materials.

Ultrasonic welding does not require high currents or external heat and there is no melting of bulk metal. Relative motion of the welding probe in a direction parallel to the work surfaces is performed in order to rub one surface against the other. However, for multicycle operations of a valve, welding is not desired since the operating life will be limited.



$r$  = radius to point in question  
 $\theta$  = polar angle  
 $a$  = inner radius  
 $b$  = outer radius  
 $u$  = radial deflection  
 $v$  = tangential deflection

Figure 5-5. Thick Cylindrical Shell Subjected to A Steady State Thermal Gradient

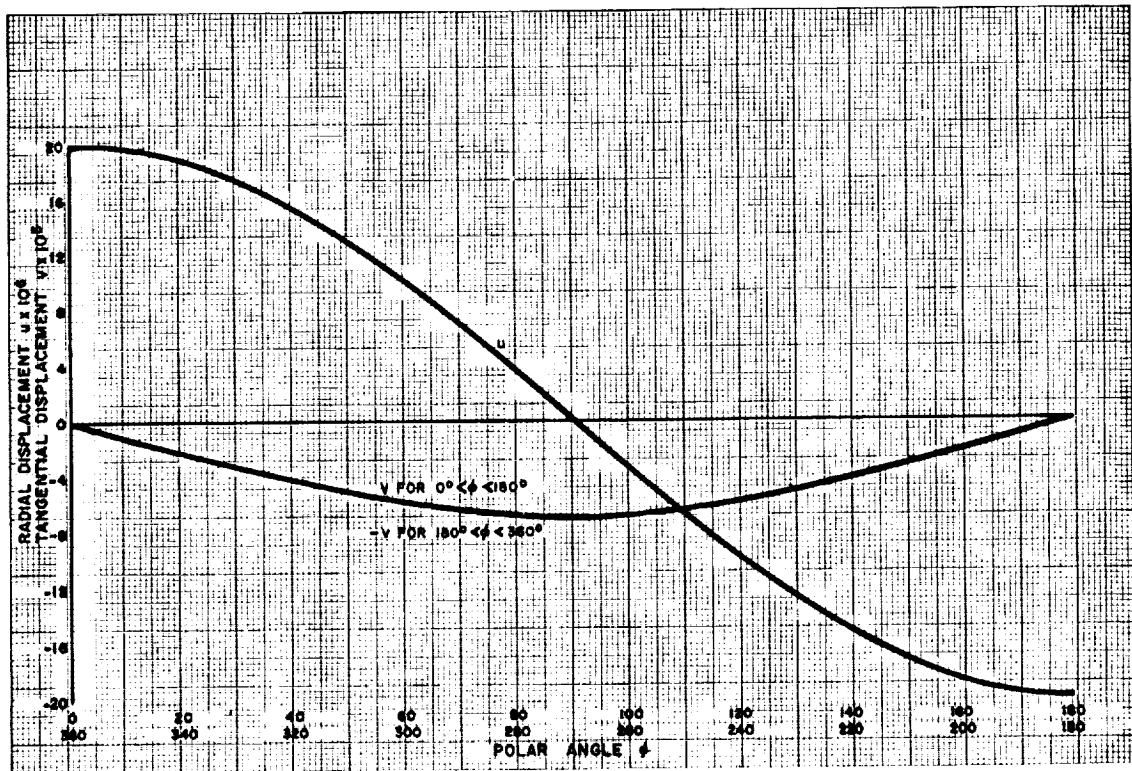


Figure 5-6. Displacements Vs. Polar Angle

Ultrasonic welding aids in plastically deforming the asperities on the metal surfaces. A transverse component of motion pushes the material from the peaks into the valleys and produces interactions of the material at the interface of the two surfaces. The ideal solution is to provide sufficient interaction such that the actuator force is adequate to separate the two surfaces with or without ultrasonic interaction.

Table 5-3 shows the combination of metals that can be welded ultrasonically (Reference 26).

Table 5-3. Combinations of Weldable Materials Using Ultrasonics

	Al	Be	Cu	Ge	Au	Fe	Mg	Mo	Ni	Nb	Pd	Pt	Si	Ag	Ta	Sn	Ti	W	U	Zr
Al and alloys	•	•	•	•	•	•	•	•	•		•	•	•	•	•	•	•	•	•	•
Be and alloys	•	•			•												•			
Cu and brass	•		•	•	•	•	•	•	•			•		•			•			•
Germanium		•										•								
Gold	•	•			•							•					•	•		•
Iron and steel	•				•	•	•	•	•			•	•	•			•	•	•	•
Mg and alloys	•												•	•			•			
Mo and alloys	•	•													•		•	•		•
Ni and alloys	•	•															•	•		
Nb and alloys	•														•					
Pd and alloys	•													•						
Pt and alloys	•	•																		
Silicon															•					
Ag and alloys	•	•																		•
Ta and alloys	•														•		•	•		
Tin																•				
Ti and alloys	•																•			
W and alloys																		•		
Uranium																			•	•
Zr and alloys																				•



5.1.5.1 Preliminary Experimental Results - The purpose of the experiment was to determine the effect of an ultrasonic field on the rate of leakage in a valve and to determine if the leakage is reduced or increased after the removal of the ultrasonic field.

A Nupro hand valve was selected for this experiment. The valve has a metal-to-metal seat. The two types of tests made are described in the following:

In the first series of tests, the valve body was cemented to the bottom surface of an ultrasonic cleaner tank with Eastman 910. The water level in the tank was about 0.25 inch above the bottom surface of the tank. After the leak was stabilized, the ultrasonic field was applied to the tank. There was no visible change observed in the meter of the CEC mass spectrometer type leak detector. This may be due to the insufficient power applied to the valve. The approximate power supplied to the valve was:

$$\begin{aligned}
 p &= \frac{\text{Average tank power} \times \text{cemented area of the valve}}{\text{Total area of the liquid}} \\
 &= \frac{300 \times 1}{110} = 2.7 \text{ watts}
 \end{aligned}$$

In the second series of tests, two piezoelectric discs 0.25 inch thick and 1.5 inches diameter were clamped between two plates, one plate being fastened to the bottom of the Nupro hand valve. The piezoelectric discs were made of Clevite PZT-4 material. The poling direction of the piezoelectric disc was such that the dynamic strains are in the same direction. The experimental setup is shown in Figure 5-7.

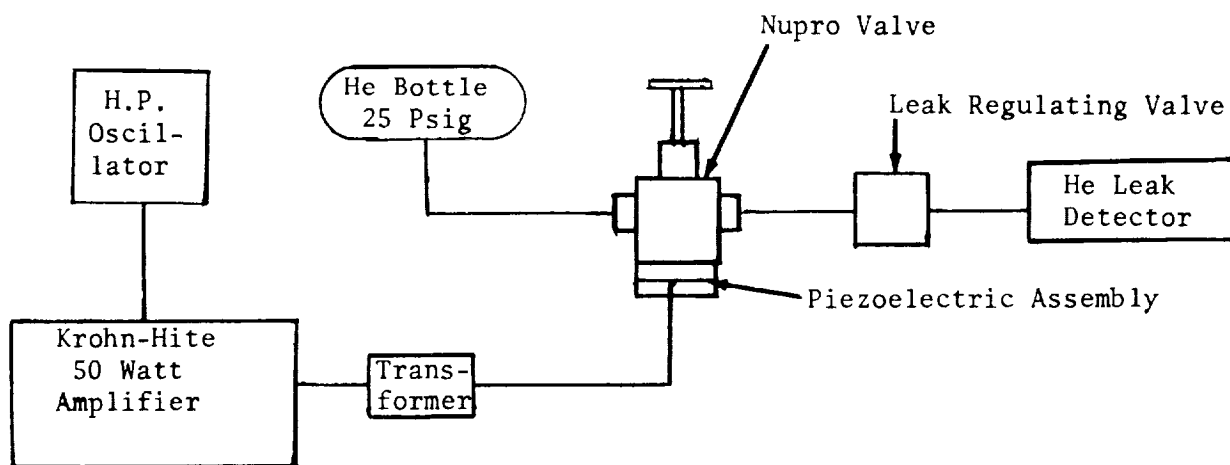


Figure 5-7. Ultrasonic Leakage Test Schematic

A transformer was introduced between the transducer and the Khrohn-Hite amplifier to provide proper matching. The power dissipated in the transducer was approximately 50 watts at 34 kcps. Since the leakage rate from the hand valve was high ( $\sim 3 \times 10^{-5}$ , scc/sec) a leak regulating valve located at the inlet port of the helium leak detector, was used to throttle the leak flow entering the mass spectrometer.

Typical test data from this second series of tests are presented in Tables 5-4 and 5-5.

The experimental results indicated that ultrasonic excitation may either reduce or increase leakage rate and that the change in leakage rate was not significant.

The test data were not conclusive, but permitted the following recommendations to be made for any future investigation of this phenomenon:

1. Increase the power to the junction of the valve seat and the poppet. In the preceding experiment a small fraction of ultrasonic power of 50 watts was dissipated at the junction.
2. The relative motion between the valve seat and the poppet should be investigated both in the direction parallel to the surfaces and perpendicular to the surfaces (as in these tests) as well as a combination such as  $45^\circ$  to the seat interface.

Further study was recommended with the following modifications:

1. Modify the test fixture to provide relative motion parallel to the seating surfaces.
2. Amplify the motion by applying a stepped horn acoustic transducer.
3. Provide a high static force. Ultrasonic pressure is superimposed on the static force.
4. Concentrate ultrasonic power at the sealing interface.

A test fixture should be designed such that all or most of the above requirements are satisfied. The parameters such as the static force and ultrasonic power should be varied to obtain a significant reduction in leakage without forming a weld between the valve seat and the poppet. The recommended test program should include the ultrasonic welding of specimens as an extreme case to determine if the technique is applicable to zero-leakage requirements.

Transducer Design - The transducer requirements are:

1. The piezoelectric disc resonates in the thickness mode. A radial mode can be used since there is always a coupling between two axes. However, the thickness mode is preferred.

Table 5-4. Test Results Showing Decrease in Leakage Rate Following Long Period of Ultrasonic Excitation

<u>Time in Minutes</u>	<u>Leakage Rate in scc/sec x 10<sup>-7</sup></u>	<u>Change in Leak Rate scc/sec/min x 10<sup>-7</sup></u>
0	12 ↓	
1	15.4 ↓	+ 3.4
2	17.4 ↓	+ 2.0
4	21 ↓	+ 1.8
6	22.7 ↓	+ 0.6
8	22.7 →	0.0
10	22.7 →	0.0
12	22.7 →	0.0

Ultrasonic power applied.

14 Power on	22.2 ↓	- 0.25
16 Power on	21.9 ↓	- 0.15
18 Power on	21.6 ↓	- 0.15

Ultrasonic power removed.

20	21.0 ↓	- 0.30
22	20.4 ↓	- 0.30
26	19.5 ↓	- 0.22
32	18.3 ↓	- 0.30
34	18 ↓	- 0.15
36	18 →	0.0

Table 5-5. Test Results Showing Decrease in Leakage Rate Following Short Period of Ultrasonic Excitation

<u>Time in Minutes</u>	<u>Leak Rate in scc/sec x 10<sup>-7</sup></u>	<u>Change in Leak Rate (scc/sec/min) x 10<sup>-7</sup></u>
0	15 ↑	
5	22.2 ↑	+ 1.44
7	23.6 ↑	+ 0.70
10	25.2 ↑	+ 0.53
12	26.2 ↑	+ 0.50

Ultrasonic power is applied for two minutes then removed.

14	25.2 ↓	- 0.50
17	24.6 ↓	- 0.20
22	24.0 ↓	- 0.12
25	21.6 ↓	- 0.8
35	20.7 ↓	- 0.1
45	18.3 ↓	- 0.24
50	17.4 ↓	- 0.19

2. The transducer horn should be designed to have the same resonant frequency as that of the piezoelectric ceramic disc. A stepped horn should be used for this purpose.
3. The stepped horn transducer should be mounted at its nodal point to minimize losses.

#### 5.1.6 Propellant Leakage in Vacuum

5.1.6.1 Introduction - As a liquid propellant flows through a restriction bounded on the upstream side by the propellant and on the downstream side by vacuum environment, there is a possibility that freezing of the liquid and eventual plugging of the flow container may occur. Freezing of propellants can be a serious problem area causing:

1. Valve response to change or complete failure of valve to actuate
2. Low temperature mechanical fit problems due to high heat of sublimation of the solid in vacuum
3. Freezing of valve hydraulic actuators where fuel is vented to vacuum
4. Delay in engine ignition
5. Explosion of hypergolic propellants.

Work conducted by Atlantic Research Corp. for NASA on freezing of propellants in vacuum has indicated freezing may have prevented the yaw thrusters from operating on Gemini 7. Two thrusters on Gemini 5 became inoperative and could have been due to freezing, however, because of valve heaters it was postulated the problem was the result of electrical failure. Problems related to the Gemini 8 valve failure were believed due to problems other than freezing. Both Gemini 7 and 8 valves had heaters on them to prevent general freezing.

A program initiated by the Air Force Rocket Propulsion Laboratory attempted to duplicate suspected flight failure mode of propellant freezing of the Transtage Engine bipropellant valve on the Titan III-4c vehicle. This propellant frosting was due to the venting of propellant leakage through the bipropellant pilot valve vent tube into the hard vacuum of space. Tests were conducted at altitudes between 400,000 and 825,000 feet. A Transtage bipropellant valve was tested under both normal and abnormal conditions, i.e., induced internal valve leakage (50% UDMH-50%  $N_2H_4$ ) ranging from 4 cc/min to 200 cc/min. Other tests included impingement of fuel leakage on the bipropellant valve as well as on adjacent engine components. The analysis of the test results revealed that internal valve leakage, at environmental temperatures of about 35°F, can result in erratic valve operation and in some cases can cause valve malfunction due to frost blockage of the bipropellant pilot valve vent tube. The impingement of fuel leakage on the bipropellant valve, from a distance of 3 inches, can cause blockage of the valve mechanical linkage as a result of propellant frost accumulation.

References 27 through 31 report work on both the NASA and Air Force programs studying the propellant freezing phenomenon. (Note: Additional work has been done on propellant freezing in vacuum since this portion of the AVT program was conducted in 1966. A typical example is Reference 32, "Hot Fire Testing of the LM Ascent and Descent Engine Restart Capabilities Test Program - Phase II" performed at Boeing, Tulalip in 1969 and reported by Grumman Aerospace Corp. This program showed conclusive proof of fuel (A-50) freezing in the injectors and in the shutoff valve actuator overboard discharge lines of both the ascent and descent engines under certain vacuum conditions.)

The Atlantic Research valve leakage study included the development of equations relating propellant thermodynamics and leakage rates and leakage testing of several propellants. As part of the AVT leakage studies, an analytical model was defined and leakage rates derived from appropriate equations. The valve leakage rates were related to freezing at the injector and are graphically plotted for 16 propellants. Leakage tests conducted under this program indicated freezing of propellants leakage occurred at the valve interface using water and nitrogen tetroxide. Future work in this area should include an analytical model of the valve interface, however, requiring a more rigorous analytical description of the environmental heating effects.

The analytical model used in this analysis consists of three primary elements: 1) a leaking valve, 2) a control or dribble volume and 3) an injector orifice.

#### 5.1.6.2 Assumptions

1. Neglect kinetic energy effects both within the control volume and within the streams entering and leaving the cavity
2. Neglect frictional effects
3. All phases within the control volume are in thermal equilibrium
4. Neglect momentum considerations within the control volume
5. Neglect volume of condensed phases in the exhaust stream
6. Evaporation rate may be described by the Knudsen relation
7. The outgoing flow from the control volume exhausts into a vacuum
8. Thermodynamic shaft work is zero
9. Neglect surface tension effects
10. The vapor follows the ideal gas law
11. The properties, i.e., temperature, phase, pressure of the exhaust stream are identical with the material within the control volume.

Discussion of Assumptions - Assumptions (1) and (4) are made as a consequence of the low velocities encountered in the physical mode. Assumptions (2) and (9) are concomitant with number (4) in that energies associated with these phenomena are also negligible in comparison with energy changes due to phase transformation.

Number (3) is reasonable since the temperature and pressure of the control volume will in general be close to the triple point of the fluid. Slight deviations of T and P between phases will only occur microscopically and would not upset the macroscopic equilibrium.

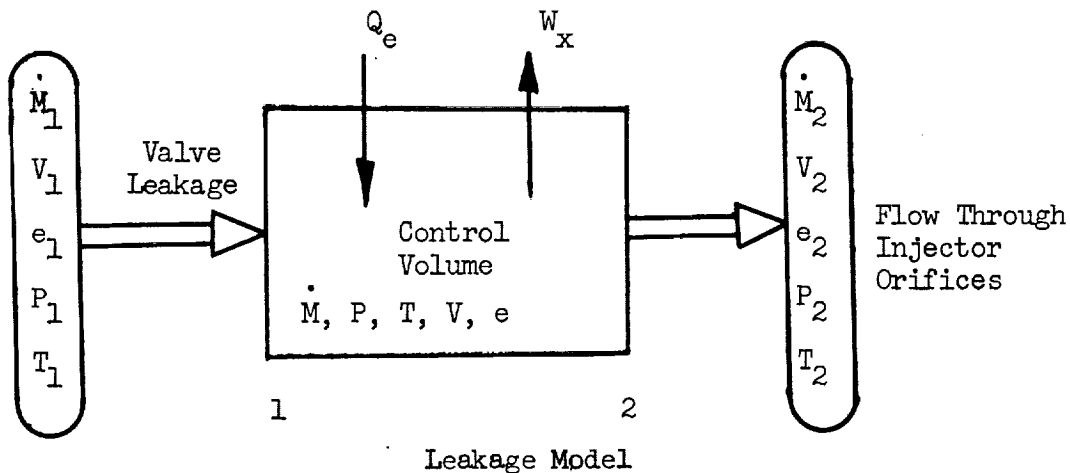
Assumptions (7) and (8) are actual conditions under which the physical model exists and are therefore exact descriptive statements.

It is a common assumption in nozzle flows where more than one phase exists to exclude the solid phase for flow volume calculations. Here we extend this to include the liquid phase, assumption (5).

Assumptions (6) and (10) describe the general relations used to describe the gas produced during the control time.

Assumption (11) assumes complete mixing within the control volume as opposed to a tubular approach which would consider property variations due to gradients within the control volume.

5.1.6.3 Analytical Model - Consider a control volume representing the volume downstream of the valve seat and upstream of injector orifices which is sometimes termed the dribble volume.



## Nomenclature

A	Area of injector orifice, in <sup>2</sup>
A <sub>s</sub>	Area of exposed surface of fluid, in <sup>2</sup>
α	Coefficient in Knudsen Equation (evaporation coefficient)
c	gJ, lb <sub>m</sub> -ft <sup>2</sup> /Btu-sec <sup>2</sup>
C <sub>v</sub>	Specific heat at constant volume, Btu/lb <sub>m</sub> -°R
C <sub>p</sub>	Specific heat at constant pressure, Btu/lb <sub>m</sub> -°R
C <sub>p</sub>	Specific heat at constant pressure, Btu/lb <sub>m</sub> -°R
$\frac{d}{dt}$	Time derivative
e	Internal energy, Btu/lb <sub>m</sub>
γ	Ratio of specific heats, C <sub>p</sub> /C <sub>v</sub>
n	Total energy in control volume, Btu/lb <sub>m</sub>
λ <sub>v</sub>	Heat of vaporization, Btu/lb <sub>m</sub>
λ <sub>v</sub>	Heat of fusion, Btu/lb <sub>m</sub>
$\dot{M}$	Flow rate, lb <sub>m</sub> /sec
h	Enthalpy, Btu/lb <sub>m</sub>
J	Proportionality factor - 778 ft - lb <sub>f</sub> /Btu
M	Mass, lb <sub>m</sub>
P	Pressure, psia
P <sub>s</sub>	Saturation pressure, psia
$\dot{Q}$	Heating rate from environment, Btu/sec
R	Specific gas constant = universal/molecular weight
ρ	Density, lb <sub>m</sub> /ft <sup>3</sup>
t	Time, seconds
T	Temperature, °R
V	Volume or velocity, ft <sup>3</sup> or ft/sec
W <sub>x</sub>	Shaft work, Btu/sec
X	Quality fraction - vapor, lb vapor/lb mix
Y	Quality fraction - liquid, lb liquid/lb mix
Z	Quality fraction - solid, lb solid/lb mix

## Subscripts

1	Entering control volume	L	liquid
2	leaving control volume	s	vapor
g	gas		

Non-numerical subscript refers to control volume

The continuity of mass requires that:

$$\frac{dM}{dt} = \dot{M}_1 - \dot{M}_2 \quad (1)$$

Assuming that three phases can exist within the volume we may write:

$$\frac{dM_g}{dt} = X \frac{dM}{dt} + M \frac{dX}{dt} \quad (2)$$

$$\frac{dM_L}{dt} = Y \frac{dM}{dt} + M \frac{dY}{dt} \quad (3)$$

$$\frac{dM_s}{dt} = Z \frac{dM}{dt} + M \frac{dZ}{dt} \quad (4)$$

where X, Y and Z represent the fraction of gas, liquid or solid compared to the total mass within the control volume.

The mass ratios (X, Y, Z) are related by:

$$\frac{dX}{dt} + \frac{dY}{dt} + \frac{dZ}{dt} = 0 \quad (5)$$

In general, the energy equation may be written as:

$$\frac{d}{dt} (\eta) = \dot{Q}_e - W_x + \dot{M}_1 \left( e_1 + \frac{P_1^J}{\rho_1} + \frac{V_1^2}{2c} \right) - \dot{M}_2 \left( e_2 + \frac{P_2^J}{\rho_2} + \frac{V_2^2}{2c} \right) \quad (6)$$

where:

$$\eta = MXe_g + MYe_L + MZe_s \quad (7)$$

Considering kinetic energy effects to be small,  $W_x = 0$ , and that we are exhausting into a vacuum environment ( $P_2 = 0$ ), Equation (6) becomes;

$$\frac{d}{dt} = \dot{Q}_e + \dot{M}_1 h_1 - \dot{M}_2 e_2 \quad (8)$$

where:

$$h_1 = e_1 + \frac{P_1^J}{\rho_1}$$

A group of auxillary equations may be used to constrain the system. If the gas produced within the control volume flows through a sonic orifice, then;



$$\dot{X}M_2 = \frac{A P (g^{1/2})}{\sqrt{T R}} \left( \gamma^{1/2} \left( \frac{2}{\gamma+1} \right)^{\frac{\gamma+1}{2(\gamma-1)}} \right) \quad (9)$$

The evaporation rate may be described by using the Knudsen relation which is based on kinetic theory:

$$\dot{M}_g = \frac{A_s}{(2\pi RT)^{1/2}} (P_s - P) \quad (10)$$

where  $\alpha$  = evaporation coefficient which was assumed equal to a value of 1.

We may assume that the evaporating liquid is described by the ideal gas equation:

$$P = \frac{M_g RT}{V} \quad (11)$$

It may be assumed that the three phases in the control volume are in thermodynamic equilibrium. Therefore, we may write;

$$T = T_2 \quad (12a)$$

$$e = e_2 \quad (12b)$$

and;

$$e_2 = X \int_{T_0}^{T_2} C_V dT + Y \int_{T_0}^{T_2} C_V dT + Z \int_{T_0}^{T_2} C_V dT + X\lambda_V - Z\lambda_F \quad (13)$$

where:  $T_0$  = an arbitrary reference temperature

$$P \leq P_1 \quad (14)$$

and, the heat fusion and evaporation are at  $T_0$  and  $P$ . If only one or two phases exist within the control volume then those terms representing the missing phases are eliminated from Equation (13). A similar expression can be written for  $h_1$ :

$$h_1 = \int_{T_0}^{T_1} C_p dT \quad (15)$$

One additional property equation is required relating vapor pressure to temperature and since the form of this equation varies, we simply write it as:

$$P_s = P_s(T) \quad (16)$$

5.1.6.4 Proposed Method of Solution - The exact solution of these equations requires knowledge of the area available for evaporation, as in Equation (10). Evaluation of this parameter will require experimental evaluation since the area of the phases available for evaporation would be dependent on the liquid surface formed by the valve leak and the agglomeration of liquid and solid phases due to geometry, gravity, or surface effects (adhesion). If it is assumed that this data is available then the previous equations are solvable according to the method described in the following paragraphs. Special cases can occur in which it is not necessary to know the exposed area available for evaporation. These cases are discussed in subsequent paragraphs.

Numerical integration will be required to solve this system of equations. Since the differential equations are first order first degree, no stability problems would be expected. A large number of integration techniques could be used. The one selected for this example is the Euler method whereby:

$$Y_{N+1} = Y_N + \left( \frac{dY}{dX} \right)_N \Delta X$$

- Step (1) - Select integration interval ( $\Delta t$ )
- (2) - Compute flow out of control from Equation (9)
- (3) - Compute accumulation in control volume from Equation (1)
- (4) - Compute amount of heat input into control volume
- (5) - Compute amount of evaporation from Equation (10)
- (6) - Compute change in gas fraction from Equation (2)
- (7) - Equations (2), (3), (4), (5) and (6) are then solved for the changes in mass between phases within the control volume. Initially when the temperature is above the triple point no solid phase will exist and when it is below the triple point no liquid phase exists. At the triple point no changes in temperature can occur until the liquid phase has been consumed. Each of these areas will require separate solutions and it will be necessary in the numerical solution to change the numerical technique at the triple point.
- (8) - Equation (11) is used to compute the change in pressure within the control volume as the condensed phase accumulates.

#### 5.1.6.5 Discussion of Limiting Cases

Case I - Steady-state, adiabatic vaporization where no solid is formed. Phenomenologically this occurs when the latent heat of vaporization is supplied by the sensible heat of the liquid and it is commonly termed "flash evaporation." Since the liquid cools by this process, freezing can occur. However, this case is restricted to a limit where there is no actual solid formation.

Mass

$$(1a) \dot{M}_1 = \dot{M}_2$$

$$(1b) X + Y = 1$$

Energy

$$(2a) \dot{M}_1 h_1 = \dot{M}_2 e_2$$

and using a result of the mass continuity equation

$$(2b) h_1 = e_2$$

Expressing this in terms of quality factors and using an arbitrary reference temperature  $T_0$  the following expression is obtained:

$$(2c) C_{P_L} (T_1 - T_0) = Y C_{V_L} (T - T_0) + X \lambda_V + X C_{V_G} (T - T_0)$$

where  $T$  is the temperature of the propellant fluid within the control volume. Assuming the exit temperature is equal to the control volume temperature and, if we choose  $T_0$  equal to the exit stream temperature, then the following expression is obtained:

$$(2d) C_{P_L} (T_1 - T) = X_V \text{ (since } T - T_2 = T_0 \text{)}$$

The auxiliary equation expressing flow from the injector is:

$$(3) X \dot{M}_2 = \frac{AP}{\sqrt{T}} \bar{K}$$

$$\text{where } \bar{K} = f(g\gamma, R)$$

Substituting this into equation (2d) for  $X$ ;

$$(4) C_{P_L} (T_1 - T) = \frac{\lambda_V AP \bar{K}}{M_2 \sqrt{T}}$$

But  $\dot{M}_2 = \dot{M}_1$  according to Equation (1a)

$$(5) \dot{M}_1 = \frac{\lambda_V AP \bar{K}}{C_{P_L} (T_1 - T) \sqrt{T}}$$

An additional equation is available in that the pressure is related to the temperature according to data available on vapor pressure:

$$(6) \quad P_s = f(T)$$

Equations (5) and (6) can be solved for the two variables P and T once the injector port area and leakage rate are specified. Alternately, since the quantity  $C_p (T_1 - T)$  decreases with temperature, the minimum valve leakage rate, below which solid will form, can be computed directly by substituting the triple point pressure directly into Equation (5). Below this point the analysis should change to reflect accumulation of solid material within the control volume through a derivation similar to the above equations by assuming the solid phase is carried out in the exit stream. It may be in fact that the system can tolerate small amounts of solid phase without enough accumulation occurring to plug or restrict the flow. If either condensed phase tends to accumulate within the control volume then the more general equations previously reported must apply; and in the event assumption (1) breaks down (i.e., due to gravity), then the equation must be rederived.

Case II - The second limiting case for the freezing zone is reached when the amount of outgoing material vapor is equal to the amount of incoming liquid leakage under steady state conditions. This situation requires a heat input from an external source to vaporize all the leaking propellant as it flows into the control volume.

The vapor flow rate will again be given by:

$$(1) \quad \dot{M}_1 = \dot{M}_2 = \frac{AP}{\sqrt{T}} \bar{K} = \frac{\alpha A_s (P_s - P)}{(2\pi RT)^{1/2}}$$

( $\alpha$  = evaporation coefficient = 1)

From the energy equation

$$(2) \quad \dot{Q}_e = -\dot{M}_1 (h_1 - e_2)$$

$$(3) \quad \text{where } e_2 = \int_{T_0}^T C_c dt + \lambda_v$$

Using the above relations

$$(4) \quad \dot{M}_1 = \frac{\dot{Q}_e}{\int_{T_0}^T C_v dt + \lambda_v - h_1 (T, P)}$$

Then for a given physical system and  $\dot{Q}_e$ , Equations (4) and (1) may be solved to predict  $M_1$  for this special case.

5.1.6.6 Discussion of Results - From the previous derivations on the thermodynamics of propellant valve leakage, three specific areas of operation can be outlined for steady-state conditions:

Case I - Condition in which there is no solid formed and only liquid and gas phases are present. The heat of vaporization is supplied by the sensible heat of the liquid. The limiting flow in this region is a function of the triple point state.

Case II - Heat inputs to the system provide sufficient heat to vaporize or sublime the entire propellant leakage.

Case III - Similar to Case I except the sensible heat of the fluid is not adequate to supply the heat of vaporization so partial freezing results. There may be three phases present at the triple point (partial freezing) but below the triple point only solid and vapor will exist.

Cases I and II are limiting cases investigated in this study.

Figures 5-8 through 5-20 present data for various propellants computed from equations developed for Case I. In this instance the minimum allowable leakage occurs when the temperature within the dribble volume is equal to the triple point. The data describing the curves was computed from Equation (5) for various propellants and as a function of injector area. In using these data a designer must know the propellant in question and the minimum inlet temperature to which the propellant will be subjected. The appropriate curve is then entered at the value of the injector orifice area and the minimum flow rate obtained for the particular inlet temperature. Corrections to other inlet conditions can be made utilizing Equation (5) only for inlet temperatures greater than the triple point. It should be noted that in this region the propellant is adiabatically expanding (heat supplied by bulk propellant) and condensing from the inlet conditions down to the triple point within the dribble volume and that the leakage out of the control volume is also at the triple state.

Figures 5-21 through 5-46 present flow rates and heat inputs required for various propellants for Case II. These data were generated from means of Equations (1) and (2) by first selecting a temperature for the propellant within the control volume and obtaining the appropriate corresponding saturated vapor pressure. The flow rate was then computed from Equation (1) and the heat input was computed from Equation (2) as a function of injector area. The bottom curve in each figure represents a limit below which solid would tend to form in the system and is nearly the same as Case I except sufficient heat is provided to evaporate the condensed phase. A designer would use these curves by ascertaining the minimum allowable temperature within the control volume which, as a general rule, should be no lower than the triple point, the lower curve in each figure. The appropriate propellant curve is then selected and entered at the value of the injector area. The appropriate maximum allowable flowrate is then obtained from the selected value of dribble volume temperature. This process is repeated to obtain the heating requirement from the corresponding figure on heat flow. This process can be varied to either adjust the maximum allowable flow rate by increasing heat input or, alternately less heat input can be accepted by decreasing leakage requirements. It should be noted that how this heat input is put into the dribble volume to prevent freezing is subject to more detailed analysis and design consideration. The required heat input can either be supplied by heat transfer from the surroundings, electrical heaters or radioisotopes.

CASE I - MAXIMUM ADIABATIC LEAKAGE RATES  
WITHOUT SOLID PHASE FORMATION

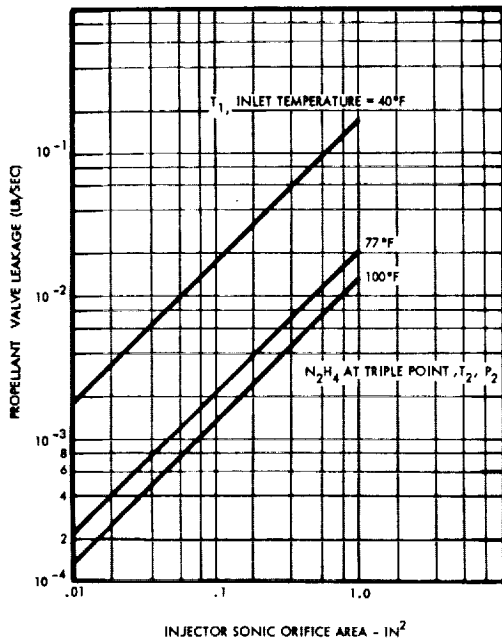


Figure 5-8. Hydrazine ( $N_2H_4$ )

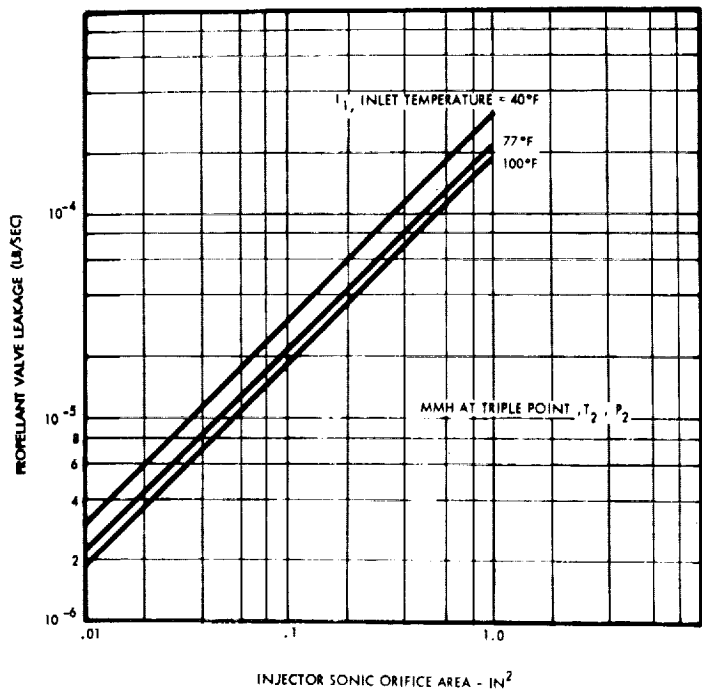


Figure 5-9. Monomethylhydrazine (MMH)

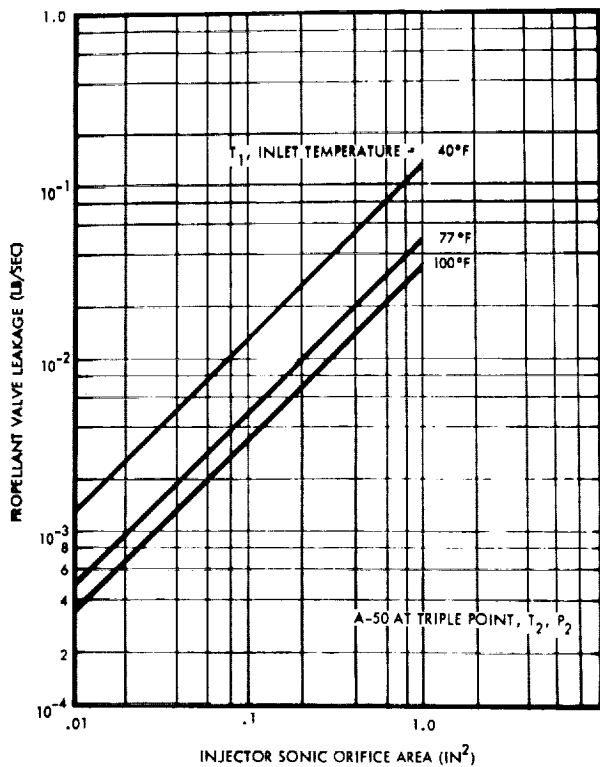


Figure 5-10. Aerozine-50

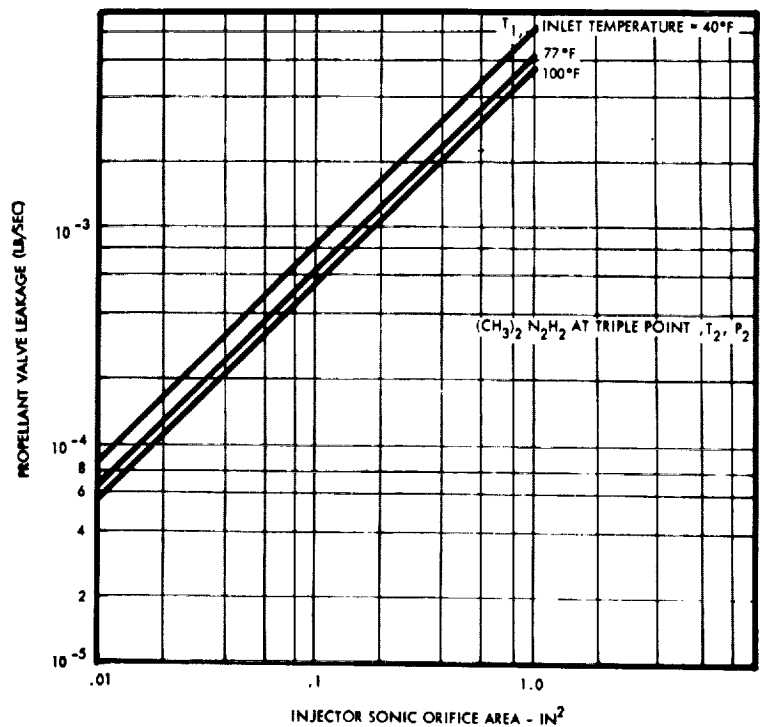


Figure 5-11. Unsymmetrical Dimethylhydrazine (UDMH)

CASE I - MAXIMUM ADIABATIC LEAKAGE RATES  
WITHOUT SOLID PHASE FORMATION

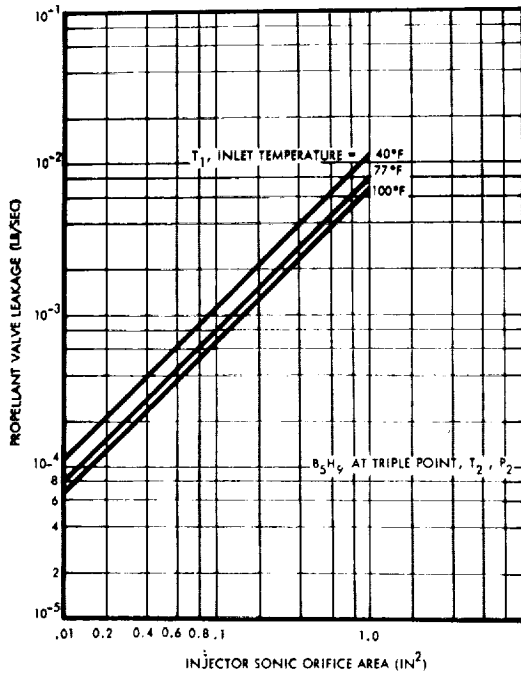


Figure 5-12. Pentaborane (B<sub>5</sub>H<sub>9</sub>)

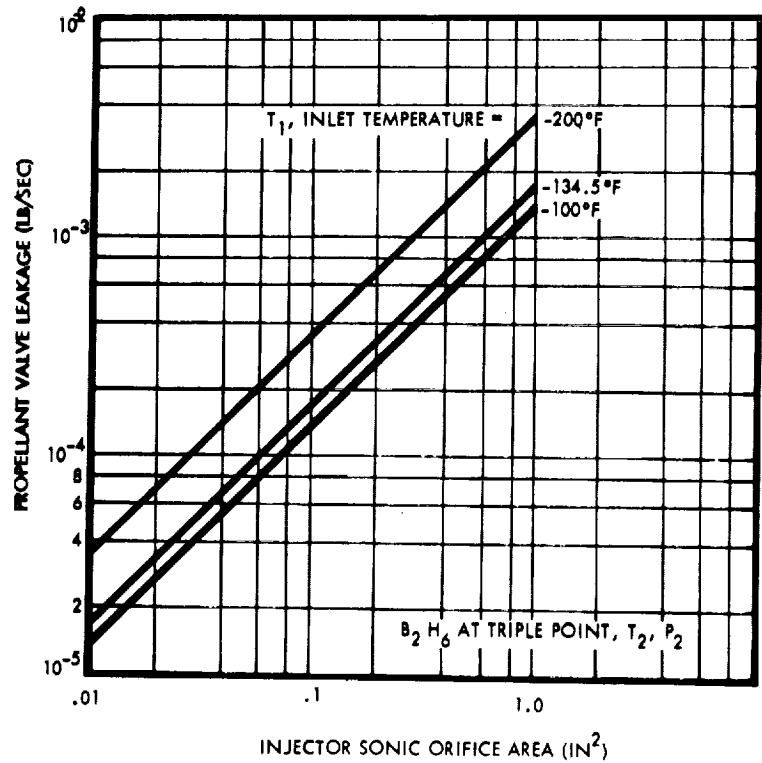


Figure 5-13. Diborane (B<sub>2</sub>H<sub>6</sub>)

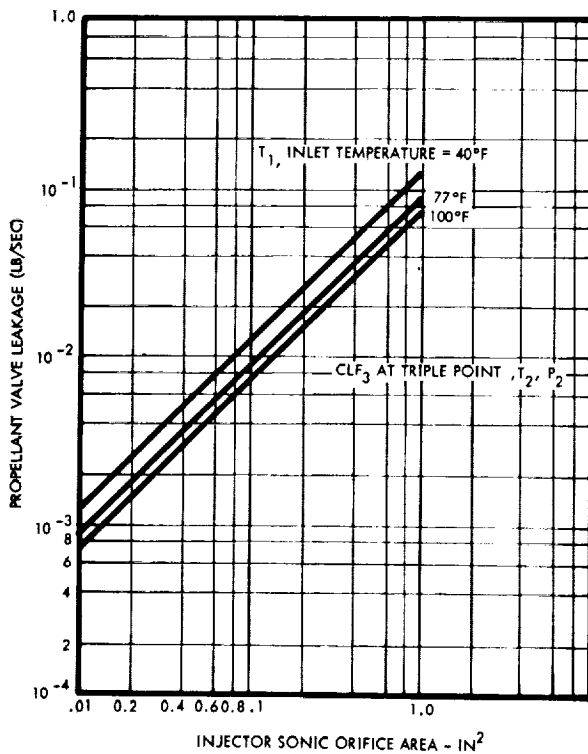


Figure 5-14. Chlorine Trifluoride (ClF<sub>3</sub>)

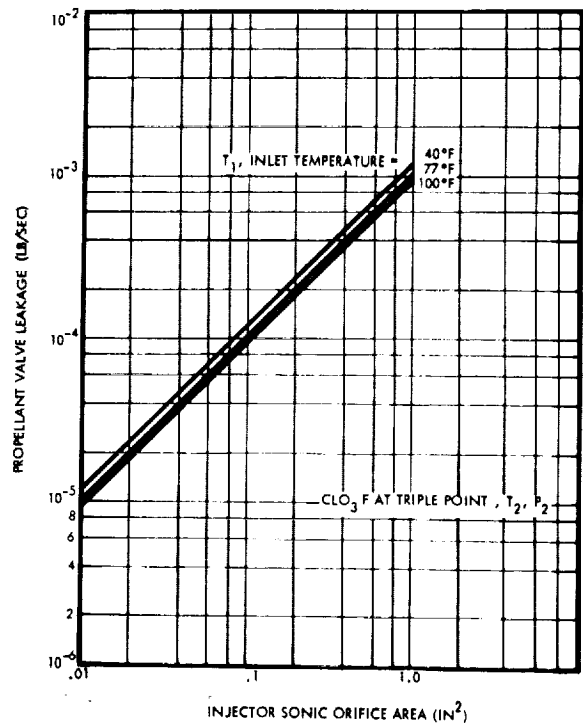


Figure 5-15. Perchloryl Fluoride (ClO<sub>3</sub>F)

CASE I - MAXIMUM ADIABATIC LEAKAGE RATES  
WITHOUT SOLID PHASE FORMATION

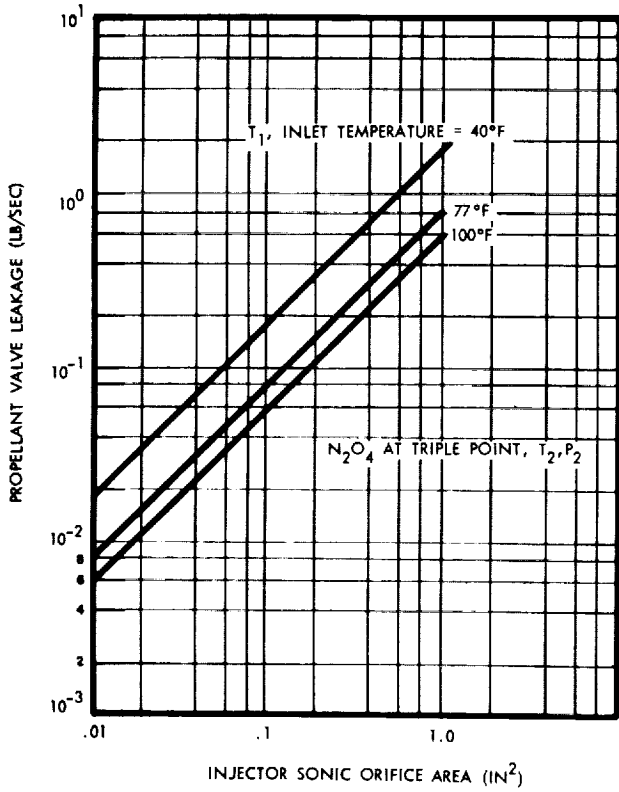


Figure 5-16. Nitrogen Tetroxide ( $N_2O_4$ )

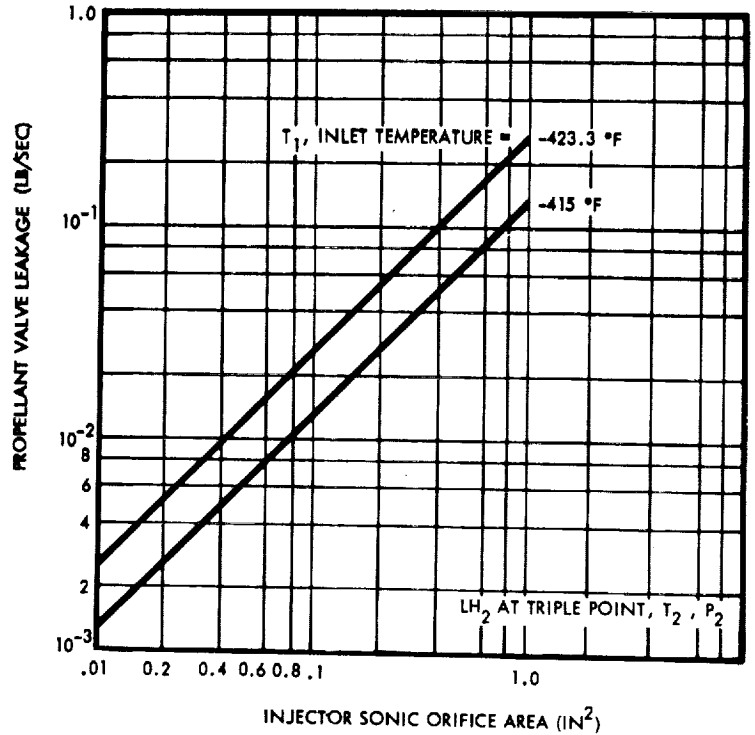


Figure 5-17. Liquid Hydrogen ( $LH_2$ )

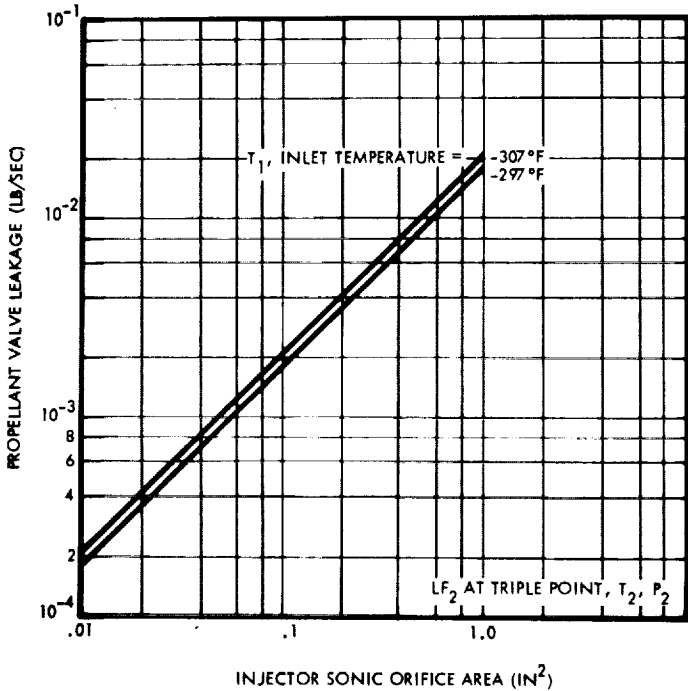


Figure 5-18. Liquid Fluorine ( $LF_2$ )

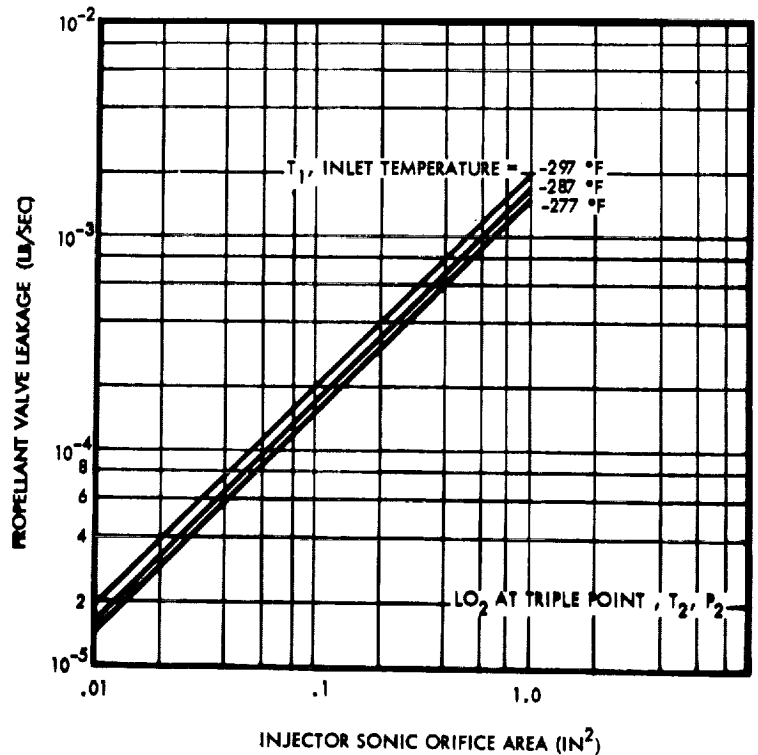


Figure 5-19. Liquid Oxygen ( $LO_2$ )



CASE I - MAXIMUM ADIABATIC LEAKAGE RATES WITHOUT SOLID PHASE FORMATION

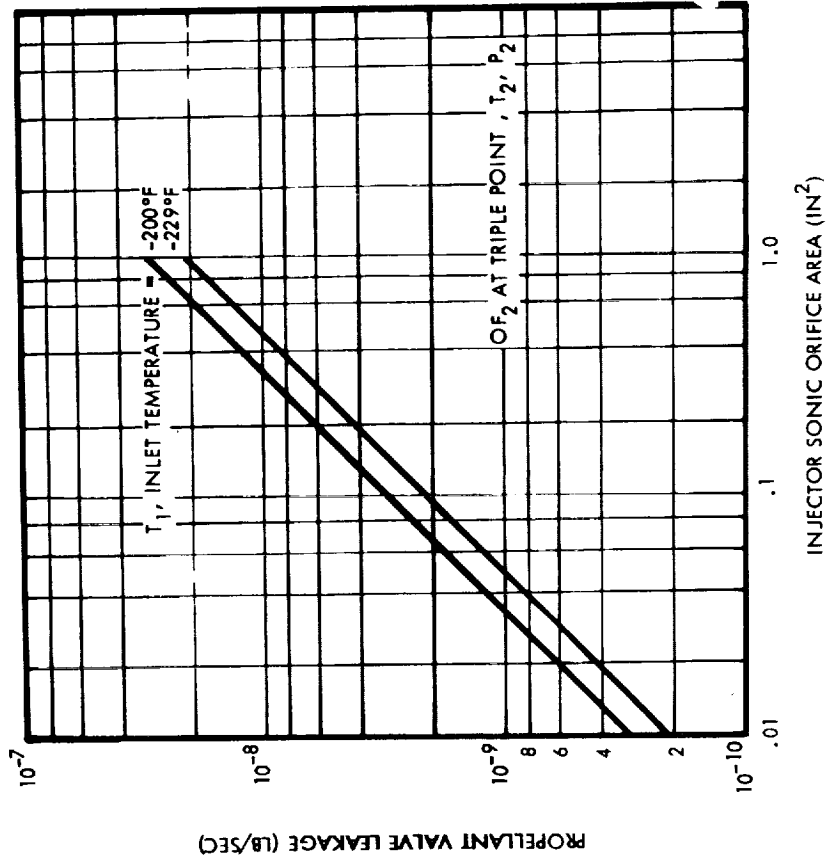


Figure 5-20. Oxygen Difluoride (OF<sub>2</sub>)

CASE II - MINIMUM FLOW RATE VS. INJECTOR ORIFICE AREA

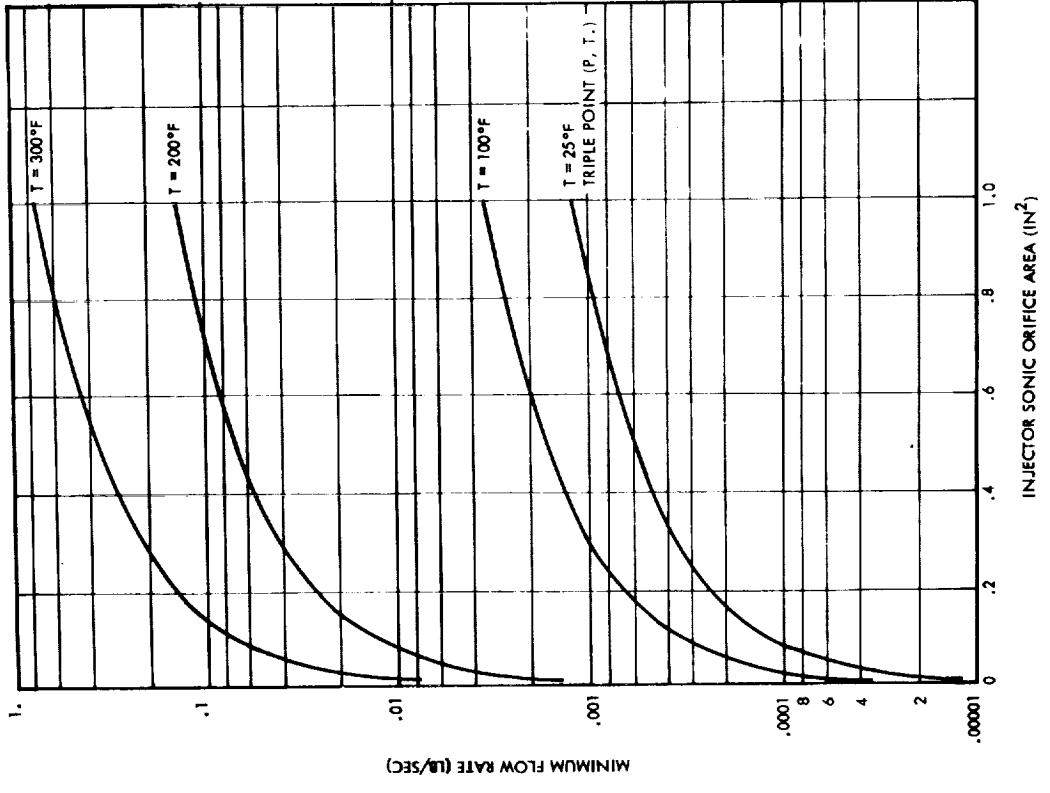


Figure 5-21. N<sub>2</sub>H<sub>4</sub>

CASE II - MINIMUM FLOW RATE VS.  
INJECTOR ORIFICE AREA

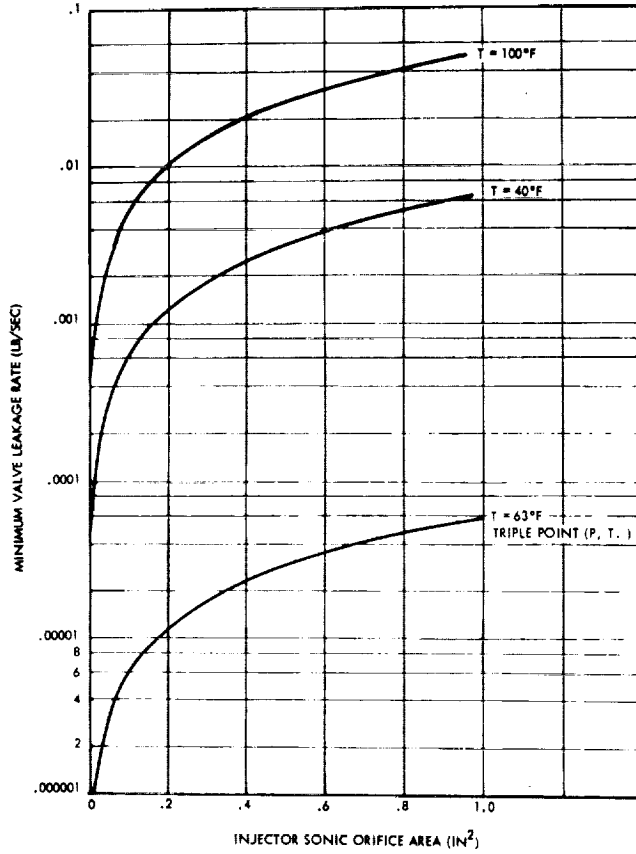


Figure 5-22. MMH

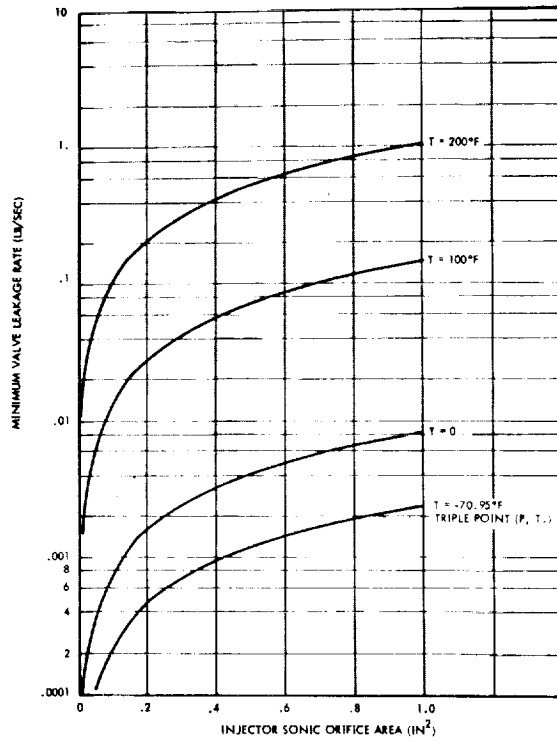


Figure 5-23. UDMH

CASE II - MINIMUM FLOW RATE VS. INJECTOR ORIFICE AREA

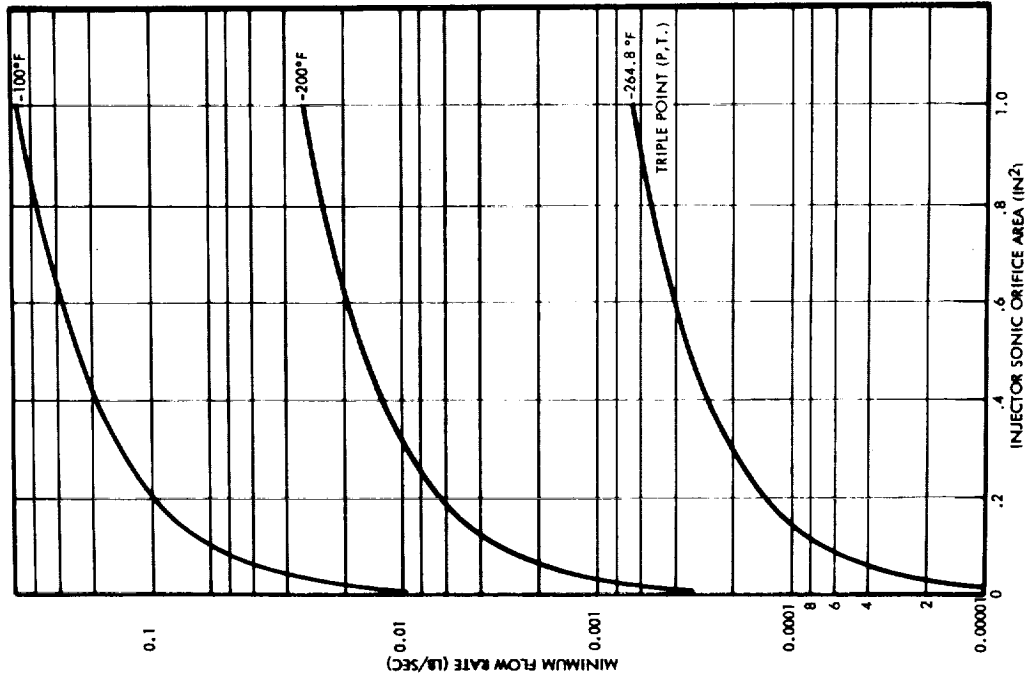


Figure 5-25. B<sub>2</sub>H<sub>6</sub>

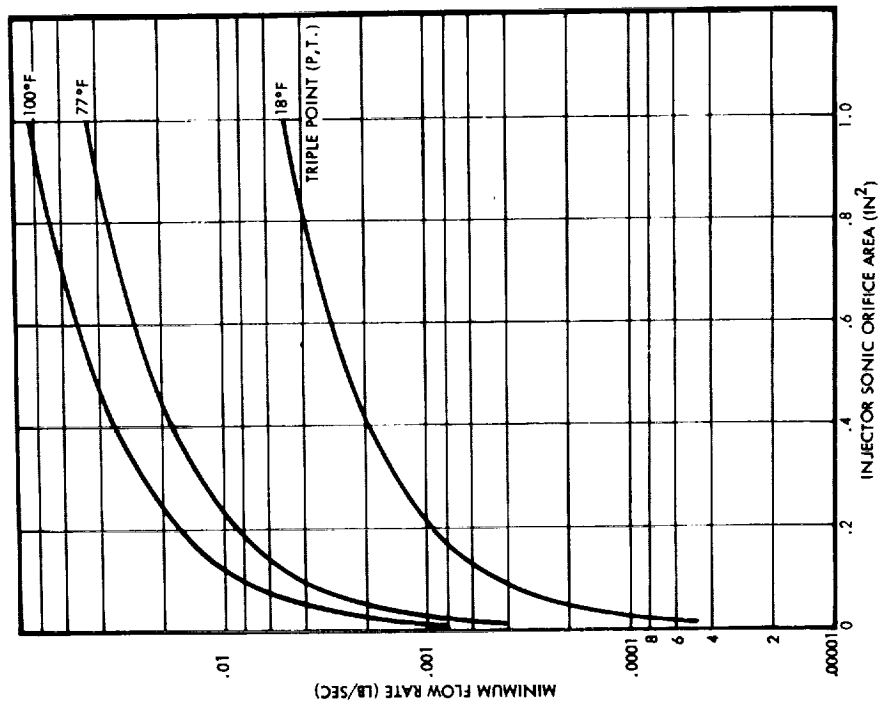


Figure 5-24. Aerozine-50

CASE II - MINIMUM FLOW RATE VS. INJECTOR ORIFICE AREA

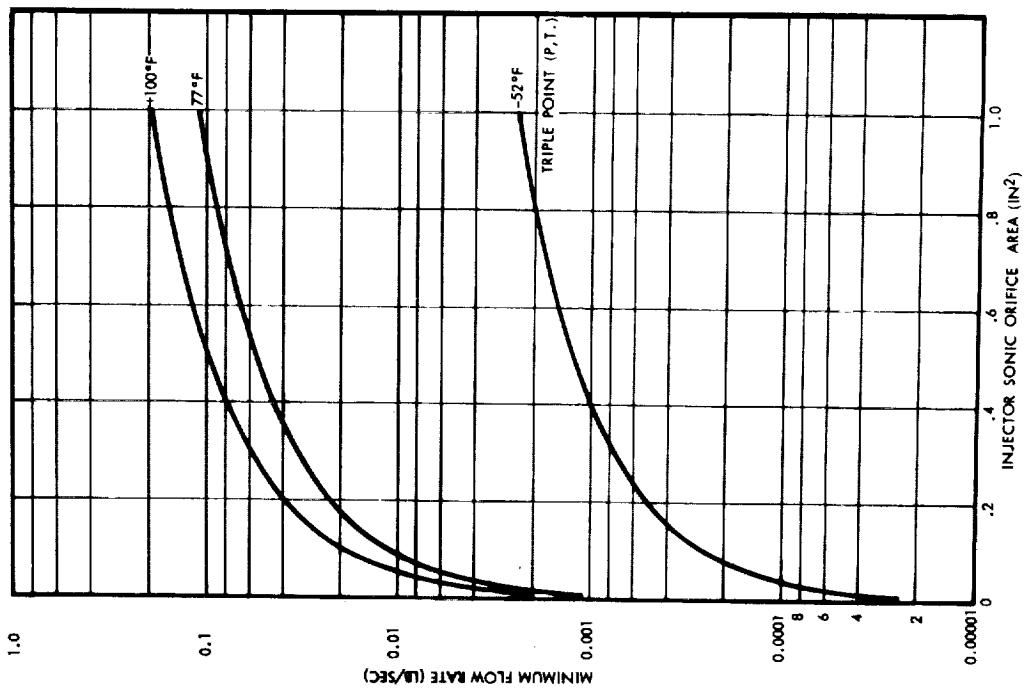


Figure 5-26. B<sub>5</sub>H<sub>9</sub>

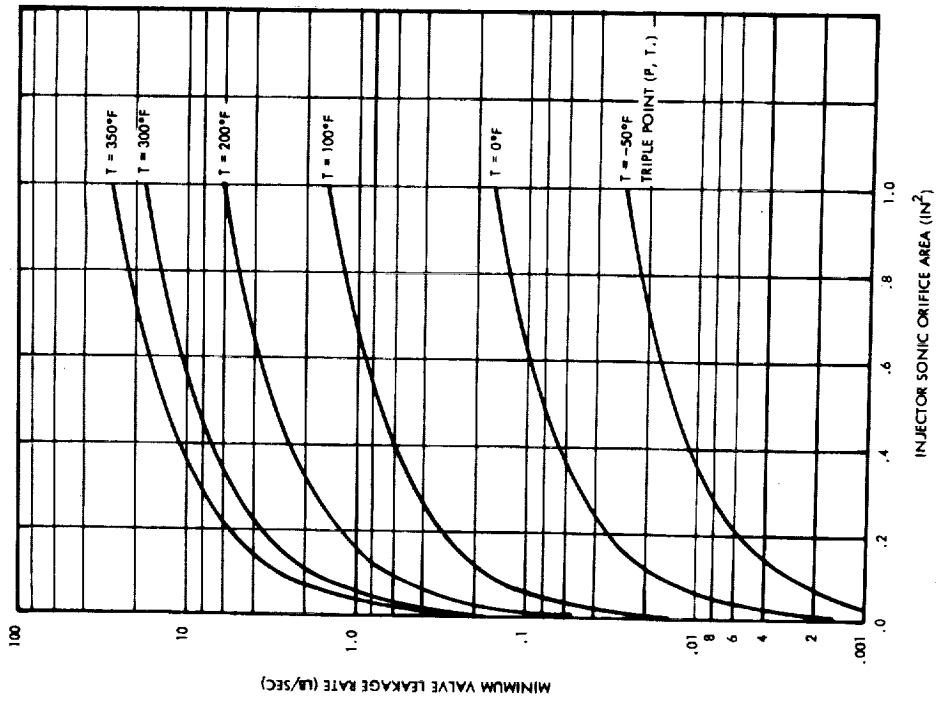


Figure 5-27. CTF

CASE II - MINIMUM FLOW RATE VS. INJECTOR ORIFICE AREA

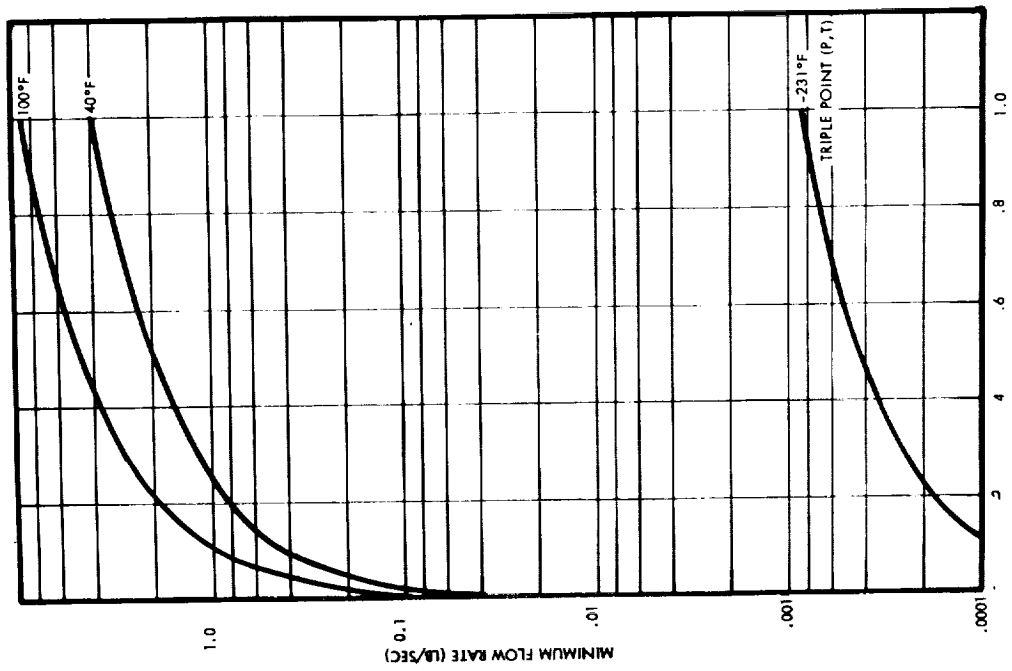


Figure 5-28. C<sub>10</sub>F<sub>3</sub>

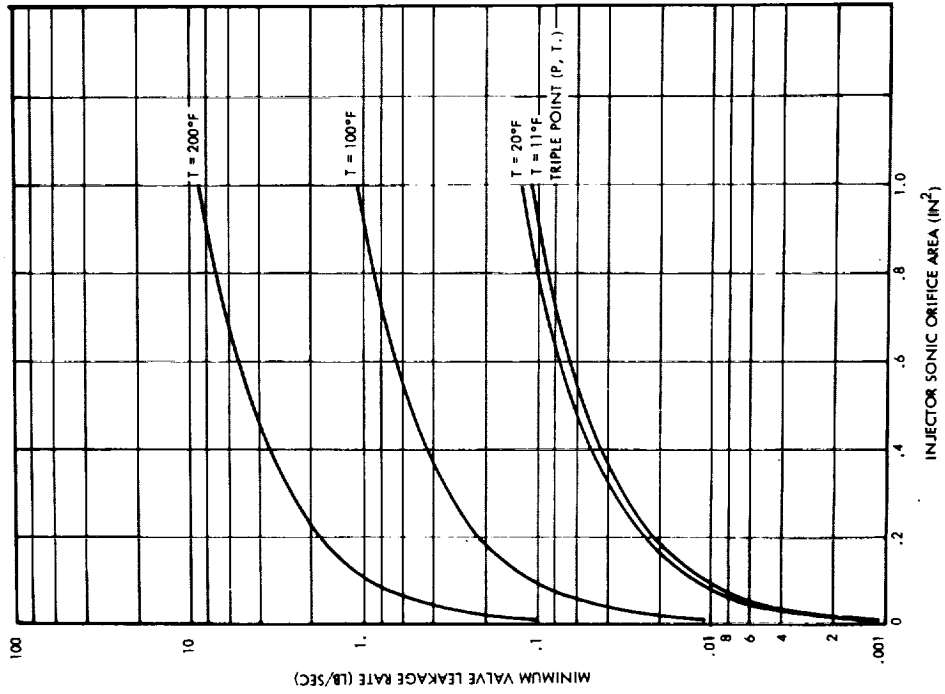


Figure 5-29. N<sub>2</sub>O<sub>4</sub>

CASE II - MINIMUM FLOW RATE VS. INJECTOR ORIFICE AREA

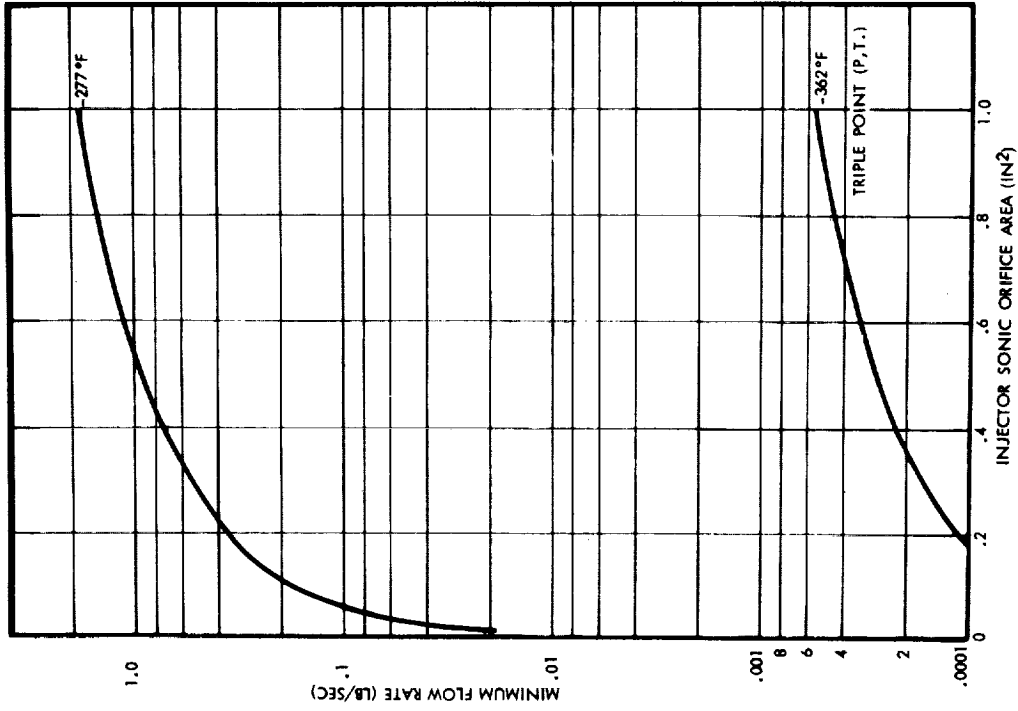


Figure 5-31. LO<sub>2</sub>

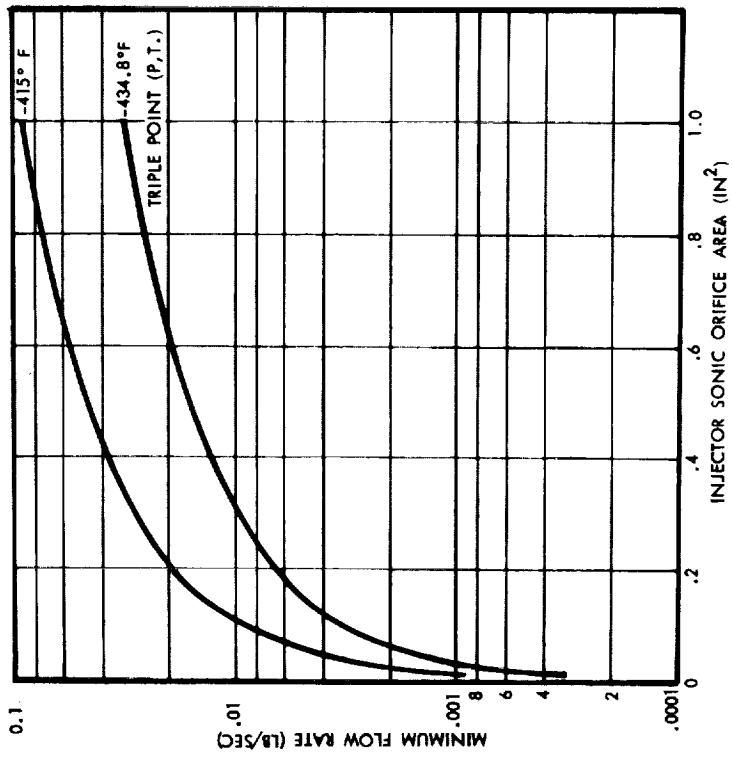


Figure 5-30. LH<sub>2</sub>

CASE II - MINIMUM FLOW RATE VS. INJECTOR ORIFICE AREA

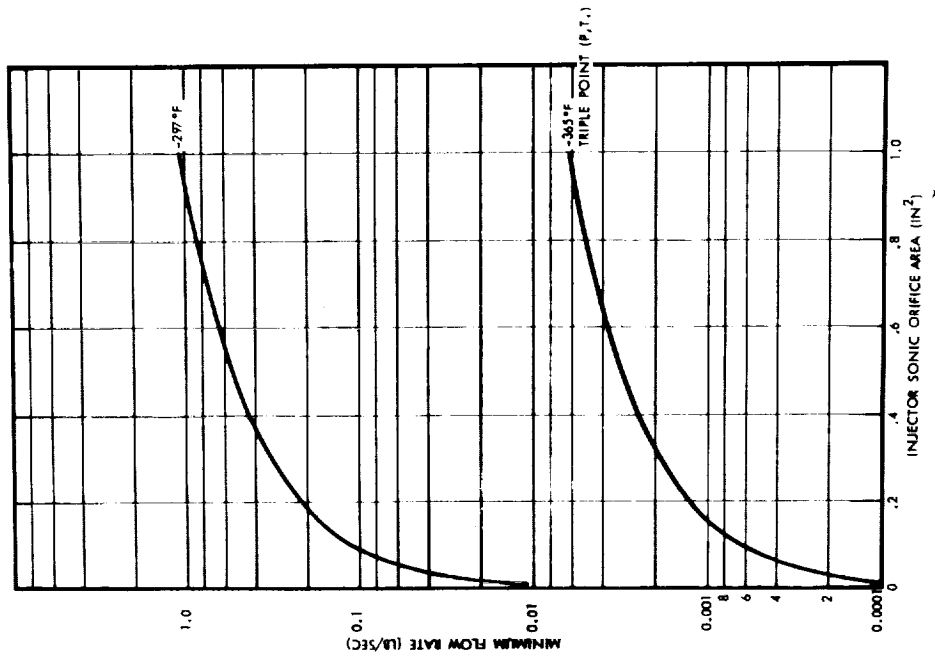
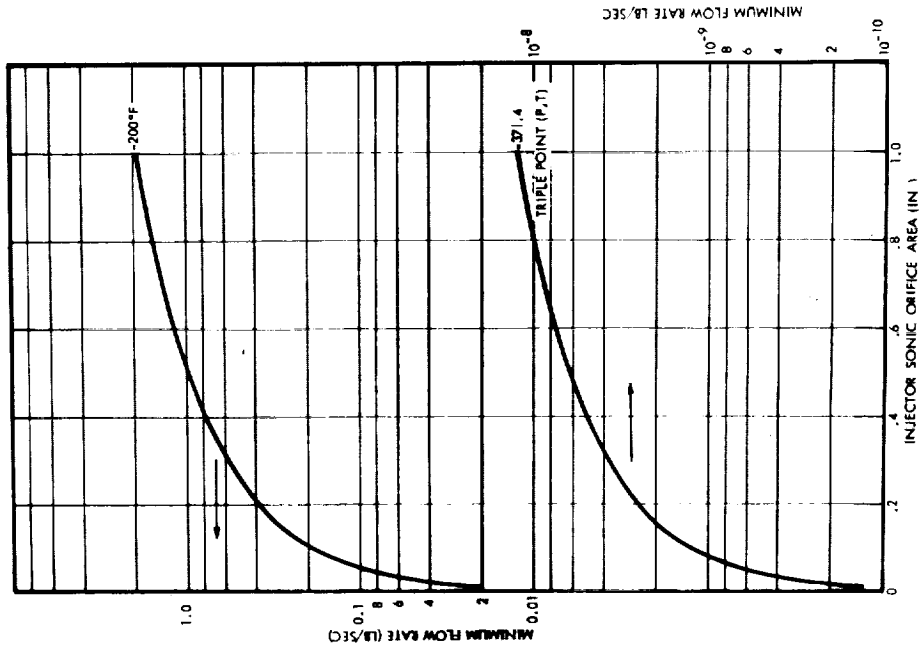


Figure 5-33. OF<sub>2</sub>

Figure 5-32. LF<sub>2</sub>

CASE II - ENVIRONMENTAL HEATING RATE VS. INJECTOR ORIFICE AREA

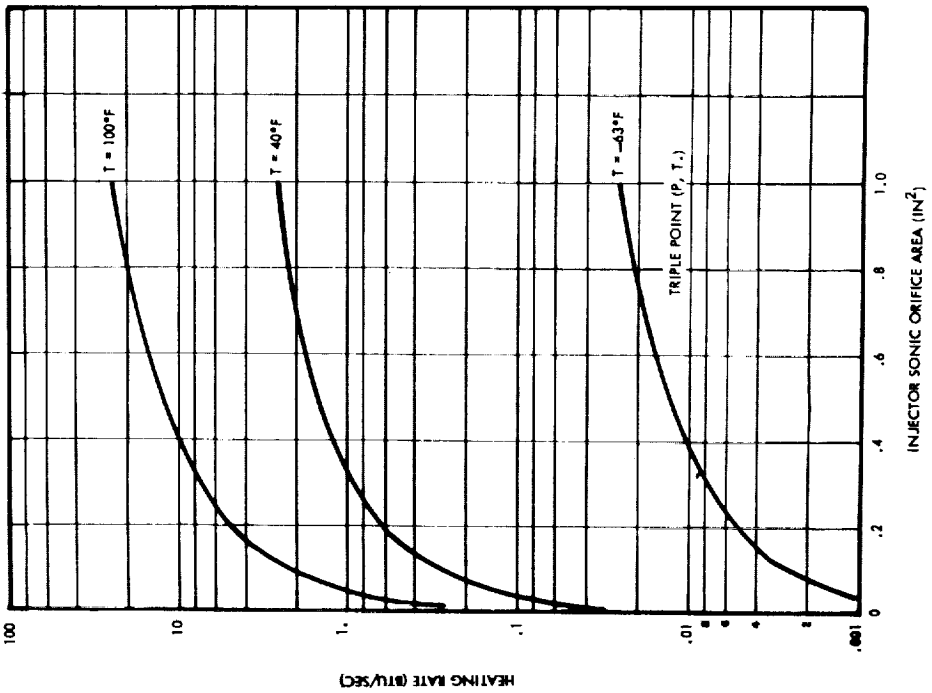


Figure 5-34.  $N_2H_4$

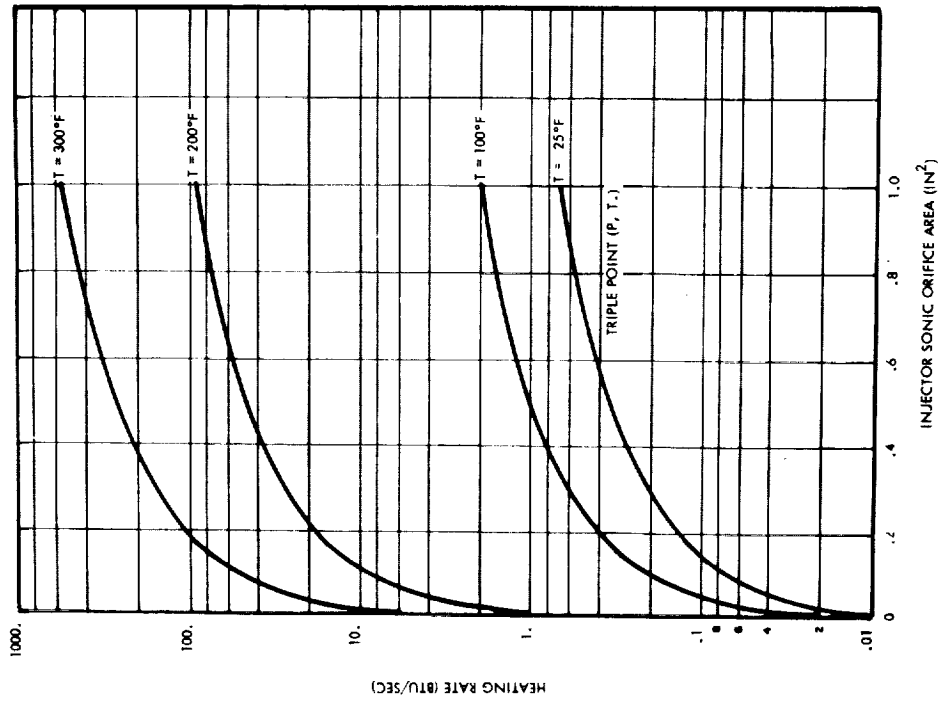


Figure 5-35. MMH



CASE II - ENVIRONMENTAL HEATING RATE VS. INJECTOR ORIFICE AREA

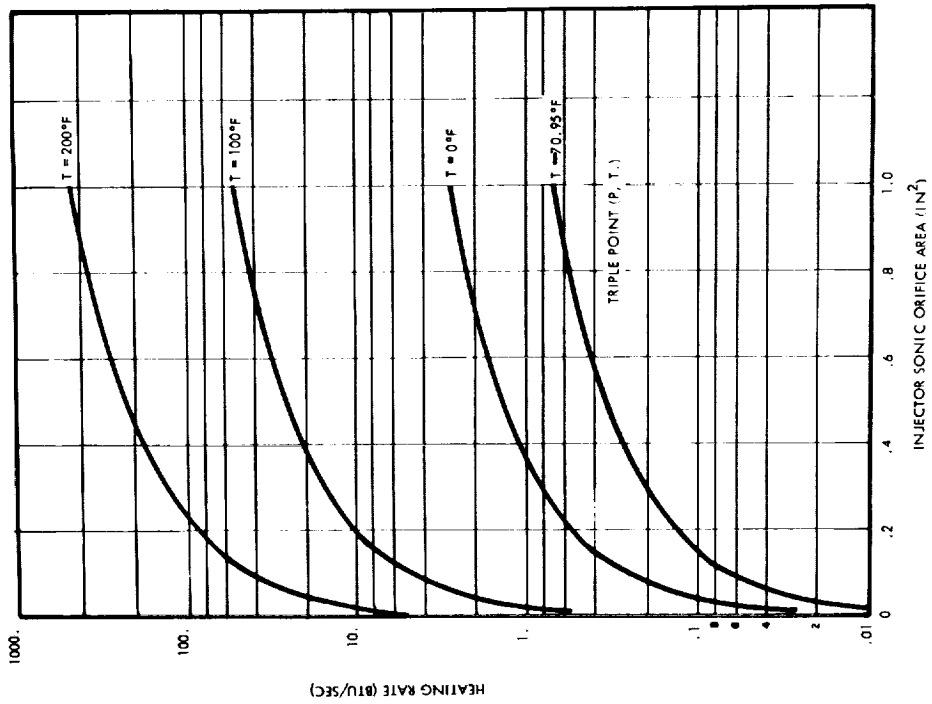


Figure 5-36. UDMH

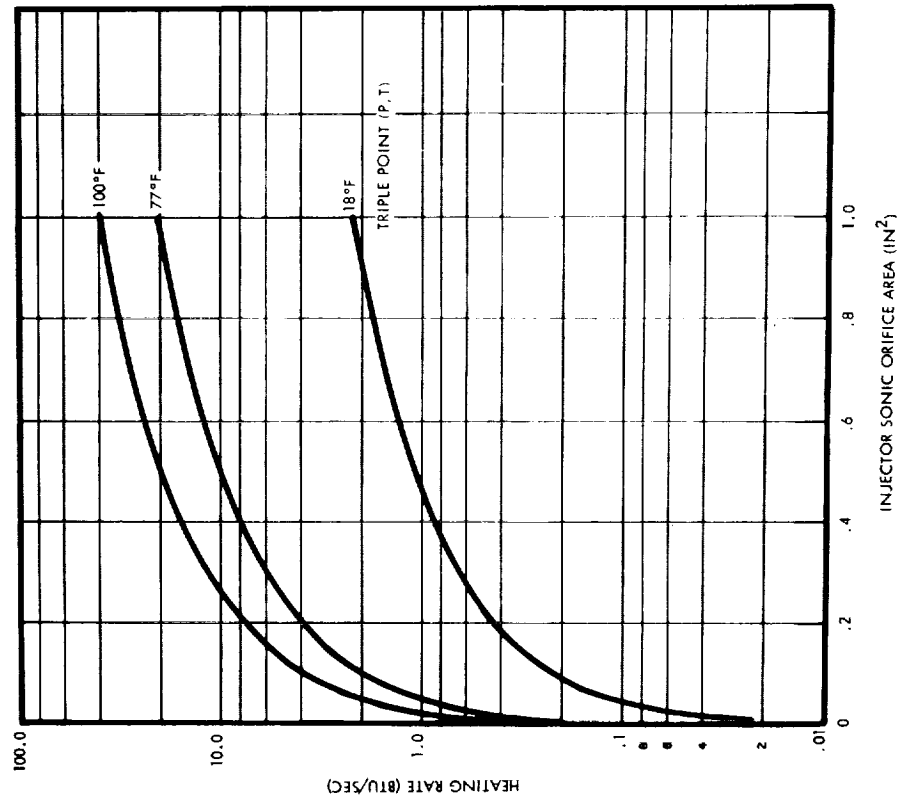


Figure 5-37. Aerozine-50

CASE II - ENVIRONMENTAL HEATING RATE VS. INJECTOR ORIFICE AREA

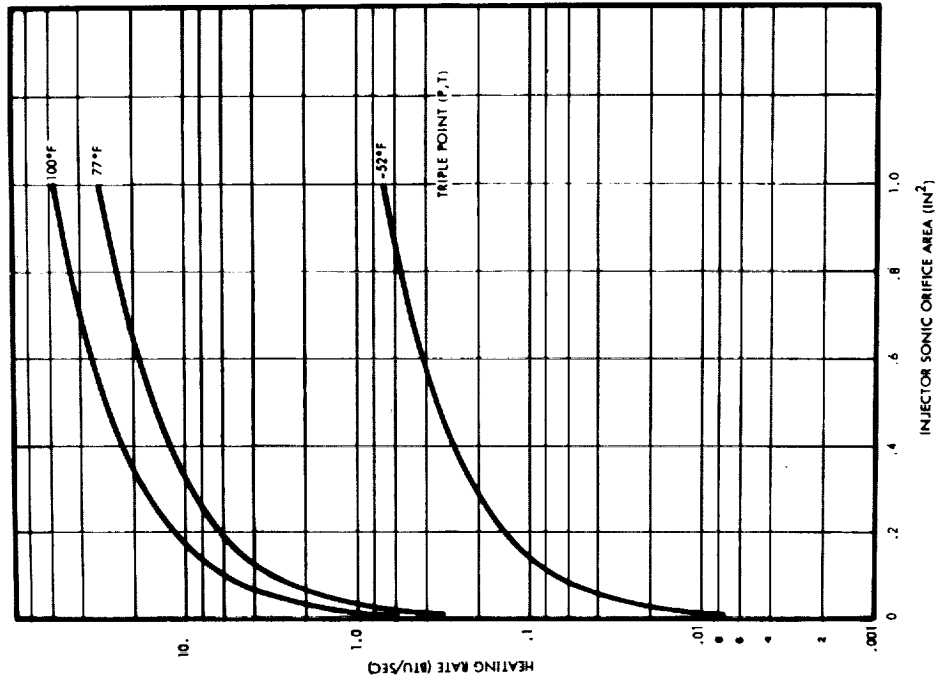


Figure 5-39. B<sub>5</sub>H<sub>9</sub>

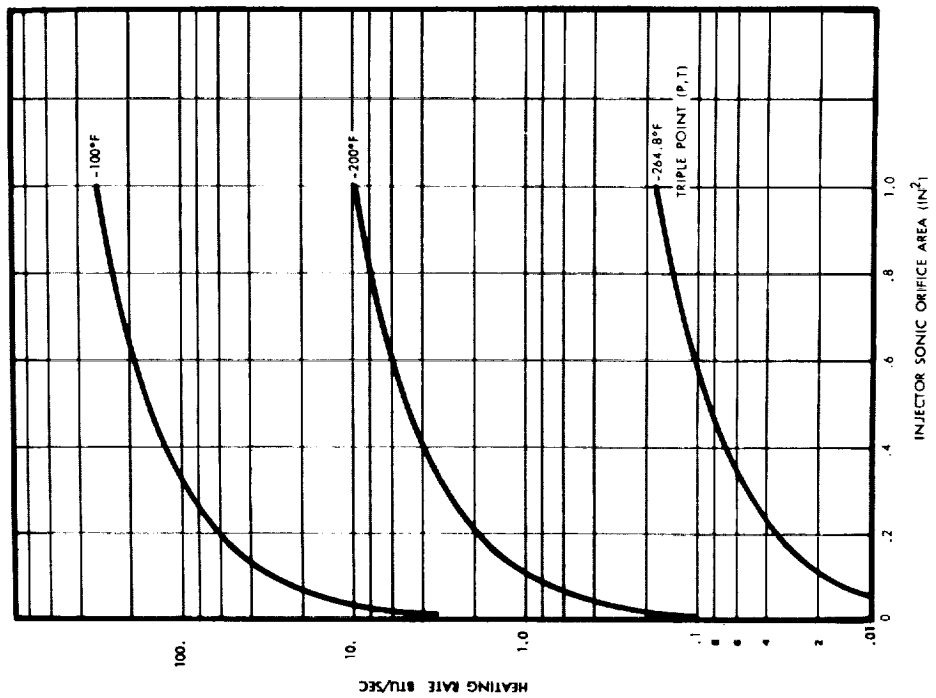


Figure 5-38. B<sub>2</sub>H<sub>6</sub>

CASE II - ENVIRONMENTAL HEATING RATE VS. INJECTOR ORIFICE AREA

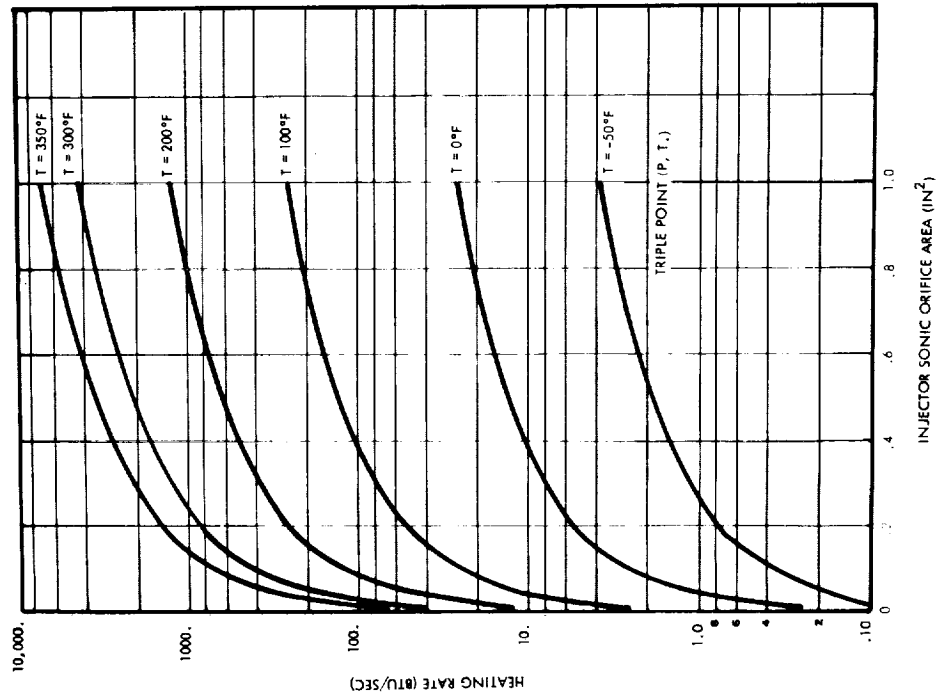


Figure 5-40. CTF

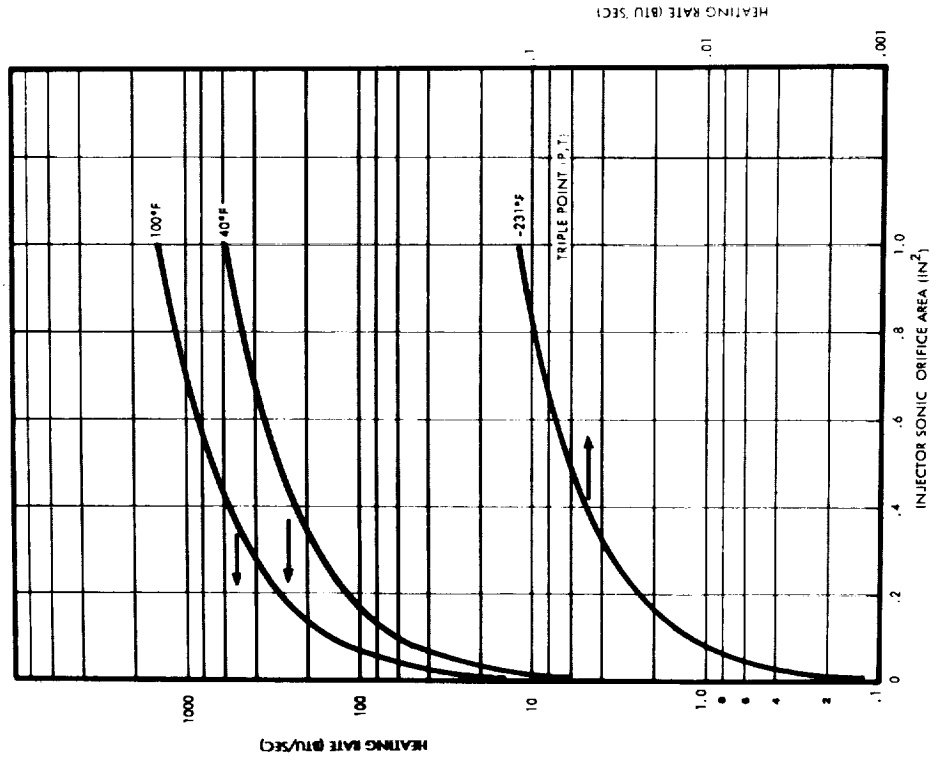


Figure 5-41. C10<sub>3</sub>F

CASE II - ENVIRONMENTAL HEATING RATE VS. INJECTOR ORIFICE AREA

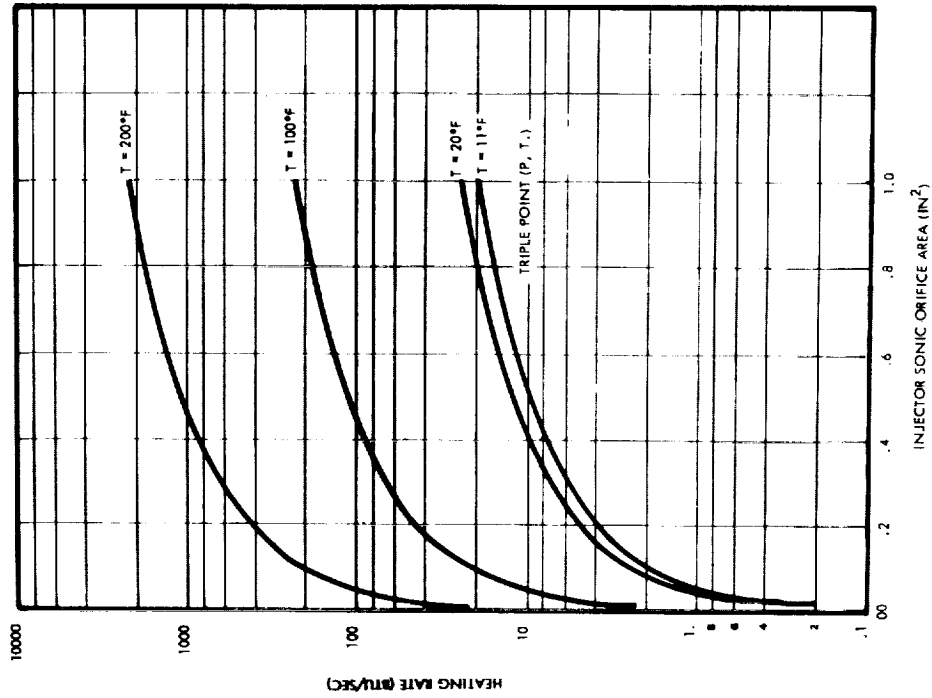


Figure 5-42. N<sub>2</sub>O<sub>4</sub>

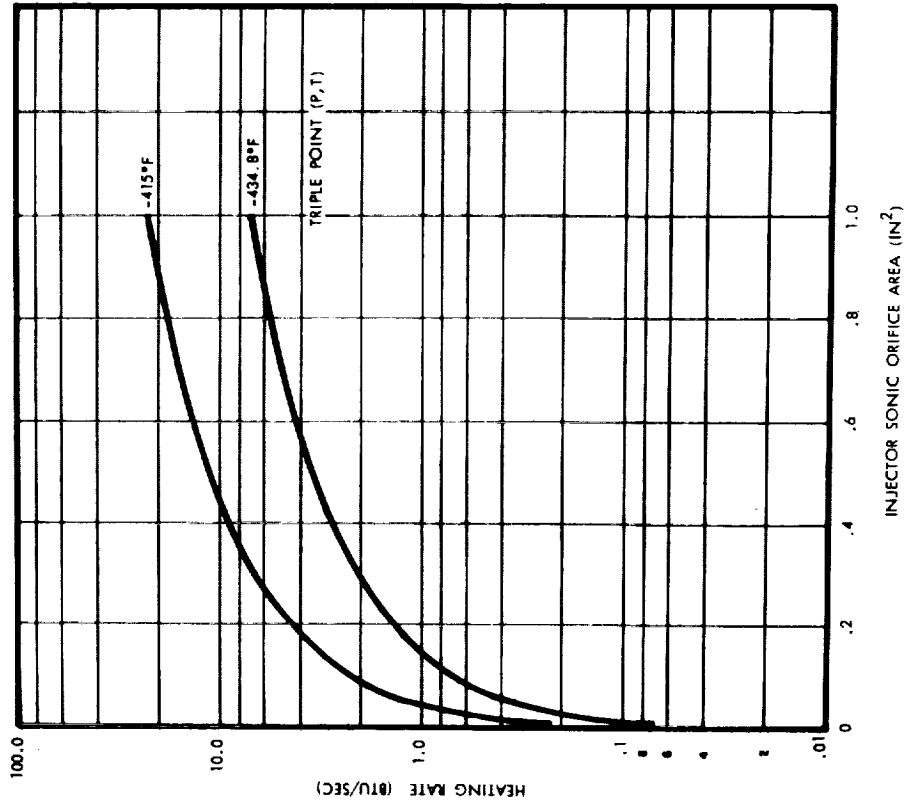


Figure 5-43. LH<sub>2</sub>

CASE II - ENVIRONMENTAL HEATING RATE VS. INJECTOR ORIFICE AREA

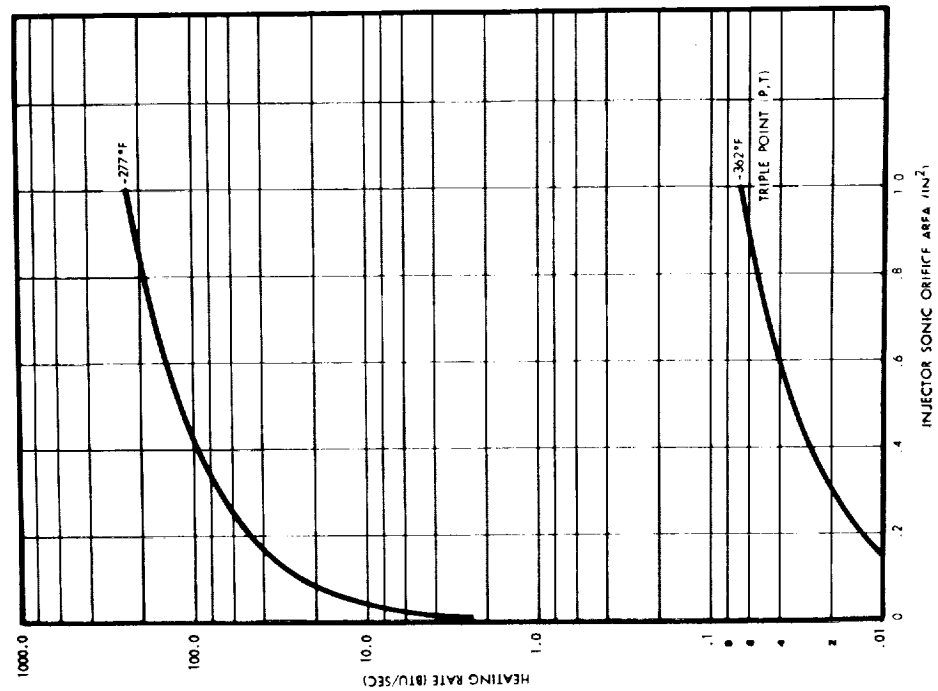


Figure 5-44. LO<sub>2</sub>

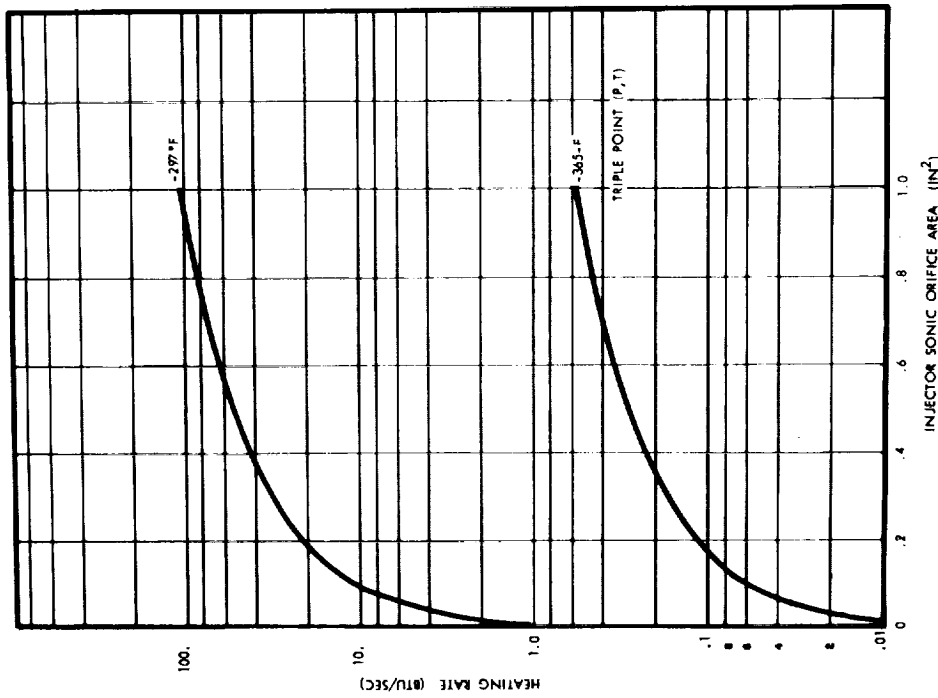


Figure 5-45. LF<sub>2</sub>

CASE II - ENVIRONMENTAL HEATING RATE VS. INJECTOR ORIFICE AREA

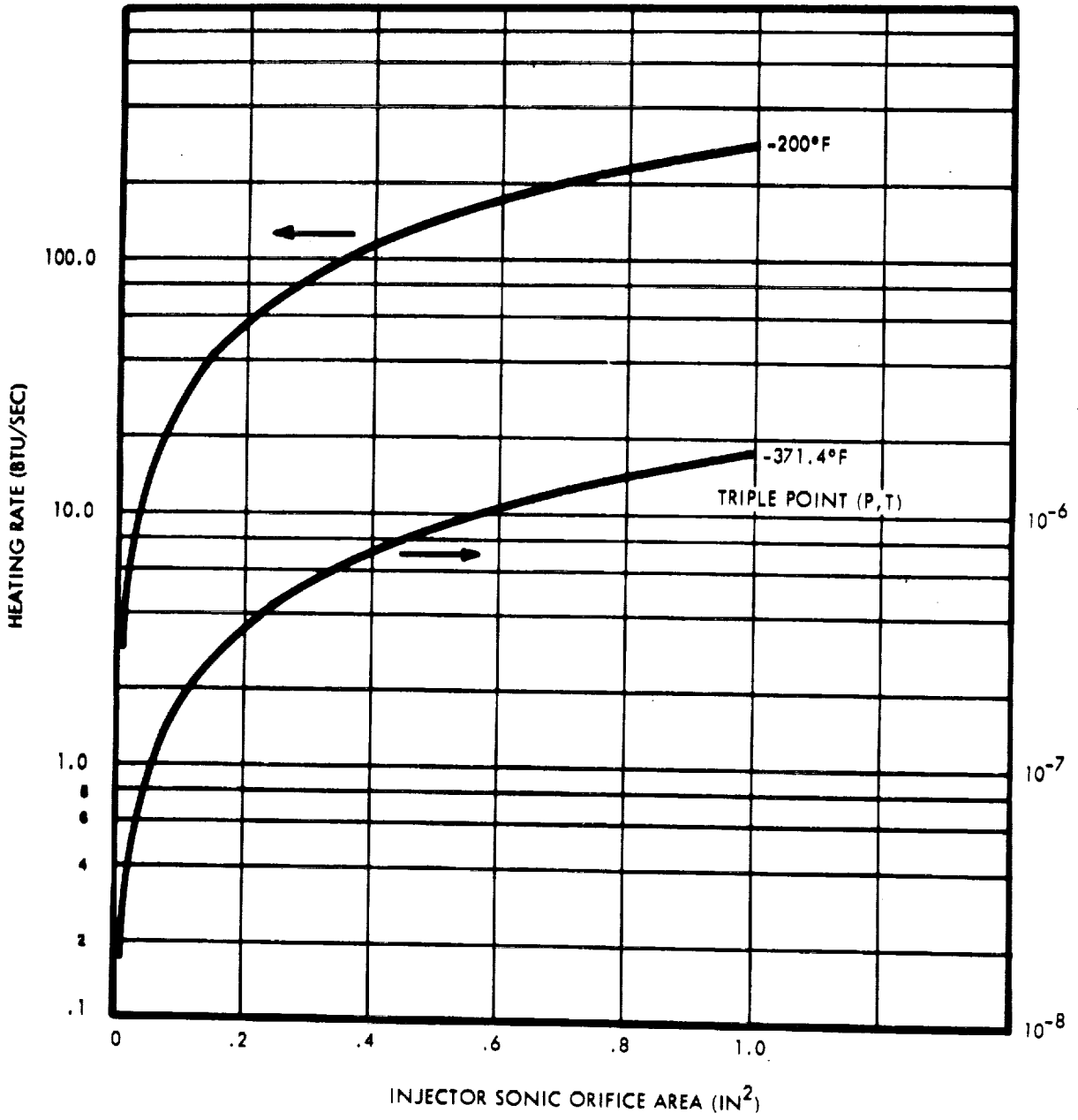


Figure 5-46. OF<sub>2</sub>

### 5.1.7 Permeation Seal Leakage

The objective of this study was to provide a greater understanding of permeation-type leakage phenomena and determine a correlation between liquid and gaseous medium permeation leakage characteristics.

The leakage study has been primarily concerned with the development of the mathematical model to aid in the predicting of leakage through seal glands containing polymeric seals. The analytical model used in the analysis takes geometry into account directly and seal properties by the introduction of the permeability coefficient. A non-dimensional geometry factor to correct for the effects of seal geometry is developed. The analysis presented here is a simplified treatment, and it is felt that a more complete analytic study including the effects of items such as seal stress vacuum conditioning and other material pre-treatments should be undertaken.

5.1.7.1 Analysis - Two basic models which closely approximate leakage past O-ring seals are the radial leakage model shown in Figure 5-47 and the axial leakage model shown in Figure 5-48 (Reference 33).

The boundary conditions for the radial flow model are:

$$C(r_o, z) = C_o$$

$$\frac{\partial C}{\partial z}(r, b) = 0$$

$$\frac{\partial C}{\partial z}(r, 0) = 0$$

$$\frac{\partial C}{\partial r}(r_i, z) = 0 \quad a \leq z \leq b$$

$$D \frac{\partial C}{\partial r}(r_i, z) = \omega \quad 0 \leq z \leq a$$

where  $C$  is the concentration of species which are leaking,  $\omega$  the leakage rate per unit length of seal material, and  $D$  the diffusivity of the seal.

The boundary conditions for the axial leakage model are:

$$C(a \leq r \leq b, 0) = C_o$$

$$\frac{\partial C}{\partial z}(b \leq r \leq R_o, 0) = 0$$

$$\frac{\partial C}{\partial z}(b \leq r \leq R_o, h) = 0$$

$$\frac{\partial C}{\partial r} (R_0, z) = 0$$

$$D \frac{\partial C}{\partial z} (a \leq r \leq b, h) = \omega$$

In the above model, it was assumed that the O-ring completely fills the groove. In reality, this is not necessarily the case.

Therefore, the case to be examined is shown in Figure 5-49. Here the boundary conditions were modified on the left-hand side leaving this edge open to the permeating gas. It can be seen that there is a great deal of similarity between the radial and axial leakage problems. That is, the boundary conditions are similar; namely, a constant concentration on one surface, impermeable boundaries normal to this surface, and diffusion through the remaining surface governed by convection from this surface.

If the dimensions  $b$  and  $c$  are very large compared with  $a$  and the diameter  $R_0$  is also compared with  $a$ , each of the models can be approximated by a model which is semi-infinite in one direction. Such a model is shown in Figure 5-50.

The solution to this problem was obtained as part of a study to analyze the permeation of high density gases and propellant vapors through single layer Teflon or Teflon structure materials and laminations performed by TRW Systems for NASA (Reference 17). The leakage rate for the above geometry is given by:

$$\frac{W}{L} = \omega = \frac{2aD C_d}{h \left[ 1 - \frac{2}{\pi^2} G \frac{a}{h} \right]} \quad (1)$$

where  $\omega$  is given is mass per unit time per unit length. For the particular problem described,  $\omega$  is multiplied by  $2\pi R_0$  ( $L \approx 2\pi R_0$ ) to obtain mass per unit time. The function  $G$  is given by:

$$G \left( \frac{a}{h} \right) = \sum_{h=0}^{\infty} \frac{\left[ I_0 \left( (h + 1/2) \pi \frac{a}{h} \right) \right]}{(h + 1/2)^2} e^{- (h + 1/2) \pi \frac{a}{h}} \quad (2)$$

where  $I_0$  denotes the zero order modified Bessel function. The details of the solution are given in Reference 17.

In the above case, both the radial and axial problems become the same, and the geometry of the problem becomes cartesian. Only the steady-state solution is presented due to the complexity involved in obtaining the transient solution in the original mathematical models.



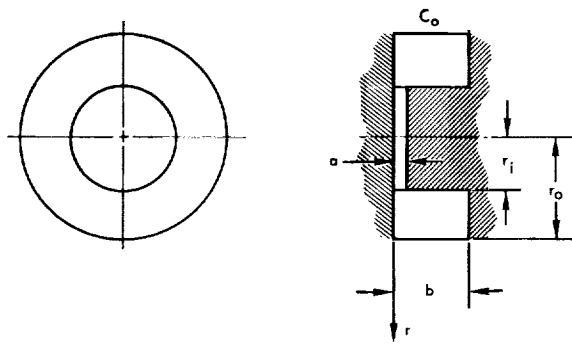


Figure 5-47. Radial Leakage Model

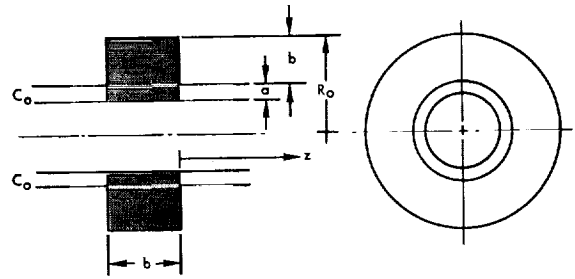


Figure 5-48. Axial Leakage

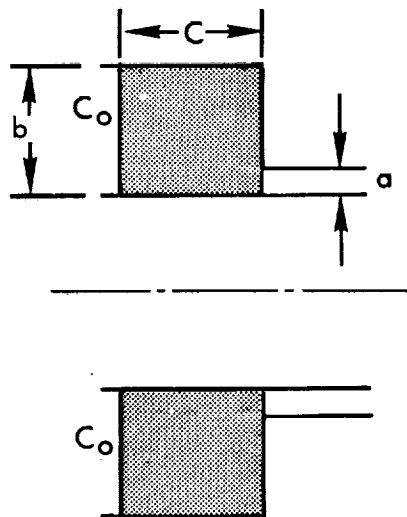


Figure 5-49. Final Permeation Leakage Model

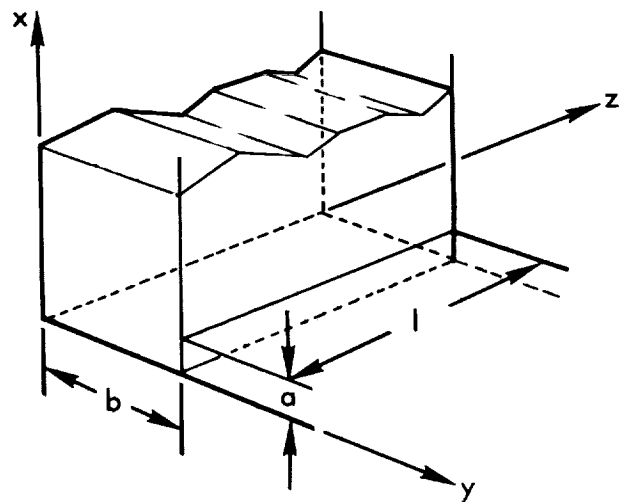


Figure 5-50. Simplified Final Permeation Leakage Model

The above discussion has not included mention of the physical properties of the seal and the leakage fluid. These properties are considered in obtaining the constants D and C<sub>0</sub> for Equation (1).

The mass transfer of a gas from one surface of a permeable material to the other involves

- Absorption on the barrier surface
- Solution in the material
- Diffusion
- Dissolution
- Evaporation at the other side

It is assumed that diffusion is the rate-controlling factor and Fick's Law is used as the starting point of the analysis. The concentration gradient in the seal will be dependent on the solubility of the leakage gas or liquid in the seal material and the pressure difference across the seal. In addition, the diffusivity D will be dependent upon such factors as the stress on the seal, and chemical reaction between the seal and the leakage fluid which may change seal surface characteristics, and on the temperature of the system.

$$\frac{\omega}{DC_0} = \frac{2\alpha}{\left[1 - \frac{2}{\pi^2} G(\alpha)\right]} \quad (3)$$

where  $\alpha = a/h$ , the ratio of the leakage path to the width of the seal. These dimensions are usually known for a gland design, and therefore leakage rate for a given seal configuration may be calculated if one knows the concentration of the fluid to which the seal will be exposed, and the diffusivity of the seal material.

Since most data on seal material is given in terms of permeability rather than diffusivities, we can transform Equation (3) by noting that Henry's Law

$$C_0 = k_p \quad (4)$$

states that the concentration is equal to the product of the solubility constant k and the absolute pressure p. In addition, the product of the solubility constant and the diffusivity is defined as the permeability. Therefore, Equation (3) becomes:

$$\frac{\omega}{S P p} = \frac{2\alpha}{\left[1 - \frac{2}{\pi^2} G(\alpha)\right]} \quad (5)$$

Figure 5-51 shows a plot of  $\frac{\omega}{P_p}$  versus  $\left[ 1 - \frac{2}{\pi^2} G(\alpha) \right]$

indicating the effects of seal geometry on leakage rate.

Sample Calculation - Consider a typical O-ring configuration which can be approximated by the situation pictured in Figure 5-52.

It is seen that  $\alpha = a/h$  is 0.025. From Figure 5-52 for this value of :

$$\frac{\omega}{P_p} = 0.65$$

Assuming that the O-ring is made of natural rubber and that the pressurant is He at one atmosphere, Reference 34 shows:

$$P_p = 23 \times 10^{-8} \frac{\text{cc(STP)}}{\text{cm/sec}}$$

Therefore

$$W = \omega (2\pi R_o)$$

i.e., the rate of flow in cc (STP)/sec is obtained by multiplying through by the circumference of the flange which is sealed. For  $R_o = 1.5$  cm the flow rate,  $w = 2.1 \times 10^{-6}$  cc/sec.

Other pertinent references concerning permeation leakage through sealing interfaces are References 1, 35, 36, 37, 38 and 39. Reference 39 is a particularly useful compilation of permeability data.

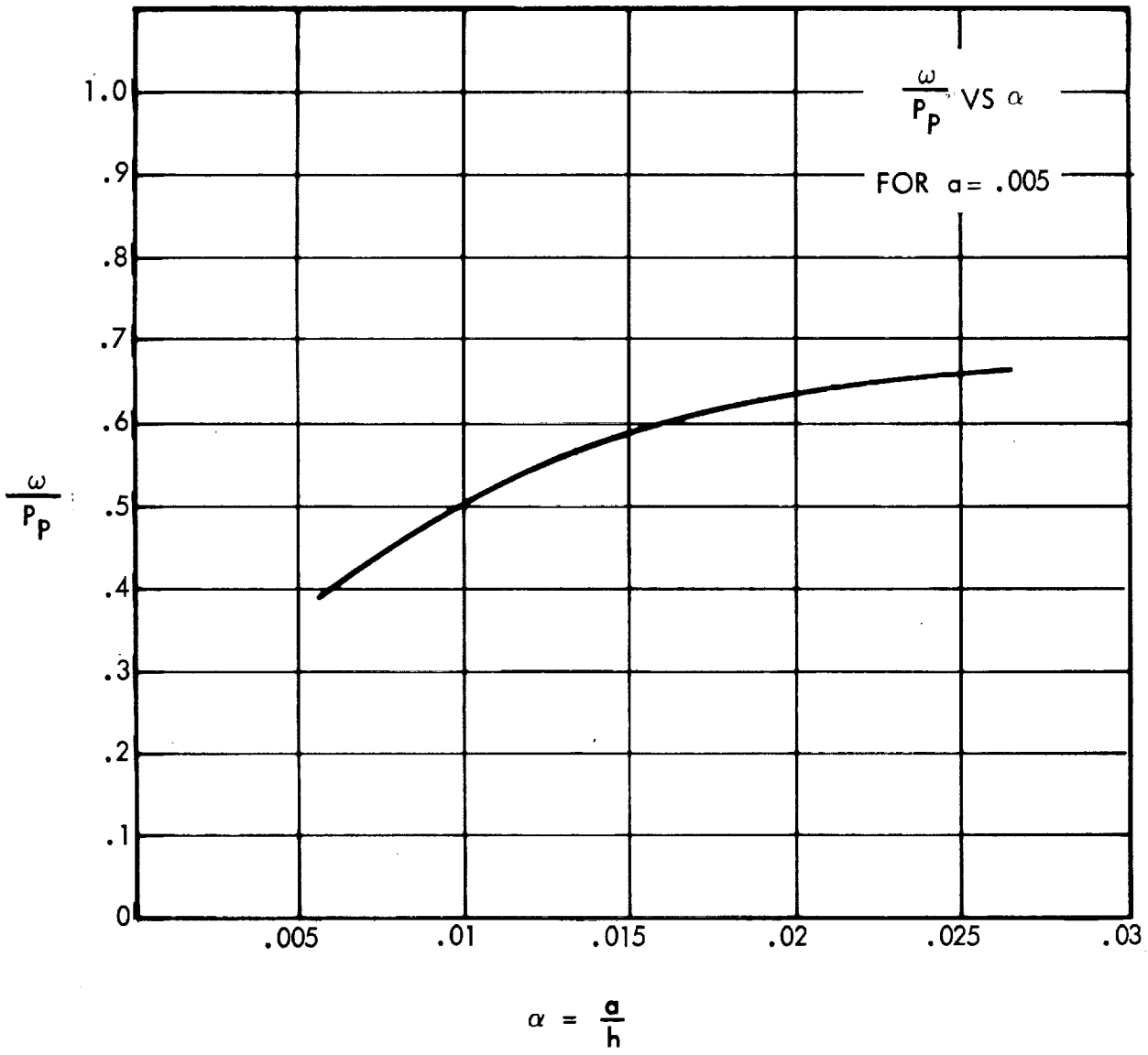


Figure 5-51. Plot of Flow Per Unit Length and Pressure Vs.  $\alpha$ , the Ratio of Gland Thickness to Leakage Gap

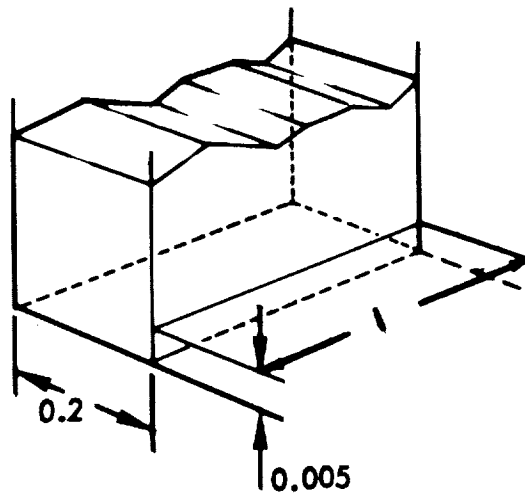


Figure 5-52. Model of Seal Configuration

## 5.2 SEALING TECHNOLOGY

### 5.2.1 State of the Art Evaluation

In 1970, the primary problems associated with static and dynamic seals for spacecraft engines remain much the same as they were in 1962. These problems include:

1. Elastomers are the most reliable means of effecting a seal, but elastomers are generally not satisfactory for use with cryogenic propellants or for the more reactive propellants such as  $N_2O_4$ ,  $OF_2$ ,  $LF$  and  $B_2H_6$ .
2. Plastics, such as Teflon, are compatible in some instances, but lack the resilience of elastomers necessary for effective sealing.
3. High temperature and some particularly difficult propellants such as  $LF_2$  and  $OF_2$  require all-metal seals.
4. Permeability of seal materials remains a major limitation to seal design. There have been no dramatic breakthroughs in sealing technology during the past eight years, but three items stand out:
  - In lieu of major breakthroughs in seal materials technology, the art of seal design has seen many design innovations to make seals work under difficult circumstances. These include the use of metal springs in Teflon seals to substitute for the lack of resilience in the plastic and the design of spring-type metal seals such as North American's NAFLEX. There have also been major advances in the mechanical design of elastomer seals for essentially incompatible applications, such as the use of butyl rubber in  $N_2O_4$  service in Titan II applications. Here the O-ring was designed to completely fill the groove (100% fill). This minimum propellant exposure has given satisfactory performance for over one year (Reference 40).
  - Both the NASA and Air Force have sponsored advanced technology seal program which have studied in detail the question of how and why seals seal. Although many questions remain unanswered and much more investigation is required, the efforts such as those reported in References 6, 7, 8, 9, 41 and 42 have provided far more insight into sealing and leakage phenomena than was available eight years ago.

- The AVT Program efforts have strived to fill a gap between the largely empirical seal improvement efforts behind the seals currently flying and the highly theoretical sealing phenomena studies by conceiving totally new sealing approaches and experimentally investigating their feasibility. These results are compiled in the remainder of Section 5.2

Sections 6.3 and 6.4 of the Aerospace Fluid Component Designers' Handbook (Reference 43) provide a good summary of the state of the art of static and dynamic seals, although this material was originally published in 1965. The NASA is presently preparing a comprehensive evaluation of the state of the art of liquid rocket engine seals as part of the Space Vehicle Design Criteria program. The liquid rocket engine seals monograph on Disconnects, Couplings, Fittings, Joints, and Seals is now in preparation under the direction of the Design Criteria Office of NASA Lewis Research Center, and when completed should accurately represent the current status of liquid rocket engine seals.

An example of the present state of the art is a current program to search out specific promising compounds and to evaluate their applicability to fluid system seals while operating with liquid oxygen and liquid hydrogen (Reference 44). This effort is being conducted under Contract NAS 9-10481 for NASA Manned Spacecraft Center, and is directed toward two basic problems associated with seal materials for these propellants. The first is that materials of closely crosslinked polymer chains (elastomers at room temperature) generally provide good physical properties but are not compatible with  $LO_2$ . The second is that materials that are compatible with  $LO_2$  are those which have, at best, only a loose crosslinking (plastics), resulting in creep under load and other undesirable physical properties. It may be seen from the necessity for program such as this that there is also a need for further investigations of advanced concepts such as those described in the following sections.

### 5.2.2 Teflon Seal Improvements

Teflon is an excellent engineering material and finds many applications in valves and other components used on spacecraft. However, two of its characteristics, the tendency to cold flow under load and its permeability to some fluids, especially  $N_2O_4$ , limits its applicability in some cases. Therefore, a study was conducted in 1963 (Reference 17) to determine if a formulation could be produced that would have improved cold flow and permeability characteristics without sacrifice of other qualities.

A search of the literature disclosed that many mixtures of Teflon and other compounds, e.g., glass fibers and metal powders had been produced, but the test data available indicated that further improvements were needed to reduce the cold flow characteristics to acceptable limits.

5.2.2.1 Initial Metal-Teflon Composite Studies - Experiments were conducted in which Teflon powder and steel wool fibers were mixed and compacted into discs of 2.0 inches diameter x 0.08 inch thick. Pressures in the order of 30,000 psi were used in the molding operation, and some of the samples were sintered while under pressure at 740°F.

A test fixture was manufactured to determine the permanent set resulting from load, and several discs for two of the mixtures were tested. The results are as follows:

Using a unit bearing stress of 2000 psi over a 24-hour period, the permanent set varied from 0.5% for a mixture of 90% steel and 10% Teflon to 3% for a mixture of 20% steel and 80% Teflon. For comparison, a permanent set of 6% for a mixture of 60% bronze and 40% Teflon represented the best commercial compound then obtainable.

A second test fixture was used to evaluate the effectiveness of the material for use in gasketing. The fixture clamped a ring of the material measuring 2.0 inches diameter x 0.10 inch landwidth x 0.08 inch thick between two flanges. Nitrogen pressure of 2000 psi was applied to the fixture for a period of 24 hours, after which a leakage measurement was made. The pressure was then reduced to zero, and then raised again to 2000 psi. The test was continued in this manner for 14 days. No leakage was recorded, and there was no observed tendency of the material to flow. This was the full extent of the preliminary Teflon seal study.

The literature search also disclosed that some experiments had been conducted with Teflon and gold foil in an attempt to reduce the permeability of Teflon to  $N_2O_4$ .<sup>\*</sup> On the basis of the favorable results obtained in this work, a procedure was devised to disperse finely divided gold powder in the mixture of the Teflon and steel wool. Unfortunately, procurement delays prevented the conclusion of this portion of the development.

It must be noted that the tests conducted on the sealing material were necessarily minimum in nature because of the time limitations of the program. Although the test results obtained were very encouraging, much additional work is required in this area.

In 1964, an additional investigation (Reference 45) was made to determine the permeability characteristics of metal-Teflon composites as seal materials.

5.2.2.2 Gold-Teflon Composite - Gold powder No. 1 in the amount of 15% by volume was added to Teflon powder which was then compressed in a mold to 10,000 psi. The composite was removed from the mold and heated in a furnace to temperatures between 710°F and 740°F for one-half hour. After removal from the furnace the composite was replaced in the mold and subjected to the dead weight of the compressing piston. It was found in testing pure Teflon samples that it was necessary to add pressure to the sample during the cooling phase to prevent warping.

Helium leakage tests were conducted to determine permeability characteristics. The composite was placed in a fixture and helium at low pressure was impressed against one side of the composite while the downstream side was evacuated and connected to a mass spectrometer. Helium leakage exceeded that which would be quantitatively measured by the mass spectrometer. It was found that helium leakage was greater through the composite than through pure Teflon. Gross leakage probably occurred because an adequate mechanical or chemical bond could not be achieved between the gold particles and the Teflon.

---

\* Quantum, Incorporated, Wallingford, Connecticut.

5.2.2.3 Iron-Teflon Composite (20% Fe by volume) - Iron-Teflon composites were also tried in the course of testing. Pressures of 10,000 and 20,000 psi and temperatures of 710°F and 740°F were used in the composite preparation. Vacuum could not be maintained across the composite sample; therefore, the helium mass spectrometer could not be used.

5.2.2.4 Silver-Teflon Composite - A silver Teflon composite was obtained through the courtesy of the Westinghouse Corporation and subjected to a helium leak test. As with the iron metal composites, vacuum could not be maintained across the composite sample.

5.2.2.5 Conclusions - These very preliminary studies showed that although improved permanent set properties could be obtained with metal-Teflon composites, permeability problems became worse than with pure Teflon, indicating a need for extensive process development if such composites were to be used for seals.

### 5.2.3 Wet Seal Study

#### 5.2.3.1 Initial Phase

Introduction - The purpose of this effort was to study the effects of surface tension on leakage by using liquid metal coatings between metal sealing surfaces and was initially reported in Reference 45. Zero leakage has been defined to be a leakage of less than  $10^{-8}$  std cc/sec helium (Reference 2). Metal-to-metal seals maintaining zero leakage are possible by plastically deforming soft metals. Static seals such as those used in flare tube fittings and flange gaskets utilize plastically deformed materials. Such seals are not recommended, however, for reuse after the joint is broken. When a large number of valve poppet cycles are required, soft metal sealing materials which are plastically deformed are unacceptable due to their low cycle life. The result is the common use of metal-to-metal seats which involve no plastic deformation and require hard seat materials with extremely fine surface finishes. A major problem with such a seat is the inherently high leakage rate and extreme sensitivity to contamination. (Reference 46 and subsequent reports describe recent Air Force attention to the problem as an outgrowth of the poppet and seat program described in References 7 and 8.)

Theory - When two highly polished surfaces are placed in contact, a small volume of porous structure can be visualized as existing between the two contacting surfaces. Numerous leakage paths result from the microscopic nonuniformity between the two surfaces.

Utilizing this concept, sealing by a liquid metal can then be visualized as the closing of the capillary leakage paths by the liquid metal. The force necessary to overcome the retention of the liquid or break down the seal is directly related to the capillary forces.

The capillary force between a liquid-solid interface depends upon the manner in which they meet. Between a liquid and a solid the contact angle is the angle between the solid and the tangent to the liquid at the point of contact. The surface tension of the solid and liquid phases and interfacial tension



between these phases determined the magnitude of the contact angle and thus the capillary force. In a confined volume the contact angle results in the formation of a meniscus. The contact angle (Reference 47) is directly related to wettability of the liquid which is described at equilibrium and neglecting gravitational effects as:

$$\lambda_{SV} = \lambda_{LS} + \lambda_{LV} \cos \theta \quad (1)$$

where:  $\lambda_{SV}$  = surface tension solid: vapor  
 $\lambda_{LS}$  = interfacial tension liquid: solid  
 $\lambda_{LV}$  = surface tension liquid: vapor

For complete wettability  $\theta = 0^\circ$  so that:

$$\lambda_{SV} = \lambda_{LS} + \lambda_{LV} \quad (2)$$

The general equation relating the pressure difference across a curved liquid surface is:

$$\Delta P = -\lambda \left( \frac{1}{R_1} + \frac{1}{R_2} \right) \quad (3)$$

where  $\lambda$  is the interfacial tension of the liquid surface film and  $R_1$  and  $R_2$  are the radius of curvature of a curved liquid surface.

For closely spaced parallel plates

$R_2 = \infty$  and  $R_1 = D/2$ ; the above equation reduces to:

$$\Delta P = -\lambda 2/D \quad (4)$$

where perfect wetting is assumed ( $\cos \theta = 1$ ).

This equation is plotted in Figure 5-53.

Figure 5-53 illustrates the significance of surface finishes for wet seals. Surface finish is important in reducing the spacing between parallel plates. For both mercury and gallium alloy liquid metal systems at room temperature, the surface tension is greater than  $500 + \text{dynes/cm}^2$ . Any contaminants present in the liquid phase or on the surface of the solid will, in general, tend to degrade wettability by lowering the surface tension.

While more rigorous mathematical solutions are available (Reference 48) for treatment of idealized geometries, their contribution does not provide more direction to the engineering problem than this simple model.

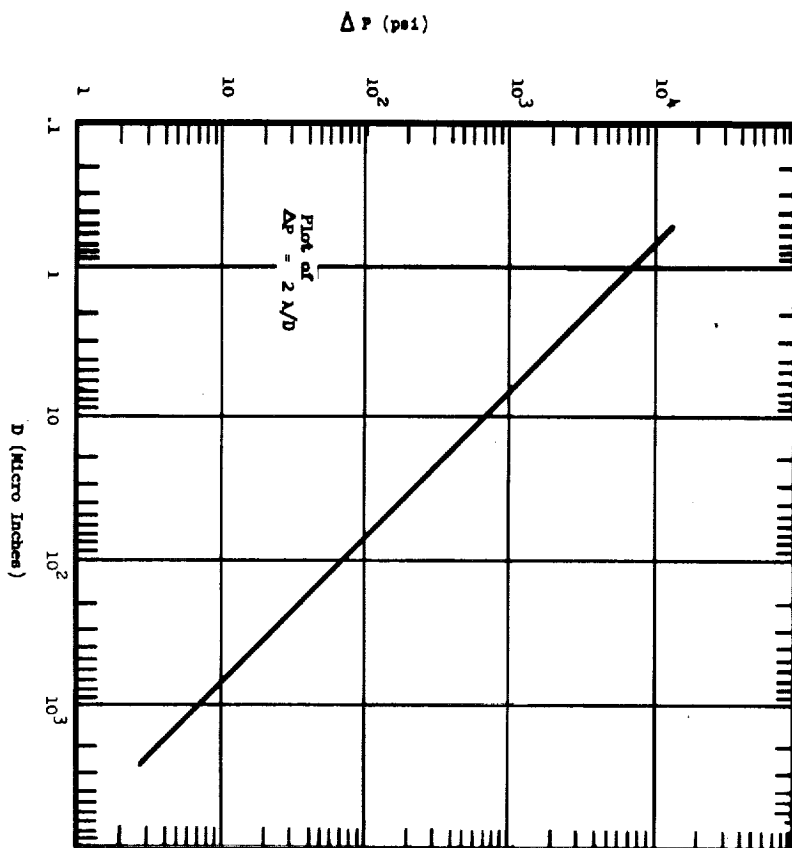


Figure 5-53. Capillary Pressure  $\Delta P$  Versus Spacing  $D$  Between Parallel Plates, Based on Surface Tension of  $\lambda = 500$  dynes/cm.

Liquid Metals and Literature Review - A partial review of the literature was made concerning applications of liquid metals to surfaces. Particular attention was given to physical properties of liquid metal systems, wettability characteristics and wetting techniques, corrosiveness, and known compatibilities, and related usage (Reference 49). As a result of the initial review, two liquid metal systems were selected for use in the experimental phase. These are mercury-indium-thallium and gallium-indium-tin. The primary considerations in selecting these two systems were their generally noted wettability for a wide range of materials and their liquid state at room temperature.

The Mercury-Indium-Thallium system was purchased from the Victor King Materials Laboratory as Viking LS232 and the Gallium-Indium-Tin from United Mineral and Chemical Corporation as UG-1 Alloy.

Compatibilities - As the surface finish is important to the sealing effectiveness of liquid metals, reactions between the liquid metal and the wetted surface which would produce roughening are of concern. Roughening could occur in the form of etching, pitting, or material buildup through amalgamation and alloying. The Aluminum Company of America (Reference 50) summarizes the compatibilities of gallium as readily alloying with all metals at elevated temperatures and forming alloys with tin, zinc, cadmium, aluminum, silver, magnesium, copper, and others at room temperature.

Tantalum resists attack up to 842°F and tungsten to 1472°F. Graphite is not attacked by gallium at any temperature and silicon base refractories are satisfactory to 1832°F. Gallium reacts with sulphuric, nitric, perchloric, and hydrochloric acids and sodium hydroxide. Aqua regia and concentrated caustics attack pure gallium very rapidly. Alcoa (Reference 51) also indicates gallium is being used as a sealant for glass joints in laboratory vacuum equipment, in particular with mass spectrometers. The Metals Department of United Mineral and Chemical Corporation (Reference 52) likewise indicates the application of gallium for vacuum seals. United Mineral indicates mild steel, stainless steels, such as the 14 percent chrome and 18/8 nickel/chrome types, Monel, nickel, copper, and brass have been wetted and left for six weeks at room temperatures and 212°F. All metals were found intact with the exception of copper and brass, which showed slight corrosion at 212°F. At temperatures over 572°F these metals are attacked by gallium and its eutectics. Columbium resists corrosion up to 842°F, beryllium up to 932°F. Tungsten, rhenium, and zirconium are not attacked at temperatures up to 1472°F. Beryllia, alumina, and silica resist attack at temperatures of 1832°F and higher. United Mineral also reports the ability of the liquid metal to withstand atmospheric pressure across a  $10^{-3}$  cm gap provided the liquid metal wets and bridges the sides continuously. They report the application of such a seal at  $10^{-7}$  torr vacuum retained a 3 psi helium pressure which corresponds well with the curve of Figure 5-53.

The mercury-thallium alloy is highly reactive with oxygen and will rapidly degrade to form thallium oxides or hydroxides. Boag (Reference 53) has found treatment with purified hydrogen can reduce the absorbed oxygen and prevent or retard additional reaction. It is the formation of the thallium oxide which probably produces the widespread wettability of this liquid metal system for most materials. For sealing purposes the presence of oxides is not clearly detrimental. The mercury-thallium system does not require special care (Reference 54) and handling, although precautions are not prohibitively complex. The alloy system is reported to have incurred no apparent degradation after nuclear exposure to  $1.35 \times 10^{16}$  n/cm<sup>2</sup> greater than 1 Mev,  $4.75 \times 10^{15}$  n/cm<sup>2</sup> greater than 2.9 Mev, and  $2.5 \times 10^8$  R gamma.

Table 5-6 (taken from Reference 55) compares the indicated corrosion resistance of gallium and mercury for a number of metals. References 56, 57, and 58 provide additional detailed solubility data on both liquid metals. While summarization of the gross compatibilities between liquid metals and substrate materials and solubilities are available in the literature, it was concluded no definitive information regarding minor surface attack or reaction kinetics appropriate to highly finished sealing surfaces was available. The known effects of liquid metals on mechanical properties have been well summarized by Rostoker, et al. (Reference 59). In addition to the alteration of mechanical properties, the possibility of liquid metals in contact between two substrate materials resulting in welding or bond formation between the solid components has been reported.

Beneficial results in applying liquid metals have been noted by using chemical attack to remove surface contaminants from metallic substrates. Lowering the sample to be coated through the cleaning agent which is floating above the

Table 5-6. Temperature °C for Good Corrosion Resistance\* (Reference 55)

<u>Solid Metal</u>	<u>Gallium</u>	<u>Mercury</u>
Graphite	800	300
Beryllium	---	300
Silicon	---	600
Zirconium	100	100
Columbium	400	600
Iron	300P	600
Molybdenum	400	600
Chromium	600P	600
Nickel	600P	100
Vanadium	---	600
Titanium	400	300L
Platinum	100	100
Tungsten	800	600
Tantalum	400	600
Cobalt	---	600

\*Unlettered temperature-corrosion less than 1 mil per year,  
L - 1-10 mpy, P >10 mpy.

liquid metal is one such technique. Likewise, the use of sonic and ultra-sonic mechanical breakdown of surface oxides while the material to be wetted is immersed in the liquid metal has been used to improve wettabilities. With the materials tested, such techniques were not found to be necessary. The results of the screening tests and wetting techniques are summarized as follows:

1. The qualitatively observed wettability for both liquid metal systems appeared very satisfactory. Tests performed prior to the wetting of seal surfaces indicated reasonable adherence to tungsten, nickel, iron, copper, tantalum, molybdenum, niobium, coil silver, sintered  $Al_2O_3$ , and glass.
2. The liquid metal was applied with a cotton bud to the surface to be wetted, and the liquid was swabbed over the desired area. Subsequent light mechanical burnishing with a disposable paper wiper insured complete coverage while striking the excess liquid metal from the wetted surface. This procedure was used on all subsequent seal surfaces.

Table 5-7 compares some of the physical properties of the liquid metals of interest.

Table 5-7. Pertinent Properties of Liquid Metal Systems

Liquid Metal System:	Ga-In-Sn	Hg-In-Tl
Melting Point:	50°F	-74°F
Surface Tension (Room Temp.):	500 + dynes/cm	532 dynes/cm

Material	Temperature (Degrees C)	Vapor Pressure (microns)	Evaporation Rate gm/cm <sup>2</sup> -sec
Ga	775	10 <sup>-2</sup>	1.52 x 10 <sup>-7</sup>
	842	10 <sup>-1</sup>	1.46 x 10 <sup>-7</sup>
	937	1	1.40 x 10 <sup>-6</sup>
In	670	10 <sup>-2</sup>	2.04 x 10 <sup>-7</sup>
	747	10 <sup>-1</sup>	1.96 x 10 <sup>-6</sup>
	837	1	1.88 x 10 <sup>-5</sup>
Sn	882	10 <sup>-2</sup>	1.87 x 10 <sup>-7</sup>
	977	10 <sup>-1</sup>	1.80 x 10 <sup>-6</sup>
	1092	1	1.72 x 10 <sup>-5</sup>
Hg	-28	10 <sup>-2</sup>	5.28 x 10 <sup>-7</sup>
	-10	10 <sup>-1</sup>	5.08 x 10 <sup>-6</sup>
	16	1	4.86 x 10 <sup>-5</sup>
Tl	412	10 <sup>-2</sup>	3.19 x 10 <sup>-7</sup>
	468	10 <sup>-1</sup>	3.06 x 10 <sup>-6</sup>
	535	---	2.93 x 10 <sup>-5</sup>

Summary of Theoretical Wet Seal Analysis - On the basis of general wettability characteristics, both the mercury and the gallium alloys appear comparable. Likewise, the surface tension of both alloys appears adequate for seal applications. However, one distinction between the two systems can be made on the basis of their solidification points. The mercury alloy may permit operation at significantly lower temperatures than the gallium system. The most attractive property of the gallium system is its relatively low vapor pressure, permitting applications as high as 800°F without significant evaporative loss. The mercury system, on the other hand, has an exceedingly high vapor pressure for elevated temperature usage and thus must be confined to ambient and below ambient applications. Because of gallium's superior vapor pressure, the primary effort in the investigation was based on the gallium.

The indicated tendency of both liquid metals to attack base metals, especially at elevated temperatures, would appear to be a significantly detrimental factor for applying them to many common valve materials. In seal applications where the surface finish is extremely critical, this becomes a dominant point. However, the results of this investigation show the importance of surface tension and on leakage control, and indicates that zero leak sealing may be possible using the effects of the surface tension of the propellant and the valve seat.

## Static Seal Tests

Preliminary Leakage Tests - A preliminary feasibility test was performed using a simple test setup and three common engineering materials. The test samples consisted of 1/2 by 2-inch long rods of ordinary drill rod stock and 304 stainless steel and a 3/8-inch diameter high-speed tool steel. The ends of these rods were surface ground to a number 16 rms finish and one of each subsequently hand polished to a burnished finish. These finishes were obtained using normal metallographic polishing practices; however, they were not checked for flatness or measured surface finish. The polished surfaces were scrubbed with MEK (methyl ethyl ketone) and the gallium liquid metal alloy applied, using the technique previously described. For all three materials the apparent wettability was excellent. In order to measure the sealing ability quantitatively, a 1/4-inch diameter hole was drilled through the 304 stainless steel rod along its longitudinal axis. One end of the rod was attached to the vacuum line of a helium mass spectrometer leak detector. The other end was coated with the liquid metal. The wetted end of the two solid materials was alternately tested by placing them on top of the drilled rod. Figure 5-54 schematically shows the specimen arrangement. With this test it was not possible to provide continuous application of helium, and leakage was determined by intermittently spraying helium from a pressurized cylinder over the joint area. The effective pressure differential across the seal consisted only of the approximately 15 psi pressure produced by the application of vacuum to the inner side of the seal. All tests were conducted at ambient temperatures. The leak detector was calibrated to have a sensitivity of  $5 \times 10^{-10}$  cc/sec/division or a minimum detectable leak of  $1 \times 10^{-9}$  std cc/sec (helium). Numerous short-term and long-term exposures of the seal were made under vacuum. Using helium probe techniques, the observed leak rate with all single contact static seals was less than  $1 \times 10^{-8}$  std cc/sec helium. The background sometimes exceeded a  $1 \times 10^{-9}$  std cc/sec leak; therefore, while no deflection was noted, a conservative figure is used for reporting the general results. On two occasions 72-hour continuous exposures were performed between the drill rod and the 304 stainless steel. From these tests no deterioration of the seal properties was observed due to the 15 psi pressure differential. However, it was determined that the seal configuration could only be separated a few times before complete loss of the seal occurred. Consequently, the surfaces were rescrubbed with MEK and rewet with gallium alloy following a few separations of the joint. Similar results were obtained with the 3/8-inch diameter high-speed tool steel sample against 304 stainless steel; that is, any leak was less than  $1 \times 10^{-8}$  std cc/sec helium. After 14 days of continuous wetting by the liquid metal, it was found the surfaces would no longer seal. It was noted the mirror-like polished surfaces showed some indications of attack as evidenced by a loss of luster. A light repolishing immediately restored the original surface finish and the effectiveness of the seal. From these tests it was concluded the gallium liquid metal served as a very adequate seal for a 15 psi pressure differential in the liquid state on metallic surfaces. It was likewise concluded the effectiveness of the seal degraded rapidly with the number of seal separations and, while the degree of liquid metal attack with the substrate material was minimal, the destruction of the surface finish would be intolerable for sealing applications.

High Pressure Tests - In order to perform static high-pressure tests, a special test cell was designed and fabricated. The purpose of this cell was to permit:

1. A quantitative measurement of leakage using helium mass spectrometer leak detector methods
2. The application of various controlled bearing loads to the seal surfaces
3. The application of controlled high-pressure helium gas to the seal.

Figure 5-55 shows the test cell assembly as designed and initially utilized in the investigation. The fixture was designed to allow testing of various seat materials by permitting interchange of the samples. While this latter flexibility was a desirable feature, it was found that the seals necessary to permit such flexibility compromised interpretation of the results. The initial problem resulted from permeation leakage of helium through the elastomeric seal between the test cell body and the lower surface of the lip seat sample. As designed, the fixture employed this seal in normal elastic compression. The inconsistency as well as the magnitude of permeation leakage compromised conclusions of the liquid metal seal at leak rates  $1 \times 10^{-8}$  std cc/sec. This resulted in modification of the fixture in order to overcome these difficulties. The initial attempt to remedy this situation consisted of placing the O-ring seal into "fluid" compression by eliminating the normal expansion volume of the O-ring groove with a filler ring. While this resulted in a marked improvement of the permeation characteristics, it did not eliminate the problem. The second solution, shown in Figure 5-56, required modification of the sample support area. The elastomeric O-ring seal was removed and replaced with a cylindrical copper shear gasket. With this seal the lipped test specimen was pressed into the test fixture housing, compressing the cylindrical copper ring gasket at the same time. While satisfactorily sealing some of the samples, it was found a fixed dimension of the gasket and housing were incompatible with variations in the sample material diameters and hardness. Therefore, this solution was abandoned as not being reproducibly leaktight to high helium pressures. The final solution eliminated the problem but no longer permitted testing of similar materials for both seal surfaces. This solution consisted of making the upper end of the test support fixture the lower sealing surface upon which the flat specimen was placed. Thus, the only possible leak to the leak detector was that of the liquid metal coated surface. To accomplish this, the upper end of the support was ground flat and subsequently polished using metallographic techniques. All results reported with 4340 steel are with the test fixture in this configuration.

The test materials used in this phase of the investigation consisted of common valve seat materials. While it was recognized that compatibility between the liquid metals and these materials might present a problem, it was decided evaluation of the severity could only be made by experiment. Table 5-8 summarizes the materials tested. Surface finishes on these samples were initially ground and lapped flat to within a few microinches

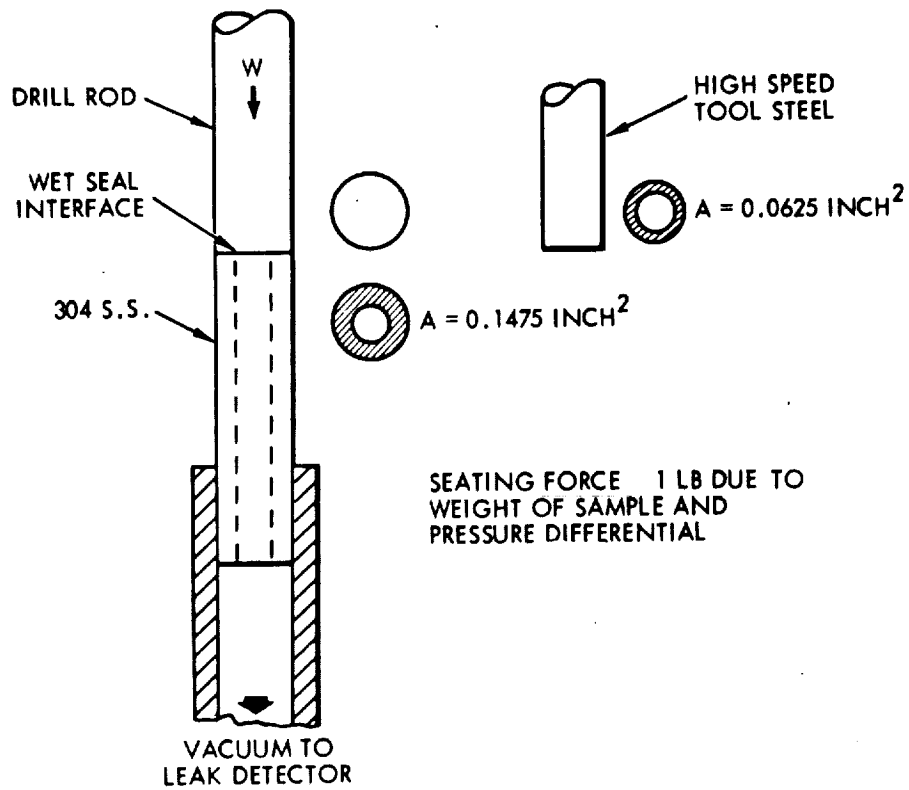


Figure 5-54. Preliminary Leak Test Configuration

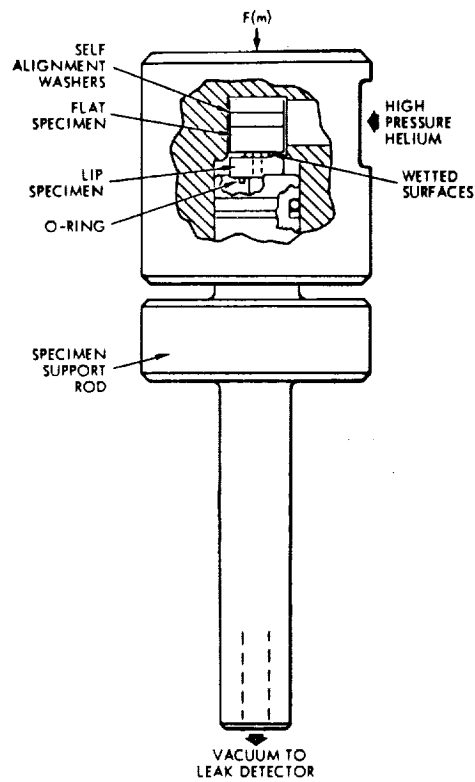


Figure 5-55. High Pressure Cell Assembly



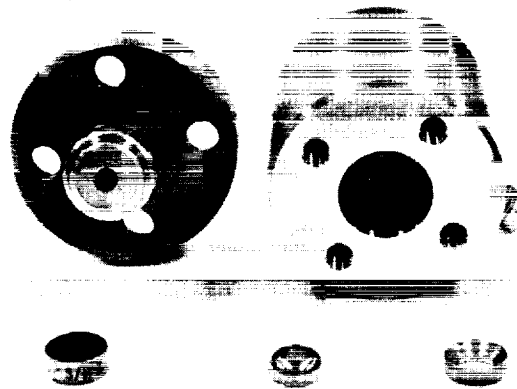


Figure 5-56. Photograph of High Pressure Test Cell Assembly Showing Lipped Specimen Copper Gasket Mounted, Flat Specimen and Alignment Washers.

Table 5-8. Materials Tested - High Pressure Test

(BC) Beryllium Copper (Berylco 25)  
 QQ-C-530. Aged three hours at  
 600°F.

(440C) 440C Stainless Steel  
 QQ-S-763. Heat Treated R/C 5560  
 MIL-H-6875.

(HSS) AISI T1 High Speed Steel  
 Heat Treated R/C 63-66 MIL-H-6875.

(4340) 4340 Steel Condition C4  
 MIL-S-5000 Heat Treated R/C 48-52  
 MIL-H-6875.

Table 5-9. Wetted Material Couples Showing No Leakage With Helium Probe Techniques

BC	versus	BC
440C	versus	440C
HSS	versus	HSS
WC	versus	HSS
WC	versus	BC
WC	versus	WC

over 90 percent of their surface area. Subsequent repolishing tended to increase curvature at the outer edges, although measurement with optical flats after each repolish indicated flatness was retained for a majority of the samples to less than one fringe.

Results of Initial Phase Tests - A number of the specimens were checked with helium probe techniques under no mechanical load. These tests were comparable to those performed in the "preliminary leakage tests." Table 5-9 gives the material couples which were wetted with the gallium alloy and helium leak checked.

As there were several samples of each material, multiple tests in each category were actually performed. With almost all the tests, the seals showed no indicated leakage when probed with helium. The leak detector background was in all cases between  $1 \times 10^{-9}$  and  $1 \times 10^{-8}$  std cc/sec (helium). A few samples would not seal under the no-load condition and were eliminated from further use.

Typical results obtained with the O-ring beneath a lipped specimen are given in tabulated form, Tables 5-10 and 5-11. The test results of Tables 5-10 and 5-11 were obtained with gallium-indium-tin wetted 440C versus 440C samples under 55-psig helium pressure. Table 5-12 shows the results of a similar test of only the O-ring using a solid flat specimen to seal the fixture.

High-pressure helium tests were performed both with copper gasketed lipped specimens and the 4340 support fixture surface. The maximum pressure used in any of these tests was 2250 psig (the limit of the bottle gas pressure). Table 5-13 summarizes the results of the high pressure tests. It was observed the seals gave no indication of leakage higher than the background of the leak detector, until either a reduction of the applied load or an increase in the helium pressure resulted in a sudden catastrophic breakdown of the seal. Examination of the seals following such breakdown showed the liquid metal to have been forced off the sealing surfaces into the center section of the solid specimen. Figure 5-57 plots the applied maximum pressure without breakdown versus a normalization factor. All tests, except as noted, were performed with the liquid gallium alloy as the sealant. The seal area for the lipped specimens was  $0.0192 \text{ in}^2$  and for the 4340 test fixture surface was  $0.185 \text{ in}^2$ .

The bearing load was applied in an Instron load frame where mechanical loading was measured with a load cell. With no internal pressure the indicated load was a direct measure of the total bearing load. Minor error due to outer O-ring friction was introduced. At higher pressures the indicated load was the sum of the initial mechanical load plus the forces of the internal gas pressure. The internal cross sectional area of the pressure cell was about  $0.4 \text{ in}^2$ . With increased internal pressure the frictional losses due to the O-ring as well as hysteresis were nonlinear so as to make the observed load only approximate. Since the mechanical load applied on the wetted surfaces was transmitted through the pressure cell to the specimen support, the result of applying internal pressure was, in effect, to reduce the applied mechanical load. Figure 5-57 is based only on the initial applied mechanical load (P) where A is the bearing area and L is the radius of the seal. Tables 5-13 and 5-14 tabulate two tests which withstood 2250 psig with no indicated leak. It should be noted the test of 4340 versus HSS of Table 5-14 was kept under 500 psi helium pressure overnight without loss of the seal.

Table 5-10

Test 440C SN1 O-ring E 515-8

Background  $3 \times 10^{-9}$  std cc/sec

(Ga-In-Sn)

Seal Bearing Area =  $0.0192 \text{ in}^2$

Time	Measured Compressive Load Lbs	Helium Pressure psig	Leak Rate Std cc/sec
1025	700	0	$3.0 \times 10^{-9}$
1027	700	55	$3.0 \times 10^{-9}$
1029	600	55	rising
1030	900	55	$1.1 \times 10^{-8}$
1035	1000	55	$1.5 \times 10^{-8}$
1036	900	55	$1.7 \times 10^{-8}$
1037	800	55	$1.95 \times 10^{-8}$
1038	700	55	$2.3 \times 10^{-8}$
1039	600	55	$2.55 \times 10^{-8}$
1040	500	55	$2.95 \times 10^{-8}$
1041	400	55	$3.2 \times 10^{-8}$
1042	300	55	$3.55 \times 10^{-8}$
1043	200	55	$3.95 \times 10^{-8}$
1044	100	55	$4.1 \times 10^{-8}$
1045	200	55	$4.25 \times 10^{-8}$
1046	300	55	$4.35 \times 10^{-8}$
1047	400	55	$4.45 \times 10^{-8}$
1048	600	55	$4.5 \times 10^{-8}$
1049	800	55	$4.5 \times 10^{-8}$
1050	1000	55	$4.5 \times 10^{-8}$
1051	1000	0	$4.75 \times 10^{-8}$
1052	1000	0	$4.9 \times 10^{-8}$

Table 5-11

Test 440C SN1 O-ring E 515-8

Background  $2.5 \times 10^{-9}$  std cc/sec

(Wet Ga-In-Sn)

Seal Bearing Area =  $0.0192 \text{ in}^2$

Time	Measured Compressive Load Lbs	Helium Pressure psig	Leak Rate Std cc/sec
1705	1000	0	$2.5 \times 10^{-9}$
1706	1000	55	$2.5 \times 10^{-9}$
1712	1000		$1.5 \times 10^{-9}$
1718	900		$1.5 \times 10^{-9}$
1723	800		$1.5 \times 10^{-9}$
1728	700		$1.5 \times 10^{-9}$
1730	600		$2.4 \times 10^{-8}$
1731	650		$1.55 \times 10^{-8}$
1732	700		$4.5 \times 10^{-9}$
1733	650		$9.0 \times 10^{-9}$
1734	600		$2.45 \times 10^{-8}$
1735	550		$4.5 \times 10^{-8}$
1736	500		$1.8 \times 10^{-7}$
1737	475		$2.25 \times 10^{-7}$
1738	450		$3.5 \times 10^{-7}$
1739	425		$4.4 \times 10^{-7}$
	400		$7.0 \times 10^{-7}$
1740	375		$9.75 \times 10^{-7}$
	350		$1.27 \times 10^{-6}$
1741	325		$1.95 \times 10^{-6}$
	300		$2.9 \times 10^{-6}$
1742	275		$4.0 \times 10^{-6}$
	250		$6.25 \times 10^{-6}$
1743	225		$9.7 \times 10^{-6}$
	200		$1.7 \times 10^{-5}$
1744	175		$2.9 \times 10^{-5}$
	150		$5.0 \times 10^{-5}$
	200		$3.35 \times 10^{-5}$
	300		$1.15 \times 10^{-5}$
	400		$3.75 \times 10^{-6}$
1745	500		$1.41 \times 10^{-6}$
	600		$5.5 \times 10^{-7}$
	700		$2.0 \times 10^{-7}$
1746	800		$9.0 \times 10^{-8}$
1747	900		$5.75 \times 10^{-8}$
1749	1000		$2.5 \times 10^{-8}$
1750	1100		$1.55 \times 10^{-8}$
	1300		$1.5 \times 10^{-8}$
	1400		$1.5 \times 10^{-8}$
1751	1500		$1.15 \times 10^{-8}$
1753	1500		$1.0 \times 10^{-8}$
	1400		$1.0 \times 10^{-8}$
	1300		$1.0 \times 10^{-8}$
	1200		$1.0 \times 10^{-8}$
	1100		$1.2 \times 10^{-8}$
1754	1000		$1.75 \times 10^{-8}$
	900		$2.95 \times 10^{-8}$
	800		$9.0 \times 10^{-8}$
1755	700		$3.1 \times 10^{-7}$
	600		$1.0 \times 10^{-7}$
	500		$3.1 \times 10^{-6}$
	400		$9.0 \times 10^{-6}$
1756	300		$2.85 \times 10^{-5}$

Table 5-12

Test O-Ring Compound E 515-8  
Background  $1 \times 10^{-9}$  std cc/sec

Time	Measured Compressive Load Lbs	Helium Pressure psig	Leak Rate Std cc/sec
1412	1000	0	0
1414	1000	5	$1.0 \times 10^{-9}$
1415	1000	10	$1.0 \times 10^{-9}$
1416	1000	20	$1.0 \times 10^{-9}$
1417	1000	30	$1.0 \times 10^{-9}$
1418	1000	40	$1.0 \times 10^{-9}$
1433	1000	55	$1.0 \times 10^{-9}$
1448	900	55	$1.0 \times 10^{-9}$
1503	800	55	$1.0 \times 10^{-9}$
1518	700	55	$1.0 \times 10^{-9}$
1533	600	55	$1.0 \times 10^{-9}$
1548	500	55	$3.0 \times 10^{-9}$
1603	400	55	$6.5 \times 10^{-9}$
1618	300	55	$1.2 \times 10^{-8}$
1633	200	55	$2.3 \times 10^{-9}$
1634	1000	55	$2.0 \times 10^{-9}$

Table 5-13

Test 4340 Vs. BC SN 6 (Hg-In-Tl)  
Background  $1.3 \times 10^{-8}$  std cc/sec  
Seal Bearing Area =  $0.185 \text{ in}^2$

Time	Measured Compressive Load Lbs	Helium Pressure psig	Leak Rate Std cc/sec
1109	500	0	$1.25 \times 10^{-8}$
1110	500	0	$1.20 \times 10^{-8}$
1112	500	0	$1.05 \times 10^{-8}$
1114	540	500	$1.0 \times 10^{-8}$
1115	560	700	$1.0 \times 10^{-8}$
1117	595	1000	$1.0 \times 10^{-8}$
1120	595	1000	$1.2 \times 10^{-8}$
1122	640	1300	$1.2 \times 10^{-8}$
1124	675	1500	$1.2 \times 10^{-8}$
1126	805	1900	$1.1 \times 10^{-8}$
1128	940	2250	$1.0 \times 10^{-9}$
1135	945	2250	$9.0 \times 10^{-9}$
1145	930	2250	$9.0 \times 10^{-9}$
1148	930	2250	$9.5 \times 10^{-9}$
1150	595	1400	$9.5 \times 10^{-9}$
1152	420	1000	$9.5 \times 10^{-9}$
1153	205	500	$9.5 \times 10^{-9}$
1157	0	0	$1.45 \times 10^{-9}$
1309	500	0	$6.5 \times 10^{-9}$
1313	935	2250	$6.5 \times 10^{-9}$

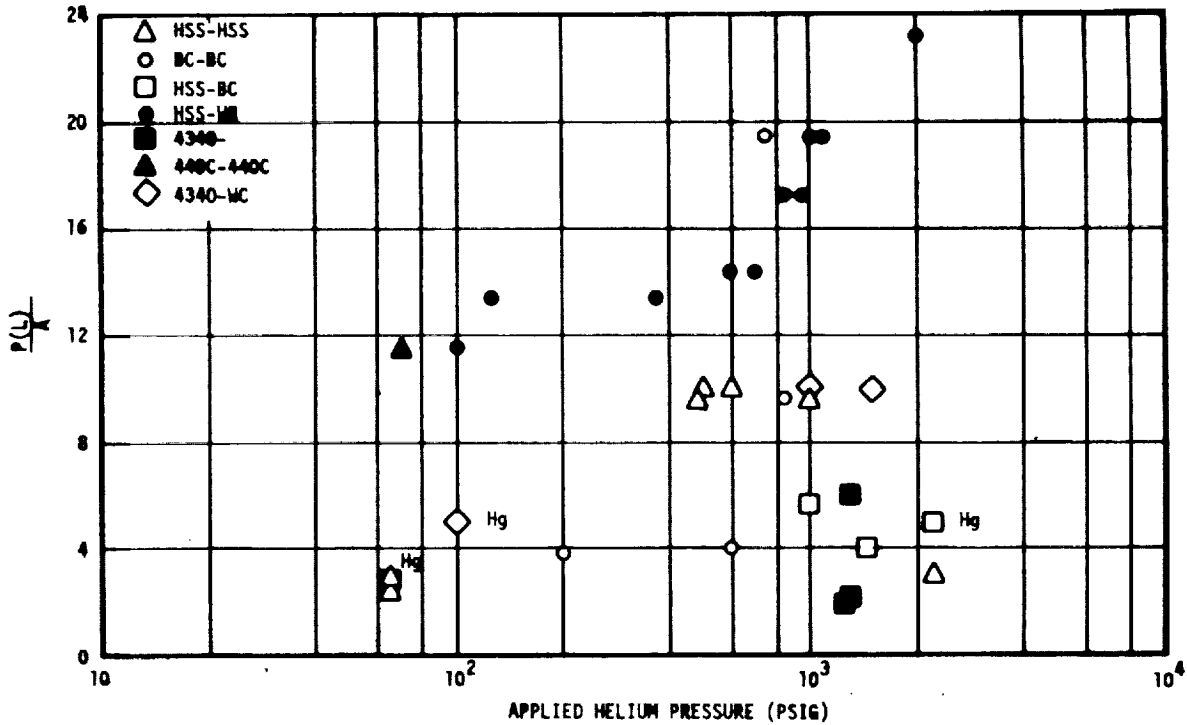


Figure 5-57. Summarization of High-Pressure Tests

Table 5-14

Test 4340 Vs. HSS SN1 (Ga-In-Sn)  
 Background  $6.5 \times 10^{-9}$  std cc/sec  
 Seal Bearing Area =  $0.185 \text{ in}^2$

Time	Measured Compressive Load Lbs	Helium Pressure psig	Leak Rate std cc/sec
1712	300	0	$6.5 \times 10^{-9}$
1714	360	500	$6.5 \times 10^{-9}$
1722	360	500	$6.5 \times 10^{-9}$
1735	360	550	$5.0 \times 10^{-9}$
0855	370	700	$2.0 \times 10^{-9}$
0908	420	900	$2.0 \times 10^{-9}$
0911	440	1000	$2.0 \times 10^{-9}$
0920	440	1000	$2.0 \times 10^{-9}$
0925	640	1000	$2.0 \times 10^{-9}$
0926	645	1100	$2.0 \times 10^{-9}$
0927	655	1200	$2.0 \times 10^{-9}$
0928	670	1300	$2.0 \times 10^{-9}$
0936	950	2250	$2.0 \times 10^{-9}$
1050	950	2250	$2.0 \times 10^{-9}$

Special Problems Discussion - While a large number of high-pressure seals were observed, several important aspects relating to the use of liquid metals for both dynamic and static seals were noted and will be discussed.

Compatibility Problems - Microscopic examination of sample surfaces which had been cleaned after being wetted and contacted showed evidence of a solid or semi-solid material buildup. This observation was noted with high-speed steel, 440C, tungsten carbide, and beryllium copper. The buildup was not uniform and appeared greatest on the bearing areas. The buildup could be easily discerned by visual observation of the lip impression on the flat specimen samples. For this reason, between each reuse of a given sample, repolishing of the surface was necessary. Initially, it was thought buildup might be associated with oxide formation and subsequently a series of weight measurements of wetted samples was performed. In addition to the weight measurements, photomicrographs of specimen surfaces before and following several days wetting by the gallium alloy were made. Also a small portion of the solid material was taken from the surface of a high-speed steel sample and an X-ray diffraction pattern obtained. The results of all three observations confirm that the buildup of a solid or semi-solid film on the surface is the result of interaction between the liquid metal and the substrate material. The weight measurements did not show any change in sample weight which would be expected should appreciable oxidation occur. Furthermore, the photomicrographs of the materials used in the leak-testing experiments clearly showed evidence of microscopic attack. The X-ray diffraction pattern of the surface material supports this same observation. The diffraction pattern appears to be characteristic of a metal-type structure rather than an oxide. Systematic review of previously identified structures relating to any of the possible binary metal compounds or metallic oxides which might have been formed failed to provide an identification.

The pattern and interplanar spacing (D) values) are reproduced as Figure 5-58 and Table 5-15. The photomicrographs, Figures 5-59, 5-60, and 5-61, show the results of wetting the test materials with the gallium liquid metal alloy. The marked difference in the rate of attack between a heat treated and untreated sample, as shown in Figure 5-59, is probably a result of the surface energy condition, as the composition is identical. While none of the samples shown in the photomicrographs were stressed during the wetting cycle, the previously noted observation of material buildup on the bearing surface would seem to relate to a higher stress condition accelerating the reaction. Shown in Figure 5-62 are photomicrographs of tantalum and porous tungsten before and after wetting. The dominant structure of the tantalum is a result of polishing. Retention of the liquid metal in the recessed areas of both materials after surface removal can be seen.

Wettability - As previously noted, wettability or the apparent achievement of wettability can be enhanced by the application of burnishing, ultrasonic, chemical, or thermal vacuum techniques to produce clean surfaces of the substrate materials. While no special problems were encountered in applying the liquid metals to the materials studied here, it must be recognized that liquid metal attack, although slight, may play a dominant role in the apparent ease with which the large number of materials are wet by both liquid metal systems.

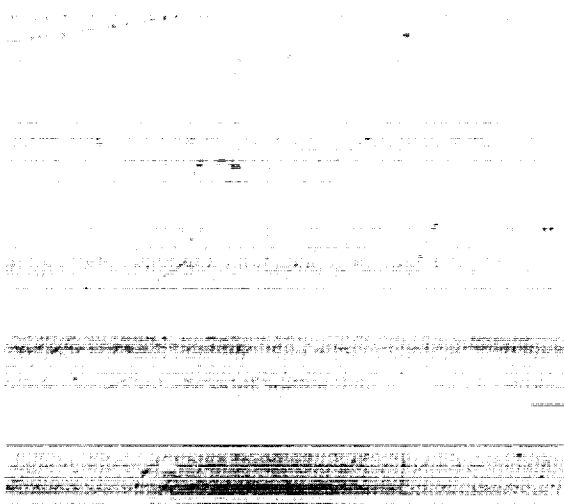
Figure 5-58. Diffraction Pattern of Unknown Compound



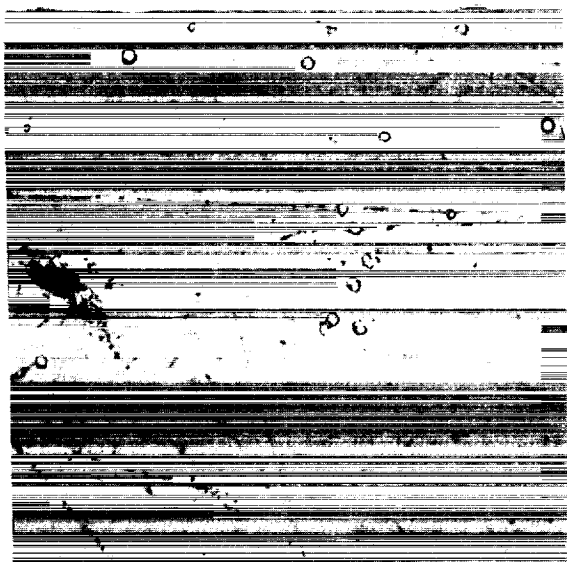
Table 5-15. Interplanar Spacing of Unidentified Compound

	<u>Intensity</u>	<u>D Value</u>	<u>Intensity</u>	<u>D Value</u>
1.		2.8944	13.	1.2619
2.	M	2.8098	14.	1.2321
3.		2.7019	15.	1.1730
4.	S2	2.5311	16.	1.1565
5.		2.4472	17.	1.1410
6.	S1	2.0183	18.	1.0749
7.	S3	1.9868	19.	1.0124
8.	M	1.9286	20.	.99908
9.		1.6431	21.	.89579
10.		1.4507	22.	.85610
11.	M	1.4076	23.	.78725
12.	M	1.3872		

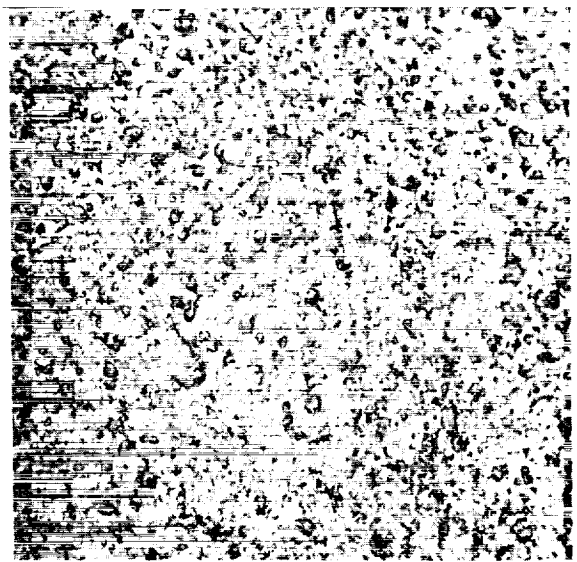




a) AISI T1 High Speed Steel X550  
Before Wetting

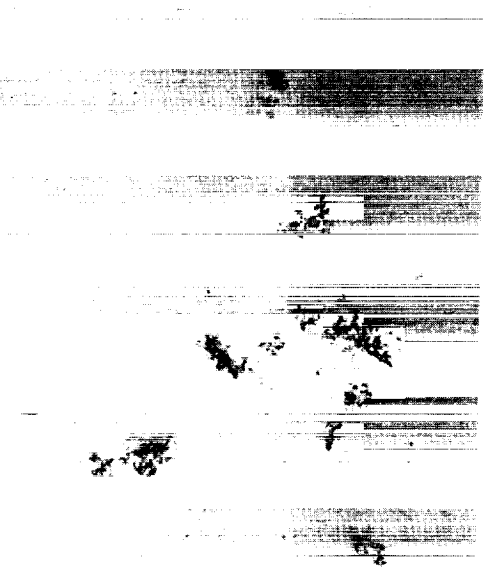


b) Not Heat Treated Sample X550  
After 72 Hours in Contact  
with Gallium Alloy

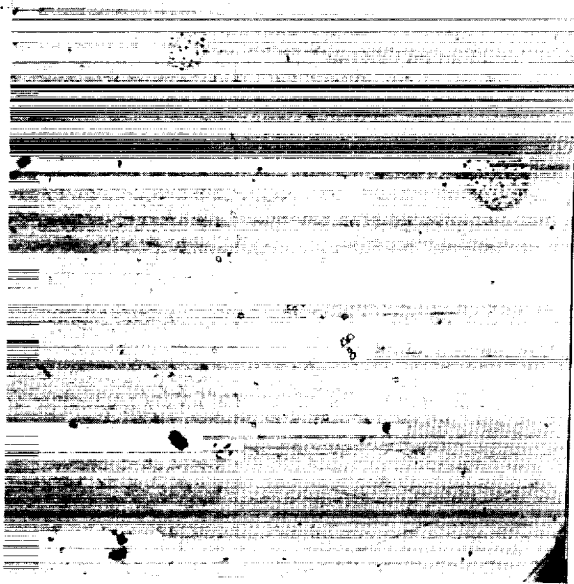


c) Heat Treated Sample X550  
After 72 Hours in Contact  
with Gallium Alloy

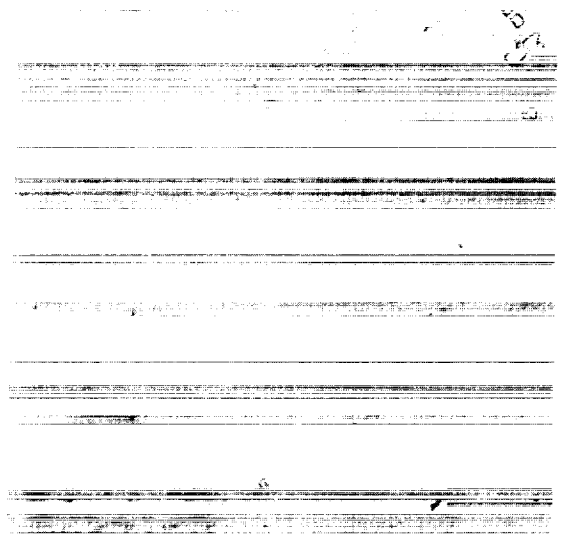
Figure 5-59



a) 440C Stainless Steel X550  
Before Wetting

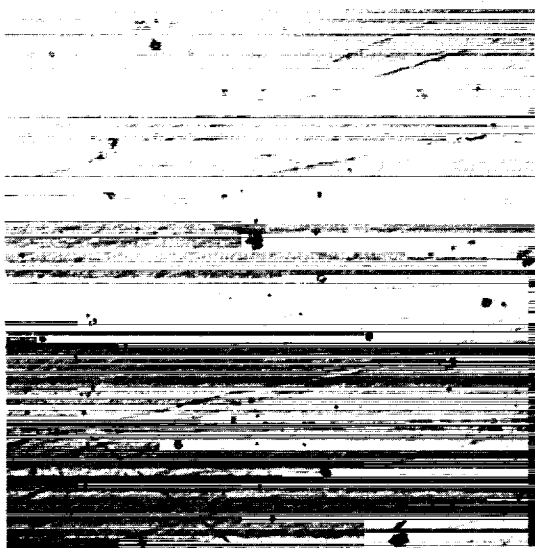


b) After 72 Hours in Contact  
with Gallium Alloy X200

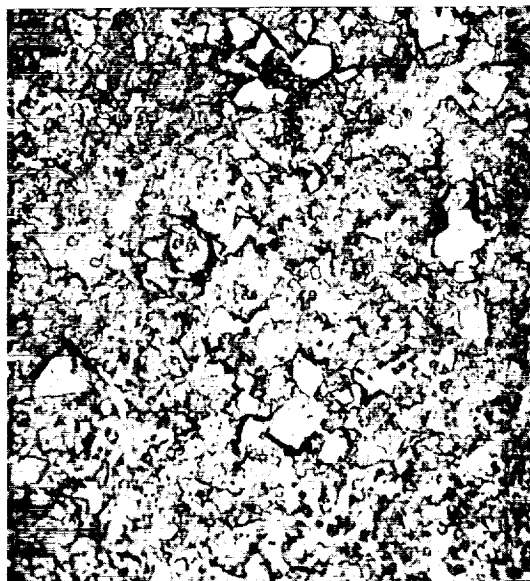


c) After 72 Hours in Contact  
with Gallium Alloy X550

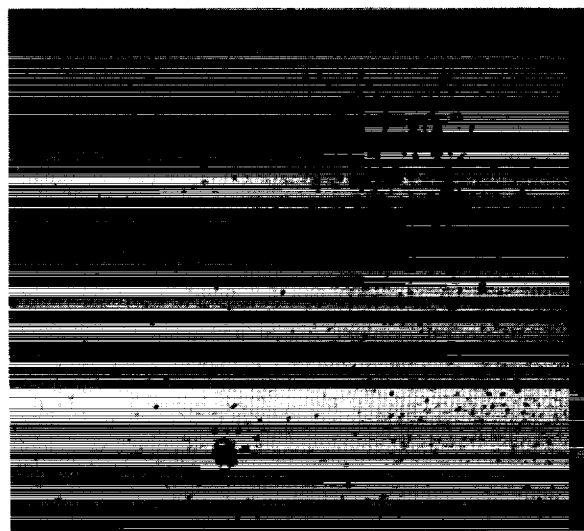
Figure 5-60



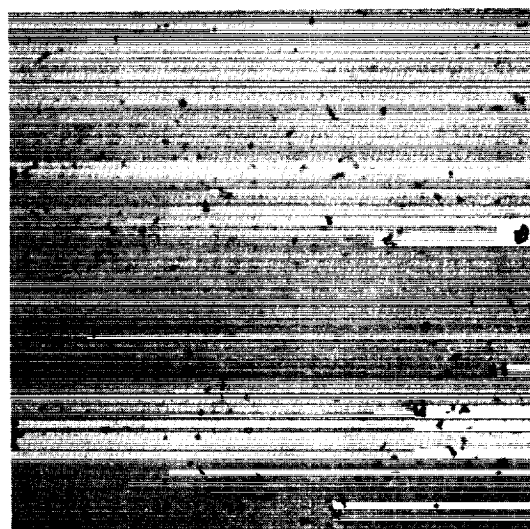
a) Beryllium-Copper X550  
Before Wetting



b) Beryllium-Copper X550  
After 72 Hours in Contact  
with Gallium Alloy

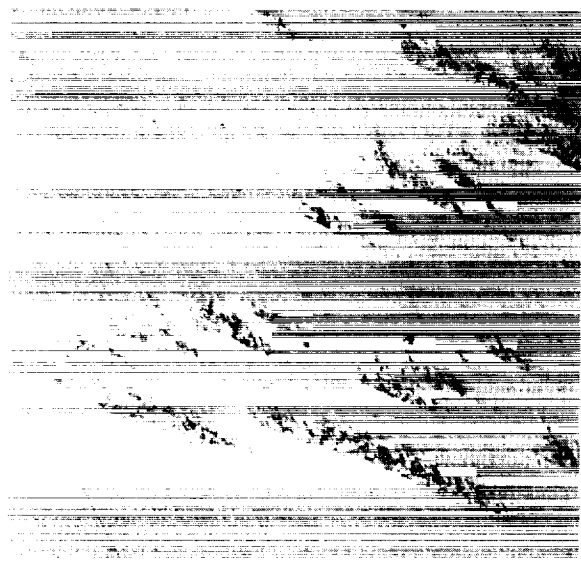


c) Tungsten-Carbide X550  
Before Wetting



d) Tungsten-Carbide X550  
After 72 Hours in Contact  
with Gallium Alloy

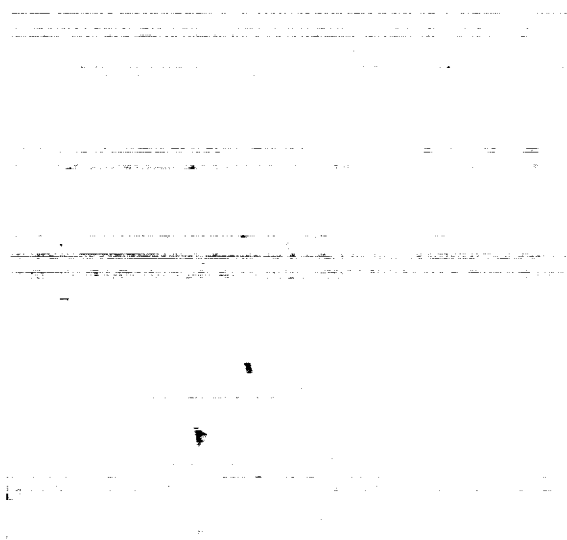
Figure 5-61



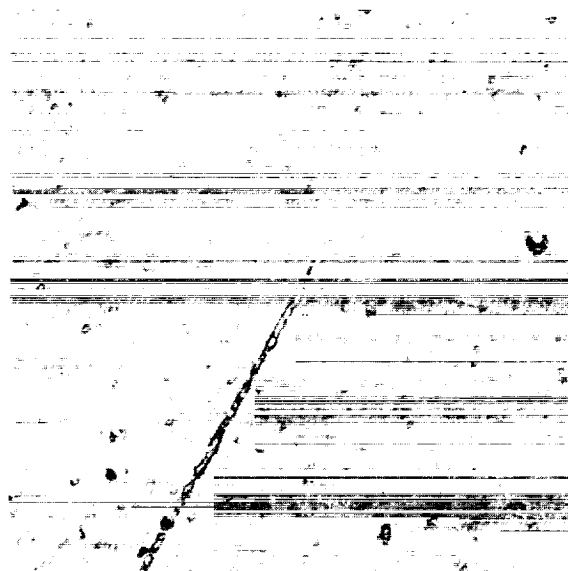
a) Tantalum X550  
Before Wetting



b) Tantalum X550  
After Wetting



c) Porous Tungsten X550  
Before Wetting



d) Porous Tungsten X550  
After Wetting

Figure 5-62

Oxidation of Liquid Metals - While the formation of oxides or complex oxide systems by both liquid metal systems may be advantageous for certain wettability considerations, the presence of an oxide scum on the surface of a thin coating would not appear desirable. Purification of the liquid metal systems to remove such contaminants and coating of the parts to be wetted in inert gas facilities could be easily implemented should a problem area of this nature be identified.

Dynamic Seal Test - The second phase of the wet seal concept evaluation studied the wet seal when used as a seal in dynamic applications such as a poppet valve seat or a sliding-type closure. Preliminary tests were performed in which a cap rotated against the face of a tube simulating a dynamic sliding type seal. The faces of the cap and tube were lapped together and then wetted with a gallium eutectic and one end of the tube was attached to the outlet hose of a helium mass spectrometer as shown in Figure 5-63. A helium probe was used around the sealed joint to provide a leak media. The simulated valve cap was rotated by hand through random, jerky, and continuous turns. Approximately 50 cycles were tried and no indication of a leak was found.

The base metal used for the cap and tube consisted of tungsten, and after several turning motions, periodic sticking was noticed, although not consistently. After examination of the surfaces, it was concluded that high frictional forces were developed as a result of galling due to poor lubricity of the reacting gallium.

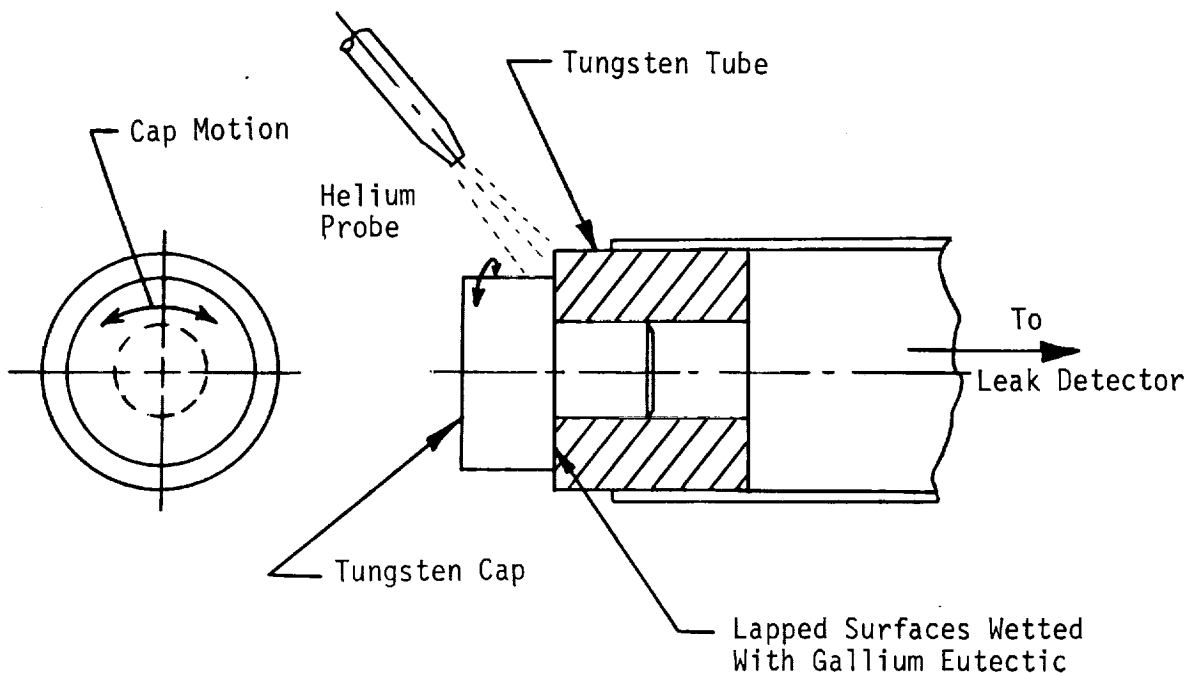


Figure 5-63. Schematic of Dynamic Wet Seal Leak Test

### Conclusions From The Initial Wet Seal Study

1. It was concluded that surface finishes for sealing surfaces are a very important condition relating to the ability of liquid metals to produce essentially zero leak seals at both high and low pressures. If nominal state of the art finishes of less than one microinch are utilized and can be maintained, both theory and the static test experimental results confirm that pressures in excess of 2,000 pounds per square inch can be sustained in a leak-free condition.
2. For both static or dynamic seals, compatibilities between the liquid metal and the sealing surface must be exceptionally good in order that long term sealing ability can be maintained. As a result of the observations obtained here, tantalum, tungsten, or their alloys would appear the most promising seat materials.
3. The limited observations indicated that seal separation, such as required by poppet action, is detrimental to the seal effectiveness. It was believed that this might be overcome through the use of porous media or other reservoir techniques to provide replenishment to the sealing services. A dynamic valve which does not utilize a poppet-type action appeared to be the next most logical step. Such a valve using rotational motion (i.e., a rotating sleeve valve) where the majority of the sealing area remains in contact, should not suffer loss of sealing properties in the liquid metal film. This suggests the consideration of valve types which are usually discounted because of traditional sealing problems.
4. Long term materials compatibility, possible enhancement of diffusion bonding, and long term stability of the seal against pressure, remained to be evaluated.

5.2.3.2 Second Phase Wet Seal Study - As a result of the initial phase experience, primary concentration during the second phase study was devoted to examining the problem of compatibility from the standpoint of attaining stable long term surface conditions including finish and wettability. Thus, the experimental activity was devoted to examining additional seal materials (other than metals) and the incorporation of low energy electron polymerized thin films on metal surfaces.

Wettability tests were performed on several non-metallic materials using the gallium-indium-tin liquid metal system. Included were high density graphite, fused alumina ( $Al_2O_3$ ), Boron nitride, zirconium oxide and magnesium silicate. Of these materials, the fused alumina was the only material exhibiting bulk vacuum tightness as determined by a helium mass spectrometer leak detector. Thus, the other materials in addition to wetting were examined for possible suitability as reservoir materials. Each will be discussed in turn.

Graphite - It has been reported that graphite is unattacked by gallium. Continuous exposure of a graphite sample for six months at ambient temperatures did not show any evidence of gallium attack. While the apparent surface wettability of graphite is good, wettability within the bulk (micro porous) structure is apparently poor. This conclusion is based upon the observation that a sample immersed in a reservoir of gallium liquid metal with a vacuum pump providing approximately 15 psia pressure differential through the sample readily transmitted liquid gallium several centimeters through the sample into the reduced pressure volume. The net result was the elimination of graphite as a possible seal material or reservoir material. The apparent adherence in the bulk is so low as to make retention of liquid gallium in any quantity with any significant pressure differential unlikely.

It is not known how much of the noted behavior is attributable to porosity with the liquid metal flowing through small capillaries or the lamellar graphite structure with gallium diffusion along the grain boundaries similar to its behavior in aluminum. Pyrolytic graphite because of its directional structure could possibly be applied under certain circumstances with different results than those obtained with conventional graphite.

Fuzed Alumina - The chemical stability of  $Al_2O_3$  is also reported good with respect to gallium attack. Wettability as determined by mechanical application and burnishing appears good. Also,  $Al_2O_3$  appears quite promising from a stability standpoint. However, zero leak seals were not obtained with low bearing loads in tests with tungsten or the other ceramics serving as the ported segment of a simulated seal.

Boron Nitride - All attempts to achieve good wetting of boron nitride with the gallium alloy were unsuccessful.

Zirconium Oxide - Wettability was very poor and some evidence of rapid attack of the sample surface was noted, following which, evidence of a sustained liquid phase could be detected.

Magnesium Silicate\* - Wettability was found to be very good, however, porosity of this material may, in part, contribute to apparent ease of wetting. Because of its high porosity, applicability as a seal surface is questionable.

In addition to mechanical application of gallium films, a special evaporator was designed and fabricated to prevent vacuum deposition of gallium coatings. This fixture was designed to permit simultaneous electron bombardment of the substrate so that composite coatings consisting of radiation polymerized monomers and gallium could be made. With this evaporator, gallium coatings were vapor deposited in vacuum on samples of boron nitride, alumina, magnesium silicate, Vycor and zirconia. These coatings lacked the bright solid metallic luster of mechanically wetted surfaces. The coatings would be easily removed by wiping, indicating the physical wetting of the substrate surfaces to be poor.

---

\*Al Si Mag 222, American Lava Co.

With selected nonmetallic samples, leakage through a seal type configuration was performed. This was accomplished by use of two cylindrical disc samples, one containing a centered hole. Coating of the interface between the discs served to simulate a seal. One end of the hollow disc was connected to the vacuum inlet of a helium mass spectrometer leak detector. The discs were fabricated of boron nitride, magnesium silicate and zirconium oxide. Tests made with mechanically burnished liquid metal coatings or evaporated gallium coatings applied to the flat faces of the discs all demonstrated leakage levels  $>1 \times 10^{-4}$  cc/sec He, the maximum detectable leak with the mass spectrometer. While some of the leakage may be attributed to the porosity of the nonmetals and permeability with respect to helium, the lack of good wettability is believed the prime contributor. Typically, a 15 psia pressure differential forced the liquid metal from between the seal surfaces into a puddle on the center of the disc specimens. Based upon the apparent wettability of the nonmetals, as previously discussed and contrasted to the liquid metal wetting of metals, this result is not surprising. As a direct seal material the  $Al_2O_3$  appears to be the only system worthy of further examination.

Rigidized polymer films produced by low energy electron bombardment in vacuum were considered as having potential application to the Wet Seal Study. The primary area of interest is for the purposes of placing the polymer film between a substrate metal and the liquid metal film. In this manner it may be possible to eliminate the long term materials compatibility problem noted with most engineering alloys in loss of surface finish as well as reduce the possibility of solution bonding under long term static contacts. This conclusion led to the extensive study of thin films reported in Section 5.2.5.

An initial test was made by forming a D.C. 705 film on a tungsten sample. Attempts to mechanically wet the film coated sample with gallium liquid metal using a burnishing technique were unsuccessful. On this basis a concept of a composite coating consisting of a mixture of an electron polymerized organic and the liquid metal was devised. Such coatings in principle could be homogeneous mixtures or graded as a function of thickness by control of the film.

Additional D.C. 705 films were formed on the metal high pressure test samples reported in the Advanced Valve Technology Final Report No. 8651-6033-SC000, Vol. II, Wet Seal Study, 19 July 1964. These samples were disc and lip specimens of beryllium-copper, high speed steel, tungsten carbide and 440C stainless steel.

All specimens were exposed to the electron beam simultaneously. However, these specimens were readily wettable with the liquid gallium system. Subsequent helium mass spectrometer leakage measurement verified zero leak seals could be attained between the various wetted material combinations. After several days with liquid metal on the surface, attack of the surface finish was noted. It is not known if these film results are typical, since there is some question as to the amount of rigidized polymer film which may have been formed on the test surfaces.



Another set of the same material samples were exposed to a simultaneous electron exposure and gallium evaporation using the evaporation source developed for this purpose. These films had the same general appearance and behavior as the pure gallium films formed on the nonmetallic materials. These coatings could be easily removed and did not achieve good seal properties. With the experimental coating no provision was available for control of the concentration of the monomer vapor. It is apparent insufficient monomer was formed and thus the composite films were extremely gallium rich.

It was concluded that the application of electron produced rigidized polymeric films to seal surfaces either as pure films or in composite structure will require the investigation of formation conditions to produce consistent and suitable structures for this purpose. To accomplish this, a systematic investigation was considered to be required, which was beyond the scope of the screening tests performed during this program.

A special composite material was investigated. This material system was considered of interest from a reservoir application standpoint. The proposed system consisted of mixing gallium liquid metal with tungsten powder to form a paste. The paste was then cold pressed isostatically at 20,000 psi to form one cm square by 25 mm thick compacts. Attempts to sinter this structure at 800°C for one hour in vacuum were unsuccessful. The mechanical properties of the cold compacted material are such that some possible application is feasible. Special porous tungsten structures which have been developed for ion emitter application are available in solid forms. A special class of this material formed by sintering spherical tungsten powder has an effective specific permeability of greater than 98 percent. This means the volume fraction of the sample which is porous is essentially all interconnected. This material is thought to offer a special class of porous materials for use with liquid metals since established material information exists to permit controlled variation of the pore diameter (capillary dimensions). This is believed directly related to incorporation, retention and removal of the liquid metal system from the porous structure.

The last observations to be reported relate to the behavior of materials placed in long term static contact with the gallium liquid metal on the interface. A beryllium-copper - beryllium copper combination and high speed steel - 440C combination were coated with gallium. These samples were extra disc samples used in the high pressure tests of the previous Wet Seal Study. Arbitrarily, these two combinations were compressed at a moderate force of unknown magnitude for 30 days by C clamps and then allowed to remain in static - no load contact for an additional five months. At the end of the six-month period, physical separation by trying to pull the couples apart by hand could not be effected. Separation was accomplished by mechanically striking the couples parallel with the contact line. Examination of the separated surfaces showed discrete areas where the gallium was no longer evident as a liquid and bonding of some sort had occurred.

A similar test was performed with magnesium silicate and tungsten carbide as the material couple. In this instance, after gallium wetting, the couple was simply left in physical contact for 30 days. As with the metal on metal couples, the samples could not be pulled apart by hand and separation was achieved in a similar manner. Examination of the separated surfaces again showed evidence of the joined areas.

Conclusions From the Second Phase Wet Seal Study - Of the non-metallic seal bearing materials investigated,  $Al_2O_3$  was the only candidate considered to show enough promise to warrant further study. While the initial application of radiation polymerized films appeared to offer positive benefits, the application was considered to best be judged after additional formation techniques had been developed. Thus, seal type studies using the radiation polymerized thin film were not recommended until additional investigation on these materials had been accomplished in the Thin Film Studies (see Section 5.2.5).

It was recommended that nonmetallic and porous metal structures receive additional study for possible application to wet seals.

#### 5.2.4 Metal-To-Metal Seals

Most of the metal-to-metal seal studies for application to valve closures have been concentrated on the simplest case, the flat poppet on the flat seat. Such studies as described in References 7, 8 and 22, have emphasized techniques for obtaining and measuring surface finish and flatness and have achieved zero leakage at very high seating stresses. Most other configurations, such as conical seats and poppets do not have a pure normal seating stress, but seal following an application of combined normal and shear stresses. The normal stress metal-to-metal seal has also been investigated in the AVT program as part of the wet seal concept discussed in Section 5.2.3 above. Another approach taken with metal-to-metal seals during the AVT program was to study the effectiveness of a seal obtained through nearly pure shear. In the experimental study described below, a ball was seated in a tube of slightly smaller internal diameter, with the only normal stress at the interface being that resulting from the elastic residual stress in the tube wall. This test program was referred to as the interference seal test.

5.2.4.1 Interference Seal Test Description - The test was performed with three tubes constructed from 17-4 PH stainless steel, and two tubes constructed from 6061-T6 aluminum, each with a different hole size, and spheres of three different materials: tungsten carbide, synthetic ruby, and pure aluminum oxide. The configuration of the interference fit ball seal test fixture is shown in Figure 5-64.

Prior to testing, the tubes and spheres were measured. The parts were then ultrasonically cleaned in Freon TF and individually bagged in clean polyethylene bags. The ruby spheres were examined under polarized light and the C axis of the sphere (which is perpendicular to the slip plane) was lightly marked with a felt pen. Precautions in handling were taken during testing to insure cleanliness of the spheres and tubes.

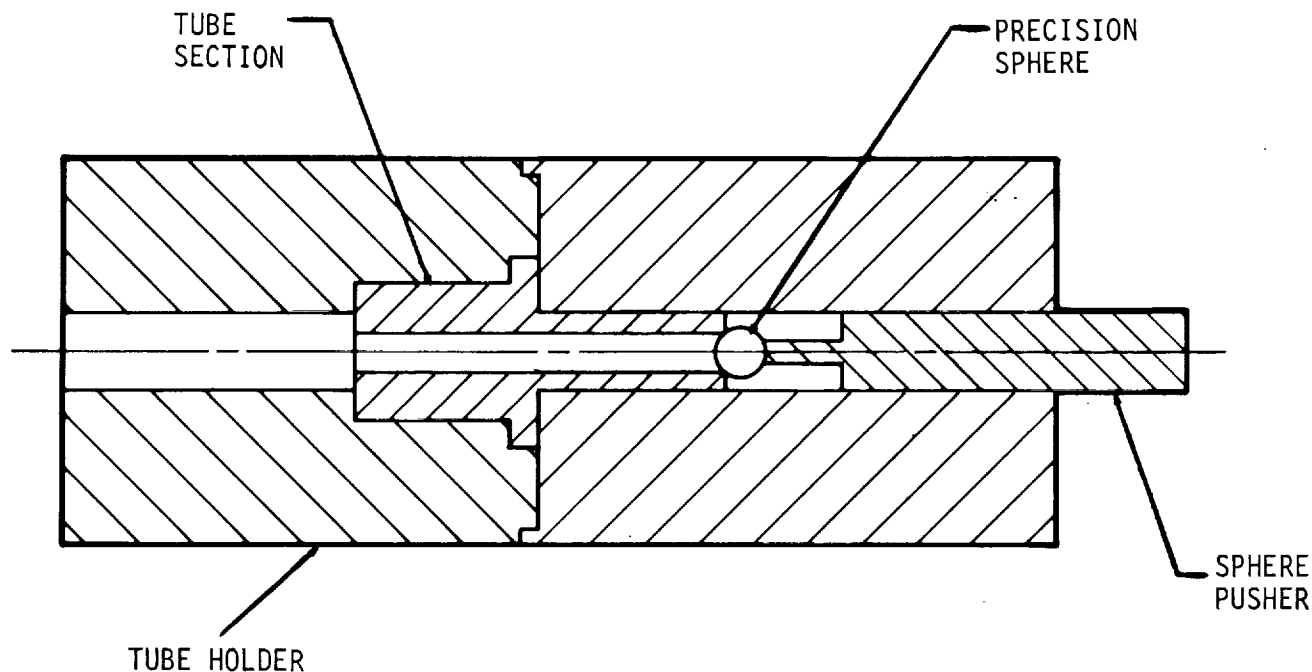


Figure 5-64. Interference Fit Ball Seal Test Fixture

To perform the test with stainless tubes, the tube O.D. was measured and then placed in the fixture. A sphere was placed at the hole entrance, and the top of the sphere was lightly marked with a felt pen to insure repeatability of reinsertion position. The test fixture was then assembled and placed in a Baldwin universal testing machine to apply the load and obtain a force readout. Load-displacement curves were plotted on an X-Y plotter. A Collins LVDT indicator was used to measure the displacement. The ball was initially forced to a depth of 0.200 inch. The tube with the captive ball was then helium leak-checked with a Veeco Model MS-9 leak detector. After the leak check, the O.D. of the tube was remeasured and the tube was reassembled into the test fixture.

The fixture was then inverted in the testing machine and the ball was forced out of the tube. This procedure was repeated at least three times with the exception that the ball reinsertion depth was 0.150 inch. In all cases, a low loading rate (30-50 pounds per minute) was used to minimize friction heating. The initial test on each tube was performed with a tungsten carbide sphere. These spheres were utilized in the initial test because the roughness traces indicated that they had the best finish of the spheres available.

Each tube was matched to a sphere to give the desired interference fit. Subsequent tests were performed on the used tubes with the alumina and ruby spheres, thus the initial interference fit is unknown for these experiments.

The test method used with the aluminum tubes consisted of initially inserting the spheres to a depth that provided at least 0.1 inch of constant diameter travel, as indicated by the load-displacement plot. The sphere was then cycled about the 0.1 inch constant diameter portion of tube without removing

the sphere. This test was performed with tungsten carbide and alumina spheres only. The method of testing of the aluminum tubes was changed from the method used for the steel tubes to provide a more precise investigation of leak rate, force, and repeatability.

5.2.4.2 Interference Seal Test Results - The test results are summarized in Table 5-16 for the stainless tubes and in Table 5-17 for the aluminum tubes. A description of each test series is discussed below.

#### 1. Stainless Tube, Tungsten Carbide Sphere

The shape of the load-displacement curve in all cases was the same: a relatively slow rise to maximum force value upon insertion, and a sharp rise to maximum force value when the sphere was pushed out, with a relatively rapid decrease in extraction force. Except for test No. 4, each traversal took a progressively larger force to move the sphere. Examination of the spheres showed that tungsten carbide sphere No. 7 had two "wear marks" on it; one at the equator, and one approximately 0.005 inch down from the equator in the insertion direction. Microscopic examination showed that the "wear" marks were smeared metal. The metal was smeared in both directions on the equatorial mark, but away from the insertion direction on the lower mark, indicating that it was made during the insertion cycle.

Examination of the tubes did not reveal any wear marks or signs of plastic deformation in the holes. Although the O.D. of the tube increased when the ball was inserted, the O.D. reverted to normal upon removal of the ball, which indicated that if plastic deformation occurred, it did not extend to the outside of the tube.

#### 2. Stainless Tube, Alumina Sphere

Examination of the roughness traces of the aluminum oxide spheres showed that they had the roughest finish of the three types of spheres (approximately 32 microinch rms). Consequently, the alumina test was performed after the tube had been used with tungsten carbide. After three cycles, the tube was visibly scored, and a relatively high leak rate was measured. A wear mark was observed on the sphere after one cycle, and after completion of the alumina tests, microscopic examination showed metal embedded on the surface of the sphere. The load cycle curves were similar in shape to tungsten carbide.

#### 3. Stainless Tube, Ruby Sphere

The tests using the ruby sphere were performed in a slightly different manner than the others. Since the tube had been used, it was decided to examine the effect of traversing the tube without removal. This was performed by inserting the sphere to a depth of 0.200 inch, leak testing, inverting the fixture and pushing the sphere back 0.150 inch, and leak testing again.

Table 5-16. Summary of Test Results For Stainless Steel Tubes

Test No.	Materials		Initial Diametral Interference (microns)	Penetration Depth (inches)	Maximum Force (pounds)		Leak Rate (scc/sec)
	Tube	Sphere			Insertion	Extraction	
1	17-4PH	Tungsten	50	0.200	33	44	$>2.5 \times 10^{-5}$ **
2	(Tube #3)	Carbide		0.150	46	49.5	$>2.5 \times 10^{-5}$ **
3		(Sphere #3)		0.150	47	51	$1.1 \times 10^{-3}$
4				0.150	36	40.5	$2.9 \times 10^{-4}$
5	17-4PH	Alumina	60*	0.150	59.5	66	$2.9 \times 10^{-3}$
6	(Tube #3)	(Sphere #21)		0.150	70	68	$4.6 \times 10^{-3}$
7				0.150	80	83	$5.5 \times 10^{-3}$
8	17-4PH	Tungsten	100	0.200	47	61	$1.2 \times 10^{-4}$
9	(Tube #1)	Carbide		0.150	70	80	$3.6 \times 10^{-5}$
10		(Sphere #2)		0.150	82	91	$6.7 \times 10^{-5}$
11				0.150	93.5	108	$4.1 \times 10^{-5}$
12	17-4PH	Tungsten	410	0.200	87	107	$1.1 \times 10^{-4}$
13	(Tube #2)	Carbide		0.150	110	123	$7.2 \times 10^{-5}$
14		(Sphere #7)		0.150	136	140	$6.3 \times 10^{-5}$
15	17-4PH	Ruby	300*	0.200	50	-	$3.9 \times 10^{-4}$
16	(Tube #2)	(Sphere #14)		0.050	72	-	$4.3 \times 10^{-4}$
17				0.200	88	-	$1.4 \times 10^{-4}$
18				0.050	105	-	$5.0 \times 10^{-4}$
19				0.200	52	76	$9.4 \times 10^{-5}$

\*Estimated

\*\*Readings were greater than leak detector maximum range - the range was increased for subsequent tests.

Table 5-17. Summary of Test Results For Aluminum Tubes

Test No.	Materials		Initial Diametral Interference (microns)	Penetration Depth (inches)	Maximum Force (pounds)		Leak Rate (scc/sec)
	Tube	Sphere			Insertion	Extraction	
1	6061-T6	Tungsten	210	0.200	22		$1.1 \times 10^{-2}$
2	(Tube #4)	Carbide (Sphere #9)		0.050		23	**
3				0.200	24	$1.2 \times 10^{-2}$	
4				0.100		23	$1.4 \times 10^{-2}$
5				0.370	24	$4.3 \times 10^{-3}$	
6				0.190		25	$9.9 \times 10^{-3}$
7				0.370	24	$5.2 \times 10^{-3}$	
8						27	-
1				6061-T6	Alumina	210*	0.300
2	(Tube #4)	(Sphere #24)		0.200		30	$3.7 \times 10^{-3}$
3				0.300	24	$1.0 \times 10^{-3}$	
4				0.200		23	$2.6 \times 10^{-3}$
5				0.300	19	$1.2 \times 10^{-3}$	
6				0		22	-
1				6061-T6	Alumina	170	0.300
2	(Tube #5)	(Sphere #23)		0.200		15	**
3				0.300	14	$1.2 \times 10^{-2}$	
4				0.200		15	**
5				0		18	-

\*Estimated

\*\*Leak rate was too great to allow pumpdown to leak detector.

The load cycle curves were different than those of the other two types of spheres. The first cycle resulted in a relatively slow rise in load to the maximum value, but the remainder of the cycles gave curves which initially had a rapid rise and then a slow taper, except for test No. 17 which had a rapid rise, then slowly increased until the end of the traversal, when it again rose rapidly.

Examination of the tube after the tests did not indicate that scoring or any wear had occurred, but the sphere had a discontinuous wear mark at the equator. Microscopic examination showed that metal was embedded in small pits on the surface of the sphere. These pits were evidently present before testing, since examination of the sphere showed random pitting over the entire surface, corroborated by the roughness trace. The ruby sphere was inserted with the force parallel to the C axis.

#### 4. Aluminum Tube, Tungsten Carbide Sphere

The shape of the load-displacement curves for the aluminum tubes differed from that of stainless tubes in that there was a sharp increase in force until movement of the ball and then the force remained constant until the force was removed. The leak rate was at least 10 times greater than with the stainless tubes, but remained constant for a given depth. In some cases the leak rate was so large that a leak measurement could not be performed. This was probably due to scratches and/or tool marks in the aluminum tube.

#### 5. Aluminum Tube, Alumina Sphere

The test with alumina spheres resulted in load-displacement curves similar to the tungsten carbide sphere. The alumina spheres did indicate a lower leak rate,  $1 \times 10^{-5}$  scc/sec, than the tungsten carbide sphere with the same insertion forces. Examination of the alumina sphere after the test showed a heavy layer of aluminum on the sphere surface. The metal layer probably resulted in the lower leak rate and provided a "tight" metal-to-metal seal.

5.2.4.3 Conclusions From the Interference Seal Tests - Minimum leak rate was observed with stainless tubes and tungsten carbide spheres and with an interference fit greater than 0.0001 inch.

Surface smoothness is extremely important to the attainment of low leak rates. Although the data are limited it appears that for low leak rates with hard materials, more than one cycle is beneficial and for soft materials the leak rate is not immediately affected by cycling.

Cycling hard materials tends to increase the required force. This phenomenon is probably the result of work hardening and increased metal-to-metal "sticktion".

5.2.4.4 Recommendations - It was recommended that further investigations be performed in the following areas:

1. Hard spheres, thin walled tubes of both hard and soft materials.
2. Thermal cycling
3. Detailed surface structure studies
4. Large interference between spheres and both soft and hard materials
5. Various tube geometries (e.g., tapered, etc.).

#### 5.2.5 Thin Film Studies

The thin film studies discussed in this section began as an outgrowth of activity originally investigated as part of the wet seal studies (Reference 60). The thin film materials of initial concern were radiation polymerized organic monomers produced in situ on the substrate surface. Later efforts (References 61, 62 and 63) considered electron polymerized films, film formation matrix studies and the application of thin films to spacecraft valves.

Thin film coatings obtained through electron polymerization of organic vapors have produced materials possessing unique properties of interest. Applications of these films may include anti-cold welding, propellant compatibility and sealing. Such applications require properties including mechanical stability, strong adhesion to the substrate, chemical and thermal stability, and continuity. It has been observed that such properties are highly structurally sensitive and depend upon formation condition variables.

As a result, subcontract university studies were initiated to study the physics of the formed films at Dartmouth College and the chemistry of formation at the University of Bradford, England. Much of the study effort has been devoted to the siloxane monomers although other thin film monomer systems have been examined. The film studies include characterizing electron polymerized coatings as a function of the electron/monomer ratio used during formation and include basic physical property measurements supplemented by observation of chemical compatibility, vacuum thermal stability and mechanical compliance.

At TRW, studies included the application of electron polymerized siloxane films to test valve seat materials for leakage and an initial evaluation of polyimide thin films.

5.2.5.1 Initial Experiments With Electron Polymerized Films - The initial experiment consisted of exposing a tungsten cylinder simultaneously to Dow Corning silicone oil DC-705 and a beam of low energy electrons. This cylinder had previously been used in the gallium dynamic seal test (Section 5.2.3 and Reference 45). The resulting surface could not be wet with liquid gallium or mercury using the technique previously employed to

satisfactorily wet uncoated samples. Removal of the film could not be effected with the following agents: kerosene, dilute nitric acid, toluene, and trichloroethylene. The tungsten coated sample was then exposed to gaseous fluorine for one minute at a rate of 2000 cc/min with again no visual change in the film.

Subsequently, four substrate materials were selected for conducting additional screening tests. The four materials were electron bombarded concurrently during a given film buildup in order to increase the number of samples obtained per vacuum exposure. The substrate materials consisted of one square inch samples of a Vycor glass, tungsten, 6061-T6 aluminum and 304 stainless steel. With this series of tests the role of formation variables were investigated.

The primary monomer utilized in these tests was Dow Corning DC-705 silicone oil, although a few films were made with Convoil 20. In these tests several preconditioning and exposure conditions in the film preparation were evaluated. The primary variables studied were thermal vacuum bakeout of the material samples prior to electron beam exposure, concentration of the monomer vapor, and electron beam current. Initial results of these film preparations indicated film adherence to be highly dependent upon formation conditions.

For both the DC-705 and Convoil 20 the best film adherence was obtained with high electron to vapor concentration ratios. A gross check of film adherence was made using mechanical abrasion as a test. All films which could be removed by vigorous scrubbing with wiper papers were eliminated from further evaluation. Those samples in which removal could not be effected by this technique were checked for chemical stability.

The films selected appeared to be unaffected when scrubbed by or soaked in solvents such as kerosene, dilute nitric acid, toluene, acetone, trichloroethylene and benzine. DC-705 films on Vycor glass, tungsten, aluminum and stainless steel were subjected to hydrazine ( $N_2H_4$ ) for six days with again no apparent change. To study edge effects, films of the Convoil oil covering sections of a Vycor and aluminum substrate were subjected to soak tests in dilute nitric acid. With both tests no apparent film degradation occurred after a five-day soak. However, after twenty-four hours the film on the aluminum substrate gave evidence of detaching at the film edge. At the end of the five-day period the film was completely freed. Examination of the substrate indicated the aluminum had been etched from under the film. No change was noted with the Vycor substrate. This result is consistent with requirements for continuous films if such are to be relied upon for protection of the base materials which are subject to attack. A summary of the experimental tests including results is presented in Table 5-18.

An additional series of tests were performed to see what effect application of electron-produced thin films might have on the permeation of Teflon. For this series of tests the helium permeation (relative) for various thicknesses of Teflon was measured before and after application of the coating. From these tests it was concluded no improvement in Teflon permeation to helium was achieved. A summary of the permeation data is presented in Table 5-19.



Table 5-18. Original Thin Film Coated Specimen Test Results

Substrate Material	Coating Monomer	Evaluation Conditions	Remarks
Tungsten (1)	Siloxane DC 705	Laboratory ambient. 5 min. scrub, 24 hr. soak in kerosene, dilute nitrate acid, toluene, trichloro- ethylene.  Ambient temperature. Exposed to direct gaseous fluorine at a rate of 2000 cc/min for 1 min.	No observed alteration.  No observed alteration.
Vycore glass (1) Tungsten (1) 6061 T6 Al (1) 304 Stainless (1)	Siloxane DC 705	Laboratory ambient. Soaked 6 days in N <sub>2</sub> H <sub>4</sub> hydrazine.	No apparent alteration.
Silicon (1)	Siloxane DC 705	Laboratory ambient. Nitric acid drop placed on film.	Nitric did not wet film.
Vycore glass (1) Tungsten (1) 6061 T6 Al (1) 304 Stainless (1)	Siloxane DC 705	Laboratory ambient. 5 min. scrub, soaked 2 hrs. in kerosene, toluene, acetone, trichloroethylene, benzine, dilute nitric acid.	No apparent alteration.
Vycore glass (1) Tungsten (1) 6061 T6 Al (1) 304 Stainless (1)	Convoil 20	Laboratory ambient. 5 min. scrub and soak kerosene, toluene, acetone, trichloroethylene, benzine.	No change
Vycore glass (1)	Convoil 20	Laboratory ambient. Soak dilute nitric acid 5 days.	No change
6061 T6 (1)	Convoil 20	Soak dilute nitric acid 5 days.	Film floated free etching substrate from underneath film.
Teflon multiple samples	Siloxane DC 705	Helium permeation.	No apparent improvement. See Table 5-19.
17-4PH Stainless (2)	Siloxane DC 704 biased	1 sample exposed to vacuum at 650°C to 700°C for 3 hrs.	No visual change.
17-4PH Stainless (3)	Siloxane DC 704	Being evaluated in hi vac coldwelding tests.	-----
17-4PH Stainless (2)	Siloxane DC 704 unbiased	1 sample exposed in vacuum 1 hr. at 800°C.	Film crazed, some dis- coloration.

Table 5-19. Thin Film Coated Teflon Helium Permeability  
 Test Results -  $\Delta P = 15$  PSIA

Before Coating Elapsed Time	$\Delta$ Concentration Helium Scale Reading*	After Coating Elapsed Time	$\Delta$ Concentration Helium Scale Reading*
<u>Teflon (PFE) 1.125" Thickness</u>			
0	0	0	0
9 min.	1	4 min.	0.025
10	8	5	10
11	10	6	10
<u>High Density Teflon 0.064" Thickness</u>			
0	0	0	0
1-15 sec.	10	1 sec	13
1-30	off scale	1-15	136
<u>High Density Teflon 0.125" Thickness</u>			
0	0	0	0
3-30 sec	.5	1 sec	6
4	4	2	4
4-15	8	3	2
4-30	8	4	4
5	20	5	12
5-30	20	6	28
<u>High Density Teflon 0.190" Thickness</u>			
0	0	0	0
3 min	.1	7 min.	0
5	.5	9	1
8	0	10	2
10	0.5	11	2
11	2	12	2
12	3	13	3
13	5	14	3
14	6	15	4
15	7	16	4
16	8	17	4

\*Scale readings are relative and no units are given.

5.2.5.2 Film Formation Matrix Studies - Two electron beam guns were utilized for production of the films. One gun was used for producing high electron flux of energy levels of 2,000 to 10,000 electron volts and the other producing low flux energy levels to 250 ev.

The films produced during the initial studies (Section 5.2.5.1 and Reference 60) using the high energy electron gun were considered in relation to the electron monomer ratio. This was a function of the experimental setup being employed and while adequately serving an initial purpose of demonstrating unique properties of the films, provided no mechanism for identifying and controlling the rate of monomer formation. As a consequence, the performance of more controlled (electron/monomer ratio) experiments was considered mandatory. Therefore, a series of films formed using the low and high energy guns were evaluated to provide a general engineering property assessment.

Film formations were performed by the Thin Film Department and the Crystal and Surface Physics Department of TRW Systems, each having special facilities available. These facilities and associated techniques have been developed over several years in conjunction with the application of electron polymerized monomer films for use as electrical insulators. Advantages of these facilities included the ability to accommodate a large substrate target area permitting incorporation of a number of samples. In addition, existing monomer vapor source evaporators and associated electronics permitted an immediate investigation of the role of electron/monomer ratio upon the resulting film properties.

The difference in film formation variables attributable to each facility is summarized as follows:

1. Low e/m ratio, low energy gun

- Initial matrix studies
- Electron energy -- 250 volts
- Electron flux --  $1.67 - 9.7 \times 10^{14}$  e/cm<sup>2</sup>/sec
- e/m ratio -- 0.6 - 4.87
- Integrated flux --  $1.45 - 8.27 \times 10^{17}$  e/cm<sup>2</sup>

2. High e/m ratio, high energy gun

- Energy dependence -- 2,000 - 10,000 volts
- Electron flux --  $10^{14} - 5 \times 10^{15}$  e/cm<sup>2</sup>/sec
- e/m ratio -- 19 - 930
- Integrated flux --  $2 \times 10^{18} - 1 \times 10^{20}$  e/cm<sup>2</sup>

Task A. Film Formation Matrix Studies, Low e/m Ratio - Fourteen sets (A-N) of four stainless steel one inch squares (see Table 5-20, Formation Conditions) were coated with thin films of various thicknesses and electron-monomer ratios. While the latter characteristic was specifically determined, film thickness was not a controlled variable. The samples were then tested for chemical, thermal and mechanical stability, as discussed in Table 5-21. Of the chemical tests, an acetone scrub, soaking in kerosene for 24 hours, applying a drop of dilute nitric acid, and coating with gallium eutectic liquid metal, only the nitric acid attacked the films. Neither a five-minute immersion in liquid nitrogen nor exposure to 500°C in vacuum and in air had any significant effect on the films. The films did become a deeper yellow upon heating, which may have been caused by oxygen diffusing through the film and reacting with the steel substrate, or possibly a carbon rich layer forming on the steel either by carbonization from the film or by migration of carbon from the substrate bulk. A glass sample coated with a thin film heated to the same temperature did not become yellow, leading to the conclusion that the film itself was not reacting to the high temperatures.

Mechanically, the films appeared stable, they were capable of conforming to the substrate as it was bent 20 degrees with a 1/4 inch radius. A summary of the test results is presented in Table 5-21.

No qualitative correlation could be made between either the thickness or electron-monomer ratio and the evaluations of the above tests. However, from previous experimentation, it had been found that an increase in the electron-monomer ratio resulted in an increased resistance to acid attack.

Task B. Film Formation Matrix Studies, High e/m Ratio - Because of the noted attack by nitric acid of all the films produced under Task A, it was decided to produce additional films of higher electron monomer ratios using the original equipment to supplement the previous results. It was also decided to briefly investigate the influence of integrated flux, electron energy dependence as well as electron/monomer ratio on the resultant film properties. Unfortunately, conclusive interpretation of the influence of all these variables was not possible as it was found the capability to maintain near constant sample temperatures during the formation periods was exceeded over the wide range of electron fluxes studied. The resultant films from these studies were evaluated for mechanical, chemical and thermal stability.

A total of ten sets (four samples/set) were prepared in this study. The formation conditions for each set are given in Table 5-22. In contrast to 250V electron produced films which had nearly uniform yellow-gold coloration, the films ranged from green, browns, golds, and purples. This was attributed to variation in thickness between the various samples. It will be noted the oil flux was kept constant for all formations so that the variation in film thickness must be a function of electron flux, energy and oil condensation-evaporation parameters. All three variables directly effect the total polymerization reaction cross-section. In a qualitative sense the following conclusions were drawn.

Table 5-20. Task A Formation Conditions

Specimen Groups 4 Each	250 ev Beam Current (ea)	Oil Source Temp °C	Deposition Time (min)	Post Deposition Electron Gun Time (min)	Thickness Å	Oil Molecule Flux mol/cm <sup>2</sup> /sec	$\Sigma \omega$	Electron Flux e/cm <sup>2</sup> /sec	$\Sigma \epsilon$	Electron $\frac{\Sigma \epsilon}{\text{Nominal}}$
A	7.5	100.75	7	3		$10.7 \times 10^{15}$	$1.55 \times 10^{17}$	$6.8 \times 10^{14}$	$4.08 \times 10^{17}$	2.63
B	2.5	100.3	7	3		11.6	1.68	2.48	1.49	0.9
C	10.0	100	12	3		10.4	2.58	7.4	6.67	2.58
D	2.5	102	12	3		11.2	2.78	1.85	1.67	0.6
E	10.0	100	10	3		10.4	2.15	6.80	5.30	2.46
F	10.0	99	8	3		10.3	1.7	8.0	5.3	3.12
G	2.6	95.5	8	6	290	8.8	1.84	1.73	1.45	0.79
H	8.0	99	10	6		10.3	2.13	6.17	5.92	2.78
I	10.0	99	8	6		10.3	1.7	9.7	8.27	4.87
J	3.0	98	8	6		10.0	1.66	1.85	1.55	0.94
K	10.0	98	8	3		10.0	1.66	7.4	4.9	2.95
L	10.0	95.5	8	3	180	8.8	2.0	6.17	4.18	2.09
M	7.0	95.5	8	6	430	8.8	1.46	5.68	4.77	2.95
N	2.0	95.5	8	12	600	8.8	1.46	1.67	2.0	1.37

Table 5-21. Task A Test Results

Specimen Grouping	Acetone Scrub	Kerosene Soak (24 Hrs)	HNO <sub>3</sub> Drop (4 Hrs)	LN <sub>2</sub> Immersion 5 Min Acetone Scrub	Heat in Vacuum to 500°C	Heat in Air to 500°C
A	NC*	NC	Attached	NC	Yellow	HNO <sub>3</sub> Spot Brown 350° Brown 470°
B	NC	NC	Attached	NC	Much Yellow	X Brown 470°
C	NC	NC	Attached	NC	Yellow	X
D	NC	NC	Attached	Hard Scrub Lightening	Lavender-Yellow at 460°	
E	NC	NC	Attached	Hard Scrub Lightening	Pink-Yellow at 400°	Brown 480°
F	NC	NC	Attached	NC	Pink-Yellow at 400°	X
G	NC	NC	Attached	X	Slightly Yellow	X
H	NC	NC	Attached	NC	Purple-Lavender at 460°	Purple-Lavender 285° Lavender-Gold 325° Brown 470°
I	NC	NC	Attached	NC	Spotty at 470°	X
J	NC	NC	Attached	NC	Slightly Yellow	HNO <sub>3</sub> Spot Brown 350°
K	NC	NC	Attached Rapidly	Hard Scrub Lightening	Yellow	X
L	NC	NC	Attached	X	Very Slightly Yellow	HNO <sub>3</sub> Spot Brown 350° Brown 470°
M	NC	NC	Attached Rapidly	X	Almost NC	Brown 470°
N	NC	NC	Attached	X	Yellow	X

\*No Change

1. Higher energy electrons 5000V and 10,000V appear to have a lower reaction cross-section than 2000V electrons.
2. At a constant energy, an increase in flux increases the rate of film formation. At 2000 eV the flux does not appear to have saturated the reaction rate.
3. Thermal effects on condensation-evaporation processes, even with high electron fluxes negated to a high degree significant amounts of film formation. This demonstrates a fairly long reaction time for the polymerization reaction, requiring long dwell times of the monomer on the substrate. Since the substrate temperatures were well below the thermally stable temperatures of films once polymerization has taken place, the effect appears to be controlling only in the reaction kinetics. Clearly, sticking coefficients near 1 are desirable and require the substrate temperature be kept well below room temperature. The evaporation rate of D.C. 704 at room temperature is approximately 1/5 the oil molecular flux directed at the substrate in these tests. For the samples H and I in which the target temperature exceeded room temperature for most of the deposition period -- the impinging oil molecules were reevaporated as fast as they arrived.

A composite color photograph of the ten sample groups was included in Reference 61 which showed a circular pattern which is the area of primary electron beam impingement. It is within this area the electron flux values are pertinent and the following film evaluations were made. The tests performed were an acetone scrub, 20-hour kerosene soak, nitric acid drop test, 460°C vacuum exposure and the mechanical bend test.

A tabulated summary of the results is given in Table 5-23.

#### Test Summary - Task A

##### Compatibility Tests

##### Acetone Scrub - Sample 1 (Group A through N)

(This test was performed after every other test). The specimens were scrubbed with acetone and a cotton bud.

##### Kerosene Soak - Sample 1 (Group A through N)

Specimens were immersed in kerosene for 24 hours with no apparent effect.

##### Dilute (20% $\text{HNO}_3$ + 80% $\text{H}_2\text{O}$ ) Nitric Acid Test - Sample 1 (Group A through N)

In all cases, dilute  $\text{HNO}_3$  attacked the films. Acid did not wet the surface immediately. Attacking of the film, in most cases, was only under the drop. A few had small "halos" around the drop, and two, K and M, had larger halos.

Table 5-22. Task B Formation Conditions

Specimen Grouping	Color	Faraday Cup Current	Electron Energy	Oil Temp.	Deposit Time	Substrate Temp. at End of Exposure	Oil Flux mol/cm <sup>2</sup> /sec	$\Sigma \omega$ mol/cm <sup>2</sup>	Electron Flux e/cm <sup>2</sup> /sec	$\Sigma e$	Electron $\Sigma$ Monomer $\Sigma \omega$
A	Green	200 $\mu$ a	2kV	80°C	6 hrs.	-47°C	$5.4 \times 10^{12}$	$1.19 \times 10^{14}$	$2.04 \times 10^{14}$	$5.32 \times 10^{18}$	38
B	Dark Brown	500 $\mu$ a	2kV	80°C	6 hrs.	-47°C	$5.4 \times 10^{12}$	$1.19 \times 10^{14}$	$5 \times 10^{14}$	$1.08 \times 10^{19}$	93
C	Dark Brown	1ma	2kV	80°C	6 hrs.	+9°C	$5.4 \times 10^{12}$	$1.19 \times 10^{14}$	$1.04 \times 10^{15}$	$2.16 \times 10^{19}$	190
D	Gold	100 $\mu$ a	5kV	80°C	6 hrs.	-78°C	$5.4 \times 10^{12}$	$1.10 \times 10^{14}$	$1.04 \times 10^{14}$	$2.16 \times 10^{18}$	19
E	Yellow	200 $\mu$ a	5kV	80°C	6 hrs.	-52°C	$5.4 \times 10^{12}$	$1.19 \times 10^{14}$	$2.04 \times 10^{14}$	$5.32 \times 10^{18}$	38
F'	Purple & Gold	500 $\mu$ a	5kV	80°C	2 hrs.	+4°C	$5.4 \times 10^{12}$	$3.96 \times 10^{15}$	$5 \times 10^{14}$	$3.6 \times 10^{18}$	93
F	Purple & Gold	500 $\mu$ a	5kV	80°C	6 hrs.	-5°C	$5.4 \times 10^{12}$	$1.19 \times 10^{16}$	$5 \times 10^{14}$	$1.08 \times 10^{19}$	93
G	Brown	1ma	5kV	80°C	6 hrs.	+37°C	$5.4 \times 10^{12}$	$1.19 \times 10^{16}$	$1.04 \times 10^{15}$	$2.16 \times 10^{14}$	190
H	Brown	5ma	5kV	80°C	6 hrs.	+214°C	$5.4 \times 10^{12}$	$1.19 \times 10^{16}$	$5 \times 10^{15}$	$1.08 \times 10^{20}$	930
I	Brown	500 $\mu$ a	10kV	80°C	6 hrs.	+47°C	$5.4 \times 10^{12}$	$1.19 \times 10^{16}$	$5 \times 10^{14}$	$1.08 \times 10^{14}$	93

Table 5-23. Task B Test Results

Specimen Grouping	Acetone Scrub	Kerosene Soak (20 hrs)	HNO <sub>3</sub> Drop	Heat in Vacuum 460°C
A	NC*	NC	NC	Duller***
B	NC	NC	NC	Duller***
C	NC	NC	NC	Duller***
D	NC	NC	Attacked under drop	Lighter
E	NC	NC	Very slight attack under drop	Lighter
F'	NC	NC	Film attacked under and around drop	Duller***
F	NC	NC	Slight attack	Duller***
G	NC	NC	Film removed** wherever scrubbed	Duller***
H	NC	NC	Attacked**	---
I	NC	NC	Attacked**	---

\*No Change - \*\*May be result of high substrate temperatures during formation.

\*\*\*All dark samples evidenced material transfer upon a cotton bud scrub with acetone.

## Thermal Stability Tests

### LN<sub>2</sub> Immersion - Sample 2 (Group A through N)

Specimens were lowered into LN<sub>2</sub> with tongs, and left for 5 minutes. Upon removal, the entire sample frosted, although frost first formed on the sample surface not coated with film. The frost melted after about 5 minutes, leaving tiny drops of water on the film, and larger more irregularly shaped drops on the uncoated parts of the specimen.

### Thermal Test in Vacuum - Sample 2 (All Temperatures °C) (Group A through N)

Specimens were placed on a hot plate under a bell jar and the vacuum was held at 10<sup>-5</sup> mm Hg for 18 hours prior to heating. The time taken to reach each temperature was: 0°-100° 6 minutes; 100°-200° 6 minutes; 200°-300° 8 minutes; 300°-400° 10 minutes; 400°-500° 25 minutes; the temperature was held at 500° for 35 minutes during which time no change was observed. The general result of this test was a yellowing of the films - this did not occur until the specimens were above 400°C. The only effect acetone scrubbing had was to make specimen H, which had been purple, and turned yellower at 460°, regain its purple cast.

### Thermal Test in Air - Sample 1 (Half the samples were treated)

This test caused the films to react more than the previous test. The time taken to reach temperature was: 0°-100° 7 minutes; 100°-200° 8 minutes; 200°-300° 10 minutes; 300°-400° 13 minutes; 400°-420° 12 minutes; heat shield put on: 420°-480° 7 minutes. All specimens began to yellow at 280°; they were quite deep gold by 400° and by 470°, all but one were brown and dull. The darkness of the specimens was noted at several temperatures. In order, from dark to light, they were:

	Room	380°	420°	470°
Darkest	H	H	H	H
	E	J	J	J
	J	C	E	M
	L	M	M	C
	A	L	C	L
	M	E	L	A
Lightest	C	A	A	E

The acetone scrub lightened all the specimens, but in general, they appeared about the same spotty brownish gold.



### Liquid Metal Wetting Test

#### Sample 3 (Group A through N)

Gallium eutectic liquid metal was burnished on each specimen with a cotton bud. In all cases, the specimens showed good wettability. Sandwiched together, A+B, C+D, etc., the 14 specimens were stacked with a 100 gm weight on top, and left for 30 days. At the end of this time all samples readily separated and upon removal of the gallium showed no evidence of film or substrate material reaction.

### Mechanical Test

#### Sample 4 (half the specimens, Group A through N)

Specimens were bent at a 20 degree angle at a quarter-inch radius, in a fixture designed to protect the film coating. An uncoated sample was similarly bent. In all cases, the texture of the specimens were more grainy at the bend, but the film appeared intact, which leads to the conclusion that all observable change in texture was in the substrate steel, rather than the film.

### Test Summary - Task B

#### Acetone Scrub

The first sample from each group (1A-1I) was scrubbed with acetone on a cotton bud, with no change in color resulting on any of the ten samples.

#### Kerosene Soak

Samples 1A-1I were immersed in kerosene for 20 hours. They were then rinsed with water and subsequently scrubbed with acetone with no apparent change in films 1F.

#### Nitric Acid Tests

A drop of concentrated (90%)  $\text{HNO}_3$  was placed on samples 1A-1I, and was left to evaporate on the film. The films were then scrubbed with acetone. Samples 1A, 1B and 1C were unaffected by the acid, but the remaining films were attacked to varying degrees, from a slight lightening of the film under the drop to apparent removal of the film from the whole sample. The general resistance of most of the films with  $e/m > 10$  was considerably better in most cases than those  $< 10$  which were attacked by 20%  $\text{HNO}_3$ . An isolated test of hydrofluoric acid showed rapid attack through the film.

## Vacuum - Thermal Treatment

Samples 2A-2I were heated to 460°C at  $10^{-6}$  torr over a period of 3 hours. Analysis by color showed that the dark purple samples (2A, 2B and 2C) became quite dull, the bright yellow samples (2D and 2E) became even brighter, and the rest of the films generally lightened. The films were then scrubbed with acetone, with a resultant lightening of all films. The dark ones lightened the most, the bright yellows hardly changed at all.

## Mechanical Bend Test

Samples 4A-4I were bent 20 degrees with a quarter-inch radius. Each film changed to the same color, light gold at the bend, regardless of the original film color. No evidence of film crazing or separation from the substrate could be noted.

## Conclusions

### Task A - Low em/ ratios - low electron energy

1. General mechanical adherence good - no damage to films from handling or scrubbing.
2. Little effect, if any, due to acetone, kerosene or gallium.
3. Substrate protected by film from gallium attack.
4. Film attacked by dilute nitric acid.
5. Thermal stability good.
6. Mechanical adherence unchanged by bending substrate.
7. No correlation between electron-monomer ratio and results of tests.

### Task B - High e/m ratios - high electron energy

1. General mechanical adherence good.
2. No effect due to acetone or kerosene.
3. No attack of films by dilute nitric acid.
4. Many films unattacked by concentrated nitric acid.
5. Thermal stability good.
6. Mechanical adherence unchanged by bending substrate.
7. Film attacked by concentrated hydrofluoric acid.
8. Qualitative relationship between electron-monomer ratio and results.

5.2.5.3 Metal-to-Metal Leakage Studies with Thin Films - These tests were undertaken to ascertain any positive benefits to be derived by placing coatings of the siloxane films on the sealing surfaces of flat metal-metal seals. Accrued benefits were ascertained by helium mass spectrometer leak detector measurements made of selected seal surface combinations before and after application of the films.

Film formation conditions were derived from the results of the Film Formation Matrix Studies discussed in Section 5.2.5.2 above. Of primary consideration was the influence of mechanical compliance and thickness as controlled variables.

This metal-to-metal leakage study entailed the use of thin films, independently and with gallium, as seals between glass, metal, and alumina. Test samples, of flat configuration, were ground and polished to optical flatness, and then leak checked before being coated. The tests performed on these samples are explained in the Test Summary.

Four sets of pyrex glass samples were coated with films; two 1500 Å and two 3000 Å thick. Leakage was greater with than without films. Application of gallium over the siloxane films did not effect sealing. Two new sets of glass substrates were coated with gallium only, and a good seal was achieved for both. They resealed after a limited number of poppet like separations. The surfaces were then cleaned, repolished, and recoated with gallium; after being checked for leaks, they were stored for 18 days. Following this time, they were leak checked with favorable results. One set resealed after several separations, the other leaked after it was first separated, and still leaked when new gallium was applied.

One set of metal samples was coated with gallium and a seal was achieved, though after repeated separations, the seal deteriorated. Two metal sets were coated with siloxane films and both leaked. Gallium was applied on one of these, yielding a seal. The set was left for 18 days and then checked and was found to leak.

Because of experimental limitations, the Task A e/m ratios could only be varied by a factor of 6.

The alumina surfaces were burnished with gallium, however, they leaked so badly that it seemed doubtful a seal could be obtained with film. Therefore, no more tests were performed.

An evaluation of the above results, which are listed in Table 5-24, indicate that due to the interaction of gallium and siloxane films the attainment of low leakage seals was not possible. Since gallium on glass provided a good static seal, and the liquid metal did not react with the substrate, the use of this material combination as a seal under some conditions appears acceptable.

Water appears to wet the thin film coated specimens. Further investigation of wettability to propellants will be accomplished. The purpose of these tests will be to support the concepts of providing a non-wettable material for valve seats; thereby preventing or improving leakage due to the surface tension of the liquid itself rather than using gallium or other wettable liquids at the seat interface (see Section 5.2.3 above).

Table 5-24. Metal-to-Metal Seal Test Results  
With Thin Films (wet and dry)

Metal Specimens	No Coating	Siloxane Film	Film Thickness	Gallium	Repeated Separations	18 Day Gallium
440 S/N 2	Leak <sup>1</sup>	Leak		No Leak <sup>3</sup>	(No leak, out of total separations)	Leak
440 S/N 3	Leak			Leak		
440 S/N 5	Leak	Leak				
Hi Speed S/N 3	Leak					
<u>Glass Specimens</u>						
1 (unpolished lip)	Leak			No Leak	5 out of 9 <sup>4</sup>	First only, out of 6
2 (unpolished lip)	Leak			No Leak	10 out of 13 <sup>4</sup>	7 out of 11 <sup>4</sup>
3	Leak	Bad Leak	3000 Å	Leak		
4	Bad Leak <sup>2</sup>	Bad Leak	3000 Å	Leak		
5	Leak	Bad Leak	1500 Å	Leak		
6	Bad Leak	Bad Leak	1500 Å	Leak		
7	Bad Leak	Bad Leak	3000 Å	Leak		

<sup>1</sup>Greater than maximum detectable helium leak.

<sup>2</sup>Throttle valve on leak detector could not be opened.

<sup>3</sup>Less than minimum detectable leak,  $1.92 \times 10^{-10}$  scc/sec.

<sup>4</sup>Seals which leaked interspersed with those which did not.

## Test Summary

### No Coating

The flat polished specimens were leak checked, using a detector with a minimum sensitivity of about  $10^{-3}$  scc/sec. None of the substrate materials were able to seal under these conditions.

### Siloxane Film Coating

Films of various thicknesses were deposited on the specimens. Care was taken in bringing the samples together, such that translation and rotation of the surfaces were minimized. All film coated samples showed leak rates so high (>leak detector minimum sensitivity), it was impossible to determine whether greater film thickness enhanced or detracted from the seal.

### Gallium Coating

Gallium eutectic liquid metal was burnished with a cotton bud on the polished substrate surfaces. The specimens were both translated and rotated to make a better seal, with no apparent damage to the glass surfaces, though scratches were noted on the metal when the gallium was removed.

### Repeated Separations

Testing for possible use in valves with poppet-type action, the specimens which had sealed in the above tests, were repeatedly separated and rejoined, each time rotating the surfaces on each other, and leak checked. The test on each set of specimens was stopped after three successive observations showed leakage.

### Gallium Over Siloxane Film

With the possibility that gallium would help seal the leaky film coated substrates, it was carefully applied on top of the films. All glass specimens still leaked, though a seal was achieved on one set of metal specimens.

### Long Term Test

The two sets of gallium coated glass specimens and one set of siloxane film and gallium coated metal specimens were left for 18 days, and then leak checked. If still sealed, they were separated and rejoined as in the above test.

## Conclusions

1. Film alone not good as a seal for metal or glass.
2. Gallium seal between metal obtainable, but it deteriorates rapidly.
3. Gallium seal between glass has zero leak rate for several days, samples reseal after poppet type separations.
4. Glass + film + gallium worse than glass + gallium.
5. Metal + film + gallium poor seal.

5.2.5.4 Application of Thin Films to Spacecraft Valves - The objective of this study was to investigate the effectiveness of the siloxane thin coatings used as a seal (Reference 63). Control (uncoated) specimens were used for purposes of providing leakage correlation. The siloxane was applied by electron beam polymerization of DC-704 silicone oil in vacuum. The test conditions for the seat specimens included inlet pressures of 5-1400 psi and clamping loads of 3 to 1000 pounds. Measurements were made with the use of water displacement and the He mass spectrometer.

Test Specimen and Fixture - The physical configuration of the test specimens used in the test are detailed in Figure 5-65. They consist of a lower specimen whose upper surface is lapped and an upper specimen, the center of which is relieved to provide a well defined flat lapped sealing lip 0.060 inch width. The lip seal and the mating surface are lapped to a flatness of better than 1/4 wave of visible light using optical lapping techniques. The specimens are fabricated of 17-4 PH H-1075 stainless steel.

A cross-section of the test fixture is shown in Figure 5-66.

The fixture holds the test specimens and allows a controlled clamping load to be applied. Freedom of motion is provided to allow free alignment of the specimens. The clamping load is applied as a pressure through the load pressure port to the loading piston. The loading piston is relieved in the center similar to the upper test specimen. This causes the load to be applied directly in line with the sealing lip and minimizes any bending loads on the test specimens. The lower seat is also supported in a manner minimizing bending loads. A pumpout port is provided between the dual seals sealing the lower test seat to the fixture leak measurement port. This allows the area between the seals to be evacuated if a vacuum leak is suspected as when a mass spectrometer leak detector is attached at the test port. It was not found necessary to use the pumpout during the test program.

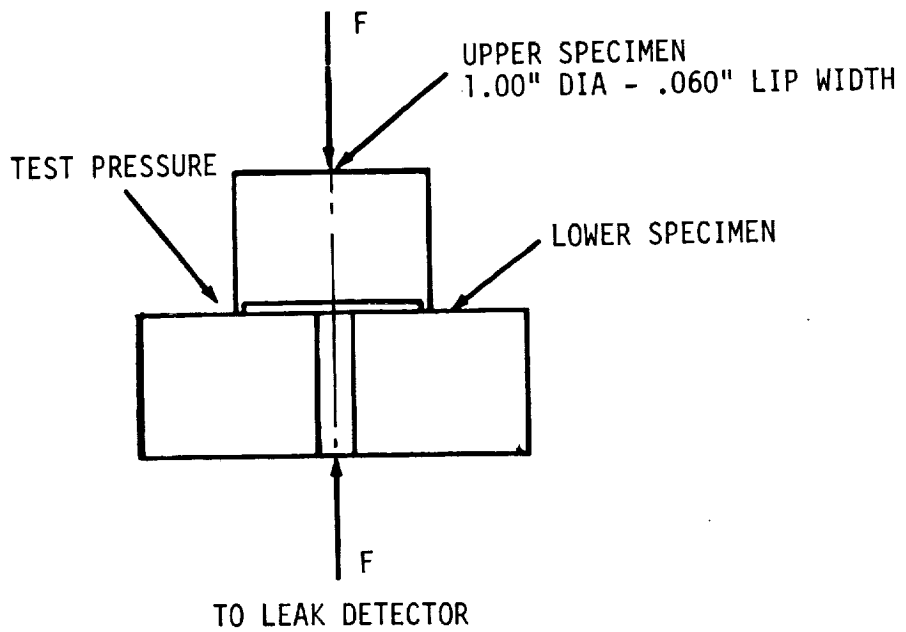


Figure 5-65. Seat Specimens for Thin Film Leakage Tests

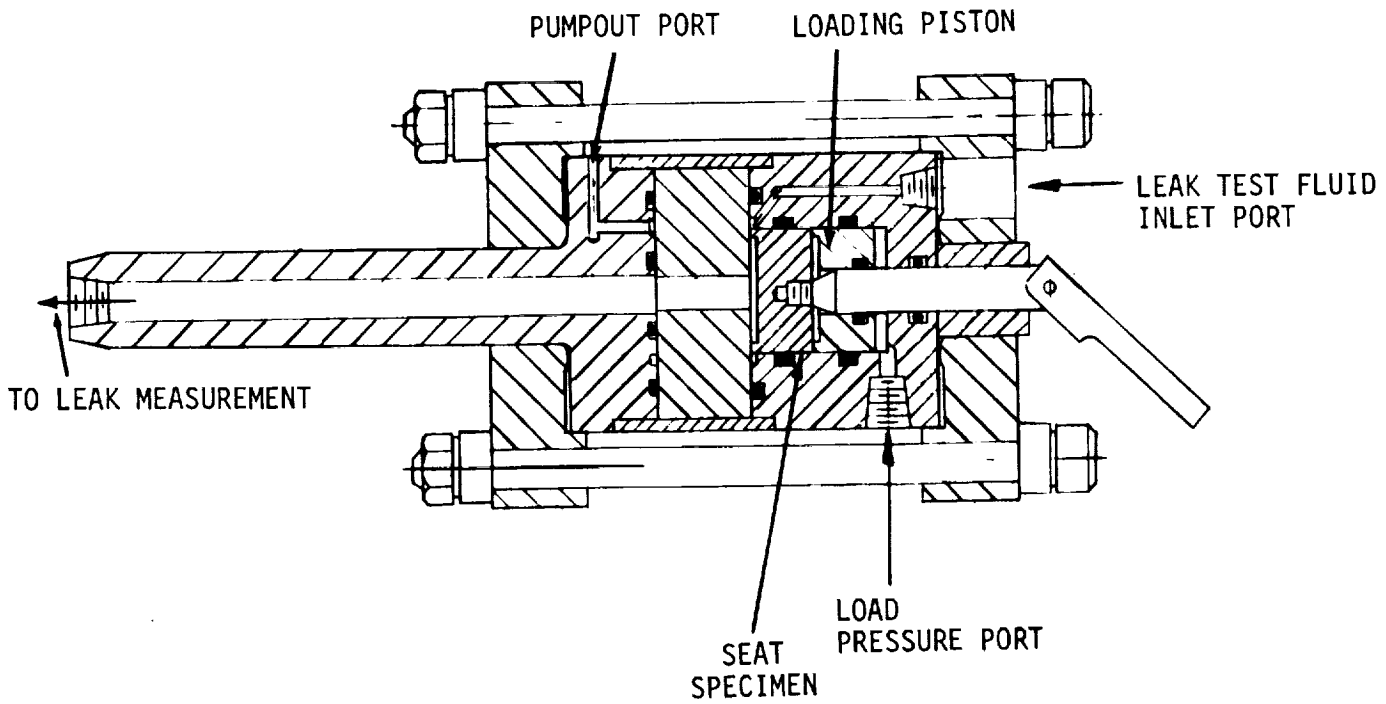


Figure 5-66. Valve Seal Leakage Fixture

Test Procedure - The specimens were thoroughly cleaned using high purity Freon TF and lens paper. The specimens were then examined and tested according to the following sequence:

1. The specimens are examined and photographed to record surface characteristics.
2. The specimens are installed in the test fixture.
3. The specimens are tested for leakage flow at a clamping load of approximately 3 pounds with inlet pressures of approximately 5, 10, 20, 40, 100, 200, 400, 800, and 1400 psig with N<sub>2</sub> as the test fluid.
4. The test series in 3 is repeated with a clamping load of approximately 30 pounds.
5. The test series in 3 is repeated with a clamping load of approximately 300 pounds.
6. The test series in 3 is repeated with a clamping load of approximately 1000 pounds.
7. Steps 3 through 6 are repeated using helium as the test fluid.
8. Steps 3 through 6 are repeated using water as the test fluid.
9. One seat specimen is coated with siloxane.
10. Steps 1 through 8 are repeated.
11. The remaining seat specimens from the set are coated.
12. Steps 1 through 8 are repeated.

Coating Procedure - The specimens were siloxane coated by electron beam polymerization of DC 704 silicone oil monomer in vacuum. The following procedure was followed in coating the specimens:

1. Sonic clean in detergent and deionized water.
2. Rinse in deionized water.
3. Wash in 10% Trisodium phosphate solution.
4. Rinse in deionized water.
5. Soak in clean deionized water and re-rinse.
6. Blow dry with clean dry nitrogen.



7. Immediately place in vacuum chamber. Heat sample to approximately 175°F and hold at  $2 \times 10^{-5}$  torr or better overnight.
8. Add LN<sub>2</sub> to cold trap and heat oil to 85°C. Irradiate with electron gun - 3KV 2.5 ma beam. Scan beam with deflector plates to assure even irradiation of the entire surface. Continue for approximately 2-1/4 hours.
9. Allow specimen and oil to cool and remove from vacuum chamber.

Test Results - Leak test results are tabulated in Tables 5-25 through 5-31 and are further described in the plots of Figure 5-67.

#### Conclusions and Recommendations

1. The nitrogen leakage at 3.4 pounds load or 18.5 psi surface stress was higher using the coated specimens.
2. The nitrogen leakage at 33.9 pounds or 185 psi surface stress was not significantly affected when the upper seat was coated. The leakage was improved at low inlet pressures when both specimens were coated, however, there was no significant difference at an inlet of 50 psi and gross leakage occurred at 100 psi. Gross leakage did not occur below 200 psi during the uncoated tests and the tests with the upper seat coated.
3. The nitrogen leakage at 339 pounds load or 1850 psi surface stress was significantly lower for the coated as compared to the uncoated specimens. The tests with both specimens coated showed higher leakage levels than those with only the upper seat coated. The tests with the upper seat coated showed an order of magnitude improvement compared to the uncoated tests while the tests with both specimens coated showed a factor of two improvement compared to the uncoated tests.
4. The nitrogen leakage at 1017 pounds load or 5550 psi surface stress was below that measurable by our apparatus over the entire inlet pressure range for the uncoated specimen tests and the upper seat coated tests. A leakage of  $1.67 \times 10^{-4}$  sccs was found in both specimen coated tests at the maximum inlet pressure of 1400 psi.
5. The helium leakage at 3.4 pounds load or 18.5 psi surface stress was beyond the range of our mass spectrometer leak detector for all coated and uncoated tests.
6. The helium leakage at 33.9 pounds load or 18.5 psi surface stress was beyond the range of our mass spectrometer leak detector except for the 5 psi inlet case with both specimens coated which showed a leak rate of  $2.1 \times 10^{-4}$  sccs.

Table 5-25. Effect of Thin Films on Seal Leakage

Sample 1A Uncoated Against 1B Uncoated Temperature 22.5°C

Leakage in SCCS N<sub>2</sub> SCCS He SCCS H<sub>2</sub>O

P Inlet Press. Psig	3.4 (18.5 psi)			33.9 (185 psi)			339 (1850 psi)			1017 (5550 psi)		
	N <sub>2</sub>	He	H <sub>2</sub> O	N <sub>2</sub>	He	H <sub>2</sub> O	N <sub>2</sub>	He	H <sub>2</sub> O	N <sub>2</sub>	He	H <sub>2</sub> O
5	1.84 x 10 <sup>-3</sup>			0			0			0 over 10 min		
10	4.74 x 10 <sup>-3</sup>			0 over 10 min			0			0		
20	20.5 x 10 <sup>-3</sup>			5 x 10 <sup>-4</sup>			0			0		
50	Gross →			(1) 3.0x10 <sup>-2</sup>			0			0		
100				0.1			0			0		
200				0.55			0 over 10 min			0		
400	Sample preset with 34 lb load			Gross @ 350 psi →			1.33 x 10 <sup>-3</sup>			0		
800							6.0x10 <sup>-3</sup>			0		
1400										0 over 10 min		

Remarks: (1) 1.17 x 10<sup>-3</sup> @ 40 psi

Table 5-26. Effect of Thin Films on Seal Leakage

Sample 2A Uncoated Against 2B Uncoated Temperature 22.5°C

Leakage in P Inlet Press. Psig	3.4 (18.5 psi)			33.9 (185 psi)			339 (1850 psi)			1017 (5550 psi)					
	SCCS	N <sub>2</sub>	He	SCCS	H <sub>2</sub> O	He	SCCS	H <sub>2</sub> O	He	SCCS	H <sub>2</sub> O	He			
5	1.39 x 10 <sup>-3</sup>						1.67 x 10 <sup>-3</sup>			0			0		
10	3.6 x 10 <sup>-2</sup>						3.34 x 10 <sup>-3</sup>			0			0		
20	0.123						7.79 x 10 <sup>-3</sup>			0			0		
50	Gross						3.08 x 10 <sup>-3</sup>			0			0		
100							0.15			0			0		
200							1.04			0 over 12 min			0		
400							Gross ↓			1.0 x 10 <sup>-3</sup>			0		
800										3.34 x 10 <sup>-3</sup>			0		
1400										25.0 x 10 <sup>-3</sup>			0 over 10 min		

Remarks:

Table 5-27. Effect of Thin Films on Seal Leakage

Sample 3A Uncoated Against 3B Uncoated Temperature 22.5°C

Leakage in SCCS N<sub>2</sub> SCCS He SCCS H<sub>2</sub>O

P Load F Inlet Press. Psig	3.4 (18.5 psi)			33.9 (185 psi)			339 (1850 psi)			1017 (5550 psi)		
	N <sub>2</sub>	He	H <sub>2</sub> O	N <sub>2</sub>	He	H <sub>2</sub> O	N <sub>2</sub>	He	H <sub>2</sub> O	N <sub>2</sub>	He	H <sub>2</sub> O
5	2.78 x 10 <sup>-2</sup>	Gross →	0	4.0 x 10 <sup>-3</sup>	Gross →	0	0	2.24 x 10 <sup>-5</sup>	0	0	4.8 x 10 <sup>-8</sup>	0
10	9.34 x 10 <sup>-2</sup>	8.34 x 10 <sup>-3</sup>	0 over 10 min	14.5 x 10 <sup>-3</sup>	0 over 10 min	0	0	Gross →	0	0	4.8 x 10 <sup>-8</sup>	0 →
20	.617	2.0	3.33 x 10 <sup>-4</sup>	3.83 x 10 <sup>-2</sup>	0	0	0	0	0	0	4.8 x 10 <sup>-8</sup>	
50	Gross ↓		5.00 x 10 <sup>-4</sup>	0.157		0 over 10 min	0		0	0	4.8 x 10 <sup>-8</sup>	
100			9.04 x 10 <sup>-4</sup>	0.617		6.77 x 10 <sup>-4</sup>	0		0	0	4.8 x 10 <sup>-8</sup>	
200			2.0 x 10 <sup>-3</sup>	.234		2.67 x 10 <sup>-3</sup>	0		0	0	4.8 x 10 <sup>-8</sup>	
400			Gross →	Gross →	Gross →	1.04 x 10 <sup>-2</sup>	0		0	0	4.8 x 10 <sup>-8</sup>	
800						8.0 x 10 <sup>-2</sup>	0		0	0	5.4 x 10 <sup>-5</sup> (1)	
1400						1.20	0 over 10 min		0 over 10 min	0 over 10 min		

Remarks: (1) 8 x 10<sup>-6</sup> @ 640 psi

Table 5-28. Effect of Thin Films on Seal Leakage

Sample 3A Siloxane Coated Against 3B Uncoated Temperature 22.5°C

Leakage in P Load F Inlet lbs. Press. Psig	3.4 (18.5 psi)		33.9 (185 psi)		339 (1850 psi)		1017 (5550 psi)	
	N <sub>2</sub>	He	N <sub>2</sub>	He	N <sub>2</sub>	He	N <sub>2</sub>	He
5	0.226	1.17 x 10 <sup>-3</sup>	6.67 x 10 <sup>-3</sup>	Gross →	0	4.8 x 10 <sup>-7</sup>	0	3.84 x 10 <sup>-8</sup>
10	Gross →	5.5 x 10 <sup>-3</sup>	6.67 x 10 <sup>-3</sup>	→	0	9.6 x 10 <sup>-7</sup>	0	6.4 x 10 <sup>-8</sup>
20		Gross →	6.67 x 10 <sup>-3</sup>	1.0x10 <sup>-3</sup> 1.67x10 <sup>-4</sup> (1)	0	1.98 x 10 <sup>-6</sup>	0	9.2 x 10 <sup>-8</sup>
50			0.267	1.0x10 <sup>-3</sup> 3.34x10 <sup>-4</sup>	0	4.6 x 10 <sup>-6</sup>	0	1.72 x 10 <sup>-7</sup>
100			1.11	1.5x10 <sup>-3</sup> 1.17x10 <sup>-3</sup>	0	1.4 x 10 <sup>-5</sup>	0	8.64 x 10 <sup>-7</sup>
200			18.4	1.0x10 <sup>-2</sup> 6.0x10 <sup>-3</sup>	0 over 10 min	1.2 x 10 <sup>-4</sup>	0	2.81 x 10 <sup>-6</sup>
400			Gross →	Gross →	1.67 x 10 <sup>-4</sup>		0	7.36 x 10 <sup>-6</sup>
800					3.0 x 10 <sup>-3</sup>		0	1.08 x 10 <sup>-4</sup>
1400					4.34 x 10 <sup>-3</sup>		0 over 10 min	0 over 10 min

Remarks: (1) Lower numbers denote leakage measured after 1 week.

Table 5-29. Effect of Thin Films on Seal Leakage

Sample 3A Siloxane Coated Against 3B Siloxane Coated Temperature 22.5°C

P Load F Inlet Press. Psig	3.4 (18.5 psi)			33.9 (185 psi)			339 (1850 psi)			1017 (5550 psi)		
	N <sub>2</sub>	He	H <sub>2</sub> O	N <sub>2</sub>	He	H <sub>2</sub> O	N <sub>2</sub>	He	H <sub>2</sub> O	N <sub>2</sub>	He	H <sub>2</sub> O
5	0.30	Gross ↓	0	0	2.1 x 10 <sup>-4</sup>	0	0	0	0	0	0	0
10	15.2		0	0	Gross ↓	0	0	0	0	0	5.4 x 10 <sup>-10</sup>	0
20	Gross ↓		5 x 10 <sup>-4</sup>	0		0	0	0	0	0	8.1 x 10 <sup>-10</sup>	0
50			4 x 10 <sup>-3</sup>	0.207		5.0 x 10 <sup>-4</sup>	0	0	0	0	10.8 x 10 <sup>-10</sup>	0
100			Gross ↓	Gross ↓		8.34 x 10 <sup>-4</sup>	0 over 10 min	10.8 x 10 <sup>-10</sup>	0	0	1.35 x 10 <sup>-9</sup>	0
200						2.67 x 10 <sup>-3</sup>	1.0 x 10 <sup>-3</sup>	3.5 x 10 <sup>-6</sup>	0	0	1.35 x 10 <sup>-9</sup>	0
400						Gross ↓	4.16 x 10 <sup>-3</sup>	6.0 x 10 <sup>-5</sup> (1)	0	0	1.62 x 10 <sup>-9</sup>	0
800							2.62 x 10 <sup>-2</sup>	Gross ↓	0	0 over 10 min	1.62 x 10 <sup>-9</sup>	0
1400							7.34 x 10 <sup>-2</sup>		0 over 10 min	1.67 x 10 <sup>-4</sup>	3.24 x 10 <sup>-9</sup>	0

Remarks: (1) At 300 psi

Table 5-30. Effect of Thin Films on Seal Leakage

Sample 4A Uncoated Against 4B Uncoated Temperature 22.5°C

Leakage in P Load F Inlet lbs. Press. Psig	3.4 (18.5 psi)			33.9 (185 psi)			339 (1850 psi)			1017 (5550 psi)				
	SCCS	N <sub>2</sub>	He	SCCS	H <sub>2</sub> O	N <sub>2</sub>	He	H <sub>2</sub> O	N <sub>2</sub>	He	H <sub>2</sub> O	N <sub>2</sub>	He	H <sub>2</sub> O
5	8.16 x 10 <sup>-2</sup>			7.5 x 10 <sup>-3</sup>	0	1.17 x 10 <sup>-3</sup>		0	0	5.4 x 10 <sup>-7</sup>	0	0	1.4 x 10 <sup>-7</sup>	
10	0.326			2.0 x 10 <sup>-2</sup>	6.67 x 10 <sup>-4</sup>	1.00 x 10 <sup>-3</sup>		0	0	6.56 x 10 <sup>-7</sup>	0	0	1.9 x 10 <sup>-7</sup>	
20	Gross →			3.84 x 10 <sup>-2</sup>	3.33 x 10 <sup>-4</sup>	1.0 x 10 <sup>-2</sup>		0 over 10 min	0	8.96 x 10 <sup>-7</sup>	0	0	2.6 x 10 <sup>-7</sup>	
50				3.24 <sup>(5)</sup>		4.5 x 10 <sup>-2</sup>				1.69 x 10 <sup>-6</sup>	0	0	3.84 x 10 <sup>-7</sup> (1)	
100					3.33 x 10 <sup>-4</sup>	6.5 x 10 <sup>-2</sup>				3.2 x 10 <sup>-6</sup>	0	0	5.7 x 10 <sup>-7</sup>	
200					6.67 x 10 <sup>-4</sup>	0.584				6.4 x 10 <sup>-6</sup>	0	0	1.05 x 10 <sup>-6</sup>	
400					3.33 x 10 <sup>-3</sup>	Gross →				1.21 x 10 <sup>-5</sup>	0	0	2.1 x 10 <sup>-6</sup>	
800										5.12 x 10 <sup>-5</sup>	0	0	3.2 x 10 <sup>-6</sup> (2)	
1400										9.6 x 10 <sup>-5</sup> (4)	0 over 10 min <sup>(6)</sup>	0 over 10 min	9.6 x 10 <sup>-6</sup> (3)	

Remarks: (1) at 40 psi (2) at 600 psi 5.7 x 10<sup>-6</sup> at 1000 psi (3) at 1500 psi (4) at 1000 psi

(5) at 30 psi (6) at 1300 psi

Table 5-31. Effect of Thin Films on Seal Leakage

Sample 4A Uncoated Against 4B Siloxane Coated Temperature 22.5°C

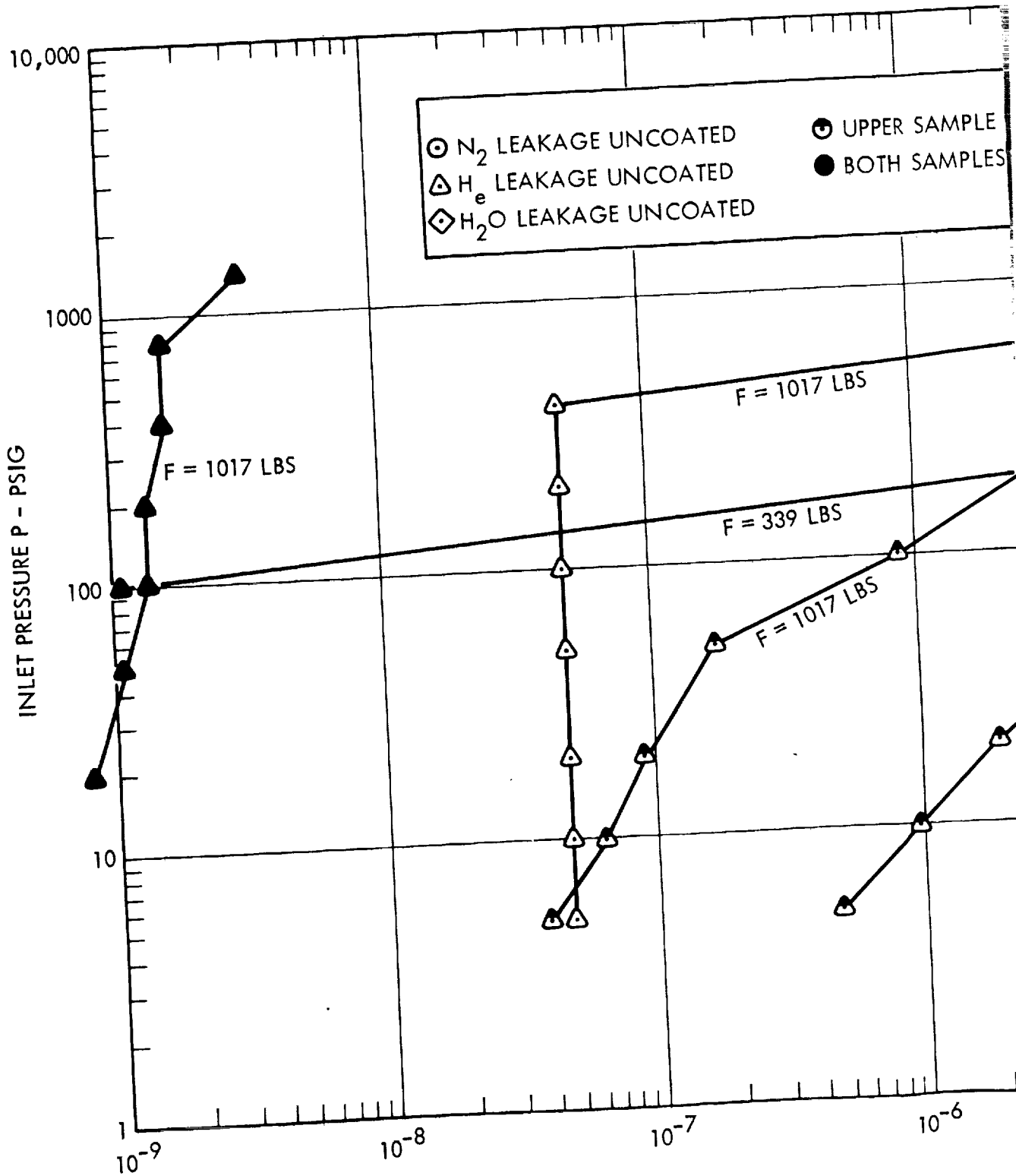
P Inlet Press. Psig	3.4 (18.5 psi)			33.9 (185 psi)			339 (1850 psi)			1017 (5550 psi)		
	N <sub>2</sub> SCCS	He SCCS	H <sub>2</sub> O SCCS	N <sub>2</sub> SCCS	He SCCS	H <sub>2</sub> O SCCS	N <sub>2</sub> SCCS	He SCCS	H <sub>2</sub> O SCCS	N <sub>2</sub> SCCS	He SCCS	H <sub>2</sub> O SCCS
5	0.327	Gross	0.274	1.17 x 10 <sup>-2</sup>		5 x 10 <sup>-5</sup>	0	8 x 10 <sup>-5</sup>	0	0	0	0
10	0.85	Gross	2.74	2.5 x 10 <sup>-2</sup>	Gross		0		0	0	0	0
20	1.62			6.34 x 10 <sup>-2</sup>		1.67 x 10 <sup>-4</sup>	0		0	0	0	0
50	Gross (5)			0.300		8.34 x 10 <sup>-4</sup>	3.33 x 10 <sup>-3</sup>		0	0	0 over 10 min	0
100				1.25		1.67 x 10 <sup>-3</sup>	9.34 x 10 <sup>-3</sup>		0	0	2.5 x 10 <sup>-6</sup> (3)	0
200				10.52		3.08 x 10 <sup>-3</sup>	2.34 x 10 <sup>-2</sup>		0	0	7 x 10 <sup>-6</sup> (2)	0
400						Gross (7)	9.34 x 10 <sup>-2</sup>		0	0	0 over 10 min	0
800							0.50		0 over 20 min	8.34 x 10 <sup>-4</sup>	3.14 x 10 <sup>-3</sup> (6)	0 over 10 min
1400							1.84 (6)		6.67 x 10 <sup>-4</sup>	3.14 x 10 <sup>-3</sup> (6)		0 over 10 min

Remarks: (1) at 3 psi inlet (2) at 150 psi inlet (3) 8 x 10<sup>-7</sup> @ 80 psi inlet; 1.3 x 10<sup>-6</sup> @ 90 psi inlet

(4) at 668 lbs load; 0 @ 5 psi inlet; 2.5 x 10<sup>-6</sup> @ 10 psi inlet; 8 x 10<sup>-6</sup> @ 15 psi inlet

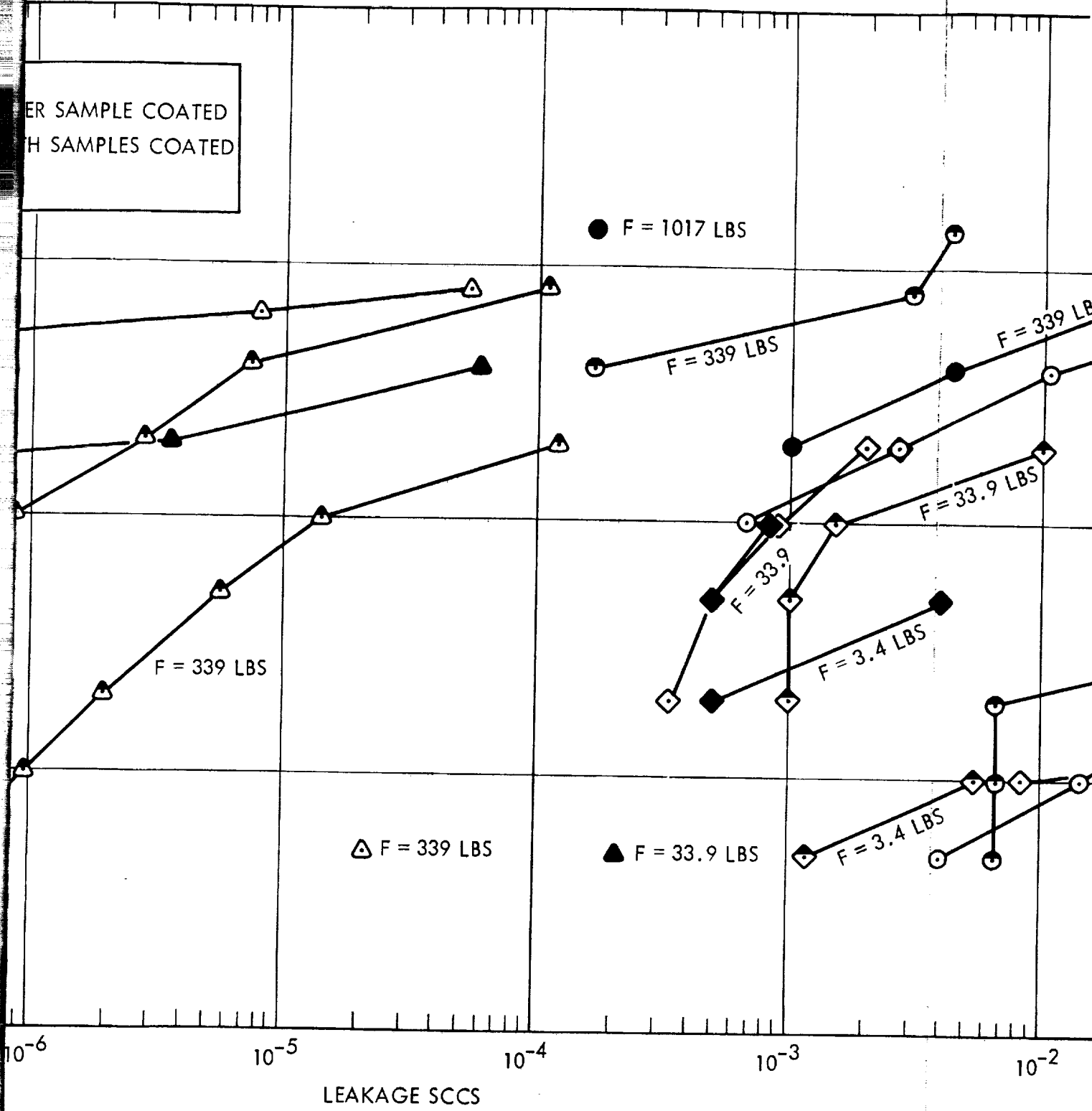
(5) Gross @ 25 psi inlet (6) at 1300 psi inlet (7) at 390 psi inlet







ER SAMPLE COATED  
H SAMPLES COATED





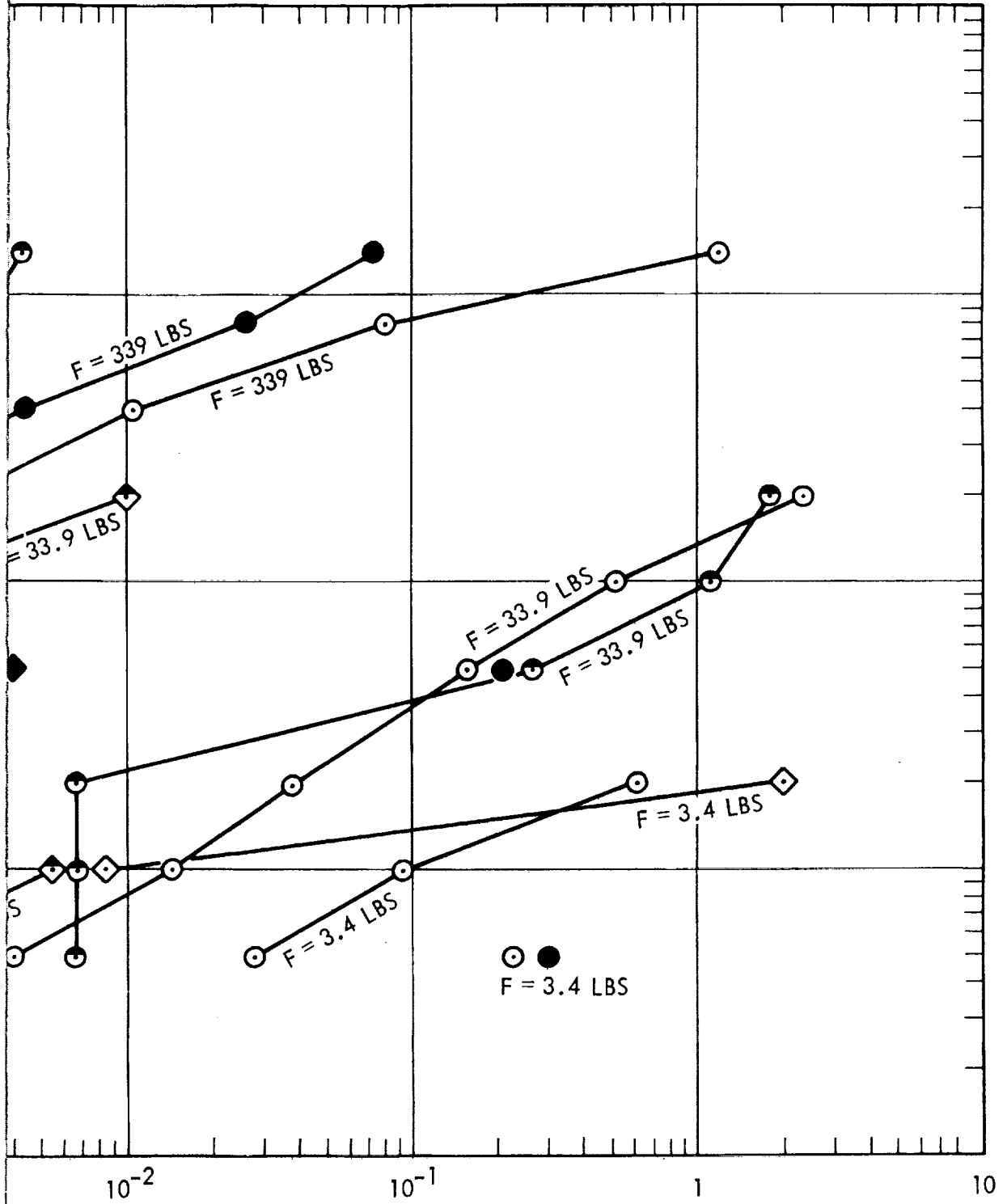


Figure 5-67. Leakage Test Data Showing Effect of Thin Films



7. The helium leakage at 339 pounds load or 1850 psi surface stress showed a marked improvement between the uncoated and upper seat coated tests and a further improvement for both specimens coated. The improvement in both cases was one to two orders of magnitude.
8. The helium leakage at 1017 pounds load or 5550 psi surface stress was higher for the upper specimen coated tests than for the uncoated tests. However, the leakage values at 5 psi and 800 psi were quite close to one another. The both samples coated tests showed leakage values more than an order of magnitude better than the uncoated tests. Even at 1400 pounds inlet the leakage was only  $3.24 \times 10^{-9}$  sccs.
9. The water leakage at 3.4 pounds load or 18.5 psi surface stress was not significantly affected by coating the upper specimen but was lower in the tests using both samples coated.
10. The water leakage at 33.9 pounds load or 185 psi surface stress was about the same for the uncoated and the both specimens coated tests. It was approximately a factor of two worse in the upper seat coated tests than in either of the other two test series.
11. The water leakage at 339 pounds load or 1850 psi surface stress was too small to be measured for all test cases.
12. The water leakage at 1017 pounds load or 5550 psi surface stress was too small to be measured for all test cases.

In general, the effects of siloxane coating seemed more pronounced at higher load levels. The tests at 3.4 pounds load showed more data scatter indicating a higher load is needed to seat the samples. A higher load was momentarily applied to the specimens before the 3.4 pound tests to help minimize the seating problem. It was noted that gross leakages as measured by water displacement and graduate normally occurred when the inlet pressure was raised slightly above the nominal surface stress induced by the clamping load on the specimens.

The use of thin film siloxane polymer coatings has been shown to have a significant effect on He and N<sub>2</sub> leakages, particularly at higher surface stresses. The effects of the coating on water leakage are inconclusive since uncoated specimen leakage were immeasurably small.

5.2.5.5 University Program Results - References 61, 62 and 63 describe in detail the investigations carried out by the University of Bradford and Dartmouth College. This section contains a brief summary of those studies.





The Formation of Surface Films by Electron Bombardment - This work was carried out at the School of Chemistry, The University of Bradford, England, by Professor M. W. Roberts, Dr. J. R. H. Ross and Mr. J. H. Wood. The initial investigation gave results on the adsorption of tetramethylsilane by evaporated films of tungsten and iron (Reference 64). Preliminary data were also obtained on the effect of electron bombardment of the adsorbed layer, in both the absence and presence of excess silane. Later studies yielded further data with the same apparatus. Additional results were obtained in a new apparatus constructed for the purpose which allowed analysis of the process to be carried out in a flow system. Results were obtained on the reaction of oxygen with the polymer formed from tetramethylsilane on evaporated metal films, and the reaction of tetramethylsilane at hot tungsten surfaces in the absence and presence of a field, in the latter case a polymer film being formed on a tungsten ribbon.

In addition, a complementary study of the effect of the emitting filament temperatures, monomer pressure, etc., on the polymerization of butadiene and in less detail of tetramethylsilane and perfluorobutene-2 was performed. The results obtained in both these studies indicated that negative ions were probably involved in the polymerization process. Therefore, in order to study the part that these play in the emission characteristics, a magnetron cell was constructed after the design of Sutton and Mayer (Reference 65).

Perfluorobutene-2 - It is found that for temperatures between 1920 and 2020°K and at pressures between  $4 \times 10^{-5}$  and  $1 \times 10^{-4}$  mm Hg, the electron emission decreases by about 60 percent on admission of gas, and this increase is more or less constant and does not increase gradually with time, as in the case of butadiene and of tetramethylsilane. Diode characteristics before and after showed the emission properties to be essentially those of polycrystalline tungsten. It would therefore appear that with the perfluoro compound no carbiding occurs, which might indicate that it is difficult to adsorb such a compound in a way which permits the adsorbed species to subsequently break down to monocarbon species and hence to carbide. This will not affect the formation of negative ions which will not require breakdown of the skeleton.

The Chemical Stability of Polymers Prepared From a Variety of Monomers - Polymers have been formed under standard conditions from a variety of monomers. Most of the solvents used have no effect on tungsten, and so any reactions noted with films on this metal will be reaction of the film. With nickel, however, any reaction could be either with the film or with the metal. It would appear that all the films are themselves resistant to attack by all the solvents used, but that they do not stop the penetration of all the solvents to the nickel substrate.

General Conclusions - We have presented evidence that in our experimental arrangements negative ions are formed from the monomer at the hot cathode and are accelerated to the anode (substrate) where they polymerize. These conclusions are very different from those of other workers in the field, and although the positioning of cathode, anode, and monomer source relative to one another must be important, we feel that our conclusions must have some relevance in other studies. The reaction at the hot filament

is accompanied by the formation of a composite material, probably tungsten carbide/silicide. It is recommended that a future program include a study of the nature of the species formed, their abundance relative to electron emission of the cathode, and the effect of other cathode materials and other monomers. Also, the program should investigate the properties of polymers formed from various monomers under rather different preparative conditions in which the filament of the electron gun is protected from monomer vapor as in most of the previous studies, and the range energies of the electrons is somewhat higher. In particular, capacitance data and wetting characteristics (from contact angle measurements) should be obtained.

Physical and Chemical Properties of Thin Polymer Films - This study was performed at Dartmouth College, Hanover, New Hampshire, by Professor Robert W. Christy (Reference 63). The purpose of this work was to elucidate the electronic structure of thin polymer films which are formed on a substrate by electron bombardment in the presence of molecules of an organic or silicone vapor. These films, which have useful dielectric, mechanical, and chemical properties, are formed by the free-radical polymerization of the molecules adsorbed on the surface, under the action of the bombarding electrons. The molecules are cross-linked by the electron beam to form a solid polymer film. The molecules used in the study were DC 704 (Dow-Corning), a tetramethyltetraphenyltrisiloxane. In the limit of large electron/molecule ratios during the formation of the film, the resulting structure could be similar to silicone monoxide with the incorporation of some organic radicals, assuming that a large fraction of the original organic radicals would be detached by the electron bombardment. The analysis of these films was approached from the standpoint of band theory of inorganic semiconductors rather than that of organic molecular crystals. The fact that the structure is amorphous instead of crystalline was expected merely to smear out the energy band edges and to lower the electron mobility.

This study yielded the following conclusions:

1. The photocurrent observed in thin polymer films, for thicknesses between 75 Å and 300 Å, is due to the optical generation of charge carriers within the bulk of the polymer. This conclusion is based on two of the most reliable experimental results, namely, that the observed photocurrent threshold is the same as the optical absorption threshold and that the photocurrent threshold does not depend on applied bias. That the photocurrent was observed to be proportional to the amount of light absorbed in the polymer, although not as reliable as the above results, is still further evidence for the bulk effect.
2. For light intensities in the range  $100 \mu\text{W}/\text{cm}^2$  the photocurrent is proportional to the light intensity. Thus, the assumption that the number of traps  $\gg$  the number of conduction electrons seems to be valid for these intensities.

3. The appropriate conduction mechanism for the dark current at room temperature and high voltage is possibly the Poole-Frenkel effect. This notion is based on the agreement between the predicted and experimentally observed dependence of dark current on applied electric field. Also, the identification of photocurrent as a bulk effect leads one to expect that the dark current should also be a bulk phenomenon.

#### 5.2.6 Energized Seal Development

Seal technology is presently inadequate to meet the requirements of zero leakage for valves controlling the flow of reactive rocket liquid propellants; specifically, oxygen difluoride, fluorine and diborane. Elastomers provide the answers to zero leakage but none have been found compatible with those propellants or suitable for use at cryogenic temperatures. Plastics such as Teflon may be compatible under static exposure to propellants and meet the low temperature requirements. However, Teflon is not sufficiently elastic to provide a zero leak seal using low actuation forces. Metal seals have been developed to meet zero leakage requirements using the flat interface design although sufficient testing has not been accomplished to prove this approach under operational requirements of high cycle life, contamination insensitivity, wear and the long term exposure to reactive propellants.

It was the purpose of this study to develop seals meeting the zero leakage requirement, provide long term operation, contamination insensitivity, and suitable for cryogenic service. The approach taken was to review the possibilities of using the elastic properties of polymers and the inherent advantages of metals. The criteria established included those possible designs which would be based on the use of state of the art materials. Dynamic flow of reactive propellants such as  $OF_2$  over the valve seat interface dictated the use of metals. Zero leakage dictated the use of polymers. It was reasoned that a possible design would include the metal seat in series with a shielded polymer seal. A polymer such as Teflon would have to be considered since it was potentially compatible to static exposure to reactive oxidizers and capable of maintaining resilience at low temperatures. However, Teflon is not an elastomer. Therefore attention was given to the design of a Teflon seal, yet maintaining the benefits of the elastomer.

It was further reasoned that since elastomers sealed well due to the filling of the seal material into the micro asperities of the mating surface, sealing with Teflon might be accomplished by flowing Teflon in a similar manner. However, Teflon cold flows with time and bearing pressures are relieved and scaling impaired. The major approach then is to design a seal fully containing the plastic preventing cold flow. The plastic must be maintained at high compressive stress levels during its sealing life.

Another problem with sealing contained plastic was the need for high force actuators if high stresses were necessary, since the compressibility of Teflon was important to the success of this approach. This was overcome by taking advantage of the energy imparted by the actuator since the actuation force moves through a distance during valve operation. The energy approach was then decided a realistic means of compressing the contained materials

whether elastomer, plastic or even metals or the combination of these. That is, the design of the seal was based on the amount of energy that could be imparted to the seal.

Three types of valves were considered: 1) shutoff, 2) pulse mode, and 3) disconnects. The common requirement for the three types, however, is zero leakage. One valve fixture was designed which could perform at least functionally within the operational characteristics of each valve type. It is recognized that design modifications or change in designs are possible for a particular application, however, the functions of sealing, actuation and the sequence of operation is common to design modifications. It is left to the interested designer to optimize these functions mechanically for suitable application since this program is not committed to an existing flight vehicle.

The design of the energized seal is shown in Figure 5-68. The seal is enclosed in a groove such that no deformation of the seal geometry is possible within the seal groove. The actuation of the poppet along the seal surface compresses the seal and at the end of the valve stroke the seal is completely entrapped under a predetermined sealing stress. The seal is energized under compression and should maintain that state until the poppet load is removed. In order to minimize the actuation load the effective piston area of the poppet is small. The energy imparted to the seal is a function of the effective piston area, A, the effective piston stroke, x, and the seal stress, P. In integral form the energy is:

$$E = A \int_{x_1}^{x_2} P dx$$

The major development focused around the seat or sealing configuration and one valve design was developed to meet the conditions of both the shutoff, pulse mode, and disconnect application. The valve then was fabricated to perform the feasibility testing of the seat configuration. The design incorporated the flexibility needed to investigate sealing techniques as well as operative functions such as its application as a disconnect or pulse mode valve.

The valve fixture design is shown in Figure 5-69. The design incorporates a flat metal seal and is the closed position in series with a polymer seal. For purposes of test economies, a pneumatic actuator was used, however, any suitable actuator can be coupled to the seat geometry. Where actuator "o" ring seals are shown, bellows may be substituted. The metal seal allows positive flow area and pulse mode operation and data is available on its leakage characteristics. The polymer seal is used for positive zero leak shutoff and is protected from dynamic flow of the propellants. Entrapment of propellants between the two seals is minimized by the cylindrical design and placement of the polymer seal.

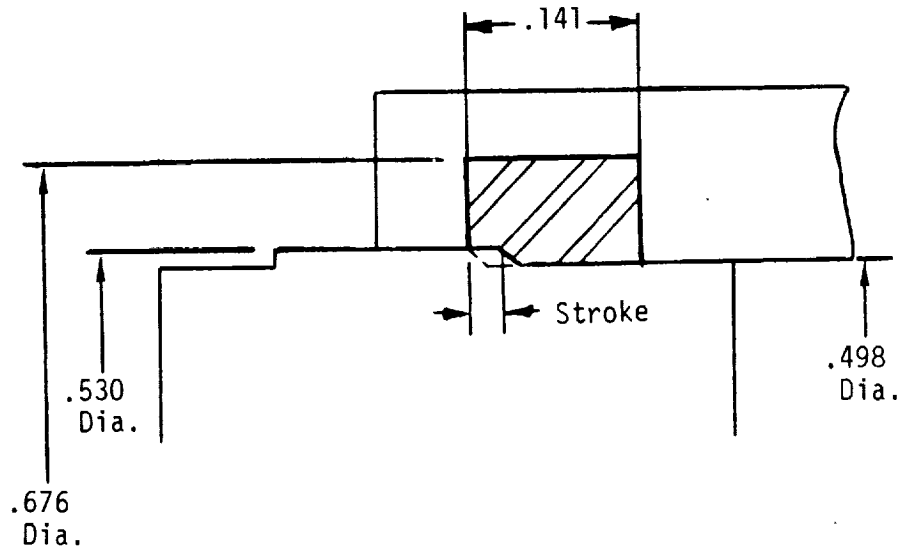


Figure 5-68. Energized Seal

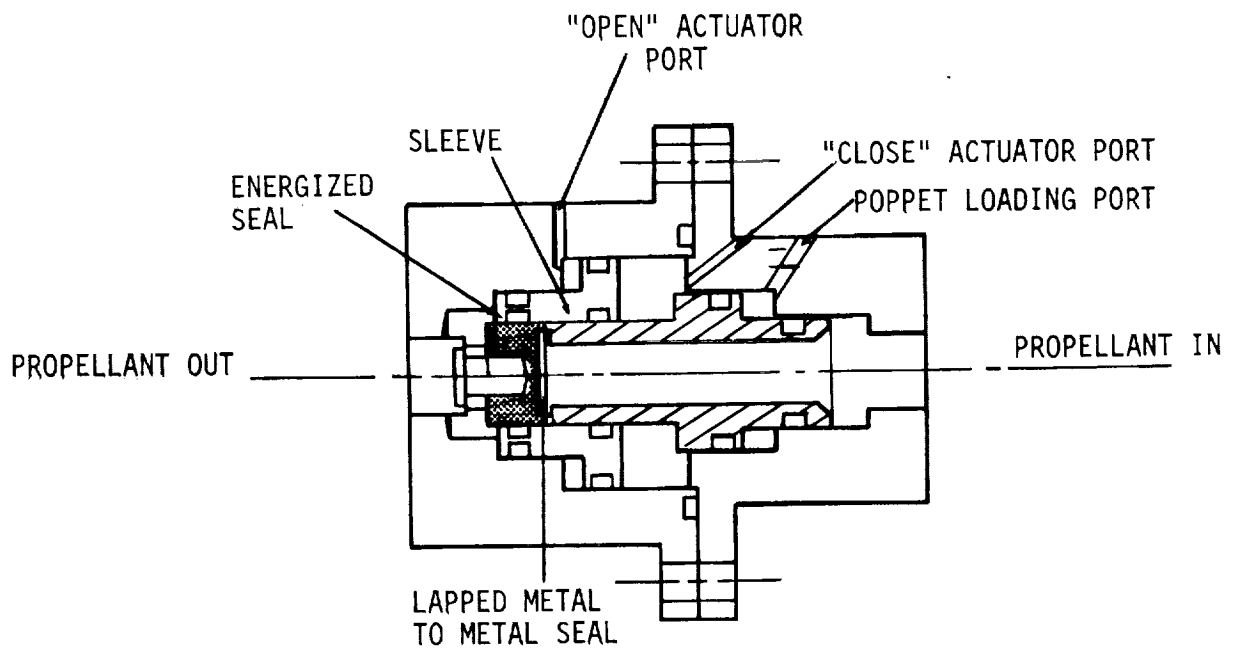


Figure 5-69. Valve and Seal Test Fixture

The flat metal seat was a machined surface and a leakage check showed gross leakage. Therefore, the flat metal seat did not effect the energized seal leakage measurements. The energized seal ring used during the test program was machined from FEP Teflon to fit closely in the seal groove. It was necessary to cut the ring at one location to facilitate installation in the seal groove. The cut was performed diagonally with an exacto-knife to minimize chances of losing quantities of seal material and to allow a good close fit upon compression.

Initial checkout after seal installation indicated gas leakages readily discernable by bubbling in water at seal hydrostatic stresses to 4000 psi and inlet pressures of 15 psi. Following these initial tests with nitrogen the test fixture was set up to allow higher seal stresses and the working fluid was changed to helium to allow the use of a helium mass spectrometer for leak detection.

A test series was then performed at inlet pressures to 500 psi and seal stresses to approximately 12,000 psi. The results of this test series are presented in Table 5-32. Initially, the leakage increased from  $3.4 \times 10^{-9}$  at 100 psi and 12,000 psi seal stress to  $4.4 \times 10^{-9}$  at 100 psi and 1000 psi seal stress. Upon continued testing the indicated leak rate increased with time, inlet pressure and applied seal stress to a final value of  $4.3 \times 10^{-7}$  at 500 psi inlet and 12,000 psi seal stress. It is felt that the seal was probably saturated with helium and the increase in seal stress compressed the material reducing the quantity of helium which could be retained. This could have resulted in an increase in apparent leakage over the short term. The long term leakage trend was upward almost regardless of inlet pressure or seal stress indicating the possibility of a permeation or molecular leak.

Several additional tests were performed varying cycle life (Table 5-32). In all cases leakage was limited to the permeation level. Over 100 cycles were made on the valve and seal.

The important accomplishment was the achievement of zero leakage with Teflon seals using low actuation forces. The design principle appears sound and at cryogenic temperatures the seal should perform equally well. Long term missions of 10 to 15 years should not be detrimental to efficient sealing. However, additional testing should establish long term effects of propellant compatibility, environments such as space radiation or onboard nuclear radiation, and aging on the seal material properties.

The actuation force to close is 1/40 times the seal stress. The piston area to close the valve is  $1.0 \text{ in}^2$  and the area of the piston to open is  $0.7 \text{ in}^2$ . It is important to note the actuation force to open was not consistent. Friction forces due the seal area and seal stress in some cases were high and did not follow the general relationship of friction force equals a constant times the normal load. The following table illustrates the changes in actuation force to open.

Table 5-32. Valve Leakage Test Data Using Energized Seal

Run	Data Point	Cycles	Time Hrs.	Gas Differential Press. (Psid)	Seal Stress (Psi)	Leakage scc/sec He	Remarks	
1	1	2	NA	30	4000	Gross	Seal preconditioned at 4000 psi by cycling twice	
	2			50	2000			
	3			50	3000			
	4			50	4000	bubble/30 sec		
	5			50	6000	" "		
	6			50	8000	0		
	7			50	10000			
	8			50	12000			
	9			15	12000	$3 \times 10^{-9}$		
	10			115	12000	3.4		
	11			141	12000	3.8		
	12			115	12000	3.6		
	13			115	10000	3.4		
	14			115	8000	3.4		
	15			115	6000	3.4		
	16			115	4000	3.8		
	17			115	2000	4.2		
	18			115	1000	4.4		
	19			30	2000	4.6		
	20			65	2000	$1.0 \times 10^{-8}$		
	21			115	2000	1.1		
	22			165	2000	8.7		
	23			265	2000	$1.3 \times 10^{-7}$		
	24			15	2000	2.0		
	25			420	2000	2.4		
	26			515	2000	2.6		
	27			515	4000	3.2		
	28			515	6000	3.4		
	29			515	8000	3.8		
	30			515	10000	4.0		
	31			515	12000	4.3		
2	1		0		2000	-	Test terminated and fixture disassembled for inspection	
	2			1.5	15	12000		$6.6 \times 10^{-8}$
	3			1.8	15	12000		5.2
	4			2.0	15	12000		5.0
	5			2.3	115	12000		5.0
	6			2.3	115	2000		4.8
	7			2.4	115	2000		4.8
	8			2.5	115	2000		5.2
	9			2.5	15	10000		5.6
	10			20.3	15	9000		8.8

Table 5-32. Valve Leakage Test Data Using Energized Seal (Con't)

Run	Data Point	Cycles	Time Hrs.	Gas Differential Press. (Psid)	Seal Stress (Psi)	Leakage scc/sec He	Remarks			
2	11	2	20.3	115	2000	$8.2 \times 10^{-8}$				
	12		20.3	115	2000	8.2				
	13		20.4	115	4000	8.4				
	14		20.5	115	2000	8.2				
	15		20.6	115	6000	8.8				
	16		25.3	115	6000	$9.4 \times 10^{-7}$				
	17		42.5	115	6000	$1.22 \times 10^{-6}$				
	18		43.3	115	6000	1.14				
	19		43.3	115	2000	1.08				
	20		44.0	115	2000	1.16				
	21		44.0	115	8000	1.20				
	22		44.7	115	2000	1.12				
	23		44.8	115	2000	1.14				
	24		45.0	115	10000	1.28				
	25		46.6	115	10000	1.18				
	26		46.6	115	2000	1.08				
	27		46.8	115	2000	1.12				
	28		46.8	215	2000	1.12				
	29		46.9	315	2000	1.12				
	3		1	1	0	115		2000	$1.8 \times 10^{-4}$	
			2		.2	115		4000	1.8	
			3		.3	115		6000	$3.0 \times 10^{-5}$	
			4		.4	115		8000	1.38	
			5		.6	115		8000	$8.0 \times 10^{-6}$	
			6		.6	115		10000	8.0	
			7		1.6	115		10000	3.6	
			8		1.6	115		2000	2.6	
	4		1	1	-	115		2000	5.2	Pressure relieved. Poppet closed with no pressure for 3 days
	5		1	-	0	115		2000	$6.0 \times 10^{-9}$	
2		.2	115		2000	$3.5 \times 10^{-8}$				
3		.4	115		2000	$8.8 \times 10^{-8}$				
4		4.6	115		2000	$1.18 \times 10^{-6}$				
6	1	1	0	115	2000	1.18				
	2		.1	115	8000	1.14				
	3		.15	115	8000	1.10				
	4		.2	115	8000	1.04				
7	1	1	-	115	8000	1.0				
8	1	1	-	115	8000	1.0				
9	1	1	-	115	8000	$9.6 \times 10^{-7}$				
10	1	1	-	115	8000	8.8				
	2		20.6	115	8000	$1.34 \times 10^{-6}$				
11	1	20	-	115	8000	$9.6 \times 10^{-7}$				
12	1	20	-	115	8000	6.8				
13	1	50	-	115	8000	5.2				



<u>Force to Open, lb<sub>f</sub></u>	<u>Seal Stress, psi</u>
32	12,000
35	2,000
37	2,000
31	2,000
28	8,000
28	8,000
28	8,000
28	8,000
28	8,000

The above forces are the breakaway forces due to friction or stiction. Probable reasons for the large variance may be due to the time the seal was allowed to remain at the stressed condition where cold flow allowed the Teflon to fill the asperities of the seal bearing area. If this is the case, smoother finishes are required. Also, the reduction of the seal material area exposed to the bearing should materially help in reducing the actuation force to open.

Another test performed showed the seal to be insensitive to particulate contaminants. The test data shown in Table 5-33 was taken during valve cyclic tests with the Teflon seal contaminated by blasting with silicon carbide grit (6 $\mu$  particles) and dipped into 25 $\mu$  to 60 $\mu$  copper particles. No effect on leakage ratio was noted due to the particles. Examination of the seat after tests showed several particles solidly imbedded in the Teflon seal.

Table 5-33. Valve Contamination Test Leakage Data, Teflon Seat

Differential Pressure	Helium Leakage Scc/sec	Remarks
115	$2.5 \times 10^{-8}$	Pretest
115	$1.2 \times 10^{-7}$	Pretest
115	$6.0 \times 10^{-8}$	Seal contaminated with 25 and 60 $\mu$ particles

### 5.3 REFERENCES

1. Leakage Testing Handbook (Revised Edition), General Electric Company, Research and Development Center, Schenectady, New York, Contract NAS 7-396. Report No. S-69-1117, July 1969.
2. Weiner, R. S., Basic Criteria and Definitions for Zero Fluid Leakage, California Institute of Technology, Jet Propulsion Laboratory, Pasadena, California., Contract NAS 7-100, Technical Report No. 32-926, 15 December 1966.
3. Hass, P. G., Aspects of Zero Leakage Technology, Proceedings of the Conference on the Design of Leak-Tight Fluid Connectors, August 4-5, 1965, George C. Marshall Space Flight Center, Huntsville, Alabama.
4. Bergeler, H., Zero Leakage Effort for Saturn Vehicles, Proceedings of the Conference on Design of Leak-Tight Separable Fluid Connectors, March 24-25, 1964, George C. Marshall Space Flight Center, Huntsville, Alabama.
5. Marr, J. W., Leakage Phenomena, Midwest Research Institute, Kansas City, Missouri, Paper presented at Valve Technology Seminar, 21-22 October, 1965.
6. Bauer, P., Analytical Techniques for the Design of Seals for Use in Rocket Propulsion Systems - Vol. I: Static Seals, Illinois Institute of Technology, Chicago, Contract AF04(611)-8020, AFRPL-TR-65-61, May 1965.
7. Tellier, G. F., Poppet and Seat Design Data for Aerospace Valves, Rocketdyne Division, North American Aviation, Inc., Canoga Park, Calif., Report R-6472, Contract AF04(611)-9712, AFRPL-TR-66-147, July 1966.
8. Tellier, G. F., Rocket Engine Valve Poppet and Seat Design Data, Rocketdyne Division of North American Aviation Inc., Canoga Park, Calif., Report R-5494, Contract AF04(611)-8392, RPL-TDR-64-68, May 1964.
9. Gitzendanner, L.G., et al, Mathematical Model of Interface Sealing Phenomena, General Electric Co., Research and Development Center, Schenectady, New York., Volume II of Final Report under Contract NAS 8-4012, 9 November 1967.
10. Santeler, D. J. and T. W. Moller, Fluid Flow Conversion in Leaks and Capillaries, General Electric Co., National Symposium on Vacuum Technology Transactions, Chicago, Illinois, October 10-12, 1956.
11. Hord, J., Correlations for Predicting Leakage Through Closed Valves, NBS Technical Note 355, August 1, 1967.
12. Hord, J., Correlations for Estimating Fluid Leakage, AIChE Paper 9E, Presented at the Symposium on Cryogenic Advances in the Space Program, Second Joint AIChE-IIQPR Meeting, Tampa, Florida, May 22-29, 1968.

13. Muyer, E. A., et al, Determination of Leakage Values of Seals, WADC Technical Report 54-16, Bjorksten Research Laboratories, November 1953.
14. Marr, J. W., Derivation of Leakage Specifications From the Fundamentals of the Leakage Phenomena, A State of the Art Report, Paper presented at the 56th Air Force/Industry Conference on Missile System Leaks and Spills, Los Angeles, Calif., February 1965.
15. Development and Demonstration of Criteria for Liquid Flowing Feed System Components, Final Report, NASA CR-72063, Douglas Aircraft Co. Report 60599, October 1967.
16. Cittadini, J. and E. U. Thomas, Hermetic Seal, Leak Rate and Vacuum Terminology, in Proceedings 1967 Electronic Component Conference by the Institute of Electrical and Electronics Engineers.
17. Advanced Valve Technology for Spacecraft Engines, TRW Systems Final Report No. 8651-6016-RU000, Contract NAS 7-107, March 1963.
18. Bowden, F. P. and D. Tabor, The Friction and Lubrication of Solids, Clarendon Press, Oxford, England 1950.
19. Rabinowicz, E., Influence of Surface Energy on Friction and Wear Phenomena, Journal of Applied Physics, Vol. 32, No. 8, August 1961.
20. Rabinowicz, E. and R. G. Foster, Final Report on the Size Distribution of Wear Fragments, Contract No. DA-19-202-ORD-4705, 10 April 1962, Massachusetts Institute of Technology.
21. Elliott, J. N., Some Studies on the Mechanism of Wear, M.S. Dissertation, Massachusetts Institute of Technology, June 1965.
22. Weichbradt, B., Tube Connector with Superfinished Seal, General Electric Co., Research and Development Center, Schenectady, New York, Volume IV of Final Report on Contract NAS 8-4012, January 1968.
23. Ferguson, M. D., G. F. Tellier and P. Mannes, Valve Design, An Industry Survey, Rocketdyne Publication No. R-3819-3, September 1962.
24. Boley, B. A. and J. H. Weiner, Theory of Thermal Stresses, John Wiley and Sons, Inc., New York 1960.
25. Melan, E. and H. Parkus, Warmespannungen, Springer-Verlag, Vienna 1953.
26. Frederick, J. R., Ultrasonic Engineering, Page 190, John Wiley and Sons, 1965.
27. Investigation of the Effects of Vacuum on Liquid Hydrogen and Other Cryogens Used on Launch Vehicles, Final Summary Report, June 26, 1963 to November 25, 1964, Contract NAS 8-11044, Control No. TPB-85441 (1F), CPB-02-1120-63, Atlantic Research Co.

28. Study of Propellant Valve Leakage in a Vacuum, Phase I Report, 7 June 1965 to 24 November 1965, Contract No. NAS 9-4494, Control No. PR No. 433-7065, Atlantic Research Co.
29. Study of Propellant Valve Leakage in a Vacuum, Phase IV Report, 10 December 1965 to 14 January 1966, Contract No. NAS 9-4494, Control No. PR No. 433-7065, Atlantic Research Co.
30. Lunar Excursion Module Propulsion Systems Valve Actuating Tests, Final Report, April 7, 1966 to July 23, 1966, Contract No. NAS 9-5937, Control No. 6054039, Atlantic Research Co.
31. Propellant Frost Effect on Operation of the Transtage Bipropellant Pilot Valve under the Low Pressure Environment, P. J. Martinkovic, Technical Report AFRPL-TR-66-141, Edwards, Calif, July 1966.
32. Hot Fire Testing of the LM Ascent and Descent Engine Restart Capabilities Test Program - Phase II, Grumman Aerospace Corp.
33. Cryenco Data Sheet, Cryogenic Engineering Company, Denver, Colorado
34. A Study to Analyze the Permeation of High Density Gases and Propellant Vapors Through Single Layer Teflon or Teflon Structure Materials and Laminations, TRW Systems Interim Final Progress Report, Contract NAS 7-505, October 25, 1967.
35. Design Data for Pressurized Gas Systems, Stanford Research Institute, Menlo Park, California, Contract NAS 7-105, November 1963.
36. Lare, P. J., et al, Investigation of the Effects of Mechanical Stress on the Permeability of Engineering Materials to Certain Cryogenic and Storable Propellants Used in Launch Vehicles, Annual Summary Report, Melpar, Inc., Falls Church, Virginia, June 30, 1964 to June 30, 1965, NASA CR-68411, Contract NAS 8-11322, September 1965.
37. Muraca, R. F., Investigation of the Storability of Pressurizing Gases, Stanford Research Institute, Menlo Park, California, Monthly Status Report No. 2, March 1962 to April 1962, Contract NAS 7-105, April 27, 1962.
38. Seal Compound Manual, Parker Seal Company, Culver City, Calif., July 1964.
39. Permeability Data for Aerospace Applications, Illinois Institute of Technology Research Institute, Chicago, Contract NAS 7-388, March 1968.
40. Howell, G. W., Use of Elastomers for Higher Performance, Lower Cost Liquid Rocket Propulsion Systems, 10th Liquid Propulsion Symposium, 19-21 November 1968, Interagency Chemical Rocket Propulsion Group, Army-Navy-Air Force-NASA.
41. Bauer, P., Analytical Techniques for the Design of Seals for Use in Rocket Propulsion Systems - Volume II: Dynamic Seals, Illinois Institute of Technology, Chicago, Ill., Contract AF04(611)-8020, AFRPL-TR-61, May 1965.

42. Bauer, P., Investigation of Leakage and Sealing Parameters, Illinois Institute of Technology, Chicago, Illinois, Contract AF04(611)-9704, AFRPL-TR-65-153, August 1965.
43. Howell, G. W. and Weathers, T. M., Aerospace Fluid Component Designers' Handbook, Revision C, RPL-TDR-64-25, November 1968, Contract F04611-67-C-0062, Volumes I and II.
44. Wright, H. W., Seal Material Development Program, Monthly Report No. 1, Report No. 4727.6-70-054, TRW Systems, March 15, 1970, Contract NAS 9-10481.
45. Advanced Valve Technology for Spacecraft Engines, Final Report No. 8651-6033-SU000, Volume II, New Concepts, Contract NAS 7-107, 19 July 1964.
46. Tellier, G. F., Survey of Contamination in Rocket Propulsion Fluid Systems, Rocketdyne, Div. of North American Rockwell Corp., Canoga Park, Calif., Contract F04611-67-C-0085, AFRPL-TR-67-290, Report No. R-7397, November 1967.
47. Udin, H., E. Funk and J. Wulff, Welding for Engineers, J. Wiley and Sons, New York, 1954.
48. Rose, W., Analytical Study of the Behavior of Fluids in Porous Solid Media, "2nd Quarterly Progress Report, University of Illinois, AD 233830, March 1960.
49. Buckley, D., and R. L. Johnson, "Gallium Rich Films as Boundary Lubricants in Air and Vacuum to  $10^{-9}$  mm Hg," prepared for ASLE-ASME Lubrication Conference, Pittsburgh, Pennsylvania.
50. Gallium and Gallium Compounds, Alcoa-Chemicals Division Data Sheet 13-11692, Aluminum Company of America, Pittsburgh, Pennsylvania.
51. Gallium as a Sealant for Laboratory Apparatus, Alcoa-Chemicals Division, Aluminum Company of America, Pittsburgh, Pennsylvania, March 1960.
52. Eutectic Alloys of Gallium Metals Fluid at Room Temperature, United Mineral and Chemical Corporation - Metals Department, New York, New York.
53. Boag, J. T., Mercury Alloy Freezes at  $-74^{\circ}\text{F}$ , Materials in Design Engineering, October 1963.
54. Sax, N. I., Dangerous Properties of Industrial Materials, Reinhold Publishing Corporation, New York, 1967.
55. Willhelm, C., Preventing Corrosion by Liquid Metals, Materials in Design Engineering, November 1963.
56. Wilkinson, W. D., A Compendium of Published Data on Gallium Alloys, ANL Report 4109, February 1948.

57. Hansen, M., Constitution of Binary Alloys, Second Edition, McGraw-Hill Book Company, New York, 1958.
58. Gladyshev, V. P., The Solubility of Metals in Mercury, Fiz. Metal, Metallored 9, No. 6, 1960, translated by V. Alford.
59. Rostoker, W., J. McCaughey, and H. Markus, Embrittlement by Liquid Metals, Reinhold Publishing Corporation, New York, 1960.
60. Advanced Valve Technology for Spacecraft Engines, TRW Systems Final Report No. 8651-6042-SU000, Contract NAS 7-107, August 1965.
61. Advanced Valve Technology, TRW Systems Interim Report No. 06641-6004-R000, Contract NAS 7-436, November 1966.
62. Advanced Valve Technology, TRW Systems Interim Report No. 06641-6014-R000, Volume II - Materials Compatibility and Liquid Propellant Study, Contract NAS 7-436, November 1967.
63. Advanced Valve Technology, TRW Systems Interim Report No. 06641-6023-R000, Volume I - Mechanical Controls, Contract NAS 7-436, January 1969.
64. Roberts, M. W., The Formation of Surface Films by Electron Bombardment, Final Report, University of Bradford, England, 9 October 1967.
65. Sutton, P. P. and J. E. Mayer, J. Chem. Phys., 3, 30, 1935.

## 6.0 VALVE ACTUATORS

### 6.1 INTRODUCTION

The Valve Actuators Section summarizes the work performed to investigate the performance, applications, and limitations of actuation devices used to operate valves for controlling the flow of liquid chemical rocket propellants. A review of actuator state of the art is given. A Rating Analysis Chart was used to summarize the results of surveys and analysis. New approaches to valve actuation were investigated and several new concepts are presented.

### 6.2 ACTUATOR STATE OF THE ART

This sections contains an appraisal of the state of the art of actuators used for actuating valves on liquid chemical propulsion systems. The study was accomplished by: a literature survey, agency interviews, analysis of applications, a determination of limitations, and a review of problem areas. A Valve Actuator Rating Analysis Chart is used to summarize the results of the study in relation to valve type, performance, functional requirements, and the effects of the space environment.

#### 6.2.1 Valve Actuator Rating Analysis Chart

A rating analysis chart (Table 6-1) was used as an aid to present the results of surveys and analysis and to define the areas where an advancement in the state of the art of valve actuation is required. A reliability rating was assigned to each type of actuator in defining its performance with propellants and in the space environment.

The ratings assigned to the various combinations of actuators and parameters are defined as follows:

#### RATING

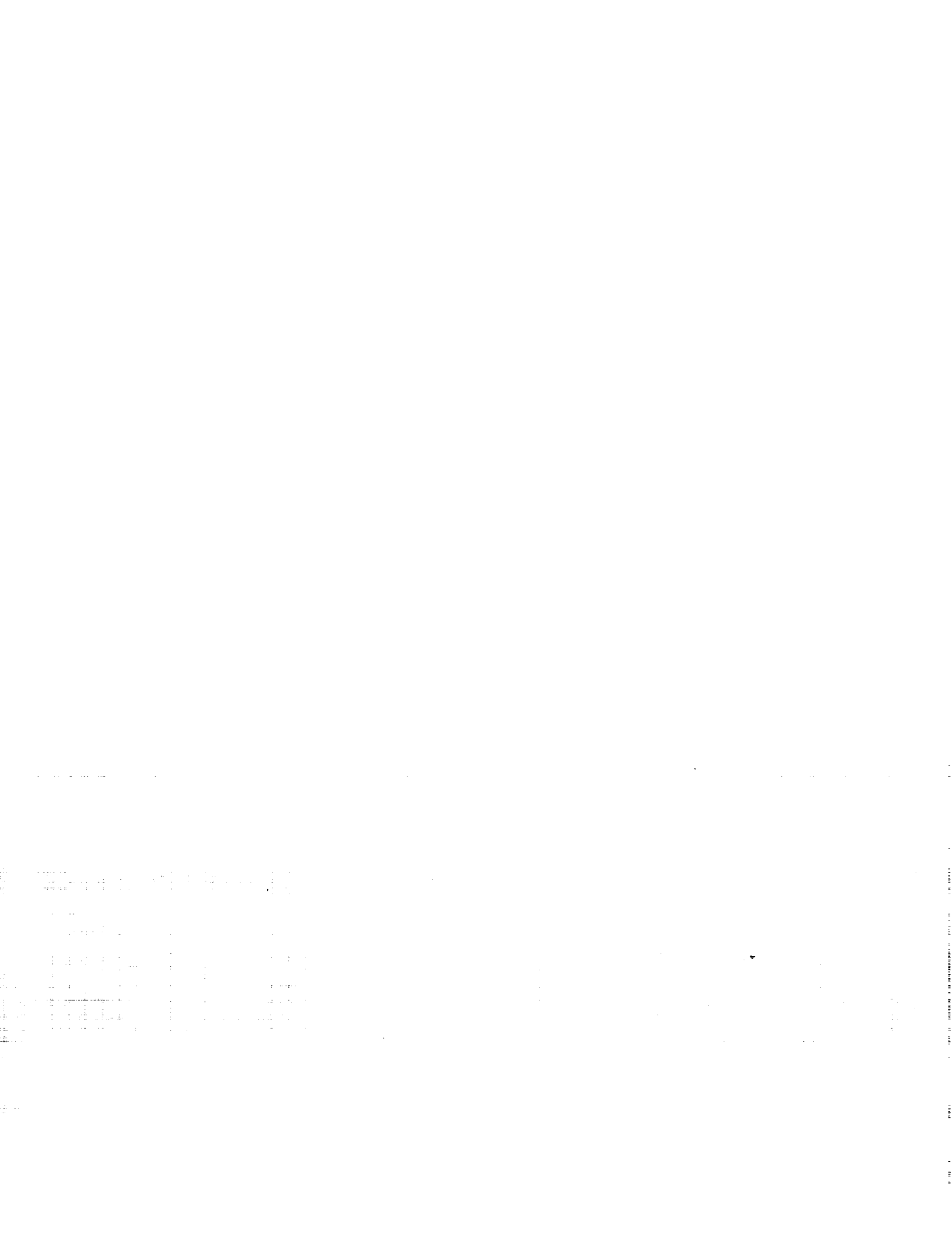
1	A problem exists for which there is no satisfactory solution under the present state of the art.
2	A problem exists but a solution may be available within the present state of the art.
3	Satisfactory - i.e., within the state of the art.
U	Necessary information upon which to base a judgment was unobtainable.
NA	Parameter not applicable.

In some cases as indicated on the chart, a differentiation in values was made for manned missions.













All the ratings were based on the actuator operating in space for up to 10 years. The time, temperature and environmental parameters, i.e., radiation and vacuum, were considered in rating the propellants, functional parameters and application-to-valve types. Ratings pertaining to actuator performance with propellants were based on compatibility of material of construction. The functional parameters were rated based on expected actuator performance requirements in the next 5 to 10 years.

#### 6.2.2 Valve Actuator Review

The various types of actuators which are or may be used for actuating valves on liquid chemical spacecraft rocket engines are briefly described. Actuator applications are discussed, but emphasis was placed on the limitations of the various actuator types which were characterized as: electromechanical, pneumatic, hydraulic, chemical, and thermal.

#### 6.2.3 Electromechanical Actuators

The electromechanical valve actuators in common use for application to liquid propulsion controls operating in space include the solenoid, torque motor, and motor drive. The solenoid and torque motor valve actuators are principally applicable to small shutoff valves and pilot valves for the control of larger pneumatic and hydraulic actuators. Motor drives are used where higher actuation forces are required and for positioning the pintle in the larger flow metering valves.

6.2.3.1 Solenoid Valve Actuators - The solenoid actuator is used with short stroke valves and valves requiring low force output and high response. Size, weight, power, and response time all increase to some degree with an increase in the solenoid stroke and force requirements (see Section 6.3.1). A limitation of the solenoid is the continuous applied current necessary to hold the plunger at the end of its stroke. If the duration of lockup is long, the coil temperature may increase and cause insulation failure. Latching solenoids which mechanically lock the plunger in position are commonly used to avoid the necessity for long term holding currents. Magnetic latching utilizing a permanent magnet which holds the plunger in position is common in small solenoid valves.

Solenoid valve actuators operating in contact with propellants represent a severe limitation since high performance, high iron magnetic core materials are attacked by a number of the fuels and oxidizers. These high iron alloys are rather difficult to plate since they exhibit surface imperfections which are difficult to bridge. If a tight plating is not accomplished, corrosion will cause rapid unit failure. Nickel and chromium have been used to plate magnetic core materials, and although they are compatible with propellants, a flaking of these platings has been observed in propellants such as hydrazine which has resulted in functional valve failures. These failures are probably caused by some small imperfection in the plating resulting from installation, or by dimensional changes due to residual stresses or magnetostriction of the core, which allows corrosion to commence under the plating, causing it to flake off.

Techniques are being sought to overcome these problems. One such technique was developed by the Parker Aircraft Company for use on the Apollo Project and consists of a vapor deposited gold barrier plating which is diffused into the core surface. This coating was successful in providing the required protection against  $N_2O_4$ , hydrazine and the nitric acid formed during subsequent water flush of the system. Chrome diffusion coatings effectively prevent core material corrosion but the temperatures involved in the diffusion process must be carefully controlled or a transition from alpha to gamma phase iron will occur with an accompanying reduction in magnetic properties. The quantity of chrome must be carefully controlled as it also degrades the magnetic properties of the materials. If wet coils are used, the core potting material must withstand the propellant, and insulation flaking must be controlled or contained to prevent valve contamination.

A technique involving the complete encapsulation of the magnetic core material with an austenitic stainless steel sheath has been employed, as have ferritic stainless steel cores. Both of these approaches markedly decrease core performance, resulting in larger coils, higher power levels, or slower valve response.

Techniques involving the use of a diaphragm to separate the core material from the propellant have been used successfully (Figure 6-1). The diaphragm also provides flexure type bearing for the valve poppet and thus eliminates sliding mechanical parts.

Solenoid actuators are within the state of the art for temperatures to  $36^\circ R$  or less, but are limited at higher temperatures ( $>1600^\circ R$ ) due to material softening, winding insulation breakdown, and loss of magnetic properties in the core material. Solenoids for use at temperatures in excess of  $1500^\circ R$  are fabricated on a special order basis. The use of beryllium as a winding material for high and low temperature solenoid applications is attractive due to its high softening temperature, tenacious insulating anodic oxide film, and low electrical resistivity. The use of beryllium for both high and low temperature applications is discussed in Section 6.5.

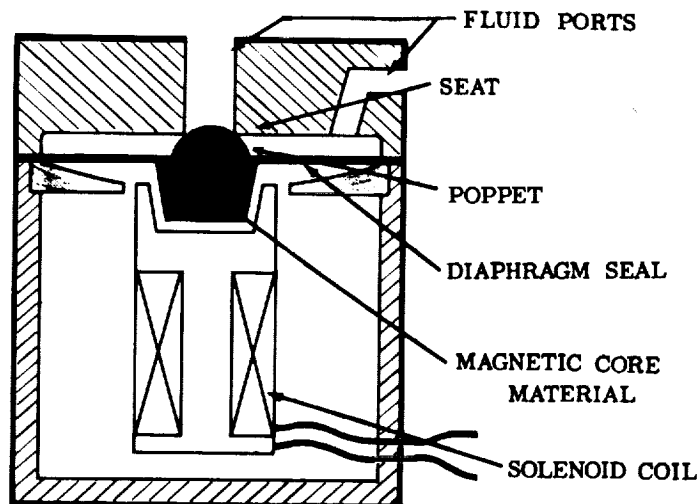


Figure 6-1. Diaphragm Sealed Solenoid Valve

6.2.3.2 Motor Drive Actuators - Electric motor driven valve actuators are used principally in large valves with modest response requirements. They are particularly useful in precision metering valves for the fine positioning of pintles and in heavily loaded shutoff valves. Material compatibility limitations with motor driven actuators are similar to those in solenoid valves when they are immersed in propellants. These have been overcome in some cases by canning the motor rotor and field in a nonmagnetic stainless steel at some sacrifice in motor performance.

Problems are caused in dc motors due to commutation requirements, i.e., immersed brushes cannot be used since many propellants are electrical conductors. In addition, the lubricants required for use on bearings and gears are not always compatible with the propellants. These problems can be overcome by sealing the motor from the propellant; however, zero leakage ( $10^{-7}$  sccs) dynamic shaft seals are not within the present state of the art. When dynamic shaft seals are used, the motor housing is often pressurized to the propellant pressure with an inert gas, such as nitrogen. This reduces the pressure difference across the seal and minimizes the possibility of leakage into the motor. Possible exposure to the propellant vapor must be assumed in this type system. Bellows or diaphragm type hermetic shaft feedthroughs may be used, but these are bulky and are limited in pressure capability and operational life.

Motor drives exposed to space vacuum may experience brush arcing, lubricant loss and cold welding of sliding parts. This may be partially alleviated by special brushes, lubricants, and materials, hermetically sealing the motor, or the use of brushless motors.

Minimizing the power input to servo motors used in positioning metering valves is an important consideration. A recent concept developed by the California Institute of Technology Jet Propulsion Laboratory minimizes the power input required to a servoactuator through the use of a spring energy storage element analogous to a hydraulic accumulator. A low-powered electric motor of .02 hp running continuously is employed to produce momentary power output of .602 hp. The system operates as follows:

The electric motor drives the spring mechanism through a gear reducer. The spring output is attached to a reversing planetary drive, which also incorporates governors for speed control. Reversal of direction is accomplished by a brake system which can hold one of the ring gears stationary while the other is left free. The output is taken through a ball-nut and converted into linear motion for use in positioning (as for a valve pintle).

The following is a brief resume of the system's design goals:

Initial breakaway force	1000 lb
Available start force (springs)	400 lb
Available operating force	200 lb
Available stroke	1 in.
Time for 1 inch stroke	.05 sec

Peak output power	.602 hp
Average input power	.02 hp

The average output power cannot exceed the steady-state input power so the duty cycle for continuous operation is 1-1/2 seconds between full stroke cycles. The springs store enough energy for 4 complete cycles without depending on the input motor.

6.2.3.3 Torque Motor Actuators - Torque motor actuators are used primarily in small-to-medium metering and shutoff valves. They are often used in positioning spool type servovalves. Torque motor actuators which are directly immersed in propellants share the magnetic material and insulation compatibility problems experienced with both the solenoid and motor driven actuators.

Several valve manufacturers have used flexible elements to isolate the torque motor from the propellant. These elements include diaphragm sealed pivots and flexing thin-walled tubes. The diaphragm seal must be kept thin to minimize torque and is therefore limited to relatively low pressures. Diaphragm deflection with pressure may also change critical air gaps, causing changes in actuator performance. This may be minimized by filling the motor cavity with an incompressible fluid such as an oil, to eliminate diaphragm flexing with line pressure changes. An oil fill has also been used as a vibration damper in the thin-walled tube designs. If improperly stressed, the thin-walled tubes have been found to fatigue under vibration, causing premature failures. There is a definite need for a reliable low torque hermetic seal for use with torque motor actuators.

6.2.3.4 Piezoelectric Valve Actuators - Although not presently used in spacecraft, piezoelectric valve actuators hold promise for use in both shutoff and metering type valves. These actuators function by the change in dimension of certain piezoelectric materials when they are electrically energized. Changes in dimension of approximately 0.1 percent are readily obtainable and produce high force levels. These deflections require relatively high voltages ranging from 300 to 3,000 volts, but this occurs at low current so the power drains are moderate.

Materials exhibiting good piezoelectric properties are normally quite brittle in nature. They have high compressive strength but relatively low (on the order of 10 times less) tensile strength. Any actuator design must take these material limitations into account. One approach to overcoming this problem is preloading the piezoelectric material in compression.

The advantages of the piezoelectric actuator include relatively low power consumption, precise positioning capabilities and high output force levels. When used on spacecraft which carry electric propulsion systems, the voltages required are easily obtained; otherwise, some type of power conditioning is required.



#### 6.2.4 Pneumatic Valve Actuators

Pneumatic actuators are used on large valves where the weight, power, and size of an electromechanical actuator is too great; and in metering valves such as pressure regulators, flow regulators, and relief valves. They are the obvious choice in gas systems. Pneumatically actuated valves are piloted with small solenoid or torque motor actuated valves when an electrical actuation signal is required.

Where liquid propellant valves are used, pneumatic pressure for actuation is supplied from a separate source. This source may be a pressurized, usually inert, cold gas cylinder or a gas generator drawing fuel from the propellant line itself. The advantages of pneumatic actuation include:

1. High actuator forces in a small lightweight package
2. Overboarding of gases is preferred over hydraulic actuators overboarding liquid propellants.

Most pressurant gases such as nitrogen, hydrogen, helium, argon, and oxygen can be exhausted directly to space vacuum when the gas is dry and initially at room temperature. Exhausting of moist gases could result in a freezing (snow) problem.

Gas system relief valves and regulators are examples of pneumatically actuated valve types applicable over a broad range of sizes. Pneumatic actuators have an extremely wide range of operating temperatures from well below 36°R to the high temperature structural limit of the material used.

The advantages of pneumatically driven piston actuators are lightweight, small size, and simplicity. Limitations are possible dynamic seal leakage and lubrication problems at temperature extremes. Piston actuators have been operated at temperatures ranging from 36°R to over 2500°R.

Bellows sealed pneumatic actuators complicate design, but provide a hermetic sealing capability over an extended range of temperatures and pressures. Bellows actuators are more sensitive to vibration than piston or diaphragm types and tend to be heavier at high pressures. Life is limited by the fatigue life of the bellows material.

Diaphragm sealed pneumatic actuators also provide a hermetic seal over a broad temperature and pressure range. They are relatively insensitive to vibration and light in weight for short stroke requirements. These actuators are limited in stroke for reasonable diaphragm diameters. Diaphragm actuators will withstand high overpressures without damage if the diaphragm is supported by a backing plate reproducing the free diaphragm contour at that deflection.

Pneumatic rotary positive displacement actuators include vane, Roots, gear and nutating disc motors. These have weight and size advantages in large valve sizes. Their complexity, leakage, and the rubbing contacts involved in the bearings, gears, seals, etc., limit their use to large-sized valves.

Pneumatic turbine actuators are small in size and weight for their power output but are relatively inefficient and require large quantities of gas for operation. This limits their use to specialized applications.

#### 6.2.5 Hydraulic Actuators

Hydraulic actuators are used for valves in spacecraft where the actuation forces required exceed the level normally attainable with solenoid actuators for the same size and weight. They are generally used to actuate large shutoff valves and metering type valves such as pressure regulators, flow regulators and relief valves. Like the pneumatic valve actuator, hydraulic units are often piloted with a small solenoid, or torque motor actuated valve.

The comments presented in the pneumatic actuator section with regard to the various actuator types generally apply also to hydraulically powered actuators. The actuator working fluid is normally the propellant itself. Long term exposure of the actuator materials to propellants may constitute a compatibility problem. This is particularly true if moisture enters the system since corrosive acids are formed when water mixes with most storable propellants.

Seal materials may also present a compatibility problem, particularly in long term use. Most elastomers are attacked to some degree by strong oxidizing agents. Such long term attack could result in seal leakages or swelling which could cause actuator malfunction.

Another problem encountered with hydraulic actuators utilizing propellants involves overboarding of the propellant upon actuation. Tests on an  $N_2O_4$  hydraulic system venting to a simulated space environment have resulted in vent valve failure due to a buildup of frozen propellant on the valve. This was solved by exhausting the propellant through an opening in a shield plate which prevented the frozen propellant from flashing back on the valve. The freezing of liquid propellants when vented to space vacuum has also been demonstrated for cryogenic propellants. Freezing is a problem which must be considered in the design of liquid propellant valves and actuators venting to space. The use of heaters has been employed in some valves and lines to control this problem as has exhaust duct design.

Hydraulic actuators must operate within a narrower range of environmental temperatures than pneumatic actuators due to the freezing and vaporization characteristics of the propellants used. Actuators utilizing a liquid at low temperatures and the vapor at elevated temperatures can be produced. The vapor characteristics as well as the liquid properties must be considered in these designs.

#### 6.2.6 Chemical Actuators

The only type of chemical valve actuators in general use on rocket engines are the squib or solid propellant explosive type. These are separated into two basic types, the deflagrating squibs and the detonating squibs. The deflagrating types are high rate gas generators and perform work by expansion of high temperature, high pressure gas. The detonators depend on a high intensity shock wave to drive the actuator.

An evaluation of squib cartridges after exposure to a variety of environmental conditions was performed as a part of previous Advanced Valve Technology studies. The data generated is presented in Section 6.6. These investigations indicated several problem areas:

1. Severe degradation in squib performance after exposure to 300°F sterilization temperatures with some propellants
2. Leakage at ceramic insulator connector pins after firing
3. Fixed volume bomb tests gave insufficient data for repeatable squib performance evaluation.

A dynamic work output tester for squibs, conceived on this program, was found to give repeatable results in evaluating squib work outputs. This device is described in more detail in Section 7.0.

Reliability testing of squib actuators can have a significant cost impact on a development program. This is due to the large number of charges which must be fired to assure proper performance in service, since the actual unit to be flown cannot be tested. Typically, ten times the required end use units from the same batch must be fired without a single failure to establish that the actuator will perform properly.

Initiation of explosive actuators in spacecraft is normally electrical. Both directly coupled and spark gap coupled bridgewires have been used. The directly coupled bridgewire type of initiator can be set off by currents induced in lead wires due to radio and radar transmission and other fluctuating electrical fields in the area. Spark gap coupled bridgewires are used to help overcome this problem. The firing of squibs by coherent radiation from a laser via a fiber optics bundle has been demonstrated by Space Ordnance Systems, Incorporated, El Segundo, California. This holds promise for future multiple squib applications.

#### 6.2.7 Thermal Actuators

Thermal actuators are not presently used for spacecraft propellant valve actuation. They are, however, used in life support and environmental control systems in manned spacecraft. They are generally applicable to valves which do not require a fast response time. Examples of thermal valve actuators in commercial use are lawn sprinkler valves and fire sprinkler valves.

Several types of thermal actuators can be devised for valve actuation (see Section 6.4.6). The type chosen will depend on force level, response, heat source and the control principle employed. One concept is described in Section 6.6. When thermal actuators are used, incorporation of the control and actuating heat source with the spacecraft thermal management system should be considered since the spacecraft may contain several heat sources which utilize a coolant loop to carry the excess heat to a space radiator. If this is the case, actuation energy may be provided by ducting the hot or cold side coolant to the valve actuator.

### 6.2.8 Manual Overrides

Manual actuator overrides are not normally required on spacecraft valving, although they have been used in aircraft and missile ground support applications. The manual override capability must be considered in the evaluations of manned spacecraft systems where it may affect overall system reliability. Manually controlled valves have been used as primary and secondary controls in the life support systems on the Mercury and Gemini capsules. The use of manually controlled functions in these applications simplified overall system design and improved reliability. Further study is required on specific missions and systems to maximize the advantages of man's adaptive and analytic nature with respect to mission success probability.

## 6.3 ELECTROMAGNETIC ACTUATOR DESIGN CONSIDERATIONS

This section considers the general requirements and characteristics of solenoid actuators and impulse solenoid drive circuits, and the practical limits on operating speed of solenoid actuators. Materials and practices and design criteria for high temperature solenoids are also covered in some detail.

### 6.3.1 Solenoid Actuator Response Time

Response time is perhaps the most important parameter considered during actuator design. Many applications require extremely short response time; requirements less than 1 millisecond have been specified for solenoid operated valves. This section reviews the factors affecting actuator response time, and the techniques for measuring response time.

The time relationships between solenoid force, valve stroke, and output fluid pressure in a normally closed solenoid actuated valve are depicted in Figure 6-2. As seen in the figure and Table 6-2, at the initiation of an opening signal ( $t_0$ ) there is a delay in valve stroke until the solenoid force is sufficient to set the valve elements in motion. There is also a discrete delay after the valve is fully stroked before the output fluid pressure reaches maximum. A differentiation is also made between the opening time and the closing time.

For the purpose of defining the response time of a solenoid actuator, the opening time and the closing time should be specified separately. The opening response time is  $t_2 - t_0$ , which is the time interval between when electrical power is first applied to the solenoid coil and when the valve or actuator is fully stroked. The closing response time is  $t_5 - t_3$ , i.e., the time interval between when the electrical power is first removed and the actuator is fully returned. These definitions are currently accepted in the industry. There are three additional ways of further specifying the actuator response time:

1. Nominal response time is obtained under the specified nominal temperature, load, and voltage supply. Sometimes the nominal response time is obtained at nominal temperature and voltage supply but with no external load.

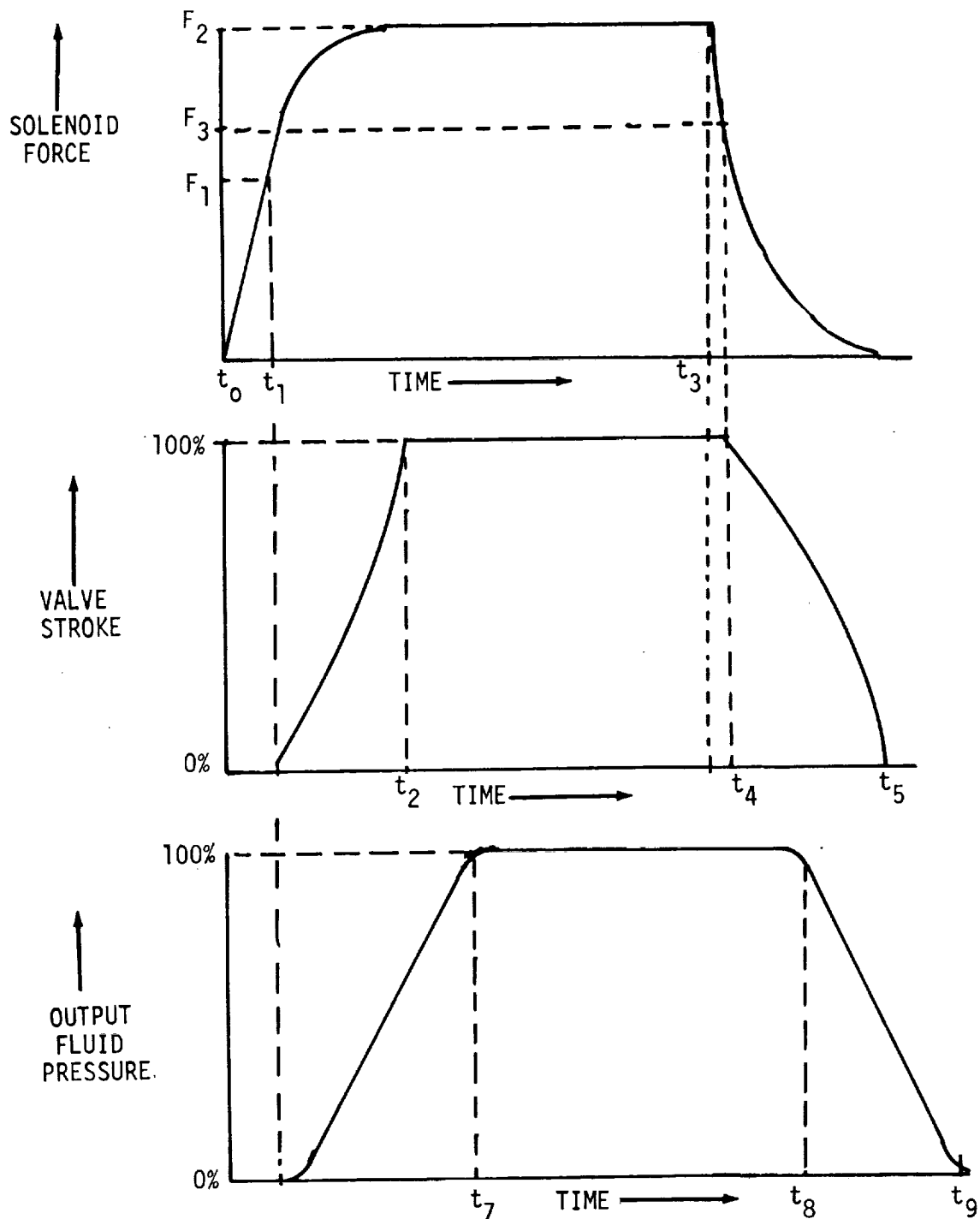


Figure 6-2. Time Relationships in Solenoid Actuated Valve

Table 6-2. Definition of Solenoid Valve Response Times

	Power Applied $t = 0$	Power Removed $t = t_3$
Time of motion of the valving element	$(t_2 - t_1)$	$(t_5 - t_4)$
Actuator lag time due to the coil inductance and friction	$(t_1 - t_0)$	$(t_4 - t_3)$
Total valve response time	$(t_2 - t_0)$	$(t_5 - t_3)$
Output response time	$(t_7 - t_0)$	$(t_9 - t_3)$

2. The longest response time is obtained under the most severe operating conditions. These are the highest environmental temperature, lowest voltage supply and maximum load.
3. The shortest or optimal response time is obtained under the most favorable conditions.

The factors affecting solenoid actuator response time are as follows:

1. Electrical Power

An increase in electrical power reduces the response time. Power, however, is limited to the upper and lower limit of the supply voltage as well as the current drain on battery supplied energy. Also limiting the power input for a given solenoid design is the maximum temperature the solenoid can tolerate before breakdown of the insulation or degradation of the magnetic core material will occur.

2. Pressure Forces

Normally the pressure forces oppose the solenoid force. The pressure forces include the return spring force and the fluid pressure acting on the effective valve seat area. The response time of the valve will be longer in the direction opposite the pressure force (normally during valve opening) and shorter during shutoff due to the pressure forces acting in the closed direction.

3. Operating Temperature

An increase in operating temperature has two effects: (a) the solenoid coil resistance increases which reduces the solenoid force and results in longer response time, and (b) the liquid viscosity decreases which tends to shorten the response time.

The response time for different temperatures can be estimated by the following formula which is used by several manufacturers.

$$\text{Response time } t = T_1 (1 + \Delta^\circ\text{F}/472)$$

where:  $T_1$  = nominal response time

$\Delta^\circ\text{F}$  = change in ambient temperature from the nominal temperature of  $78^\circ\text{F}$

Maximum variation allowed is  $\Delta\text{F} = \pm 100^\circ\text{F}$

4. Friction

The effect of friction is to increase the response time in both directions since it always opposes the motion. Friction will be insignificant in valves which are designed to operate without sliding elements such as a diaphragm valve.

Refer to Reference 3 for a detailed consideration of solenoid actuator lag time, plunger stroke time, temperature effect on response, load pressure effect, response time measurement, lag measurement, and a method for improving response time.

### 6.3.2 High Temperature Electromagnetic Actuators - Materials and Practices

This section presents possible performance characteristics which may be used to define design and development objectives for high temperature solenoid actuators. The materials and practices considered here include high temperature magnetic wire, insulation, potting, impregnation, and the effect of temperature and environment on solenoid construction.

Solenoid actuators operating at temperatures up to 250°C with an operating life exceeding 40,000 hours are possible with available materials. Materials and electromagnetic devices for operating temperatures up to 540°C maximum are available and a solenoid actuator with a life less than 100 hours at temperatures not exceeding 800°C is available. The upper temperature limit for presently available efficient magnetic core materials is about 1000°C. A lightweight solenoid actuator using beryllium magnet wire has been fabricated and shown capable of operation at 1000°C (see Section 6.5).

6.4.2.1 High Temperature Magnet Wire and Insulation - Recent developments and applications of high temperature organic and inorganic insulating materials provide insulations suitable for an operating temperature of 250°C for as long as 40,000 hours. Copper wire conductors with organic film and fiberglass insulation are not resistant to oxidation for long exposures at temperatures exceeding 180°C. Nickel plating, nickel-clad or aluminum-clad copper wire may be used to obtain resistance to oxidation up to 250°C. Silver, aluminum and anodized aluminum wire are suitable for use with high temperature organic insulations up to 250°C. Above 250°C, additional oxidation protection for magnet wire may be required and compatible organic insulations must be used.

6.3.2.2 Temperature and Radiation Resistance - The radiation resistance of materials is approximately related to the temperature resistance as follows:

$$\text{Log (Megarads)} = 8.80 - \frac{3200}{^{\circ}\text{K}}$$

Table 6-3 gives a summary of the temperature and radiation limits for materials used in construction of electromagnetic devices.

Temperature effects such as oxidation, diffusion, or chemical reactions of cladding or insulation, melting point, and grain growth are important in establishing the useful operating range of magnet wire and insulation material combinations (References 4 and 5).

Table 6-3. Radiation Exposure and Temperature Limits for Electromagnetic Materials (100 Hour Total Exposure)

Material Class	100 Megarads at 10 <sup>5</sup> to 10 <sup>6</sup> rads/hr (180°C Max.)	1000 Megarads at 10 <sup>6</sup> to 10 <sup>7</sup> rads/hr (250°C Max.)	10 <sup>4</sup> Megarads at 10 <sup>7</sup> to 10 <sup>8</sup> rads/hr (400°C Max.)	10 <sup>5</sup> Megarads at 10 <sup>8</sup> to 10 <sup>9</sup> rads/hr (650°C Max.)	10 <sup>6</sup> Megarads at 10 <sup>9</sup> to 10 <sup>10</sup> rads/hr (1000°C Max.)	10 <sup>7</sup> Megarads at 10 <sup>10</sup> to 10 <sup>11</sup> rads/hr (1500°C Max.)
Electrical insulation	Silicones, glass mica, asbestos, polyesters, epoxys, and combinations	Polyimide film and varnish, silicone varnish, composite, glass, mica, asbestos, ceramic	Ceramic coating and embedding, special fiber-glass, glass, glass enamel, glass bonded mica, mica, paper, asbestos, anodic films	Glass bonded fibers, glass ceramic, glass bonded mica, glass enamel ceramic embedding and extrusions, vapor depositions, films, vapor deposited films	Special glasses, ceramics, quartz, ceramic and glass fibers, ceramic embedding and extrusions, vapor deposited films	Oxide ceramics, alumina, beryllia, magnesia, sapphire
Conductors	copper, aluminum, silver, beryllium	nickel plated copper, aluminum clad copper, silver, beryllium, aluminum, anodized aluminum, beryllium	nickel plated copper, nickel clad copper, aluminum, silver, beryllium, nickel clad silver, anodized aluminum, anodized beryllium	nickel clad copper, stainless steel clad copper, nickel iron clad copper, nickel clad copper, nickel clad silver, nickel clad silver, dispersion hardened aluminum, anodized aluminum, anodized beryllium	Inconel + barrier on dispersion hardened copper, Inconel on silver Inconel on dispersion hardened silver, anodized dispersion hardened beryllium in protective atmosphere	platinum
Magnetic materials	ingot iron, silicone iron, silicone-aluminum iron, nickel iron, cobalt iron	ingot iron, silicone irons, silicone-aluminum iron, nickel iron, cobalt iron	ingot iron, silicone iron, silicone-aluminum iron, nickel iron, cobalt iron	ingot iron to 500°C, cobalt iron	Cobalt iron, cobalt	none



6.3.2.3 Oxidation Protection - Above 200°C, insulated copper magnet wire requires protection from oxidation. Four percent nickel plating is reasonably effective to 400°C and ten percent nickel plating is more effective. For wires finer than AWG 22 and temperatures exceeding 400°C, nickel-clad copper wire is required. Above 500°C, the nickel sheath diffuses into the copper base metal increasing the electrical resistance after sustained high temperature operation, although operation at 700°C is not harmful for a short time. The high temperature diffusion of nickel and copper may be avoided by use of a non-diffusing barrier layer such as iron between the copper and nickel sheath. Stainless steel cladding may also be used.

Operations of copper wire at high temperatures causes grain growth which impairs the strength of the wire or may cause surface boundary shifts of the grain boundaries causing failure of the conductor and insulation. Grain growth may be greatly inhibited, with only a slight increase in electrical resistance, by dispersion of a small amount of metallic oxide, aluminum oxide, magnesium oxide, thorium oxide, or beryllium oxide in the base metal. A copper wire dispersion hardened with aluminum oxide has been used at temperatures near its melting point, 1083°C. Commercial clad copper wires are available for operation up to 650°C. Nickel plated anodized aluminum clad copper has a useful life of 2000 hours at 300°C. Nickel or iron-clad copper has a life of about 1500 hours at 400°C.

Aluminum is a good magnet wire material for temperatures above 250°C because of the protective insulating aluminum oxide film which may be formed on its surface. The aluminum oxide film serves to protect the aluminum from oxidation and is used for electrical insulation. Good operating life is obtained with anodized aluminum magnet wire at 400°C. Dispersion hardened anodized aluminum magnet wire is useful at temperatures up to 600°C. Aluminum oxide insulating film is a superior high temperature insulator having an insulation resistance which is at least 100 times greater than available ceramic magnet wire insulations.

The advantage of anodized aluminum combined with the low resistivity of copper or silver may be realized at temperatures above 200°C by cladding copper with a silver barrier and an anodized aluminum sheath or anodized aluminum clad silver wire. Pure gold and dispersion-hardened gold may be used to 1063°C. Low resistivity and ductility make gold very attractive for magnet wire, but high cost precludes its general use.

Above 1000°C to 1500°C, corrosion resistant alloys such as Inconel X containing nickel are required. These alloys have a high resistivity when compared to copper, silver, gold or aluminum and should be used only when solenoid valve design requirements necessitate solenoid coil operation at temperatures above 1000°C. Magnetic material performance above 1000°C is very inefficient and is a compelling reason for designing electromagnets to operate below 1000°C.

6.3.2.4 Operation in Protective Atmospheres and High Vacuums - In applications where oxidizing or corrosive atmospheres may be excluded, the excellent electrical properties of unclad dispersion-hardened copper and silver may be utilized to temperatures approaching their melting point. The existing ceramic insulating films are not suitable for unclad copper or silver because the

thermal expansion coefficients of the available insulation coatings are too low.

High-temperature insulating coatings with expansion coefficients nearly matching silver and copper or possessing sufficient ductility are required. Oxidation and corrosion protective electrical insulating coatings with the necessary mechanical and electrical requirements for temperatures from 180°C to 1000°C are not available for copper or silver.

The ends of copper, aluminum or silver magnet wire coils must be protected from sublimation at high temperature in space vacuum by a suitable insulating encapsulant or metal sheath. Most brazes or solders used for terminal connections must also be protected.

6.3.2.5 Radioactive Activation - Table 6-3 shows that high temperature wire, insulation, and magnetic materials are very resistant to space and nuclear radiation; however, if silver is operated in neutron flux densities existing in a reactor pile or neutron shield, it is converted to a radioactive isotope, Ag<sup>110</sup>, with a half-life of 253 days. Cobalt, which is used in magnetic alloys and other high-temperature-resistant alloys, is likewise activated to Co<sup>60</sup> which has a half-life of 5.25 years. Personnel or sensitive equipment should not be subsequently exposed to silver or cobalt which has been activated by high neutron flux densities.

6.3.2.6 High Temperature Impregnation, Encapsulation, and Potting - Insulating impregnation, encapsulation, and/or potting of high temperature magnet wire coils are required to improve shock and vibration resistance, support the coil structure and assembly, improve thermal transfer, reduce sublimation of the magnet wire in high vacuum, prevent oxidation and corrosion, and restrain creep and sag of the coil wire. The materials used must be good electrical insulators which are compatible with the magnet wire and insulation at the highest desired operating temperature.

Coils are usually impregnated by running the magnet wire through a water suspension or slurry of ceramic while the coil is wound. The coil is dried and cured after winding. The coil is cured after drying by heating to a high temperature in vacuum to remove all organic binders and moisture, and to sinter the coil assembly into a solid porous mass. The porous cured impregnating material will absorb moisture if exposed to the atmosphere and should be protected from moisture by a compatible vitreous encapsulating material or hermetic sealing for operation in moist or corrosive atmospheres. Hermetic sealing after vacuum drying is preferable for long life.

A commercially available solenoid coil, with an operating life of less than 100 hours at 800°C, is fabricated by extruding the insulation on the wire before winding the coil with the damp ceramic extrusion coated wire (green extrusion). The coil is cured at high temperatures to obtain a rigid bonded coil without additional impregnation. The moisture content of the extruded insulation is 14.2 + .1%. The particle size distribution is selected to obtain maximum cured density and minimum shrinkage.

6.3.2.7 Effect of Temperature on Magnetic Materials - The magnetic properties of materials are affected by temperature. Ferromagnetic materials are magnetic below a critical temperature called the Curie temperature and essentially nonmagnetic above the Curie temperature. The Curie temperature is the upper limit for operation of ferromagnetic materials. Practical applications require a lower operating temperature than the Curie point to obtain useful magnetic induction with useable magnetizing current densities.

The relative saturation magnetization,  $I_s/I_o$ , of ferromagnetic materials is approximately given given by the simplified "Curie-Weiss Law" (Reference 6).

$$\frac{I_s}{I_o} = \text{Tanh} \left( \frac{I_s/I_o}{T/\theta} \right)$$

where:  $I_s$  = Saturation magnetization at absolute temperature T  
 $I_o$  = Saturation magnetization at absolute zero temperature  
T = Absolute temperature in same units as  $\theta$   
 $\theta$  = Curie temperature (magnetic transition temperature) of the magnetic material

Bloch (Reference 6) has derived a relation which conforms better to the measured saturation  $I_s$  for  $T/\theta \leq 0.4$ .

$$\frac{I_s}{I_o} = 1 - AT^{3/2}$$

The "Curie-Weiss Law" and the 3/2 power law gives a general behavior of the magnetic saturation characteristics for all useful ferromagnetic materials; however, the shape of the magnetization curve and hysteresis loop cannot be defined analytically. In general, the magnetization curve of ferromagnetic materials is a variable which is influenced by magnetic, thermal and mechanical history. Typical experimental magnetization curves for specific material samples are useful for design purposes and care must be used to assure the magnetic materials used for construction are nearly represented by the magnetization curves used for design.

Figure 6-3 illustrates typical relative saturated magnetization curves for useful magnetic materials. The abrupt magnetic transition of cobalt-iron alloys at a temperature below the inferred Curie temperature is believed due to an  $\alpha$  to  $\gamma$  phase transformation. The  $\gamma$  phase is nonmagnetic.

6.3.2.8 High Vacuum Operation - Available published data on magnetic core materials suitable for high temperature solenoids indicate the magnetic properties of most magnetic materials may be improved by high temperature operation in high vacuum due to gradual sublimation of many entrained impurities such as sulphur, phosphorous, oxygen, nitrogen, carbon dioxide and carbon monoxide if the magnetic properties are not otherwise impaired by high temperature operation. An exception is vacuum purification and annealing of nickel iron alloys in which the oxygen content is essential for good magnetic properties (Reference 7).

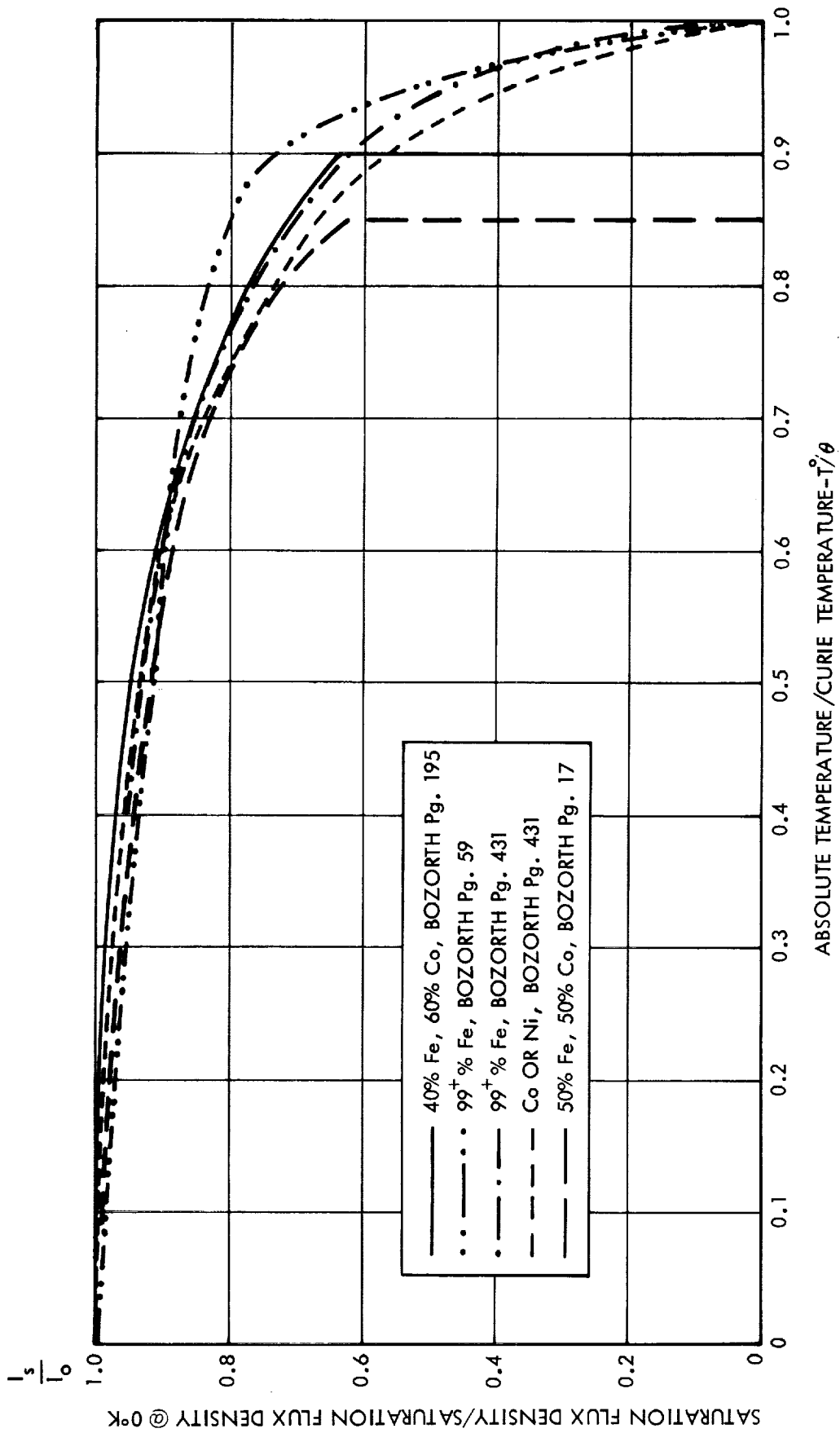


Figure 6-3. Saturation Flux Density Ratio vs. Temperature for Ferromagnetic Materials

### 6.3.3 High Temperature Solenoid Design Criteria

Compact, efficient, low-weight electromagnetic actuators for high temperature valves are considered a requirement for future spacecraft applications. The ultimate performance of high temperature solenoids utilizing available materials is not generally obtained in commercially available actuators. The design criteria in Reference 8, should be helpful in providing improvements in weight, size, power consumption, efficiency, and radiation resistance of high temperature solenoids.

### 6.3.4 High Speed Solenoid Valve Drive Circuits

Solenoid actuated valves for use on spacecraft rocket propulsion systems are designed for minimum weight, minimum size, low electrical power consumption and high speed. These requirements can be enhanced when solenoid valve actuators are driven by circuits which provide a large electrical energy impulse during actuation and automatically switch to a modest holding power required during steady-state operation. The electrical impulse supplied from the electrical drive circuit should provide maximum energy force without reducing the steady-state holding force. The electrical impulse energy required during actuation is stored in single or multiple capacitors which are electrically charged slowly. This technique avoids an impulse demand on the spacecraft electrical power source.

The characteristics of solenoid actuator circuits are studied by use of the general nonlinear variable coefficient differential equation describing the current-voltage characteristic of an active solenoid actuator. This equation is linearized for limited time intervals by appropriate adjustment of coefficients during selected portions of the operating transient. Appropriate operating intervals are selected by consideration of typical current-voltage characteristics. Armature motion effects are included by using variable coefficients for armature position and velocity during the motion interval.

6.3.4.1 Principles of Operation - A dc solenoid valve actuator usually obtains the electrical actuation power from a constant voltage, low impedance dc power supply. A semi-conductor circuit is usually used to obtain nearly ideal switching. The solenoid actuator includes an iron or iron alloy magnetic circuit which has a nonlinear relationship between magnetizing current and magnetic flux density; hence, accurate analysis is not possible using a single linear differential equation with constant coefficients. It is possible to understand the current-voltage, pull-in time behavior of solenoid actuators by using a linear differential equation with variable coefficients to account for armature motion. The nonlinear current flux density relationship is conveniently accounted for by readjusting the initial parameter conditions at selected intervals during the operation transient.

Figure 6-4 represents a simplified solenoid actuator circuit suitable for analyses of the current-voltage relationship of a solenoid actuator. The general nonlinear differential equation describing the current-voltage relationship of an active solenoid actuator is:

$$E(t) = \frac{d}{dt} [L(x,i) i(t)] + R i(t) \quad (1)$$

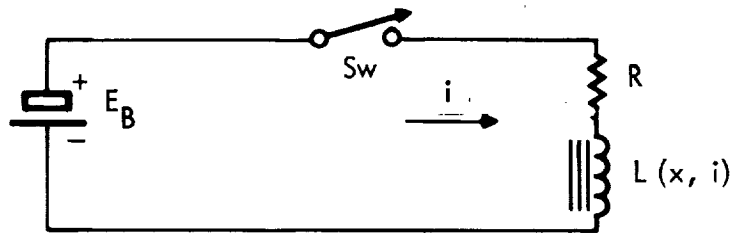


Figure 6-4. Solenoid Actuator Circuit

- where:  $E(t)$  = voltage applied to solenoid actuator as a function of time
- $L(x, i)$  = apparent inductance of solenoid actuator as a function of armature position,  $x$ , and current  $i(t)$
- $i(t)$  = electric current flowing in the solenoid actuator as a function of time

The time intervals (Figure 6-5) are defined as follows:

1. The time o-a, immediately following application of electrical power but prior to armature motion.
2. The time a-b, from initiation of armature motion until the armature reaches nearly full travel but has not decelerated.
3. The time b-c, when deceleration and rebound of the armature appears near full travel.
4. The time c-d, after armature motion following actuation has ceased.

During this initial premotion interval, o-a, after application of power, the magnetizing current is low due to current rate limiting by the solenoid inductance. The solenoid inductance is much lower than the inductance at higher currents when the armature is partially closed. The inductance is low at low magnetizing currents because the nonlinear characteristic of iron and iron alloys results in a low initial magnetic permeability at low magnetizing forces and the air gap. The air gap accounts for most of the magnetizing force. Equation (2) may be used for the current-voltage characteristic during the initial interval o-a.

$$E_{oa}(t) = L_{oa} \frac{di}{dt} + Ri, \quad 0 \leq t \leq a, \quad i(0) = 0 \quad (2)$$

- where:  $L_{oa}$  = the initial inductance (assumed constant)
- $E_{oa}(t)$  = actuator applied voltage during interval o-a

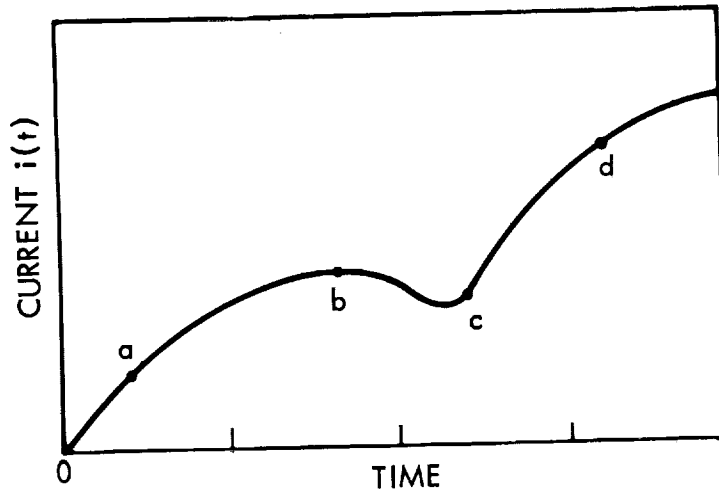


Figure 6-5. Typical Current Transient Characteristic Curve for Solenoid Valve Actuator

During the initial motion interval a-b, the inductance increases with time due to armature motion and the increasing magnetizing force applied to the magnetic circuit. The inductance is a function of current and armature position during this interval; however, a suitable inductance,  $L_{ab}(x)$ , which is a function of armature position but independent of current, may be selected to fit this portion of the characteristic. For  $L_{ab}(x)$ , which is position dependent only, Equation (1) becomes Equation (3).

The circuit inductance in Equation (1) is a function of current,  $i(t)$ , and armature position,  $x$ , and hence requires an a priori knowledge of  $L$  for all expected operating combinations of  $i$  and  $x$ ; this is not usually available. Approximate values of  $L$  which are independent of  $i$  may be selected for appropriate time intervals of a typical current-voltage transient.

This approximation simplifies Equation (1) and enables an understanding of the current-voltage/time characteristic including the effects of armature position and velocity. The typical current-voltage transient of an active solenoid actuator, Figure 6-5, illustrates the choice of time intervals and provides the basis for the appropriate simplified differential equations which are applicable during each selected time interval.

$$E(t) = \frac{d}{dt} \left[ L_{ab}(x) i(t) \right] + R i(t)$$

$$E_{ab}(t) = i(t) \frac{d}{dt} L_{ab}(x) + L_{ab}(x) \frac{d i(t)}{dt} + R i(t)$$

$$E_{ab}(t) = i(t) \frac{dL_{ab}(x)}{dx} \frac{dx}{dt} + L_{ab}(x) \frac{d i(t)}{dt} + R i(t) \quad (3)$$

for  $a \leq t \leq b$ ,  $i(a) \leq i(t) \leq i(b)$

where  $L(x)_{ab}$  = inductance for  $x(a) \leq x \leq x(b)$

$E_{ab}(t)$  = applied voltage for interval a-b

Equation (3) differs from the nonmotion Equation (2) by the addition of a velocity dependent voltage and a position dependent coefficient for the rate of change of current.

During the final motion interval when deceleration and rebound exist, the inductance,  $L(x)$ , is nearly constant at a final position value  $L_c$ , hence for the final motion interval, b-c-d, depicted in Figure 6-5.

$$E_{bd}(t) = i(t) \frac{dL_c}{dx} \frac{dx}{dt} + L_c(x) \frac{di(t)}{dt} + R i(t) \quad (3a)$$

$i(b) \leq i(t) \leq i(d)$ ,  $b \leq t \leq d$

$E_{bd}(t)$  = applied voltage for interval b-d

During the interval when armature motion ceases after application of power  $L(x) = L_d$  and  $\frac{dL(x)}{dx} = 0$ , hence:

$$E_{de}(t) = L_d \frac{di(t)}{dt} + R i(t), \quad d \leq t \leq e \quad (4)$$

$E_{de}(t)$  = applied voltage for interval d-e

6.3.4.2 Breakaway Time - During the initial linear operating interval (o-a, Figure 6-5), prior to breakaway, the armature force and breakaway speed will be proportional to the applied voltage from Equation (1)  
 $E_b = L_{oa} \frac{dI_o}{dt}$ ,  $I(o) = 0$ , at  $t = 0$

hence,  $\frac{dI(o)}{dt} = \frac{E_b}{L_{oa}}$ ,  $\frac{\Delta I_{oa}}{\Delta t_{oa}} \cong \frac{E_b}{L_{oa}}$  (5)

and  $\Delta t_{oa} \cong L_{oa} \frac{\Delta I_{oa}}{E_b}$ ,



where:  $\Delta t_{oa}$  = breakaway time

$\Delta I_{oa}$  = breakaway current

$L_{oa}$  = initial inductance of the solenoid actuator

$E_b$  = voltage applied to the solenoid actuator

6.3.4.3 Operating Time - Subsequent to breakaway, the armature velocity,  $dx/dt$ , will be proportional to the applied voltage; hence, the armature pull-in speed is proportional to applied voltage for linear circuit operation. If the magnetic force is a monotonically increasing function of current but is less than a proportional rate of increase, a diminishing improvement in pull-in velocity will result with increasing current.

The cusps in the  $I(t)$  curve of Figure 6-5 between b and d are due to armature bounce. This characteristic will depend on construction of the actuator. For example, a stiff spring and hard stop for the armature at the full limit of travel may have conspicuous bounce cusps unless the armature motion is damped by fluid damping and armature friction. The bounce characteristic cannot be used as final criteria of solenoid quality since poppet clearances, stop hardness, fluid viscosity, pressure, etc., will differ between valves. It is obvious that a fast solenoid actuated valve with conspicuous bounce characteristics is unsuitable for controlling pulses of fluid flow whose pulse width is comparable to the bounce interval.

6.3.4.4 Electrical Impulse Drivers - High actuator speed may usually be obtained from electrical impulse solenoid drivers. Spacecraft power supplies are usually low voltage and may provide a limited peak demand and steady power to a solenoid actuator. The actuator power consumption is also limited by size, weight, and temperature rise. An impulse electrical supply may supply high peak powers to a solenoid actuator during actuation without excessive actuator heating. The transient and steady power demand of the impulse supply may be small compared to the solenoid holding power. The weight and power consumption of an impulse driver should be less than required for a larger solenoid actuator to achieve a corresponding result from a constant voltage supply. In addition, a fail-safe circuit is desired which will provide power at reduced impulse if a component malfunction develops. A capacitor storage impulse driver can meet these basic weight and power requirements.

The capacitor storage impulse driver charges  $N$  capacitors in parallel while the solenoid actuator is off or in a steady holding condition. The capacitors automatically connect with their voltage in series aiding with the power supply when the valve is actuated. When the capacitor stored energy is depleted, the capacitor automatically connects for recharge and standby until a valve actuation requires the impulse energy. This capacitor switching logic corresponds to the practice used for many years for high voltage impulse generators exemplified by the Marx trigger circuit. Figure 6-6 illustrates the logic of a capacitor storage solenoid actuator driver.

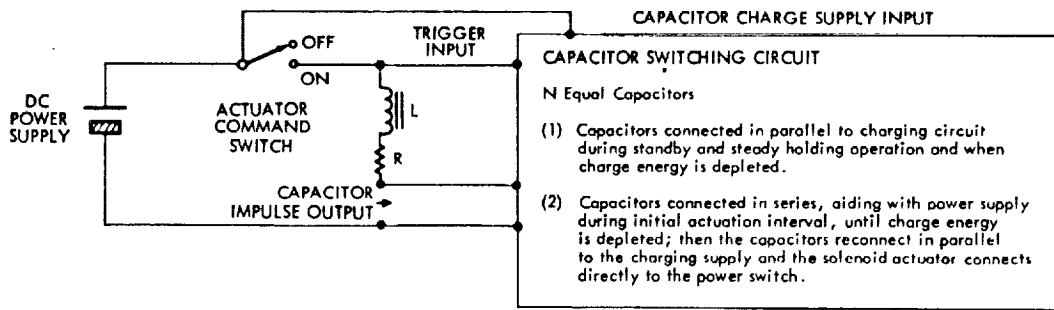


Figure 6-6. Capacitor Impulse Actuator Driver

The breakaway time may be reduced by a factor  $1/(N+1)$  times by  $N$  series connected capacitors charged to the power supply voltage. For  $N$  capacitors the breakaway time,  $\Delta t_{oaN}$ , is:

$$t_{oaN} = \frac{L_{oa} \Delta I_{oa}}{(N+1)E_b} = \frac{\Delta t_{oa}}{(N+1)} \quad (6)$$

If we select an approximate initial inductance value for  $L(x)_{ab}$  which is independent of magnetizing current, the pull-in time,  $\Delta t_{ac}$  is also improved by the factor,  $1/N+1$ , when  $N$  charged capacitors are series connected.

For  $N$  capacitors, the pull-in time,  $\Delta t_{acN}$ , is:

$$\Delta t_{acN} = \frac{\Delta i_{ac}}{(N+1)} \quad (7)$$

The actual improvement in  $\Delta t_{acN}$  will be less than given by Equation (7), depending on the degree of magnetic circuit saturation.

Equations (5) and (6) assume the charge stored in each of the  $N$  capacitors is sufficient to supply the solenoid current for the time intervals  $\Delta t_{oaN}$  and  $\Delta t_{acN}$  with a negligible decrease in capacitor voltage; however, a decrease in capacitor voltage is required to supply the current to the solenoid actuator. If we assume the rate of change of current is constant at the initial value at  $t = 0$ ,  $di(o)/dt$ , we can make a conservative estimate of the capacity and number of capacitors required for a desired improvement in pull-in time,  $\Delta t_{ac}$ . The pull-in speed improvement factor,  $A$ , assuming a linear differential equation is:

$$A = N + 1 = \frac{\Delta t_{ac}}{\Delta t_{acN}} \quad (8)$$

where:  $N$  = number of series capacitors in the current impulse supply

$\Delta t_{acN}$  = pull-in time with  $N$  capacitors

$\Delta t_{ac}$  = pull-in time with only the constant voltage supply

$A$  = pull-in speed improvement factor for  $N$  capacitors

The capacitors supply the solenoid current ( $i(t)$ ) for a time  $\Delta t_{ocN}$  with a corresponding decrease in charge,  $\Delta Q_c$ , and voltage,  $\Delta E_c$ ,

$$\Delta Q_c = C \Delta E_c = \int_0^{\Delta t_{oc}} i(t) dt \quad (9)$$

where:  $\Delta Q$  = decrease in charge of each capacitor  
 $\Delta E_c$  = decrease in voltage of each capacitor

Using the conservative assumption that

$$\frac{di}{dt} \sim \frac{d i(o)}{dt}$$

$$\Delta Q_c = \int_0^{\Delta t_{oc}} i(t) dt \sim \int_0^{\Delta t_{oc}} t \frac{d i_o}{dt} dt$$

$$\Delta Q_c \sim \frac{\Delta t_{oc}^2}{2} \frac{d i_o}{dt} \quad (10)$$

$$\frac{d i_o}{dt} = \frac{(N+1)E_b}{L_o}$$

For  $N$  capacitors,  $\Delta Q_N$  and  $C_N$  are:

$$\Delta Q_N \sim \frac{\Delta t_{oc}^2}{2} \left( \frac{(N+1)E_b}{L_o} \right) \cong C \Delta E_c \quad (11)$$

$$C_N \sim \frac{(N+1)E_b \Delta t_{oc}^2}{2L_o \Delta E} \quad (12)$$

Equation (12) will give the required capacity for each capacity,  $C$ , corresponding to a given decrease in capacitor voltage,  $\Delta E$ , during the time,  $\Delta t_{oc}$ . A conservative value of  $\Delta E$  is 10 percent of  $E_b$ . For  $\Delta E = .1 E_b$ , Equation (12) becomes:

$$C_N \approx \frac{(N+1) \Delta t_{oc}^2}{.2L} \quad (13)$$

from Equation (8) the number of capacitors, N, is:

$$N \approx \frac{\Delta t_{oc}}{\Delta t_{ocN}} - 1 = A - 1 \quad (14)$$

Equations (11) and (12) give a conservative value for the capacity of each capacitor,  $C_N$ , and the number of capacitors, N. It is possible to obtain the same speed improvement with a larger N than given by Equation (13) with a corresponding decrease in C; however, the capacitor total weight and energy storage density does not improve and additional switching components are required. A lower value of C than given by Equation (12) may produce the desired speed improvement factor A since the Equation (12) is a conservative approximation. Experimental success approximations based on an initial trial value given by Equation (11) is an appropriate method to determine a precise value of  $C_N$  required for the desired  $\Delta t_{acN}$ .

6.3.4.5 Electrical Requirements of Impulse Circuits - The current, power, and energy requirements for the capacitor discharge solenoid driver may be determined when the capacity,  $C_N$ , the number of capacitors, N, and the power supply voltage,  $E_b$ , are selected. The capacity  $C_N$  and N are determined by speed requirements using Equations (13) and (14).

The total stored energy,  $T_{cN}$ , in the N capacitors, is:

$$T_{cN} = \frac{N C E_b^2}{2} \quad (15)$$

where:  $T_{cN}$  is the total capacitor stored energy in Joules or Watt seconds

$C_N$  is in Farads

$E_b$  is in Practical Volts

The energy loss in the capacitors is small; hence, most of the energy stored in the capacitors is delivered to the solenoid during the driving impulse.

The energy supplied by the power supply circuit to charge the capacitors exceeds the energy stored in the capacitor by the charging circuit losses,  $T_r$ , which are largely dissipated in the charging resistance. The charging circuit loss is always equal to the energy stored in the capacitor.

$$\text{For N capacitors: } T_{rN} = T_{cN} = \frac{N C E_B^2}{2} \quad (16)$$

The total energy delivered by the power supply,  $T_b$ , to charge the capacitors is for  $N$  capacitors:

$$T_b = N C E_b^2 \quad (17)$$

The peak charging current for  $N$  capacitors,  $\hat{I}_c$ , is:

$$\hat{I}_{cN} = \frac{N E_b}{R_c} \quad (18)$$

where  $R_c$  is the charging circuit resistance in ohms, the charging current,  $I_{cN}(t)$ , is for  $N$  capacitors:

$$I_{cN}(t) = \frac{N E_b}{R_c} e^{-t/R_c C_N} \quad (19)$$

where:  $t$  is the time in seconds after application of the charging voltage,  $E_b$ , in volts, and  $e$  is the natural base = 2.718.

The voltage on the charging capacitor,  $E_c(t)$ , is:

$$E_c(t) = E_b \left[ 1 - e^{-\frac{t}{RC_N}} \right] \quad (20)$$

Typical values of  $\frac{E_c(t)}{E_b}$  for selected values of  $t/RC_N$  are given in the following table:

$t/RC_N$	4.6	3	2.3	1.61
$\frac{E_c(t)}{E_b}$	.99	.95	.90	.80

The power demand from the battery  $P_b(t)$ , during charging is for  $N$  capacitors

$$P_b(t) = \frac{N E_b^2}{R} e^{-t/R_c C_N} \quad (21)$$

The capacitor charging time,  $t_1$ , to a specified fraction of the supply voltage,  $\frac{E_c(t)_1}{E_b}$ , will also determine  $\hat{I}_c$  for a given  $C$ ,  $t_1$  is:

$$t_1 = -R_c C \ln \left( 1 - \frac{E_c(t_1)}{E_b} \right) \quad (22)$$

The  $\hat{I}_{cN}$  corresponding to  $t_1$  is for N capacitors:

$$\hat{I}_{cN} = \frac{N E_b}{R_c} = \frac{N C E_b \ln \left( 1 - E_c(t_1)/E_b \right)}{-t_1} \quad (23)$$

An independent choice of charging time  $t_1$  and  $\hat{I}_{cN}$  is not possible unless C is permitted to vary from the value defined by Equation (13). Since the C determined by Equation (13) is a conservative estimate for C, some reduction in C is possible. If  $\hat{I}_{cN}$  is limited by the power supply capability then the value of charging time,  $t_1$ , corresponding to the permitted peak charging current,  $I_{cN}$ , must be used. Hence:

$$t_1 = \frac{N C E_b \ln \left( 1 - E_c(t_1)/E_b \right)}{I_{cN}} \quad (24)$$

**6.3.4.6 Limiting Speed of Operation** - Equation (12) suggests the speed improvement factor A will continue to increase in proportion to N; however, there are practical limits to A beyond which a diminishing improvement in A is obtained with increasing N. Some of the factors causing severe deviations from the linear relationship of Equation (8) are:

1. The bulk of the magnetic material becomes saturated at  $\Delta t < \Delta t_{ocN}$ .
2. The rate of increase of current and magnetic induction is too rapid to permit full penetration of the magnetic field into the magnetic structure, thus limiting the possible rate of increase of the total magnetic force.
3. The breakaway force required for a solenoid armature has been assumed constant; however, it may have additional force requirements which are dependent on the rate of application of breakaway force.
4. The mechanical friction forces are assumed to be proportional to velocity. Additional nonlinear forces proportional to the square of the velocity may be important when valve fluid loads with velocity squared forces are important.
5. Good magnetic materials are subject to inelastic deformation and plastic or fluid flow when the rate of application of magnetic stress exceeds the stress propagation velocity in the magnetic material.

The above five limiting factors show improved operating speed can be obtained with an electrical impulse driver for low values of the improvement factor A. The speed limits which may be realized in properly constructed solenoid actuators can approach the speeds obtained by magnaforming or explosive actuated actuators; however, repeated cycle operation will obviously be sacrificed. The upper speed limit of the electrical impulse solenoid driver corresponds to the speed of magnaforming techniques.

6.3.4.7 Improvement of Limiting Speed - When the practical operating speed limit of existing solenoid actuators have been realized with an electrical impulse driver, the above five factors limiting further speed improvement may be considered to select methods which will yield the greatest improvement in speed.

Some of the methods for improvement of each limiting factor are:

1. Improvement of Bulk Saturation Flux Density

If the active magnetic structure is saturated for  $\Delta t < \Delta t_p$ , the depth of penetration due to a rapid buildup of magnetizing induction is not limiting the actuation speed. A higher acceleration force and speed may be obtained by using a magnetic material with a higher saturation flux density obtainable by improved heat treatment and/or alloy composition. If this is not possible, it is necessary to increase the active cross-sectional area of the magnetic circuit transverse to the direction of magnetic field. In the case of the moving armature, this change should be accomplished without increasing the mass of the armature; i.e., the increased armature cross-sectional area must be accompanied by an equal squared thickness or length reduction.

In cases where higher saturation magnetic materials are available, the pull-in speed is improved in direct proportion to the square of the saturation flux density, assuming the magnetic field penetration remains complete.

$$\frac{\Delta t_{p1}}{\Delta t_{p2}} = \frac{B_{2\text{ sat}}^2}{B_{1\text{ sat}}^2} \quad (25)$$

where:  $\Delta t_{p1}$  = pull-in time with magnetic material No. 1  
 $\Delta t_{p2}$  = pull-in time with magnetic material No. 2  
 $B_{1\text{ sat}}$  = saturation flux density of magnetic material No. 1  
 $B_{2\text{ sat}}$  = saturation flux density of magnetic material No. 2

A common example of improvement in magnetic material is the substitution of optimum annealed permendur<sup>R</sup> for low carbon steel or pure ingot iron. The saturation flux density by this substitution may be improved from 12 to 15 kilogauss for low alloy iron to 20 to 22 kilogauss when permendur is used. The corresponding pull-in speed ratio would be:

$$\frac{\Delta t_{p1}}{\Delta t_{p2}} = \left( \frac{B_{2 \text{ sat}}}{B_{1 \text{ sat}}} \right)^2 = \left( \frac{22}{12} \right)^2 = 3.68 \text{ times}$$

## 2. Improvement of Magnetic Field Penetration Velocity

When the rate of increase of magnetic force on the armature is limited by the rate of increase of magnetic field penetration to the full dimension of the armature and magnetic circuit, improvement in performance requires a material or construction change which allows a faster buildup of the magnetic field. A decrease in electrical conductivity or magnetic material thickness will permit a faster increase in magnetic field. The propagation constant for a magnetic wave in a conducting, homogeneous, isotropic, linear magnetic material is:

$$\gamma = \sqrt{j \omega \mu g} = \alpha + jB ; \alpha = B = \sqrt{\frac{\omega \mu g}{2}} \quad (26)$$

where:

- $\gamma$  = the complex magnetic wave propagation constant
- $\alpha$  = the magnetic wave attenuation constant in nepers per meter
- $B$  = the magnetic wave phase constant in radius per meter
- $j$  =  $\sqrt{-1}$  the imaginary factor
- $\omega$  =  $2\pi f$  where  $f$  is the real wave frequency
- $\mu$  = permeability of the magnetic material in Henry's per meter
- $g$  = conductivity of the magnetic material in ohm meters

The attenuation of the magnetic wave in the magnetic material may be reduced by reducing  $\mu$  or  $g$  or both. The reduction of  $\mu$  is somewhat unattractive because a higher magnetizing current is required to obtain a desired flux density and mechanical force. The conductivity may be reduced by appropriate alloying elements and heat treatment. The conductivity reduction should not be accomplished by a corresponding reduction of permeability,  $\mu$ , or saturation flux density,  $B_{\text{sat}}$ . The bulk conductivity of a given material may be reduced by compressing small insulated particles together to obtain the bulk configuration. Insulated laminations assembled to fit the desired physical shape may also be used. The method of subdivision and assembly must cause a minimum degradation of the apparent bulk magnetic properties. Examples of magnetic wave attenuation improvement by alloying are the substitution of silicon steel for high purity ingot iron and the substitution of 2 percent vanadium permendur for 50/50 permendur.



The use of high purity compressed insulated iron powder or flake for bulk iron magnetic structures is not attractive for high force solenoid actuators because of the poorer bulk magnetic properties of the compressed materials. Magnetic materials with low conductivity and low magnetic wave attenuation such as ferrites are available; however, their saturation flux density of 4 kilogauss precludes their use in high force density actuators.

A survey of methods to improve the speed of magnetic field penetration and the consequent limiting speed of armature force buildup indicates bonded laminates of high saturation magnetic alloys will produce the highest actuator speed and force density. Laminates of .001-inch-thick sheets are available resulting in apparent bulk permeabilities and saturation flux densities which are 90 to 95 percent of the static characteristics for the solid material. It is possible by use of insulated magnetic laminates to obtain full magnetic force speeds less than 0.1 millisecond. The laminate bonding must have sufficient strength to endure the acceleration and shock loads which are possible with high speed buildup or decay of magnetic force.

### 3. Improvement of Breakaway Speed

A solenoid actuator usually works against a spring force which is installed to insure return of the actuator armature to a required unenergized position. An initial preload force is included in the spring to assure armature return for all operating conditions and maintain stability under environmental accelerations. Reduction of spring preload will reduce the breakaway time and the minimum shock and acceleration tolerance. It is assumed that materials and surface finishes are selected to minimize static friction.

### 4. Improvement of Dynamic Friction

Dynamic friction will limit the speed of operation for a given applied magnetic force. Valve actuators are required to move a valve closure against a fluid stream velocity and pressure. It is possible to design valve closure mechanisms which balance the fluid forces on the closure element with identical forces on a balancing element. This technique may complicate the design and reduce reliability; hence, the application must be carefully considered.

### 5. Improving Speed Limit by Inelastic Deformation of Actuator Materials

The maximum saturated magnetic pressure obtainable from the best available magnetic materials is approximately 600 psi which is much lower than the permissible stress in most structural and magnetic materials; hence, this inelastic deformation of actuator materials is not limiting for efficient solenoid actuators operating at near saturation flux densities. Electromagnetic forming or deformation requires much higher magnetic field intensities for the transformation of the electrical energy into mechanical kinetic energy prior to the material deformation. This electromagnetic forming transformation of electrical energy to mechanical forming forces does not appear to be an efficient method of operating solenoid actuators.

6.3.4.8 Ideal Impulse Voltage Characteristic - The electromechanical factors limiting speed of electromechanical actuators and the basic requirements to improve the speed with a multiple capacitor impulse driven circuit have been considered. Voltage time characteristics obtained with the multiple capacitor impulse driver is not an ideal characteristic, but it does represent a good compromise consistent with requirements of reliability and simplicity. An ideal impulse drive voltage characteristic may be established which will give maximum speed for minimum electrical energy consistent with electrical and mechanical stress limits. Figure 6-7 represents an idealized impulse voltage time characteristic considering the material stress limits.

The maximum impulse voltage  $E_{ab}$  (Figure 6-7) of the ideal impulse driver is determined by the coil electrical insulation requirements. This voltage represents the greatest rate of change of current and magnetic force obtainable with acceptable electrical insulation life. The impulse voltage must be applied and removed at a limited rate during intervals 0-a and b-c (Figure 6-7) because the impulse voltage propagates the coil at a low velocity, causing large voltage differences between adjacent turns and layers of the actuator coil. The large voltage differences can cause voltage overstress of the interturn and interlayer insulation. For maximum speed, the full impulse voltage,  $E_{ab}$  (Figure 6-7), must be sustained during armature motion. After the armature position is static following actuation, the actuator voltage may be gradually reduced to a voltage,  $E_{ce}$ , which is sufficient to hold the armature position against the return spring, fluid and external acceleration forces.

It is possible to construct a circuit which will generate a nearly ideal turn-on pulse similar to Figure 6-7 for driving solenoid actuators; however, the component, weight and reliability will not compare favorably with the multiple capacitor impulse driver. The switching logic for the low voltage trapezoid impulse driver circuit can be identical to the capacitor circuit, except the capacitor energy storage components are replaced by lumped or uniformly distributed L-C transmission line elements with a round trip propagation time equal to the desired impulse time.

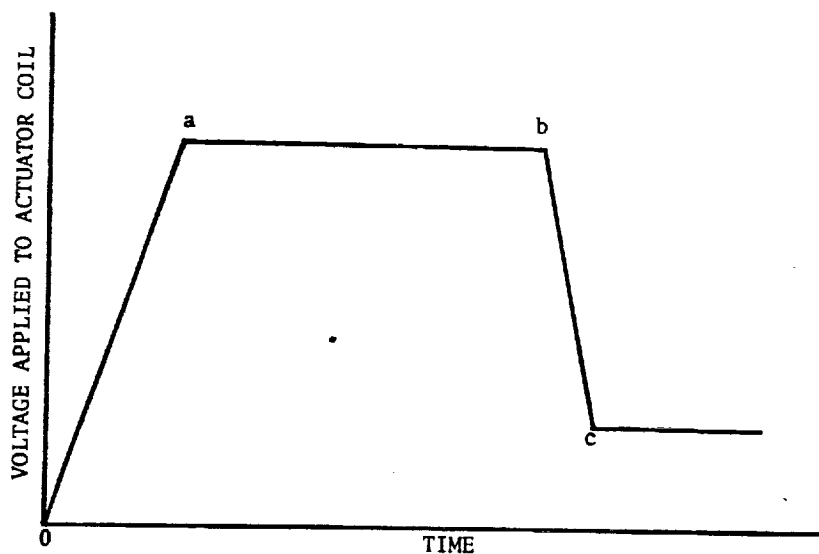


Figure 6-7. Ideal Solenoid Drive Impulse

## 6.4 CONCEPTUAL ACTUATOR DESIGNS

This section reviews the actuators conceived for use in the actuation of liquid propellant valves. The valves of primary interest are those intended for control of  $\text{OF}_2\text{-B}_2\text{H}_6$  rocket engines at thrust levels up to 1000 pounds. Consideration was also given to miniature valve actuators for use with micro thrusters or as fluidic system shutoffs. Work was accomplished in the areas of monopropellant, bipropellant, electrodynamic, piezoelectric, superconductive, and thermal actuators.

### 6.4.1 Monopropellant Chemical Actuator Concept

Liquid hydrazine monopropellant gas generators have been developed for use in spacecraft rocket engines and for spacecraft propellant pressurization systems. A concept incorporating an integral actuator and monopropellant gas generator is capable of producing high pressures from small quantities of fuel, resulting in high actuation forces. The measured work output of the unit compared very favorably to that of squib type actuators.

The operation of the monopropellant unit shown in Figure 6-8 is as follows: Since the valve is shown normally open, initially there is flow through the valve. When turn-off is desired, a pilot valve is pulsed, allowing a predetermined amount of monopropellant to flow through the check valve and catalyst, into the actuator's pressure chamber. The pressure thus formed, acts against the piston or bellows head of the actuator to close the valve. The effects of high pressure on the pilot valve are minimized by the check valve, which prevents back flow in the actuated condition. When the valve is to be opened, the pilot vent valve is opened, venting the pressure from the actuator. The vented gas may be directed back into the line or overboard. If more positive opening is desired, a second actuator similar to the first but arranged to act in the opposite direction may be used. Three-way pilot valves may be used to replace the separate pilot and pilot vent valves. The advantage of using two separate valves for piloting is that they need to be opened only momentarily for valve actuation, reducing power requirements without the use of latching solenoid type valves.

6.4.1.1 Feasibility Tests - A monopropellant actuator was constructed and tested to determine the feasibility of this concept. The system used in performing these tests is shown schematically in Figure 6-9. Recordings were taken of valve current, injected fuel volume, actuator stroke, actuation pressure and restraining pressure versus time. Hydrazine was used as the working fluid. Successful actuations with restraining loads to 265 pounds were demonstrated. Piston transfer times as low as 60 ms for a 2.75 inch stroke were observed.

The test firings were performed for fuel supply pressures ranging from 150 to 350 psig and restraining pressures from 100 to 600 psig. A typical plot of pressure and displacement versus time is shown in Figure 6-10. After a total of 25 test firings the actuator was disassembled for examination. A strong odor of ammonia typical of hydrazine reactions was noted, and the presence of catalyst "fines" was observed in the actuation chamber. The actuator elastomeric seals seemed unaffected by the test firings and no erosion of the actuator internal surfaces was evident. A photograph of the disassembled actuator after test is shown in Figure 6-11.

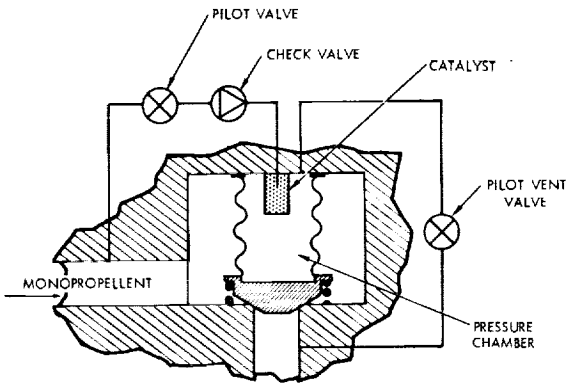


Figure 6-8. Monopropellant Chemical Actuator (Normally Open Valve)

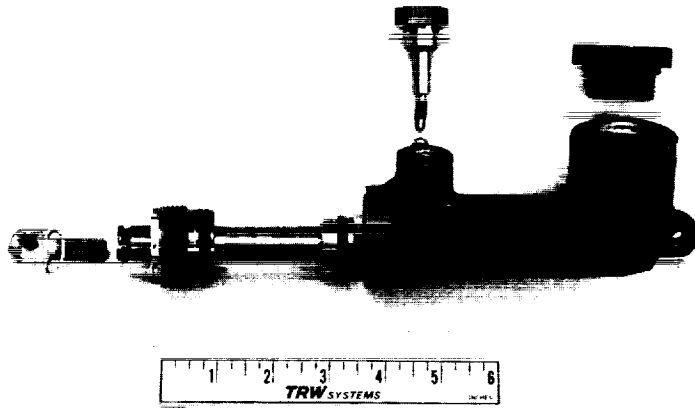


Figure 6-11. Monopropellant Chemical Actuator Test Unit

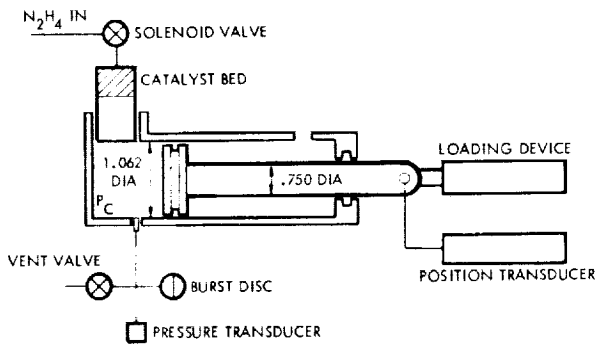


Figure 6-9. Monopropellant Chemical Actuator Test Schematic

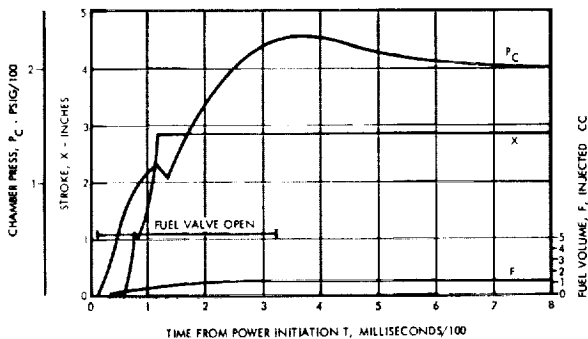


Figure 6-10. Monopropellant Chemical Actuator - Performance Curve

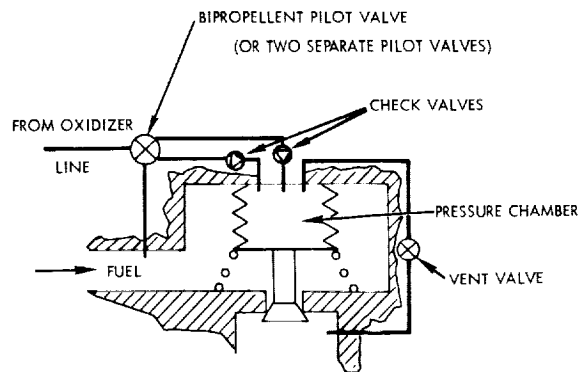


Figure 6-12. Bipropellant Chemical Actuator (Normally Closed Valve)

The monopropellant actuator provides actuation with high force levels and with fuel consumption an order of magnitude less than if direct line piloting was used. This approach has promise for applications in spacecraft valves and may also find application in other spacecraft actuation functions such as boom extension, spacecraft positioning on planet surfaces, and in powering tools for space maintenance functions.

#### 6.4.2 Bipropellant Chemical Actuator Concept

The bipropellant actuator is very similar to the monopropellant unit described above. It is apparent that a hybrid (liquid-solid) actuator containing a quantity of fuel or oxidizer internally could also be utilized. Figure 6-12 illustrates a bipropellant chemical actuator applied to a normally closed valve. Operation is very similar to the monopropellant unit except that both fuel and oxidizer injection is necessary. Positive actuation in both directions may also be obtained, eliminating the spring used for closure. The bipropellant actuation concept may also be applied to other spacecraft actuation functions requiring high force levels. The advantages of using propellant combustion for actuation are similar to those for squibs used for actuating explosive valves, except that many actuation cycles are possible.

#### 6.4.3 Electrodynamic Actuators

Electrodynamic actuators are used to produce sound in loud speakers. The important difference between the loud speaker and the electrodynamic actuator is that the light paper cone is replaced by a metal diaphragm (Figure 6-13). The motion generated can be described by reference to Faraday's Law, which states that in a magnetic field the force on a conductor is proportional to the product of the magnetic flux density, the current in the conductor, and the length of the conductor, provided that the conductor and the flux density are perpendicular to each other. The direction of the force is perpendicular to the plane of the conductor and the flux density.

The force density in electrodynamic actuators is expressed by the vector equation  $\mathbf{J} \times \mathbf{B}$ , where  $\mathbf{B}$  is the flux density in the air gap and  $\mathbf{J}$  is the current density in the moving coil attached to the diaphragm or bellows closing or opening the valve. If  $\mathbf{J}$  and  $\mathbf{B}$  are orthogonal, the force can be expressed in terms of current  $I$ , length of the conductor  $L$  and flux density  $B$  giving  $F = BIL$ . To maximize the force, it is necessary to optimize the flux density  $B$  for a given size of magnet. It is believed that the most appropriate shape for minimum leakage flux, is the one used in acoustic loud speakers with concentric air gap geometry (configuration (a) of Figure 6-13). For this shape it is feasible to have a complete magnetic circuit made of anisotropic magnetic material such as Alnico 5DG. This will require special techniques for fabrication and magnetization. For example, winding the coil in the square air gap window and exciting it with a high current, should magnetize the material provided the material has the preferred axis along the axis of magnetization; that is, the material exhibits magnetic anisotropy. It should be noted that the air gap is formed between soft iron pole pieces (like Permendur) to obtain the maximum flux density in the air gap.

If it is not desirable to fabricate the entire magnetic circuit of anisotropic magnetic material, then soft magnetic material is used wherever there is a change in the direction of the flux path, (configuration (b) of Figure 6-13). Too many interfaces are not desirable in a magnetic circuit since each interface will have an air gap, causing an increase in the reluctance of the magnetic circuit. For a given magnet and its air gap, the greatest volumetric efficiency is obtained by maximizing the product  $B_m H_m$ , where  $B_m$  is the flux density and  $H_m$  is the magnetizing force.

An approximate value of magnetic flux densities for different magnetic assemblies is shown in Table 6-4.

Beyond the optimized value of  $B_m = 20,000$  to  $22,000$  gauss, the reluctance of the magnetic circuit increases greatly due to saturation. Therefore,  $B_m = 20,000$  gauss is taken as the limiting value of the flux density. This can be increased significantly only if the operation of the device is at cryogenic conditions. It should be noted that  $B_m = 20,000$  gauss can be obtained even for a magnetic circuit of half the size by decreasing the gap width to half.

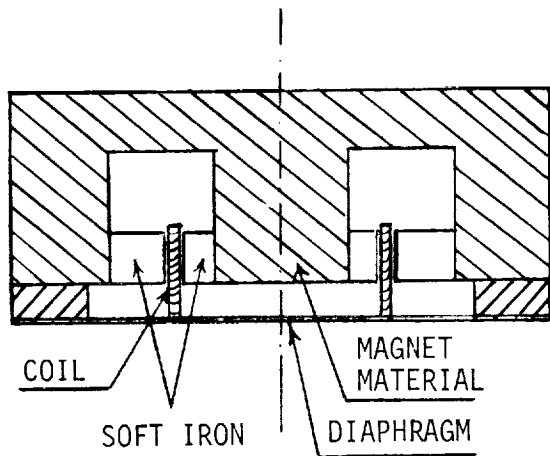
The temperature dependence can be explained as follows: As the temperature of a ferromagnetic material is raised the measured intensity of magnetization will steadily decrease, which is due to the increasing thermal agitation of the elementary spin alignment.

The relative magnetization change with temperature is shown in Figure 6-14 derived from the modified Langerin-Weiss Theory. Also, in general, the intrinsic saturation induction (gauss) increases with decrease in temperature.

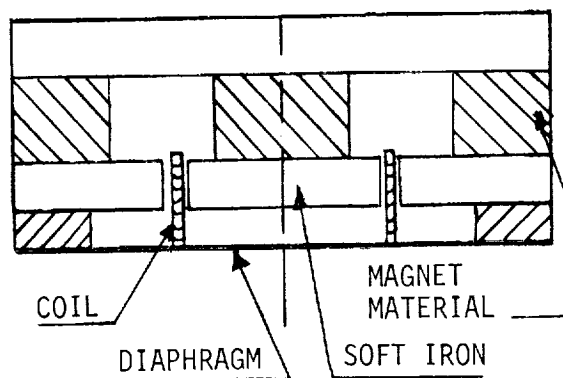
The coil design is optimized by the following considerations: From the force relation,  $F = BIL$ , it is apparent that for a given gap volume which defines the flux density  $B$ , the maximum safe power is dissipated in the coil for a given temperature rise, if the coil volume approaches the gap volume. Since the coil needs to be insulated, and it is not allowed to have contact with the gap walls, the ratio of the coil volume to the gap volume will always be less than one. To maximize this ratio, the coil wire cross-section should be rectangular, and the number of turns should be minimum so as to minimize the wire insulation volume.

The advantages of electrodynamic actuators are:

1. Time response is improved in comparison with the time response of solenoid actuators of similar characteristics (see Table 6-5).
2. Sliding friction is eliminated so that service life and reliability are improved.
3. The actuator magnet and coil can be isolated from propellants by using a diaphragm provided the pressure across the diaphragm is equalized. However, if the coil is submerged in the fluid, which will enhance the heat transfer from the coil, higher power can be applied to obtain a greater magnitude of force.



(a)



(b)

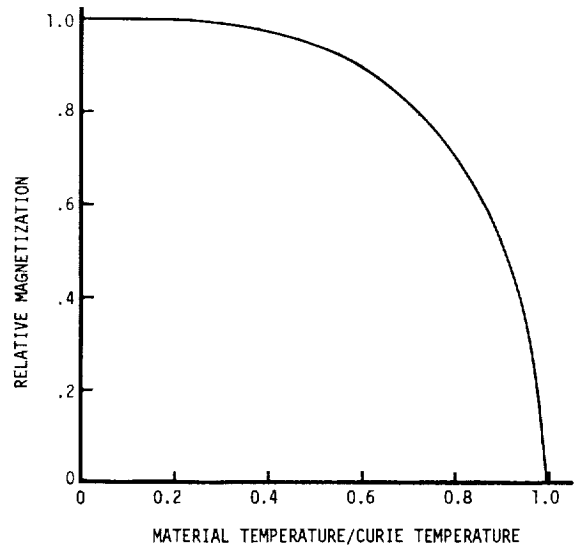


Figure 6-13. Typical Electrodynamic Actuator Configurations

Figure 6-14. Relative Magnetization Change with Temperature

Table 6-4. Comparison of Magnetic Assemblies

Type	Weight (oz.)	Gap Energy (ergs x 10 <sup>6</sup> )	Flux Density (gauss)
EIA Standard	6.8	2.3	12,600
Dual Diameter Type	6.3	2.9	16,200
Optimized Magnetic Circuit (Estimate)	6.3		20,000

Mean gap diameter = 1 inch  
 Gap width = 0.030 inch  
 Gap length = 0.25 inch

Table 6-5. Comparison of Solenoid and Electrodynamic Actuators

Power = 5 watts. Displacement = 0.01". Weight ≈ 5 oz.	
Solenoid Actuator	Electrodynamic Actuator
(A) <u>Force</u> = 5 lbs at zero displacement; Force = 10 lbs at maximum displacement; Voltage vs force relationship is non-linear.	Force = 1.9 lbs at zero displacement; Force <1.9 lbs at maximum displacement depending upon the spring stiffness*. Voltage vs force relationship is fairly linear.
(B) <u>Friction:</u> About 10% of initial force.	<u>Friction:</u> None.
(C) <u>Time Response:</u> Moving mass = 9.1 gms. Coil inductance ≈ 0.69 h. R = 220Ω Electrical time constant: ≈ 3.1 m sec. Total time to open: 9 m. sec.	<u>Time Response:</u> Moving mass = 2.22 gms. Coil inductance ≈ 1100 micro henries. R ≈ 4.75 Ω Electrical time constant: ≤ 0.5 m. sec. Approximate time to open: < 2 m. sec.

\*Stiffness of the diaphragm of 2" diameter and 0.005" thickness is much smaller than external spring.

Table 6-6. Comparison of Solenoid and Electrodynamic Actuators

Force = 5 lbs. Displacement = 0.01". Weight = 5 oz.	
Solenoid Actuator	Electrodynamic Actuator
(A) <u>Power:</u> 5 watts	<u>Power:</u> 28.5 watts
(B) <u>Friction:</u> 10% of initial force.	<u>Friction:</u> None.
(C) <u>Time Response:</u> Moving mass = 9.1 gms. Coil inductance 0.69 h. R = 220 Electrical time constant: 3.1 Total time to open: 9 m. sec.	<u>Time Response:</u> Much less than 2 m. sec.



The limitations of electrodynamic actuators are:

1. To obtain larger force, greater power is required (see Table 6-6).
2. The weight required per unit of force and power is higher in electrodynamic actuators than in solenoid actuators.

#### 6.4.4 Piezoelectric Actuators

The operation of piezoelectric ceramic actuators is based on the enhanced electrostrictive effect of the special dielectric materials called ferro-electrics. Electrostriction is a dielectric phenomenon where the application of a field across the dielectric changes the dimension of the dielectric material. The material considered here is lead zirconate-titanate, which is equivalent to PZT-4 and PZT-5 of the Clevite Corporation.

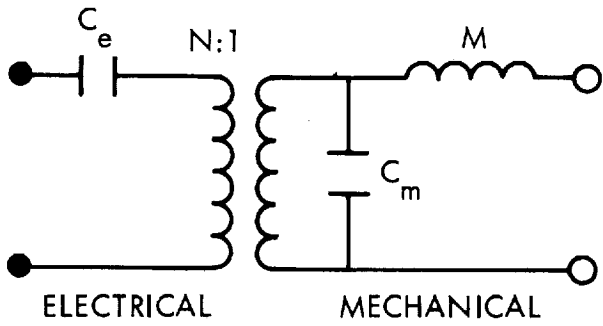
The equivalent circuit of a piezoelectric transducer is shown in Figure 6-15. From this circuit, the free displacement and the blocked force can be computed for a particular actuator design. The power dissipation is essentially that due to the dielectric leakage resistance and the losses in the voltage step up process. See Reference 3 for piezoelectric actuator design criteria.

A PZT-5A piezoelectric ceramic disc of 0.021-inch thickness and 1-inch diameter was tested unloaded with an applied field of 3000 volts per inch. The disc was clamped with "O" rings as shown in Figure 6-16. The measured maximum deflection was 0.00017 inch, which was only half of the computed deflection for a free disc. This test pointed out the importance of the disc installation in a piezoelectric actuator, i.e., the use of an unclamped mount.

In a disc, the piezoelectric force can be increased by increasing the disc thickness, however, the displacement is reduced. To increase the displacement, discs can be stacked in pairs as shown in Figure 6-17, so that the direction of polarization of each of the two discs in the pair is opposite. Then the total force generated is the same as the force produced by each disc separately, however, the displacement is amplified by a factor equal to the number of discs. In Figure 6-17, the displacement is six times that produced by one disc.

Another way to improve the displacement of a piezoelectric actuator, is to use a piezoelectric bender bimorph cantilever. However, to obtain sufficient force and displacement, the length and thickness of the bender have to be quite large. To solve this problem, at least in theory, it should be possible to make a piezoelectric coil with rectangular cross-section as shown in Figure 6-18.

The prominent advantages of piezoelectric actuators are improved time response, no sliding friction, low power dissipation, and ruggedness. The primary limitation is short stroke.



where:  $N$  = electro-mechanical linear transducer ratio in volts/Newton  
 $C_e$  = electrical capacitance in farads  
 $C_m$  = mechanical compliance in meters/Newton  
 $M$  = effective mass in kilograms

Figure 6-15. Equivalent Circuit of a Piezoelectric Transducer

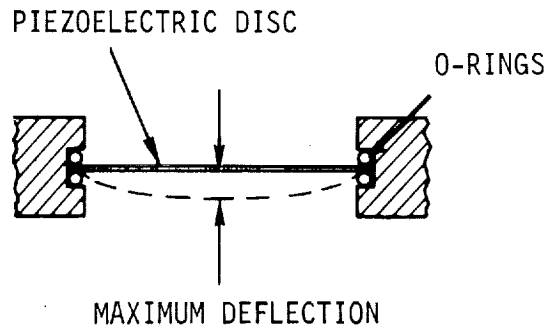


Figure 6-16. Piezoelectric Ceramic Disc Test Installation

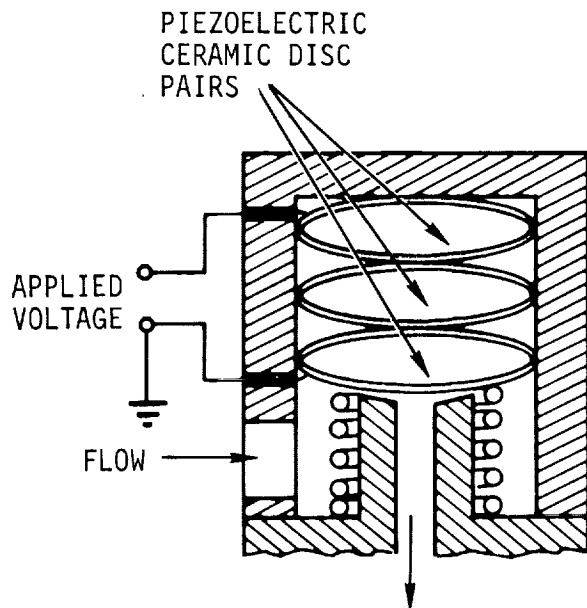


Figure 6-17. Piezoelectric Actuator Using Stacked Discs

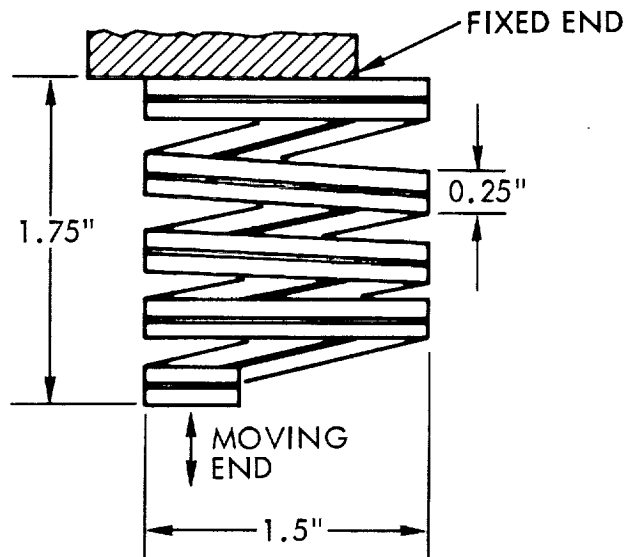


Figure 6-18. Piezoelectric Helical Actuator

#### 6.4.5 Superconductive Actuators

A state of matter, called the superconductive state, is obtained for certain metals where they show zero ohmic resistance below certain temperatures called the critical temperature. Critical temperatures for a number of elements are shown below.

##### Critical Temperature of Some Important Superconductors

<u>Element</u>	<u>°K</u>
Aluminum	1.2
Indium	3.4
Tin	3.72
Mercury	4.15
Tantalum	4.45
Lead	7.19
Niobium	9.6

A superconductor will become a normal conductor in the presence of a magnetic field above critical field value  $H_c$ , but will return to the superconductivity state when the field is removed.

An approximate relationship of critical field as a function of temperature is:

$$H_c = H_0 \left[ 1 - \left( \frac{T}{T_c} \right)^2 \right]$$

where:  $H_0$  = critical field at absolute zero °K

$T$  = temperature in °K

$T_c$  = critical temperature

Figure 6-19 shows the critical field vs. temperatures for various superconducting metals.

The phenomenon of superconductivity is essentially based on the process which involves the condensation of pairs of conduction electrons into a lower energy level or phase. This condensation process is found to be associated with the interaction between the conduction electrons and the crystal lattice, a process that is also responsible for the electrical resistance of metals in the nonsuperconductive state. For this reason, superconductivity occurs in the poorer metallic conductors rather than in better conductors such as copper, silver or gold.

From the periodic table of elements, the following regularities are observed which so far hold for elements as well as alloys and compounds.

1. Superconductivity is observed in metals.
2. Superconductivity is found only in elements for which the number of valence electrons lies between 2 and 8. For compounds and alloys the limits can be slightly lower than 2 and higher than 8.

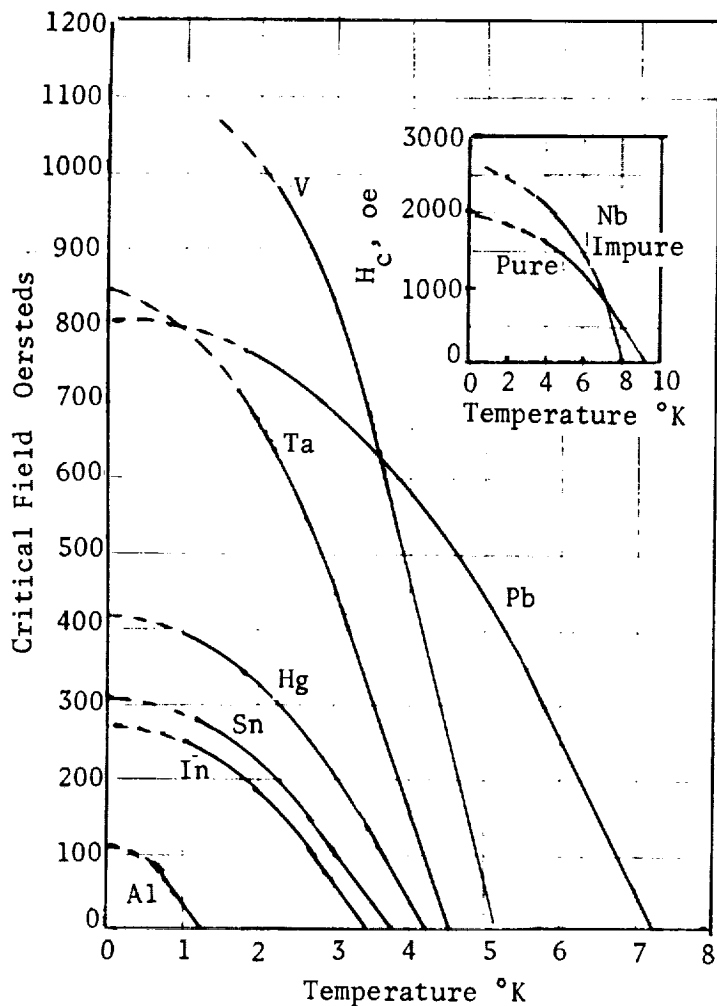


Figure 6-19. Critical Field Curves of Some Superconductors

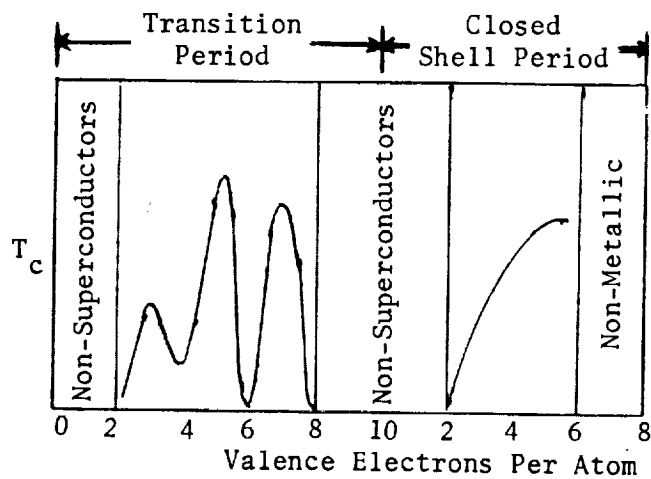


Figure 6-20. Variation of Critical Temperature With Number of Valence Electrons

3. No ferromagnetic or antiferromagnetic elements are superconductors.
4. For non-transition element superconductors,  $T_c$  increases with the number of valence electrons (Figure 6-20).

Since superconducting wire has no ohmic resistance it is possible to construct superconducting solenoids that produce no joule heating. At the present, superconductive solenoids are used to produce a high dc magnetic field in laboratory apparatus and in connection with low temperature devices such as the maser.

Solenoids used in conventional actuators cannot be used in the superconductive state since the current will exceed the critical current during the transition period. The best magnetic field obtainable in ferromagnetic materials used in conventional solenoid actuators is 20 kiloersteds, due to saturation of the material. However, superconductive solenoids can be used to generate fields as high as 100 kiloersteds in air. To obtain mechanical motion for actuation in a high magnetic field, electrodynamic actuator concepts can be used where the conductors interact with the static magnetic field. The magnet used in electrodynamic solenoids is replaced by the superconductive solenoid. Since conductors such as copper or silver have very low resistance, under the cryogenic conditions, the losses are very small. Therefore, the advantages of the superconductive electrodynamic actuators are high static forces and very low heat losses.

The primary problem encountered in the present state of the art is the need for very low temperatures. However, metallic and intermetallic compounds have been developed with critical temperatures as high as 30°K, so that liquid hydrogen can be used for refrigeration.

According to Dr. W. A. Little's thesis (Stanford University, Palo Alto, California), a special class of organic materials can remain superconducting at very high temperatures. Work performed at the Synvar Corporation, Palo Alto, California, appears to support Dr. Little's thesis, and a small amount of organic superconductive material has been produced. If room temperature superconductors become available, their possible applications in actuator design cannot be disregarded.

#### 6.4.6 Thermal Actuators

Thermal actuation is accomplished by solid differential expansion, liquid or vapor expansion, state change, and phase change (Polyphase) actuators. Some mechanizations of this type of actuator are shown in Figures 6-21 and 6-22.

The time response of thermal actuators is slower than solenoid actuated valves due to the thermal lags associated with transferring heat into or out of a system. These lags are controlled by the relative temperature difference between the heater and the object to be heated, the heat transfer

coefficient between the two, and the thermal inertia of both. For constant heater output and constant specific heat, the time rate of change of temperature may be described as:

$$\frac{dT}{dt} = \frac{Q}{(W_1 C_{p1} + W_2 C_{p2} + \dots)}$$

where: T = temperature  
t = time  
Q = heat input into area to be heated  
W = weight of heated part  
C<sub>p</sub> = specific heat of heated part

The actual temperature of the part at any time t may then be described as:

$$T = T_o + \frac{Qt}{(W_1 C_{p1} + W_2 C_{p2} + \dots)}$$

where: T<sub>o</sub> = the initial temperature of the part

From the above equation it is evident that the valve time response may be improved by increasing the heat input and decreasing the mass and specific heat of the actuating part.

Figure 6-23 schematically illustrates an actuator concept where this has been considered. In this valve a thin bimetallic diaphragm is used to provide high actuation forces in a snap acting manner while minimizing the mass of the actuating element. Heat is introduced directly to the actuation diaphragm either electrically or from a separate source so as to open the valve. The flowing propellant then impinges on the diaphragm and removes excess heat which allows rapid valve closure when the heater is turned off.

A state change actuator concept for multiple operation is illustrated in Figure 6-24. A quantity of state change material is confined in a sealed housing by a diaphragm which also forms the valve seal. The diaphragm is the only moving element. The material is solid in the valve open position and liquified by heat addition to close the valve.

A valve concept utilizing a thermal state change actuator intended for single cycle operation is illustrated in Figure 6-25. The operation is similar to that of a squib valve where the ends of the tubes are sheared off. The magnets are provided to insure that the sheared tube ends remain clear of the flow stream.

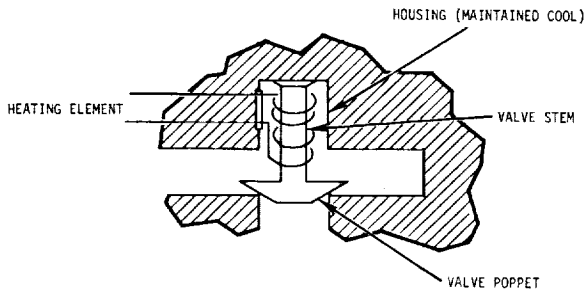


Figure 6-21. Differential Expansion Actuated Valve

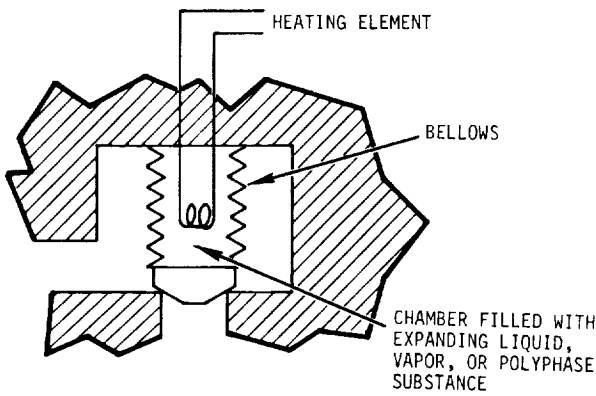


Figure 6-22. Fluid Expansion Actuated Valve

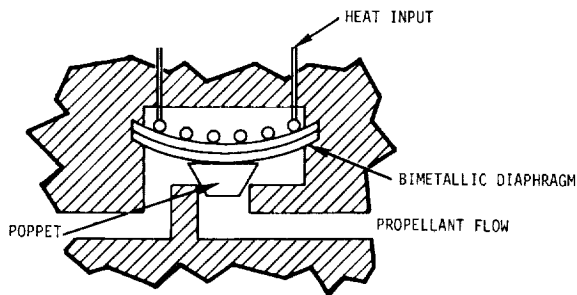


Figure 6-23. Snap Action Differential Expansion Actuated Valve

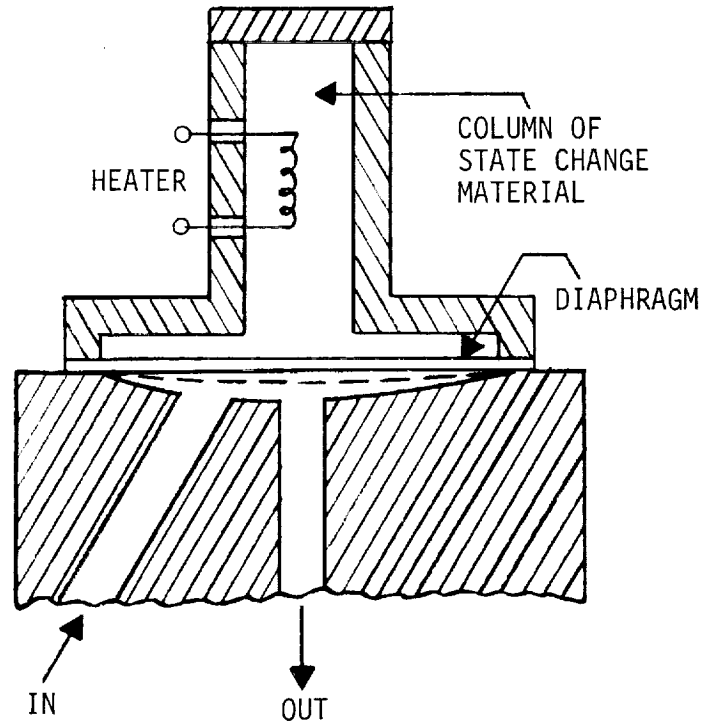


Figure 6-24. State Change Actuator for Multicycle Operation

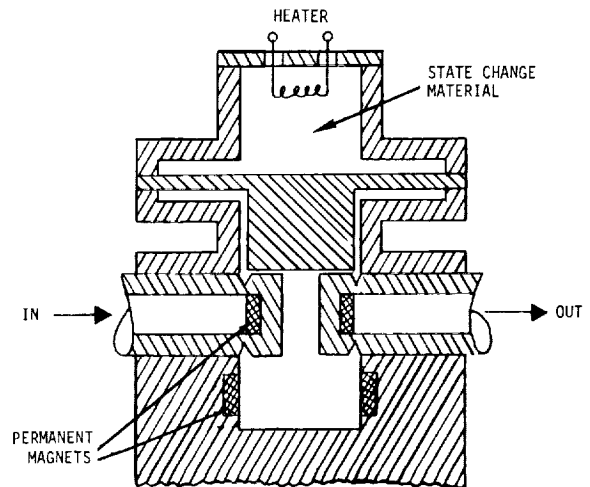


Figure 6-25. State Change Actuator for Single Cycle Operation

## 6.5 LIGHTWEIGHT SOLENOID ACTUATOR

### 6.5.1 Introduction

From earlier studies it was determined that both the weight and the high and low temperature characteristics of solenoid valve actuators could be significantly improved through the use of beryllium wire as a magnet coil material. This section describes efforts made to investigate and develop a lightweight solenoid actuator for operation of valves on spacecraft propulsion engines.

Solenoids operating at temperatures up to 250°C with an operating life in excess of 40,000 hours are considered within the present state of the art. A solenoid actuator with an operating life of about 100 hours has been developed for operation at temperatures up to 800°C and with potential life up to 1000°C. Presently available efficient magnetic core materials also have an upper temperature limit of 1000°C.

Valve actuators and other electrical machinery operating at extreme low temperatures have lower electrical power losses by several hundred times compared to room temperature operation. Corresponding reductions in size and weight and increases in power rating are possible. The optimum reduction in system weight effected by the proper combination of refrigerant or refrigerator and cryogenic electrical equipment for space applications will depend on mission requirements. The greatly reduced electrical resistivity of cryogenic beryllium offers an opportunity for power densities and electrical actuator performance which are impossible to achieve by other methods, including superconductors, which have limited current capacity due to their transition flux and current density limitations.

Two French companies have recognized the advantage of cryogenic beryllium electrical conductors in electrical machinery. A cooperative program has been recently initiated between Societe Alstom and Pechiney for development of a practical and economic cryogenic beryllium technology applied to large electrical apparatus (100 to 1000 megavolt amperes). One area of investigation involves the deliberate controlled addition of impurities to commercially pure beryllium to obtain very low cryogenic resistivity and other favorable characteristics.

The potential application of beryllium is also attractive for high and low temperature spacecraft electrical machines; for example, a high temperature beryllium turboelectric generator could result in great weight savings. This is due to the combination of low density, high tensile strength, and high Young's modulus, which permits much higher operating speeds at 1000°C than with other good electrical conductors. Beryllium has also been considered in the construction of rocket engines. Low temperature applications are most attractive when cryogenics are on board for other purposes. A cryogenic beryllium ac machine offers the greatest possible power, efficiency and weight reduction of any electrical conductor. Cryogenic ac turboelectric generators could be coupled to nuclear reactor power supplies with a negligible weight requirement for electrical machines.



## 6.5.2 Beryllium Technology

Beryllium metal has electrical and physical characteristics which make it inherently superior to other electrical conductors for high temperature electrical machinery operating at temperatures to 1000°C and cryogenic temperatures near -200°C. Some of the salient characteristics which make beryllium most attractive when compared to conventional electrical conductors are:

1. Low density
2. High tensile strength
3. High Young's modulus
4. Thin adherent self-electrical insulating anodize film
5. Good thermal and electrical conductivity
6. Best combinations of above properties at 1000°C and -200°C

At high temperatures near 1000°C or above, beryllium is the only good electrical conductor, offering a near optimum combination of high thermal conductivity, high space factor insulation, and good mechanical properties.

At low temperatures near -200°C, beryllium has the highest electrical conductivity in combination with the best overall mechanical properties.

Data on the electrical and physical properties of beryllium and other commercial metals used for electrical conductors is given in Table 6-7, along with data on two good high-temperature ceramic insulating materials. Table 6-8 gives a comparison of the properties of copper and beryllium, and Table 6-9 a comparison of beryllia and alumina.

The Nuclear Metals Corporation has generated data on ultra refined high purity Pechiney commercial beryllium and very pure copper as shown in Figures 6-26 and 6-27. Figure 6-26 compares the resistivity of ultra refined beryllium and very pure copper from cryogenic temperatures to 1800°F, and Figure 6-27 compares the resistivity density product of the two materials. The resistivity density product is a more significant figure of merit for comparison of electrical conductors in spacecraft actuator and electrical applications since minimum system weight is a dominant requirement.

6.5.2.1 Beryllium Wire and Insulation - Number 14 A.W.G. square wire (.064 inch square) was considered attractive for use in winding the solenoid coils which were subsequently evaluated in this program. This wire would provide a high space factor and ease of winding without random imbedding into the turns of adjacent layers. At the time (1964) manufacturing technology for square beryllium wire was not well established, so that number 14 A.W.G. round wire was felt a reasonable compromise.

Ductile square beryllium wire can now be obtained from Nuclear Metals Corporation, and other sources. The use of ductile square wire will enable winding of beryllium coils at room temperature with approximately 20 percent

Table 6-7. Data on Electrical Conductors and Ceramic Insulators

MATERIAL	DENSITY LBS/CU IN.	MELTING TEMPERATURE °C	SPECIFIC HEAT CAL/GM		ELECTRICAL RESISTIVITY Ω/CM		THERMAL CONDUCTIVITY GM CAL/SEC CM <sup>2</sup> °C		YOUNG'S MODULUS PSI X 10 <sup>-6</sup>		ULTIMATE TENSILE STRENGTH PSI X 10 <sup>-3</sup>	
			@25°C	@1000°C	@25°C	@1000°C	@45°C	@1000°C	@25°C	@1000°C	@25°C	@1000°C
ALUMINUM Al	0.100	653	0.214		2.824		0.504		10.1	0	30	0
BERYLLIUM Be	0.066	1283	0.425	0.79	4	40	0.45	0.15	44	LOW	50-70	2.5
COBALT Co	0.321	1480	0.100	0.187	6.24	77.4	0.165		30		30-100	12
COPPER Cu	0.323	1083	0.092		1.724	9.42	0.918		15		30	
GOLD Au	0.698	1063	0.031		2.44	12.52	0.700		11.3		20-46	
NICKEL Ni	0.321	1452	0.105		6.8	48	0.206		30		120	5.2
SILVER Ag	0.379	960	0.0558		1.59		1.00		11.2	0	42	0
IRON Fe	0.27	1539	0.107		10	116	0.161	0.191	30		25	
ALUMINA Al <sub>2</sub> O <sub>3</sub>	0.1395	2050	0.18	0.28	>10 <sup>20</sup>	2 X 10 <sup>12</sup>	0.88	0.25	50		35	21+
BERYLLIA BeO	0.109	2550	0.240	0.5+	>10 <sup>21</sup>	8 X 10 <sup>19</sup>	0.63	>0.07	50	37	21	13.5

Table 6-8. Comparison of Beryllium and Copper

DENSITY RATIO $\rho_{Be}/\rho_{Cu}$	0.204
SPECIFIC HEAT RATIO $C_{pBe}/C_{pCu}$	4.62
VOLUME RESISTIVITY RATIO $R_{Be}/R_{Cu}$	@ 25°C 2.32
	@ 1000°C 4.25
THERMAL CONDUCTIVITY RATIO $G_{Be}/G_{Cu}$	0.49
TENSILE MODULUS RATIO $E_{Be}/E_{Cu}$	2.93
TENSILE STRENGTH RATIO $S_{Be}/S_{Cu}$	≈ 2
RESISTIVITY RATIO × DENSITY RATIO $R_{Be}/R_{Cu} × \rho_{Be}/\rho_{Cu}$	@ 25°C 0.483
	@ 1000°C 0.868
THERMAL CONDUCTIVITY RATIO ÷ DENSITY RATIO $G_{Be}/G_{Cu} ÷ \rho_{Be}/\rho_{Cu}$	2.4
MODULUS RATIO ÷ DENSITY RATIO $E_{Be}/E_{Cu} ÷ \rho_{Be}/\rho_{Cu}$	14.36
TENSILE STRENGTH RATIO ÷ DENSITY RATIO $S_{Be}/S_{Cu} ÷ \rho_{Be}/\rho_{Cu}$	≈ 9.8
YIELD STRENGTH RATIO ÷ DENSITY RATIO $G_{Be}/G_{Cu} ÷ \rho_{Be}/\rho_{Cu}$	≈ 26

Table 6-9. Comparison of Beryllia and Alumina

DENSITY RATIO $\rho_{BeO}/\rho_{Al_2O_3}$	0.778
SPECIFIC HEAT RATIO $C_{pBeO}/C_{pAl_2O_3}$	@ 25°C 1.333
	@ 1000°C 1.788
VOLUME RESISTIVITY RATIO $R_{BeO}/R_{Al_2O_3}$	@ 25°C 10
	@ 1000°C $4 × 10^7$
THERMAL CONDUCTIVITY RATIO $G_{BeO}/G_{Al_2O_3}$	@ 25°C 7.1
	@ 1000°C >2.8
TENSILE MODULUS RATIO $E_{BeO}/E_{Al_2O_3}$	1
TENSILE STRENGTH RATIO $S_{BeO}/S_{Al_2O_3}$	0.6
RESISTIVITY RATIO ÷ DENSITY RATIO $R_{BeO}/R_{Al_2O_3} ÷ \rho_{BeO}/\rho_{Al_2O_3}$	@ 25°C 12.86
	@ 1000°C $5.14 × 10^7$
THERMAL CONDUCTIVITY RATIO ÷ DENSITY RATIO $G_{BeO}/G_{Al_2O_3} ÷ \rho_{BeO}/\rho_{Al_2O_3}$	@ 25°C 9.03
	@ 1000°C >3.6
MODULUS RATIO ÷ DENSITY RATIO $E_{BeO}/E_{Al_2O_3} ÷ \rho_{BeO}/\rho_{Al_2O_3}$	@ 25°C 3.77
	@ 1000°C 0.77
TENSILE STRENGTH RATIO ÷ DENSITY RATIO $S_{BeO}/S_{Al_2O_3} ÷ \rho_{BeO}/\rho_{Al_2O_3}$	0.77

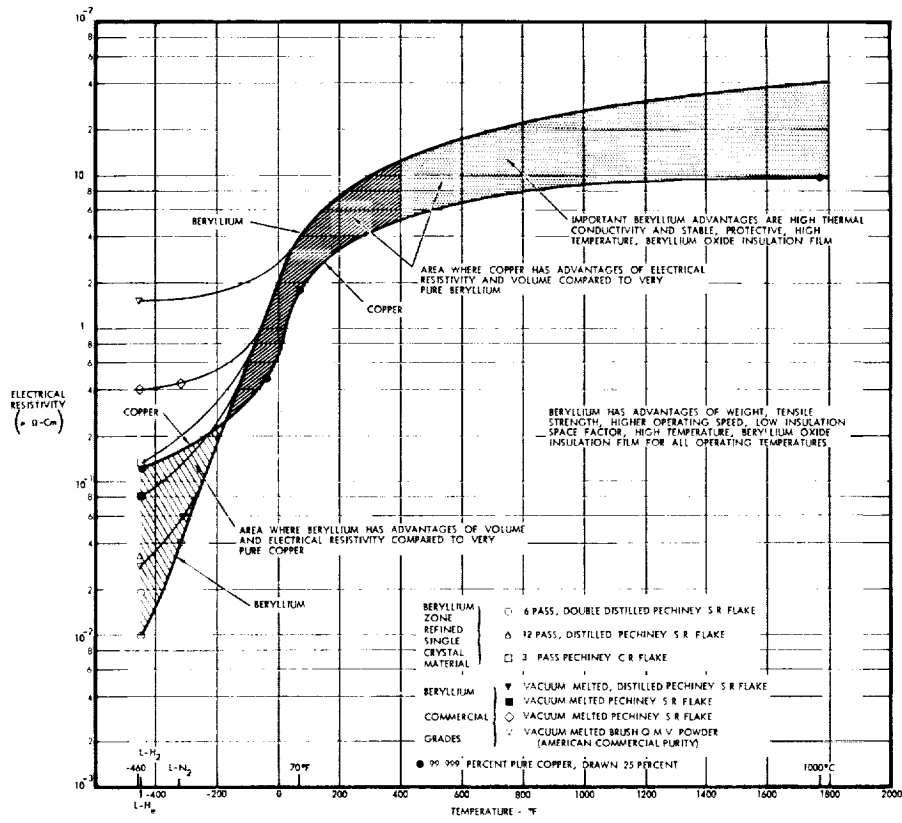


Figure 6-26. Resistivity of Ultra Pure Beryllium and Copper

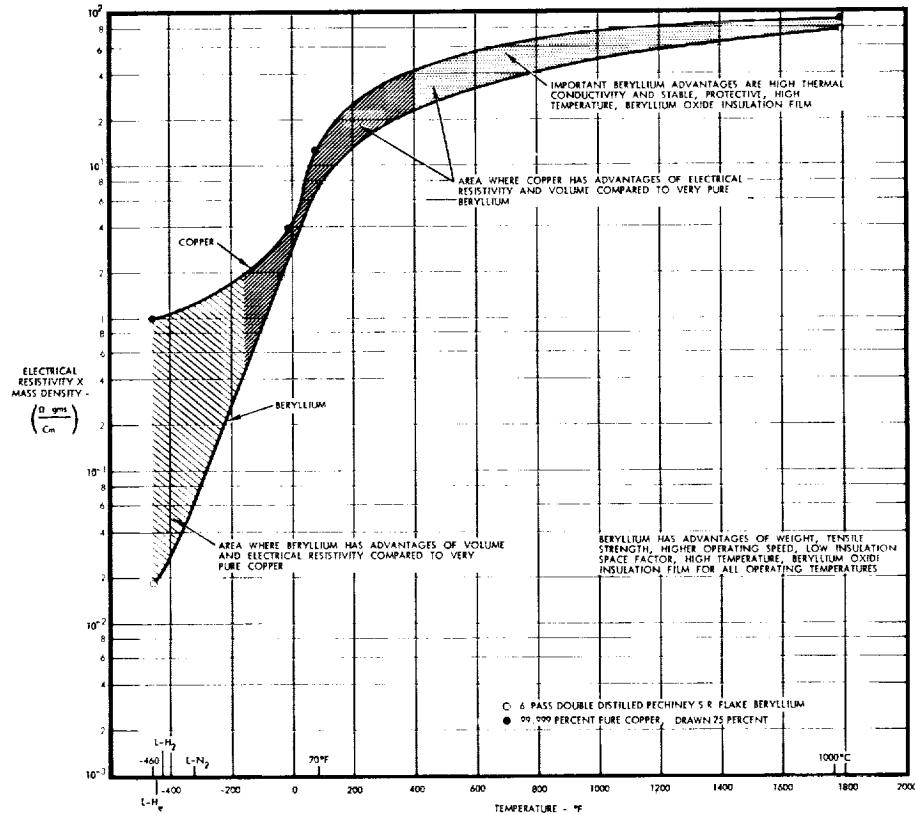


Figure 6-27. Resistivity-Density Product of Pure Beryllium and Copper

improvement in winding space factor. The winding irregularities caused by interlayer embedding of multilayer round wire coils are also eliminated. The interlayer contact between square wire windings is much greater than obtained with round wire, so that the interlayer thermal resistance is greatly reduced with square wire. The reduced interlayer thermal resistance will permit a proportionate increase in thermal dissipation density and current density within the coil winding. The increased current density of square wire coils will also permit the use of smaller coils to obtain a specified magnetizing ampere turn.

Three lots of anodized (beryllium oxide) beryllium wire were tested before a selection was made for use in winding the test solenoid coils. These tests demonstrated that anodized beryllium wire may be used at temperatures up to 1000°C in vacuum. Insulation breakdown in air was experienced at approximately 800°C. Reasons for the breakdown are presently not completely understood, however, it is believed an anodized coating can be developed which will meet the 1000°C temperature requirement in air. It is apparent from the insulation tests completed and experience in anodizing beryllium wire that an effort to obtain an improved anodize for electrical applications is likely to be effective since no effort has been directed specifically to this objective. The interior defects and inclusions of the base metal wire have an effect on the anodize insulation performance at high temperatures and any improvement in the basic quality of the wire will show as a corresponding improvement in anodize insulation performance.

The performance qualities of beryllium anodized wire for application to high current density and high temperature solenoid actuator coils is limited by defects in the wire, which are believed to be caused by inclusions of aluminum and silicone impurities. Utilization of commercially available low aluminum content beryllium wire with other impurity levels carefully controlled is expected to result in beryllium wire product quality suitable for electrical applications.

A summary of the important advantages of beryllium-oxide-insulated beryllium magnet wire in electromagnetic device coils is as follows:

1. Lighter Weight

1/5 the weight of typical magnet wire materials.

2. High-Temperature Operation to 1000°C

Be melts at 1283°C

BeO melts at 2550°C

BeO insulation is adherent, protective and compatible with Be metal to 1000°C.

3. Good Electrical Conductivity

Be has 40% the volume electrical conductivity of copper at 25°C.

Be has 2.07 times the electrical conductivity of copper on a weight basis at 25°C.

4. Good Thermal Conductivity

Be and BeO have superior thermal conductivity assuring cool operation at high power densities.

5. Superior Mechanical Properties for Rotating Machine Applications

The low density, high Young's modulus, and high tensile strength provide a combination of mechanical properties which improve the high-speed performance. Up to 15 times the power rating may be obtained when compared to the usual conductor materials used in high-speed rotating machines in cases where the peripheral speed limit of the rotor windings limits the power rating.

Methods of applying a beryllium oxide coating to beryllium wire which may be suitable for electrical insulation are:

1. Deposition and curing a film from a beryllium oxide slurry.
2. Extrusion and curing of a wet plastic beryllium oxide film.
3. Direct surface boundary oxidation by using a controlled atmosphere and temperature.
4. Deposition by electrophoresis from a colloidal beryllium oxide suspension.
5. Vacuum vapor deposition.
6. Spray coating of molten beryllium oxide.
7. Application of an anodized film by an electromechanical process.

For more detailed information on investigations of beryllium wire and insulation, see References 2 and 8.

6.5.2.2 Beryllium Thin Films - It was thought possible to fabricate beryllium electrical conductors having the desirable characteristics of low resistivity and high ductility by the deposition of beryllium film on a substrate in a continuous process. The film may be used on the substrate or removed for the electrical application. Beryllium was deposited on selected substrates by electron beam evaporation to ascertain the properties of vapor deposited films on fused silica and beryllium oxide substrates.

A series of beryllium thin films were prepared using electron beam heating evaporation techniques. The material used was 99.99 percent pure beryllium obtained from Electronic Space Products, Inc. (No. K-446B, Grade 4N). Typical impurities listed by the supplier are: 1 ppm Cr, 3 ppm Fe, 5 ppm Mn, 2 ppm Ni, and 30 ppm Si.

Film deposits were made by supporting target substrates above the beryllium evaporation source on a chimney. With this configuration, a circular target plane of approximately 6.5 cm was formed. Films were deposited on SiO<sub>2</sub> (quartz), Al<sub>2</sub>O<sub>3</sub> (aluminum oxide), and BeO (beryllium oxide) substrates.<sup>2</sup> A mask for the standard Hall specimen configuration was used for test samples (Figure 6-28).

Films not exceeding 1000Å thickness could be formed on quartz; thicker films showed a matte surface and separated completely from the substrate. Films formed on BeO and Al<sub>2</sub>O<sub>3</sub> had a matte surface similar to the substrate surface. The characteristics of all of the thin films tested were directly related to the film thickness, i.e., no significant difference was found between the three substrates used.

Three beryllium films with different thicknesses were measured for total solar absorptance ( $\alpha$ ) and normal emittance ( $\epsilon$ ), and are compared in Table 6-10. The tabulated film thickness values are approximate values calculated from an assumed bulk resistivity of  $2.78 \times 10^{-6}$  ohm cm. Experimental interferometer measurements were unsuccessful, because beryllium is a "dark" metal with significant spectral absorption in the near ultraviolet and visible wavelengths.

The typical electrical measurements made were Surface Resistance (with a 4 point probe), Film Thickness (with a 4 point probe, assuming the  $\alpha$  of Be =  $2.78 \times 10^{-6}$  ohm cm @ 25°C), Bulk Resistivity (bridge method), Hall Coefficient, and Hall Mobility. The three Be thin films on quartz were evaluated at room temperature to determine the above characteristics (Table 6-11). Subsequent measurements of relative bulk resistivity (bridge method) down to LN<sub>2</sub> temperatures were also made. The results are shown in Figure 6-29. Where the data points are not given at LN<sub>2</sub> temperature, electrical contact separation occurred on the sample. For comparison, the bulk resistance curves of iron and copper are also shown in Figure 6-29. The resistivity curve shown for Film B is not believed to be accurate, because of the uncertainty in the film thickness.

The slope of the three Be thin film resistance curves in comparison to the bulk iron/copper data is most significant. Electrical conductivity of thinner beryllium film is nearly temperature independent, because bulk and surface scattering processes limit electron or hole transport. For thin film geometries, the critical path length ( $L_c$ ) is important.  $L_c$  is defined as the value of the charge carrier mean free path ( $\lambda$ ) at which boundary surface scattering processes equal bulk scattering effects. For a thin film,  $L_c$  can be greater than the film thickness. Bulk resistance decreases with temperature by decreasing the effect of bulk scattering centers. Surface controlled scattering processes apparently are temperature insensitive. Low bulk resistivity requires a long charge carrier mean free path. Values as large as one millimeter have been calculated from experimental measurements made for metals at cryogenic temperatures.

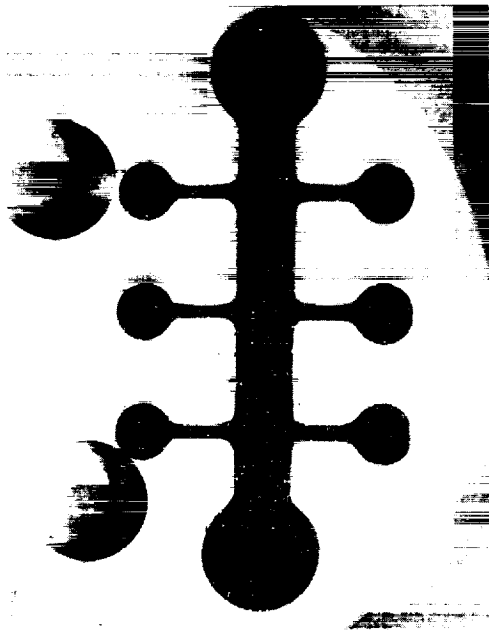


Figure 6-28. Beryllium Film Deposited on Beryllium Oxide Substrate

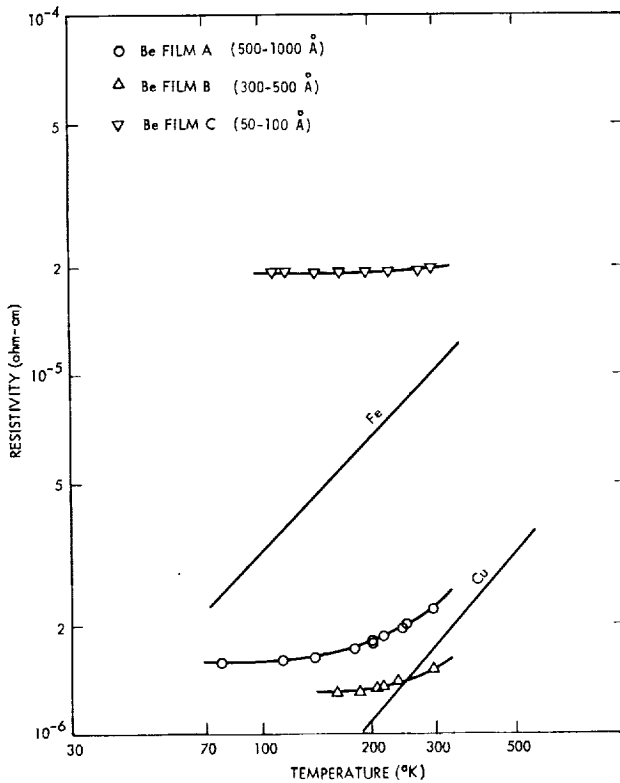


Figure 6-29. Bulk Resistivity Data for Evaporated Beryllium Thin Films

Table 6-10. Characteristics of Beryllium Films on Quartz

Film	Description	—	—
A	Thick Film (500-1000Å)	.45	.06
B	Moderate Thickness Film (300-500A)	.61	.10
C	Very Thin (50-100Å) Slightly Transmitting	.66*	.20*

\*Some quartz effect

Table 6-11. Electrical Properties of Beryllium Films on Quartz

Parameter	Film A	Film B	Film C	Published Bulk Values
Surface Resistance, $R_s$ (ohm/square)	0.245	1.335	76-174	
Thickness, $t$ , (Å)	1130	208	37-16	
Bulk Resistivity, $\rho$ @ 25°C (ohm cm)	$2.2 \times 10^{-6}$	$1.53 \times 10^{-6}$	$19.5 \times 10^{-6}$	$2.78 \times 10^{-6}$
Hall Coefficient, $R_H$ @25°C (cm <sup>3</sup> /coulomb)	$1.32 \times 10^{-4}$	$9.4 \times 10^{-5}$	$9.8 \times 10^{-5}$	$2.4 \times 10^{-4}$
Hall Mobility, $\mu_H$ @25°C (cm <sup>2</sup> /volt-sec)	60.0	61.5	5.0	86.5

Table 6-12. Resistivity of a Beryllium Film on Beryllium Oxide

Temperature °C	Resistivity ohm-cm
-196	$2.4 \times 10^{-6}$
38	$3.0 \times 10^{-6}$
60	$3.0 \times 10^{-6}$
77	$3.1 \times 10^{-6}$
93	$3.13 \times 10^{-6}$
116	$3.28 \times 10^{-6}$

Films with a thickness less than  $L_c$  have a film resistance which is temperature insensitive. The thinner the film, the less the temperature dependence because bulk scattering effects are decreased. For thicker films, some temperature effect is apparent; however, when temperature decreases, the effective bulk carrier mean free path exceeds the film thickness, and surface scattering again dominates the film resistance. This is illustrated in the three film resistance curves of Figure 6-29, in which the relative resistance change as a function of temperature is approximately proportional to the film thickness. Measured resistance values of a beryllium film from  $-196^\circ\text{C}$  to  $116^\circ\text{C}$  are tabulated in Table 6-12.

The application of beryllium thin films to high precision, high stability resistors, and high power resistors for electronic and electrical power applications deserves investigation because the results obtained here are superior to the corresponding characteristics of commercially available thin film resistors. The thin beryllium films tested exhibit a very low temperature coefficient of resistance which is approximately 3 times better than other commercially used thin film resistance materials. Beryllium thin films are especially interesting for precision and power resistor applications because of the protective oxidation resistant property of beryllium at high temperatures and the high recrystallization temperature.

Pure beryllium films prepared by the experimental method described above are not suitable for high efficiency solenoid actuator windings where the low bulk resistivity of high purity beryllium is required. This limitation of resistivity of deposited films is due to the limited thickness of the films which were produced by the vapor deposition methods used. Thin films have higher resistivity than the observed bulk resistivity because surface boundary controlled scattering of charge carriers dominates the conduction process.

### 6.5.3 Solenoid Actuator Evaluation

Design, fabrication, and test of a solenoid actuator assembly was completed utilizing No. 14 A.W. Ground anodized beryllium wire. The detailed procedures and test results are covered in Reference 2.

Two solenoid coils were tested at temperatures up to  $1000^\circ\text{C}$  and currents up to 100 amperes. Both coils failed early during the test program. Failure was attributed to hot spots due to uneven application of the anodize or flaws in the beryllium wire, which were inclusions, cracks, or sectional defects. Since melting and runout from pinholes occurred during furnace insulation tests at temperatures of  $1000^\circ\text{C}$  or less, it was concluded that some of the flaws must be inclusions of lower melting point materials.

The most likely impurities causing this behavior are aluminum and silicone. Beryllium is recovered from the ore beryl, a complex aluminum beryllium silicate with a nominal chemical formula  $3 \text{BeO} \cdot \text{Al}_2\text{O}_3 \cdot 6 \text{SiO}_2$ . Aluminum and silicone appear throughout the processing of beryllium and small amounts as impurities are not ordinarily considered detrimental. The cold solubility of aluminum and silicone in beryllium is very low and they are most likely to appear as interstitial impurities or inclusions. Interstitial aluminum



is ordinarily regarded as a beneficial impurity because it improves low temperature ductility and is sometimes deliberately added for this purpose. The melting point of some of the aluminum silicone beryllium combinations which may be possible in the inclusions are:

Al-Be-Si Eutectic	435°C
Al-Be Eutectic	640°C
Al	660°C
Al-Si Eutectic	577.2°C
Be-Si Eutectic	1090°C
Si	1430°C
Be	1283°C

Pure beryllium, Be-Si and Si will not melt at temperatures up to 1000°C. Beryllium wire with very low aluminum content is obtainable and may greatly alleviate the undesirable effect of inclusions for high temperature electrical winding applications.

A two-foot section from a ninety-foot lot of beryllium wire was nondestructively tested on a Magnaflux eddy current wire tester. The tester indicated one large flaw to induced circumferential current and numerous smaller flaws in the two-foot length tested. The location and magnitude of the flaws could be consistently determined in repeated tests with the Magnaflux tester. This type of tester is promising for the production monitoring of beryllium wire manufactured for electrical and other applications.

Before additional solenoid high temperature testing can be accomplished, improvement in the beryllium wire quality and anodizing process is required. Based on the information and experience obtained from the tests conducted under this program, it is believed that the necessary technology for producing a high quality insulated beryllium wire is within the present state of the art. Specific recommendations are as follows:

1. Develop a high purity beryllium magnet wire in a broad range of wire gauge sizes.
2. Investigate the anodizing process for the purpose of providing a continuous uniform adherent electrical insulation coating for high temperature service, which is capable of withstanding coil winding stresses.
3. Find a high temperature (melting point >1000°C) additive, which will improve the room temperature ductility of beryllium wire.
4. Investigate the use of the Magnaflux eddy current inspection process for qualifying wire. A 5 percent reduction in maximum current due to flaw magnitude or distribution should be reason for rejection.

## 6.6 THERMAL EXPANSION ACTUATOR

A thermal expansion actuator was designed which operated due to the change in volume of an amorphous material upon the application of thermal energy. Subsequent testing showed that this concept, although slower in response than a solenoid actuator, can supply higher force outputs in a smaller size and weight and with a lower peak power input.

### 6.6.1 Conceptual Design

The stroke of a thermal expansion actuator utilizing a sealed chamber filled with either a liquid or an amorphous material can be calculated from the actuator geometry, the material properties and the temperature change.

The following simplified relations hold for a simple thermal expansion actuator as illustrated in Figure 6-30.

$$x - x_o = \left( \frac{V_m - V_{mo}}{A} \right) - \left( \frac{V_c - V_{co}}{A} \right)$$

where:  $x$  = output piston position

$V_m$  = volume of heat sensitive material

$V_c$  = cavity volume

$A$  = piston area

the subscript o refers to the initial state.

The volume change of the heat sensitive material is:

$$V_m - V_{mo} = v_{mo} \xi_m (T_m - T_{mo})$$

where:  $\xi_m$  = volume expansion coefficient of the heat sensitive material

$T_m$  = temperature of the heat sensitive material

the cavity volume change

$$V_c - V_{co} = V_{co} \xi_c (T_c - T_{co})$$

where:  $\xi_c$  = volume expansion coefficient of the cavity

$T_c$  = temperature of the material forming the cavity

The above three equations are combined to give:

$$(x - x_o) = \frac{1}{A} \left\{ \left[ V_{m1} \xi_m (T_m - T_{mo}) \right] - \left[ V_{co} \xi_c (T_c - T_{co}) \right] \right\}$$

In most situations of interest, the value of  $\xi_m$  is much greater than that of  $\xi_c$  and  $(T_c - T_{c0})$  is small compared to  $(T_m - T_{m0})$ . For such cases the second term may be safely ignored and the above equation reduces to:

$$(x - x_0) = \frac{V_{m0}}{A} \xi_m (T_m - T_0)$$

If it is assumed that the heat sensitive material fully fills the cavity with no voids, the above equation may also be stated as:

$$(x - x_0) = \frac{V_{c0}}{A} \xi_m (T_m - T_0)$$

These equations assume that no stresses are induced in the heat sensitive material, e.g., the initial force on the piston is zero and no stresses are induced in extruding the material from the large cavity diameter to the piston bore diameter. This is an exact assumption in the case of a smaller lightly loaded piston (no compressibility) utilizing an expanding liquid as the heat sensitive material. There are, however, some errors in the case of high piston loads using compressible liquids and when semi-solid materials are used as the heat sensitive material.

#### 6.6.2 Prototype Evaluation

A prototype thermal expansion actuator was fabricated in the configuration shown in Figure 6-31. Photographs of the test unit are shown in Figures 6-32 and 6-33. The test actuator consists of five basic parts: the base, the body, the heater, the piston, and the heat sensitive material. In addition, a thermistor was introduced into the actuator cavity to monitor the temperature of the heat sensitive material. The base, body and piston were fabricated of stainless steel, the heater is a 50 ohm 1/4 watt wire wound resistor, and the heat sensitive material is a quantity of General Electric RTV-11 silicone rubber. The rubber is an initially pourable liquid which was cast in place and vacuum degassed to minimize the possibility of gas pockets and voids. The rubber was allowed to cure for two days at room temperature.

Testing of the actuator consisted of applying known loads, energizing the heater to a predetermined power level, and recording the values of stroke  $(x - x_0)$  and temperature as a function of time. The stroke and temperature versus time curves were automatically plotted on a dual channel X-Y recorder to simplify data taking and to provide a continuous record over each run. The test setup used is described in Figure 6-34.

The friction in the loading cylinder was measured and found to be approximately 1.8 pounds or the force generated by 2 psig pressure. The cylinder area was 0.89 in<sup>2</sup>. Voltage and current were measured on standard laboratory meters and recorded manually for each test run. No significant variation occurred over the run. The overall accuracy of the recorded stroke data is estimated as approximately 3 percent. After the first 21 runs the actuator was subjected to 2360 cycles of operation at 10 pounds load and 1.9 watts power input on an automated setup.

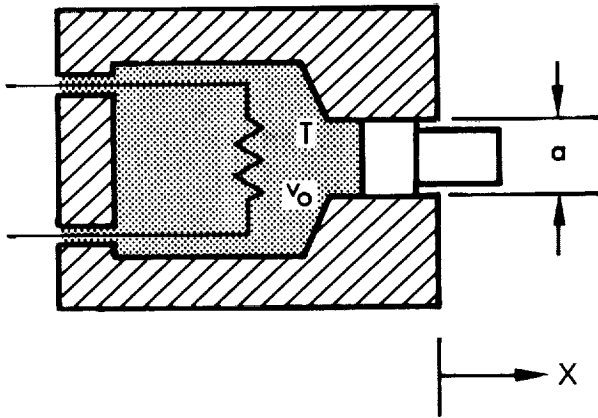


Figure 6-30. Thermal Expansion Actuator Parameters

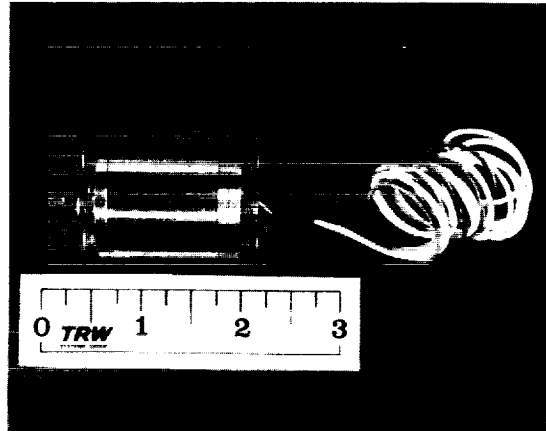


Figure 6-32. Thermal Expansion Actuator Assembly

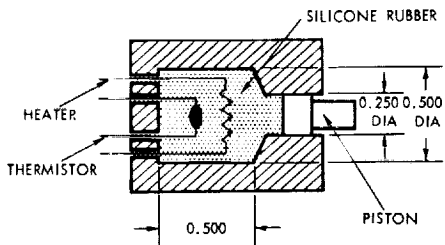


Figure 6-31. Prototype Thermal Expansion Actuator

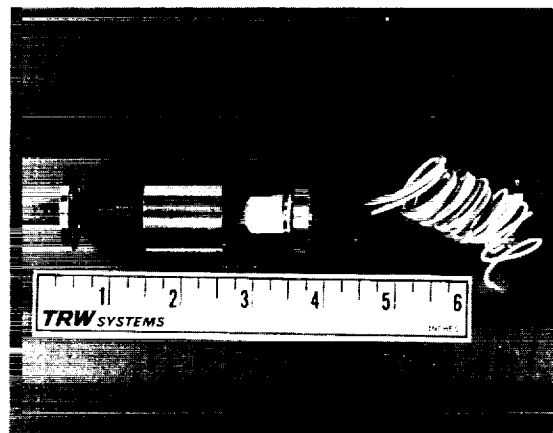


Figure 6-33. Thermal Expansion Actuator Subcomponents

### 6.6.3 Test Results and Conclusions

The test results at various power levels are presented as curves of Stroke vs Time, Temperature vs Time, and Stroke vs Temperature in Figures 6-35 through 6-39. A summary of recorded test runs and strokes after fixed time intervals of 8.3 and 16.6 minutes including load data is included as Table 6-13. Strokes as high as .115 inch were observed at 10 pounds load with approximately 11 watts input power. At 105 pounds load, a stroke of .032 inch was attained with a power input of 2.58 watts.

The thermal expansion actuator has been shown to be an effective device for obtaining high forces and strokes with low peak input power levels. In spacecraft application waste heat may be utilized where it is available to further minimize the power requirements. Care must be taken to use an actuator material which is compatible with the working fluid or to isolate the actuator from the working fluid in propellant valve applications. The thermal actuator should be considered where size, weight, and peak power requirements are more critical than response time.

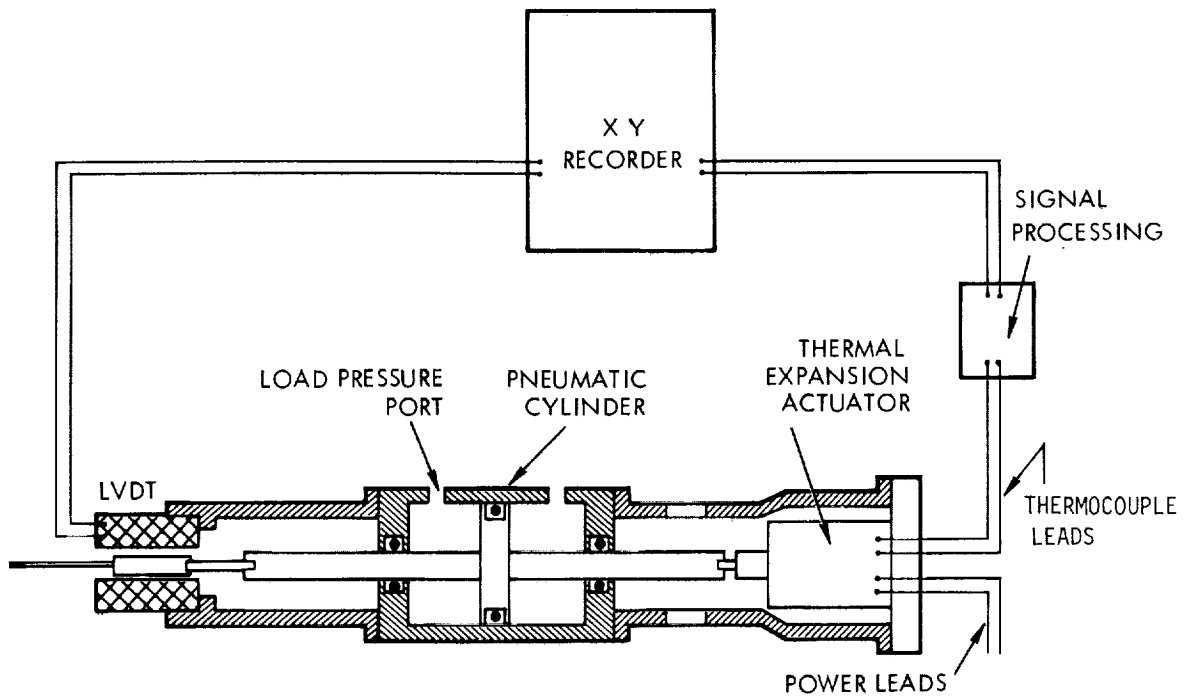


Figure 6-34. Test Setup for Thermal Actuator Evaluation

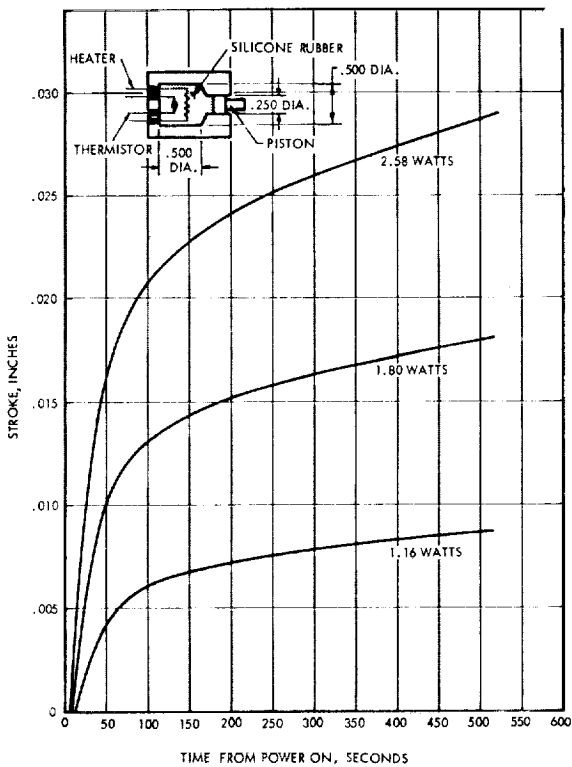


Figure 6-35. Thermal Actuator Stroke Vs. Time for 80 lb Load

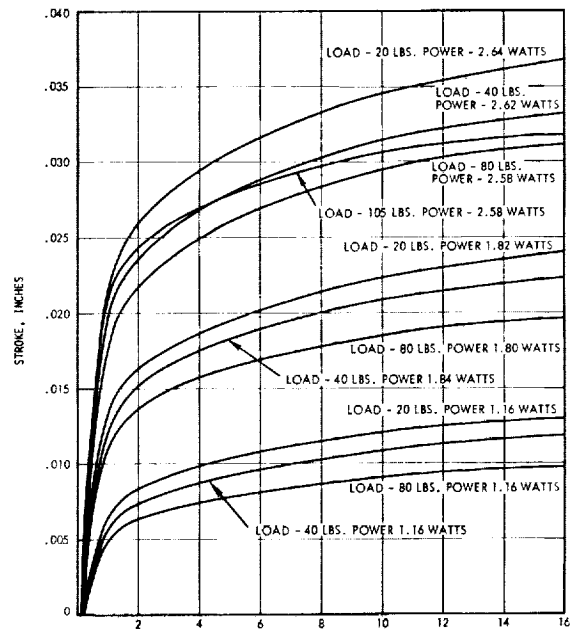


Figure 6-36. Thermal Actuator Stroke Vs. Time for Several Loads

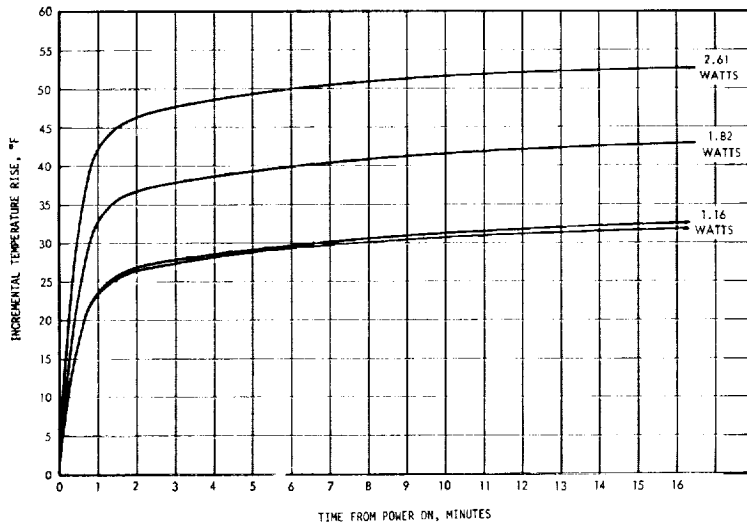


Figure 6-37. Thermal Actuator Temperature Rise Vs. Time

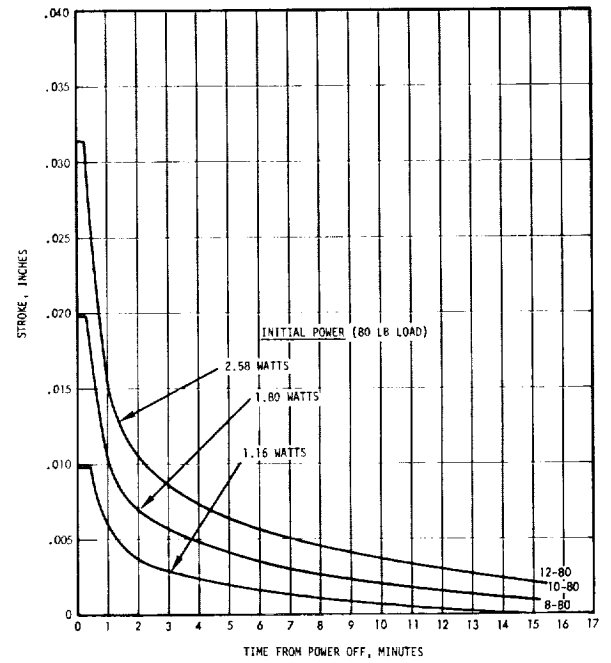


Figure 6-39. Thermal Actuator Stroke Vs. Time from Power Off With 80 lb Load

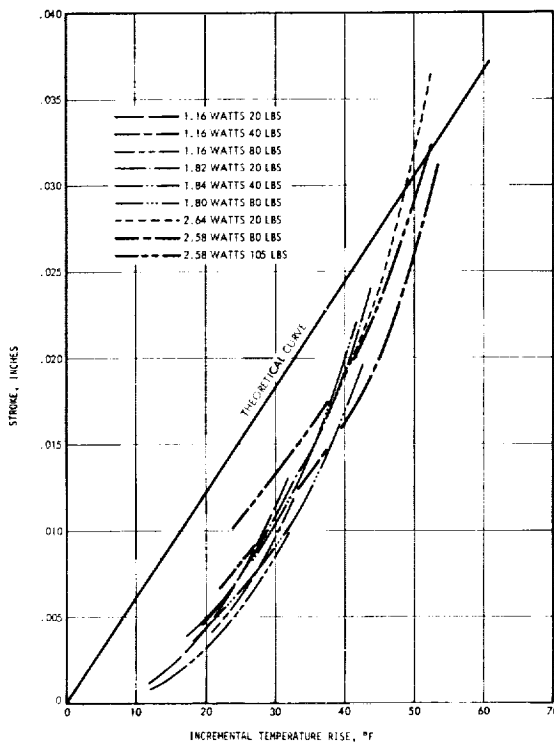


Figure 6-38. Thermal Actuator Stroke Vs. Temperature Rise

Table 6-13. Summary of Thermal Actuator Test Runs

Run No.	Restraining Load (lbs)	Power Input (watts)	Stroke After 8.3 min. (inches)	Stroke After 16.6 min. (inches)
1	<0.5	1.28	.0080	.0106
2	<0.5	1.65	.0130	-
3	5.0	1.30	.0071	.0088
4	5.0	1.67	.0126	.0148
5	5.0	2.02	.0187	.0215
6	5.0	2.37	.0244	.0275
7	5.0	2.70	.0282	.0325
8	10.0	2.70	.0340	.0365
9	10.0	1.85	.0219	.0244
10	10.0	1.16	.0112	.0128
11	20.0	1.16	.0116	.0132
12	20.0	1.82	.0216	.0242
13	20.0	2.64	.0338	.0362
14	40.0	2.62	.0305	.0334
15	40.0	1.84	.0204	.0226
16	40.0	1.16	.0104	.0119
17	80.0	1.16	.0088	.0098
18	80.0	1.80	.0168	.0185
19	80.0	2.58	.0286	.0313
20	105.0	2.58	.0299	.0320
21	10.0	3.36	.0459	.0508
22	10.0	initially 4.4 jumped to 11.2 due to short in heater	.115 after 5.6 min.	-
23	10.0	6.8 - 7.0	.075 after 1.1 min.	-

## 6.7 ELECTROPYROTECHNIC ACTUATOR CARTRIDGE STUDY

The purpose of this study was to investigate the effects of space and sterilization environments on squib cartridges and on the reliability of ceramic seals employed as insulators for the electrical connector pins. Environmental tests included sterilization, radiation, and vacuum exposure. A new electric initiation concept was evaluated. The cartridges studied were of the type used to actuate valves on liquid propellant spacecraft engines.

### 6.7.1 Background

Remote, single-cycle actuation of valves in spacecraft is often accomplished with an electrically initiated pyrotechnic generation cartridge. There are, at present, two main types of electrical initiation elements in use: a low voltage-low current squib type and an exploding bridge-wire (EBW) initiator. Figures 6-40 and 6-41 illustrate the two types of electropyrotechnic cartridges, with block diagrams of the electrical systems necessary for element actuation.

The low-voltage-low current squib type cartridge consists of a fine metal wire suspended between two electrical contact posts. The wire is beaded with a primary, heat-sensitive explosive, or the material is placed in a squib cup adjacent to the wire. The gas generation portion of the cartridge consists of a less sensitive secondary explosive placed next to the primary explosive.

The EBW initiator consists of a wire connected between the two electrical contact posts. The secondary explosive utilized in the gas generation portion of the cartridge is formed directly around the wire. The explosive material used in the EBW configuration may be more sensitive than the secondary material used in the low voltage squib.

Both elements perform the same function: they initiate an explosive by transformation of electrical energy to heat. The method of initiation, however, differs. In the low voltage squib, the fine metal wire is heated electrically and the heat initiates the primary explosive which then releases enough energy to initiate the secondary explosive. The fine wire in the EBW initiator receives a large electrical power pulse, which vaporizes the wire and creates a plasma. The magnetic field generated by the current contains this dense plasma until enough energy is received to break it apart, forming a shock wave of hot metal particles which directly initiates the explosive.

The energy necessary for valve actuation can normally be met by small amounts of explosive materials, therefore, both types of electropyrotechnic cartridges are relatively small and are interchangeable at the point of initiation. The complete ordnance system, however, and the advantages and disadvantages of the two systems are so different that a careful appraisal is necessary to determine if one system is superior to the other for the particular mission requirements.



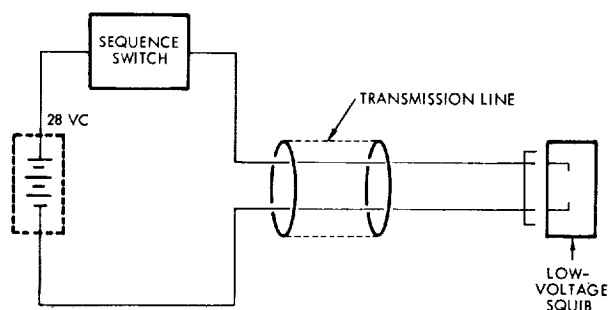
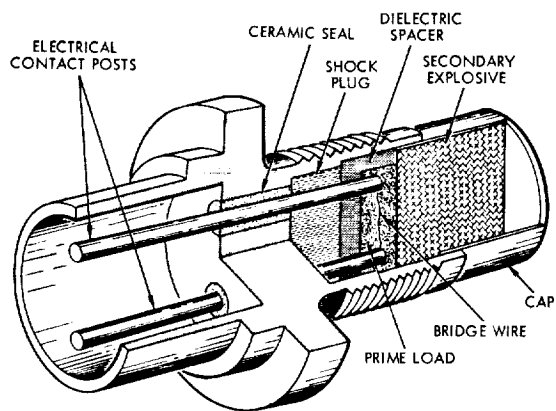


Figure 6-40. Low Voltage Electropyrotechnic Cartridge and Associated Firing Circuit

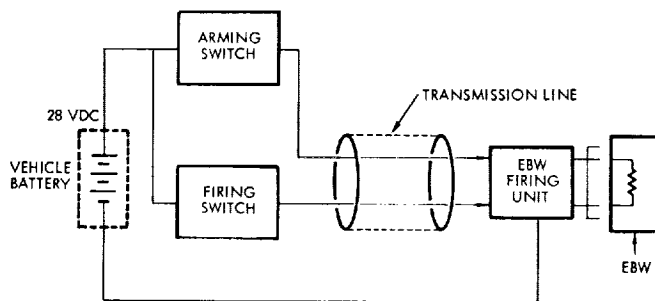
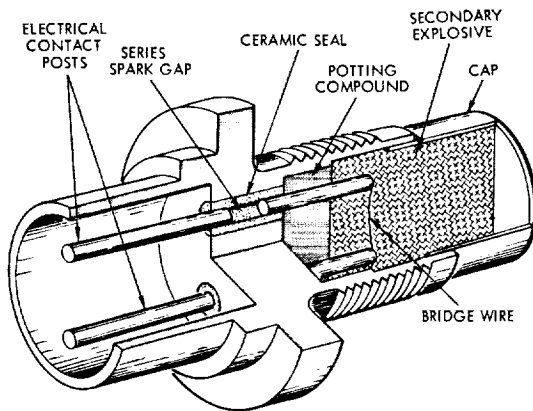


Figure 6-41. Exploding Bridgewire (EBW) Pyrotechnic Cartridge and Associated Firing Circuit

Table 6-14 presents a summary of the advantages and disadvantages of the two electropyrotechnic systems. The most serious disadvantages common to both systems (from an overall systems standpoint) are:

1. Sensitivity to electromagnetic radiation in the radar frequency range

An electrical current is induced in long lengths of wire due to coupling of the wire with an electromagnetic radiation source (the "antenna effect"). If the induced current is large enough, the device will either prematurely fire, or the heat will degrade the primary explosive to the point of incipient malfunction. This is particularly true of low voltage squibs. Range requirements (device survivability in fields of 2 watts/meter<sup>2</sup> from 150 kilocycles to 50 megacycles, 100 watts/m<sup>2</sup> from 50 megacycles and above) may dictate the necessity of safe/arm switches, shorting devices, and/or RF shielding for low voltage squibs to meet these safety requirements. These requirements increase system complexity.

The EBW system is inherently less sensitive to electromagnetic radiation, but it is still sensitive to radiation spikes which could trigger the firing circuit. An attenuator is usually built into the system as an added safety factor.

2. Sensitivity to electromagnetic radiation in the solar (X-ray and gamma ray) range

Some explosives are radiation sensitive, due to radiation induced decomposition of the material. Since an EBW firing circuit is capacitance-discharged, the firing circuitry is also sensitive to radiation, and at a far lower intensity than that necessary to cause explosive degradation. Thus, if the EBW system will be exposed to radiation (such as that from an intense solar storm), the firing circuitry must be shielded from this energy source.

3. Low thermal tolerance to repeated heat soaks

For certain space mission requirements, such as planetary landings, the electropyrotechnic must survive a sterilization cycle (e.g., 300°F for 60 hours, 6 cycles).

4. Reliability of ceramic insulation seal - incipient failures

Failures have been reported in ceramic-to-metal seals due to cracking. This allows propellant gases to escape. These gases may affect the sensitivity of instruments or optical devices used in spacecraft, and in certain applications may result in a leakage path for a primary fluid. The existence of this leakage problem has been confirmed as a result of tests conducted on this program.

5. Reliability of complex initiation components

As the number of components in a given system increases, the overall system reliability decreases for single given component reliability. In view of the high reliability required of systems on board spacecraft, this entails testing of large numbers of systems. The cost of an EBW system or a low voltage squib with a shorting mechanism is high, and the cost of qualifying these devices is a significant factor in overall system cost.

6. Weight penalty on either safe/arm or firing system components

The electropyrrotechnic cartridge itself is lightweight, weighing at most a few ounces. The components which may be necessary to prevent the squib cartridge from premature initiation (the safe/arm or shorting device) could weigh several pounds. Redundant EBW firing systems exhibit potential weight penalties for high performance space missions, particularly where a number of separate devices are required.

These disadvantages have been noted on various ballistic missile programs where system destruct and stage disconnect as well as actuation requirements have been necessary.

Table 6-14. Relative Advantages and Disadvantages of Exploding Bridgewire and Low Voltage Elements

Device	Approximate Actuation Voltage and Current	Advantages	Disadvantages
Low Voltage Squib Element	Requires 6 to 28V and 1 to 5 A depending on desired initiation parameters	<ol style="list-style-type: none"> <li>1) Can utilize vehicle power directly.</li> <li>2) System can be checked in de-energized condition for continuity before usage.</li> </ol>	<ol style="list-style-type: none"> <li>1) Squibs sensitive to electromagnetic radiation in the radio frequency to radar range.</li> <li>2) System may require an electromechanical shorting device to suppress accidental activation.</li> <li>3) Some ignition elements are relatively sensitive to shock.</li> <li>4) Some secondary explosive may be sensitive to sterilization temperature cycling.</li> <li>5) Initiation wire is difficult to quality during assembly</li> </ol>
Exploding Bridgewire (EBW element)	Requires 1 to 2000V and 1 to 2000 A depending on desired initiation parameters.	<ol style="list-style-type: none"> <li>1) Fast response time (order of 10 microseconds).</li> <li>2) Relatively insensitive to changes in temperature, shock, and electromagnetic hazards.</li> </ol>	<ol style="list-style-type: none"> <li>1) Large number of components in firing system, with commensurate decrease in reliability.</li> <li>2) System weight penalty.</li> <li>3) Firing circuit may be discharged by X-ray or gamma ray radiation.</li> <li>4) Cannot be tested before installation.</li> <li>5) Capacitance type firing system cannot be immediately de-energized if a launch abort occurs; therefore, it is possible to launch a malfunctioning system by shutdown transients. (Normally applies to destruct systems)</li> <li>6) Cannot use vehicle power directly.</li> </ol>

## 6.7.2 Electropyrotechnic Cartridge Environmental Tests

The purpose of these tests was to determine the effects of space and sterilization environments on squib cartridges and the reliability of the ceramic seals employed as insulators for the electrical connector pins. The environmental tests included simulated space radiation and vacuum exposures, sterilization temperature cycling, and ethylene oxide exposure. The results obtained are intended to establish probable problem areas which reflect the state of the art.

6.7.2.1 General Description - Forty-four low voltage squib type cartridges were purchased from Horex Corporation for these tests. No EBW initiated cartridges were tested. The cartridges were tested in four groups, each group receiving a different test schedule. Of the forty-four squibs, twenty-nine (Group I, II, III) were charged with 188 milligrams of Hercules Hi-Temp (Horex No. 72) propellant purchased from the Horex Corporation per Horex Part No. 3511-1 (TRW Drawing No. C1011530). The remaining 15 cartridges (Group IV) were charged with 188 milligrams of Horex No. 74 load, Horex Part No. 4360-1. This propellant is comprised of boron potassium nitrate. Both types of cartridges contain the TRW Universal Ignition Element. The loads described are of the gas generation or deflagration type; however, the boron potassium used in the 4360-1 cartridge should have a much lower impetus than the Hercules Hi-Temp used in 3511-1.

All cartridges were serialized for identification within their respective groups. A description of each test is as follows:

1. Resistance Check - The cartridges necessary for this test were checked with an Alinco Ohmmeter and their resistances recorded.
2. One Watt Test - This test included subjecting the cartridges to a direct current for five minutes of a level such that one watt of power was dissipated in the bridgewire element.
3. Weight Check - Several cartridges were checked for weight loss or gain after exposure to sterilization, radiation, and vacuum environments. The cartridges were weighed using an enclosed pulp type balance, 200-gram capacity and 1-milligram sensitivity.
4. Sterilization Test - This test consisted of a thermal cycling test followed by 12 percent ethylene oxide, 88 percent Freon exposure for eight hours.

The thermal cycling tests included a 24-hour 300°F soak for the 3511-1 type cartridge and a 36-hour 300°F soak for the 4360-1 type cartridge. After the 300°F temperature soak, the cartridges were then cooled to ambient conditions and repeated a maximum of 6 times.

5. Radiation Exposure - X-rays were the radiation environment chosen. This approach was taken because the geometry of the cartridges and their typical location in space vehicles renders them relatively well shielded against primary charged particle radiation but subject to the penetrating Bremsstrahlung X-rays. To simulate this environment the TRW 1 Mev electron Van de Graaff accelerator was used. A tungsten target was utilized to convert the primary electron beam to Bremsstrahlung X-rays. The energy is typical of the forward scattered Bremsstrahlung spectrum produced by 1.1 Mev electrons. The radiation intensity was measured with a Nuclear Chicago "cutie-pie" radiation monitor Model 2586 with a Model P-18 high-range ionization chamber. The accuracy of this instrument is + 10 percent of full scale. The response of the chamber as a function of X-ray energy is linear to within + 10 percent over the energy range of 50 kev to 2 Mev. The accuracy of the dosimetry for this experiment can therefore be expected to be within + 10 percent with a maximum uncertainty of + 20 percent. The intensity used in the performance of the cartridge irradiations varied considerably, depending upon the operating characteristics of the electron accelerator at the time of the test to a maximum intensity of  $10^5$  roentgens/hr (r/hr).

The cartridges were irradiated to an exposure of  $10^6$ r. Due to the large amount of energy dissipation in the target and the relative closeness of the target to the exposed cartridge, provisions for cooling the cartridges during the irradiation were necessitated. During some initial runs cooling was provided by packing the accelerator drift tube and target assembly with dry ice. This produced a relatively large fluctuation in monitored cartridge temperature.

A water-cooled cartridge holder assembly was constructed to minimize cartridge temperature excursions. The remaining cartridges were irradiated after completion of the water-cooled cartridge holder. Table 6-15 shows the maximum temperature excursions received by each cartridge. The cartridges noted, exposed to consistent temperatures between 58°F to 74°F were irradiated utilizing the water cooling technique.

6. High Vacuum Environmental Test - This test consisted of a vacuum thermal cycle of the squibs followed by vacuum firings. The thermal cycle test for each squib type is as follows:

Type 4360-1	+300°F to -300°F	3 cycles
Type 3511-1	+200°F to -300°F	3 cycles

After the vacuum thermal cycle exposure a number of squib cartridges of each type were returned to the vacuum chamber and fired at a given temperature extreme.

Table 6-15. Electropyrotechnic Cartridge Group I Test Results

Cartridge Serial No. Note 1	Resistance (Ohms)	1 Watt 5 Minutes	Resistance (Ohms)	300°F 24-Hr Cycle 6 Cycles	Resistance (Ohms)	Zero Volume Chamber Firing Cartridge Pres. (psi)	Disposition
576	.94	X	.95	X	.96	2000	Fired
577	.91	X	.94	X	Fired		Fired
579	.97	X	.98	X	.98	2500	Fired
582	.92	X	.94	X	.94		Disassembled & Inspected
586	.97	X	1.00	X	Fired		Fired
587	.94	X	.96	X	.96	2500	Fired
588	.93	X	.96	X	.96	2000	Fired
590	.97	X	.97	X	.99		Disassembled & Inspected

Note 1: Manufactured by Horex, Inc., Hollister, Calif.

The chamber volume is 20 cubic feet and has a pressure capability in the low  $10^{-10}$  torr region. The pumping system consists of two oil diffusion pumps in series backed by a mechanical roughing pump. These pumps are supplemented by cryogenic traps and cryogenically cooled surfaces in the working volume. Elevated temperature cycling and exposure were achieved by heating the copper support fixture with a hermetically sealed calrod heater. Temperature measurements and temperature control were obtained by two thermocouples mechanically attached to selected squibs. Because of the high conductivity of the copper support fixture, the two measurements are believed representative of the average temperature for all squibs to within  $5^{\circ}\text{F}$ . One of the two thermocouples was used for automatic control purposes, the other for a millivolt temperature indicator. The cold temperature cycle was achieved by the use of liquid nitrogen as a coolant.

Pressure measurements were made with a Nottingham-type hot-filament ionization gauge with the entrance approximately 12 inches from the test item. Previous tests of this gauge by inter-comparison with fully nude and partially nude gauges mounted in the test volume have shown no significant discrepancy between the two types of gauges and, therefore, the measured pressures are believed representative of the vacuum conditions at the test items.

7. Pressure Firing - All cartridges were fired in a fixed-volume bomb cavity initiated by a square wave pulse of 20 milliseconds and 5 amperes. The information recorded from this test was the bridgewire burnout and peak pressure, versus time.
8. Leak Test - All cartridges were subjected to a leak test using a helium mass spectrometer to determine the integrity of the ceramic seals. Helium pressure was applied to the squib on the igniter side of the ceramic-to-metal seals. Two series of leak tests were performed; a low-pressure (50 psig) and a high-pressure (2,000 psig) helium leak test.

6.7.2.2 Group I Cartridge Test - Eight cartridges were exposed to a sterilization test, which involved a thermal cycle (ambient to  $300^{\circ}\text{F}$  for 24 hours, six times) exposure. Two cartridges inadvertently fired during the test and the remaining six were no longer hermetically sealed, the seals having been widened by melted and resolidified solder used on the cans. Four of these six cartridges were fired in a test block and pressures to 2500 psi were recorded, indicating severe degradation of the cartridge (see Table 6-15).

## Test Procedures and Results

1. One Watt Test - Eight Halex cartridges (TRW P/N 101530) were checked with an Alinco ohmmeter and their resistances recorded in Table 6-15 of this report. The cartridges were then subjected to a direct current for five minutes. The current was of a level such that one watt of power was dissipated in the resistance element (bridgewire) of each cartridge. All cartridges qualified.
2. Sterilization Test - Eight of the cartridges exposed to one watt for five minutes in One Watt Test above were assembled in a test and holding fixture and placed in a temperature chamber. The cartridges were exposed to six cycles of temperature as follows:

Raised to 300°F and held for 24 hours  
Cooled to ambient temperature

After this exposure the cartridges were examined. Cartridges S/N 577 and S/N 586 inadvertently fired during the six 24-hour 300-degree temperature cycles. Cartridges S/N 582 and S/N 590 (Figure 6-42) were disassembled after the temperature soak and the base charge was found to be replaced by a brownish crust on the inside of the cartridge cans. The mylar disc over the prime mix was blackened. Except for cartridges S/N 577 and S/N 586 which inadvertently fired, all cartridges had swollen cases and some of the solder on the cans was found to have melted and resolidified as beads along the edge of the cartridge cans (see Figure 6-42). The ethylene oxide exposure test was therefore suspended.

After examination of temperature recordings from the Sterilization Test described above, a rerun using the test block instrumented with three thermocouples was made. One thermocouple was in the block, one thermocouple was on the base of a cartridge can and one thermocouple was exposed to air in the temperature chamber. The heater voltages and recorded temperatures of Run 4 were duplicated. The temperature during Run 4 was recorded at 1-hour intervals. During this rerun, temperature was recorded every two minutes and a maximum overshoot temperature of 325°F was recorded on the cartridge can and 322°F on the test block. At the equivalent time that the next temperature recording had been made in Run 4, the thermocouple reading on the block was down to 300°F.

3. Pressure Firing - Four of the cartridges (S/N's 576, 579, 587 and 588) were fired in a test block with a high pressure transducer (0-70,000 psi) and pressure peaks of 2000 psi to 2500 psi were recorded (see Table 6-15).



4. Leak Test - Six cartridges (S/N's 576, 577, 579, 586, 587 and 588) gave no indication of a definitive leak larger than the background of the leak detector which ranged from less than  $2 \times 10^{-10}$  to  $2.4 \times 10^{-9}$  standard cc/sec helium (see Table 6-26). One squib (S/N 579) did give an indication of a time dependent or permeation type leak under the low (50 psi) pressure test. However, the same squib gave no such indication in the high pressure test. With the exception of one of the low pressure test of this squib, at no time did any of the six squibs indicate a leak rate greater than  $1 \times 10^{-8}$  standard cc/sec. All six cartridges tested in Group I were degraded during the thermal cycle such that the peak pressures developed on firing did not exceed 2500 psi. The normal peak pressures developed for these squibs are much higher.

6.7.2.3 Group II Cartridge Tests - Seven cartridges (S/N's 580, 581, 583, 584, 585, 591 and 592) were subjected to tests as outlined in Table 6-16. Data sheets are given in Table 6-17. The results of these tests are summarized as follows:

1. Two cartridges (S/N's 580 and 581) were exposed to six cycles of 300°F for 24 hours each cycle, exposed to ethylene oxide vapor for 8 hours, then fired. The pressure generated on firing was measured and found to be equivalent to the pressure generated by a cartridge with a prime mix and no main load (3000 psi). During the six 24-hour soak cycles, the cartridge weights decreased by 155 and 163 milligrams, respectively.
2. Two cartridges (S/N's 583 and 584) were installed in test blocks and fired. The pressure recorded (53,000 psi) was much greater than that recorded for the cartridges exposed to long-term heat soaking.
3. Two cartridges (S/N's 585 and 591) were modified by replacement of the main load with 35 milligrams of powdered pentaerythrite tetranitrate (PETN). The cartridges were fired in a block with a minimum clearance cavity and the pressures recorded (15,000 and 20,000 psi) being about half that measured on unmodified cartridges. Initial pressure spikes of 20,000 and 28,000 psi were recorded and may have been detonation shock effects.
4. One cartridge (S/N 592) was modified by removal of the load can, main charge, and mylar cover of the prime mix. A thermocouple was installed in contact with the prime mix. The cartridge was placed in an insulated box and one watt of DC power was dissipated through the bridgewire for fifteen minutes. The thermocouple indicated a maximum temperature of 256°F. The cartridges did not fire.

CART. NO. 582



Figure 6-42. Electropyrotechnic Cartridge S/N 582  
After Six 300°F 24-Hr Temperature  
Cycle Sterilization Test

Table 6-16. Flow Chart - Electropyrotechnic  
Cartridge Group II Test

Cartridge Serial No. Note 1	Resistance (Ohms)	1 Watt 5 Min.	Resistance (Ohms)	300°F 24-Hr.Cycle 6 Cycles	Ethylene Oxide 8 Hours	Changes Made to Cartridge
580	.94	Yes	.95	Yes	Yes	None
581	.94	Yes	.95	Yes	Yes	None
583	.94	Yes	.96	No	No	None
584	.95	Yes	.96	No	No	None
585	.93	Yes	.94	No	No	Removed Horex #72 Load; replaced with 35 mg PETN
591	.94	No	No	No	No	Removed Horex #72 Load; replaced with 35 mg PETN
592	.92	No	No	No	No	Load can removed and thermocouple placed on primer

Note 1: Manufactured by Horex, Inc., Hollister, California.

Table 6-17. Data Sheet - 3511-1 Electropyrotechnic Cartridge Group II Test Results

TEST 1: THERMAL CYCLES AND ETHYLENE OXIDE LOCK

	<u>Temperature</u>	<u>Cartridge S/N 580</u>		<u>Cartridge S/N 581</u>	
		<u>Weight (Grams)</u>	<u>Resistance (Ohms)</u>	<u>Weight (Grams)</u>	<u>Resistance (Ohms)</u>
		9.333	.95	9.269	.95
(Thermocouple attached to cartridge can)					
1st 24-hr cycle	299-300°F	9.295	.95	9.230	.95
2nd 24-hr cycle	298-301°F	9.182	.95	9.126	.96
3rd 24-hr cycle	297-302°F	9.175	.95	9.118	.95
4th 24-hr cycle	296-302°F	9.171	.95	9.114	.95
5th 24-hr cycle	294-300°F	9.170	.95	9.114	.95
6th 24-hr cycle	297-302°F	9.170	.95	9.114	.95
8-hr ethylene oxide exposure		9.172	.95	9.116	.95
Firing current		5 amperes		5 amperes	
Bridgewire burnout		9 milliseconds		10 milliseconds	
Pressure		3000 psi		3000 psi with 5500 psi initial spike	

TEST 2: PRESSURE FIRING OF UNCONDITIONED CARTRIDGES

	<u>Cartridge S/N 583</u>	<u>Cartridge S/N 584</u>
Exposed to 1 watt for 5 minutes	Yes	Yes
Firing current	5 amperes	5 amperes
Bridgewire burnout	9 milliseconds	9 milliseconds
Pressure	63,000 psi spike at 12 milliseconds then zero as cartridge separates	63,000 psi at 15 milliseconds, decreased to 40,000 psi by 80 milliseconds

TEST 3: PRESSURE FIRING OF PETN LOADED CARTRIDGES

	<u>Cartridge S/N 585</u>	<u>Cartridge S/N 591</u>
Firing current	5 amperes	5 amperes
Bridgewire burnout	9 milliseconds	12 milliseconds
Pressure	28,000 psi at 12 ms	20,000 psi spike at 15 ms
	20,000 psi sustained pressure	15,000 psi sustained pressure

TEST 4: ONE WATT EXPOSURE

	<u>Resistance</u>	<u>Cartridge S/N 592</u>
	.95 ohms	
Thermocouple attached to prime mix		
<u>Time From Start of One Watt Application</u>		<u>Temperature at Prime Mix</u>
0		73°F
2 seconds		97°F
10 "		146°F
18 "		166°F
26 "		177.5°F
34 "		186°F
42 "		192°F
50 "		200°F
1 minute		205°F
2 "		220°F
3 "		227°F
4 "		234°F
5 "		237°F
6 "		241°F
7 "		244°F
8 "		247°F
9 "		248°F
10 "		250°F
11 "		252°F
12 "		253°F
13 "		254°F
14 "		255°F
15 "		256°F

The cartridge was enclosed in a box which was lined with about two inches of styrofoam during this test.

5. All cartridges were leak tested using a helium mass spectrometer to determine the integrity of the ceramic seals. The results of the leak test are given in Table 6-26. All cartridges were leak checked in the as-fired condition; however, cartridges S/N 584 and 591 were leak checked again after the epoxy plug had been removed.

Cartridges S/N 583 and 584 showed gross leakage. These two squibs developed pressures of 63,000 and 53,000 psi on firing. Cartridges S/N 585 and 591 were loaded with a detonating type propellant PETN and peak firing pressures recorded were 20,000 and 15,000 psi, respectively. Of the two, only S/N 591 showed slight leakage in the range  $10^{-7}$  scc/sec helium.

Examination of Ceramic Insulators - Cartridges S/N's 583, 584, 585 and 591 were sectioned through the ceramic insulator surrounding the electrical contact pins. The sectioned parts are shown in Figures 6-43 through 6-46. The sectioned samples were examined to determine the effects of the firing loads on the ceramic material.

The four samples shown were carefully hand cut to expose the ceramic inserts and mounted with a room temperature potting compound to allow metallurgical polishing and microscopic examination.

6.7.2.4 Group III Cartridge Tests - Sixteen cartridges (Holex No. 3511-1) were tested according to the schedule shown in Table 6-18. Five cartridges were exposed to the radiation tests and their weight recorded before and after exposure. Ten cartridges underwent a thermal cycling test in a high vacuum environment, four of which were returned to the vacuum chamber for firing.

Table 6-20 shows the maximum temperature excursion received by each cartridge during radiation exposure.

Tables 6-21 and 6-22 presents a description of the vacuum thermal cycle test and the vacuum firing tests. Table 6-18 includes the results of the firing tests. The results of the helium leak test of all cartridges are shown in Table 6-26.

The cartridges seemed unaffected by the simulated space radiation and vacuum exposure. These X-ray radiation exposure test results may not be typical, and conclusions based on the test results given here apply only to the propellants and cartridges tested.

6.7.2.5 Group IV Cartridge Tests - Sixteen cartridges (Holex No. 4360-1) were tested according to the schedule shown in Table 6-19. The 4360-1 squib contains 188 milligrams of boron potassium nitrate (Holex No. 74 load) and is expected to withstand temperature in excess of 300°F for indefinite periods of time. The Group IV cartridges underwent sterilization, radiation and high vacuum testing.

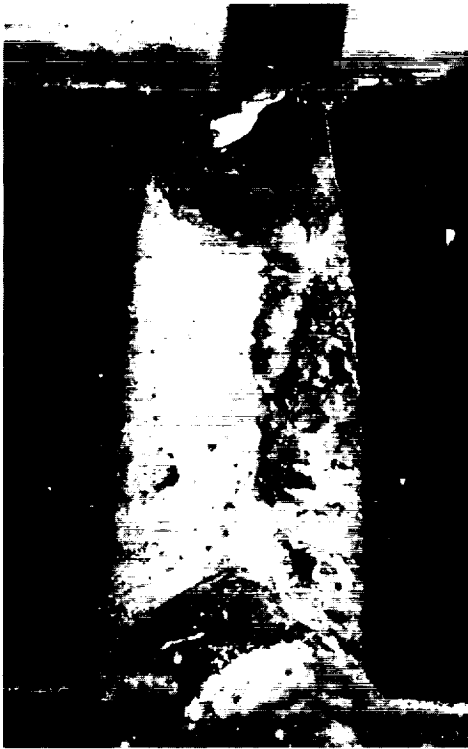


Figure 6-43. Photomicrograph of Electropyrotechnic Cartridge S/N 583 Showing Ceramic Insert After Firing. Deflagration pressures reached 63,000 psi.



Figure 6-44. Photomicrograph of Electropyrotechnic Cartridge S/N 584 Showing Ceramic Insert After Firing. Deflagration pressures reached 53,000 psi.

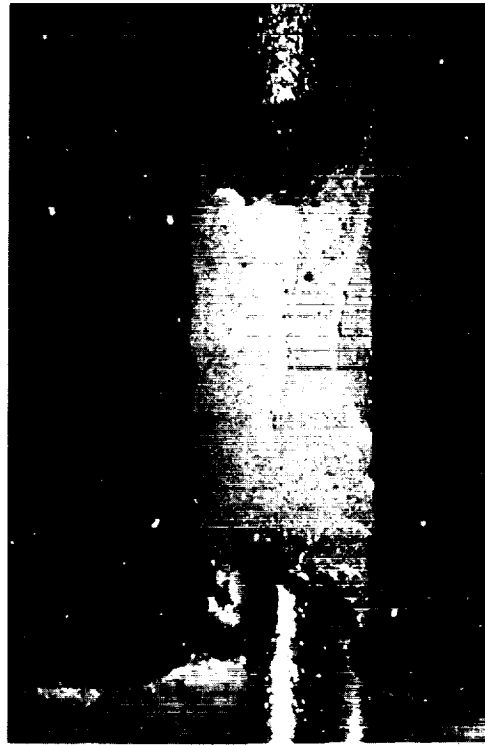


Figure 6-45. Photomicrograph of Electropyrotechnic Cartridge S/N 585 Showing Ceramic Insert After Firing. Detonation pressure reached 28,000 psi.



Figure 6-46. Photomicrograph of Electropyrotechnic Cartridge S/N 591 Showing Ceramic Insert After Firing. Detonation pressure reached 20,000 psi.

Table 6-18. 3511-1 Electropyrotechnic Cartridge Group II Test

S/N	Resist. (Ohms)	Watt. 5 Min.	Resist. (Ohms)	Weight (grams)	Resist. (Ohms)	Weight (grams)	Resist. (Ohms)	Weight (grams)	Watt. 5 Min.	Max. Pressure (psi)	Max. Pressure Time Delay (milli-sec)	High Vacuum Pk. (psi)	Max. Pressure Time Delay (milli-sec)
1	.93	X	.94	8,958	X	.94	8,957	8,957	X	+203°F	33,000	+203°F	11
2	.92	X	.94	8,920	X	.95	8,919	8,919	X	-296°F	34,000	-296°F	15
3	.92	X	.92	8,923	X	.94	8,922	8,922	X				
5	.93	X	.93	8,908	X	.93	8,903	8,906	X				
6	.94	X	.95	8,914	X	.93	8,917	8,917	X				
7	.93	X	.94	8,875	X	.94	8,874	8,939	X				
8	.95	X	.96	8,939	X	.96	8,939	8,939	X				
9	.97	X	.98	8,880	X	.96	8,879	8,879	X				
10	.94	X	.95	8,945	X	.95	8,945	8,945	X				
12	.95	X	.96	8,959	X	.95	8,957	8,957	X				
13	.97	X	.98	8,889	X	.96	8,888	8,888	X	No Data			
14	.96	X	.97	8,946	X	.96	8,946	8,946	X				
15	.98	X	.98	8,970	X	.96	8,970	8,970	X				
16													

Notes: 1. Bomb pressure tester working volume = 1.2 cc  
 2. Time from current initiation (switch closed) to max. pressure

Table 6-19. 4360-1 Electropyrotechnic Cartridge Group IV Test

S/N	Resist. (Ohms)	Watt. 5 Min.	Resist. (Ohms)	Watt. 5 Min.	Resist. (Ohms)	Watt. 5 Min.	Resist. (Ohms)	Watt. 5 Min.	Resist. (Ohms)	Watt. 5 Min.	Low Vacuum		High Vacuum	
											Port. Press. (psi)	Time Delay (milli-sec)	Port. Press. (psi)	Time Delay (milli-sec)
1	.95	X	.95	X	.95	X	.95	X	.95	X	-302	5000**	+300	5000**
2	.94	X	.94	X	.94	X	.94	X	.94	X				
3	.99	X	.99	X	.99	X	.99	X	.99	X				
4	.95	X	.96	X	.96	X	.96	X	.96	X				
6	.97	X	.98	X	.98	X	.98	X	.98	X				
7	.95	X	.95	X	.95	X	.95	X	.95	X				
8	.97	X	.97	X	.97	X	.97	X	.97	X				
9	.97	X	.98	X	.98	X	.98	X	.98	X				
10	.96	X	.94	X	.94	X	.94	X	.94	X				
11	.98	X	.96	X	.96	X	.96	X	.96	X				
12	.96	X	.96	X	.96	X	.96	X	.96	X				
13	.97	X	.96	X	.96	X	.96	X	.96	X				
14	.96	X	.96	X	.96	X	.96	X	.96	X				
15														
16														

\* Bomb pressure tester working volume = 0.9 cc  
 \*\* Volume increased from .9 cc to 1.2 cc

Table 6-21. 3511-1 Group III Thermal Cycle Vacuum Soak Test Description, S/N 1,2,3,5,6,8,9,10,12 & 13

Table 6-20. Temperature Extremes During Radiation Exposure  $10^5$  r/hr.

4360-1 Cartridge

<u>S/N No.</u>	<u>Temperature °F</u>
1	58 to 61
2	58 to 60
3	58 to 61
6	57 to 74
7	59 to 60
8	58 to 62
10	-10 to 102
11	-8 to 95
13	32 to 101

3511-1 Cartridge

1	14 to 94
2	-3 to 97
3	2 to 97
5	10 to 85
7	-5 to 85

1. Soaked at ambient temperature for 48 hrs. in  $10^{-8}$  torr vacuum.
2. Temperature raised to 200°F 1 hr., low  $10^{-8}$  torr vacuum held at 200°F for 17 hrs. low  $10^{-9}$  scale.
3. Temperature lowered to -146°F in 8 hrs.
4. Temperature raised to 200°F in 1 hr., middle  $10^{-8}$  torr vacuum held at 200°F for 15-1/2 hrs. low  $10^{-8}$  - high  $10^{-9}$  torr.
5. Temperature lowered to -140°F in 8 hrs. low  $10^{-9}$  torr.
6. Temperature raised to +200°F 1 hr., low  $10^{-8}$  torr held at 200°F for 15-1/2 hrs. high  $10^{-9}$  scale.
7. Temperature lowered to -131°F 7 hrs., low  $10^{-9}$  scale.

Total vacuum exposure 117 hours.

Total vacuum exposure at reduced temperature - 23 hours.

Total vacuum exposure at elevated temperature 200°F - 51 hours.

Table 6-22. 3511-1 Group III Vacuum Firing Test Description

- |       |  |
|-------|--|
| S/N-1 | <ol style="list-style-type: none"> <li>1. Soaked 3-1/2 hours at ambient temperature in vacuum</li> <li>2. Temperature raised to 140°F, held for 13 hours</li> <li>3. Temperature raised to 200°F, held for 25 hours</li> <li>4. Fired in <math>4 \times 10^{-9}</math> torr vacuum</li> <li>5. Total vacuum exposure 28-1/2 hours</li> </ol> |
| S/N-2 | <ol style="list-style-type: none"> <li>1. Soaked 16 hours ambient temperature in vacuum</li> <li>2. Temperature lowered to -296°F in 7 hours</li> <li>3. Squib fired in <math>1.3 \times 10^{-8}</math> torr vacuum</li> <li>4. Total vacuum exposure 23 hours</li> </ol>  |
| S/N-8 | <ol style="list-style-type: none"> <li>1. Soaked 2 hours at ambient temperature in vacuum</li> <li>2. Temperature raised to 200°F, held 90 hours</li> <li>3. Fired in <math>4 \times 10^{-9}</math> torr vacuum</li> <li>4. Squib pin lost</li> <li>5. Total vacuum exposure 92 hours</li> </ol>   |
| S/N-9 | <ol style="list-style-type: none"> <li>1. Soaked 1 hour at ambient temperature in vacuum</li> <li>2. Temperature lowered to -294°F in 6 hours</li> <li>3. Squib fired in <math>3.5 \times 10^{-8}</math> torr vacuum</li> <li>4. Total vacuum exposure 7 hours</li> </ol>  |

Table 6-20 shows the maximum temperature excursion of each cartridge during radiation exposure.

Table 6-23 is a tabulation of the weight and resistance measurements before and after sterilization-thermal cycle tests.

Tables 6-24 and 6-25 present a description of the vacuum thermal cycle test and the vacuum firing tests. Table 6-19 includes the results of the firing tests. The results of the helium leak tests are shown in Table 6-26.

The cartridges seemed unaffected by the simulated space radiation and vacuum exposure. The X-ray radiation exposure test results may not be typical for deflagration propellants and conclusions based on the test results given here apply only to the propellants and cartridges tested.

6.7.2.6 Weight Loss of Electropyrotechnic Cartridge Materials - Measurements were made to determine the weight loss of the sub-component materials comprising the squib, when exposed to sterilization temperatures of 300°F. The results of these measurements are given in Table 6-27. The majority of the weight loss observed was due to the Horex No. 72 (Hercules Hi-Temp) propellant charge. Minor weight loss or thermal instability was noted for all other organics.

A few minutes after the start of the test on the Horex No. 72, a smoke was noted rising from the material. Upon continued exposure (less than 70 minutes) a white crystalline structure developed. This material change is shown in the photographs given in Figures 6-47 and 6-48. A short term thermal vacuum exposure of the other organic materials was performed. Test conditions consisted of exposure to 300°F and  $3 \times 10^{-5}$  torr vacuum (Horex No. 72 tested in air) for a period of 70 minutes. Weight measurements were performed in air before and after the test.

#### 6.7.2.7 Conclusions

1. Type 3511-1 cartridge utilizing Hercules Hi-Temp propellant are not recommended for spacecraft application requiring sterilization thermal exposure to 300°F.
2. Sterilization thermal exposure to 300°F - 6 cycles had no apparent effect on the 4360-1 cartridges utilizing the boron potassium nitrate propellant.
3. All cartridge ceramic electrical insulators showed indication of helium leakage around the connector pins. Helium leakage is interpreted to be indicative of incipient failure of the ceramic seals.



4. No apparent effects on the pressure-time relationship during firing of the cartridges were noted after exposure to simulated radiation and/or vacuum environments. However, the firing of all cartridges was accomplished in a fixed volume bomb cavity; therefore, the resulting pressure-time data are not indicative of the total work output of a squib cartridge. Application of squibs to valve actuators requires a knowledge of work output. The inability to test for total work output of a single squib cartridge is a definite liability in evaluating electropyrotechnic devices and is especially important to small quantity testing. A specially designed electropyrotechnic dynamic tester capable of measuring work output is described in Section 7.0.

Table 6-23. Group IV 4360-1 Electropyrotechnic Cartridge Sterilization-Thermal Cycle Test

		WEIGHT (GRAMS) - RESISTANCE (OHMS) BEFORE AND AFTER THERMAL CYCLE															
		1		2		3		4		6		7		8		9	
START	S/N	9.102	.95	9.121	.94	9.086	.99	9.100	.96	9.107	.98	9.127	.95	9.066	.97	9.116	.98
		(Grams)	( $\Omega$ )														
1st Thermal Cycle to 300°F		9.101	.97	9.120	.97	9.081	1.00	9.098	.98	9.106	.99	9.136	.97	9.065	.96	9.125	.98
2nd " " " "		9.102	.98	9.119	.95	9.093	.98	9.098	.97	9.105	.98	9.137	.96	9.064	.94	9.125	.96
3rd " " " "		9.102	.99	9.120	.94	9.080	.99	9.098	.98	9.106	.98	9.136	.96	9.064	.96	9.124	.99
4th " " " "		-	-	-	-	-	-	-	-	9.106	.99	9.137	.95	9.066	.98	9.125	.97
5th " " " "		-	-	-	-	-	-	-	-	9.106	.99	9.136	.97	9.065	.97	9.125	.97
6th " " " "		-	-	-	-	-	-	-	-	9.105	.98	9.136	.98	9.064	.97	9.124	.97

Table 6-24. 4360-1 Thermal Cycle Vacuum Soak Test  
Description, S/N 1,2,3,6,7,8,10,11 & 12

1. Soaked two days in low  $10^{-8}$  torr vacuum at ambient temperature.
2. Temperature lowered to 203°F over 6-hour period - vacuum pressure middle  $10^{-9}$  torr scale.
3. Temperature raised to 300°F in one-hour period - pressure rose to  $10^{-7}$  torr.
4. Held at 300°F for 17 hours at low  $10^{-8}$  torr pressure.
5. Temperature lowered to -214°F over 7-hour period - pressure middle  $10^{-9}$  torr scale.
6. Temperature raised to 300°F in 1 hour - pressure rose to middle  $10^{-8}$ .
7. Held at 300°F for 16 hours middle  $10^{-8}$  torr.
8. Temperature lowered to -211°F in 7 hours - pressure low  $10^{-9}$  scale.
9. Temperature raised to +300°F in 1 hour - pressure rose to low  $10^{-8}$ , held at 300°F for 16 hours on high  $10^{-9}$  scale.

Total vacuum exposure - 108 hours.

Total vacuum exposure at reduced temperature - 20 hours

Total vacuum exposure at elevated temperature 300°F - 51 hours.

Table 6-25. 4360-1 Vacuum Firing Test Description

- |        |   |
|--------|---|
| S/N 1  | <ol style="list-style-type: none"> <li>1. Soaked 72 hours at ambient temperature in vacuum</li> <li>2. Heated for 5 hours at 300°F</li> <li>3. Returned to atmospheric conditions</li> <li>4. Soaked 2 hours at ambient temperature in vacuum</li> <li>5. Heated for 5 hours at 300°F</li> <li>6. Returned to atmospheric conditions</li> <li>7. Soaked 18 hours at ambient temperature in vacuum</li> <li>8. Heated for 4 hours 300°F</li> <li>9. Fired in <math>2.8 \times 10^{-8}</math> torr vacuum</li> <li>10. Total vacuum exposure 106 hours</li> </ol> |
| S/N 2  | <ol style="list-style-type: none"> <li>1. Soaked 17 hours at ambient temperature in vacuum</li> <li>2. Cooled down over 7-1/2 hours to -303°F</li> <li>3. Squib fired in vacuum (pressure <math>6 \times 10^{-9}</math> torr)</li> <li>4. Total vacuum exposure 24-1/2 hours</li> </ol>   |
| S/N 6  | <ol style="list-style-type: none"> <li>1. Soaked 4 hours at ambient temperature in vacuum</li> <li>2. Heated 23 hours at 300°F</li> <li>3. Fired in <math>4.4 \times 10^{-9}</math> torr vacuum</li> <li>4. Total vacuum exposure 27 hours</li> </ol>   |
| S/N 7  | <ol style="list-style-type: none"> <li>1. Soaked 2 hours at ambient temperature in vacuum</li> <li>2. Cooled down over 5 hours to -288°F</li> <li>3. Squib fired in vacuum (pressure <math>2.8 \times 10^{-8}</math> torr)</li> <li>4. Total vacuum exposure 7 hours</li> </ol>   |
| S/N 10 | <ol style="list-style-type: none"> <li>1. Soaked 6 hours at ambient temperature in vacuum</li> <li>2. Heated 18 hours at 300°F</li> <li>3. Fired in <math>5 \times 10^{-9}</math> torr vacuum</li> <li>4. Total vacuum exposure 24 hours</li> </ol>   |
| S/N 11 | <ol style="list-style-type: none"> <li>1. Soaked 2 hours at ambient temperature in vacuum</li> <li>2. Cooled down over 6 hours to -303°F</li> <li>3. Squib fired in vacuum (pressure <math>1.1 \times 10^{-8}</math> torr)</li> <li>4. Total vacuum exposure 8 hours</li> </ol>   |

Table 6-26. Electropyrotechnic Cartridge Helium Leak Check

Cartridge S/N	Fired Max. Bomb Pressure (psi)	Helium Leak Gage Pressure (psi)	Helium Leakage Std. cc/sec
<u>Group I</u>			
576	2,000	50	No indicated leak
"	"	2,000	No indicated leak
577	Note 1	50	No indicated leak
"	"	2,000	No indicated leak
579	2,500	50	1.3 x 10 <sup>-8</sup>
"	"	2,000	No indicated leak
586	Note 1	50	No indicated leak
"	"	2,000	No indicated leak
587	2,500	50	No indicated leak
"	"	2,000	No indicated leak
588	2,000	50	No indicated leak
"	"	2,000	No indicated leak
<u>Group II</u>			
583	63,000	Helium Probe	Gross leakage Note 2
584	53,000	Helium Probe	No indicated leak
"	"	50	No indicated leak
"	"	50 Note 3	No indicated leak
"	"	2,000	Gross leakage
585	20,000	Helium Probe	No indicated leak
"	"	50	No indicated leak
"	"	2,000	No indicated leak
591	15,000	Helium Probe	10 <sup>-7</sup>
"	"	50	10 <sup>-7</sup>
"	"	50 Note 3	4 x 10 <sup>-7</sup>
<u>Group III</u>			
1	33,000	Helium Probe	
"	"	600	3.6 x 10 <sup>-6</sup>
2	34,000	Helium Probe	Gross leakage
3	33,000	Helium Probe	4.8 x 10 <sup>-6</sup>
5	27,000	Helium Probe	Gross leakage
6	34,000	Helium Probe	Gross leakage
7	30,000	Helium Probe	Gross leakage
8	No leak test - connector pin blew out on firing		
9	26,000	Helium Probe	Gross leakage
10	31,000	Helium Probe	Gross leakage
12	34,000	Helium Probe	Gross leakage
13	Approx. 35,000	Helium Probe	No indicated leak
"	"	375	Gross leakage
14	36,000	Helium Probe	No indicated leak
"	"	600	Gross leakage
15	33,000	Helium Probe	Gross leakage
16	33,000	Helium Probe	Gross leakage
<u>Group IV</u>			
1	8,000	Helium Probe	Gross leakage
2	8,000	Helium Probe	Gross leakage
3	11,000	Helium Probe	No indicated leak
"	"	500	Gross leakage
4	11,000	Helium Probe	Gross leakage
6	No Data	Helium Probe	Gross leakage
7	11,000	Helium Probe	Gross leakage
8	11,000	Helium Probe	No indicated leak
"	"	200	Gross leakage
9	10,000	Helium Probe	4.8 x 10 <sup>-6</sup>
10	11,000	Helium Probe	Gross leakage
11	10,000	Helium Probe	Gross leakage
12	11,000	Helium Probe	No indicated leak
"	"	550	Gross leakage
13	No Data	Helium Probe	7.2 x 10 <sup>-6</sup>
14	10,000	Helium Probe	No indicated leak
"	"	600	Gross leakage
15	11,000	Helium Probe	No indicated leak
"	"	550	Gross leakage
16	8,000	Helium Probe	0.8 x 10 <sup>-5</sup>

Note 1: Cartridges 577 and 586 inadvertently fired during sterilization thermal cycle test.

Note 2: Gross leakage is the result of saturation of the mass spectrometer and indicates a leak greater than 2 x 10<sup>-5</sup> scc/sec helium.

Note 3: Epoxy plug removed.

Table 6-27. Weight Loss of Electropyrotechnic Cartridges Materials

Temperature Soak at 300°F for One Hour

Material	Exposure During Temp. Soak	Weight Grams		Percent Loss
		Before Temp. Soak	After Temp. Soak	
Potting Compound	Vacuum	1.908	1.904	.21
Potting Compound	Air	1.810	1.805	.27
Q Dope	Vacuum	.05116	Adhered to Glass	---
Spacer	Vacuum	.11532	.11475	.005
Mylar	Vacuum	.284	.2828	.042
Holex No. 72 Propellant	Air	.05659	.03145	45.00



Figure 6-47. Holex #72 Propellant Before 300°F Thermal Exposure



Figure 6-48. Holex #72 Propellant After 300°F Thermal Exposure

## 6.8 REFERENCES

1. Advanced Valve Technology for Spacecraft Engines, Final Report No. 8651-6032-SU000, Volume I, Valve Study, TRW Systems Group, July 19, 1964.
2. Advanced Valve Technology for Spacecraft Engines, Final Report No. 8651-6042-SU000, TRW Systems Group, August 1965.
3. Advanced Valve Technology, Final Report No. 06641-6023-R000, Volume I, Mechanical Controls, TRW Systems Group, January 1969.
4. W. W. Pendleton, Advanced Magnet Wire Systems, Electro-Technology, October 1963.
5. Thin Film Aluminum Oxide Wire and Strip, Permaluster, Inc., Burbank, California.
6. R. M. Bozorth, Ferromagnetism, Van Nostrand Company, Inc., New York, New York.
7. E. A. Nesbitt, R. D. Heindenreich and A. J. Williams, A Necessary Factor for Heat Treatment of the Permalloys in a Magnetic Material, Supplement to the Journal of Applied Physics, Vol. 31, pp. 228S-229S, McGraw-Hill, New York, 1960.
8. Advanced Valve Technology for Spacecraft Engines, Final Report No. 8651-6033-SC000, Volume II, New Concepts, TRW Systems Group, July 19, 1964.
9. Advanced Valve Technology, Interim Report No. 06641-6014-R000, Volume I, Spacecraft Valve Technology, TRW Systems Group, November 1967.



## 7.0 INSTRUMENTATION AND MEASUREMENTS

### 7.1 INTRODUCTION

The qualification of valves and other control components for use in space is accomplished by testing or experiments during space flights and by testing on the ground in a simulated space environment. Testing in space, although costly, can provide important design criteria. However, as the tempo of the space program is increased, such testing becomes impractical. The more practical solution is to test in a simulated space environment, which is limited by our present knowledge and the inability to duplicate the entire space environment in a combined test.

Instrumentation and measurement techniques are discussed in this section which are considered adaptable to the qualification of valves and components for spaceflight. The space environment is covered in detail in Section 2.0 Operational Considerations.

### 7.2 VALVE POSITION INDICATORS

#### 7.2.1 Solenoid Valve Position Indicators

Position indication for solenoid valves can be obtained from the transient current and voltage characteristic of the actuator coil. However, in some cases the current and voltage time traces are not properly interpreted resulting in rejection of the valve during qualification tests. Other position indication techniques utilize a mechanical linkage coupling a position transducer such as an LVDT, resistance potentiometer, or photometric device to the linkage. On or off status may also be confirmed by precisely located switching devices coupled to the linkage. Many actuators do not couple to the valve mechanism through a mechanical linkage and conventional position indicating and measuring devices cannot be used. Solenoid valves without external position measuring devices may use various in-situ methods for position determination which are constructed as part of the actuator assembly. Position measuring methods suitable for solenoid valves which do not permit mechanically coupled external measuring devices are also considered.

7.2.1.1 Current and Voltage Transient Data - There is a relationship between armature velocity-position characteristic and the transient current-voltage characteristic. This relationship is complicated and a simple, unique, direct and linear relationship does not exist between actuator armature position and the transient current-voltage characteristic. Information obtained from the actuator current/voltage on-off transient is useful for laboratory study where carefully controlled conditions can be used to obtain consistent results. For example, consistent on-off transients can usually be obtained for solenoid actuators by using a gated, precision regulated power supply in a temperature and humidity controlled laboratory. The on-time of the gate is adjusted slightly in excess of the on transient time of the solenoid actuator. This procedure reduces the heating usually caused by steady actuator coil excitation, which affects the final coil current and

the time constant of the transient characteristic. A one shot multivibrator or triggered single cycle square wave generator or pulse width time switch may be used for gating the power supply. Figure 7-1 illustrates a system which is useful for obtaining consistent, repetitive, on-off current and voltage transients for a solenoid actuator coil. Figure 7-2 is an illustration of a current and voltage-on transient trace for a solenoid valve obtained with the system shown in Figure 7-1.

The current transient obtained with the solenoid poppet locked closed is a useful reference for comparison. The current transient obtained with a moving poppet may be compared to determine the starting time for armature motion. A blocked armature current transient with a distinctly faster than normal rise time is indicative of shorted actuator coil turns. It is also possible to detect shorted turns with the poppet blocked closed, by measuring the incremental inductance on a low level audio frequency bridge. Low bridge excitation at high audio frequencies will minimize or eliminate the effects of poppet motion or buzz, 1 to 10 kilohertz should be sufficient. Low inductance relative to a statistically normal production inductance is indicative of shorted turns. Shorted turns should be cause for rejection because it is indicative of faulty coil windings and will usually cause a large change in pull-in time.

Comparison of blocked and moving poppet current transients of a solenoid valve will give information on the time of motion initiation. A double exposure photograph with both transients on one photograph will give a precise overlay comparison of both transients or a memory oscilloscope may be used for direct visual comparisons. The results of such a visual or photographic comparison may be similar to Figure 7-2. It is apparent that point a in Figure 7-2 is the point where the unblocked poppet motion begins because this is where the two current traces begin to depart from each other due to poppet motion. The deviation from the blocked armature transient on path a-b is small due to low armature velocity during this interval; hence, existing practice has assumed armature motion begins at b and is complete at c. It is possible for a solenoid actuator to have a current transient similar to the dashed curve in Figure 7-2 with normal armature travel and with conditions of high viscous or fluid damping, in this case the completion of armature travel is not well defined, yet the fluid flow characteristics of the valve opening may be acceptable.

Actuator motion data inferred by processing the on-off current and voltage transient of solenoid actuator coils does not provide a simple dependable means of measuring on and off actuator position errors. This type of data is invaluable in laboratory studies of actuator performance where controlled conditions enable consistent results.

7.2.1.2 LVDT Coils - Linear variable displacement transformer (LVDT) coils can be built into a solenoid valve actuator to provide position indication. A matched pair of differentially opposed coils may be installed on the end of the driving solenoid coil to produce a null output for either the fully closed or fully open position. Three coils may be installed to enable



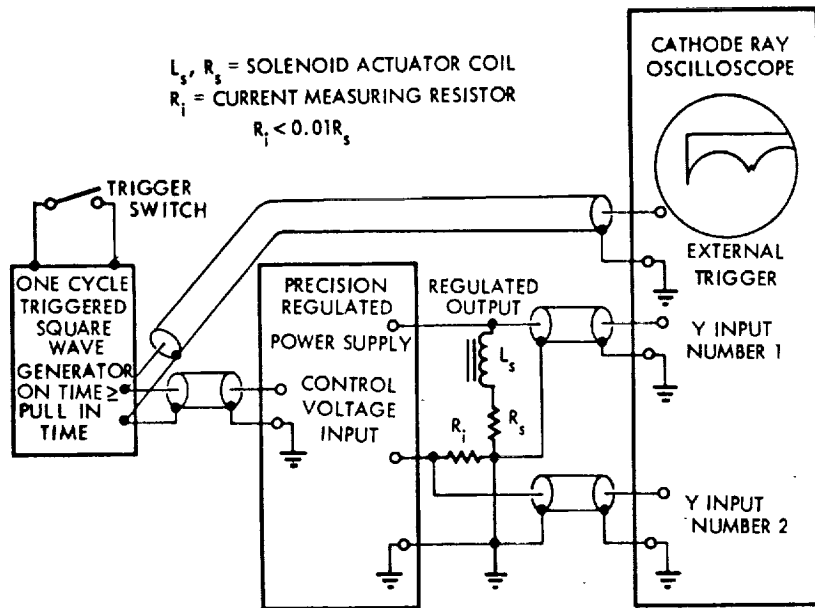


Figure 7-1. Solenoid Actuator On-Off Transient Test Setup

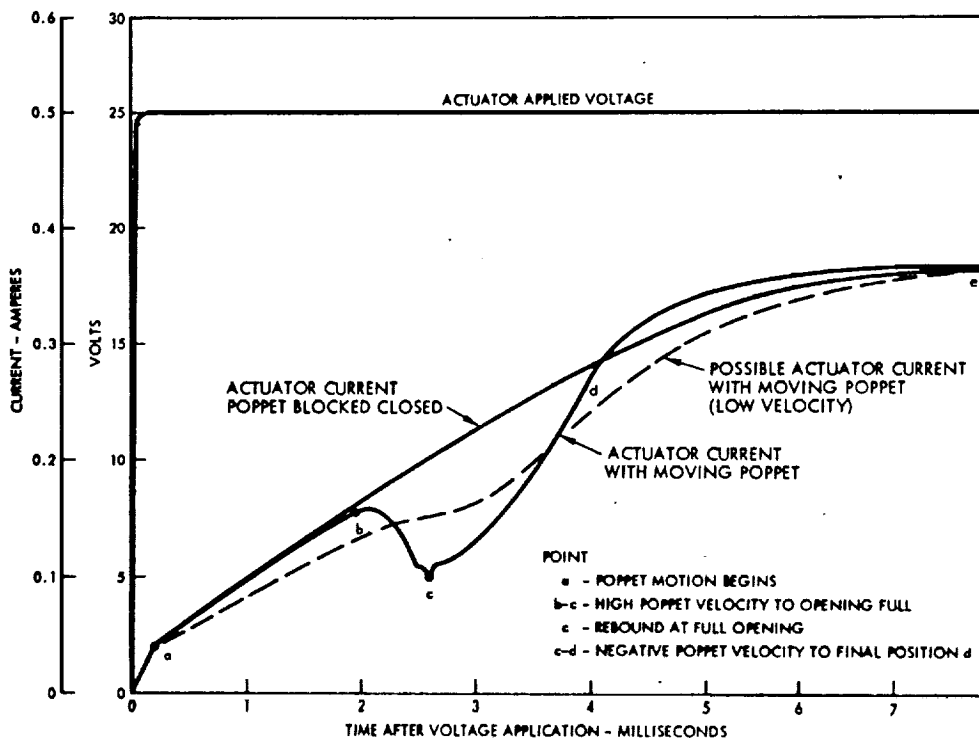


Figure 7-2. Typical Current Voltage Transient Characteristics of a Solenoid Valve

measurement of deviations from fully open and fully closed position as shown in Figure 7-3. One pair of the three provides null output at the fully open position and the second pair is null output at the fully closed position. The real time position information obtainable during switching transients is limited because the changing actuator field caused by the solenoid coil current transient contributes somewhat to the LVDT output indication. The static null position measurements can be very accurate and quantitative nominal deviations from null are affected only slightly by environmental factors and coil excitation.

Figure 7-4 is a diagram illustrating the use of builtin LVDT coils for measurement of the static on and off position of the solenoid actuator. Carefully located LVDT coils promise to be a sensitive and precise method of measurement for static on and off position errors for in-flight and laboratory measurements.

7.2.1.2 Magneto Resistive Sensors - An electrical resistance which changes when exposed to a magnetic field can be used in a position sensor technique. The resistance is temperature sensitive, consequently, matched pairs of magneto resistors exposed to identical temperature must be used in a differential opposing circuit to cancel out temperature effects. Three magneto resistors may be installed in a solenoid actuator to obtain null outputs for the desired on and off actuator positions. The null outputs are insensitive to actuation coil transient excitation, operating, and environmental conditions. Figure 7-5 illustrates the installation of three matched magneto resistors to assure immunity from temperature changes and Figure 7-6 illustrates a typical position error measuring system. The magneto resistive error sensing system can give real time actuator position information during actuator on-off transients if the inductive coupling of switching transients to the magneto resistance sensor circuits is precisely compensated by an identical opposing inductive coupling. Magneto resistive sensors offer advantages of accurate real time transient and static position information, simple power supply requirements and high position error sensitivity.

7.2.1.3 Hall Effect Position Sensors - A Hall effect transducer produces an output voltage proportional to the magnetic flux density perpendicular to the sensor surface. The installation and characteristics are similar to the magneto resistive sensors described previously. Hall effect transducers are less sensitive than the corresponding magneto resistive transducer and also require a resistance null error balance adjustment.

7.2.1.4 Photometric Position Error Sensing - Compact, solid state, infrared or visible light sources and sensors are available which may be built into solenoid actuators. The light source sensor system is installed with the light beam transverse to the actuator motion and properly located with respect to the actuator armature end boundary to obtain a null output from the photometric system at the desired on or off position. The circuit concepts and performance characteristics are comparable to the magneto resistive sensor system, however, a transparent, nearly constant light transmission path must be available transverse to the armature motion. If the armature is operated in the propellant, the fluid must offer little attenuation to the transverse light beam.

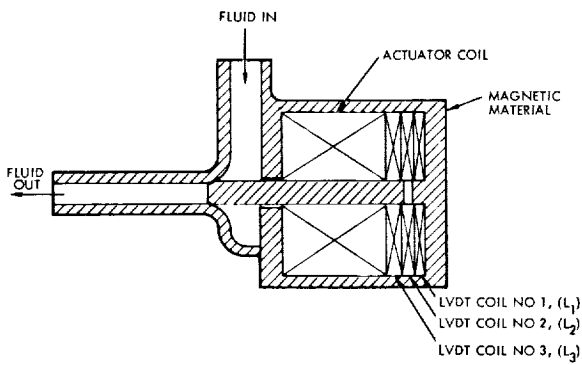


Figure 7-3. Solenoid Valve With Built-in LVDT Position Sensor

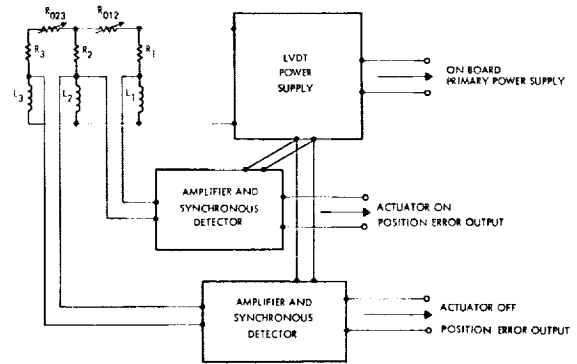


Figure 7-4. LVDT Position Error Measuring System

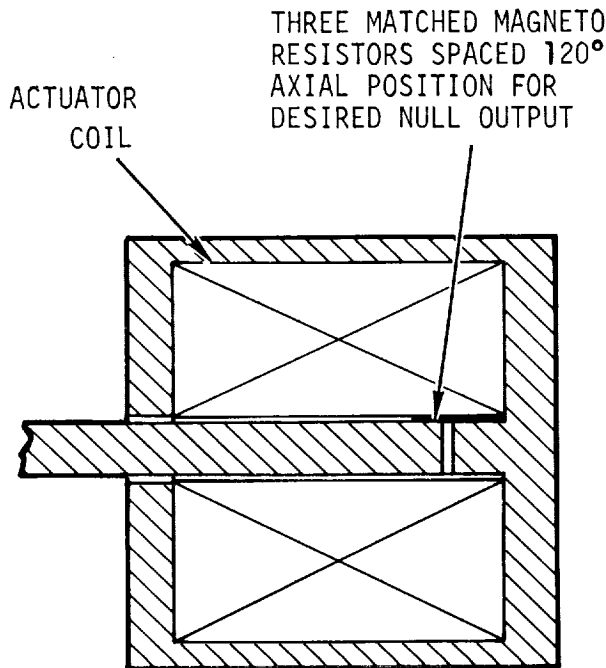


Figure 7-5. Solenoid Valve With Built-in Magneto Resistance Position Sensors

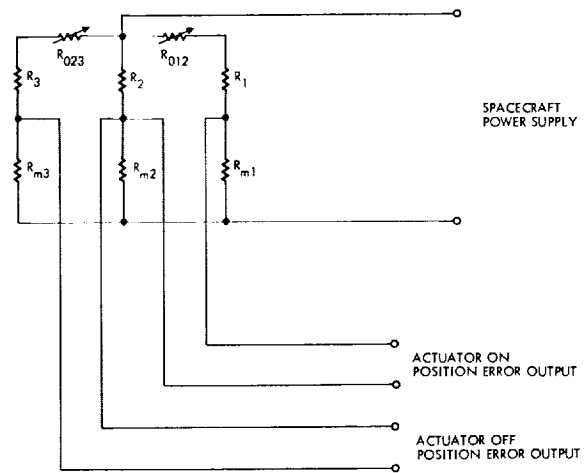


Figure 7-6. Magneto Resistance Position Error Measuring System

## 7.2.2 Radioactive Proximeter

In view of the fact that a radioactive source may be made small and light-weight and that no contact is required between the radioactive source and the detector to obtain a meaningful output, it was felt that the employment of a radioisotope in a valve position indicating device would provide significant advantages over more conventional techniques. In concept (Figure 7-7), valve position would be measured by a source-detector system in which the radioisotope is the particle source: the number of particles striking the particle detector (beryllium target) per unit time becomes a measure of the relative displacement between the source and the detector.

To demonstrate the feasibility of the use of a radioisotope in a valve position indicating system, the valve actuator of the Lunar Module (LM) descent engine was selected as a specific case for analysis. The requirements associated with the present position measuring device, which utilizes potentiometers, provide a realistic basis for analysis of a positioning device employing a radiating source. Three configurations involving both angular and linear displacement between source and detector were considered. See Reference 1 for a detailed analytical description of these radioactive proximeter schemes.

7.2.2.1 Linear Displacement Proximeter - Figure 7-7 shows the general arrangement of source, target and electronic devices required in the linear displacement proximeter. Alpha particles from the source, S, travel to the target, T, where they react with the beryllium and produce carbon-12 and a neutron. About 70 percent of the carbon-12 atoms produced are in an excited state and return to the stable or ground state by emitting a 4.4 mev gamma ray. A certain portion of these gammas striking the detector result in voltage pulses which are amplified and then counted by the count rate meter. Thus, the count rate is directly proportional to the number of alphas striking the beryllium target per unit time. The number of alphas, in turn, striking the beryllium target per unit time is proportional to the solid angle subtended by the source on the target. This is a function of the target radius,  $r$ , and the source-to-target distance,  $d$ . Thus for a fixed target radius the change in count rate measured by the count rate meter is proportional to the change in  $d$ .

The major advantage of the above system is the fact that a meaningful detector output may be obtained even though some material is interposed between the target and detector. The major disadvantage of the alpha source/beryllium target approach is the large quantity of alpha source required to give reasonable accuracy in the position measurement: the radiation hazard is a direct function of source quantity. Large source quantities are a result of the low probability that an alpha particle will produce a 4.4 mev gamma.

Using the LM valve actuator design as a test bed, source quantity calculations were performed for the alpha source, beryllium target, and detector arrangement as shown in Figure 7-8. An alpha source size of about one megacurie was found necessary to meet the LM valve total resolution

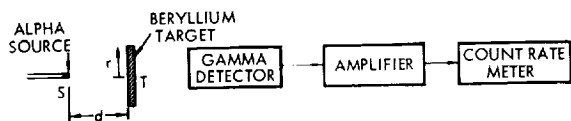


Figure 7-7. Alpha Source, Beryllium Target Positioner

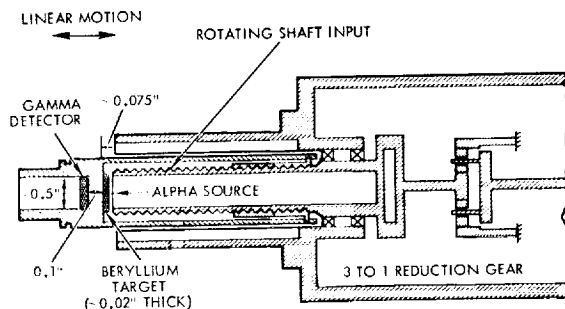


Figure 7-8. Linear Displacement Proxi-meter in LM Valve Actuator

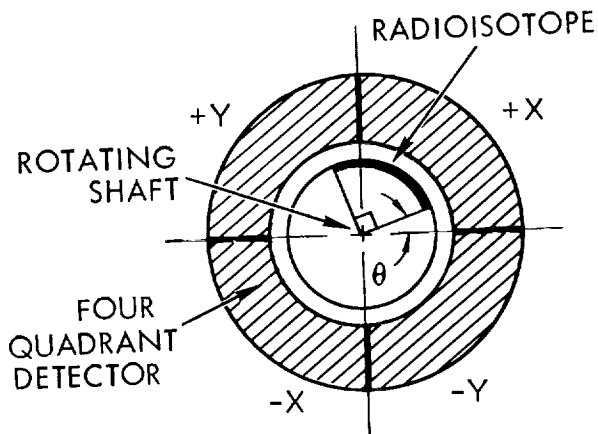


Figure 7-9. Four Quadrant Position Indicator

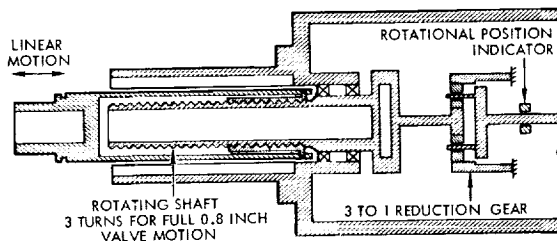


Figure 7-10. Four Quadrant Position Indicator Installation

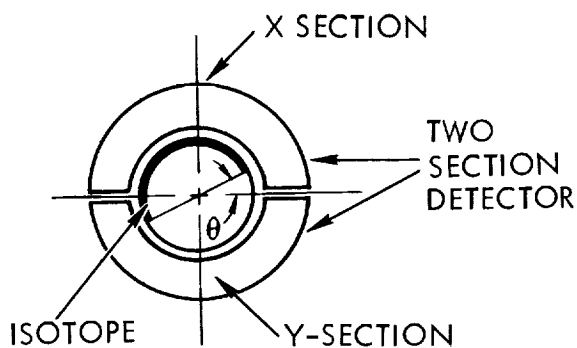


Figure 7-11. Linear Output Rotational Source With Split Detector

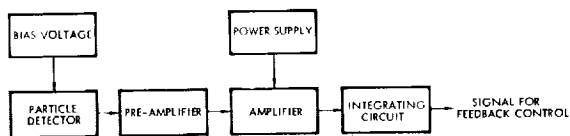


Figure 7-12. Radioisotope Positioner Electronic Components

requirement of 0.6 percent of full stroke. Megacurie source sizes are much too large to consider from a practical handling standpoint. Based upon the AEC tolerable dose rate of 2.5 millirem/hr and considering a distance of 6 inches from the point source, the upper limit on a Polonium-210 alpha source with about 6 millimeters of tungsten shielding is about 15 curies. In view of this fact the alpha source, beryllium target linear displacement configuration was not considered feasible for use with the LM valve actuator.

7.2.2.2 Four Quadrant Position Indicator - Since the change in solid angle approach did not appear attractive for use with the LM valve actuator, an alternate approach was sought which would result in smaller source requirements. The result was the source detector arrangement shown in Figure 7-9. In concept, the rotating shaft has a quadrant of its surface coated with a radioisotope. The shaft is surrounded by a four-quadrant detector which has four outputs: plus x, plus y, minus x and minus y. The X-Y output from the detector defines the angle,  $\theta$ , through which the shaft has rotated from a zero position. Analyn's showed that a source of about one millicurie is required to attain the LM specified resolution if the counting efficiency of a solid state detector is assumed to be unity and a geometry factor of 0.5 is used; i.e., half of the particles leaving the source are counted. Thus, source sizes are down by a factor of about  $10^3$  from the source sizes required for the solid angle approach. There are two reasons why the source sizes are so greatly reduced. One is the fact that the geometry factor for the rotational approach is about a factor of 50 times the geometry factor for the solid angle device. The other is the fact that the sensitivity of the rotational device is much greater; i.e., small changes in valve motion result in large changes in the output signal from the detector.

Figure 7-10 shows the location of the four quadrant position indicator in the LM valve actuator. A source size of one millicurie does not represent a radiation hazard: based on a dose rate of 2.5 millirem/hr, a distance of 6 inches and a typical shield thickness of 6 millimeters of tungsten, the tolerable curie levels for representative alpha, beta and gamma sources are, respectively, about 15 curies of Polonium-210, about 45 millicuries of Strontium-90, and about 60 microcuries of Cobalt-60.

Although the four-quadrant detector is attractive from the standpoint of source size, analysis shows that the output signal from the detector is nonlinear. A nonlinear signal must be linearized for use in feedback control. The circuitry required to provide a useful signal for feedback to the LM valve actuator motors adds complexity and decreases the reliability of the system.

7.2.2.3 Linear Output Split Detector - Realizing the desirability of a linear output for feedback control, source-detector configurations were investigated which would yield a linear output. Figure 7-11 shows a concept which yields a detector output which is directly proportional to angular shaft motion. Half of the circumference of the shaft is coated with a radioisotope, and the difference between the outputs from the two detectors yields a linear response. For the LM valve actuator, the source size as a function of total resolution requirement was found to be about 50 millicuries.

This source size is reasonable from a radiation hazard standpoint, although the count rate at the detector is relatively high. An advantage of the radioisotope detector lies in the fact that no contact between source and detector must be made and the inertia effects attributable to the measuring device are very small: the weight of a 50 millicurie beta source is of the order of  $10^{-3}$  gm.

Since the divided detector yields a reasonable source size and a linear response, a particular system based upon its use was considered for the LM valve actuator. It was determined that the circuitry required for the proximeter approach would be more complex than the circuitry required for each potentiometer of the system presently employed in the LM valve actuator, although the power requirements for the two systems would be quite similar. Since the anticipated reliability of a developed source and detector will be high, the total circuitry is expected to be reduced by the need for fewer source/detector units.

A pictorial representation of the electronic system required for the proximeter, utilizing a detector with a linear output, is shown in Figure 7-12. Estimates of the weights and volume of the electronic components are 1 to 1.5 pounds and 25 cubic inches, respectively. The weight of the present LM valve potentiometer circuitry is of the order of 0.25 pound. Consideration of the count rate circuitry of the two systems on a one-to-one basis would, therefore, appear to present a possible reduction in reliability for the proximeter configuration; i.e., the mean time to failure for the radioisotope system would be lower. The volume of circuitry is important from the standpoint of system reliability, since the addition of components normally is detrimental. On a one-for-one basis, assuming validity in estimated weights and volumes, this would show the proximeter to be inferior. However, because of the relative insensitivity of the proximeter to vibration, temperature, fluid environment, etc., it is anticipated that one or, at most, only two proximeters and their associated electronics would be required to replace the four potentiometers (and associated electronics) now used. The net effect here, and in most systems so constituted, is expected to be a reduction in total circuitry.

7.2.2.4 Summary - It appears that a positioning device based upon the use of a radioisotope is feasible, however, the following qualifications must be made:

1. For non-critical missions where the environment will permit a single potentiometer to operate continuously with high reliability, a radioisotope-based position indicator would appear to add complexity and weight.
2. When environmental, physical, and thermal factors dictate the use of redundant potentiometers to achieve desired system reliability, the radioactive proximeter technique appears to provide a method for increasing overall reliability.

3. An additional area of potential usage for this concept is one in which no contact is permitted with the device whose position is to be detected and no detectable loading of that device can be tolerated. Although available test components based on the use of magnetic fields fulfill the first of these needs, they generally impose objectionable inertia loads.

In general, it appears that a source-detector device based upon the change in solid angle approach may be used to indicate valve position for valves which move in a linear manner at moderate speeds. Either the four-quadrant detector or the divided detector may be used to indicate valve position for valves which move in a rotary manner.

The two major problems associated with a radioisotope position indicator are the counting time required to obtain good statistical accuracy and the circuitry required to analyze the detector output. If feedback control is required, an additional burden is placed on the source-detector system in that a linear detector output becomes desirable. Laboratory testing of the devices shown in Figures 7-9 and 7-11 would be desirable for the purpose of obtaining practical knowledge with respect to the fabrication and testing of such devices. A detailed analysis of the electrical circuits required to obtain an output from the four-quadrant detector would also be useful.



## 7.3 FLOW AND LEAKAGE MEASUREMENT

### 7.3.1 In-Flight Leakage Measurement

In-flight leakage measurement requirements include a sensitivity of  $10^{-7}$  sccs operation in zero-g and high vacuum environments, and proper function after launch accelerations and vibrations. Accuracy of the instrument should be better than 5 percent, and traceability to NBS standards is preferred.

The principle methods which have been considered for in-flight leakage measurement are discussed below.

Table 7-1 presents a rating comparison of the various leakage measurement techniques considered. These ratings are based on ground performance and do not reflect size or weight considerations.

7.3.1.1 Electrothermal Flowmeters - These meters operate on the principle that the heat transfer from a warm body in a flow stream varies with the Reynolds number of the flow. The electrothermal flowmeter is extremely simple and requires no moving parts. The parts exposed to propellants may be easily encapsulated in a compatible material. The limitations of the instrument include a lack of sense information, errors due to convective currents when used in a gravity field and cryopumping errors when used in some cryogenic propellant applications. Leakage sensitivities of 25 cch of liquid propellant have been obtained in a 0.625 inch diameter line. This is probably close to the lower limit of Reynolds numbers detectable by this method. A marked improvement in sensitivity may be attained by reducing the diameter of the flow channel in the sensing area, so as to increase the flow velocity.

7.3.1.2 Fuel Cells - A fuel cell operates on a reverse electrolysis principle wherein a voltage is generated between two plates during the reaction of an oxidizer and a reducing agent. This principle has been applied to commercial oxygen and hydrogen concentration monitors, which generate a voltage proportional to the partial pressure of the oxygen or hydrogen present in the atmosphere exposed to the detector. An advantage of this type of sensor is that it generates its own power which is sometimes sufficient for operating a sensitive relay. Disadvantages include a lifetime limited by the quantity of oxidizer (or reducing agent) packaged in the unit and by its exposure to the reducing agent (or oxidizer) being sensed. Errors have occurred in  $H_2$  sensors due to  $O_2$  entering the cell, resulting in a reaction similar to that occurring in catalytic sensors. Sensitivities on the order of 1 percent of the lower explosion limit of hydrogen in air mixtures have been attained.

7.3.1.3 Catalytic Sensors - These devices measure the heat dissipated in a reaction between the fluid being sensed and an oxidizer (or reducing agent) in a catalytic burner. This type of sensor has been used in laboratory and commercial installations for measuring  $O_2$  and  $H_2$  concentrations. The oxidizer must be stored within the unit or supplied from an externally stored supply.

Table 7-1. Comparison of In-Flight Leakage Measurement Methods

INSTRUMENT	External Leakage	Internal Leakage	Sensitivity	Accuracy	Gases	Liquids	Propellant Limitations
Electrothermal Flow Meters	3 <sup>a</sup>	3	2 (7 x 10 <sup>-3</sup> ccs liquid)	2	3	3	None.
Fuel Cell	2 <sup>a</sup>	2	U	2	2	2	Oxidizers & Reducing Agents Only.
Catalytic Sensor	2 <sup>a</sup>	2	U	2	2	2	Oxidizers & Reducing Agents Only.
Radiation Sensor	3 <sup>a</sup>	3	3	3	3	3	None.
Mass Spectrometer	3 <sup>a</sup>	3	3 10 <sup>-11</sup> sccs	2	3	Vapors Only	Vapors Only.
Acoustic Sensor	2 <sup>a</sup>	2	U	2	3	3	None.
Burst Diaphragm	2 <sup>a</sup>	2	1-3	1	3	3	None.
Thermal Leak Sensor	3 <sup>a</sup>	3	3 (4.5 x 10 <sup>-7</sup> ccs liquid)	2	1-2	2-3	None.

a - Leakage must be collected and delivered to sensor.

Ratings: 1 - Poor, 2 - Fair, 3 - Good, U - Unknown

7.3.1.4 Radiation Sensors - These sensors sense the radiation level in a line or area into which a fluid component could leak. This radiation is supplied by a radioactive tracer material added to the leaking fluid. The tracer material may be mixed with the propellant initially or it may be added as part of the leak sensing operation. An example of the latter case is a system in which the leakage is passed through a platinum dioxide sponge impregnated with  $Kr_{85}$ . As the leaking fluid passes through the sponge it entrains some of the radioactive  $Kr_{85}$  which is sensed by a radiation detector in a shielded area downstream. The sensitivity of these systems depends on the quantity of the tracer added to the leaking fluid. When a radioactive material is added to the bulk propellant, sensitivity is limited by the undesirable effects of radiation on the propellant, structure, and personnel in the area. When the entrainment approach is used the sensitivity and life of the system must be traded off; the higher the sensitivity, the shorter the life for a given size limit.

7.3.1.5 Mass Spectrometers - A mass spectrometer measures the anode to cathode current in a magnetically deflected beam of ions. Ionization is normally accomplished by passing the sample over a hot wire. The electric and magnetic fields are adjusted so that only the ions with the proper charge to mass ratio strike the cathode.

Mass spectrometers are in general use in ground leakage measurements of hydrogen and helium and other gases and their use has been proposed for flight systems. They may also be used as an analytic tool to determine leakage sample composition. Successful operation of a mass spectrometer tube at cryogenic temperatures has been demonstrated. Further work in this area is required to produce a spaceborne system. The mass spectrometer has higher sensitivities than any of the methods listed with the possible exception of the radiation type sensor.

7.3.1.6 Acoustic Sensors - Acoustic leakage sensors normally measure the velocity of an acoustic wave transmitted in the direction of flow and compare it with the velocity of one transmitted against the direction of flow. This approach has been used in commercial flowmeters and has relatively high sensitivity.

7.3.1.7 Burst Diaphragms - Go-no-go and long term inspection leakage surveillance in rocket engines can be accomplished with burst diaphragms. The diaphragm closes off a cavity into which leakage will potentially flow. When a certain quantity of fluid leakage has occurred the diaphragm ruptures. A problem is encountered when this approach is used with cryogenic propellants. Cryogens may cause cryopumping in the measurement cavity with resulting diaphragm implosion. This may be partially overcome by venting the measurement cavity through a small orifice but this markedly reduces sensitivity. Remote readout may be provided to indicate diaphragm failure. Data is principally qualitative and once failure occurs, no further leakage monitoring is possible.

7.3.1.8 Thermal Sensors - Thermal leakage sensors sense the temperature change due to the isenthalpic expansion of the leaking fluid across the valve seal and compare it to the bulk fluid temperature. These sensors are extremely simple and they may be easily encapsulated in propellant compatible materials. Sensitivities of  $3.66 \times 10^{-6}$  in<sup>3</sup>/hr with water and  $4 \times 10^{-4}$  in<sup>3</sup>/hr with hydrazine have been obtained.

### 7.3.2 Electromagnetic Flowmeter

The electromagnetic meter concept (References 2 and 3) traces back to Faraday, however, it still has basic advantages for high reliability systems in that it has no moving mechanical parts. The principle involved is that motion of a substance in a magnetic field results in an induced voltage. Figure 7-13 shows a flowmeter concept utilizing an ac magnetic field to allow flow measurement of insulating and poorly conducting fluids in a duct. The use of a periodically varying magnetic field also eliminates problems due to electrolysis, polarization, stray electromagnetic fields, and flow induced electrostatic fields.

The meter's output is described by the following equation:

$$V = \oint (\mathbf{v} \times \mathbf{B}) \cdot d\mathbf{l} - \iint \frac{\partial \mathbf{B}}{\partial t} \cdot d\mathbf{s}$$

where:  $V$  = fluid velocity perpendicular to the magnetic field

$B$  = magnetic field vector

$v$  = induced voltage across the fluid duct

$l$  = width of flow channel

$d$  = incremental duct area

However, the meter in Figure 7-13 utilizes two magnetic fields in opposite directions to cancel the effects of the second term. The induced voltage for each coil is then described by:

$$V = \oint (\mathbf{v} \times \mathbf{B}) \cdot d\mathbf{l}$$

where, if the magnetic field is varying sinusoidally

$$B = B_0 \cos \omega t$$

By substituting for  $B$  we obtain

$$V = v l B_0 \cos \omega t$$

Since two coils were used with opposing magnetic fields, the effects of spurious fields are cancelled. By connecting the coils in series, as shown in the sketch Figure 7-13, the output signal is doubled, i.e.

$$V = 2 v l B_0 \cos \omega t$$

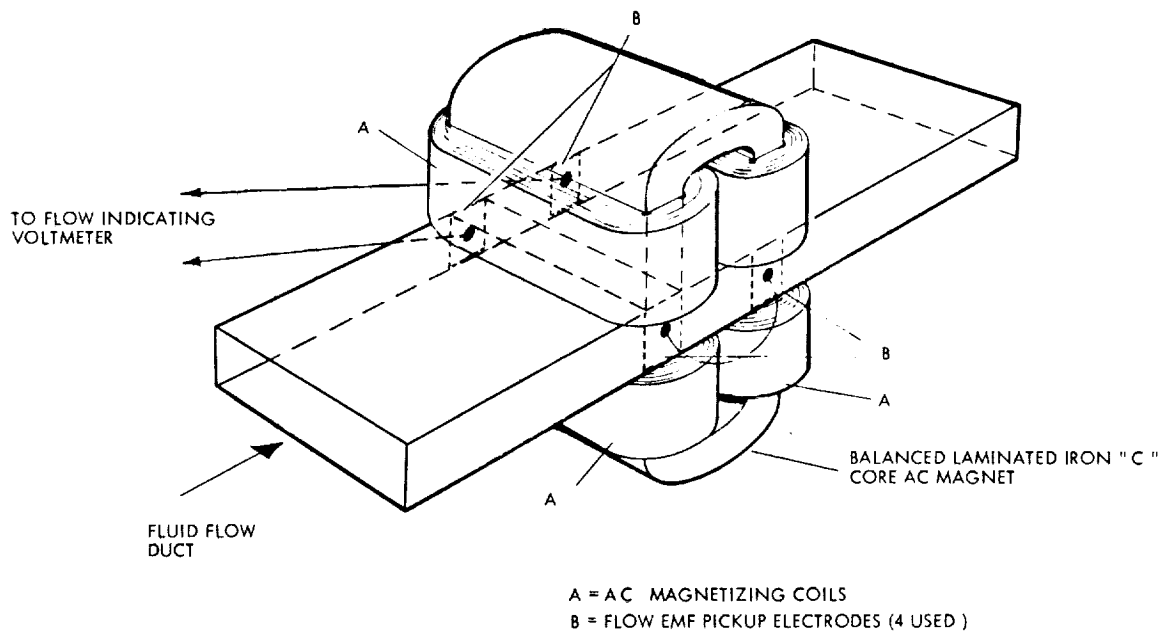


Figure 7-13. AC Electrohydrodynamic Flowmeter

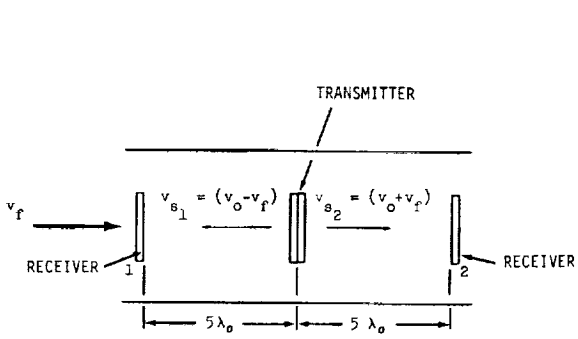


Figure 7-14. Acoustic Flowmeter Concept

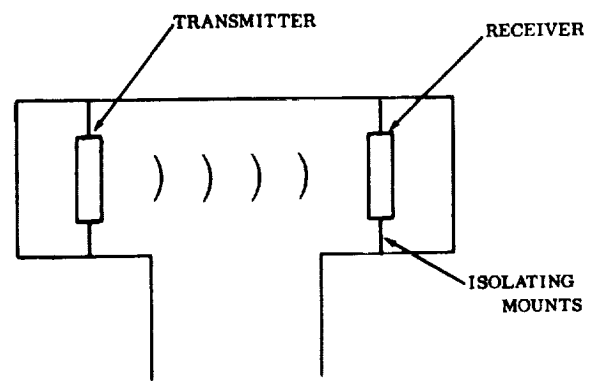


Figure 7-15. Acoustic Pressure Measuring Device

For a duct 4 cm wide by 0.4 cm high, the sensitivity is approximately 0.244 in<sup>3</sup>/hr. The sensitivity will be considerably higher for smaller ducts. More sophisticated voltage measurements could improve the sensitivity by as much as a factor of a thousand. Sensitivities of approximately 25 in<sup>3</sup>/hr are presently attained with electrothermal type flowmeters.

### 7.3.3 Acoustic Flowmeters

Acoustic meters have been made which measure the deflection of an acoustic beam transmitted perpendicular to a fluid flow. The frequency measurement of the repetition rate of a self triggered acoustic wave transmitted over a known distance with and against a fluid flow has also been used. A more sensitive acoustic flowmeter may be made which measures the Doppler phase shift of a sound wave when traveling with, and against the fluid velocity in a duct. This phase shift is directly translatable into a fluid velocity measurement and therefore gives a flow measurement. A possible arrangement is shown schematically in Figure 7-14.

The time for the sound wave to travel between the transmitter and the upstream receiver is:

$$t_1 = \frac{5\lambda_0}{v_{s_1}}$$

and between the transmitter and downstream receiver

$$t_2 = \frac{5\lambda_0}{v_{s_2}}$$

With no flow the time becomes:

$$t_0 = \frac{5\lambda_0}{v_0} \text{ in both cases.}$$

Now, if we compare the phase of the wave arriving at the upstream receiver to that arriving at the downstream receiver, the time difference is:

$$t_\phi = (t_1 - t_0) + (t_0 - t_2)$$

or

$$t_\phi = t_1 - t_2$$

then

$$t_{\phi} = \frac{5 \lambda_0}{v_{s_1}} - \frac{5 \lambda_0}{v_{s_2}}$$

$$t_{\phi} = 5 \lambda_0 \left( \frac{1}{v_{s_1}} - \frac{1}{v_{s_2}} \right)$$

the time required for one wave to occur is

$$T = \frac{1}{f}$$

then the phase shift is

$$\phi = f \cdot t_{\phi} \cdot 360 \text{ degrees}$$

this gives

$$t_{\phi} = \frac{1.8 \times 10^{-4}}{360 \times 10^5}$$

$$t_{\phi_{\min}} = 5 \times 10^{-13} \text{ sec}$$

Substituting for  $v_{s_1}$  and  $v_{s_2}$

$$t_{\phi} = 5 \lambda_0 \left( \frac{1}{(v_0 - v_f)} - \frac{1}{(v_0 + v_f)} \right)$$
$$t_{\phi} = \frac{10 \lambda_0 v_f}{v_0^2} \left[ \frac{1}{\left(1 - \frac{v_f}{v_0}\right) \left(1 + \frac{v_f}{v_0}\right)} \right]$$

Since  $v_f$  is small compared to  $v_0$ , in our case this reduces to:

$$t_{\phi} = \frac{10 \lambda_0 v_f}{v_0^2}$$

then for the example

$$t_{\phi} = \frac{10 \times 5 \times 10^{-2} \times .33 \text{ ft/sec}}{(5 \times 10^3)^2 \frac{\text{ft}^2}{\text{sec}^2}}$$

$$t_{\phi} = 6.6 \times 10^{-9} \text{ sec}$$

If we choose a tube area of  $1.6 \text{ cm}^2$ , as before, the flow rate,  $q$ , is

$$q = 16 \frac{\text{cm}^3}{\text{sec}}$$

then

$$\begin{aligned} q_{\min} &= \frac{t_{\phi \min} q}{t_{\phi}} \\ &= \frac{5 \times 10^{-13}}{6.6 \times 10^{-9}} \times 16 \\ &= 1.21 \times 10^{-3} \frac{\text{cm}^3}{\text{sec}} \end{aligned}$$

For a flow tube area of  $1.6 \text{ cm}^2$  the minimum measurable flow rate or sensitivity was calculated to be  $0.266 \text{ in}^3/\text{hr}$ . This is two orders of magnitude better than electrothermal flowmeters and might be improved further with more sophisticated sensing techniques and optimized tube geometry.

#### 7.3.4 Acoustic Pressure - Leakage Measurement Technique

This technique is based on measuring the acoustic impedance or transmission characteristics of a chamber or line. A sound wave is produced by exciting the input transducer (transmitter) at a known level, and the intensity of the wave at the receiver or output transducer is then examined (Figure 7-15).

The pressure is calculated from the wave intensity and physical dimensions of the transmitter receiver, and chamber and the fluid present. Preliminary calculations indicate a receiver intensity of  $1.63 \times 10^{-16} \text{ watts/cm}^2$  (0 db) for mean chamber pressures of  $10^{-8}$  torr and an input transducer motion of  $10^{-4}$  times the chamber volume is possible. This signal strength should be easily detectable. Leakage measurements may be made by monitoring pressure over a known time with a known chamber volume. Since chamber volume may be precisely determined, an extremely sensitive leakage measurement is obtainable.



The acoustical method of pressure and leakage measurement has the advantage of being insensitive to the pressure or absence of gravity fields. It may be made quite rugged to withstand a spacecraft launch environment or allow field use on the ground.

### 7.3.5 Accelerometer Valve Control Concept

All of the transducer/gauging elements considered as engine valve control elements obtain the control signal from functions which have an indirect but proportional relationship to the desired final function for which control is required, i.e., thrust or total impulse. It is possible and probably most accurate and practical to directly utilize the thrust or impulse measurement with an accelerometer or integrating accelerometer for engine valve controls. Variations of this method have been used in spacecraft engine control systems. The control loop has been directly closed by an on-board system with predetermined thrust or impulse programming. Ground station control computers and corrective decision programming of impulse and thrust are also used.

The direct use of acceleration and impulse sensors for spacecraft engine valve controls appears to be the most precise and practical method of closed loop valve control. Force balancing accelerometers have been developed and used for space applications which are capable of resolution to 1 part in  $10^6$ . The problem of direct exposure of the control transducer to the active propellant is avoided and the accelerometer may be installed in any location which minimizes spacecraft environmental disturbances.

Figure 7-16 illustrates a control system utilizing an accelerometer for the engine thrust control valve. The total impulse and thrust level control loops may be used separately or jointly. An on-board or ground control signal may be used for thrust or total impulse control programming. This reference control signal must also account for changes in the mass of the spacecraft.

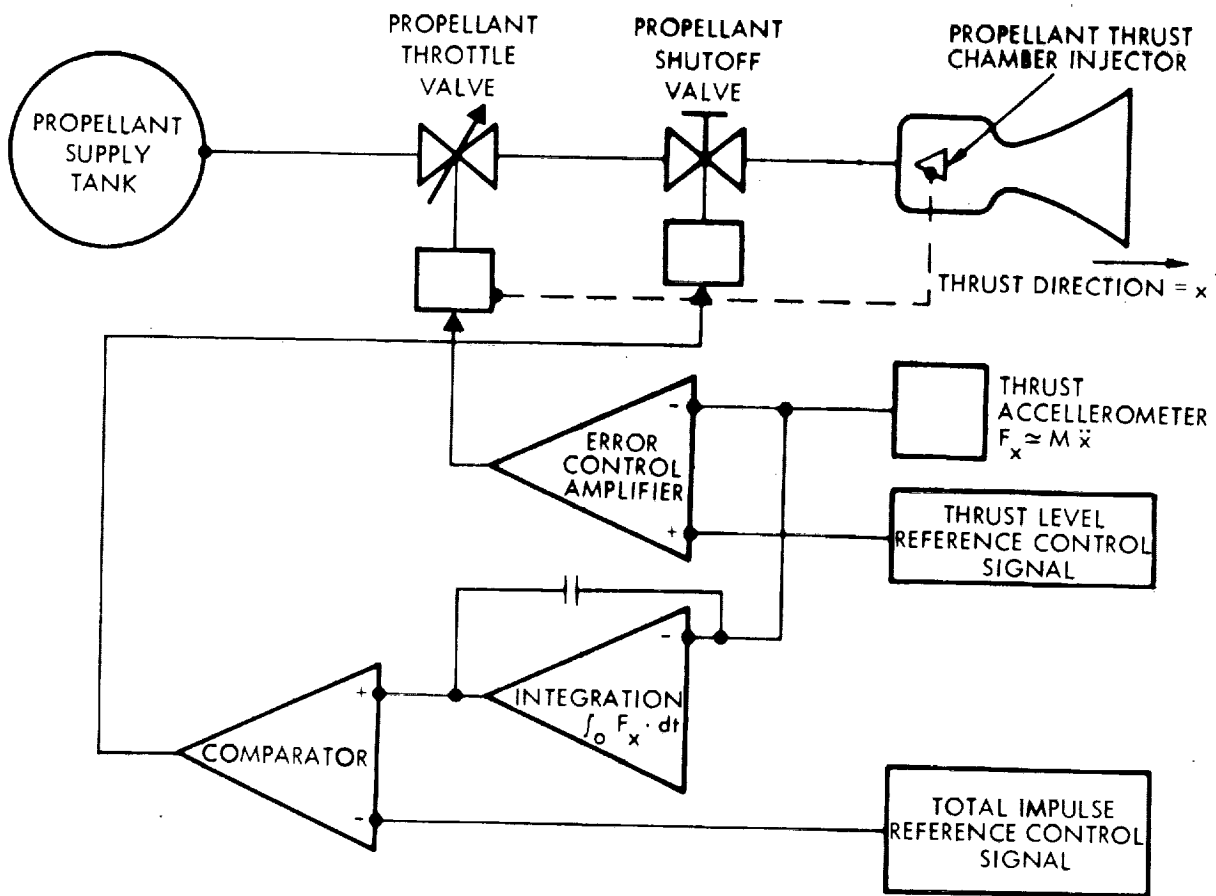


Figure 7-16. Accelerometer Control System for Spacecraft Engine Valves

## 7.4 LEAKAGE MEASUREMENT CONCEPT - ABLEAK

### 7.4.1 Introduction

Leakage is a perennial valve problem. Spacecraft valve leakage measurements are required to establish propellant losses which may affect spacecraft mission duration, cause damage to materials, interfere with onboard space experiments, or cause fire and explosion and toxic hazards. Spacecraft valve leakage requirements may range from over 25 scc of nitrogen to zero-leakage helium. "Zero" gas leakage is defined by the Jet Propulsion Laboratory in Figure 7-17 (from Reference 4). For many propulsion valve applications, "zero" leakage for a range of gas pressure from 20 to 1000 psi is determined from Figure 7-17 to be  $10^{-7}$  sccs helium. Measurements of this magnitude are accomplished using the helium mass spectrometer as a leak detector.

For purposes of qualification, valve leakage is commonly specified as gas even though the actual fluid is a liquid (usually a highly reactive propellant). At present, there is no acceptable measurement method of converting leak rates of one medium to another and no acceptable measurement device has been found for measuring liquid propellant leakage. Other investigators at the Advanced Technology Laboratories of General Electric have contributed much, under NASA sponsorship, to determine the accuracy of leakage measuring equipment, calibrate leakage standards, and establish standard leakage units (References 5, 6, and 7).

Investigators at TRW were directed toward the development of a device which can measure gross to zero leakage of either liquid or gas, the measurements being independent of temperature and pressure and traceable to NBS standards. Conceptual evaluation of a device which measured the buoyancy change on a ball suspended in the leak media was completed (References 8 and 9). In operation, leaking gas is directed into a volume ( $V_c$ ) to cause a buoyant force on a ball suspended in the gas. This buoyant force  $F$  is measured using an electrobalance. The cavity volume ( $V_c$ ), the volume of the ball ( $V_b$ ), and the measured buoyant force ( $F$ ) as a function of time can then be combined in the following equation to yield the leakage ( $\dot{W}$ ) in mass flow units:

$$\dot{W} = V_c/V_b F$$

For a liquid leak, the chamber pressure is held below the vapor pressure of the liquid. The liquid then vaporizes in the chamber causing a buoyant force on the ball, so that the leak rate can be established as with a gas leak.

Two measurement instruments were constructed using this principle of operation. The measuring devices were identified by the coined term ABLEAK. ABLEAK 1, the first measuring instrument developed at TRW Systems (Reference 9), used a Cahn electrobalance with a 1 gram capacity for force measurement. ABLEAK 100 utilized a 100 gram capacity Cahn Electrobalance. The ABLEAK instruments are capable of measuring gaseous or liquid leakage continuously over a wide range, and are capable of measuring both internal and external

"ZERO" GAS LEAKAGE

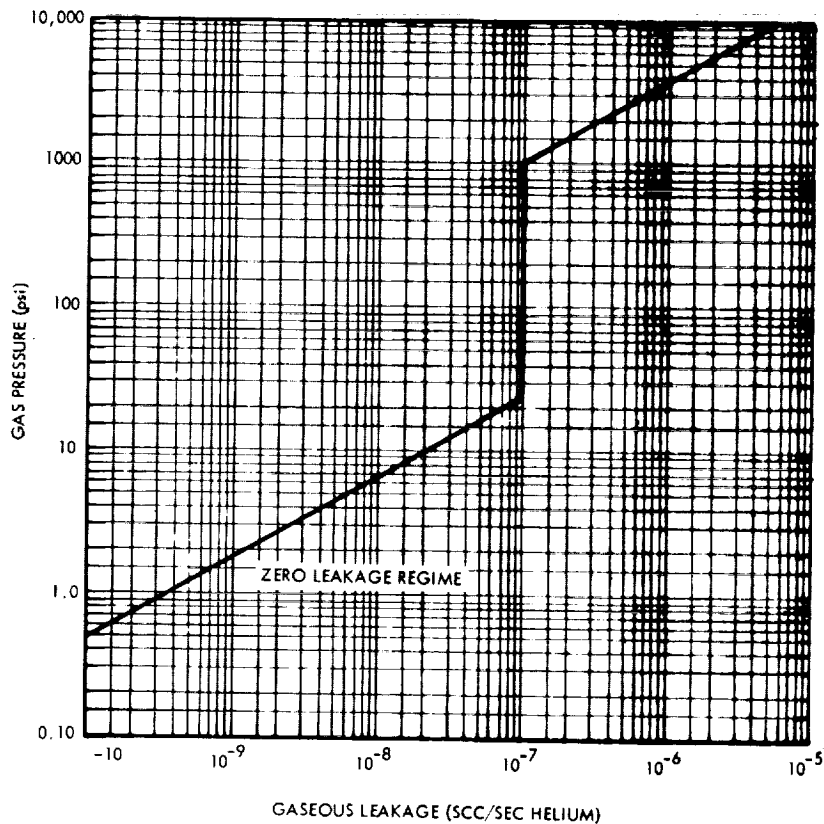


Figure 7-17. Definition of Zero Gas Leakage  
(Courtesy of Jet Propulsion Laboratory)

leakage. Leakage is measured directly in units of mass per unit time with a sensitivity of  $1 \times 10^{-7}$  grams.

The important characteristics and observations made during the evaluation of ABLEAK are summarized as follows:

1. The measured mass leak rate is nearly independent of the upstream species of liquid or gas when the downstream accumulation is allgaseous.
2. If the leak path is not altered due to cycling or pressure loading, the mass leak rate is proportional to the differential pressure across the leak.
3. Small liquid leaks into low pressure may result in sustained freeze plugging of the leak. Such freezing in spacecraft valves may cause serious operational problems during actual space missions. Spacecraft valve qualification tests should recognize and properly evaluate freezing caused by liquid leaks into vacuum.
4. Flexible valve seal materials may evidence greatly reduced leakage after sustained liquid exposure.

5. Accurate leakage measurements of accumulated downstream condensible gases can be made when the downstream accumulation is superheated or supersaturated. Accuracy is lost, however, when progressive downstream condensation commences.
6. Currently accepted leakage testing techniques do not simulate the actual downstream conditions of space operation. The valve leak experimental methods utilizing ABLEAK are practical for realistic space simulation testing.

#### 7.4.2 ABLEAK Concept

ABLEAK utilizes a container with a sensitive weight measuring device to measure the change in weight of an evacuated sphere due to the buoyancy of the gas within the container which surrounds the sphere. The container is first evacuated to an adequately low pressure and the leak whose mass flow rate is to be determined is admitted to the container. A schematic of the system is shown in Figure 7-18 and a photograph of the ABLEAK 1 measuring instrument in Figure 7-19.

The mass flow rate measured by ABLEAK is given by the system leak equation:

$$\frac{\dot{\Delta W}}{\Delta t} = \frac{\Delta W}{\Delta t} \frac{V_c}{V_s}$$

- where:
- $\Delta W$  = indicated weight increment (buoyancy force) on the sensitive weight scale during the time interval  $\Delta t$
  - $\dot{\Delta W}$  = total mass of fluid (leak) introduced into the detector chamber during the time interval  $\Delta t$
  - $V_c$  = net active gas volume of the chamber containing the weight balance device and evacuated sphere
  - $V_s$  = displacement volume of the evacuated sphere.

For any given time interval  $\Delta t$ ,

$$\dot{\Delta W} = \Delta \rho V_c$$

$$\Delta W = \Delta \rho V_s$$

Where  $\Delta \rho$  is the added change in density of the chamber media. Eliminating  $\Delta \rho$  and for any given time interval the leak equation reduces to:

$$\dot{\Delta W} = \Delta W \frac{V_c}{V_s}$$

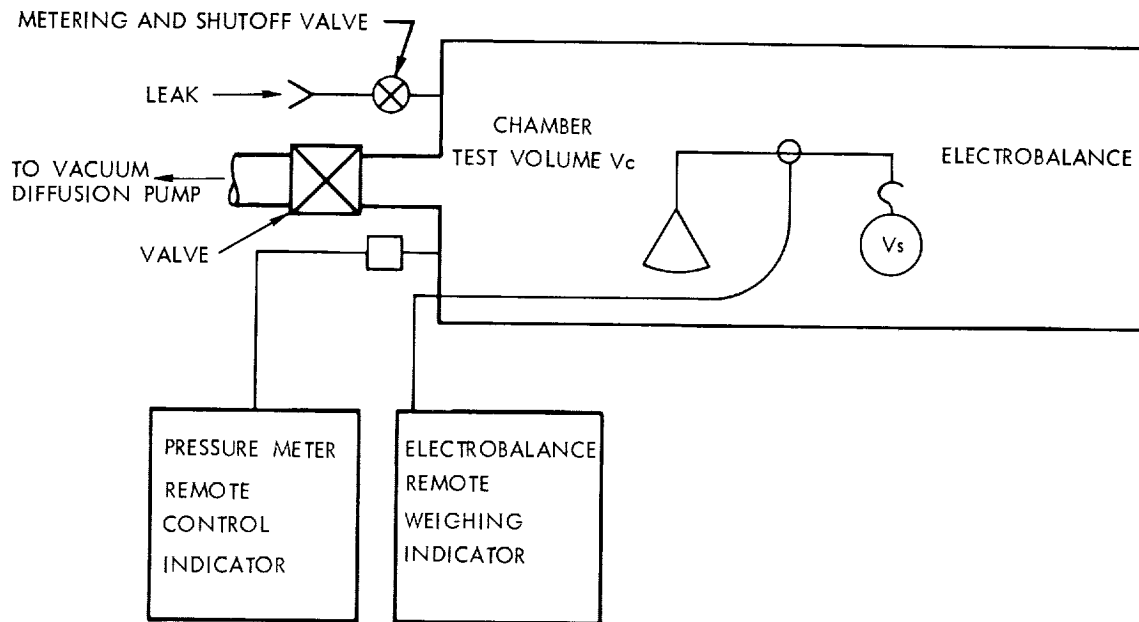


Figure 7-18. Schematic of ABLEAK 1



Figure 7-19. ABLEAK 1 Mass Leak Measurement System

### 7.4.3 Valve Leak Investigations

ABLEAK 1 was used to measure air, nitrogen, argon, methanol and nitrogen tetroxide leakage from the oxidizer shutoff valve of the Lunar Module Descent Engine (LMDE). Figures 7-20 and 7-21 show the test configuration used for the leak tests on the LMDE shutoff valve. A summary of the results is given in Table 7-2. The LMDE oxidizer shutoff valve tested consists of two ball valve elements in series in a single aluminum body. The internal ball seals and the external shaft seals are spring loaded Teflon lip seals. A single seal is located on the upstream side of each ball.

7.4.3.1 External Air Leakage - External atmospheric air leakage through the shaft seals was measured with both ball valves open to vacuum. The inlet was closed by the supply valve (Figure 7-20). A downstream leak rate of 0.35 milligrams of air per minute was measured. Subsequent internal leakage tests (see Table 7-2) were conducted with a downstream vacuum without a guard vacuum external to the valve, so that external air leakage would be included in the total measured leakage. Air leakage through both ball shaft seals must be considered with only the upstream ball valve closed.

7.4.3.2 Nitrogen Leakage - Nitrogen leakage measurements were made with gaseous supply pressures of 40, 80, 120 and 150 psig and all valve closure combinations as summarized in Table 7-2. Measurements on the downstream valve only showed a consistent predictable leak rate given by:

$$\Delta\dot{W}/\Delta t = 0.0364 P + 0.556$$

where:  $\Delta\dot{W}/\Delta t$  = milligrams/minute leakage and P = supply pressure in psig.

The inlet valve section leaked excessively and results were not consistent or predictable. As expected, the leakage with both sections closed was initially low due to low initial pressure between valve sections. The leakage approached that of the best valve section after approximately one hour operation.

7.4.3.3 Methanol Leakage - Liquid methanol was selected for leak tests because the low freezing temperature would minimize the possibility of freeze plugging and the molecular weight was compared to other materials tested. During the first two hours of test the mass leak rate was comparable to the leakage of other fluids tested. However, the test was repeated after the valve soaked for a period of approximately 16 hours in an upstream supply of liquid methanol and the measured leak rate was negligible. The apparent leakage after the soak period was less than the calibrated external air leakage. The low methanol leakage was apparently due to swelling of the seals.

7.4.3.4 Argon Leakage - The argon mass leak rate was comparable to other fluids tested.

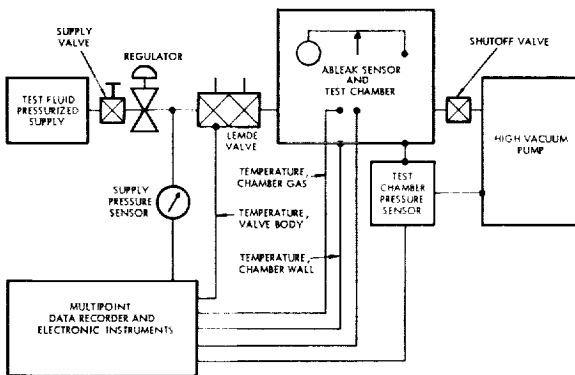


Figure 7-20. ABLEAK LMDE Valve Test Arrangement

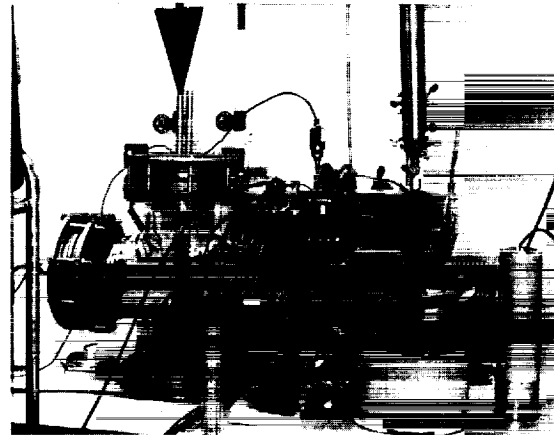


Figure 7-21. LMDE Oxidizer Shutoff Valve Test Setup

Table 7-2. LMDE Oxidizer Shutoff Valve Test Data

Test Fluid	Supply Pressure (psig)	Typical Average Leak Rate (milligrams/minute)	Valve Position
External Air	0	0.35	Both open
N <sub>2</sub> Gas	6.6	1.45	Both closed
N <sub>2</sub> Gas	40.0	1.4 2.5 at 60 min.	Both closed
N <sub>2</sub> Gas	40.0	2.15	Downstream closed
N <sub>2</sub> Gas	40.0	9.4	Upstream closed
N <sub>2</sub> Gas	80.0	1.2 3.8 at 60 min.	Both closed
N <sub>2</sub> Gas	80.0	3.8 calculated 3.35 measured	Downstream closed
N <sub>2</sub> Gas	80.0	11.2 typical	Upstream closed
N <sub>2</sub> Gas	120.0	1.2 3.2 at 60 min.	Both closed
N <sub>2</sub> Gas	120.0	5.25 average	Downstream closed
N <sub>2</sub> Gas	120.0	7.8 typical	Upstream closed
N <sub>2</sub> Gas	150.0	0.8 2.4 at 60 min.	Both closed
N <sub>2</sub> Gas	150.0	5.9 or 6 typical	Downstream closed
N <sub>2</sub> Gas	150.0	11.5 typical	Upstream closed
CH <sub>3</sub> OH Liquid 1st Day Test	80.0	3.8 typical	Downstream closed
CH <sub>3</sub> OH Liquid Soaked Overnight	80.0	0.32 typical = air leak	Downstream closed
Argon Gas	80.0	3.0	Downstream closed
N <sub>2</sub> O <sub>4</sub> Liquid	15.0	1.12 average $\Delta M/\Delta T$ before freezing	Downstream Closed

NOTE: 1.0 milligram/minute of N<sub>2</sub> = 50 scch



7.4.3.5 Nitrogen Tetroxide Leakage - An attempt was made to measure leakage of liquid nitrogen tetroxide, but freeze plugging rapidly sealed the valve. Leakage was observed when the liquid nitrogen tetroxide was first admitted under its own vapor pressure (approximately 1 atmosphere). Complete freeze plugging occurred about 4 minutes after the supply was introduced. The mass leak rate of nitrogen tetroxide before freeze plugging was approximately equal to other fluids tested.

Figure 7-22 illustrates the behavior of the LMDE valve during the first 5 minutes of the  $N_2O_4$  test. The rate of chamber pressure,  $P_c$ , increase during the first minute of leakage indicates the highest leak rate progressing to negligible pressure change and leak rate after the first 4 minutes of the test. The mass leak rate  $\Delta\dot{W}/\Delta t$  indicated by the buoyancy sensor was low during the first minute, increasing to a maximum at point a after 2 minutes freeze plugging. The apparent low rate during the first 2 minutes is caused by the counteracting negative buoyancy effect of  $N_2O_4$  adsorption on the spherical sensor surface.

#### 7.4.4 Evaluation of ABLEAK 100

ABLEAK 100 (Figure 7-23) was found to be approximately 100 times more sensitive than the early prototype ABLEAK 1. The primary limitation to further improvement is the ability to measure a more sensitive force with present technology. This limitation is directly attributed to the sensitivity of the Cahn Electrobalance, which has been improved to  $1 \times 10^{-7}$  gram by modifications made at TRW.

The performance parameters of ABLEAK 100 were measured by injecting an accurately measured volume and weight of argon into the closed, evacuated test chamber of the leak measurement equipment. The injection rate was controlled to minimize the aerodynamic disturbance to the weight measuring equipment. Details are given in Reference 10.

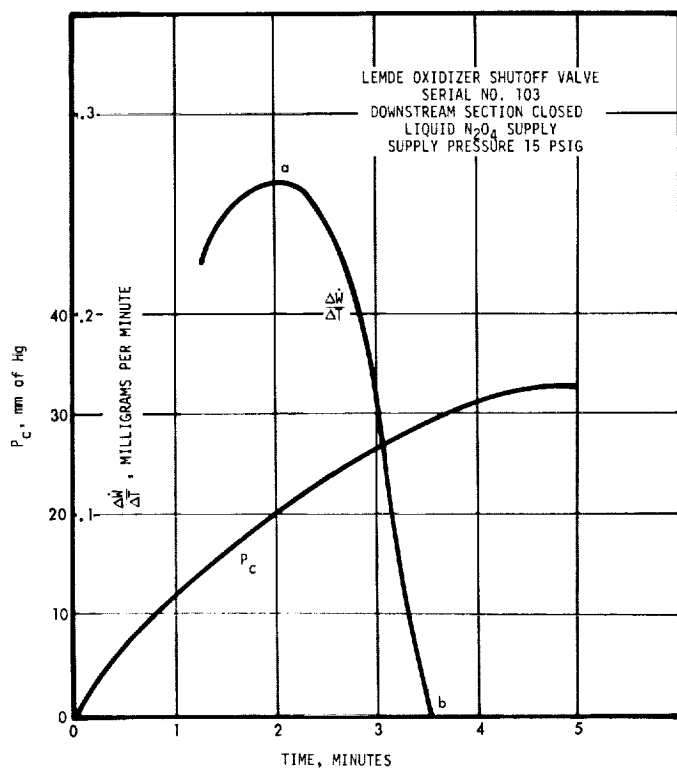


Figure 7-22. LMDE Valve N<sub>2</sub>O<sub>4</sub> Leakage

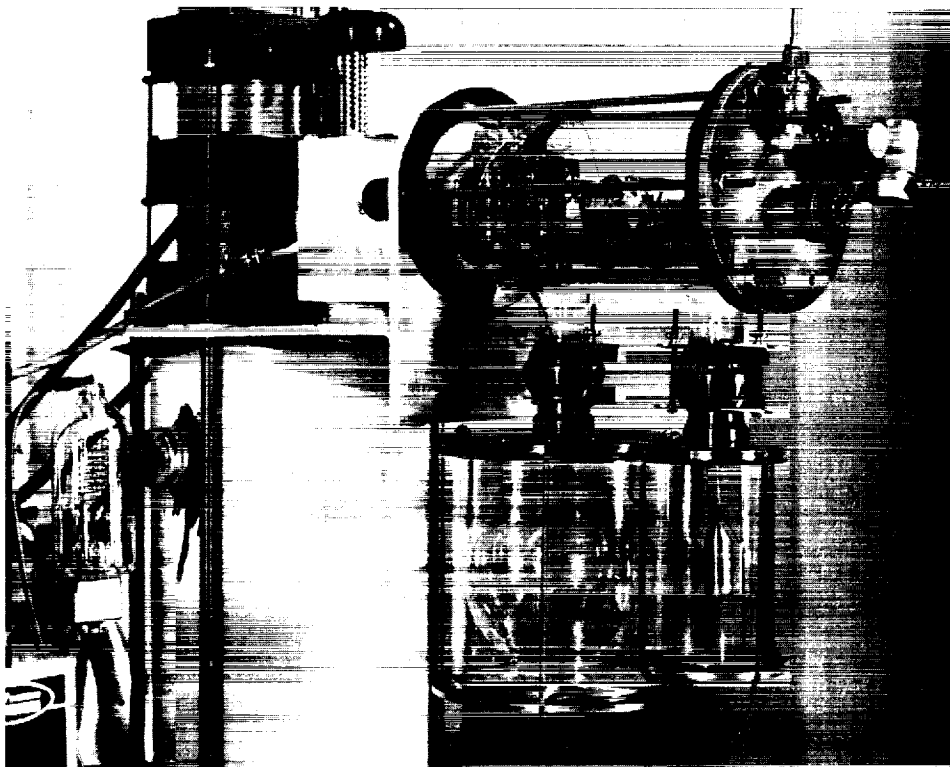


Figure 7-23. ABLEAK 100 Mass Leak Measurement System

## 7.5 ELECTROPYROTECHNIC CARTRIDGE TESTER

### 7.5.1 Introduction

Deflagration squib cartridge tests performed during this program (Reference 8), revealed a weakness in evaluating any degradation of the cartridges after exposure to the space environmental tests. Normal test procedure involved firing the cartridges in a fixed-volume bomb and recording pressure versus time on an oscillograph. Squib cartridges used for valve actuation require propellant charges of the deflagration type in which the expanding high temperature, high pressure combustion gases do work against a movable piston. The pressure-time information obtained from the fixed bomb does not represent this work output. Degradation of work output due to environmental exposure could escape detection if the squib was evaluated by the fixed-volume bomb test method.

A squib tester in which the energy generated by the squib is absorbed by a liquid spring shock absorber was conceived on this program as a possible solution to problems involving test of squibs after exposure to radiation, vacuum, and sterilization. Such a device, incorporating a piston-driven liquid compressibility element as well as a dashpot for absorbing energy, was designed and developed by a private manufacturing company, Integrated Dynamics, Inc., Buffalo, New York. A cutaway view of the tester is depicted in Figure 7-24.

The following measurements can be made with the dynamic tester:

1. Work output - pressure or force versus displacement
2. Impulse - pressure or force versus time
3. Displacement versus time
4. Acceleration

The tester is also adaptable to changes in the initial volume, piston diameter, piston stroke, and mounting port. These changes are possible because of removable cylinder heads, piston, and spring-shocks. It is estimated that three spring-shocks and two different size pistons can represent the work output of a significant portion of the ordnance devices used in spacecraft applications including valve actuators.

### 7.5.2 Advantages of the Dynamic Tester

7.5.2.1 Qualification - Thousands of dollars are spent qualifying squibs by destructive testing of pyrotechnic actuated devices. The dynamic tester can provide a means of qualifying the squib cartridge itself. This can be achieved by establishing a tolerance band on the work output of a sample of cartridges.

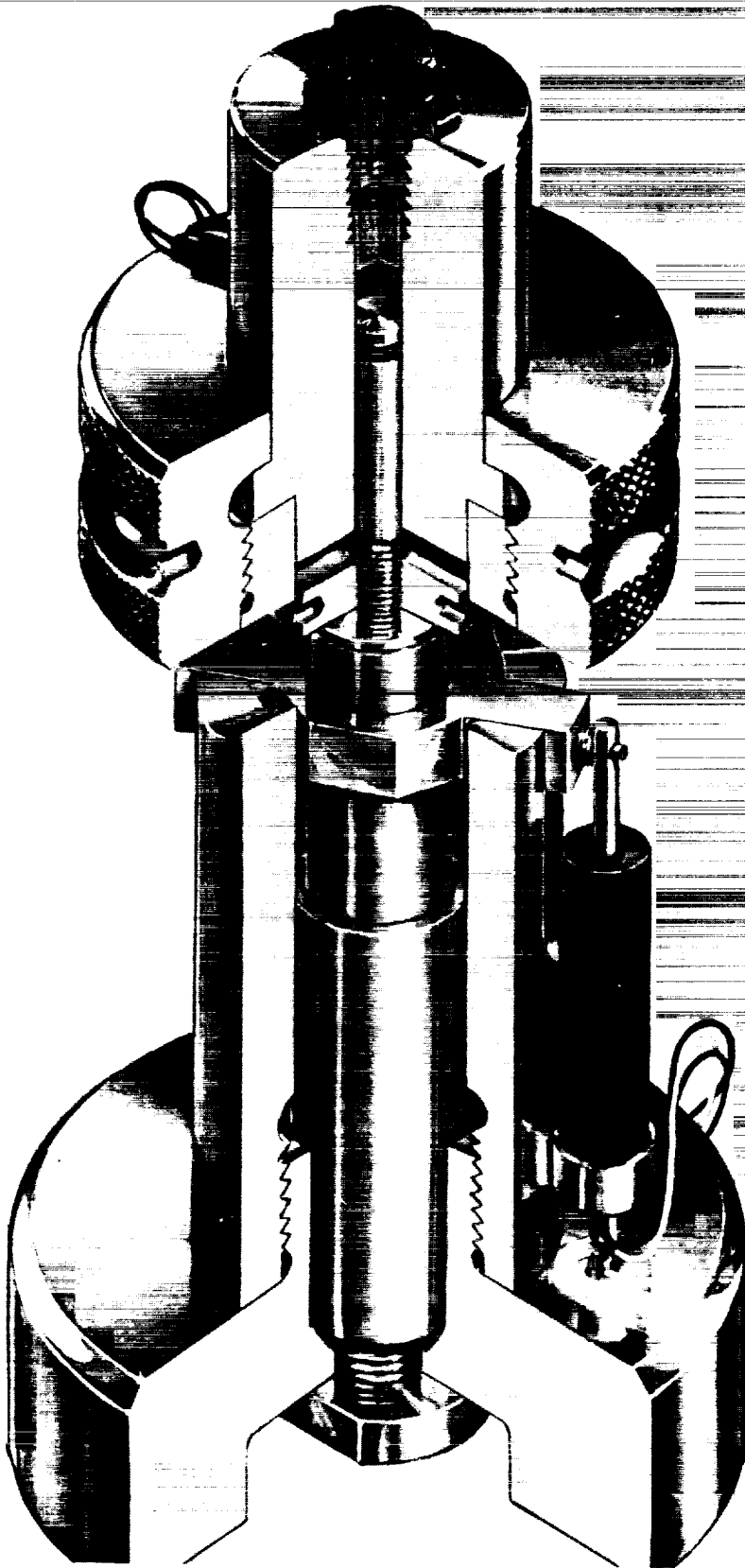


Figure 7-24. Dynamic Squib Tester (Pyromite Model 1040)

7.5.2.2 Research and Development - The dynamic tester may be used in optimizing propellants used in deflagration type explosives, including grain size and amount. Testing of new propellants and new concepts involving unique means of initiation is also possible with the dynamic tester.

7.5.2.3 Environmental Testing - Degradation of propellants after exposure to environments such as radiation, vacuum, humidity, vibration, and high temperature may be measured by comparing the work output of exposed squibs to a control sample. Work output data may also be used in determining propellant degradation due to shelf life.

7.5.2.4 Design - It would be possible to establish characteristic work output curves to aid designers in selecting propellant type and load for a particular application. Peak pressure and work output would provide the necessary design information in selecting pyrotechnics for actuation of mechanisms.

7.5.2.5 Quality Control - Chemical composition of propellants may vary between batches resulting in changes in work output. Once a set of characteristic curves is obtained, such as the work curve, any differences between batches would be easily detected. Quality control can also be inexpensively maintained on items stored over a long time period.

7.5.2.6 Simulation Testing - In some cases the dynamic tester may be used to simulate the end item hardware, such as a valve actuator. If a known "actuation" force is required, a spring-shock can be designed with a given preload. The piston will not begin its stroke until the preload force is overcome, thus simulating the minimum force required to shear a pin or bolt.

### 7.5.3 Test Instrumentation

There are many approaches to the instrumentation with this device. The minimum instrumentation required to obtain usable data would consist of a pressure or force transducer with its associated circuits, a linear motion potentiometer, an oscilloscope capable of having its horizontal sweep driven by an external signal, and an oscilloscope camera. The basic requirement is to measure force and piston displacement with respect to time, or with respect to each other. A brief discussion of several possible methods used in measuring these parameters and recording and reducing the data follows.

7.5.3.1 Force Measurement - The use of strain gages for force measurement requires an external balance circuit, an excitation voltage, an operational amplifier, and a system for calibrating the gaged member. Strain gages may be applied to the piston shaft, or a special load collar. If a collar is used, extreme care is required in the choice of materials and the machining of mating surfaces. The collar should be calibrated as an assembly, with all of its mating components. Strain gages are subject to damage from careless handling, and to both mechanical and electrical overloads.

A load cell with an electrostatic charge amplifier can also be used for force measurement. Most commercial crystal load cells require only periodic calibration checks, and some may be statically calibrated. Force may also be inferred from chamber pressure measurements by multiplying pressure by the piston area.

7.5.3.2 Position Measurement - A linear motion potentiometer is the most convenient method of measuring position. The only additional requirement is a voltage source. These disadvantages associated with wirewound potentiometers are wiper bounce and accelerated wear at high velocities. Potentiometers with conductive film or plastic resistive elements generally have considerably less wiper bounce, and better wear characteristics.

A linear variable differential transformer (LVDT) would eliminate all of the disadvantages of the linear motion potentiometer, since there are no sliding mechanical parts. The only limitation to the use of the LVDT would be the available carrier excitation frequency.

Either velocity or acceleration may also be measured, and the results integrated to obtain position data at some sacrifice in accuracy.

#### 7.5.4 Evaluation

The Pyromite Model 1040 tester was used during several squib cartridge evaluation programs at TRW to provide an entirely new concept and method for gaining detailed information on the possible variation of energy output from one cartridge to another within the same family or lot. These programs verified the usability of such a tester to qualify squib cartridges for use in missiles and spacecraft. In brief, the tester provides accurate and reproducible data with approximately one percent accuracy on pressure versus time, displacement versus time, force versus time, pressure versus displacement and force versus displacement.

## 7.6 CORROSION MEASUREMENT BY HOLOGRAPHY

A hologram is capable of recording a complex optical wave so that when the hologram is reilluminated later, another optical wave is generated identical to the original. It is this property which makes it possible to use a hologram to generate either the test beam or a comparison beam, or both as an interferometric analytical technique.

Holographic interferometry may be considered as a form of common path interferometry (normally not used with conventional light sources due to various optical distortions) except that the test and comparison beams are separated in time. It is the use of this feature, the stored beam interferometric method, that is of interest here. When the comparison beam is holographically recorded and "stored", and the reconstructed comparison beam is compared with the actual subject and test beam, then the real time behavior of the subject can be seen interferometrically. Thus, the stored-beam holographic interferometric method offers not only real time information but also a means for acquiring time-lapse or moving picture records during the course of the reaction.

Figure 7-25 schematically illustrates the process for obtaining stored beam interferograms. The test environment (in this case a concentrated  $\text{HNO}_3$ ) is superimposed upon a holographic comparison beam and the complete comparison beam is developed. After development, the stored-beam reference plate is repositioned, and reilluminated by the holographic reference beam, and positioned such that reference interferometric test pattern is formed. The material to be tested is inserted into the test environment, and the reaction between the material and the test environment is recorded.

### 7.6.1 Test Setup

Figure 7-26 shows the test apparatus used to evaluate this technique. The prism deflects the laser beam and directs it toward the reference plate in order to make the original stored-beam reference plate. The laser used was a model 124 Spectra-Physics 23 milliwatt helium-neon gas laser operating in the TEM mode. A 35 mm camera was used to record the events during these tests, however, a movie camera could also be used to resolve the more rapidly occurring initial events.

Reagent grade (70% assay) concentrated nitric acid was used as the corrodent. The basic metal used was commercial 1020 cold-rolled steel, with a standard 32 micron finish; one sample consisting of the bare metal, the other case hardened by carburizing. Each sample was 3.0 inches long by 0.50 inch wide by 0.10 inch thick. The coupons, electrically isolated from one another, were immersed into the nitric acid test tank after the reference fringes were recorded, and pictures were taken every thirty seconds for the first five minutes of immersion, and every minute thereafter, until initial, near passivation was evident in the most severely attacked case.

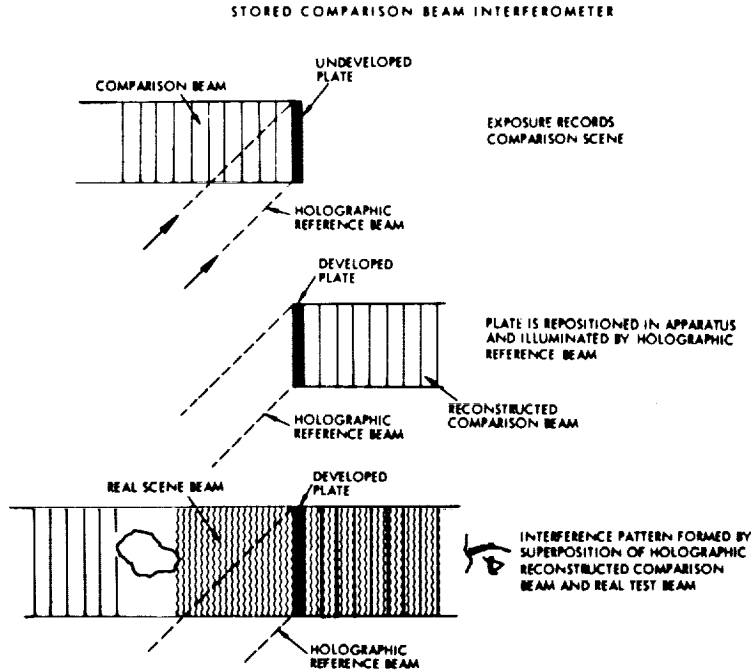


Figure 7-25. Stored Beam Holographic Interferometer Technique

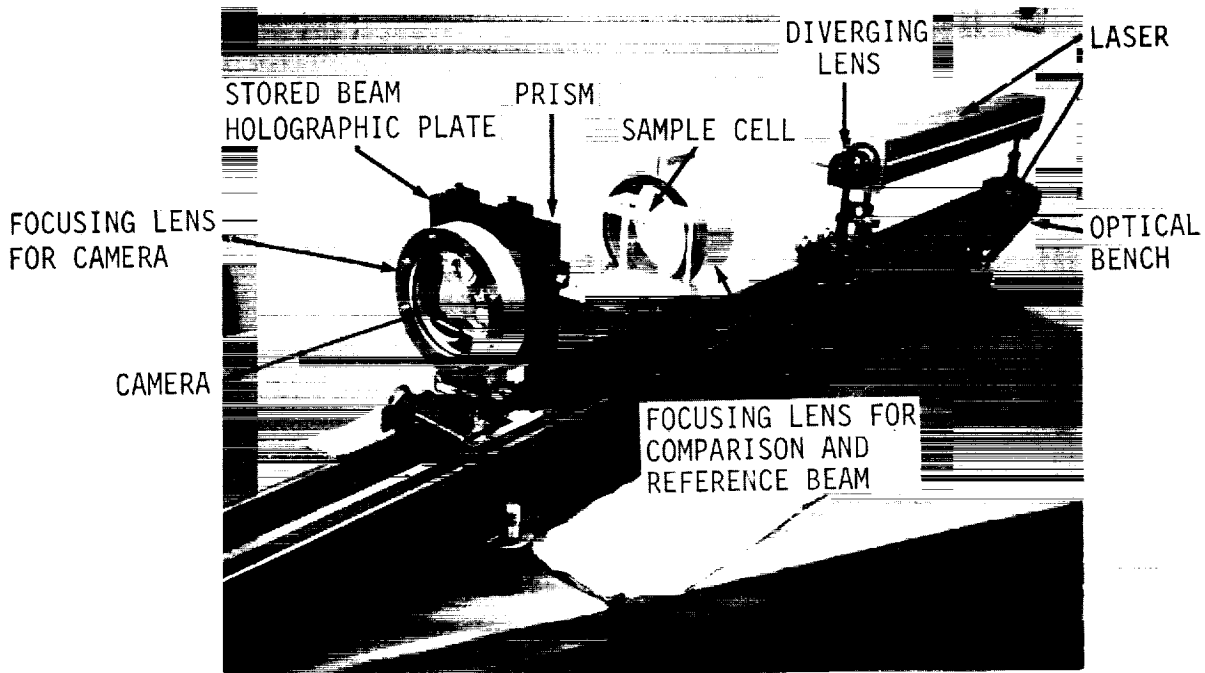


Figure 7-26. Stored Beam Holographic Interferometer Apparatus



## 7.6.2 Test Results

7.6.2.1 Unprotected Specimens - Figure 7-27 shows the selected time events and reactions during the course of the interaction between the specimens and the corrodent. In all cases, the case-hardened specimen is on the left. As can be seen, the basic reference fringe pattern shows all of the inhomogeneities of the test setup, so that the basic distortions in the test apparatus can easily be distinguished from the events occurring during reaction. The specimens are shown edge-on, so that reactions across the main sample area can be observed.

After immersion, there was an intense, initial reaction on both specimens, probably due to reaction of the nitric acid with surface contaminants. The picture at 30 seconds shows a slight initial reaction with the case-hardened specimen, as seen by the distortion of the fringes below the specimen. The two dark spherical shapes on the bottom edge of the case-hardened specimen are bubbles which were formed upon immersion and are of no significance to the test.

After one minute, a very vigorous reaction occurred with the case-hardened specimen, as evidenced by the extreme fringe shift and the distortion of the fringes below the specimen from reaction products streaming down toward the bottom of the tank. Some reaction is occurring at the surface of the regular steel specimen, but not to the extent of the case-hardened specimen.

The pictures at 1.5, 3.0, 3.5 and 5.0 minutes, however, show that the reactions between the nitric acid and the case-hardened and regular steel specimens begin to reverse. The case-hardened specimen gradually passivates while progressively, the regular specimen reacts more vigorously with the nitric acid.

At the end of ten minutes reaction time, the case-hardened specimen is nearly passivated, as indicated by the nearly parallel fringes, whereas some reaction is still progressing on the surface of the regular specimen. The specimens progressively became more passivated by the nitric acid until at the end of the experiment, shown in the last photograph at 28 minutes, both the case-hardened and the regular specimens are nearly completely passivated. This is evident by the appearance of the fringes, which are nearly parallel across the picture, as in the reference frame, and also are nearly perpendicular to the faces of the specimens. Some slight reaction is still occurring, since a small amount of fringe shift is evident; for the most part however, a passivation layer has developed over the bulk of the specimens. It should be emphasized that these reactions could be observed indefinitely, as long as the apparatus is not disturbed. Thus, intermittent observations could be made over a much longer time span than was done in these series of experiments.

7.6.2.2 Thin Film Protected Specimens - Figure 7-28 shows the interaction between the protected specimen and the corrodent. Time events, experimental procedures, and mounting techniques were identical to the tests performed on the unprotected specimens, with the exception that one surface of each specimen was protected by a thin polymerized film. Figure 7-29 schematically illustrates the arrangement of the specimens with respect to the protective film.

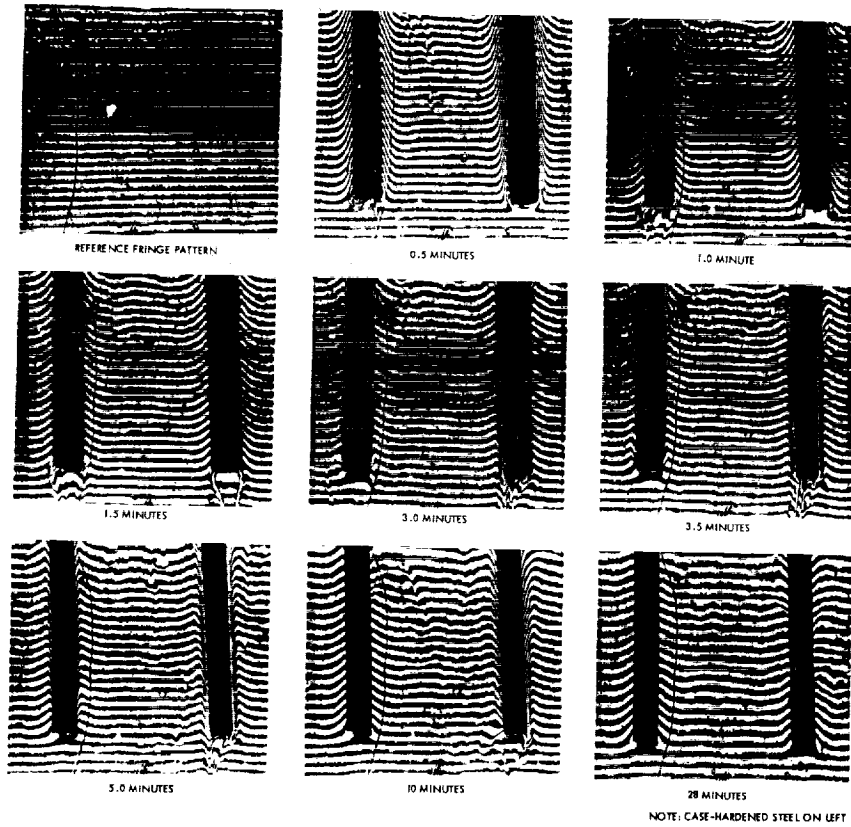


Figure 7-27. Holographic Interferometer Photographs of Steel Corrosion in Nitric Acid

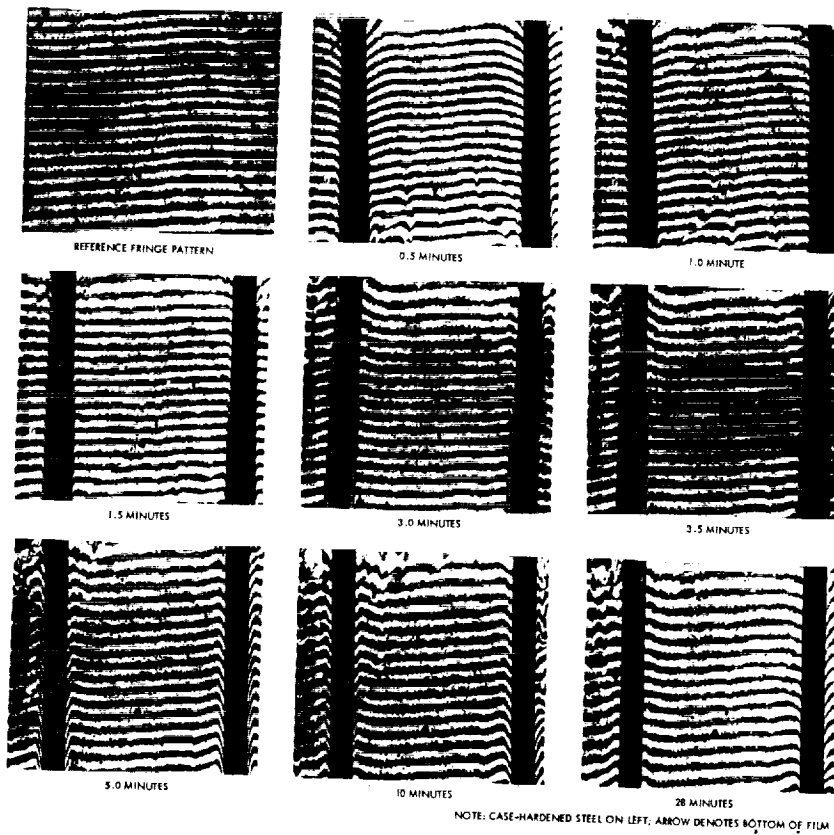


Figure 7-28. Holographic Interferometer Photographs of Thin-Film Protected Steel Corrosion in Nitric Acid

In order to observe the differences between the film protected surface and the unprotected surface, as well as any film-metal interface reactions, the bottom portion of the specimens did not have the protective film, as shown in Figure 7-29.

The film was polymerized on the specimen surfaces as follows: the specimens, as targets, were placed in a holding fixture and installed in a vacuum chamber. The silicone polymer precursor (Dow Corning DC 705 silicone oil) was placed in an evaporation boiler with the outlet orifice directed toward the target. An electron beam gun was positioned perpendicular to the specimens, and the vacuum chamber evacuated. After the appropriate vacuum was achieved, the boiler was activated and the oil vapor was impinged upon the specimens. At the same time, the electron beam gun was turned on and the surface of the specimens were bombarded with electrons. The electron beam was rastered by the use of deflection plates so that the entire surface was uniformly covered by the beam. The interaction of the electrons with the oil at the specimen surface produces a tenacious, polymerized film. After the surfaces of the specimen were covered by the film, the boiler was cooled, the electron beam gun turned off, and the vacuum chamber was back filled with air and the specimens recovered and cleaned. The unprotected ends of the specimens were obtained by shadow masking so that no film was formed in the area.

After immersion in the test cell, the unprotected portions of the specimen underwent the same initial, intense reaction with the nitric acid. The protected portion of the specimens, however, did not react to any extent, as shown by the relatively small fringe shift above the reference mark. The film protected the specimens for 3.5 minutes, as evidenced by the small fringe shift in the film protected area (Figure 7-28) as contrasted to the unprotected bottom and back sides of the specimens. After this time period, however, the film-metal interface started reacting with the nitric acid, and some reaction occurred above the interface edge. Distortion of the fringes in the bulk of the tank away from the specimens as illustrated by the picture taken at 10 minutes (Figure 7-28) is probably due to small pieces of film floating down from the top portion of the specimen not shown in the picture.

As with the unprotected specimens shown in Figure 7-27, these specimens also became passivated at the end of the experiment, as shown in the picture taken at 28 minutes in Figure 7-28.

Microscopic examination of the specimens after the test showed that although the film-metal interface was attacked by nitric acid which slowly worked its way under the film, the bulk of the film-covered surface was protected except at minor pinpoint areas over the surface. This was probably due to the thinness of the film in areas where the roughness of the metal surface prevented the film from being uniformly thick over the total surface area of the specimen. This is schematically illustrated in Figure 7-30. This defect could be remedied by either utilizing a smoother metal finish, or thicker films.

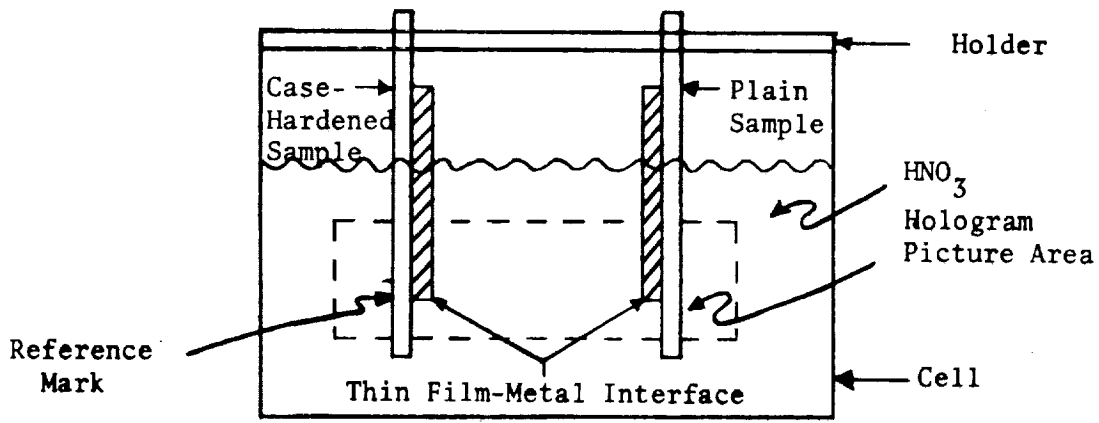


Figure 7-29. Arrangement of Coated Specimens in Cell

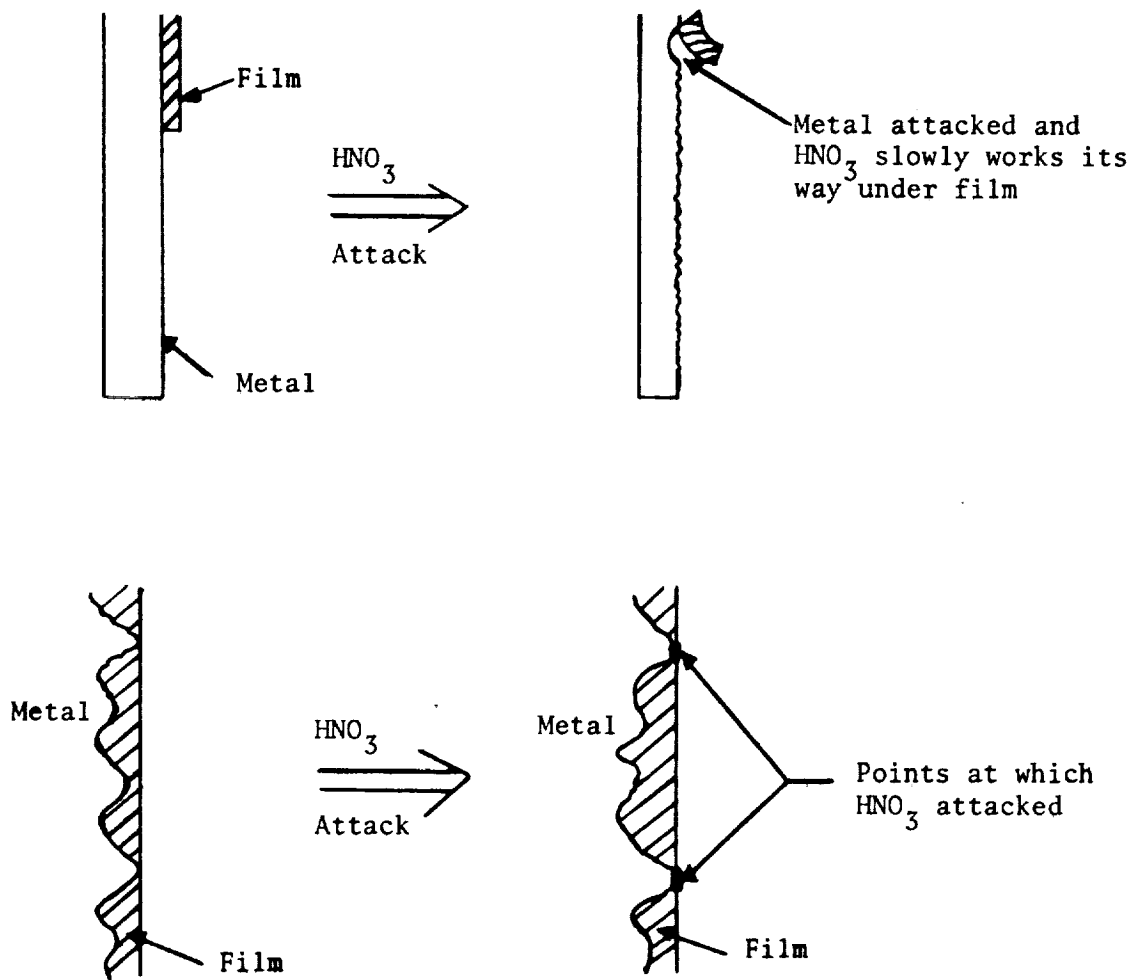


Figure 7-30. Representation of Nitric Acid Attack on Coated Steel Specimens

### 7.6.3 Conclusions

The test results have demonstrated that reactions occurring in small time spans can be studied readily and conveniently by holographic interferometry. With other techniques, similar results are either impossible or extremely difficult to obtain. Further, there is no time limitation imposed on the observations, so that minute interactions between the material and the corrodent which may occur later may also be examined. The technique is not limited to metals, in that any material which interacts with the test media may be investigated. The important area of experimentation necessary is the correlation of the fringe shift with the interactions occurring.

This method, when coupled with other referencing techniques, should give the information necessary for determination of materials compatibility for long duration spacecraft missions.

## 7.7 REFERENCES

1. Advanced Valve Technology for Spacecraft Engines, Final Report No. 8651-6033-SC000, Volume II New Concepts, TRW Systems Group, July 19, 1964.
2. Kraus, J. D., Electromagnetics, McGraw-Hill, New York, New York, 1953.
3. Shercliff, J. A., Electromagnetic Flow Measurement, Cambridge University Press, Great Britain, 1962.
4. Weiner, Richard S., Basic Criteria and Definitions for Zero Fluid Leakage, JPL Technical Report No. 32-926, December 15, 1966.
5. Marr, J. W., Leak Measurement and Evaluation, General Electric Report 64GL163, October 12, 1964.
6. Marr, J. W., Leak Detection and Measurement, General Electric Report 65GL28, February 1, 1965.
7. Research and Development Center, Study of Dynamic and Static Seals for Liquid Rocket Engines, General Electric Final Report, NASA Contract NAS 7-102.
8. Advanced Valve Technology for Spacecraft Engines, Final Report No. 8651-6032-SU000, Volume I Valve Study, TRW Systems Group, July 19, 1964.
9. Advanced Valve Technology for Spacecraft Engines, Final Report No. 8651-6042-SU000, TRW Systems Group, August 1965.
10. Advanced Valve Technology, Interim Report No. 06641-6004-R000, TRW Systems Group, November 1966.

FINAL REPORT DISTRIBUTION LIST  
CONTRACT NAS 7-717

	<u>Copies</u>
NASA Headquarters Washington, D. C. 20546 Contracting Officer	1
NASA Lewis Research Center 2100 Brookpark Road Cleveland, Ohio 44135 Office of Technical Information	1
NASA Manned Spacecraft Center Houston, Texas 77001 Office of Technical Information	1
NASA Marshall Space Flight Center Huntsville, Alabama 35812 Office of Technical Information, MS-IP Technical Library Dale Burrows S&E - ASTN - PJ	2 1 1
Jet Propulsion Laboratory 4800 Oak Grove Drive Pasadena, California 91103 Louis Toth	2
Chief, Liquid Propulsion Technology RPL Office of Advanced Research and Technology NASA Headquarters Washington, D. C. 20546	3
Director, Technology Utilization Division Office of Technology Utilization NASA Headquarters Washington, D. C. 20546	1
NASA Scientific and Technical Information Facility P. O. Box 33 College Park, Maryland 20740	25
Director, Launch Vehicles and Propulsion, SV Office of Space Science and Applications NASA Headquarters Washington, D. C. 20546	1
Director, Advanced Manned Missions, MT Office of Manned Space Flight NASA Headquarters Washington, D. C. 20546	1

	<u>Copies</u>
<u>NASA FIELD CENTERS</u>	
Ames Research Center Moffett Field, California 94035	1
Goddard Space Flight Center Greenbelt, Maryland 20771	1
Jet Propulsion Laboratory California Institute of Technology 4800 Oak Grove Drive Pasadena, California 91103	2
Langley Research Center Langley Station Hampton, Virginia 23365	1
Lewis Research Center 21000 Brookpark Road Cleveland, Ohio 44135	1
Marshall Space Flight Center Huntsville, Alabama 35812	1
Manned Spacecraft Center Houston, Texas 77001	2
John F. Kennedy Space Center, NASA Cocoa Beach, Florida 32931	1
<u>GOVERNMENT INSTALLATIONS</u>	
Aeronautical Systems Division Air Force Systems Command Wright-Patterson Air Force Base Dayton, Ohio 45433	1
Air Force Missile Development Center Holloman Air Force Base New Mexico 88330	1
Air Force Missile Test Center Patrick Air Force Base, Florida	1
Space and Missile Systems Organization Air Force Unit Post Office Los Angeles, California 90045	1
Arnold Engineering Development Center Arnold Air Force Station Tullahoma, Tennessee 37388	1



	<u>Copies</u>
Bureau of Naval Weapons Department of the Navy Washington, D. C. 20546	1
Defense Documentation Center Headquarters Cameron Station, Building 5 5010 Duke Street Alexandria, Virginia 22314 Attn: TISIA	1
Headquarters, U. S. Air Force Washington, D. C. 20546	1
Picatinny Arsenal Dover, New Jersey 07801	1
Air Force Rocket Propulsion Laboratory Research and Technology Division Air Force Systems Command Edwards, California 93523	2
U. S. Army Missile Command Redstone Arsenal Alabama 35809	1
U. S. Naval Ordnance Test Station China Lake California 93557	1
<u>CPIA</u>	
Chemical Propulsion Information Agency Applied Physics Laboratory 8621 Georgia Avenue Silver Spring, Maryland 20910	1
<u>INDUSTRY CONTRACTORS</u>	
Aerojet-General Corporation P. O. Box 296 Azusa, California 91703	1
Aerojet-General Corporation P. O. Box 1947 Technical Library, Bldg. 2015, Dept. 2410 Sacramento, California 95809	1
Space Division Aerojet-General Corporation 9200 East Flair Drive El Monte, California	1

	<u>Copies</u>
Aerospace Corporation 2400 East El Segundo Blvd. P. O. Box 95085 Los Angeles, California 90045	1
Atlantic Research Company Edsall Road and Shirley Highway Alexandria, Virginia 22314	1
Avco Systems Division Wilmington, Massachusetts	1
Beech Aircraft Corporation Boulder Division Box 631 Boulder, Colorado	1
Bell Aerosystems Company P. O. Box 1 Buffalo, New York 14240	1
Bellcomm 955 L'Enfant Plaza, S. W. Washington, D. C.	1
Bendix Systems Division Bendix Corporation 3300 Plymouth Road Ann Arbor, Michigan 48105	1
Boeing Company P. O. Box 3707 Seattle, Washington 98124	2
Boeing Company 1625 K Street, N. W. Washington, D. C. 20006	1
Missile Division Chrysler Corporation P. O. Box 2628 Detroit, Michigan 48231	1
Wright Aeronautical Division Curtiss-Wright Corporation Woodridge, New Jersey 07075	1
Research Center Fairchild Hiller Corporation Germantown, Maryland	1

	<u>Copies</u>
Republic Aviation Corporation Fairchild Hiller Corporation Farmingdale, Long Island, New York	1
General Dynamics, Convair Division Library & Information Services (128-00) P. O. Box 1128 San Diego, California 92112	1
Missile and Space Systems Center General Electric Company Valley Forge Space Technology Center P. O. Box 8555 Philadelphia, Pa.	1
Grumman Aircraft Engineering Corp. Bethpage, Long Island New York 11714	1
Honeywell, Inc. Aerospace Division 2600 Ridgway Road Minneapolis, Minnesota	1
Hughes Aircraft Co. Aerospace Group Centinela and Teale Streets Culver City, California 90230	1
Walter Kidde and Company, Inc. Aerospace Operations 567 Main Street Belleville, New Jersey	1
Ling-Temco-Vought Corporation P. O. Box 5907 Dallas, Texas 75222	1
Arthur D. Little, Inc. 20 Acorn Park Cambridge, Massachusetts 02140	1
Lockheed Missiles and Space Co. Attn: Technical Information Center P. O. Box 504 Sunnyvale, California 94088	1
Lockheed Propulsion Company P. O. Box 111 Redlands, California 92374	1

	<u>Copies</u>
The Marquardt Corporation 16555 Saticoy Street Van Nuys, California 91409	1
Baltimore Division Martin Marietta Corporation Baltimore, Maryland 21203	1
Denver Division Martin Marietta Corporation P. O. Box 179 Denver, Colorado 80201	1
Astropower Laboratory McDonnell-Douglas Aircraft Company 2121 Paularino Newport Beach, California 92663	1
McDonnell-Douglas Aircraft Company P. O. Box 516 Municipal Airport St. Louis, Missouri 63166	1
Missile and Space Systems Division McDonnell-Douglas Aircraft Company 3000 Ocean Park Boulevard Santa Monica, California 90406	1
Space and Information Systems Division North American Rockwell 12214 Lakewood Boulevard Downey, California 90241	1
Rocketdyne (Library 586-306) 6633 Canoga Avenue Canoga Park, Calif. 91304	1
Northrop Space Laboratories 3401 West Broadway Hawthorne, California 90250	1
Aeronutronic Division Philco Corporation Ford Road Newport Beach, California 92663	1
Astro-Electronics Division Radio Corporation of America Princeton, New Jersey 08540	1
Rocket Research Corporation 520 South Portland Street Seattle, Washington 98108	1

	<u>Copies</u>
Sunstrand Aviation 2421 11th Street Rockford, Illinois 61101	1
Stanford Research Institute 333 Ravenswood Avenue Menlo Park, California 94025	1
TRW Systems Group TRW Incorporated One Space Park Redondo Beach, California 90278	1
Tapco Division TRW Incorporated 23555 Euclid Avenue Cleveland, Ohio 44117	1
Thiokol Chemical Corporation Aerospace Services Elkton Division Bristol, Pennsylvania	1
Research Laboratories United Aircraft Corp. 400 Main Street East Hartford, Connecticut 06108	1
Hamilton Standard Division United Aircraft Corp. Windsor Locks, Connecticut 06096	1
United Technology Center 587 Methilda Avenue P. O. Box 358 Sunnyvale, California 94088	1
Florida Research and Development Pratt and Whitney Aircraft United Aircraft Corporation P. O. Box 2691 West Palm Beach, Florida 33402	1
Vickers, Inc. Box 302 Troy, Michigan	1
Calmec Manufacturing Corporation 5825 District Blvd. Los Angeles, California 90022	1

	<u>Copies</u>
Carleton Controls Corporation East Aurora, New York 14052	1
J. C. Carter Company 671 W. Seventeenth Street Costa Mesa, California 92626	1
Holex Incorporated 2751 San Juan Road Hollister, California 95023	1
M. C. Manufacturing Company P. O. Box 126 Lake Orion, Michigan 90501	1
Moog Servocontrols, Inc. Proner Airport East Aurora, New York 14052	1
National Waterlift Company 2200 Palmer Avenue Kalamazoo, Michigan 49001	1
Ordnance Engineering Associates, Inc. 1030 East North Avenue Des Plaines, Illinois	1
Parker Aircraft 18321 Jamboree Road Irvine, California 92264	1
Pelmec Division Quantic Industries, Inc. 1011 Commercial Street San Carlos, California	1
Pyronetics, Inc. 10025 Shoemaker Avenue Santa Fe Springs, California 90670	1
Stratos Western Division of Fairchild-Hiller Corporation 1800 Rosecrans Boulevard Manhattan Beach, California	1
Solar Division of International Harvester Co. 2200 Pacific Avenue San Diego, California	1
Vacco Valve Company 10350 Vacco Street South El Monte, California	1

	<u>Copies</u>
Valcor Engineering Corporation 365 Carnegie Avenue Kenilworth, New Jersey 07033	1
Vickers, Inc. Division of Sperry Rand Corporation 2160 E. Imperial Highway El Segundo, California	1
Whittaker Corporation 9601 Canoga Avenue Chatsworth, California 91311	1
Wintec Corporation 343 Glasgow Inglewood, California	1

